

### **Long term test of buffer material at the Äspö Hard Rock Laboratory, LOT project**

#### **Final report on the A2 test parcel**

Ola Karnland, Siv Olsson, Ann Dueck, Martin Birgersson,  
Ulf Nilsson, Tania Hernan-Håkansson  
Clay Technology AB

Karsten Pedersen  
Microbial Analytics Sweden AB and Göteborg University  
Department of Cell and Molecular Biology

Sara Nilsson, Trygve E Eriksen  
School of Chemical Science and Engineering  
Nuclear chemistry, KTH

Bo Rosborg  
Rosborg Consulting

November 2009

**Svensk Kärnbränslehantering AB**  
Swedish Nuclear Fuel  
and Waste Management Co  
Box 250, SE-101 24 Stockholm  
Phone +46 8 459 84 00



# **Long term test of buffer material at the Äspö Hard Rock Laboratory, LOT project**

## **Final report on the A2 test parcel**

Ola Karnland, Siv Olsson, Ann Dueck, Martin Birgersson,  
Ulf Nilsson, Tania Hernan-Håkansson  
Clay Technology AB

Karsten Pedersen  
Microbial Analytics Sweden AB and Göteborg University  
Department of Cell and Molecular Biology

Sara Nilsson, Trygve E Eriksen  
School of Chemical Science and Engineering  
Nuclear chemistry, KTH

Bo Rosborg  
Rosborg Consulting

November 2009

*Keywords:* Bacteria, Bentonite, Buffer, Clay, Copper corrosion, Diffusion, Field experiment, LOT, Mineralogy, Montmorillonite, Physical properties, Radioactive waste, Repository, Äspö.

This report concerns a study which was conducted for SKB. The conclusions and viewpoints presented in the report are those of the authors and do not necessarily coincide with those of the client.

A pdf version of this document can be downloaded from [www.skb.se](http://www.skb.se).

# Abstract

In the Swedish repository concept for nuclear waste (KBS-3 concept), the spent nuclear fuel will be stored in copper canisters surrounded by compacted bentonite. The decaying power of the fuel will increase the temperature in the repository which, in combination with the uptake of ground-water, are expected to result in minor mineralogical changes in the bentonite.

The ongoing LOT test series at the Äspö Hard Rock Laboratory (HRL) are focused on identifying and quantifying such mineralogical alterations in the bentonite exposed to typical repository-like conditions. Further, buffer-related processes concerning copper corrosion, cation transport, and bacterial survival/activity are studied. In total, the LOT project includes seven test parcels, which contain a central Cu-tube surrounded by cylindrical bentonite blocks with a diameter of 30 cm, and gauges for temperature, total pressure, water pressure and humidity. Electrical heaters placed inside the copper tube are used to simulate the heat generation from the decaying spent fuel. Three parcels are exposed to standard KBS-3 conditions (maximum temperature below 100°C) and four parcels to adverse conditions (maximum temperature below ~140°C). Both the standard and the adverse test series include short term tests (1 to 2 years), medium term tests (>5 years) and long term tests (>10 years).

The present report concerns the A2 test parcel, which was a medium term test exposed to adverse conditions. Cu-coupons, <sup>60</sup>Co tracers and specific chemical substances were placed in the bentonite at defined positions. After field exposure, the entire test parcel was released from the rock by overlapping percussion drilling and wire sawing. The parcel was lifted and divided at the test site and the bentonite material was sampled for specified analyses performed by nine different laboratories in five countries. The main aspects of the various tests and analyses may be summarized in the following items:

- physical properties (water content, density, swelling pressure, hydraulic conductivity, and rheology),
- mineralogical alteration of the bentonite,
- distribution of added substances (e.g. diffusional transport of <sup>60</sup>Co),
- copper corrosion,
- bacterial survival/activity.

The main focus was on bentonite mineralogy, which, was studied by Andra, BGR, Nagra, and Posiva in addition to SKB. The results of the former studies are reported in separate appendices. Reference and exposed bentonite material were analyzed by the various groups for a number of parameters by use of an array of techniques such as mineralogy by X-ray diffraction, exchange of cations, element distribution and electron microscopy. Some specific results of interest may be summarized by the following items:

- reorganization of easily dissolved accessory minerals in the bentonite, in particular CaSO<sub>4</sub>,
- increase in cation exchange capacity of the bentonite in parts exposed to high temperature,
- no formation of illite or other typical montmorillonite alteration minerals,
- decrease in strain at failure of bentonite exposed to high temperature,
- diffusive transport of trace elements in accordance with previous studies,
- corrosion rate of metallic copper in agreement with model predictions and previous tests,
- a minor survival of bacteria.

An overarching conclusion is that the observed mineralogical alterations, as a consequence of the water saturation process and the exposure to high temperature, are relatively small and that these alterations did not change the physical properties to such an extent that the buffer function is jeopardized.

# Sammanfattning

I det svenska KBS-3-konceptet för slutförvar av utbränt kärnbränsle förvaras bränslet i kopparkapslar vilka omges av kompakterad bentonit. Bränslets radioaktiva sönderfall kommer att höja temperaturen i förvaret vilket tillsammans med upptag av grundvatten förväntas orsaka mindre mineralogiska förändringar i bentoniten.

Det nu pågående LOT-projektet vid Äspö berglaboratorium syftar till att identifiera och kvantifiera sådana mineralogiska förändringar i bentoniten som följd av exponering för en förvaringsliknande miljö. Dessutom undersöks relaterade processer i bentoniten som rör kopparkorrosion, diffusion av katjoner, samt överlevnad och aktivitet hos bakterier. Totalt används sju försökspaket, vilka innehåller ett centralt cirka 4 m långt kopparrör omgivet av cylinderringar av kompakterad bentonit. Elektriska värmare inne i kopparröret används för att simulera resteffekten från det utbrända bränslet. Temperatur, totaltryck, vattentryck och fuktighet mäts via givare som placerats i bentoniten. Projektet innefattar tre paket som är utsatta för typiska KBS-3-förhållanden med en maximal temperatur som understiger 100 °C, och fyra försökspaket som är utsatta för speciellt ogynnsamma förhållanden, framförallt förhöjd temperatur till maximalt cirka 140 °C. Båda försökstyperna genomförs som korttids- (1 till 2 år), medellånga (>5 år) och långtidsförsök (>10 år).

Den nu aktuella rapporten avser A2-försöket, vilket var ett medellångt försök där bentoniten utsattes för ogynnsamma förhållanden. Vidare placerades kopparkuponger, <sup>60</sup>Co spårämne, och utvalda mineral på bestämda positioner i bentoniten. Efter cirka 6 års exponering i fält friborrades A2-paketet varefter det lyftes, delades och provtogs för specificerade analyser av nio olika laboratorier i fem länder. Huvudintresset för de genomförda testerna och analyserna avsåg följande punkter:

- bentonitens fysikaliska egenskaper (vatteninnehåll, densitet, svälltryck, hydraulisk konduktivitet och reologiska egenskaper),
- mineralogiska förändringar i bentoniten,
- fördelning i bentoniten av tillförda substanser (t ex gips och <sup>60</sup>Co),
- korrosion av kopparkupongerna,
- överlevnad och aktivitet hos bakterier i bentoniten.

Merparten av analyserna avsåg bentonitens mineralogi. Förutom SKB har Andra, BGR, Nagra och Posiva bidragit med rapporter vilka här redovisas i form av bilagor. Referensmaterial och exponerat försöksmaterial har undersökts med en bred uppsättning mineralogiska analysmetoder såsom röntgendiffraktometri, katjonbytesanalys, elementanalys och elektronmikroskopi enligt ett huvudsakligen förutbestämt testprogram. De mest betydelsefulla resultaten från alla genomförda analyser och tester kan sammanfattas i följande punkter:

- omfördelning av lättlösliga mineral i bentoniten, speciellt gäller detta kalciumsulfat (gips),
- en mindre ökning av katjonbyteskapaciteten i de delar av bentoniten som utsatts för höga temperaturer,
- ingen nybildning av illit eller andra typiska omvandlingsmineral från montmorillonit,
- minskning av brottöjning i bentonit som utsatts för höga temperaturer,
- diffusionsegenskaperna hos <sup>60</sup>Co som överensstämmer med tidigare undersökningar,
- uppmätt korrosionshastighet av metallisk koppar överensstämmer med resultat från tidigare försök samt med modellberäkningar,
- minimal överlevnad av bakterier.

En övergripande slutsats är att endast små mineralogiska förändringar har skett i bentoniten som följd av vattenmättnaden och exponeringen för höga temperaturer, och att dessa förändringar inte har lett till påtagligt försämrade fysikaliska egenskaper.

# Contents

<b>1</b>	<b>Background</b>	7
1.1	General	7
<b>2</b>	<b>Objectives</b>	9
2.1	General	9
2.2	Physical buffer properties	9
2.3	Buffer stability	10
	2.3.1 General	10
	2.3.2 Dissolution and precipitation	11
	2.3.3 Smectite-to-illite conversion	12
	2.3.4 Effects of cement pore water	13
2.4	Microbiology	13
2.5	Cation migration	14
2.6	Copper corrosion	14
2.7	Gas transport	14
<b>3</b>	<b>Experimental concept</b>	15
3.1	General	15
	3.1.1 Principles	15
	3.1.2 Adverse conditions	15
3.2	Experimental configuration	16
	3.2.1 Test program	16
3.3	Test site	16
	3.3.1 General	16
	3.3.2 Pilot holes	17
	3.3.3 Test holes	18
3.4	Test parcel construction	18
	3.4.1 General	18
	3.4.2 Heater	18
	3.4.3 Central tubes	19
	3.4.4 Blocks	19
	3.4.5 Test plugs	21
3.5	Instrumentation	22
	3.5.1 General	22
	3.5.2 Thermocouples	24
	3.5.3 Pressure gauges	24
	3.5.4 Moisture gauges	24
	3.5.5 Data collection and registration system	25
<b>4</b>	<b>Field operation</b>	27
4.1	Preparation	27
	4.1.1 Parcel assembly	27
	4.1.2 Installation	28
4.2	Heating phase	28
	4.2.1 Temperature control	28
	4.2.2 Water supply	29
4.3	Field results	29
	4.3.1 General	29
	4.3.2 Temperature	29
	4.3.3 Total and water pressure	30
	4.3.4 Moisture	31
4.4	Termination of the field activity	32
	4.4.1 Termination, drilling and uplift	32
	4.4.2 Partitioning of the parcel	33

<b>5</b>	<b>Laboratory analyses – general</b>	35
5.1	Test philosophy	35
5.2	Test material	35
<b>6</b>	<b>Basic geotechnical properties</b>	37
6.1	Test principles	37
6.2	Results	37
<b>7</b>	<b>Sealing properties</b>	41
7.1	Test principles	41
7.2	Results	42
<b>8</b>	<b>Rheological properties</b>	45
8.1	Triaxial tests	45
8.1.1	Test principles	45
8.1.2	Equipment	45
8.1.3	Sample preparation	46
8.1.4	Test procedure	46
8.1.5	Data flow and evaluation	46
8.1.6	Results	46
8.1.7	Discussion and conclusions	47
8.2	Unconfined compression tests	48
8.2.1	Test principle	48
8.2.2	Equipment	51
8.2.3	Test procedure	51
8.2.4	Data flow and evaluation	51
8.2.5	Results and discussion	52
8.2.6	Additional analyses	59
8.2.7	Conclusions	59
<b>9</b>	<b>Mineralogy and chemical composition</b>	61
9.1	Introduction	61
9.2	Standard blocks of the A2 parcel	61
9.2.1	Materials and methods	61
9.2.2	Results	65
9.2.3	Summary and conclusions	88
9.3	Blocks with additives	88
9.3.1	Materials and methods	88
9.3.2	Results	92
9.3.3	Summary and conclusions	110
	<b>References</b>	111
	<b>Appendices</b>	
	<i>SKB contributions</i>	
1	Microbial analyses	113
2	Co <sup>2+</sup> diffusion	131
3	Copper coupons	143
4	Bentonite block description and sensor configuration	157
	<i>External contributions</i>	
5	Water analyses Posiva	167
6	Mineralogy ANDRA	191
7	Mineralogy BGR	225
8	Mineralogy NAGRA	251

# 1 Background

## 1.1 General

Bentonite clay has been proposed as buffer material in several concepts for HLW repositories. In the Swedish KBS-3 concept the demands on the bentonite buffer are to serve as mechanical support for the canister, reduce the effects on the canister of a possible rock displacement, and minimize water flow over the deposition holes. The transport through the buffer is expected to be controlled principally by diffusion, both with respect to corrosive components in the groundwater and to corrosion products and escaping radionuclides in case of a canister failure.

Comprehensive research and development work has been carried out during the last thirty years in order to determine the basic behavior of unaltered bentonite material. The results have been reported in technical reports, and tentative computer codes concerning both unsaturated and saturated buffer conditions are at hand /e.g. Børgesson et al. 1995/. The models are believed to well describe the function of an unaltered MX-80 bentonite buffer after water saturation with respect to physical properties, e.g. swelling pressure, hydraulic conductivity and rheological behavior. Further, techniques for bentonite block production and application have been developed in order to fulfill the requirements concerning density, homogeneity, handling etc /Johannesson et al. 1995/.

The decaying spent fuel in the HLW canisters will increase temperature of the bentonite buffer. Initially there will also be a thermal gradient over the buffer by which original water will be redistributed parallel to an uptake of water from the surrounding rock. A number of laboratory test series, made by different research groups, have resulted in various buffer alteration models which are discussed in /Karlund and Birgersson 2006/. According to these models no significant alteration of the buffer is expected to take place at the prevailing physico-chemical conditions in a KBS-3 repository neither during, nor after water saturation. The models may to a certain degree be validated in long term field tests. Former large scale field tests in Sweden, Canada, Switzerland and Japan have in different respects deviated from possible KBS-3 repository conditions and the testing periods have generally been dominated by initial processes, i.e. water uptake and temperature increase.

The present LOT test series is consequently focused on the long term performance of the bentonite buffer, i.e. the conditions after water saturation, and on buffer related processes in a water-saturated bentonite buffer concerning microbiology, cation transport, and copper corrosion. Long term in this context does of course not refer to the full time span of a repository. However, a considerable part of the heating period in a KBS-3 repository is being covered with respect to kinetic reactions by the use of adverse conditions in the present A2 test parcel.

This report concerns the A2 parcel with respect to:

- background
- construction
- field results
- results from laboratory analyses of field exposed material concerning
  - physical properties
  - mineralogy
  - bacterial activity
  - cobalt diffusion
  - copper corrosion

The mineralogical processes are not discussed in detail in this report, but will be reported separately within the separate LOT modeling project.

The project was initiated and is financed by SKB (Sweden). Posiva has contributed from project start by financing clay water analyses performed by VTT. As from the present A2 parcel, also ANDRA (France), BGR (Germany) and Nagra (Switzerland) have joined the project by financing parallel independent mineralogical analyses performed by laboratories in these countries, respectively.

## 2 Objectives

### 2.1 General

The bentonite buffer material in the KBS-3 concept is a natural mixture of montmorillonite and several common accessory minerals, e.g. quartz, feldspar, calcite, siderite and pyrite. The bentonite material is chosen because of the specific physico-chemical properties, which primarily are due to interaction between the montmorillonite component and water. These properties are of fundamental importance for the repository function during the entire lifetime of the repository. The stability of the montmorillonite mineral is therefore of vital importance for the buffer performance and is one of the main issues in the LOT project. Also possible changes of the accessory minerals may be important as they may dissolve and precipitate and thereby may alter especially the rheological properties of the buffer material.

Main aspects of the previously accomplished LOT medium term (6 years) tests were to check that compaction, placement and water saturation did not significantly change the physical properties of the buffer. In this part of the project, i.e. medium long term exposure to repository similar conditions, the main aspects are to check that the repository temperature and geochemical conditions after water saturation do not significantly change the physical properties of the buffer.

The test layout also makes it possible to study other important processes in the canister-buffer-rock system. The general objectives in the LOT test series may be summarized in the following items, and the specific issues of interest are described in the following sections:

- Collect data for validation of models concerning buffer performance under quasi-steady state conditions after water saturation, e.g. swelling pressure, hydraulic conductivity and rheological properties.
- Check of existing models concerning buffer degrading processes, e.g. mineral redistribution and montmorillonite alteration.
- Produce data concerning “critical gas penetration pressure” and gas transport capacity. This option has not been used in the present A2 test parcel.
- Check of existing models concerning cation diffusion in bentonite.
- Collect information concerning survival, activity and migration of bacteria in bentonite under repository-like conditions.
- Check of calculated data concerning copper corrosion, and collect information regarding the character of possible corrosion products.
- Collect information, which may facilitate the realization of the full-scale test series (e.g. the Prototype project) with respect to preparation, instrumentation, retrieval, subsequent analyses, evaluation and data handling.

### 2.2 Physical buffer properties

The clay/water system in a KBS-3 repository is expected to have well known physical properties, of which swelling pressure, hydraulic conductivity and plasticity are the most important. A large number of data from laboratory tests are available in reports produced by SKB and corresponding organizations in other countries (e.g. AECL, Andra, Enresa, Nagra, PNC and Posiva).

A main hypothesis in this project is that the initial swelling pressure, hydraulic conductivity and plasticity of the water saturated bentonite material are well described and possible to predict for a KBS-3 construction by present laboratory results and models.

## 2.3 Buffer stability

### 2.3.1 General

One reason for choosing bentonite as buffer material is its long term stability in nature. It is frequently found in very old geological formations also in relation to the lifetime of a HLW repository. As an example, the Wyoming formation from which the commercial MX-80 bentonite is produced is from the Cretaceous period (~65 million years ago) /Slaughter and Earley 1965/. In a future repository, however, the bentonite will be exposed to a new environment with respect mainly to temperature and groundwater chemistry (Figure 2-1). Consequently, different alteration processes have been studied with respect to repository conditions, and to a larger extent, much work has been made mainly in relation to oil exploration. A large number of articles concerning measured natural alteration and alteration models have been published over the last 50 years in scientific clay literature, e.g. Clay Minerals, Clays and Clay Minerals, and Applied Clay Science, and several books have been written on this subject /Karlund and Birgersson 2006/.

The design criteria for the KBS-3 repository stipulate that the temperature in the buffer should not exceed 100°C, including a safety margin of 10°C, in any position at any time.

The expected temperature evolution has been calculated for the present repository layout to lead to a maximum temperature below 90°C, and a maximum temperature gradient below 24°C over the 0.35 m thick buffer material (Figure 2-2) /Hökmark and Fälth 2003/.

Chemical/mineralogical changes of possible importance in a KBS-3 repository may be listed as follows:

- Enrichment of substances emanating from the groundwater
- Dissolution and precipitation of accessory minerals
- Montmorillonite surface reactions
  - ion exchange, e.g. from sodium to calcium
  - sorption of ions
  - pH buffering of the montmorillonite
- Montmorillonite structural alteration
  - in situ alteration e.g. into illite
  - incongruent dissolution, e.g. release of silica
  - congruent dissolution

Depending on the overall conditions all these types of processes may result in significant changes of the buffer physical properties.

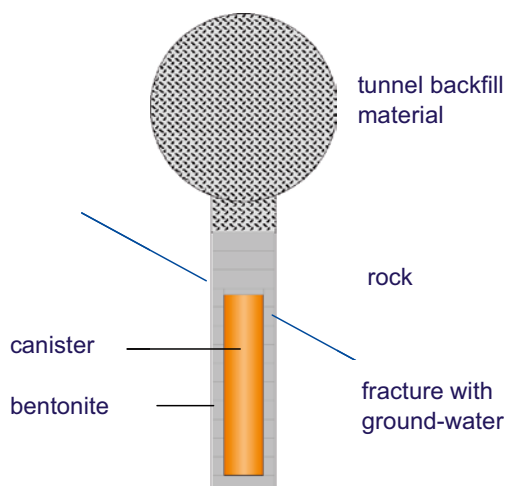


**Figure 2-1.** Schematic view of a cross section through a deposition tunnel and deposition hole in a KBS-3 repository.

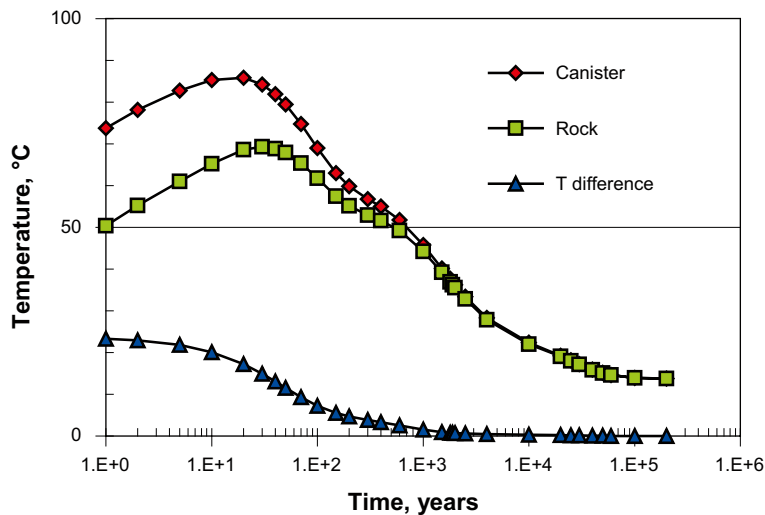


**Figure 2-2.** Calculated temperature evolution in a typical KBS-3 deposition hole showing the buffer temperatures at the interfaces to the canister and the rock, and the temperature gradient over the buffer, respectively. Calculated from data in /Hökmark and Fälth 2003/.

### 2.3.2 Dissolution and precipitation

Different enrichment processes of dissolved substances may take place due to the temperature gradient which prevails over the KBS-3 buffer during the elevated temperature phase, i.e. ~10,000 years. Precipitations may cement the buffer and change mainly the rheological properties of the buffer functions /Pusch et al. 1992/. One such possible process is ion transport parallel to water uptake from the outer cooler parts of the bentonite, or from the surrounding groundwater, to the wetting front in the originally unsaturated bentonite. The transport is assumed to take place by an evaporation/condensation process in which water is sucked in from cooler parts and evaporates at the wetting front. Dissolved salts will thereby be deposited at the wetting front.

A second possible process is precipitation of minerals, which have lower solubility at higher temperature, e.g. calcium sulfate (gypsum/anhydrite) and calcium carbonate (calcite). This process may take place also in a fully water saturated bentonite and the potential problem is consequently larger. The process will come to a standstill after limited enrichment if the buffer material alone is the source of the original pore water concentration. The total maximum effect will then be possible to calculate. On the other hand, if the surrounding groundwater is the source of substances then the enrichment process may continue until the precipitation stops due to spatial limitations.

According to laboratory experiments the following conditions reduces enrichment of easily dissolved minerals in a bentonite buffer /Karlund 1995/.

- High buffer density.
- Low content of accessory minerals in the buffer.
- Low electrolyte content in the surrounding water.
- High water pressure.

The use of water pre-saturated bentonite blocks, supply of low electrolyte water in open slots, and a fast restoration of the hydrostatic pressure may consequently reduce mineral redistribution and enrichment in a KBS-3 repository. No such preventive techniques were used in the present test, since the aim is to study the magnitude and consequences of such reactions. Instead, the initial water to solid mass ratio was low and the slots were filled with groundwater in order to maximize the precipitation effects. Further, the processes were enhanced in the current A2 parcel by elevated temperature, and higher temperature gradient compared to KBS-3 conditions, and by placing reactive substances at specified positions in the parcel.

The hypothesis is that the precipitation reactions will be limited and that no major cementation of the buffer will take place at normal repository conditions.

### 2.3.3 Smectite-to-illite conversion

Depending on the conditions, alteration of minerals in the smectite group, to which montmorillonite belongs, may take place and form a number of related minerals, e.g. illite, chlorite or zeolites. In nature the most common smectite alteration at elevated temperature is transformation into illite. This type of conversion has also been considered as the most probable, or rather least improbable, under repository conditions. Fortunately, the smectite-to-illite reaction has been extensively studied for several decades mainly because of its relevance to oil prospecting. Different parameters have been proposed as kinetic controlling factors, but there is no general consensus on the reactions involved in the conversion. Based on geological analogues and laboratory experiments i.a. the following factors have been proposed as kinetic controlling factors (no ranking):

- Overburden pressure /Weaver 1959/
- Temperature /Perry and Hower 1970/
- Potassium activity /Hower et al. 1976/
- Aluminum activity /Boles and Frank 1979/
- pH /Eberl et al. 1993/
- Dehydration /Couture 1985/
- Silica activity /Abercrombie et al. 1994/

According to the kinetic model proposed by /Huang et al. 1993/, the overall kinetics of the smectite-to-illite reaction can be described by the equation:

$$\frac{dS}{dt} = A \cdot [K^+] \cdot S^2 \cdot \exp\left(\frac{-E_a}{R \cdot T}\right) \quad \text{Equation 2-1}$$

where  $S$  is the smectite fraction in the illite/smectite material,  $t$  is time,  $A$  is frequency factor,  $E_a$  is activation energy and  $R$  is the universal gas constant, and  $T$  is temperature. After integration of Equation 2-1, the smectite content at a certain time can be calculated according to:

$$S = \frac{S_0}{1 + S_0 \cdot [K^+] \cdot A \cdot \exp\left(\frac{-E_a}{R \cdot T}\right) \cdot t} \quad \text{Equation 2-2}$$

Where  $S_0$  is the smectite fraction at  $t = 0$ . The potassium concentrations in the Äspö groundwater are measured to be in the range of a few ppm up to 45 ppm /Laaksoharju et al. 1995/. According to the model, practically no clay conversion will take place in a KBS-3 repository at these conditions as shown in Figure 2-3. However, the reaction relationship and the constants are determined from relatively short-term laboratory experiments at temperatures significantly higher than repository conditions (250–325°C), and from geological analogues, which differ from repository conditions in several aspects. The uncertainty in calculated conversion increases with the difference in temperature between test condition and calculated condition /Karnland and Birgersson 2006/.

Therefore, the LOT test series aims at checking the model results and exclude that the reaction rate is not substantially faster than predicted by the model. The experiments are performed at “as repository like conditions” as possible in standard (S) type experiments, and at moderately increased temperature (maximum 140°C) and controlled high potassium concentration in the adverse (A) type experiments. The latter tests are further conservative in that sense that the transport of potassium, which is considered as one of the major hindrances for illitization in a repository is leaped over by the internal potassium source.

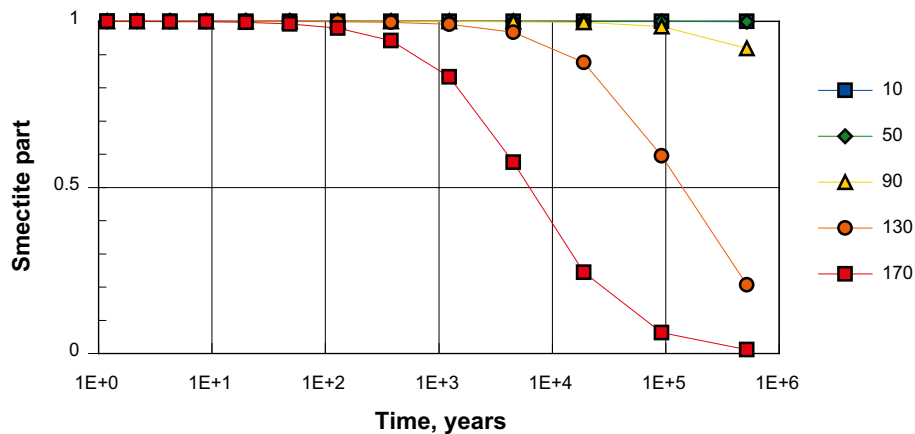


**Figure 2-3.** Remaining smectite part for different temperatures in a hydrothermal system with  $[K^+] = 0.002$  mole/litre (80 ppm) according to the /Huang et al. 1993/ kinetic model and laboratory determined constants ( $E_a = 27.4$  kcal/mole and  $A = 8.5E4$ ).

### 2.3.4 Effects of cement pore water

Possible effects on the bentonite of exposure to cement pore water are believed to give the following reactions /Eberl et al. 1993, Karnland and Birgersson 2006, Karnland et al. 2007/:

- Replacement of the original charge balancing cations, e.g. sodium against calcium.
- Cementation of the bentonite due to precipitation of cement matter (e.g. calcium-silica-hydrates and calcite) in clay pore space.
- Attack on the accessory minerals (e.g. cristobalite) in the bentonite.
- Alteration of clay mineral due to the induced high pH.

The hypothesis is that bentonite under repository conditions resists short-term attack from cement pore water without major alteration. The main aspects of this part of the project are to confirm/reject results from former laboratory experiments, which showed ion exchange, minor mineral dissolution/neo-formation and no or minor clay lattice alteration.

## 2.4 Microbiology

The survival of bacteria in bentonite has been suggested to depend on the water activity. Laboratory tests have shown that two different species of sulfate reducing bacteria were killed when the water activity was decreased to 0.96, corresponding to the conditions in an un-pressurized and fully saturated clay at a density of  $2,000 \text{ kg/m}^3$  /Motamedi et al. 1995/. It may, however, be argued that other, more halo-tolerant sulfate reducing bacteria could survive and be active.

The main hypothesis is that bacterial survival is governed by water activity/induced swelling pressure. The low water activity/high swelling pressure in compacted bentonite around waste canisters is expected to act as a strong limiting factor for bacterial survival and activity, thereby reducing or eliminating the risk for bacterial production of gas and corrosive metabolic products.

Further, it has been argued that bacteria should be able to colonize the buffer from the groundwater. The presence of viable bacteria in deep clay sediment is usually interpreted as if the bacteria were mixed in with the clay during burial. Theoretically, the pore size of compacted bentonite is much smaller (nanometers), compared to microorganisms (microns), which makes migration into the buffer from groundwater improbable.

## 2.5 Cation migration

The diffusion of radionuclides in compacted bentonite has been studied rather extensively in laboratory experiments with synthetic groundwater. The pore water diffusion model, generally used to interpret the experimental data, is based on the assumption that diffusion takes place in pore water and is retarded by sorption of the diffusing species on the solid phase. This model may be adequate for cations sorbed on the solid phase by surface complexation mechanisms, e.g.  $\text{Co}^{2+}$ . For cationic species present in the clay due to ion exchange, e.g.  $\text{Cs}^+$  and  $\text{Sr}^{2+}$ , experimental data indicate an additional diffusion mechanism in which migration takes place within the nano-sized interlayer space between the montmorillonite surfaces. The diffusivities of  $\text{Cs}^+$  and  $\text{Co}^{2+}$  in compacted bentonite saturated with groundwater of different ionic strength (salinity) are rather well documented at room temperature and, in principle, it should be possible to model the diffusive transport of these cations in the actual bentonite system.

A common theory is that cation transport may take place by two different transport mechanisms i.e. by diffusion in pore water which is not affected by the montmorillonite and by an additional migration between individual montmorillonite mineral layers next to the mineral surface. Recently, it has been shown that the interlayer volumes play an important role in compacted bentonite in general, and that laboratory diffusion data may principally be explained by two interlayer ion equilibrium processes; Donnan equilibrium and ion exchange /Birgersson and Karnland 2009/.

A difference in diffusive transport is expected between cations sorbed by surface complexation mechanisms e.g.  $\text{Co}^{2+}$  and cationic species present as exchangeable ions e.g.  $\text{Cs}^+$  and  $\text{Sr}^{2+}$ . A faster transport is therefore expected to take place for the latter cations. In the present A2 parcel the diffusive behavior of  $^{60}\text{Co}^{2+}$  was studied.

## 2.6 Copper corrosion

The corrosion rate of the canister is in principle determined by the chemical reactivity at the canister surface and the mass transfer to and from this surface. For a specific canister, the corrosion rate depends on the geochemical conditions of the close vicinity of the copper surface, i.e. the type, content and mobility of dissolved constituents in the surrounding bentonite buffer. Thermodynamic calculations show that alteration products of copper are stable and that the corrosion process is expected to be affected by the redox conditions of the clay medium /Wersin et al. 1993/.

In general there are different types of uncertainties associated with estimation of the corrosion rate of copper in bentonite:

- Model validity
- Time scale of oxic/anoxic transition
- Pitting factor
- Transport properties of the clay

Modeling which takes into account diffusive transport in addition to flow, equilibrium reactions and kinetic processes at the bentonite-canister interface has been made /Wersin et al. 1994/. The results indicate conservative corrosion rates of  $2 \cdot 10^{-8}$  and  $7 \cdot 10^{-6}$  m/y for anoxic and oxic conditions, respectively. A sensitivity analysis indicates that the main uncertainties arise from the diffusion properties of the clay.

The present test aims at determining the mean corrosion rate, and identifying possible pitting and corrosion products. The main hypothesis is that the mean corrosion rate under the initial oxic conditions will be less than  $7 \cdot 10^{-6}$  m/y.

## 2.7 Gas transport

No gas pressure test was included in the A2 parcel program, mainly because the focus has been on the ongoing full scale Lasgit project at the Äspö HRL.

## 3 Experimental concept

### 3.1 General

#### 3.1.1 Principles

The LOT test series may be described as a multi-task experiment in which relatively small test parcels are exposed to field conditions at Äspö HRL. The series include three parcels which are exposed to conditions similar to those in a KBS-3 repository and four parcels which are exposed to conditions which accelerate alteration processes. The test parcels contain prefabricated bentonite blocks placed around a copper tube, which are placed in vertical boreholes in granitic rock. After exposure to field conditions for a defined period of time a parcel is extracted by overlapping core drilling outside the original borehole, and the whole test parcel are lifted and partitioned. Material from defined positions in the parcel and reference material are thereafter examined by well-defined tests and analyses in order to provide data for the different objectives.

The dimensions of the parcels are kept considerably smaller, especially the diameter, compared to a KBS-3 deposition hole in order to:

- Shorten the water saturation period and thereby have saturated condition during a substantial part of the test period.
- Get a higher temperature gradient over the buffer material.
- Facilitate sampling, i.e. release and up-lift of the exposed test parcel in one piece.

#### 3.1.2 Adverse conditions

Mineralogical stability of the bentonite clay is one of the grounds for the choice of bentonite as buffer material. Nevertheless, alteration processes will take place in the buffer but are predicted to be very slow under KBS-3 repository conditions. The following accelerating conditions compared to KBS-3 conditions were therefore used in order to make it possible to study slow alteration processes in the relatively short duration time of the experiments:

- Higher temperature.
- Higher temperature gradient.
- Higher content of accessory minerals (calcite, gypsum, K-feldspar).
- Introduction of new substances (Portland cement).

The expected effect of these accelerating conditions (buffer adverse conditions) may be summarized in the following discussion.

The initial reaction rate of a reaction



can be described by the standard rate law

$$\text{Rate} = k [A]^n [B]^m \quad \text{Equation 3-2}$$

here  $n$  and  $m$  are constants, and  $k$  is a rate constant which can be expressed by the Arrhenius relationship

$$k = zp \cdot \exp(-E_a/RT) \quad \text{Equation 3-3}$$

where  $z$  is the collision frequency factor,  $p$  is the steric factor,  $E_a$  is activation energy,  $R$  is the gas constant and  $T$  is the temperature. This reaction rate theory consequently implies:

- The reaction rate increases with increasing concentration of a reactant.
- The reaction rate increases with increasing temperature.
- The temperature effect increases with increasing activation energy.
- The temperature increase effect is reduced with increasing temperature.

For the case of illitization with the high activation energy (114,700 J/mole), measured by /Huang et al. 1993/, a temperature increase of 10 K results in an almost tripled reaction rate. Consequently, the increase from 90°C, which is the upper temperature limit in the KBS-3 buffer, to the maximum temperature in the adverse conditions parcels (130°C) leads to an increased illitization reaction rate of around 40 times according to the Huang et al. model. The calculated maximum temperature hundred years after fuel deposition is around 70°C and the corresponding temperature after 1,000 years is 50°C (Figure 2-2). The temperature in the outermost part of the bentonite will initially be around 20°C lower. A comparison between the 130°C in the adverse condition parcel and the maximum bentonite temperature after 100 years (70°C) gives a reaction rate factor of almost 400 times. A 6-year test at 130°C consequently represents a significant part of the thermal load in a KBS-3 repository with respect to kinetically controlled slow processes.

Consequently, the LOT A2 test is expected to show mineralogical effects of processes governed by the kinetics of the involved reactions provided the corresponding activation energies are sufficiently large. If the activation energies are small then the reactions are relatively fast and the effects should likely also be revealed. The introduction of additional substances will accelerate also processes, which are governed by the transport of reactants in a repository, e.g. limitation of illitization by potassium transport.

However, reactions governed by the removal of reaction products cannot be generally accelerated in a simple way. The adverse conditions in the present A2 parcel do consequently not accelerate such processes generally, although the increase in temperature will increase e.g. the precipitation rate of quartz.

## 3.2 Experimental configuration

### 3.2.1 Test program

In total, the LOT test series includes seven test parcels (Table 3-1) of which three are exposed to standard KBS-3 conditions, and four test parcels which are exposed to adverse conditions. The present report concerns the A2 parcel.

## 3.3 Test site

### 3.3.1 General

The LOT main test series are run in the G tunnel situated in the western part of the present Äspö hard rock laboratory (Figure 3-1). The depth from surface is around 450 m and the rock consists mainly of Äspö diorite, which is crossed by some pegmatite dikes and bands of fine-grained granite. A few water-bearing fractures are visible, but the tunnel may be considered dry relative to the average Äspö rock volume.

**Table 3-1. Test program for the “Long Term Test of Buffer Material” series. A = adverse conditions, S = standard conditions, T = temperature, [K+] = potassium concentration, pH = high pH from cement, am = accessory minerals added.**

Type	No.	Max T, °C	Controlled parameter	Time, years	Remark
A	1	130	T, [K+], pH, am	1–2	pilot test
A	0	120–150	T, [K+], pH, am	1–2	A1 complement
A	2	120–150	T, [K+], pH, am	>5	main test
A	3	120–150	T	>>5	main test
S	1	90	T	1–2	pilot test
S	2	90	T	>5	main test
S	3	90	T	>>5	main test

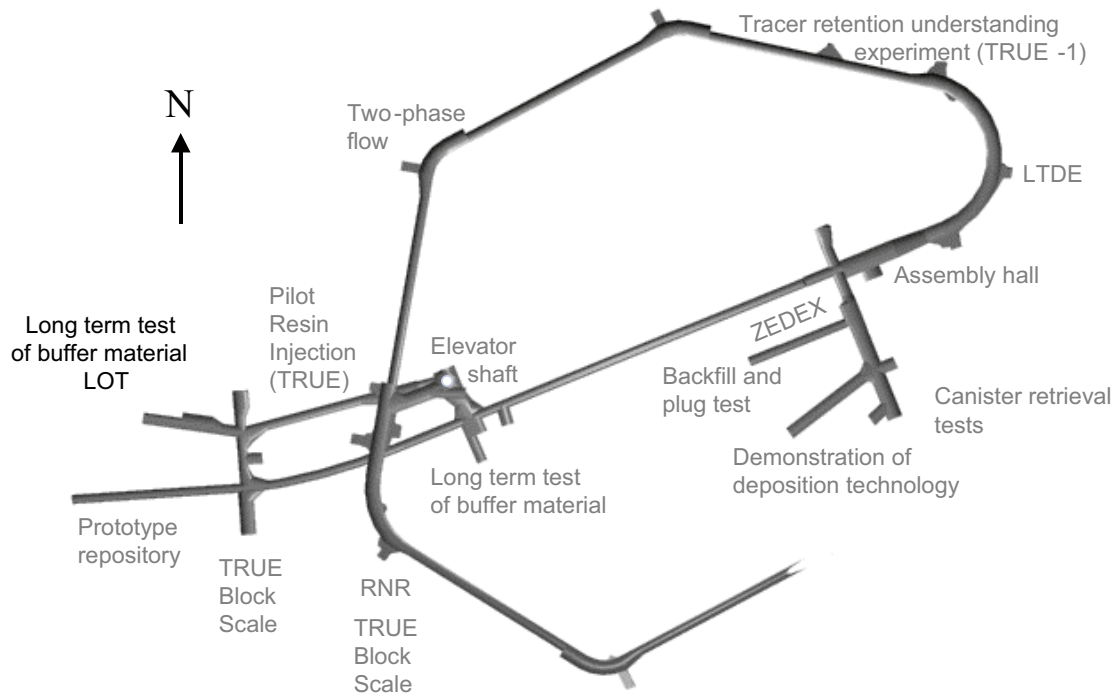


**Figure 3-1.** The present LOT test site is located in the G-tunnel in the western part of the research area, and close to the lowest part of the Äspö tunnel.

### 3.3.2 Pilot holes

Five 76 mm vertical pilot holes were drilled in line on the northern side of the G-tunnel between March 2nd and March 4th 1999. The holes were approximately 8 m deep and with a relative distance of 4.5 m. The holes were termed KG0033G01, KG0037G01, KG0042G01, KG0046G01 and KG0051G01, where K denotes core-drilled, G denotes the G-tunnel, 0033 denotes the length in meters from tunnel entrance, G denotes floor position. The KG0037G01 hole was used for the present A2 test.

No definite suitability criteria were defined for the test holes, but the water pressure in the holes has to be higher than the vapor pressure at the chosen test temperature. Further, water inflow had to be low enough to allow the placement of the test parcels and to exclude the risk of piping and erosion after closure.

Shortly after drilling, mechanical packers were installed. The boreholes were shut in and kept closed until the start of flow and pressure measurements were performed. The flow measurements were made by use of double packers with 1 m spacing in the upper 4 m and a single packer was used for the bottom part (4 m to 8 m). The results of the flow measurements are presented in Table 3-2.

**Table 3-2.** Flow rates (ml/min) measured in intervals of the five pilot boreholes for the LOT tests in the G-tunnel of ÄSPÖ HRL, April 1999. The pilot hole for the A2 test is marked by bold text.

Section	Borehole:				
	KG0033G01	KG0037G01	KG0042G01	KG0046G01	KG0051G01
1.4 – 8.05	0.025	<b>0.02</b>	-0.12	1.3	0.025
1.00 – 2.00	0.07	<b>0.09</b>	±0	0.1	0.07
2.00 – 3.00	0.07	<b>0.07</b>	0.04	0.14	0.01
3.00 – 4.00	0.06	<b>0.14</b>	0.05	0.08	0.07
4.00 – 8.05	0.01	<b>0.06</b>	0.01	0.60	0.01

The general conclusions from the pilot hole characterization program were that the water inflow was low, and that the water inlet points were few in all holes. The test time was therefore expected to be much longer than acceptable. Instead of abandon the site it was decided to add external groundwater into the test holes during the test period. A water supply hole (HG0038B01) was drilled into the northern wall where a water-bearing fracture was found a few meters into the rock. The water pressure was determined to be around 1.2 MPa and the flow was more than sufficient to support all test holes. The water supply hole was packed off and a system of titanium tubes was used to inject water into the test holes.

The groundwater composition has been measured in borehole HG0038B01 within the Äspö HRL campaigns and typical composition of main elements is given in Table 3-3.

### 3.3.3 Test holes

The five pilot holes were enlarged to a diameter of 300 mm to a depth of 4 m. The enlargement was made by percussion drilling because this technique was thought to best simulate the core TBM-type drilling with respect to surface damage and thereby to water conductivity. The test holes were named according to the standard Äspö database nomenclature; HG0033G01, HG0037G01, HG0042G01, HG0046G01 and HG0051G01. The test hole HG0037G01 was used for the present A2 parcel.

The diameter and the straightness of the test holes were checked and the diameter was measured to exceed 300 mm by up to 10 mm in some parts.

## 3.4 Test parcel construction

### 3.4.1 General

The basic demand for the test parcel construction was to keep a defined maximum temperature in the central part of the clay column during the test time span. An important part of the system was therefore the temperature measurement and power regulation system. A central heater inside an open tube was chosen, as this allows for heater change during the test period in case of a failure. The central tube was made of copper in order to simulate the KBS-3 copper canister, and thereby keep as realistic chemical conditions as possible. The A2 test parcel contained heater, central tube, bentonite blocks, sensors and additives, which are individually described in the following sections.

### 3.4.2 Heater

Specially designed electric heater from Backer Elektro-värme AB, Sösdala, Sweden was used. The total length was 4,650 mm, and the active bottom part had a length of 2,000 mm. Three individual stainless steel (SS2348) elements with a diameter of 14 mm were brazed into a stainless steel (SS2343) flange, which was designed in order to let the heater hang down from the top of the copper tube. The maximum power was decided to be 2 kW (230/400 V, AC), i.e. each element has a maximum power of 667 W (230 V) corresponding to 0.7 W/cm<sup>2</sup>. The expected power need was based on the previously performed pilot tests A1 and S1, which were in agreement with scoping calculations made by MICROFIELD finite element computer code performed by Harald Hökmark, Clay Technology AB.

**Table 3-3. Main composition of the ground-water in water supply bore hole HG0038B01 in 2000, 2001 and 2006.**

HG0038B01 Units	Na mM	K mM	Ca mM	Mg mM	HCO <sub>3</sub> mM	Cl mM	SO <sub>4</sub> mM	Br mM	F mM	Si mM	HS mM	pH	E.C. mS/m
2000-04-14	98.7	0.236	43.4	2.21	0.852	185	4.84	0.504		0.178		7.4	1,750
2001-09-26	104	0.246	49.6	2.15	0.705	195	4.94	0.617	0.125	0.196	0.000604	7.40	1,930
2006-10-02	98.7	0.261	56.6	1.90	0.215	219	5.57	0.617	0.076	0.208	0.000332	7.62	2,170

### 3.4.3 Central tubes

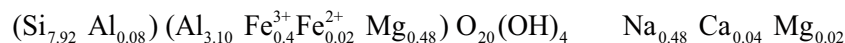
The copper tube (SS 5015-04), simulating the canister, had a length of 4,700 mm, an inner diameter of 100 mm and a wall thickness of 4 mm. At the bottom end a copper plate and 4 copper reinforcement parts were brazed by use of soldering silver. A detachable lifting device was placed at the top of the tube during the placement. The maximum possible external pressure acting on the outside of the central tube was expected to be less than 10 MPa (bentonite swelling pressure plus hydrostatic water pressure), which corresponds to a maximum compression stress of 140 MPa acting at the inner radius. The used hard-drawn copper quality has a yield point exceeding 200 MPa, which consequently was sufficient.

No water/steam leakage into the tube could be accepted with respect to both the heater function and the mass transport conditions. The impenetrability was therefore tested after the soldering by use of a helium source inside the copper tube and an external detector.

### 3.4.4 Blocks

Wyoming bentonite with the commercial name MX-80 was the source material for all bentonite components in the system. It was delivered by Askania AB and manufactured by Volclay LTD, Mersyaside, UK. The material was delivered in 25 kg sacks in one consignment.

The material is dominated by natural mainly sodium montmorillonite clay (~80% by weight). Accessory minerals are quartz (~4%), tridymite (~4%), cristobalite (~3%), feldspars (~4%), muscovite/illite (~4%) sulfides (~0.2%), and small amounts of several other minerals and organic carbon (~0.4%). Dispersed in distilled water the clay fraction (grain size <2 µm) makes up around 80%. The mean mineralogical composition of the montmorillonite part is given by:



The cation exchange capacity is around 0.75 eq/kg bulk material and around 0.85 eq/kg clay in the minus 2 µm fraction. The natural exchangeable cations are sodium (~70%), calcium (~20%), magnesium (~6%) and small amounts of potassium (~2%). The specific surface area is around  $5.5 \cdot 10^5 \text{ m}^2/\text{kg}$  material and the grain density is around  $2,750 \text{ kg/m}^3$  /Karlund and Birgersson 2006/.

The various blocks and plugs produced for the A2 parcel may be divided in the following groups:

- Standard blocks with maximum original diameter of 281 mm and a height of 100 mm.
- Special blocks, which were prepared from standard blocks, with excavations for reinforcements, instruments, copper plates or 20 mm test plugs.
- 20 mm diameter bentonite plugs with or without different additives, used in the tracer tests, the bacteria tests, and accessory mineral enrichment tests.

The choice of block compaction technique was based on experiences from previous SKB projects concerning block production /Johannesson et al. 1995/. A uniaxial compaction device was constructed in order to make it possible to produce blocks with the accurate dimensions, density and composition. A slight axial conic form and chamfered edges between mantle and end sides were used in order to facilitate the expulsion after compaction and to avoid subsequent stress induced cracks. A small amount of molybdenum sulfide grease was used to smear the mantel surfaces in order to reduce friction.

The bentonite material was compacted without pre-treatment. Water to solid mass ratio was measured in each 25 kg sack in order to determine the amount of solid bentonite in each block batch. The governing figure for the production was a final density of  $2,000 \text{ kg/m}^3$  in the test hole after expansion by water uptake, since this is the reference KBS-3 bentonite bulk density. The accomplished calculations were made by use of a bentonite solid density of  $2,750 \text{ kg/m}^3$ , a mean block radius of 139.3 mm and an inner radius of 56 mm, a borehole radius of 150 mm, copper tube radius of 54 mm, and the measured water to solid mass ratio in the bentonite, which was 10% ( $\pm 0.9\%$ ). Extra blocks were made in the production series in order to be dissected and analyzed with respect to homogeneity. For each produced block, approximately 250 g of the same material, i.e. from the same 25 kg sack, was marked and stored as reference material for background analyses.

The blocks predestined for gauges or plugs were made from standard blocks by drilling and carving out the necessary volume. The bentonite material is well suited for this technique and the produced unintentional gaps between the gauges and the bentonite are small and insignificant with respect to the final buffer density

The special blocks produced for the A2 parcel had the following modifications:

<b>block no.</b>	<b>modifications/excavations for</b>
01	copper bottom-plate reinforcements
02	3 thermocouples
05	20 mm cylindrical holes for tracer tests, 2 filters/tubes
08	5 thermocouples, 1 total pressure gauge, 1 water pressure gauge, 1 relative humidity gauge
10	4 plugs of 10% CaCO <sub>3</sub> of and 1 water sampling cup
12	4 plugs of 10% CaSO <sub>4</sub> and 1 water sampling cup
14	5+1 thermocouples, 1 total pressure gauge, 1 water pressure gauge, 2 relative humidity gauges
16	3×4 plugs of 50% K-feldspar and 1 water sampling cup
18	3 water sampling cups and 2 tubes with filters
20	5 thermocouples, 1 total pressure gauge, 1 water pressure gauge, 1 relative humidity gauges
22	2 copper plates
24	2×3 cement plugs
26	3 thermocouples
28	2 tubes with filters
30	2 copper plates
32	1 thermocouple, 3 water sampling cups, 1 tube with filter
34	2×3 cement plugs
36	3×ECN sensors (for a separate copper corrosion study)
38	1 thermocouple

All blocks were designed for defined positions in the test parcels and given a specific denomination. The blocks were theoretically partitioned in 9 sections in order to get a system for instrumentation and sampling. The first section ranging from the inner mantle surface and 2 cm outwards was termed section 1, and the following volume, i.e. between 2 and 4 cm from the inner mantle surface, was termed section 3, etc. The last section was consequently 9, and this section only had an initial extension outwards of ~1 cm. After swelling, due to water uptake, section 9 represented the volume between 8 and ~10 cm (rock wall). Furthermore, the point of the compass was used to describe the horizontal orientation. The denomination of a specific point (centre of a volume) is according to the example 08ASE3 where

- 08 block number (counted from the bottom of the parcel),
- A vertical level in the block,
- SE direction of compass in the test hole,
- 3 radial distance in centimeter from the inner mantle surface to the centre of the specimen.

The reference material was related to an imaginary point. Reference material from a specific block was termed according to the example A209R where

- R reference material,
- A2 parcel type and number,
- 09 block number (counted from the bottom of the parcel).

The layout of all special blocks is schematically shown in Appendix 4.

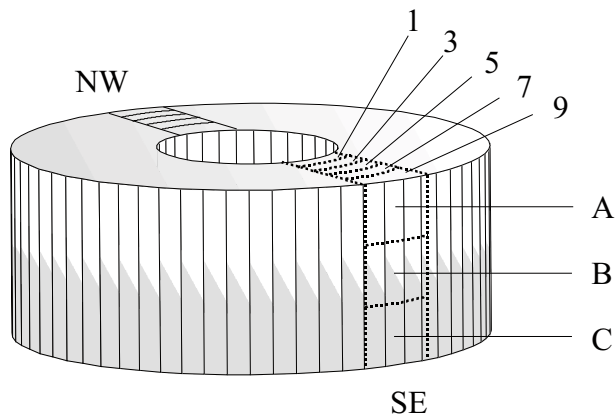


**Figure 3-2.** Schematic block partition. SE and NW denote the directions of compass in the test-hole, figures denote the centre of the specimens expressed in centimeters measured from the block inner mantle surface, and A, B and C denotes the analyzed three vertical position in the blocks.

### 3.4.5 Test plugs

All bentonite-containing plugs had a cylindrical form with a length and diameter of 20 mm. They were compacted in a laboratory compaction device working by the same principle as the block compaction device, but no grease was used. The plugs were compacted to a bulk density of  $\sim 2,070 \text{ kg/m}^3$ , corresponding to the target density of  $2,000 \text{ kg/m}^3$  after full water saturation regardless of the additives. The compaction was accordingly controlled by the final sample volume and not by the maximum compaction pressure.

The plugs were placed in cylindrical holes, which were drilled from the mantle surface into the specified blocks halfway between, and parallel to, the end surfaces. The hole diameter was constantly 21 mm, while the depth depended on the purpose of the test. The outer plugs were sprayed with a small amount of deionized water before they were inserted in order to let the bentonite swell slightly and thereby seal the slots. The positions of the plugs were marked by millimeter thick titanium wires inserted into drilled holes placed 10 mm above the centre of the plugs. Two wires marked the northern position, and one wire marked the other three main directions of compass. The positions of all test plugs are shown schematically in Figure 3-3 and Appendix 4.

**The calcite plugs** had a 10 wt% content of calcite. The calcite material was a finely ground pure quality which was thoroughly mixed with the bentonite and compacted to cylindrical plugs with a diameter of 20 mm and a height of 20 mm. Four holes were drilled at mid height from the cardinal points of the outer surface into block A210 to a depth of  $\sim 30 \text{ mm}$ . A test plug was placed at the bottom of each hole, and the outermost part of the holes was sealed by a slightly wetted bentonite plug without additives just before the placement of the parcel.

**The gypsum plugs** had a 10 wt% content of gypsum. The used  $\text{CaSO}_4 \cdot 2 \text{H}_2\text{O}$  material was a finely ground pure quality which was thoroughly mixed with the bentonite and compacted to cylindrical plugs with a diameter of 20 mm and a height of 20 mm. Four holes were drilled at mid height from the cardinal points of the outer surface into block A212 to a depth of  $\sim 30 \text{ mm}$ . A test plug was placed at the bottom of each hole, and the outermost part of the holes was sealed by a slightly wetted bentonite plug without additives just before the placement of the parcel.

**The feldspar plugs** had a 50 wt% content of K-feldspar (chemical analyses in Table 9-8). The material was finely ground and mixed with the bentonite and compacted to cylindrical plugs with a diameter of 20 mm and a height of 20 mm. Four holes were drilled at mid height from the cardinal points of the outer surface into block A216 to a depth of  $\sim 70 \text{ mm}$ . Three test plugs were placed at the bottom of each hole, and the outermost part of the holes was sealed by a slightly wetted bentonite plug without additives just before the placement of the parcel.

**The cement plugs** were cast to a water-to-cement ratio (w/c) of 0.8 by use of an Aalborg white Portland cement and de-ionized water. The cement was allowed to harden in water for 14 days before the emplacement. Two cylindrical holes were drilled into block A224, and A234 from the north and from the south side to a depth of 80 mm. Four plugs were placed in each hole. No bentonite plugs were used for sealing.

**The <sup>60</sup>Co-tracer doped plugs.** A few cubic millimeters of bentonite were ion-exchanged to contain 1 MBq of <sup>60</sup>Co. The prepared material was placed in the centre of two bentonite plugs. Cylindrical holes were drilled from the north and south side into the mantle surface in block A205. The diameter of the holes was 21 mm and the depth was 50 mm, meaning that the doped part was placed close to the centre of the bentonite, halfway between the rock and the copper tube. The tracer-doped plugs were placed into the block during the submerging of the parcels.

**The copper samples** were placed in tiny slots drilled and sawed from the upper side of the blocks. The copper coupons were placed in the blocks during the pile up of the bentonite column. The samples were pre-characterized and marked with letters, for identification, and with smaller marks for localization during the post test investigation.

## 3.5 Instrumentation

### 3.5.1 General

The basic aim for the field activity in the LOT tests is to expose the bentonite clay to conditions similar to those in a KBS-3 repository, and to expose the clay to adverse physico-chemical conditions, mainly by an increased temperature. A fundamental demand was therefore to measure the temperature in order to regulate power, and to register the obtained temperature distribution in the whole A2 parcel. Relative humidity, porewater pressure and swelling pressure reveal the state of saturation and were therefore also measured. An additional objective with the LOT series was to test equipment for the subsequent full scale buffer tests at Äspö. These demands in combination with the relatively limited volume in the clay and the potential risk for artifacts due to the instrumentation led to the following compromise concerning instrumentation of the A2 parcel:

- 24 thermocouples,
- 3 total pressure gauges,
- 3 water pressure gauges,
- 7 water filters of which some are equipped with external pressure gauges,
- 4 relative humidity sensors.

The gauges and sensors were placed in the parcels as shown in Figure 3-3 and Appendix 4. The equipment was termed in accordance with the following example:

A2084P where

A2 parcel type and the number of the test,

08 block number counted from the bottom,

4 position in the block (according to Section 3.4.4),

P type of measuring equipment.

The following abbreviations of measuring equipment were used:

E temperature in the pressure gauges,

M relative humidity sensors,

P total pressure gauges,

T thermocouples,

W water pressure gauges.

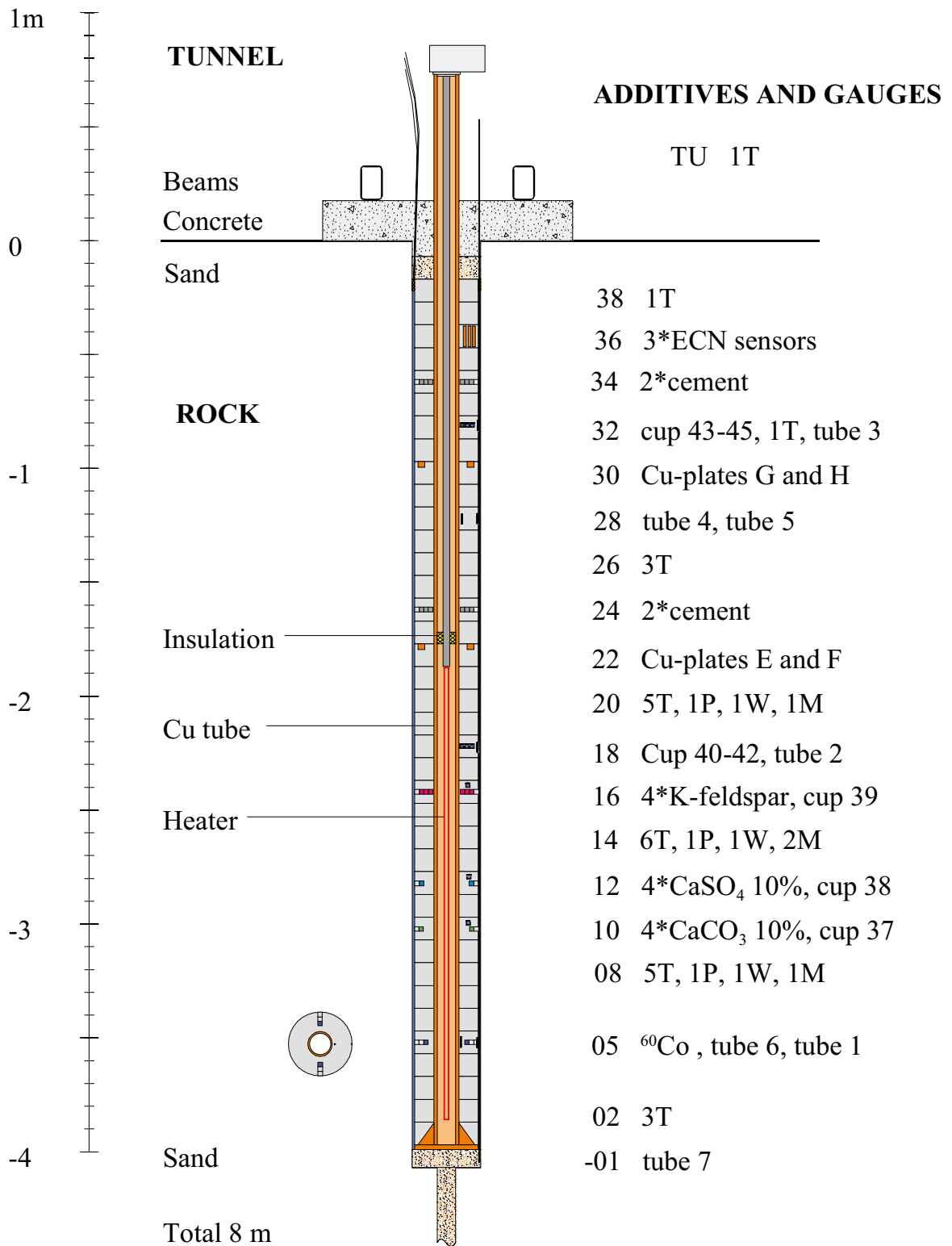


**Figure 3-3.** Scaled schematic drawing of the A2 test parcel. Abbreviations are explained in Section 3.4.4 to Section 3.5.4.

### 3.5.2 Thermocouples

Temperature was generally measured by thermocouples with a hot junction type J according to IEC 584 standard. Additional temperature information was given by the pressure and humidity sensors, which had thermistors and Pt-100 sensors built-in, respectively. The thermocouples were delivered by BICC Thermoheat Limited, Hedgeley Road, Hebburn, Tyne & Wear NE31 1XR, England. The soldering spots were isolated by cupro-nickel alloy, which also jackets the wires up to the tunnel and into the measuring cabinet.

The placing strategy was to concentrate the thermocouples in the clay volume around the heater in order to monitor the temperature gradient over the bentonite in detail. Thermocouples were placed in position 1, 3, 5, 7, and 9 in the blocks 08, 14, and 20. In block 14 there was an additional sensor on the copper surface. Below the most interesting sections, three thermocouples were placed in position 1, 5 and 9 in block 02. And above, three thermocouples were placed in position 1, 5 and 9 in blocks 26. One thermocouple was placed in position 4 in block 32 and 38, respectively. All measuring soldering points were placed from the upper surface of the blocks, into pre-drilled holes, down to a depth of 35 mm.

Calibration is generally not needed for thermocouples, however, a function control was made by connecting all thermocouples to the actual data collecting system and a check was made that the thermocouples showed the prevailing temperature before installation.

### 3.5.3 Pressure gauges

Two quite different types of pressure gauges were used in order to make the pressure measurements redundant. The placing strategy was to place the optical gauges in block 08 and 20, and in between the vibrating wire gauges in block 14.

The optical gauges, model FOP, were manufactured and delivered by Roctest Ltd, 665 Pine Avenue, Saint-Lambert, Canada. The gauges were delivered with signed individual calibration data sheets and traceability numbers.

The vibrating wire gauges, model no. 4500TI-1500, were manufactured and delivered by Geokon Inc., 48 Spencer St. Lebanon, N.H. 03766, USA. The gauges were delivered with signed individual calibration data sheets and traceability numbers according to ANSI Z540-1.

The water pressure transferred by titanium tubes was measured by external gauges placed in the tunnel above the parcels. The gauges were produced by Druck Limited, Fir tree Lane, Groby, Leicester LE6 0FH, and delivered by AMTELE AB Box 66, SE-12722 Skärholmen, Sweden. Individual data sheets, including gauge serial no, were delivered with the sensors.

The factory calibrations and temperature compensations were used for all three types of pressure gauges in the following presentation of results.

### 3.5.4 Moisture gauges

The measuring principle for the humidity sensors was electrical capacity change which gives a large measuring span and sufficient accuracy in order to follow the water uptake. The sensors were manufactured by Vaisala Oyj, Vanha Nurmijärventie 21, Fin-01670 Vantaa, Finland. The gauges were delivered with signed individual calibration data sheets. Traceability is guaranteed by the Vaisala Oyj.

The sensors were individually calibrated in order to check the delivery calibration data both with respect to relative humidity and to temperature dependence. The sensors were connected to the actual data collecting system, including all cables etc. The gauges were placed in specially designed plastic boxes, which were partly filled with different saturated salt solutions. Saturated solutions of  $(\text{NH}_4)_2\text{SO}_4$ , KCl,  $\text{BaCl}_2$  and  $\text{KH}_2\text{PO}_4$  were used. The temperature was kept at 22°C and the equilibrium relative humidity 81.2, 84.8, 90.4 and 94%, respectively, were used for the calibration.

The BaCl<sub>2</sub> solution was also used for the temperature compensation calibration, since the humidity equilibrium is relatively stable in the examined temperature range. Temperatures close to 40, 50 and 60°C were used and a linear function, describing apparent dRH as a function of T, was determined for each sensor. No significant differences between the factory calibration and the Clay Technology laboratory calibration were noticed with respect to relative humidity. The factory calibration and temperature compensation were therefore used in the following presentation of results.

### **3.5.5 Data collection and registration system**

All measuring sensors and gauges were connected to DATASCAN units, which in turn were connected to computer working under Windows NT placed in a cabin close to the test site. The software was named Orchestrator and was manufactured by Eurosoft Technology, UK. MSS AB, Åkersberga, delivered the software and DATASCAN units. The program has a range of output/input drivers and real time data acquisition which i.a. admitted the use of event-governed logging in addition to periodic logging and alarm functions. The standard logging interval was set to 1 hour during the entire test period. The alarm system was used in order to detect overheating, and the system was connected to the control room at the CLAB facility at the nearby nuclear power plant for 24 h supervision.

A standard interval of 1 hour was used for all collection of data since the course of events was expected to be relatively slow. In addition, an event governed data collection was programmed for each type of measuring equipment. The triggering measuring event was exceeding or falling short of a fixed value, or a fixed interval related to the previous measured value. The configuration was made in such a way that all channels related to the test was read off if an event-triggered measurement was started by a single instrument.

The recording and real time handling of data may be divided in three levels of importance. The handling of data used for regulating the system was of course most important since a malfunction may have lead to a fast destruction of the system. Of second most importance were the data needed for the evaluation of the test conditions, and finally there is a group of data which is of general interest but which is not necessary for the accomplishment of the test. In consequence, several levels of alarm function were used in the monitoring system. Different measures were stipulated depending on the type of released alarm, ranging from simple notes to immediate actions from the safety guard at the nuclear power plant.

All recorded data were stored in the specific project computer and backup was regularly made at the Äspö HRL. The standard recorded data concerning temperature, pressure and humidity were copied approximately once a month from Clay Technology and stored in an SQL-database. The data were processed by means of MS EXCEL and thereafter stored in the SICADA database at Äspö.

## 4 Field operation

### 4.1 Preparation

#### 4.1.1 Parcel assembly

The entire parcel systems were prepared and checked in laboratories in Lund, dismantled and loaded on to a lorry for transport to Äspö HRL. At the test site, the water in the test hole was pumped and the bottom part was filled with sand up to approximately 10 cm from the bottom. The central 8 m deep pilot hole with a diameter of 76 mm was thereby also filled with sand. The test hole was covered with a building board and the copper tube was vertically fixed at a bottom support right on top of the test hole. The predestined blocks were thread onto the copper tube from above one by one from a scaffold (Figure 4-1).

The gauges and sensors were placed in shaped cavities before the successive block was placed. The instruments were held in position only by the weight of the overlying blocks without additional equipment. All tubes, that is, tubes intended for water and gas, and wire protecting tubes from each instrument were individually placed in tracks excavated in the outer mantle surface of the blocks above the instrument. The tubes were fixed during the construction of the parcels, but released during the parcel submersion in order to admit movements during the subsequent swelling of the bentonite. A few thin copper wires were though left to keep the tubes in place during the placement (Figure 4-1). The various plugs were placed in position after all bentonite blocks were in position. The plugs were fixed and sealed by adding a small amount of water on the outer plug surface before they were pressed into position. The tracer test plugs were the last to be placed in order to minimize the risk for contamination with  $^{60}\text{Co}$ . The entire mounting procedure of the A2 parcel at the test site was achieved within two days (although quite long days) since all blocks were prepared and the parcel partly test built in the laboratory”.



**Figure 4-1.** Left: Finalizing the construction of the A2 parcel at test site, note the large number of wire protecting tubes from sensors. Right: Insertion of the plug containing  $^{60}\text{Co}$  during lowering the parcel into the test hole. Note the limited amount of tubes in the lower hot section.

## 4.1.2 Installation

The A2 parcel was installed into test hole HG0037G01 on October 29, 1999. The top of the copper tube was connected to the lift device mounted in the roof above the test hole. The parcel was slightly heaved and the bottom support and building board were removed. The test hole was again emptied on water and the parcel was carefully centered and slowly lowered into the test hole. The total submergence procedures took approximately 15 minutes. The upper slot between the bentonite and the rock was sealed with mineral insulation (Rockwool) in order to avoid sand penetrate downwards. An approximately 10 cm thick sand layer was placed on top of the clay column and the wire protecting tubes from all gauges and tubes from filters were brought together above the bentonite and fixed. The uppermost 10 cm of the test-hole and a square-formed reinforced concrete top plug were cast. After hardening, the plug was prevented from heaving, due to bentonite swelling and water pressure, by use of two steel beams, which in turn were fixed by 4 rock bolts (Figure 4-2). The sensor and heater cables were connected to measuring and regulating equipment placed in cabinets on top of the test hole, and the cabinets were covered by a simple drip shelter. The measuring equipment was connected to computers in a hut at about 10 m distance. These computers were in turn connected to the general backup system at the Äspö HRL.

## 4.2 Heating phase

### 4.2.1 Temperature control

There are in principle two main options to control the temperature in this kind of tests, i.e. regulation of the heater power to a fixed value, and to regulate the power to give a defined temperature at a certain position. Constant power best simulates the heat production of spent fuel and constant temperature excludes overheating. The power was first turned on February 2, 2000, and regulated to give a constant maximum temperature of 50°C. A mean value of the three thermocouples A208T1, A214T1 and A220T1 were initially used to govern the power in order to ensure that no overheating took place. The maximum temperature target was thereafter increased in steps of 10°C. On April 19, 2000 the regulation was changed to a fixed power of 480 W. The power was thereafter increased in steps to a final power of 850 W which was reached on June 17, 2000.

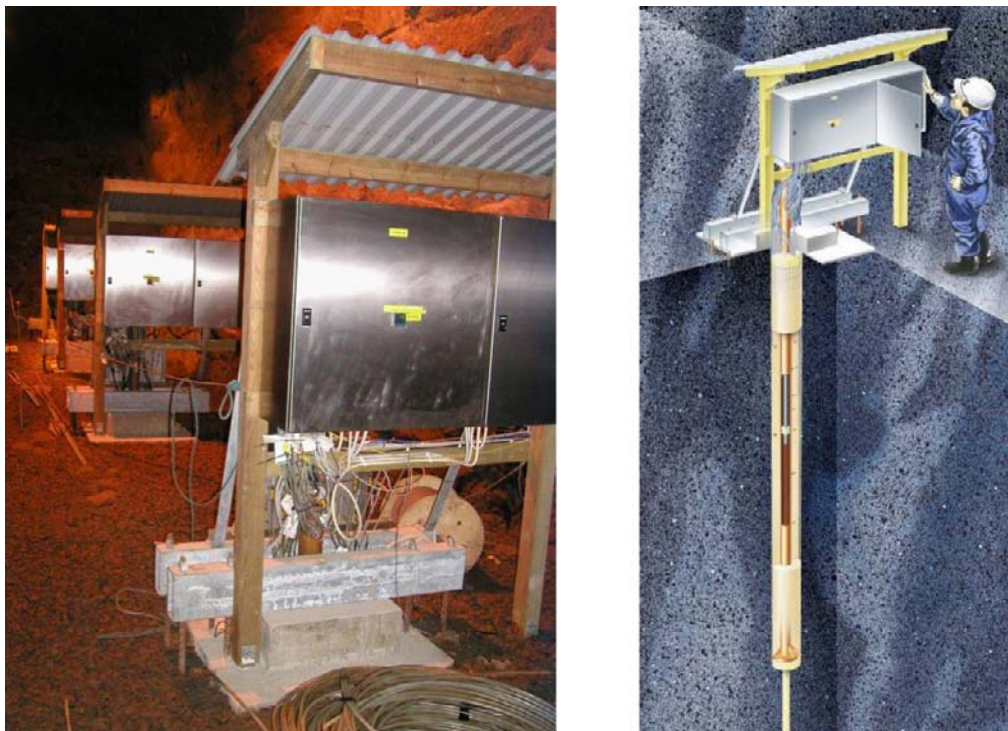


*Figure 4-2. Left: Picture of the test site with parcel A2 in the front. Right: Schematic drawing of the final appearance of the A2 test after installation.*

## 4.2.2 Water supply

The slot between the clay column and the rock was slowly water filled on February 2, 2000 in parallel with the onset of heating. The filling was made with groundwater from the adjacent borehole (HG0038B01) by use of the fixed installed titanium tube and bottom filter (filter no 7) placed in the sand below the parcel and close to the rock wall. The valve connected to the bottom filter was closed at the time when the groundwater had reached the uppermost filter (Filter 3 in block 32), which so far was open against air. This filter was instead connected to the groundwater supply, and the intention was to leave it open to ensure saturation in the upper cold part of the parcel in order to prevent steam to escape along the copper tube. However, the system did not seal completely, likely due to the large number of various tubes intersecting in the uppermost part (Figure 4-1). The supply of groundwater was therefore moved to the next lower filter in order to ensure a sufficient groundwater pressure and thereby prevent boiling.

## 4.3 Field results

### 4.3.1 General

The field regulating and measuring systems worked very well during the entire six years of operation, and no malfunction of importance occurred. Most important was that no overheating or unplanned temperature drops took place. Minor incidents with logging units and service stops in logging can be seen in the various results.

### 4.3.2 Temperature

The temperature recordings were of special importance as this parameter is of such importance for the reaction rate of chemical processes. The large number of sensors gave a clear picture of the temperature distribution within the parcel. Figure 4-3 shows the measured temperature evolution in the warmest section (block 14). Uppermost curve shows the temperature at the copper tube surface, and the underlying curves show the temperatures of points successively 2 cm closer to the rock. The lowest curve consequently represents a point approximately 1 cm from the rock.

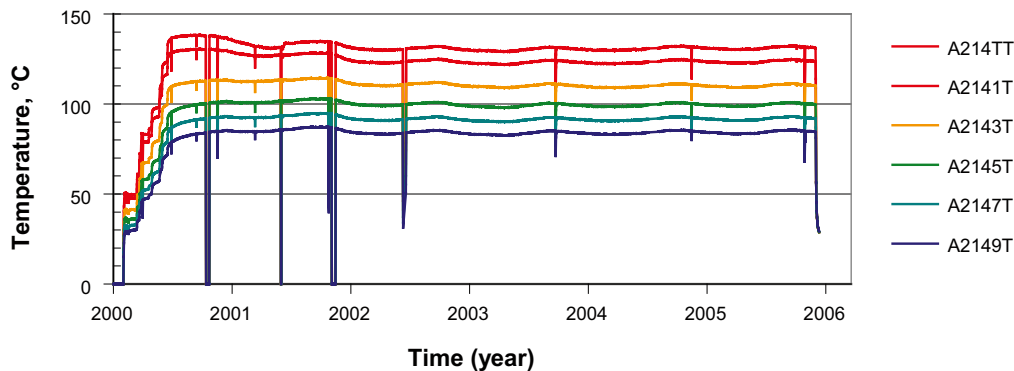


**Figure 4-3.** Temperature results from the thermocouples in block no. 14. Uppermost curve shows the temperature at the copper tube surface, and the underlying curves show the temperatures of points successively 2 cm closer to the rock. The lowest curve represents a point approximately 1 cm from the rock.

A certain annual cyclic variation is noticed, which can be correlated to the temperature in the ventilated tunnel, and represents the combined effect of the thermal conductivity of the bentonite, copper tube and surrounding rock. A minor temperature decrease in the innermost positions over the first 3 years is noticed in all warm positions, and is a strong indication of the course of water saturation. Figure 4-4 (left) shows the temperature distribution in the parcel during the major part of the field exposure, and Figure 4-4 (right) shows the distribution in the cooled parcel seven days after power termination.

### 4.3.3 Total and water pressure

The two types of pressure sensors, i.e. optical sensors in block 08 and 20 and vibrating wire sensors in block 14 show similar results, both with respect to total pressure and water pressure (Figure 4-5). The results show that the sensors worked quite well, but still one has to be careful with the absolute values, because of the high temperature and long time elapsed after calibration. Qualitatively, it is clear that the bentonite was fully water saturated after less than 2 years at the measuring points, which is in agreement with the temperature indications. The measured maximum water pressure is close to the applied groundwater pressure (~1.2 MPa) in the supply filter, indicating the accuracy of the measurement. An unintended closure of the water supply in January 2002 led to a significant pressure drop in all three monitored levels, both with respect to total and water pressure. The water supply was deliberately not turned on until September 2002 in order to study the natural pressure evolution. A quick response was noticed after the opening the closed valve.

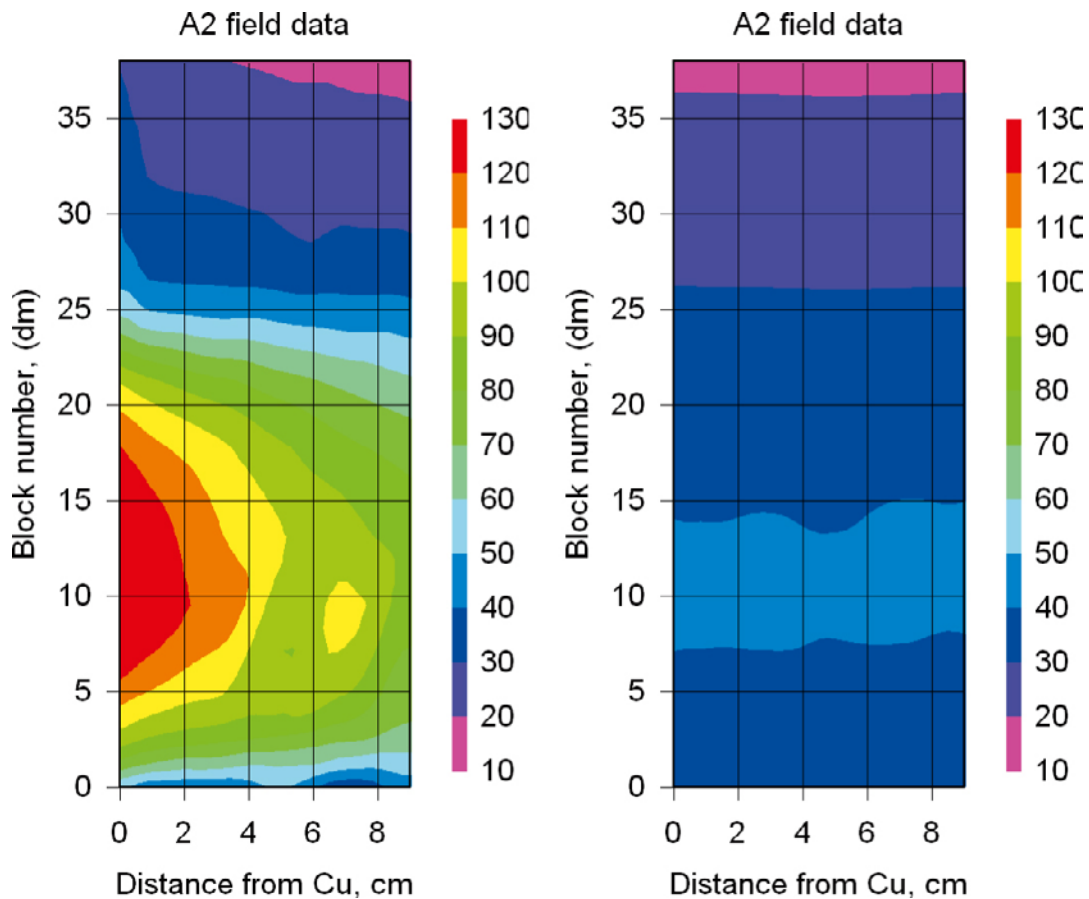


**Figure 4-4.** Left: temperature distribution at termination of the heating, which also represents the major part of the field exposure time (see Figure 4-3). Right: temperature distribution one week after termination of the heating.

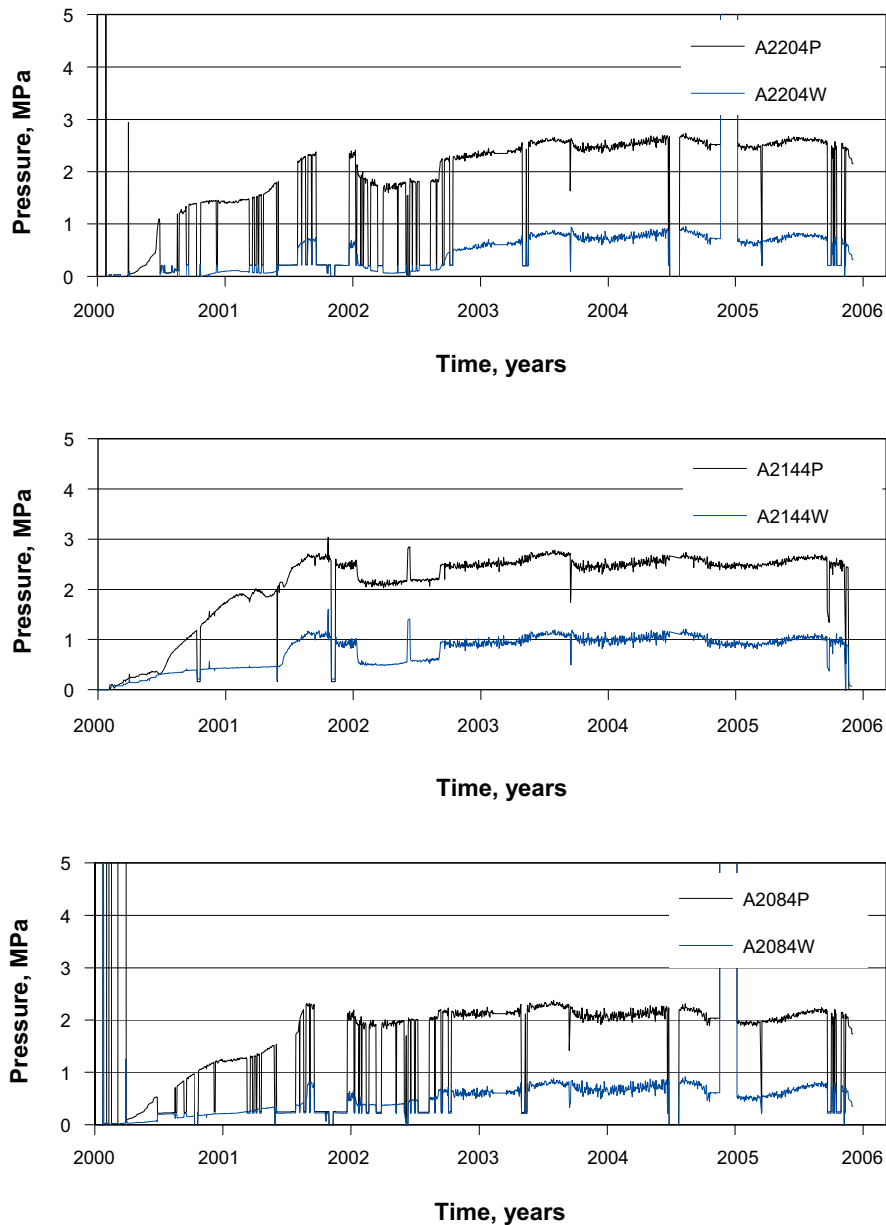


*Figure 4-5. Total pressure (black lines) and water pressure (blue lines) versus time in block 20 (upper), 14 (mid) and in block 8 (lower) at mid position between the copper tube and the rock.*

#### 4.3.4 Moisture

High quality moisture measurements are difficult to perform over long time, especially in the very harsh environment in bentonite at high temperature. At full water saturation of the bentonite the fragile moisture sensors normally get contaminated of the saline water. This commonly leads to subsequent erroneous results, which however is a good indication of full water saturation. Figure 4-6 shows the results from three moisture and accessory temperature sensors from block A208, A214 and A220, respectively. All moisture sensors indicate a rather fast increase in humidity to over 90% within the first half year. A complete failure of both the moisture and temperature sensors took place around mid 2001 for all sensors. Such a failure is usually due to liquid water intrusion and consequently indicates full water saturation. These results are consequently in good agreement with the indications from the pressure sensors and thermocouples with respect to water saturation.

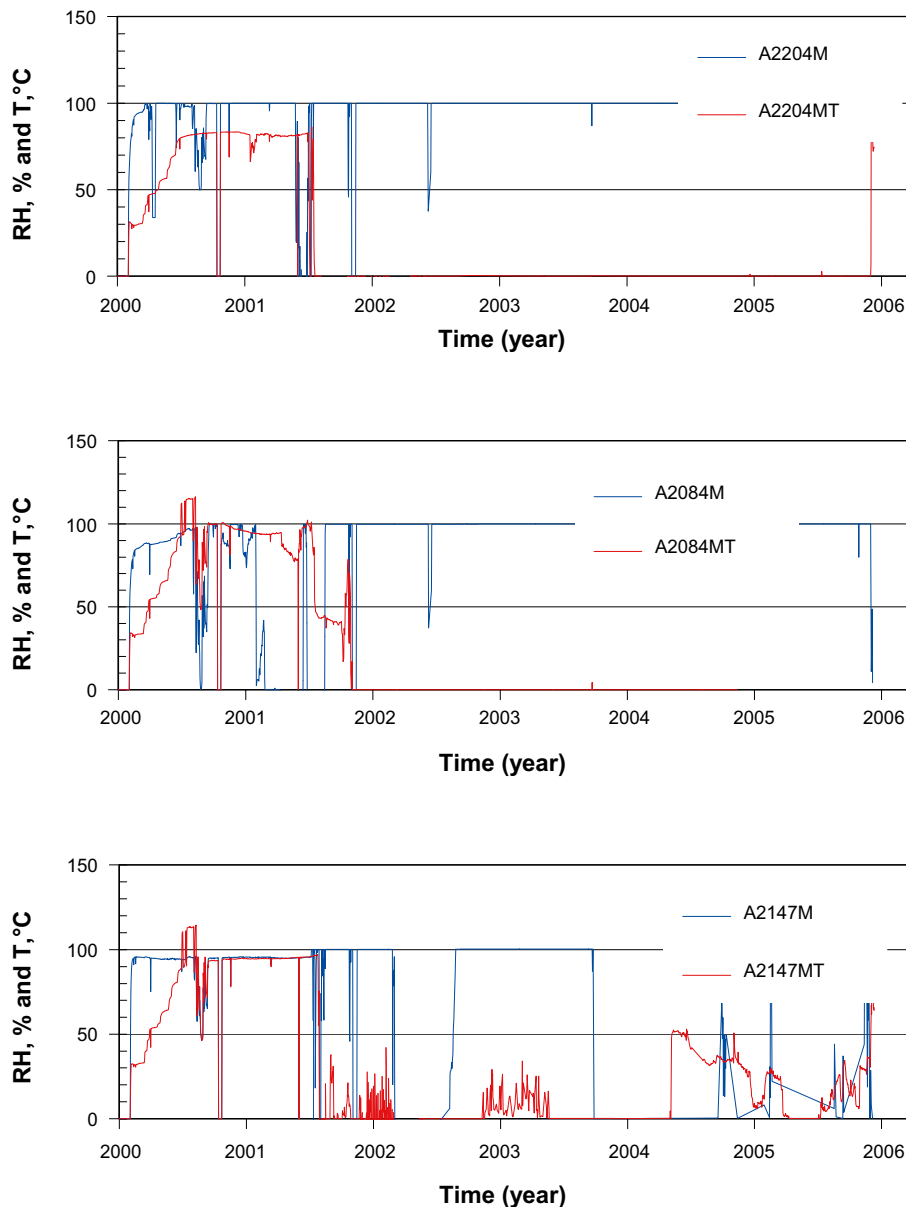


**Figure 4-6.** Results from the Vaisala moisture sensors showing temperature (red lines) and the in situ relative humidity (blue lines) in equilibrium with the bentonite in block A208, A214 and A220.

## 4.4 Termination of the field activity

### 4.4.1 Termination, drilling and uplift

The heater power was reduced to zero on December 6, 2005. The temperature dropped relatively fast and was below 50°C within a week (Figure 4-4, right). The uncovering drilling operation is described in the Äspö HRL activity plan AP TD F62-05-023.

In short, the test parcel was partly released by overlapping percussion drilling in the surrounding rock. The diameter of the boreholes was 89 mm diameter and the depth was around 4.5 m. The final part of the circumference was core drilled with a diameter of 280 mm (Figure 4-7). The choice of percussion technique was motivated partly by economic reasons, but mostly by the fact that no cooling water was necessary. The core drilling technique was used to finalize the slot around the parcel, since the rock support normally is poor at this stage which makes the steering of a percussion boring head cumbersome. The large diameter of the core drilled holes was motivated by the wire sawing



*Figure 4-7. Left: Top part of the parcel with attached lifting device. Note the surrounding slot made by overlapping percussion drill holes and the larger core drilled holes. Right: Entire A2 test parcel with rock-cover being placed on a lorry for transport.*

equipment which was used to release the bottom of the rock column. The released block containing parcel and rock-cover was lifted by a crane lorry and transported to a dry niche for examination and sampling. The total weight of the rock/parcel block was around 4,000 kg, and the diameter was around 65 cm. i.e. the rock cover of the test parcel was of a good size.

#### **4.4.2 Partitioning of the parcel**

The uncovering of rock and subsequent sampling operation started on January 17, 2006 and was finalized after two days of intense work. The operation is described in the Äspö HRL activity plan AP TD F62-06-001, and the course of events is described in detail in the appurtenant Daily log (stored at Äspö HRL).

In short, the covering rock was successively removed in approximately 0.5 m long pieces by sawing, use of wedges, and natural weaknesses in the rock (Figure 4-8). The approximate position of the original block interfaces were identified in the exposed bentonite by use of the various kinds of tubes going in to defined positions and by measuring. The bentonite blocks were cut by sawing and successively removed from the copper tube. The blocks were marked according to the activity plan and placed in plastic bags. Air was evacuated by use of a vacuum pump, and the bags were sealed and placed in plastic boxes which were closed. The main part of the material was transported to Clay Technology laboratory in Lund for analyses and further distribution to the involved laboratories. Special care was taken in handling the blocks aimed for water analyses at VTT, mineralogical analyses performed by University of Bern, bacterial analyses by Micans laboratory, copper coupon analyses, and the bottom 6 blocks aimed for <sup>60</sup>Co tracer analyses at KTH. The VTT blocks were placed in metal containers and air was replaced by an argon atmosphere in order to prevent redox reaction during transport. The University of Bern block was transported directly after release to the Äspö surface laboratory for partitioning and storing. The blocks aimed for bacterial activity analyses were quickly brought to an anaerobic box at the nearby underground bacterial test site at Äspö. The blocks containing copper coupons were sealed and transported directly for analyses at e.g. Studsvik AB. Finally, the KTH bottom part of the parcel was placed in a special box for prompt transport to the Department of Nuclear Chemistry at KTH, Stockholm.



*Figure 4-8. Left: Photo taken just after the removal of the first piece of rock from the upper part of the parcel. Note the well covered sensor wire protecting tubes and the tight interface between bentonite and the covering rock. Right: Sawing cuts were made approximately at the original block interfaces and the released blocks were successively removed from the copper tube.*

## 5 Laboratory analyses – general

### 5.1 Test philosophy

Reference material and material from defined positions in the A2 parcel material were tested and analyzed. The results were compared with respect to changes in physical properties and mineralogy. The present LOT A2 parcel material was analyzed with respect to mineralogy/chemistry not only by SKB and Posiva, but also by the four additional independent laboratories BGR in Germany, University of Bern in Switzerland, G2R and LEM from Nancy University in France, which were financed by BGR, NAGRA and ANDRA respectively.

The large number of performed physical tests and mineralogical/chemical analyses of the material were made without close contact between the different laboratories. The purpose was to get independent results based on the techniques normally used by the different laboratories, which to some extent differs by tradition. The most striking example is the cation exchange capacity, which was determined without using the same technique in two laboratories. The risk for systematic artifacts are thereby believed to be reduced significantly.

Since absolute quantitative data are difficult to procure for some of the properties, the aim has been to reveal possible systematic discrepancies between the reference material and parcel material from different positions.

### 5.2 Test material

The six bottom blocks for the  $^{60}\text{Co}$  tracer analyses were only analyzed at KTH, Stockholm and the results are presented in Appendix 2. Block 13 was only analyzed by the University of Bern and the results are presented in Appendix 8. One part of block 15 was analyzed by BGR, and the results are presented in Appendix 7, and another part of the same block was analyzed by the G2R and LEM laboratories and their results are presented in Appendix 6.

The main part of the blocks was transported to Clay Technology's laboratory, and selected blocks were divided by use of an electric band saw in order to produce test material according to Figure 3-2. The rough partitioning of the clay at the test site enabled a relatively fast and precise sampling of the bentonite and additive zones of interest. The partition was made within a few days in order to reduce redistribution of elements in the material. The sawn samples were made large enough to admit several tests from a specific position. In other words, material with the same specimen denomination was used for several different kinds of tests and analyses. The denomination of a specific point (centre of a volume) was according to the following example:

08ASE3 where

08 block number (counted from the bottom of the parcel),

A vertical level in the block,

SE direction of compass in the test hole,

3 radial distance in centimeters from the inner mantle surface to the centre of the specimen.

## 6 Basic geotechnical properties

### 6.1 Test principles

Basic geotechnical properties were determined for a large number of positions in the test material in order to give a general picture of especially density and the water distribution. Block no. 7, and every second block above, except block 13, were analyzed with respect to water to solid mass ratio ( $w$ ) and bulk density ( $D_b$ ) from which the degree of saturation ( $S_r$ ) was calculated. No specific preparation of the test material was made except for sawing specimens to a size corresponding to approximately 20 grams. The relatively large samples and quick handling after sawing were used in order to minimize drying artifacts.

All samples were taken at the mid height (B position) of the western side of the blocks in order to minimize interference from gauges and other test devices. An exception is block 19 where the south section was used. The sample bulk density ( $D_b = \text{total mass}/\text{total volume}$ ) determined by weighing the material in air and submerged in paraffin oil. The bulk density was thereafter calculated according to:

$$D_b = \frac{m \cdot D_{\text{paraffin}}}{m_{\text{paraffin}}} \quad \text{Equation 6-1}$$

where  $m$  is the mass of the specimen,  $D_{\text{paraffin}}$  is the density of the paraffin oil, and  $m_{\text{paraffin}}$  is the mass of displaced paraffin oil. All bulk density results are compiled in (Table 6-1).

The water to solid mass ratio ( $w$ ) was determined by drying the material in a laboratory furnace at 105°C for 24 h, and the water to solid mass ratio was calculated according to:

$$w = \frac{m - m_d}{m_d} \quad \text{Equation 6-2}$$

where  $m_d$  is the mass of the dry sample. All water to solid mass ratio results are compiled in (Table 6-2).

The degree of saturation ( $S_r$ ) was calculated from sample density ( $D_b$ ) and water to solid mass ratio ( $w$ ) according to:

$$S_r = \frac{w \cdot D_b \cdot D_s}{D_w (D_s (w + 1) - D_b)} \quad \text{Equation 6-3}$$

where  $D_s$  is the mean grain density,  $D_w$  is the water density. A mean grain density of 2,750 kg/m<sup>3</sup> was used for the bentonite /Karlund and Birgersson 2006/. All results of calculated degree of saturation are compiled in (Table 6-3).

### 6.2 Results

The results show that there was a significant density distribution in the parcel bentonite mass (Figure 6-1). One extreme being the denser lower part close to the hot copper tube with a density around the KBS-3 target density, and the other extreme was the uppermost outer part close to the rock. All tested samples were fully water saturated within the accuracy of the measurements, which by definition means that the saturated densities were equal to the measured bulk densities.

The raw and calculated data are stored in Excel files and transferred to the SICADA database. The individual specimens were denominated according to the general description scheme. A typical denomination of a specimen is consequently A238BW1b, where A2 is the parcel, 38 is the block number, B is the mid height in the block, W is the western direction, 1 is the radial position, and finally the b denotes that it concerns the bulk material.

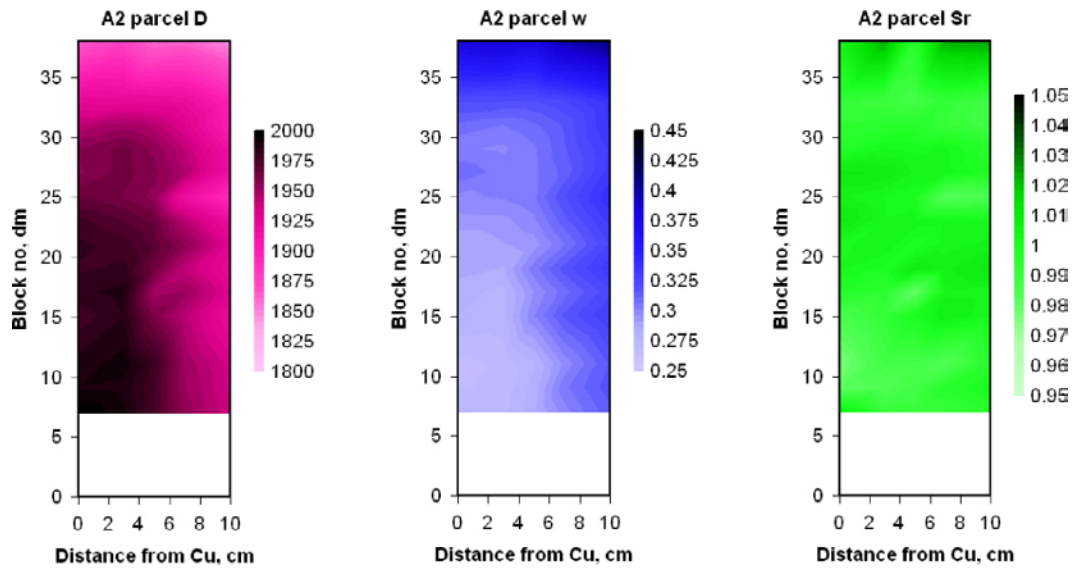


*Figure 6-1. Bulk density,  $D$  (left), water to solid mass ratio,  $w$  (center) and degree of water saturation,  $S_r$  (right) in the LOT A2 parcel.*

**Table 6-1. Measured bulk density in kg/m<sup>3</sup> of blocks 07 to 38 in parcel A2.**

Block no.	Position, in cm from Cu tube				
	1	3	5	7	9
38	1,864	1,876	1,859	1,862	1,847
33	1,923	1,922	1,920	1,918	1,897
31	1,941	1,948	1,943	1,930	1,898
29	1,955	1,962	1,954	1,941	1,912
27	1,954	1,962	1,957	1,945	1,912
25	1,965	1,960	1,953	1,916	1,890
23	1,977	1,971	1,964	1,943	1,917
21	1,982	1,978	1,969	1,955	1,928
19	1,979	1,981	1,962	1,940	1,921
17	1,983	1,987	1,948	1,951	1,928
15	1,977	1,985	1,959	1,942	1,919
11	1,987	1,993	1,979	1,950	1,933
09	1,990	1,988	1,975	1,951	1,934
07	2,000	1,991	1,975	1,954	1,936

**Table 6-2. Measured water-to-solid mass ratio of blocks 07 to 38 in parcel A2.**

Block no.	Position, in cm from Cu tube				
	1	3	5	7	9
38	0.376	0.380	0.374	0.393	0.408
33	0.321	0.321	0.320	0.325	0.337
31	0.309	0.305	0.309	0.316	0.336
29	0.301	0.299	0.304	0.314	0.331
27	0.309	0.303	0.304	0.312	0.333
25	0.299	0.301	0.304	0.320	0.340
23	0.293	0.293	0.299	0.313	0.332
21	0.285	0.289	0.293	0.304	0.326
19	0.287	0.285	0.303	0.317	0.333
17	0.282	0.278	0.295	0.308	0.324
15	0.280	0.279	0.300	0.316	0.330
11	0.268	0.271	0.279	0.297	0.316
09	0.269	0.271	0.282	0.303	0.318
07	0.275	0.274	0.283	0.298	0.314

**Table 6-3. Calculated degree of saturation ( $S_r$ ) of blocks 07 to 38 in parcel A2.**

Block no.	Position, in cm from Cu tube				
	1	3	5	7	9
38	1.00	1.02	1.00	1.02	1.02
33	0.99	0.99	0.99	0.99	0.99
31	0.99	1.00	1.00	0.99	0.99
29	1.00	1.00	1.00	1.00	1.00
27	1.01	1.01	1.00	1.00	1.00
25	1.00	1.00	1.00	0.98	0.98
23	1.01	1.00	1.00	1.00	1.00
21	1.00	1.00	1.00	1.00	1.00
19	1.00	1.00	1.01	1.01	1.01
17	1.00	1.00	0.98	1.00	1.00
15	0.99	0.99	1.00	1.01	1.00
11	0.98	0.99	0.99	0.98	1.00
09	0.98	0.98	0.99	1.00	1.00
07	1.01	0.99	0.99	0.99	1.00
Mean	1.00	1.00	1.00	1.00	1.00

## 7 Sealing properties

### 7.1 Test principles

The hydraulic conductivity and swelling pressure were determined in combined tests on material chosen from strategic positions within the test parcel and on the corresponding reference material. The test series includes the following sub-series and all results are summarized in Table 7-1:

- reference material, air-dried and compacted, Äspö-water, 6 samples,
- parcel material, air-dried, crushed and recompact to buffer density, Äspö-water, 6 samples,
- parcel material, naturally saturated, sawn and trimmed to fit the test cells, Äspö-water, 6 samples.

Six purpose-built swelling pressure test cells were used (Figure 7-1). The samples were confined by cylinder rings with a diameter of 20 mm and stainless steel filters at the top and bottom. The test volumes were sealed by o-rings placed between the bottom plates and the cylinder rings and between the pistons and the cylinder rings. At test start the height of the test volumes were fixed to 10 mm by the flanges on the moveable pistons. The axial force from the sample was determined by the transducer placed between the piston and the upper lid. The displacement of the piston due to transducer deformation is 100  $\mu\text{m}$  at maximum force, which consequently correspond to 1% of the sample height and is considered insignificant.

Reference samples were prepared from material saved from block production. Parcel samples were prepared from extracted material in two ways,

- air-dried and crushed to a grain size similar to the original MX-80 powder and re-compacted to a density of 2,000  $\text{kg}/\text{m}^3$ ,
- sawn by a cylindrical saw and trimmed to fit the test cells and thus had a density close to but slightly lower than the field value.

Äspö ground water from borehole HG0038B01 was initially circulated below the lower filter in order to let air out through the upper filter during the saturation. The water uptake was indirectly monitored by the force transducer (Figure 7-1). At constant swelling pressure, the solution was circulated also above the upper filter. Stable force conditions were reached within 1 week. At this point a water pressure of maximum 50% of the measured swelling pressure was applied in the bottom filter in order to establish percolation. The volumes of the percolated water solution were registered daily by visual observations of the water/air interface meniscus. The water pressure was thereafter reduced to zero and the tests were terminated when the recorded axial forces had stabilized.

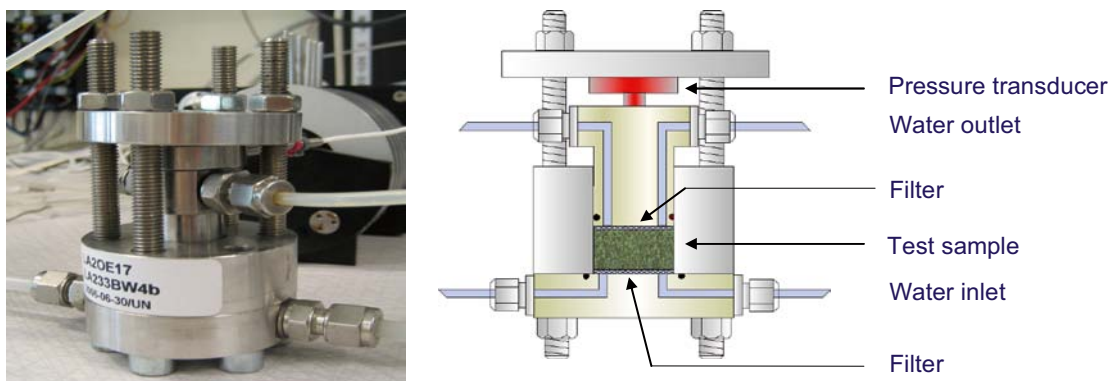


**Figure 7-1.** Photo and schematic drawing of the test cell used for determination of swelling pressure and hydraulic conductivity.

The swelling pressure  $P_s$  (Pa) was calculated from the measured force at zero water pressure according to:

$$P_s = \frac{F}{A} \quad \text{Equation 7-1}$$

where  $F$  is the axial force (N) and  $A$  is the sample area acting on the piston ( $\text{m}^2$ ). The accuracy of the measured values is governed by the force transducers which were calibrated against a standard force ring before and after each test.

The hydraulic conductivity  $k$  (m/s) was evaluated from the percolated water volume according to Darcy's law:

$$k = \frac{V \cdot l}{A \cdot h \cdot t} \quad \text{Equation 7-2}$$

where  $V$  is the percolated volume ( $\text{m}^3$ ),  $l$  is the sample length (m),  $A$  is the sample area ( $\text{m}^2$ ),  $h$  is the water pressure difference over the sample expressed as water column (m) and  $t$  is the time (s).

At test termination, the samples were split in two halves and the sample bulk density ( $D_b$ ) and water to solid mass ratio ( $w$ ) were determined by the same technique as described in Section 6.1. The samples may be considered fully water saturated due to the test conditions, and the dry density, void ratio and porosity can be calculated since the grain density is known.

## 7.2 Results

Measured swelling pressures and hydraulic conductivities are presented in Table 7-1.

**Table 7-1. Results from swelling pressure and hydraulic conductivity tests. Äspö groundwater from borehole HG0038B01 was used in all tests.**

Test material	Preparation	Water to solid mass ratio	Bulk density, $D_b$ , $\text{kg/m}^3$	Swelling pressure, $P_s$ , MPa	Hydraulic conductivity, $C_h$ , m/s
LA2R	air-dry	0.494	1,742	0.25	2.8E-12
LA2R	air-dry	0.436	1,796	0.80	7.8E-13
LA2R	air-dry	0.359	1,881	2.60	2.7E-13
LA2R	air-dry	0.327	1,922	5.0	1.3E-13
LA2R	air-dry	0.285	1,981	8.1	7.7E-14
LA2R	air-dry	0.259	2,022	12.1	5.0E-14
LA209BS4b	air-dry	0.303	1,955	5.1	1.9E-13
LA209BS8b	air-dry	0.278	1,992	7.9	1.4E-13
LA211BS4b	air-dry	0.306	1,951	5.0	1.7E-13
LA211BS8b	air-dry	0.281	1,987	6.2	1.2E-13
LA233BW4b	air-dry	0.281	1,987	6.7	1.5E-13
LA233BW8b	air-dry	0.297	1,963	6.3	1.7E-13
LA209BS4b	trimmed	0.284	1,983	8.4	5.1E-14
LA209BS8b	trimmed	0.303	1,954	7.0	5.1E-14
LA211BS4b	trimmed	0.290	1,974	6.9	6.2E-14
LA211BS8b	trimmed	0.316	1,937	4.8	7.5E-14
LA233BW4b	trimmed	0.309	1,946	5.2	7.4E-14
LA233BW8b	trimmed	0.302	1,955	5.6	7.2E-14

The scatter in density of the sawn and trimmed samples are likely due to the preparation technique and are not directly related to the previous field conditions (Figure 7-2). No differences were found in the results from warm positions compared to those from the upper cool positions or from the reference material. The results from the A2 parcel are also in good agreement with previously measured results, e.g. from the short term test parcel A0 and reference material /Karnland et al. 2009/.

There is a minor but significant shift in hydraulic conductivity as a function of density between trimmed and re-compacted samples (Figure 7-3). There is, however, no significant difference between samples from different positions in the parcel. The slightly lower conductivity in the trimmed samples can consequently not be related to temperature or temperature gradients.

The raw and calculated data have been stored in Excel files and transferred to the SICADA database. The test series was termed LA2OE and the individual specimens were denominated according to the general scheme, e.g. LA209BS4b.

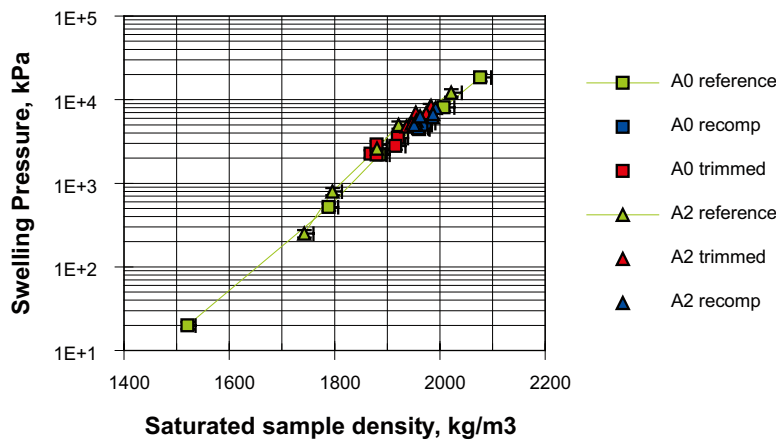


**Figure 7-2.** Measured swelling pressure results from the A2 parcel material compared with reference material and to the previous short term test material (A0).

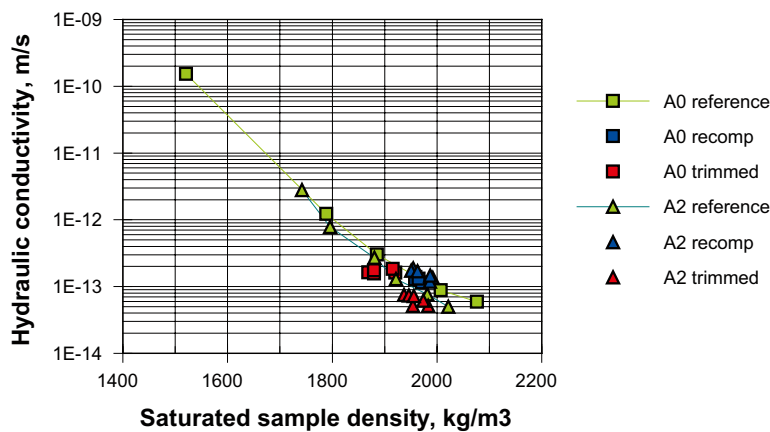


**Figure 7-3.** Measured hydraulic conductivity results from the A2 parcel material compared with results from reference material and to the previous short term test material (A0).

# 8 Rheological properties

Ann Dueck, Clay Technology AB

## 8.1 Triaxial tests

### 8.1.1 Test principles

The strength properties of soil materials can preferably be evaluated from triaxial tests. A description concerning technique and evaluation is given by /Börgesson et al. 1995/. The technique requires relatively large test specimens and is resource consuming, both with respect to time and active work. The test series were therefore limited to three samples from the parcel material and one reference sample (Table 8-1).

Two tests on parcel material represented high temperature conditions (blocks 09 and 11), and one represented low temperature condition (block 33). The specimens were sawn from the inner part of the block cylinder ring (position 0 to 4 in the radial direction).

### 8.1.2 Equipment

The test specimens were pre-saturated in a cylindrical saturation device equipped with an axial and cylindrical steel filter to achieve radial saturation. A piston allowed for measurement of the axial swelling pressure parallel to the saturation. The central part of the device was comprised of two half cylinders in order to enable removal of the specimens without use of axial force.

A high pressure triaxial cell was used for all tests. The cell was equipped with standard strain gauges, force transducers and pore-pressure transducers according to Figure 8-1.

Table 8-1. The LOT A2 triaxial test series (LA2TL).

Test ID	Material	Preparation	Solution	Density, kg/m <sup>3</sup>	Max temperature, °C
LA2TL01	LA209BS2b	sawn	LOT	parcel	125
LA2TL02	LA211BS2b	sawn	LOT	parcel	125
LA2TL03	LA233BS2b	sawn	LOT	parcel	30
LA2TL04	MX-80 LA2R	air-dry	LOT	1,950	room

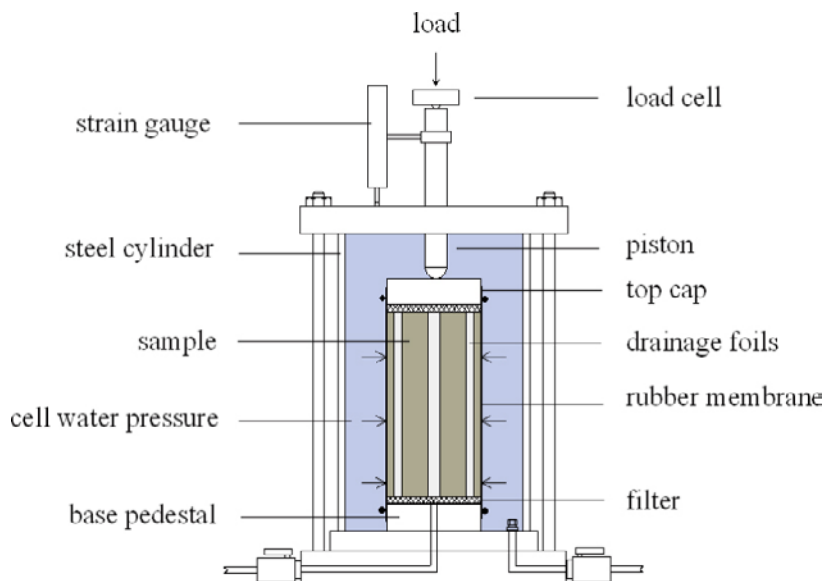


Figure 8-1. Triaxial test equipment used in combination with a hydraulic press.

### 8.1.3 Sample preparation

Cylindrical specimens were prepared from the parcel material by sawing rough work pieces which were trimmed to a cylindrical form with a diameter of 35 mm and a height of 70 mm. The reference sample was compacted from air-dry powder to the same dimensions, and water saturated in the same saturating device as used for the parcel samples. After 4 weeks in the saturation device each sample was mounted in the triaxial cell (Figure 8-1), and a cell pressure corresponding to the measured swelling pressure was applied in the cell. The valve to the pedestal was kept closed during an equilibration period and the pore pressure ( $u$ ) at the base pedestal was measured. Filter paper drains along the samples were used to accelerate the equalization of the pore pressure over the sample height.

### 8.1.4 Test procedure

The cell was loaded by use of a mechanical press when the pore pressure was considered stable with time, i.e. when pressure equilibrium was reached. A constant shear rate of 7.5 mm/week ( $7.4 \cdot 10^{-4}$  mm/min) was applied. In all tests the pore pressure was 200 kPa or higher at the start of the shearing, in order to avoid problems with air. The sample was undrained during the course of shearing. After failure the water to solid mass ratio and density of the specimens were determined. The water to solid mass ratio and the density were determined according to Section 6.1.

### 8.1.5 Data flow and evaluation

The cell pressure ( $\sigma_3$ ), pore pressure ( $u$ ), deformation ( $\Delta l$ ), and axial force ( $F$ ) were measured. The samples were considered as undrained during shearing and no volume change was taken into account. The deviator stress was calculated from:

$$q = \frac{F}{A_0} \left( \frac{l_0 - \Delta l}{l_0} \right) \quad \text{Equation 8-1}$$

where  $A_0$  is the specimen initial cross section area and  $l_0$  the initial length of the sample. The contact area between load piston and top-cap was considered insignificant.

The vertical total stress ( $\sigma_1$ ) was calculated from:

$$\sigma_1 = q + \sigma_3 \quad \text{Equation 8-2}$$

The average effective stress ( $p'$ ) was calculated from:

$$p' = \frac{1}{3} (\sigma_1 + 2\sigma_3 - 3u) \quad \text{Equation 8-3}$$

The strain ( $\varepsilon$ ) was calculated from:

$$\varepsilon = \frac{\Delta l}{l_0} \quad \text{Equation 8-4}$$

The measured cell pressure, pore pressure, deformation, and axial force versus time were stored together with the calculated stresses, strain, water to solid mass ratio and density data in an Excel file. The test series were termed LA2TL (TL for triaxial test) and the individual specimens were denominated according to the general LOT scheme, e.g. LA209BS2b. In the result section this individual specimen is denoted 09\_2 which means block number\_distance in cm from the Cu-tube.

### 8.1.6 Results

Deviator stress versus strain resulting from the triaxial tests are shown in Figure 8-2. The stress path is plotted as deviator stress versus mean effective stress in Figure 8-3. In Table 8-2 final water to solid mass ratio ( $w$ ) and saturated density ( $D_b$ ) are noted for each sample together with the swelling pressure ( $P_s$ ) measured during saturation. Stresses and strain at maximum deviator stress during shearing are also noted in Table 8-2.

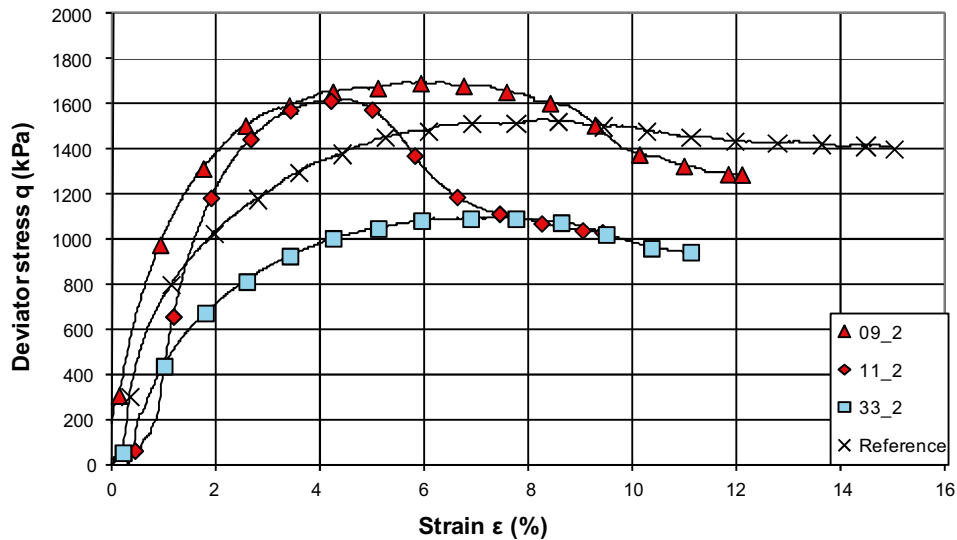


Figure 8-2. Deviator stress versus strain resulting from the triaxial tests.

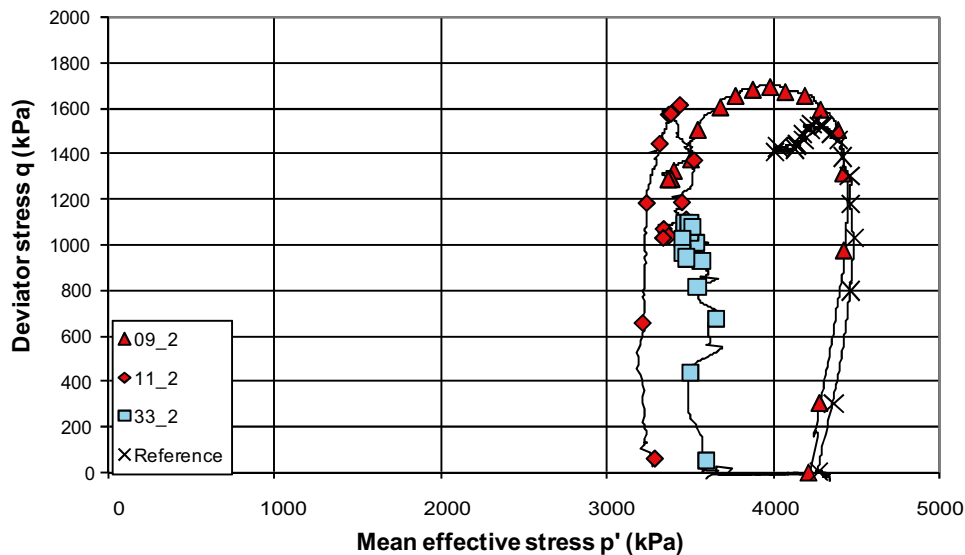


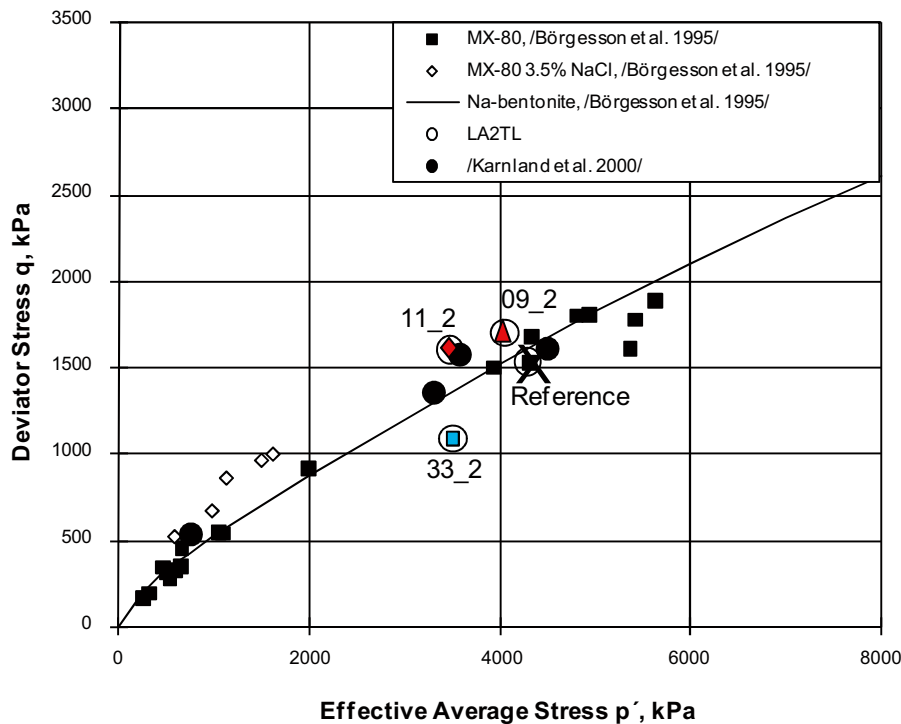
Figure 8-3. Stress paths plotted as deviator stress versus mean effective stress.

Table 8-2. Results from the triaxial tests. Sample position indicates block no.\_position in block.

Test ID	Sample position	Results at failure					Final average values		
		$P_s$ kPa	$q$ kPa	$p'$ kPa	$\epsilon$ %	$\sigma_3$ kPa	$u$ kPa	$D_b$ kg/m <sup>3</sup>	$w$ %
LA2TL01	09_2	4,400	1,696	4,043	6	4,498	1,020	1,940	32.2
LA2TL02	11_2	4,000	1,600	3,458	5	4,848	1,924	1,950	31.1
LA2TL03	33_2	3,400	1,087	3,497	6	4,675	1,540	1,910	34.3
LA2TL04	Reference	3,580	1,531	4,279	8	4,515	746	1,940	32.0

### 8.1.7 Discussion and conclusions

The present results are presented in Figure 8-4 with values from the literature. No significant discrepancies are seen between the reference and parcel material with respect to shear strength and shear course. The present results, representing LOT groundwater, are expected to fall on a line slightly above the results for MX-80, since salt seems to influence the resulting deviator stress (cf. MX-80 3.5% NaCl) in a previous study by /Börgesson et al. 1995/.



**Figure 8-4.** Maximum deviator stress versus effective average stress for different bentonites. Results from the present investigation are shown with circles around the symbols (triangle, diamond, square, cross) denoting the block or reference (09, 11, 33, LA2R). The results are presented with results from /Karnland et al. 2000/ and /Börgeesson et al. 1995/. The open diamonds represent MX-80 saturated with a 3.5% NaCl solution.

Sample 33\_2 suffered from leakage problems and was therefore dismantled and re-mounted in the triaxial cell. The pore water pressure response was still not sufficiently fast, and the sample was likely not in equilibrium. The results for this sample are thus considered as unrepresentative.

The present study shows no significant discrepancies from earlier reported results regarding shear strength. However, a tendency towards less strain at maximum deviator stress is noticed in the sample from block 11 (test LA2TL02).

## 8.2 Unconfined compression tests

### 8.2.1 Test principle

The stress-strain properties were used as indicator for evaluating relative rheological changes between different positions in the test parcel and the reference material. A simplified method to determine these properties is to perform unconfined compression tests, in which a sample is compressed axially with a constant rate of strain with no radial confinement or external radial stress. Unconfined compression tests on saturated bentonite have been reported by /Börgeesson et al. 2003/.

Two test series were run, one with field exposed material and reference material (Series I), and one with oven exposed material and reference material (Series II). Groundwater from the LOT test site was used in most tests in Series I, and deionized water was consequently used in test Series II. The dimension of the test samples was minimized in order to get spatial resolution of the test parcel and to ensure full water saturation. Cylindrical samples with a diameter and height of 2 cm were used. The results should therefore only be used to evaluate relative changes, since the height normally is kept twice the diameter.

A relatively large number of specimens were tested in the test Series I (Table 8-3) representing high temperature parcel material (LA2UC01 to LA2UC12), low temperature parcel material (LA2UC13 to LA2UC18) and reference material (LA2UC19 to LA2UC30). Samples were sawn from the 5 radial positions 1, 3, 5, 7, 9 cm in block no. 9, 11 and 33. The sixth sample in each block was a doublet from the radial position 1 cm. A series of unexposed reference material was run in order to determine the relationship between sample density and the stress-strain properties. In addition, one complementary set of tests was run with parcel material including both high and low temperature material (LA2UC101-106). Finally, three specimens with air-dried, milled and re-compacted material from the warmest part of block 11 (LA2UC231-233) were run. The purpose of this series was to examine the stability of possible changes.

**Table 8-3. Test Series I with unconfined compression tests including LOT field exposed material. The maximum field exposure temperatures ( $T_{max}$ ) are evaluated from Figure 4-4.**

Test ID	Material	Preparation	Solution	Density kg/m <sup>3</sup>	$T_{max}$ °C
LA2UC01	LA209BS1b	drilled	LOT	parcel	125
LA2UC02	LA209BS3b	drilled	LOT	parcel	115
LA2UC03	LA209BS5b	drilled	LOT	parcel	100
LA2UC04	LA209BS7b	drilled	LOT	parcel	95
LA2UC05	LA209BS9b	drilled	LOT	parcel	80
LA2UC06	LA209BS1b	drilled	LOT	parcel	125
LA2UC07	LA211BS1b	drilled	LOT	parcel	125
LA2UC08	LA211BS3b	drilled	LOT	parcel	115
LA2UC09	LA211BS5b	drilled	LOT	parcel	100
LA2UC10	LA211BS7b	drilled	LOT	parcel	95
LA2UC11	LA211BS9b	drilled	LOT	parcel	80
LA2UC12	LA211BS1b	drilled	LOT	parcel	125
LA2UC13	LA233BS1b	drilled	LOT	parcel	35
LA2UC14	LA233BS3b	drilled	LOT	parcel	25
LA2UC15	LA233BS5b	drilled	LOT	parcel	25
LA2UC16	LA233BS7b	drilled	LOT	parcel	25
LA2UC17	LA233BS9b	drilled	LOT	parcel	25
LA2UC18	LA233BS1b	drilled	LOT	parcel	35
LA2UC19	MX-80 LA2R	compacted	de-ionized	1,850	20
LA2UC20	MX-80 LA2R	compacted	LOT	1,850	20
LA2UC21	MX-80 LA2R	compacted	de-ionized	1,950	20
LA2UC22	MX-80 LA2R	compacted	LOT	1,950	20
LA2UC23	MX-80 LA2R	compacted	de-ionized	2,050	20
LA2UC24	MX-80 LA2R	compacted	LOT	2,050	20
LA2UC25	MX-80 LA2R	compacted	LOT	1,850	20
LA2UC26	MX-80 LA2R	compacted	LOT	1,850	20
LA2UC27	MX-80 LA2R	compacted	LOT	1,950	20
LA2UC28	MX-80 LA2R	compacted	LOT	1,950	20
LA2UC29	MX-80 LA2R	compacted	LOT	2,050	20
LA2UC30	MX-80 LA2R	compacted	LOT	2,050	20
LA2UC101	LA211BN5b	drilled	LOT	parcel	100
LA2UC102	LA233BSE5b	drilled	LOT	parcel	25
LA2UC103	LA211BN5b	drilled	LOT	parcel	100
LA2UC104	LA233BN5b	drilled	LOT	parcel	25
LA2UC105	LA211BN5b	drilled	LOT	parcel	100
LA2UC106	LA233BN5b	drilled	LOT	parcel	25
LA2UC231	LA211BSE1b	milled and re-compacted	LOT	1,970	125
LA2UC232	LA211BSE1b	milled and re-compacted	LOT	1,970	125
LA2UC233	LA211BSE1b	milled and re-compacted	LOT	1,970	125

Test Series II was performed in order to further investigate the influence of increased temperature (Table 8-4). The objectives of this series were to examine the stress-strain behaviour after short term exposure to:

- 20°C, 90°C, 120°C and 150°C after water saturation (LA2UC201-218).
- repeated change in temperature between 20°C and 120°C (LA2UC219-224).
- 120°C before water saturation (LA2UC234-236).
- high water pressure (LA2UC237-242).

The water pressure used for the study of the influence of high water pressure was at least twice as high as the water pressure used for the water saturation in the same series. The maximum water pressure used was 1,900 kPa.

Tests were also made to verify the influence of density (LA2UC225-230). MX-80 reference material R1 /Karlund et al. 2006/ was used in all tests. A laboratory oven was used for the short term temperature exposure.

**Table 8-4. Test Series II layout.**

Test ID	Material	Preparation	Solution	Density kg/m <sup>3</sup>	Temperature °C
LA2UC201	MX-80 R1	compacted	de-ionized	1,970	20
LA2UC202	MX-80 R1	compacted	de-ionized	1,970	20
LA2UC203	MX-80 R1	compacted	de-ionized	1,970	20
LA2UC204	MX-80 R1	compacted	de-ionized	1,970	120
LA2UC205	MX-80 R1	compacted	de-ionized	1,970	120
LA2UC206	MX-80 R1	compacted	de-ionized	1,970	120
LA2UC207	MX-80 R1	compacted	de-ionized	1,970	20
LA2UC208	MX-80 R1	compacted	de-ionized	1,970	20
LA2UC209	MX-80 R1	compacted	de-ionized	1,970	20
LA2UC210	MX-80 R1	compacted	de-ionized	1,970	150
LA2UC211	MX-80 R1	compacted	de-ionized	1,970	150
LA2UC212	MX-80 R1	compacted	de-ionized	1,970	150
LA2UC213	MX-80 R1	compacted	de-ionized	1,970	90
LA2UC214	MX-80 R1	compacted	de-ionized	1,970	90
LA2UC215	MX-80 R1	compacted	de-ionized	1,970	90
LA2UC216	MX-80 R1	compacted	de-ionized	1,970	120
LA2UC217	MX-80 R1	compacted	de-ionized	1,970	120
LA2UC218	MX-80 R1	compacted	de-ionized	1,970	120
LA2UC219	MX-80 R1	compacted	de-ionized	1,970	120
LA2UC220	MX-80 R1	compacted	de-ionized	1,970	120
LA2UC221	MX-80 R1	compacted	de-ionized	1,970	120
LA2UC222	MX-80 R1	compacted	de-ionized	1,970	120
LA2UC223	MX-80 R1	compacted	de-ionized	1,970	120
LA2UC224	MX-80 R1	compacted	de-ionized	1,970	120
LA2UC225	MX-80 R1	compacted	de-ionized	1,850	20
LA2UC226	MX-80 R1	compacted	de-ionized	1,950	20
LA2UC227	MX-80 R1	compacted	de-ionized	2,050	20
LA2UC228	MX-80 R1	compacted	de-ionized	1,850	20
LA2UC229	MX-80 R1	compacted	de-ionized	1,950	20
LA2UC230	MX-80 R1	compacted	de-ionized	2,050	20
LA2UC234	MX-80 R1	compacted	de-ionized	1,970	120
LA2UC235	MX-80 R1	compacted	de-ionized	1,970	120
LA2UC236	MX-80 R1	compacted	de-ionized	1,970	120
LA2UC237	MX-80 R1	compacted	de-ionized	1,970	20
LA2UC238	MX-80 R1	compacted	de-ionized	1,970	20
LA2UC239	MX-80 R1	compacted	de-ionized	1,970	20
LA2UC240	MX-80 R1	compacted	de-ionized	1,970	20
LA2UC241	MX-80 R1	compacted	de-ionized	1,970	20
LA2UC242	MX-80 R1	compacted	de-ionized	1,970	20

## 8.2.2 Equipment

The test specimens were saturated in two different special designed devices prior to the shear tests in order to ensure full saturation. In one of the devices the central part comprised of two symmetric pieces made of steel and this device was used for the samples LA2UC01-06, LA2UC19-30. The central part of the other device was made in one piece and made of PEEK and this device was used for LA2UC07-18, LA2UC101-106, LA2UC201-242. The shearing was made by a mechanical press and the sample set-up is shown in Figure 8-5. The deformation and the applied force were measured during the test by means of laboratory force and strain transducers. The transducers were controlled before and after every set of six sample measurements.

## 8.2.3 Test procedure

In test Series I (Table 8-3) cylindrical specimens were prepared from the parcel material by core drilling cylindrical samples with 20 mm in diameter which were cut to the height 20 mm. The non-parcel samples were prepared in a compaction device from air-dry MX-80 powder and then saturated. All samples in Series I were placed in a saturation device for at least 2 weeks, and the saturating solution was circulated over the filters on both sides, except for samples 231–234 which were saturated by a 20 cm water column.

In the Series II (Table 8-4) the specimens were prepared in a compaction device from air-dry MX-80 powder and then saturated. The heated samples were exposed to maximum temperature during 24 h in the saturation device. The increase and decrease in temperature were made in steps of 30°C and each temperature was kept for a minimum of 5 h, except in tests 222–224 where the repeated changes were made in one step. A water pressure was applied to all specimens during heating, and thereafter reduced to zero water pressure for 12 h before the dismantling. Finally, the samples were left to stress relaxation for 12 h after dismantling.

The load-applied sample surfaces were lubricated by use of vacuum grease, and the samples were placed in the mechanical press. The shearing was made at a constant rate of strain (0.16 mm/min). After failure the water to solid mass ratio was determined according to Section 6.1. The density was calculated from the mass of the samples and the volume of saturation device.

## 8.2.4 Data flow and evaluation

The samples were considered as undrained during shearing and no volume change was taken into account. The deviator stress was evaluated from Equation 8-1, and the strain from Equation 8-4.

The axial force and deformation versus time were stored together with the calculated stress, strain, water to solid mass ratio and density data in Excel files. The test series was termed LA2UC (UC for unconfined compression test) and individual specimens were denominated according to general scheme e.g. A211BS2b. In the result section this individual specimen is denoted x\_11\_2 which indicates test number\_block number\_distance in cm from the Cu-tube.

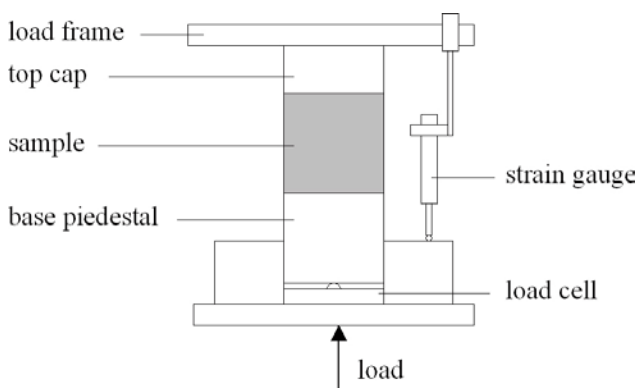


**Figure 8-5.** Schematic drawing of the set-up used for the unconfined compression tests. See also photos in Figure 8-12.

## 8.2.5 Results and discussion

Table 8-5 shows all results from test Series I, except the results from six samples (19, 21, 23, 25, 27 and 29) which are missing due to technical problems. From the reference samples (20, 22, 24, 26, 28, 30) the influence of density is clearly seen i.e. the higher density the higher maximum deviator stress ( $q_{max}$ ) and the smaller corresponding strain. Densities are calculated from measured mass of the sample and volume in the saturation device.

The test results from the parcel material are shown as deviator stress versus strain in Figure 8-6 to Figure 8-8. The colours refer to the temperature coupled to the position of the specimen in the LOT parcel and given in Section 4.3.2. From the warmest to the coldest the colours red, orange, yellow, green, blue and purple represent the average temperatures 125, 115, 100, 90, 40 and 20°C, respectively. The density of each specimen is shown to the right in each diagram.

**Table 8-5. Results from test Series I including all field exposed material. Maximum temperature, maximum deviator stress ( $q_{max}$ ), strain at  $q_{max}$  ( $\epsilon$ ), final water to solid mass ratio ( $w$ ), degree of saturation ( $S_r$ ) and bulk density ( $D_b$ ).**

Test ID	Label Number_block _distance	$D_b$ kg/m <sup>3</sup>	$w$ %	$S_r$ %	At shearing		Max $T$ °C
					$q_{max}$ kPa	$\epsilon$ %	
LA2UC01	1_09_1	1,980	29.4	101	1,562	3.5	125
LA2UC02	2_09_3	1,980	29.5	102	1,694	4.8	115
LA2UC03	3_09_5	1,950	29.9	99	1,736	4.3	100
LA2UC04	4_09_7	1,950	31.7	101	1,509	5.4	95
LA2UC05	5_09_9	1,960	32.5	104	1,327	7	80
LA2UC06	6_09_1	1,980	31.4	105	1,296	3	125
LA2UC07	7_11_1	1,960	29.8	100	1,818	5.1	125
LA2UC08	8_11_3	1,960	30.4	101	1,614	6.1	115
LA2UC09	9_11_5	1,950	30.6	100	1,658	6.5	100
LA2UC10	10_11_7	1,920	32.8	101	1,283	4.7	95
LA2UC11	11_11_9	1,900	34.8	101	1,002	7.5	80
LA2UC12	12_11_1	1,960	31.0	101	1,444	6.4	125
LA2UC13	13_33_1	1,930	31.8	100	1,378	10	35
LA2UC14	14_33_3	1,950	31.4	101	1,535	9.5	25
LA2UC15	15_33_5	1,930	31.8	100	1,405	9.3	25
LA2UC16	16_33_7	1,940	31.7	101	1,437	8.3	25
LA2UC17	17_33_9	1,930	32.5	100	1,298	8.1	25
LA2UC18	18_33_1	1,960	30.8	101	1,602	9.5	35
LA2UC20	20_LA2R	1,860	37.9	101	734	11.7	20
LA2UC22	22_LA2R	1,970	30.6	103	1,603	9.1	20
LA2UC24	24_LA2R	2,090	22.8	102	2,926	4.9	20
LA2UC26	26_LA2R	1,870	37.9	101	726	12.2	20
LA2UC28	28_LA2R	1,970	30.7	103	1,534	9.9	20
LA2UC30	30_LA2R	2,110	21.5	102	4,968	5.8	20
LA2UC101	101_11_5	1,950	31.1	101	1,649	4.1	100
LA2UC102	102_33_5	1,890	35.0	99	1,018	8.2	25
LA2UC103	103_11_5	1,970	30.0	101	2,074	5.1	100
LA2UC104	104_33_5	1,930	32.3	100	1,401	9.7	25
LA2UC105	105_11_5	1,970	30.3	102	1,954	5.2	100
LA2UC106	106_33_5	1,910	33.1	100	1,332	9.1	25
LA2UC231	231_11_1_dry	1,970	30.0	101	2,008	10	125
LA2UC232	232_11_1_dry	1,970	30.3	101	2,060	10	125
LA2UC233	233_11_1_dry	1,970	30.0	101	2,005	10	125

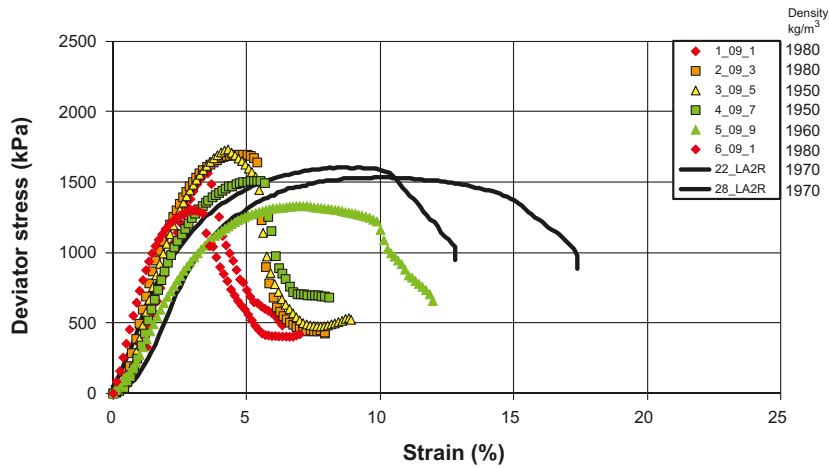


Figure 8-6. Test results from specimens from block 09. The labels denote the test number\_block\_distance from the canister. The two reference tests (22 and 28) are also shown.

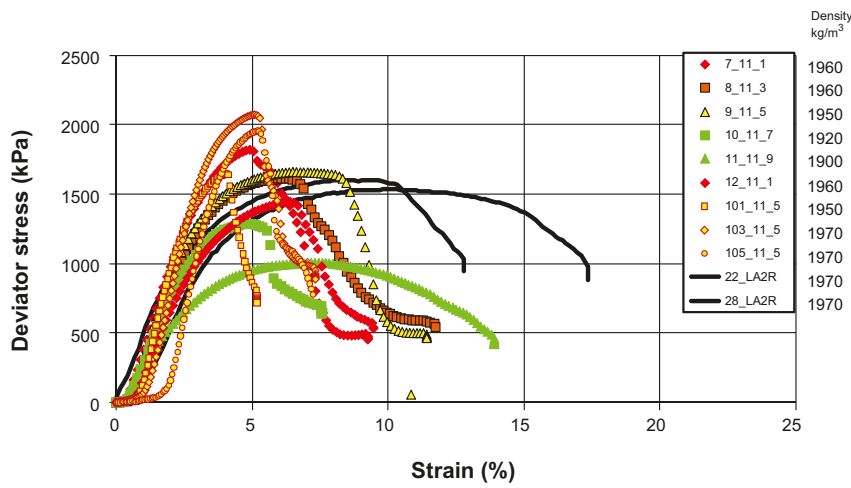


Figure 8-7. Test results from specimens from block 11. The labels denote the number of the test\_the\_block\_distance from the canister in cm. The two reference tests (22 and 28) are also shown.

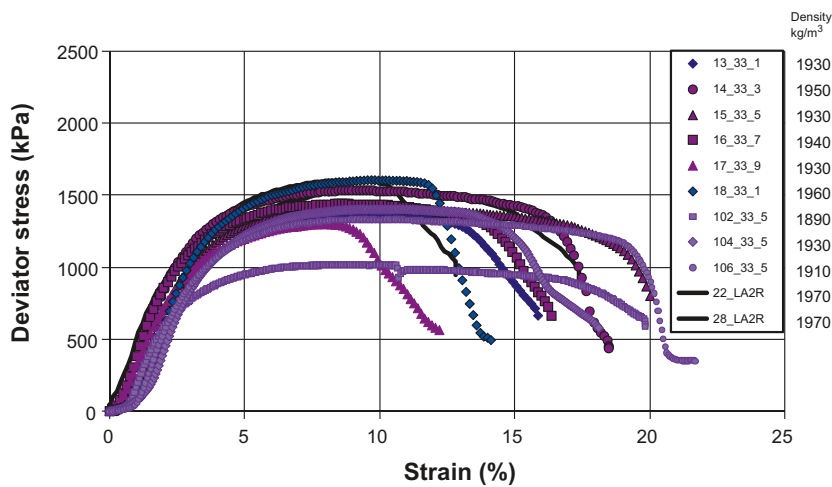
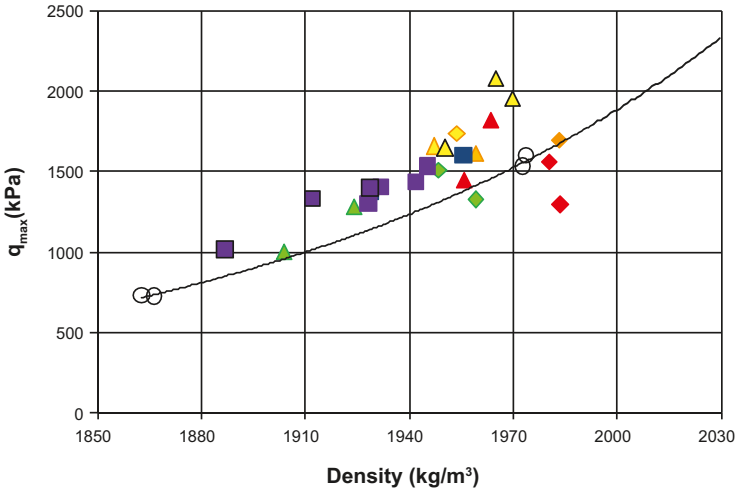


Figure 8-8. Test results from specimens from block 33. The labels denote the number of the test\_the\_block\_distance from the canister in cm. The two reference tests (22 and 28) are also shown.

The maximum deviator stress ( $q_{max}$ ) and the corresponding strain ( $\epsilon$ ) are plotted versus density in Figure 8-9 and Figure 8-10. A large scatter is noticed in maximum deviator stress ( $q_{max}$ ) for the material exposed to the highest temperatures (Figure 8-9). Notably is that the coarse of shearing is qualitatively different in these samples with a more pronounced failure (Figure 8-6 to Figure 8-7).

The results from the disturbed, i.e. air-dried, milled and re-compacted, specimens are shown in Figure 8-11. The maximum deviator stresses ( $q_{max}$ ) fall within the scatter of the undisturbed samples. However, the strain at maximum deviator stress is in the same range as for the reference samples, i.e. the pronounced failure observed in the undisturbed samples was restored to reference levels after milling and re-compacting.

The shape of the failure surfaces differed between the individual specimens. Some of the specimens taken from block 09 and 11 showed a nearly vertical failure surface, exemplified in Figure 8-12 (upper left). This shape was not seen on specimens taken in block 33 or in laboratory heat exposed samples. The failure surfaces shown in Figure 8-12 represent specimens from block 33 (upper right), dried and milled material from block 11 (lower left) and specimen exposed to high temperature in an oven in the laboratory (lower right).



**Figure 8-9.** Maximum deviator stress versus density for the drilled specimens in the test Series I. The colors refer to the exposed temperature in the LOT parcel from the warmest to the coldest (red, orange, yellow, green, blue and purple). Open circles are reference tests linked with a solid best fit line, diamonds indicate block no. 9, triangles block no. 11 and squares block no.33.

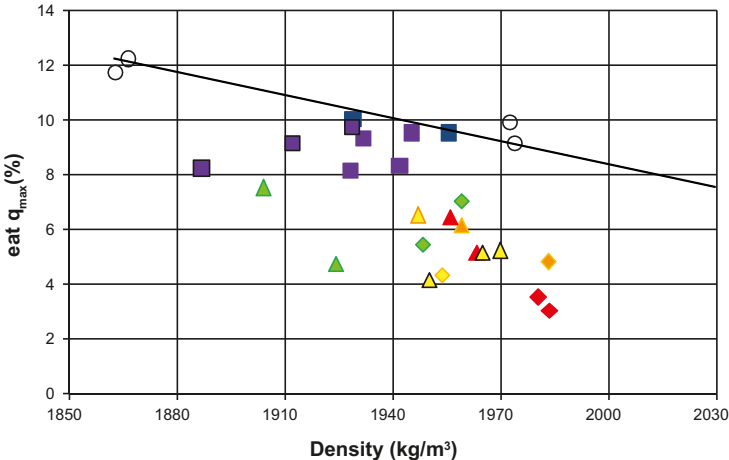


**Figure 8-10.** Strain at maximum deviator stress vs. density for the drilled specimens in the test Series I. The colors refer to the exposed temperature in the LOT parcel from the warmest to the coldest (red, orange, yellow, green, blue and purple). Open circles are reference tests linked with a best fit solid line, diamonds indicate block no. 9, triangles block no. 11 and squares block no.33.

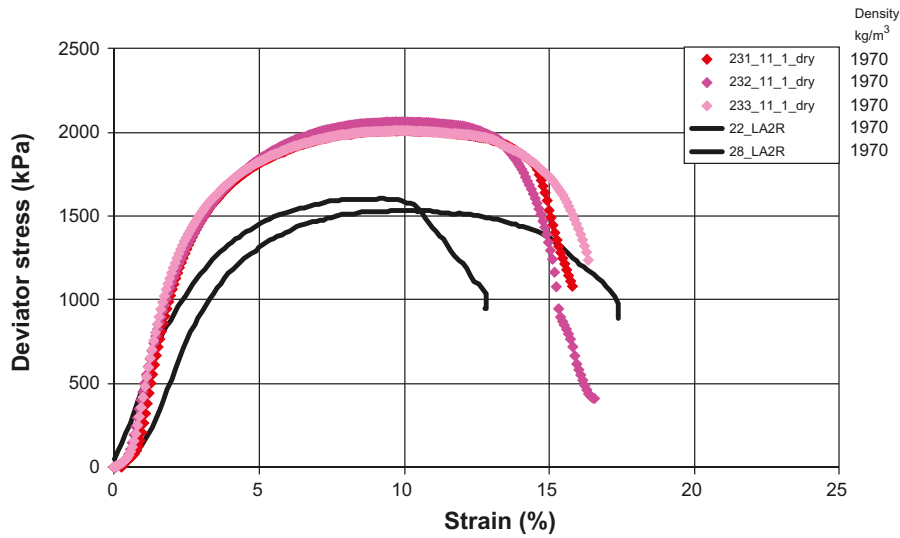


**Figure 8-11.** Test results from the disturbed, i.e. air dried, milled and re-compacted, samples taken from block 11. The labels denote the number of the test\_the block\_distance from the canister in cm. Two reference tests are also shown.



**Figure 8-12.** Photos of selected specimens after failure. The specimens represent block 09 position 1 cm (upper left), block 33 position 1 cm (upper right), air dried, milled and re-compacted material from block 11 position 1 cm (lower left) and compacted specimen exposed to 150°C in an oven in the laboratory (lower right).

Results from all tests in the test Series II are shown in Table 8-6. Densities ( $D_b$ ) are calculated from measured mass of the sample and volume in the saturation device.

The set-up used for the specimens 225–230 and 201–206 was found less rigid than during the other tests in the test Series II (Table 8-6). The stiffness of the different set-ups were measured and corrected for in the presented results from samples 225–230 and 201–206.

**Table 8-6. Results at shearing from the test Series II including the subsequent laboratory study. Maximum temperature, maximum deviator stress ( $q_{max}$ ) and corresponding strain ( $\epsilon$ ), final water to solid mass ratio ( $w$ ), degree of saturation ( $S_r$ ) and bulk density ( $D_b$ ). C denotes that the values are corrected for less stiffness in the set up.**

Test ID	$T_{max}$ °C	$D_b$ kg/cm <sup>3</sup>	$w$ %	$S_r$ %	$q_{max}$ kPa	$\epsilon$ %	Remark
LA2UC201	20	1,960	30.3	100	1,650	10.1	C
LA2UC202	20	1,970	31.1	103	1,600	10	C
LA2UC203	20	1,970	31.0	103	1,650	9.8	C
LA2UC204	120	1,960	30.8	102	1,970	7.5	C
LA2UC205	120	1,960	30.4	101	1,900	9	C
LA2UC206	120	1,960	31.2	102	1,910	8.6	C
LA2UC207	20	1,960	30.8	102	1,800	9.5	
LA2UC208	20	1,970	30.7	102	1,760	10	
LA2UC209	20	1,970	30.9	103	1,760	10	
LA2UC210	150	1,960	31.7	103	1,940	7	
LA2UC211	150	1,970	31.3	104	2,200	5.8	
LA2UC212	150	1,970	31.5	104	2,140	7	
LA2UC213	90	1,960	30.7	102	1,950	8.5	
LA2UC214	90	1,970	31.3	103	1,970	9	
LA2UC215	90	1,960	31.2	102	1,900	8	
LA2UC216	120	1,960	31.1	102	2,030	6.5	
LA2UC217	120	1,970	31.1	103	2,130	7	
LA2UC218	120	1,960	31.2	102	2,010	7.5	
LA2UC219	120	1,970	31.3	103	2,185	7.5	
LA2UC220	120	1,970	30.7	102	2,115	7.8	
LA2UC221	120	1,970	31.1	103	2,130	8	
LA2UC222	120	1,960	31.6	103	2,150	6.1	repeated
LA2UC223	120	1,960	30.8	101	2,240	7	change
LA2UC224	120	1,950	32.1	103	1,960	6.4	20°C/120°C
LA2UC225	20	1,860	38.5	101	750	10.3	C
LA2UC226	20	1,970	30.9	102	1,670	11.5	C
LA2UC227	20	2,060	24.8	103	3,110	10.5	C
LA2UC228	20	1,860	38.6	101	730	11	C
LA2UC229	20	1,960	30.9	101	1,690	11.6	C
LA2UC230	20	2,060	25.1	103	3,150	10.6	C
LA2UC234	120	1,970	30.1	101	1,770	8.5	dried at
LA2UC235	120	1,970	30.1	101	1,770	8.5	120°C then
LA2UC236	120	1,970	30.2	102	1,730	8.7	saturated
LA2UC237	20	1,970	30.7	102	1,883	8.8	
LA2UC238	20	1,970	30.7	102	1,807	8.3	
LA2UC239	20	1,970	30.8	102	1,880	9.3	
LA2UC240	20	1,970	30.4	102	1,835	11	high
LA2UC241	20	1,970	30.5	102	1,870	10.3	water
LA2UC242	20	1,970	30.3	101	1,913	8.9	pressure

Results from test Series II are shown in Figure 8-13 to Figure 8-17 where the labels denote *test number\_maximum temperature*. The influences of the following factors are illustrated:

- exposure to 20°C, 90°C, 120°C and 150°C (Figure 8-13 to Figure 8-14).
- repeated changes in temperature between 20°C and 120°C (Figure 8-15 left).
- exposure to 120°C before the water saturation (Figure 8-15 right).
- influence of high water pressure (Figure 8-16).
- influence of density (Figure 8-17).

Some selected results from test Series II are shown in Figure 8-13 to illustrate the influence also of a short term temperature pulse on the stress-strain behaviour. Significantly lower strain at maximum deviator stress ( $q_{max}$ ) and significant increase in maximum deviator stress ( $q_{max}$ ) with increasing temperature were measured.

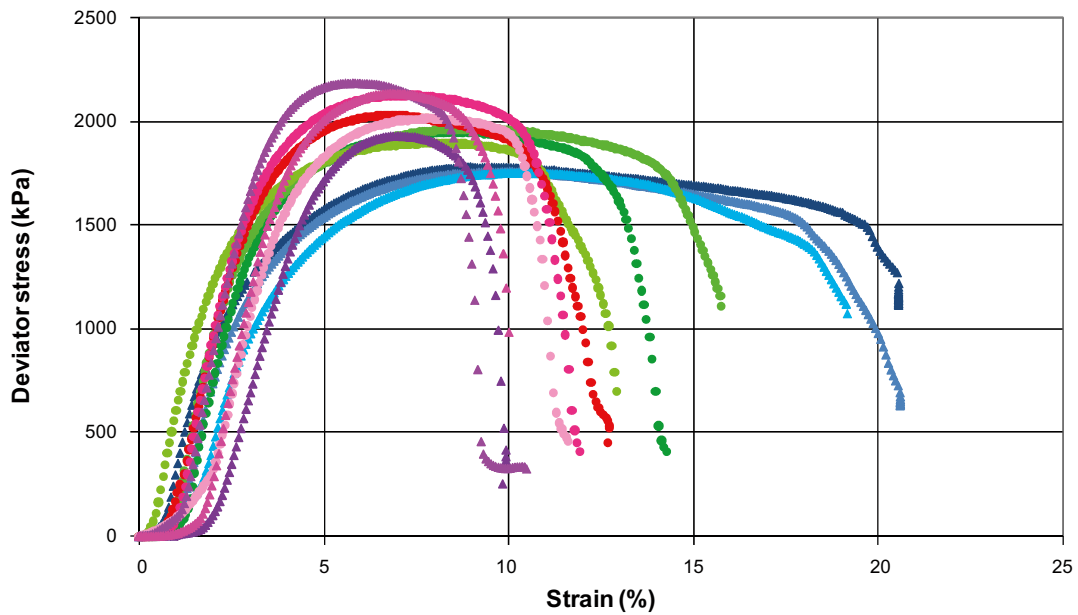


**Figure 8-13.** Selected results from the test Series II (samples 207 to 218). The colors (lilac, red, green, blue) denote the temperatures (150°C, 120°C, 90°C, 20°C).

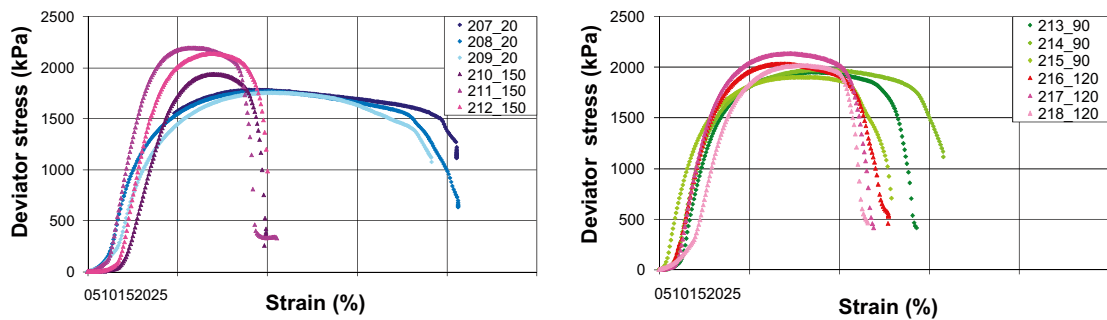


**Figure 8-14.** Illustration of influence of temperature. The colors (lilac, red, green, blue) denote the temperatures (150°C, 120°C, 90°C, 20°C). The labels show test number\_temperature.

Repeated changes of temperature seem to influence the stress-strain behaviour (Figure 8-15 left). Drying the specimens before the saturation (Figure 8-15 right) as well as the use of high water pressure (Figure 8-16) seem not to influence the stress-strain behaviour.

The results from the references material in Series II, presented in Figure 8-17, illustrate the density dependence of strain, maximum deviator stress, and the general shape of the curves. The decrease of strain at failure with increasing density is slightly different from what was found in Series I. This difference may be due to the different preparation techniques used between the two series, for example with respect to relaxation time. Insofar as the sample stress history may influence measured results, only those samples tested against identical protocols can be directly compared.

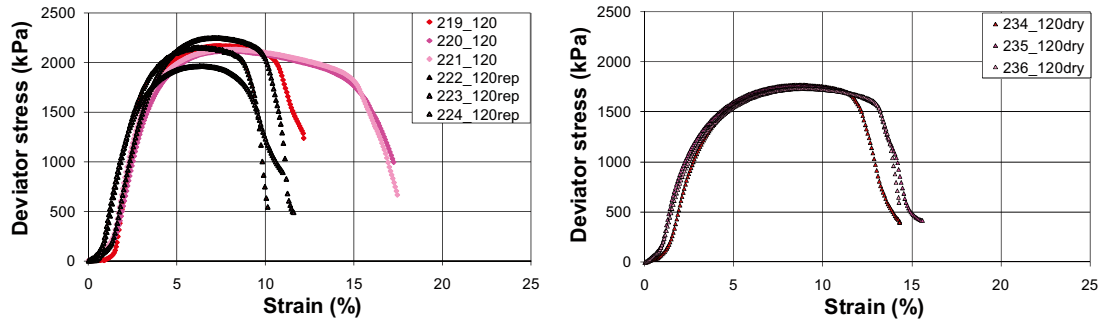


Figure 8-15. Illustration of influence of repeated changes (*rep*) of the temperature between 120°C/20°C (left) and drying before the water saturation (right). The labels show test number \_ temperature.

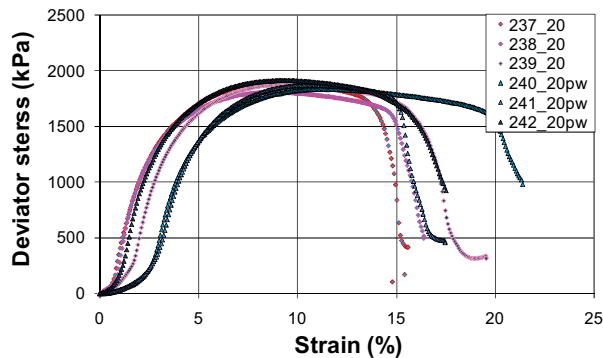


Figure 8-16. Illustration of the non-significant influence of high water pressure. The labels show test number \_ temperature, *pw* indicate high pore-water pressure.

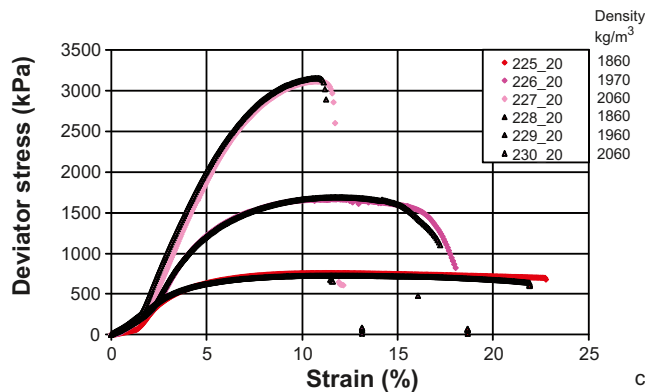


Figure 8-17. Illustration of influence of density (note the scale). The labels show test number \_ temperature.

### 8.2.6 Additional analyses

The procedure used for the specimens exposed to increased temperature in the laboratory was further analysed by a hydro-mechanical model. The modelling of hydro-mechanical processes in the test Series II was done in a similar way as reported by /Börgesson and Hernelind 1999/. The focus of the analysis was mainly to study the occurrence of excess pore water pressure in the specimens caused by the increase and decrease in temperature. It was found that enough time was given to avoid excess pore water pressure in the specimens. The calculation also showed that the 12 h elapsing from the removal of the applied pore water pressure to the dismantling of the specimens was enough to equalize the pore water pressure.

Twelve samples representing the temperatures 20, 90, 120 and 150°C from test Series II were analysed with respect to CEC, cation exchange capacity, according to Section 9.2.1, Cation exchange capacity (CEC) and exchangeable cations (EC). The results show values between 80 and 83 cmol<sup>+</sup>/kg clay, i.e. close to reference results (Table 9-4), and no significant trend with temperature was seen.

### 8.2.7 Conclusions

The major conclusions from the performed measurements may be summarized in the following items for the field exposed material;

- A significantly reduced strain at failure was measured in material from the warm sections.
- A qualitatively different course of shearing involving a more pronounced failure was noticed in the material from the warm sections.
- A nearly vertical failure surface was developed in several of the samples from the warm sections.
- The decrease in strain and pronounced failure in the material from the warm sections disappeared when the material was dried, milled and re-compacted.

and from the short term (24 h) laboratory tests;

- A clear correlation between lower strain at failure and increasing temperature was found. The measured strains at the highest temperatures were similar to those measured in the warmest field exposed material despite the very short exposure time.
- An increase in stress at failure with increasing temperature was measured.
- The above changes in stress-strain properties were not correlated to changes in cation exchange capacity.

## 9 Mineralogy and chemical composition

Siv Olsson, Ola Karnland, Martin Birgersson, Ulf Nilsson, Tania Hernan-Håkansson

### 9.1 Introduction

The chemical and mineralogical characteristics of bentonite from defined positions in the LOT A2 parcel have been compared with reference materials consisting of the specific batch of MX-80 that was used for fabrication of the individual blocks of the A2 parcel. The aim of the study has been to elucidate how the bentonite has altered after the medium term (~6 years) exposure to the adverse conditions of the A2 test, which means both higher temperature and steeper temperature gradient compared to KBS-3 conditions. Two test series of bentonite blocks from the A2 parcel, in the following referred to as standard blocks and special blocks, have been analyzed. The standard block series comprises two blocks from the hottest section and one block from the cool section of the parcel. The special block series comprises five blocks in which cylindrical bentonite plugs containing either calcite, gypsum, K-feldspar or cement have been embedded in order to simulate various adverse chemical conditions that might accelerate the alteration processes.

### 9.2 Standard blocks of the A2 parcel

#### 9.2.1 Materials and methods

##### *Sampling and sample nomenclature*

The standard block series comprises blocks 09 and 11 from the hot section and block 33 from the cool section of the parcel. The entire volume of blocks 09 and 11 has been exposed to temperatures >80°C, and the innermost 4 centimeters to temperatures exceeding 100°C. Block no. 33 was never exposed to temperatures exceeding 30°C, apart from the innermost centimeter. These blocks were sampled contiguously at five positions along the radius in the B-level (Figure 3-2). A 1–2 mm thick layer of the contact surfaces bentonite/Cu-tube and bentonite/bedrock were removed before the sampling which was made by use of a band saw. The contact bentonite/Cu-tube (radial position 0) was sampled separately in one of the hot blocks (no. 12) by scraping off a 1–2 mm thick layer from the bentonite surface with a knife of stain-less steel. Bentonite used for and stored since the fabrication of the blocks has been used as reference material.

The analytical test protocol for the standard blocks is summarized in Table 9-1, where individual samples have been given an identity code according to the general nomenclature, e.g. A209BW1b means that the sample is from the LOT **A2** parcel, block no. **09**, level **B** of the **W**estern sector of the block, radial position **1**. The **bulk** of the material has been analyzed (**c** is used if the material analyzed is the clay fraction). The identity code of the corresponding reference sample is A209Rb (or c for the clay fraction).

##### *Sample preparation*

Both the bulk material and the clay fraction of the bentonite samples have been analyzed when relevant (Table 9-1). The bulk material was not subject to any pre-treatments prior to the analyses, apart from drying at 60°C and grinding.

The clay-sized fraction (<2 µm) was separated by centrifuged sedimentation. In order to prepare a stable dispersion of the bentonite that allowed a separation of different size fractions, soluble salts were first dissolved by centrifuge-washing with water. After complete dispersion of the bentonite the suspension was left to rest for 10 minutes to allow sedimentation of the coarsest particles. The supernatant was thereafter collected in centrifuge bottles and centrifuged at 850 rounds/minute for 5 minutes. The centrifugation time and speed required for sedimentation of particles >2 µm was calculated by use of the integrated form of Stokes' Law.

After centrifugation the supernatants were collected in plastic containers and concentrated by evaporation at 60°C in a ventilated oven.

**Table 9-1. Sample nomenclature and analytical test protocol for the standard blocks 09, 11 and 33 of the LOT A2 parcel.**

SICADA test code b=bulk;c=clay fraction Sample identity	Chemical analysis	Cation exchange capacity	Exchangeable cations	X-ray diffraction analysis		Aqueous leaching
	LA2EA b/c	LA2CEC b/c	LA2EC b	LA2XRD b random	c oriented	LA2WA b
<b>Reference bentonite samples</b>						
A2(01-05)Rb	X	X	X	X		X
A2(01-05)Rc	X	X			X	
A211Rb	X	X	X	X		X
A211Rc	X	X			X	
A233Rb	X	X	X	X		X
A233Rc	X	X			X	
A224Rb	X	X	X	X		X
A224Rc		X			X	
A234Rb	X	X	X	X		X
A234Rc		X			X	
<b>Standard block series</b>						
A209BW1b	X	X	X	X		X
A209BW1c	X	X			X	
A209BW3b	X	X	X	X		X
A209BW3c	X	X			X	
A209BW5b	X	X	X	X		X
A209BW5c	X	X			X	
A209BW7b	X	X	X	X		X
A209BW7c	X	X			X	
A209BW9b	X	X	X	X		X
A209BW9c	X	X			X	
A211BW1b	X	X	X	X		X
A211BW1c	X	X			X	
A211BW3b	X	X	X	X		X
A211BW3c	X	X			X	
A211BW5b	X	X	X	X		X
A211BW5c	X	X			X	
A211BW7b	X	X	X	X		X
A211BW7c	X	X			X	
A211BW9b	X	X	X	X		X
A211BW9c	X	X			X	
A212(A-C)N0b	X	X	X	X		X
A212(A-C)N0c	X	X			X	
A233BW1b	X	X	X	X		X
A233BW1c	X	X			X	
A233BW3b	X	X	X	X		X
A233BW3c	X	X			X	
A233BW5b	X	X	X	X		X
A233BW5c	X	X			X	
A233BW7b	X	X	X	X		X
A233BW7c	X	X			X	
A233BW9b	X	X	X	X		X
A233BW9c	X	X			X	

### **Chemical analysis of the bentonite**

The chemical composition of the reference and the parcel bentonite was determined by ICP emission spectrometry (AES) and ICP mass spectrometry (MS) at an ISO 9001 certified laboratory (ACME Analytical Laboratories, Canada), using standard techniques for silicate analysis (fusion with LiBO<sub>2</sub> followed by nitric acid digestion). These analyses include major (Si, Al, Fe, Ca, Mg, K, Na, Mn, P, Ti), minor and trace elements (Ba, Co, Ce, Cr, Cu, Nb, Ni, Sc, Sr, Ta, Y, Zn, Zr). Loss on ignition (LOI) was determined as the difference in weight of the dried (105°C) and ignited (1,000°C) sample.

Total carbon and sulfur were determined by evolved gas analysis (EGA) at the same laboratory by combustion of the samples in a Leco furnace, equipped with IR-detectors for CO<sub>2</sub> and SO<sub>2</sub>. Carbonate carbon was determined as CO<sub>2</sub> evolved on treatment with hot 15% HCl.

Prior to the chemical analysis of the clay fractions, carbonates were removed by treatment with an acetic acid-sodium acetate buffer with pH 5 /e.g. Newman and Brown 1987/. The purified clay was thereafter converted to homo-ionic Na-clay by repeated washings with 1 M NaCl solution (analytical grade reagent). Excess salts were removed by repeated centrifuge-washing with water followed by dialysis (Spectrapore 3, 3500 MWCO dialysis membrane) against deionized water until the electrical conductivity of the external solution remained <10 µS/cm for five days. The purpose of saturating the exchange sites with one single cation is to make the allocation of cations to exchange and structural sites, respectively, less ambiguous.

All samples were ground, dried at 105°C and stored in desiccators prior to the analysis, i.e. all analytical results are expressed in wt% (major oxides) or ppm (trace elements) of the dry mass of the sample. The data have been stored in the SICADA database in a matrix in which concentration values are given for each parcel position using an identity code according to the general nomenclature.

### **Cation exchange capacity (CEC) and exchangeable cations (EC)**

The cation exchange capacity (CEC) of bulk materials and of clay fractions was determined by exchange with copper(II)triethylenetetramine following the procedure of /Meier and Kahr 1999/, modified according to /Ammann et al. 2005/ to ensure complete exchange. The ground sample (400 mg) was dispersed in 50 ml deionized water by ultrasonic treatment and shaking overnight. 20 ml of 15 mM Cu(II)-triethylenetetramine solution was added to the suspension, which was left to react for 30 minutes on a vibrating table. After centrifugation the absorbance at 620 nm of the supernatant was measured using a spectrophotometer (Shimadzu). CEC was calculated on the basis of the uptake of Cu by the clay and is expressed in centimole of charge per kilogram clay (cmol<sup>+</sup> kg<sup>-1</sup>), which is numerically equivalent to milliequivalents per 100 g (meq/100 g). The water to solid mass ratio of the clay was determined for a separate sample dried at 105°C to a constant weight. All CEC determinations were duplicated.

The exchangeable cations of the bulk bentonite were also extracted into alcoholic ammonium chloride solution (0,15 M NH<sub>4</sub>Cl in 80% ethanol) according to a procedure originally recommended for CEC determinations of gypsiferous/calcareous soils, /e.g. Belyayeva 1967, Jackson 1975/. An alcoholic solution is used to minimize dissolution of gypsum and calcite, which are soluble or relatively soluble in aqueous solutions. Ideally, i.e. when the content of easily soluble salts, such as chlorides and carbonates of alkali metals, is low, the sum of cations extracted should be equivalent to the CEC of the sample.

0.8 g of the ground sample was shaken for 30 minutes in approximately one third of a total volume of 50 ml of the extractant. After centrifugation the supernatant was collected in a volumetric flask. The treatment was repeated twice. The concentration of Ca, Mg, Cu, Na and K in the extracts was determined by use of an ICP-AES equipment at the Department of Ecology, Lund University. The concentration of exchangeable cations is expressed in centimole of charge per kilogram (cmol<sup>+</sup> kg<sup>-1</sup>). The water to solid mass ratio of the bentonite was determined for a separate sample.

The results have been delivered in Excel files from the laboratories involved and transferred to the SICADA database as a matrix in which calculated CEC values/exchangeable cation concentrations are given for each parcel position using an identity code according to the general scheme.

### **Aqueous leachates**

Aqueous leaching of the bulk samples was used to obtain information about the pore water composition and the spatial distribution of soluble/sparingly soluble salts within the blocks. The dried and ground bentonite was dispersed in deionized water (solid : solution ratio 1:100) by ultrasonic treatment for 30 minutes and stirring overnight. The suspension was left for 7 days at room temperature to allow equilibration. The supernatant was collected in centrifuge bottles and centrifuged at 3,000 rounds/minute for half an hour, and thereafter ultra-filtered through 0.8 and 0.2  $\mu\text{m}$  syringe filters (Acrodisc PF Syringe Filters) prior to analysis. Major cations were determined by ICP-AES and anions by use of ion chromatography (IC) at the Department of Ecology, Lund University.

The results have been delivered from the laboratory in Excel files in which concentration values are given for each parcel position. The code for the sample positions follows the general nomenclature.

### **X-ray diffraction analysis (XRD)**

The mineralogical composition was determined by X-ray diffraction analysis of two different types of preparations, one type consisting of unsorted and randomly oriented powders of the bulk materials, the other type consisting of aggregates with maximized preferred orientation of the clay minerals.

The random powder of the bulk sample produces “three-dimensional fingerprints” of all minerals and are needed for a general characterization of the materials. Also the distinction between di- and trioctahedral types of clay minerals by measurements of  $d(060)$  requires an X-ray diffraction profile of a randomly oriented sample.

The bulk material was ground in an agate mortar to a grain-size  $<10 \mu\text{m}$ . The montmorillonite of the parent bentonite is predominantly Na-saturated, giving a basal spacing around  $12.5 \text{ \AA}$  under normal laboratory conditions. In order to improve the resolution of the  $10 \text{ \AA}$  region to allow for a better detection of micaceous minerals, the samples were equilibrated in desiccators at a relative humidity of 75% (over saturated NaCl-solution) during a minimum of 5 days. X-ray scans were made as soon as possible after removal of the samples from the desiccators, but there was no RH control of the goniometer chamber during the scanning. The random powders were scanned with a step size of  $0.02^\circ 2\theta$  in the  $2\theta$  interval  $2-66^\circ$ .

The oriented specimen of the clay fraction gives strongly enhanced basal ( $00l$ ) reflections, and little or no evidence of the  $hk$  reflections of clay minerals. This type of preparation is useful for identification of the clay minerals and of interstratified structures and is also used for tests of the swelling properties of the clay after the clay has been solvated with a polyalcohol, such as ethylene glycol. However, the diffraction characteristics of smectites both in the air-dried and the ethylene glycol solvated state depend on the type of cation that is held in the exchange sites. Therefore, in order to give unambiguous diffraction characteristics, all clay samples were saturated with one single cation (Mg) prior to the X-ray scanning.

The clay fractions were deflocculated in deionized water, saturated with Mg ( $0.5 \text{ M MgCl}_2$ ) and thereafter washed free of excess salt by centrifuge-washing with water. Oriented aggregates were prepared of the clay slurry according to the “smear-on-glass” method /Moore and Reynolds 1989/ and dried at room temperature. The oriented mounts were X-ray scanned with a step size of  $0.02^\circ 2\theta$  in the  $2\theta$  interval  $2-36^\circ$ . In order to test the swelling properties the samples were re-scanned after solvation with ethylene glycol (EG) at  $60^\circ\text{C}$  for 48 hours.

A Seifert 3000 TT X-ray diffractometer with  $\text{CuK}\alpha$  radiation and automatic slits was used for the X-ray diffraction analyses.

The results have been stored in the SICADA database in Excel files in which the intensity values and the corresponding  $2\theta$  values are listed. No interpretation is given in the SICADA database. The code for the sample positions follows the general scheme.

## 9.2.2 Results

### Material color

A visual inspection of the bentonite revealed a difference in color between samples from different positions in the parcel. Powders of the bentonite located proximal to the Cu-tube (sample 0 and 1) in the hottest parts had a dull reddish grey color which contrasted with the light grey color of the powdered bentonite from other positions. The color was probably imparted when grinding the minute, brick red, soft “grains” which occurred only in the innermost two centimeters of the blocks (Figure 9-1). Efforts to characterize the soft “grains” by XRD-analysis of a concentrate picked by hand under a microscope were negative – the red “grains” appear to be X-ray amorphous.

### Aqueous leachates

The content of soluble sulfate and chloride determined by dispersion of the bentonite in water (s:l 1:100) are given in Table 9-2 together with the chloride and sulfate concentration in the groundwater at Äspö, sampled in 2006. The latter data have been extracted from Table 3-3. Focus has been laid on the major anions since the concentration of the cations is strongly affected by the exchange reactions that take place when divalent cations are released from dissolving minerals during the contact with water. Moreover, the source of some of the cations, such as Al, Fe and some Si and Mg, are most likely suspended ultra-fine clay particles which the filtering method failed to remove from the solution. Evidence for this is a strong correlation ( $R^2=0.98$ ) between Al and Fe and also the fact that the concentrations of these cations are at a minimum in samples with maximum sulfate concentrations, because dissolution of salts during the extraction promoted flocculation and sedimentation of clay particles.

The radial concentration profiles of chloride and sulfate, expressed as mg/g dry bentonite and as the molar concentration of the pore water, are presented in Figure 9-2. In the calculations of the molar concentration, the water-to-solid ratios of the samples given in Table 6-2 have been used. The pore water concentration of chloride is more or less constant in all three blocks but has increased compared with the chloride concentration of the reference bentonite. Thus, the groundwater must be the essential source of chloride (cf. Table 9-2). However, the pore water chloride concentration is still only half of that of the Äspö groundwater, which may be explained by mixing of original water in the bentonite with incoming groundwater, or alternatively by ion equilibrium theory /Birgersson and Karnland 2009/.



**Figure 9-1.** The section 0–3 cm of block 11 from the LOT A2 parcel. Note the brick-red “grains” occurring in the innermost 2 cm of the block. Fissures formed during storage.

**Table 9-2. Major anions (mg/g dry clay) extracted by dispersion of bentonite in deionised water in a solid:liquid ratio of 1:100. Data for blocks 09, 11 and 33 together with one contact sample and five reference samples for the LOT A2 parcel. Included is also the concentration of chloride and sulfate in Äspö groundwater sampled in October 2006 (complete data in Table 3-3)**

Sample id.	Cl <sup>-</sup>	CO <sub>3</sub> <sup>2-</sup> -C mg/g dry clay	S <sub>tot</sub>	SO <sub>4</sub> <sup>2-</sup> -S
A212(A-C)N0b	0.965	0.109	1.030	0.973
A209BS1b	1.070	0.100	1.599	1.430
A209BS3b	1.039	0.091	3.732	4.018
A209BS5b	1.068	0.104	2.222	2.164
A209BS7b	1.145	0.104	0.553	0.579
A209BS9b	1.284	0.095	0.631	0.509
A211BW1b	1.005	0.107	1.556	1.565
A211BW3b	1.031	0.123	3.320	2.876
A211BW5b	1.045	0.113	1.598	1.586
A211BW7b	1.248	0.111	0.430	0.529
A211BW9b	1.349	0.108	0.468	0.371
A233BW1b	1.303	0.090	1.336	1.300
A233BW3b	1.353	0.121	1.353	1.288
A233BW5b	1.282	0.108	1.241	1.235
A233BW7b	1.230	0.104	1.255	1.229
A233BW9b	1.351	0.083	1.209	1.213
A2(1-5)Rb	0.134	0.103	1.102	1.093
A211Rb	0.148	0.158	1.038	1.089
A224Rb	0.124	0.019	1.008	1.128
A233Rb	0.149	0.094	0.975	0.945
A234Rb	0.122	0.019	1.050	1.142
mM				
Äspö ground-water 2006	219			5.6

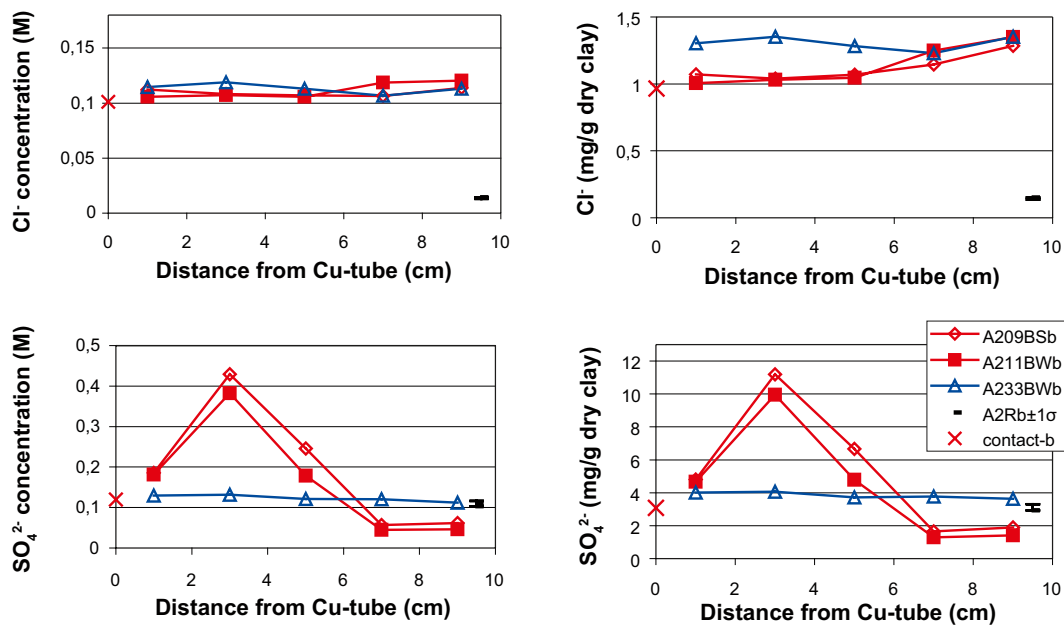


**Figure 9-2.** The radial distribution of Cl<sup>-</sup> and SO<sub>4</sub><sup>2-</sup> in water extracts of bulk samples from blocks 09, 11 and 33 of the LOT A2 parcel. The concentration of the reference samples (A2Rb) is shown at position 9.5 cm as the mean ±1 standard deviation of five samples.

The sulfate concentration of the pore water in all blocks is significantly higher than that of the Äspö groundwater (cf. Table 9-2 and Figure 9-2). Accordingly, the essential source must be the inventory of soluble sulfates initially present in the parent bentonite MX-80 as gypsum. The concentration in the cool block no. 33 is constant and more or less the same as that of the reference bentonite. In contrast, both hot blocks display an irregular distribution pattern with maxima 2–6 cm from the central heater and minima in the peripheral parts of the blocks, where the concentration is lower than that of the reference samples. Thus, it is evident that calcium sulfate has been redistributed along the thermal gradient in the blocks. The spatial distribution pattern is confirmed by other chemical data (Section 9.2.2, Bentonite composition) and by the XRD analysis (Section 9.2.2, Bentonite mineralogy), which shows that the re-precipitated calcium sulfate in the hot zone is anhydrite (CaSO<sub>4</sub>).

### **Exchangeable cations**

The data on the cations extracted by exchange with ammonium in alcoholic solutions are summarized in Table 9-3. The sum of cations is generally somewhat lower than the CEC of the sample (cf. Table 9-4) and varies quite randomly within the blocks. This fact probably reflects the problems inherent with the extraction method: the requirement of minimal dissolution of Ca sulfates and carbonates, the dissolution of which would inevitably lead to erroneous results for the exchangeable cations, may, on the other hand, lead to incomplete extraction.

The concentrations of the major exchangeable cations, K, Na, Mg and Ca, have been plotted against the distance from the Cu-tube in Figure 9-3.

Block 33 from the cool part of the parcel has essentially the same pool of exchangeable cations as the reference samples, i.e. almost 70% of the exchange sites are occupied by sodium, 22–23% by calcium and 7% by Mg. In contrast, sodium has been replaced by Ca and Mg in the hot blocks, where divalent cations constitute a gradually increasing proportion of the cation pool towards the heater. This is clearly demonstrated by the plot of the ratios Na/Ca and Na/Mg in Figure 9-4. It is also notable that the overall proportion of Mg has increased in the hot blocks, particularly in their hottest parts. As shown by the chemical analysis of the clay fraction (Section 9.2.2, Bentonite composition), the increase in exchangeable Mg is paralleled by increasing content of non-exchangeable Mg in the clay.

**Table 9-3 Exchangeable cations of the samples of blocks 03, 11 and 33 from the LOT A2 parcel. Included are also five reference samples and one sample (0) from the Cu-tube/bentonite contact. Cations extracted by exchange with NH<sub>4</sub><sup>+</sup> in alcoholic solution.**

Sample ID	Ca cmol*kg <sup>-1</sup>	Cu cmol*kg <sup>-1</sup>	K cmol*kg <sup>-1</sup>	Mg cmol*kg <sup>-1</sup>	Na cmol*kg <sup>-1</sup>	Sum cmol*kg <sup>-1</sup>
A209BW1b	17.2	0.2	1.1	8.5	45.6	73
A209BW3b	17.5	0.0	1.3	8.5	48.6	76
A209BW5b	17.4	0.0	1.4	8.2	51.5	79
A209BW7b	17.1	0.0	1.3	8.0	54.8	81
A209BW9b	15.8	0.0	1.2	7.5	51.7	76
A211BW1b	18.2	0.3	1.2	8.3	46.3	74
A211BW3b	17.6	0.0	1.2	7.6	47.6	74
A211BW5b	16.5	0.0	1.2	7.3	48.1	73
A211BW7b	15.8	0.0	1.2	7.0	51.3	75
A211BW9b	15.3	0.0	1.1	6.6	49.0	72
A212(A–C)N0b	18.5	1.4	1.1	9.7	47.4	78
A233BW1b	16.3	0.0	1.2	5.5	49.2	72
A233BW3b	17.6	0.0	1.3	5.3	52.8	77
A233BW5b	16.6	0.0	1.4	5.2	50.8	74
A233BW7b	16.4	0.0	1.2	5.1	49.1	72
A233BW9b	16.0	0.0	1.1	5.0	50.4	73
A2(5–1)Rb	16.5	0.0	1.2	4.4	49.9	72
A211Rb	15.9	0.0	1.2	4.7	49.7	72
A224Rb	16.8	n.d.	1.3	6.1	56.6	81
A233Rb	16.2	0.0	1.3	4.9	50.5	73
A234Rb	17.1	n.d.	1.3	6.5	56.3	81

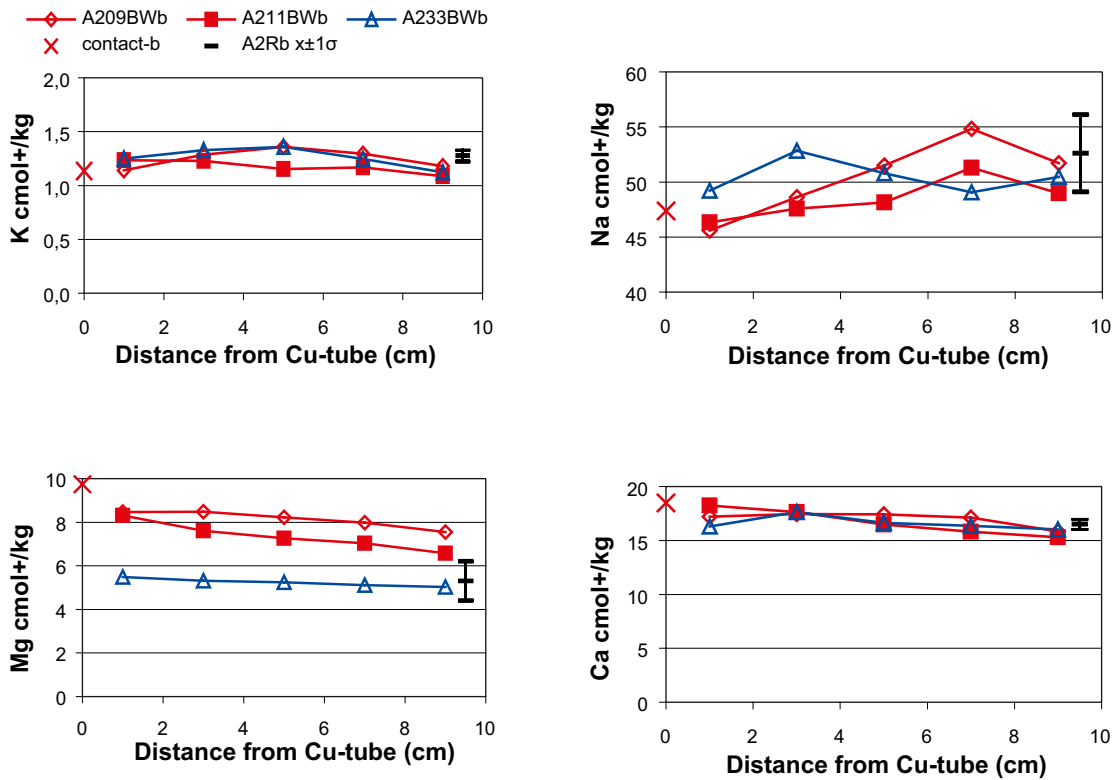


Figure 9-3. Plots of exchangeable K, Na, Mg and Ca, respectively, versus the distance from the Cu-tube for blocks 09, 11 and 33 of the LOT A2 parcel. Values of the reference samples (A2Rb) are shown at position 9.5 cm as the mean  $\pm 1$  standard deviation of five samples.

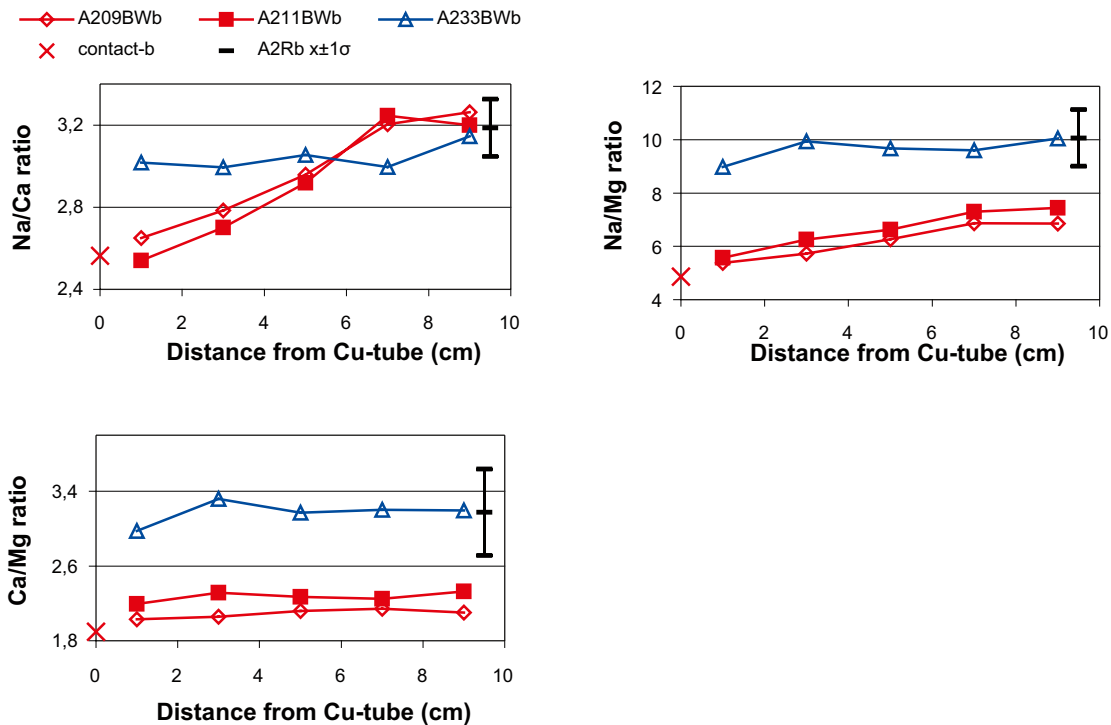


Figure 9-4. Plot of the ratios of exchangeable Na/Ca, Na/Mg, and Ca/Mg, respectively, versus the distance from the Cu-tube. Samples of blocks 09, 11 and 33 of the LOT A2 parcel. Values for the reference samples (A2R) are shown at position 9.5 cm as the mean  $\pm 1$  standard deviation of five samples.

Cu concentrations in excess of the analytical detection limit were found only in extracts of the innermost samples (samples no. 0 and 1) of the hot blocks (cf. Table 9-3). The extractable amount is, however, generally less than 1% of the total exchangeable cation pool and make up 9% at most of the maximum available amount of Cu (4,951 ppm Cu in the contact surface of block 12 is equivalent to 16 cmol<sup>+</sup>kg<sup>-1</sup>, but the extracted amount is less than 1.5 cmol<sup>+</sup>kg<sup>-1</sup>). This fact suggests that Cu has been incorporated in the bentonite matrix mainly in a form that is not readily soluble or accessible for cation exchange.

### **Cation exchange capacity**

The data on the cation exchange capacity (Cu-CEC) of bulk samples and of clay fractions are compiled in Table 9-4.

The mean CEC value of five LOT A2 reference bentonites, 81 cmol<sup>+</sup>kg<sup>-1</sup> (std. dev. 0.64) matches the Cu-CEC value previously reported for the bentonite MX-80, that was used for the LOT parcels /Karnland et al. 2000/. The samples from the cool part of parcel A2, block 33, have essentially the same CEC (mean CEC 80 cmol<sup>+</sup>kg<sup>-1</sup>, std. dev. 0.34) as the reference samples, whereas CEC values of the samples from the two hot blocks are more variable and have higher means (mean CEC 82 cmol<sup>+</sup>kg<sup>-1</sup>, std. dev. 0.96 for block 09; mean CEC 83 cmol<sup>+</sup>kg<sup>-1</sup>, std. dev. 0.94 for block 11).

**Table 9-4. Cation exchange capacity (CEC) in cmol<sup>+</sup>kg<sup>-1</sup> of bulk samples (left) and of clay fractions (right) from blocks 09, 11 and 33 together with one sample of the contact surface (sample 0) and five reference samples for the LOT A2 parcel. CEC determined by exchange with the Cu-triethylene tetramine complex.**

Bulk sample				Clay fraction <2 μm			
Sample id.	CEC <sub>1</sub>	CEC <sub>2</sub>	CEC <sub>mean</sub>	Sample id.	CEC <sub>1</sub>	CEC <sub>2</sub>	CEC <sub>mean</sub>
A209BW1b	84	83	84	A209BS1c	92	90	91
A209BW3b	81	82	82	A209BS3c	88	90	89
A209BW5b	81	82	81	A209BS5c	89	88	88
A209BW7b	82	82	82	A209BS7c	89	87	88
A209BW9b	81	81	81	A209BS9c	89	88	89
block mean ± 1σ			82±0.96				89±1.14
A211BW1b	84	84	84	A211BW1c	94	93	94
A211BW3b	83	84	83	A211BW3c	89	89	89
A211BW5b	83	82	83	A211BW5c	88	89	89
A211BW7b	82	82	82	A211BW7c	89	90	89
A211BW9b	82	82	82	A211BW9c	88	86	87
block mean ± 1σ			83±0.94				90±2.45
A212(A-C)N0b	85	84	85	A212(A-C)N0c	94	94	94
A233BW1b	80	80	80	A233BW1c	86	87	86
A233BW3b	80	80	80	A233BW3c	86	86	86
A233BW5b	80	81	81	A233BW5c	85	86	86
A233BW7b	79	80	80	A233BW7c	85	86	85
A233BW9b	79	81	80	A233BW9c	85	85	85
block mean ± 1σ			80±0.34				86±0.55
A2(1-5)Rb	80	81	81	A2R(1-5)c	87	86	87
A211Rb	81	80	80	A211Rc	86	87	87
A224Rb	82	81	81	A233Rc	87	86	87
A233Rb	80	79	80	A224Rc	88	88	88
A2R34b	81	81	81	A234Rc	88	87	88
reference mean ± 1σ			81±0.64				87±0.68

These rather subtle differences in CEC may simply reflect the range of variation in CEC measurements of fairly inhomogeneous materials like bentonites. Moreover, differential mineral dissolution/precipitation along the thermal gradient has increased the inhomogeneity of the hot blocks.

It is notable, however, that the CEC of both bulk samples and of clay fractions of the hot blocks display a tendency to increase in the two innermost samples (1 and 0), as shown by the plot of CEC against the radial distance in Figure 9-5. Interestingly enough, these samples are distinguished also by higher contents of non-exchangeable Mg in the clay (cf. Table 9-5 and Table 9-6; and Section 9.2.2, Bentonite composition) and higher Mg-concentrations in the pore water. The possibility of an interconnection between these parameters will be further studied.

### Bentonite composition

The chemical composition of the bentonite samples is given in Table 9-5 (bulk samples) and Table 9-6 (clay fractions).

Initial air and sulfides in the bentonite are potential causes of copper corrosion and of subsequent Cu uptake into the bentonite. The radial Cu-distribution within the blocks (Figure 9-6) clearly shows that copper has been incorporated into the bentonite matrix proximal to the Cu-tube at all temperatures, although the content in the hot blocks is 10 to 20 times higher than that of the cool block. The increase in Cu is seen only in the innermost samples, i.e. sample 0 and 1, (sample 1 with a 1-2 mm thick layer of the contact surface removed). All samples beyond 2 cm from the Cu tube have concentrations similar to those of the references. A small increase in Cu, which is paralleled by an increase in Ni in the peripheral sample of block 33 (cf. Table 9-5) suggests that the Cu in this case emanates from the thermocouple tubing of Cu-Ni alloy that were aligned on the outer surface of the blocks during the field exposure.

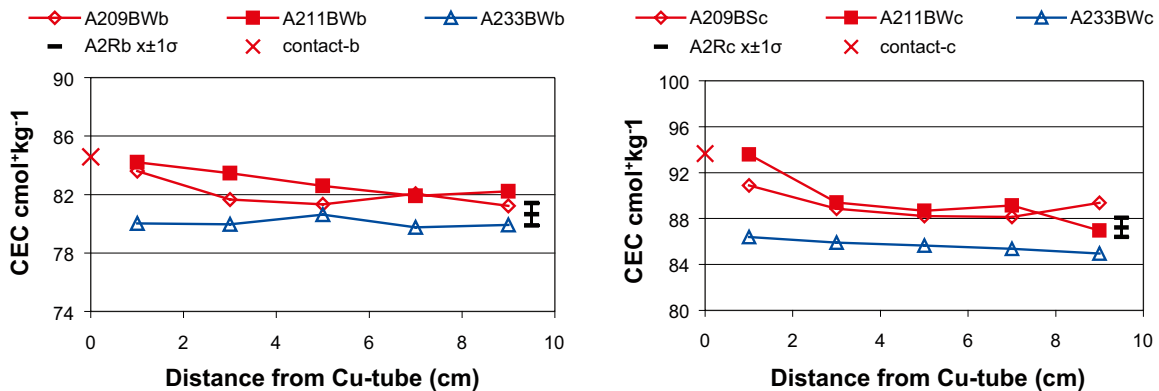


Figure 9-5. Plot of the CEC of bulk samples (left) and of clay fractions (right) versus radial distance for blocks 09, 11 and 33 of the LOT A2 parcel. Values for the reference samples (A2R) are shown at position 9.5 cm as the mean  $\pm 1$  standard deviation of five samples.

**Table 9-5. Chemical composition of the bulk bentonite samples of blocks 09, 11 and 33 together with one sample of the contact surface (sample 0) and five reference samples of the LOT A2 parcel. Major elements by ICP-AES, trace elements by ICP-MS except for samples A224Rb and A234Rb (different detection limits for AES and MS), S and C by evolved gas analysis. n.d.=not determined.**

Sample id.	SiO <sub>2</sub> %	Al <sub>2</sub> O <sub>3</sub> %	Fe <sub>2</sub> O <sub>3</sub> %	MgO %	CaO %	Na <sub>2</sub> O %	K <sub>2</sub> O %	TiO <sub>2</sub> %	P <sub>2</sub> O <sub>5</sub> %	MnO %	Cr <sub>2</sub> O <sub>3</sub> %	LOI %	TOT/C %	CO <sub>2</sub> -C %	TOT/S %	SUM %	Ni ppm	Sc ppm	Cu ppm	Zn ppm	Ba ppm	Co ppm	Nb ppm	Sr ppm	Ta ppm	Zr ppm	Y ppm	Ce ppm
A209BW1b	62.48	19.00	3.68	2.47	1.12	1.99	0.51	0.14	0.05	0.01	0.003	8.1	0.28	0.068	0.27	99.94	5	5	2325	88	257	5	29	234	5	177	44	102
A209BW3b	63.01	18.96	3.60	2.20	1.55	2.07	0.53	0.14	0.05	0.01	0.001	7.8	0.29	0.085	0.48	100.06	5	5	5	112	356	5	29	313	7	171	44	108
A209BW3b-2	62.91	19.03	3.66	2.26	1.44	2.06	0.53	0.14	0.05	0.01	0.001	7.7	0.33	n.d.	0.43	99.94	5	5	5	99	411	5	32	303	7	176	46	104
A209BW5b	63.01	18.86	3.74	2.34	1.59	2.07	0.55	0.15	0.05	0.01	0.005	7.7	0.35	0.155	0.43	100.07	5	5	5	93	261	1.2	27	325	3	177	46	123
A209BW7b	63.21	19.18	3.71	2.27	1.47	2.07	0.53	0.15	0.05	0.02	0.002	7.4	0.37	0.142	0.27	100.06	5	5	5	78	465	1	28	344	3	182	46	127
A209BW9b	63.51	19.06	3.78	2.25	1.22	2.12	0.54	0.15	0.05	0.01	0.004	7.4	0.35	0.153	0.16	100.09	9	5	8	96	279	1	28	273	3	197	48	130
Sample mean	63.02	19.02	3.70	2.30	1.40	2.06	0.53	0.15	0.05	0.01	0.003	7.68	0.33	0.121	0.34	100.03	5.7	5	392	94	338	3	29	299	5	180	46	116
A211BW1b	62.96	18.91	3.70	2.55	1.11	2.03	0.50	0.15	0.05	0.01	0.001	7.9	0.27	0.057	0.24	99.87	5	5	1600	72	196	0.9	28	237	3	187	47	128
A211BW3b	62.93	18.97	3.75	2.39	1.38	2.04	0.52	0.15	0.05	0.01	0.003	7.9	0.29	0.085	0.35	100.09	5	5	6	91	258	0.8	27	274	3	198	45	124
A211BW5b	63.50	18.77	3.77	2.25	1.30	2.04	0.51	0.14	0.05	0.02	0.001	7.7	0.38	0.136	0.22	100.05	5	5	4	94	589	1	27	330	3	185	47	124
A211BW7b	63.59	18.88	3.75	2.29	1.25	2.11	0.51	0.14	0.05	0.01	0.011	7.5	0.35	0.139	0.14	100.1	5	6	4	68	174	1	28	229	3	197	47	125
A211BW9b	62.84	19.09	3.66	2.24	1.32	2.12	0.50	0.15	0.06	0.01	0.001	8.1	0.39	0.139	0.16	100.09	5	5	11	68	204	1	28	271	3	183	50	131
Sample mean	63.16	18.92	3.73	2.34	1.27	2.07	0.51	0.15	0.05	0.01	0.003	7.82	0.34	0.111	0.22	100.04	5.0	5.2	325	79	284	0.94	28	268	3.2	190	47	126
A212(A-C)N0b	62.51	18.84	3.64	2.65	1.05	2.03	0.50	0.14	0.05	0.01	0.003	8.0	0.31	0.063	0.2	99.43	5	5	4951	52	188	0.8	28	238	3	189	47	126
A233BW1b	63.38	19.11	3.82	2.36	1.40	2.15	0.52	0.15	0.06	0.01	0.001	7.1	0.37	n.d.	0.33	100.06	5	5	149	82	295	0.9	28	291	3	184	47	129
A233BW3b	62.94	19.44	3.83	2.41	1.39	2.12	0.54	0.15	0.05	0.01	0.005	7.2	0.37	n.d.	0.27	100.09	6	5	4	85	373	1.6	28	298	3	197	46	130
A233BW5b	63.90	18.86	3.80	2.32	1.34	2.12	0.52	0.15	0.05	0.01	0.009	7.0	0.36	n.d.	0.29	100.08	7	5	4	91	323	1.1	28	301	3	188	48	133
A233BW7b	63.61	18.81	3.84	2.35	1.35	2.08	0.53	0.15	0.05	0.01	0.001	7.3	0.37	n.d.	0.26	100.08	5	5	4	96	283	1	28	291	3	185	46	129
A233BW9b	62.99	19.10	3.68	2.31	1.33	2.14	0.50	0.15	0.05	0.01	0.006	7.8	0.37	n.d.	0.29	100.07	63	5	162	88	273	0.9	27	273	3	192	45	126
Sample mean	63.36	19.06	3.79	2.35	1.36	2.12	0.52	0.15	0.05	0.01	0.004	7.28	0.37	n.d.	0.29	100.08	17	5	65	88	309	1.10	28	291	3.26	189	46	129
A2(1-5)Rb	63.46	19.03	3.81	2.38	1.35	2.08	0.55	0.15	0.06	0.01	0.005	7.2	0.38	0.145	0.26	100.08	7	5	4	76	442	1	28	289	3	206	46	130
A211Rb	62.84	19.01	3.70	2.30	1.27	2.06	0.51	0.14	0.05	0.01	0.002	8.2	0.36	0.131	0.26	100.1	5	5	4	69	240	0.9	27	270	3	185	47	129
A224Rb	63.42	19.68	3.70	2.39	1.17	2.14	0.51	0.14	0.05	0.01	0.001	6.6	0.37	0.145	0.13	99.93	<5	6	<10	74	258	<5	32	275	<20	192	45	94
A233Rb	63.65	19.13	3.74	2.35	1.30	2.09	0.53	0.15	0.05	0.01	0.001	7.1	0.34	0.134	0.28	100.1	5	5	4	82	257	0.9	29	276	3	200	47	135
A234Rb	64.12	19.28	3.64	2.33	1.21	2.09	0.53	0.14	0.04	0.01	0.002	6.4	0.37	0.145	0.14	99.93	<5	5	<10	103	395	<5	33	287	<20	187	44	90
Reference mean	63.50	19.23	3.72	2.35	1.26	2.09	0.53	0.14	0.05	0.01	0.002	7.10	0.36	0.140	0.21	100.03		5.2		81	318		30	279		194	46	115

**Table 9-6. Chemical composition of the Na-saturated clay fractions of samples from blocks 09, 11 and 33 together with one sample of the contact surface Cu-tube/bentonite (sample 0) and three reference samples of the LOT A2 parcel. Analyses by ICP-AES.**

Sample id.	SiO <sub>2</sub> %	Al <sub>2</sub> O <sub>3</sub> %	Fe <sub>2</sub> O <sub>3</sub> %	MgO %	CaO %	Na <sub>2</sub> O %	K <sub>2</sub> O %	TiO <sub>2</sub> %	P <sub>2</sub> O <sub>5</sub> %	MnO %	Cr <sub>2</sub> O <sub>3</sub> %	LOI %	TOT/C %	TOT/S %	SUM %	Ba ppm	Cu ppm	Zn ppm	Ni ppm	Co ppm	Sr ppm	Zr ppm	Ce ppm	Y ppm	Nb ppm	Sc ppm	Ta ppm
A209BS1c	63.20	21.25	3.81	2.63	0.06	2.33	0.07	0.13	0.03	0.01	0.001	6.3	0.24	0.01	99.94	11	642	89	5	5	13	149	83	35	32	6	5
A209BS3c	64.05	20.32	3.83	2.44	0.06	2.31	0.12	0.13	0.03	0.01	0.002	6.7	0.27	0.01	100.06	35	27	57	10	25	18	151	104	38	36	6	9
A209BS5c	63.68	20.64	3.86	2.42	0.04	2.30	0.10	0.13	0.03	0.01	0.001	6.8	0.36	0.01	100.07	32	24	39	8	5	17	151	91	37	29	6	5
A209BS7c	64.19	20.39	3.82	2.34	0.12	2.20	0.13	0.14	0.03	0.01	0.001	6.5	0.25	0.01	99.93	37	24	56	5	5	18	155	99	40	32	6	7
A209BS9c	63.86	20.40	3.85	2.40	0.10	2.24	0.08	0.13	0.03	0.01	0.001	6.9	0.27	0.01	100.05	19	25	42	5	6	17	150	88	34	34	6	5
<i>Sample mean</i>	<i>63.80</i>	<i>20.60</i>	<i>3.83</i>	<i>2.45</i>	<i>0.08</i>	<i>2.28</i>	<i>0.10</i>	<i>0.13</i>	<i>0.03</i>	<i>0.01</i>	<i>0.00</i>	<i>6.64</i>	<i>0.28</i>	<i>0.01</i>	<i>100.01</i>	<i>27</i>	<i>148</i>	<i>57</i>	<i>7</i>	<i>9</i>	<i>17</i>	<i>151</i>	<i>93</i>	<i>37</i>	<i>33</i>	<i>6</i>	<i>6</i>
A211BW1c	63.28	21.19	3.81	2.58	0.03	2.21	0.07	0.12	0.02	0.01	0.001	6.5	0.19	0.01	99.93	18	479	77	5	5	12	148	79	35	34	6	8
A211BW3c	64.27	20.17	3.54	2.37	0.05	2.33	0.09	0.12	0.02	0.01	0.002	6.9	0.26	0.01	99.93	26	5	52	5	8	18	156	135	37	33	6	5
A211BW5c	64.50	20.20	3.59	2.28	0.04	2.32	0.10	0.13	0.02	0.01	0.001	6.7	0.27	0.01	99.94	52	5	37	5	8	19	156	114	37	37	5	5
A211BW7c	65.17	19.98	3.51	2.22	0.04	2.28	0.11	0.13	0.02	0.01	0.002	6.4	0.27	0.01	99.93	30	17	36	22	5	16	157	124	38	39	6	5
A211BW9c	64.94	20.09	3.64	2.26	0.14	2.24	0.11	0.13	0.01	0.01	0.001	6.3	0.27	0.01	99.93	26	44	54	43	5	18	157	111	38	36	6	5
<i>Sample mean</i>	<i>64.43</i>	<i>20.33</i>	<i>3.62</i>	<i>2.34</i>	<i>0.06</i>	<i>2.28</i>	<i>0.10</i>	<i>0.13</i>	<i>0.02</i>	<i>0.01</i>	<i>0.00156.56</i>	<i>6.3</i>	<i>0.25</i>	<i>0.01</i>	<i>99.93</i>	<i>30</i>	<i>110</i>	<i>51</i>	<i>16</i>	<i>6</i>	<i>17</i>	<i>155</i>	<i>113</i>	<i>37</i>	<i>36</i>	<i>6</i>	<i>6</i>
A212(A-C)N0c	63.00	21.29	3.82	2.71	0.04	2.38	0.07	0.13	0.02	0.01	0.001	6.3	0.37	0.01	99.93	12	932	67	5	5	15	148	95	37	33	6	5
A233BS1c	63.96	20.53	3.70	2.37	0.06	2.25	0.13	0.13	0.04	0.01	0.001	6.8	0.30	0.01	100.06	40	241	38	5	5	19	155	100	40	34	6	10
A233BS3c	64.00	20.73	3.73	2.41	0.06	2.27	0.14	0.13	0.03	0.01	0.001	6.5	0.26	0.01	100.07	39	15	38	5	6	19	153	92	41	32	6	5
A233BS5c	64.22	20.40	3.75	2.39	0.09	2.33	0.15	0.14	0.03	0.01	0.001	6.5	0.26	0.01	100.07	46	42	44	5	5	21	155	100	40	27	6	5
A233BS7c	64.27	20.44	3.70	2.37	0.06	2.26	0.13	0.13	0.03	0.01	0.001	6.6	0.26	0.01	100.06	39	40	37	5	7	19	152	91	39	36	6	5
A233BS9c	63.71	20.25	3.71	2.41	0.12	2.12	0.12	0.13	0.03	0.01	0.001	7.4	0.29	0.01	100.07	34	28	53	5	5	18	153	96	38	28	6	5
<i>Sample mean</i>	<i>64.03</i>	<i>20.47</i>	<i>3.718</i>	<i>2.39</i>	<i>0.078</i>	<i>2.246</i>	<i>0.134</i>	<i>0.132</i>	<i>0.032</i>	<i>0.01</i>	<i>0.001</i>	<i>6.76</i>	<i>0.274</i>	<i>0.01</i>	<i>100.06640</i>	<i>73</i>	<i>42</i>	<i>5</i>	<i>6</i>	<i>19</i>	<i>154</i>	<i>96</i>	<i>40</i>	<i>31</i>	<i>6</i>	<i>6</i>	
A2(1-5)Rc	64.06	21.06	3.56	2.36	0.03	2.18	0.08	0.12	0.03	0.01	0.001	6.4	0.39	0.01	99.93	14	11	27	5	5	13	146	91	35	32	6	5
A211Rc	64.17	20.85	3.62	2.34	0.04	2.21	0.11	0.13	0.03	0.01	0.001	6.5	0.27	0.01	100.06	29	39	32	5	5	15	151	110	38	34	6	6
A233Rc	63.78	21.40	3.67	2.34	0.04	2.21	0.10	0.13	0.03	0.01	0.001	6.3	0.28	0.01	100.07	36	38	35	5	5	13	153	105	38	30	6	5
A233Rc-2	63.88	21.23	3.64	2.35	0.04	2.26	0.11	0.13	0.03	0.01	0.001	6.2	0.27	0.01	99.93	37	41	34	5	5	13	154	89	39	33	6	5
<i>Reference mean</i>	<i>63.97</i>	<i>21.14</i>	<i>3.62</i>	<i>2.35</i>	<i>0.04</i>	<i>2.22</i>	<i>0.10</i>	<i>0.13</i>	<i>0.03</i>	<i>0.01</i>	<i>0.001</i>	<i>6.35</i>	<i>0.30</i>	<i>0.01</i>	<i>100.00</i>	<i>29</i>	<i>32</i>	<i>32</i>	<i>5</i>	<i>5</i>	<i>13.5</i>	<i>151</i>	<i>99</i>	<i>38</i>	<i>32</i>	<i>6</i>	<i>5</i>

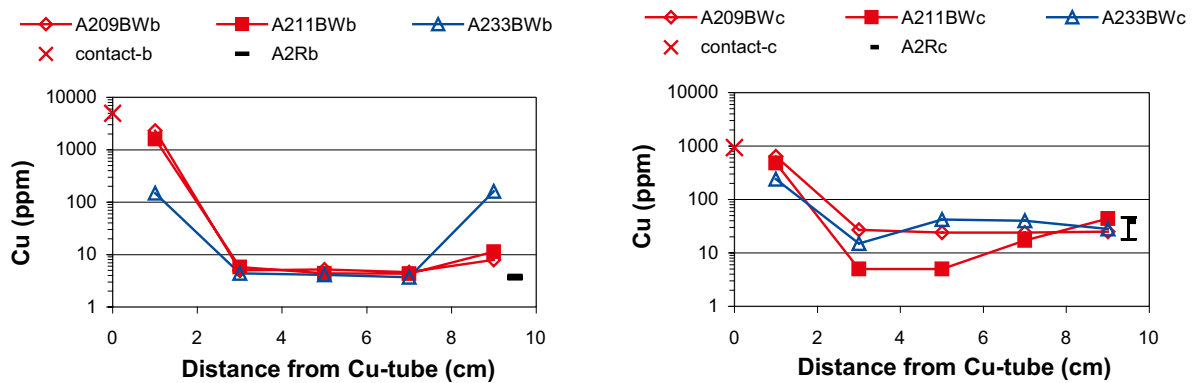


**Figure 9-6.** Plot of the Cu concentration in bulk samples (left) and clay fractions (right) versus the distance from the Cu-tube for blocks 09, 11 and 33 of the LOT A2 parcel. Values for the reference samples (A2R) are shown at position 9.5 cm as the mean  $\pm 1$  standard deviation of five samples.

The content and distribution of Cu may at least partly be explained by the initial low degree of water saturation in the bentonite. The incoming saturating ground-water leads to an outer rim of fully saturated bentonite which principally traps the major part of the air in the bentonite. The mean air filled porosity of a single block was 0.74 dm<sup>3</sup>, based on total volume, initial water-to-solid mass ratio, and total porosity of the blocks. This corresponds to 0.013 moles of oxygen calculated from an air density of 1.29 kg/m<sup>3</sup> and 21% oxygen in air. Assuming only Cu (II) was formed, this corresponds to 0.8 grams of Cu, which gives a mean Cu content of approximately 80 ppm in a block. Distributed only in the innermost section this content corresponds to approximately 700 ppm Cu, which can be compared with the measured maximum value of 2,325 ppm in block A209, 1,600 ppm in block A211, and 149 ppm in block A233. The large difference between the warm and cold sections may be explained by higher reaction rate at higher temperatures, and by the fact that the warmest part of the bentonite principally is the last to be water saturated and thereby the last volume to contain a gaseous phase.

A comparison of the results of the medium term (6-years) A2 test with those of the short term (< 2 years) A0 test /Karlund et al. 2009/ reveals that the Cu content (on ignited basis) of the analyzed hot A2 blocks has increased by approximately 15% compared to the concentration of the equivalent blocks from the A0 parcel. This fact suggests that the rate of copper incorporation in the bentonite is not linearly related to the duration of the test conditions but seems to have proceeded at a higher rate during an early stage of the test.

The Cu concentration of the clay fraction of the contact samples is 20–30% of that of the corresponding bulk samples. Provided that the clay fraction extracted is representative of the entire sample volume, this fact indicates that the major fraction of Cu is not incorporated in the structure of the montmorillonite. The form in which copper has been incorporated has not been identified but, as previously described, 9% at most is extractable into the alcoholic ammonium chloride solution used for the extraction of the exchangeable cations (cf. Section 9.2.2, Exchangeable cations)

The sulfate and carbonate minerals are trace constituents (<1.5%) in the parent bentonite MX-80 but attention is paid to these minerals because of their temperature-dependant solubility – that is, the solubility decreases with increasing temperature. Under non-isothermal conditions with steep temperature gradients these salts may consequently accumulate in the warmer parts of the buffer, which would affect both the rheology of the bentonite and the composition of the pore water.

The mean concentration of total sulfur in the reference bentonite samples is 0.21% (std.dev. 0.07; N=5; DL=0.02%). According to the data on water-soluble salts (Table 9-2) approximately 40% of the total sulfur content is derived from water-soluble minerals (mainly gypsum, CaSO<sub>4</sub> · 2H<sub>2</sub>O). The source of the remaining fraction, 0.10–0.15% S, is sulfides and, possibly, also sulfates of low solubility (e.g. BaSO<sub>4</sub>). The distribution of total sulfur plotted in Figure 9-7 matches the results of the analysis of aqueous leachates (cf. Figure 9-2), and shows that the sulfur distribution in the cool block has remained more or less unaffected during the LOT test. In the hot blocks the total sulfur content has increased by 40–90% in the interval 3–6 cm from the heater where CaSO<sub>4</sub> has accumulated, whereas the peripheral parts appear to be depleted in sulfur.

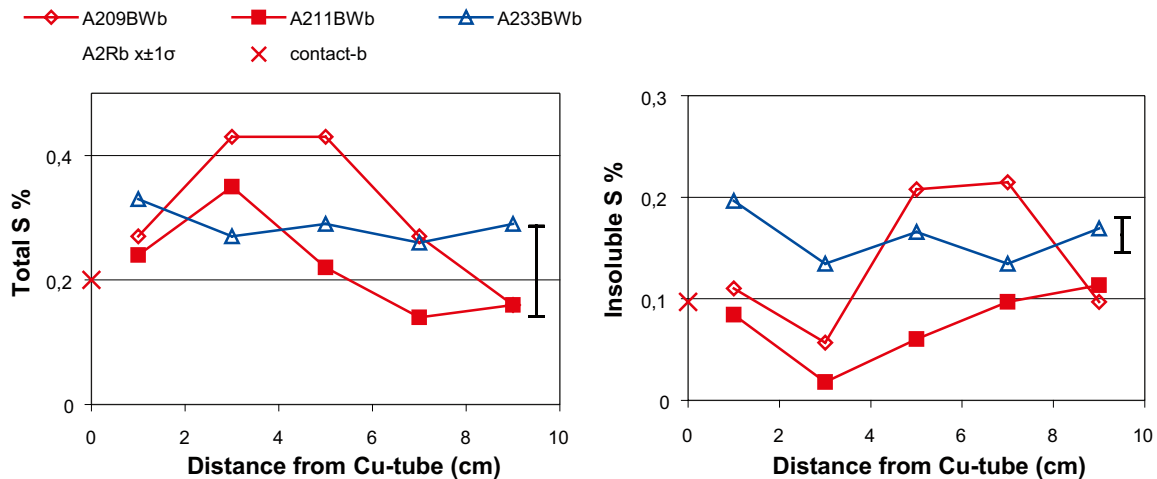


**Figure 9-7.** The content of total (left) and water-insoluble sulfur (right) in bulk samples of block 09, 11 and 33 of the LOT A2 parcel. Values for the reference samples (A2Rb) are shown at position 9.5 cm as the mean  $\pm 1$  standard deviation of five samples.

No separate analysis of sulfide was made, but the insoluble fraction of S (i.e. the differences between total and water-soluble S) is most likely dominated by iron sulfide (pyrite  $\text{FeS}_2$ ) although no precautions were taken to prevent oxidation during the leaching with water. The distribution pattern of this fraction of sulfur (Figure 9-7) suggests that a supplementary sulfide analysis might provide useful information about differences in iron sulfide stability between hot and cool blocks and should therefore be considered in future investigations of the LOT parcels.

The average total carbon content of the reference samples is 0.36% (std.dev. 0.02; N=5; DL=0.02%). The content of acid-soluble carbon, which is derived mainly from carbonate phases, is 0.14% C. The source of the remaining, acid-insoluble fraction is most likely organic matter.

The plots of the distribution of the different fractions of carbon (Figure 9-8) show that the acid-insoluble fraction of carbon is more or less constant in all blocks irrespective of the block temperature. The content of carbonate carbon, on the other hand, decreases in the interval 0–5 cm from the Cu-tube in the hot blocks, suggesting that carbonate dissolution has increased with increasing temperature. This somewhat unexpected distribution pattern of the carbonates was observed also in the ANDRA studies presented in Appendix 6.

The exact composition of the carbonate phase is not known but a normative calculation based on the CaO content remaining after allocating Ca to sulfate and to exchangeable Ca, suggests that Ca-carbonate is predominant. Dissolution/precipitation reactions involving both sulfates and carbonates of calcium have necessarily influenced the composition of the pore water in the hot blocks and, consequently, explain some of the changes in the pool of the exchangeable cations indicated in Figure 9-3 and Figure 9-4.

Calculation of the structural formulas of the smectite based on the available chemical data was considered too uncertain, since it is obvious from the XRD-analysis that the  $\text{SiO}_2$  content of the clay fraction is derived not only from smectite but also from fine-grained quartz and cristobalite. Nevertheless, some clear trends can be seen in the composition of the silicate fraction, which are demonstrated in Figure 9-9 to Figure 9-11 by some selected parameters extracted from the chemical data on the clay fraction (Table 9-6). Prior to the chemical analysis, carbonates and sulfates were removed from the clay, which thereafter was saturated with sodium (and dialyzed) in order to make the allocation of cations to exchange and structural sites, respectively, less ambiguous. Therefore, exchangeable sodium is the predominant interlayer cation but any calcium carbonate/sulfate that survived the pre-treatments will dissolve during the dialysis, supplying calcium for exchange. The same would be true for magnesium but no soluble Mg-bearing phase has been identified (cf. below). Potassium in the clay is, on the other hand, derived predominantly from illitic layers (cf. Section 9.2.2, Bentonite mineralogy) and thus fixed in the interlayers. Accordingly, the equivalent ratio  $(\text{Ca}+\text{Na})/\text{K}$  reflect the proportion between the exchangeable and non-exchangeable interlayer cations. As shown in Figure 9-9, this ratio has changed during the long term test in samples proximal to the heater, apparently due to loss of some potassium.

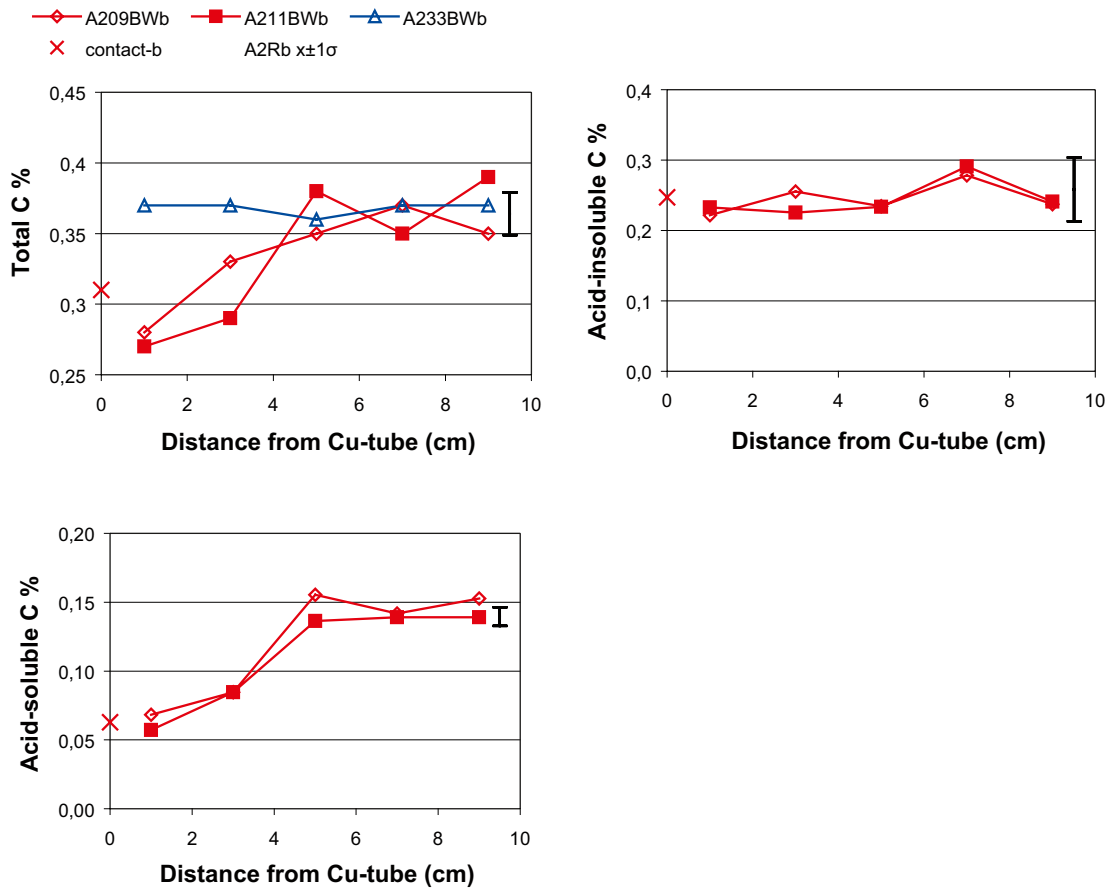


**Figure 9-8.** Total, acid-insoluble and acid-soluble carbon in bulk samples of block 09, 11 and 33 of the LOT A2 parcel (for block 33 only total carbon). Values for the reference samples (A2Rb) are shown at position 9.5 cm as the mean  $\pm 1$  standard deviation of five samples.

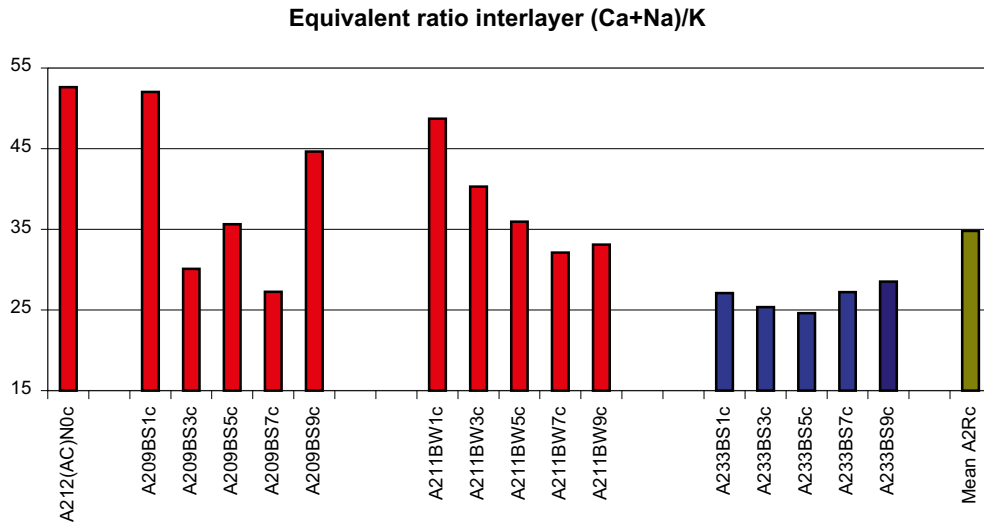


**Figure 9-9.** The equivalent ratio of interlayer  $(Ca+Na)/K$  of the Na-saturated  $< 2 \mu m$  fractions of sample 1–9 from the hot blocks 9 and 11 and from the cool block 33 of the LOT A2 parcel. One sample from the contact with the Cu-tube (sample 0) and the mean of three reference samples are also included.

Also the MgO content of the clay fractions (Figure 9-10) displays a clear gradient towards the Cu-tube in the hot blocks and has increased from 2.35% (mean of references) to ca. 2.6% in the innermost samples, whereas the peripheral parts of the blocks appear to be depleted in magnesium. The MgO-values plotted in Figure 9-10 have been re-calculated on an ignited basis to avoid the artifacts that may arise due to variable amounts of volatiles among the samples. Mg in exchange positions can be assumed to contribute insignificantly to the total MgO content in the Na-saturated clay. No other Mg-bearing mineral phase than montmorillonite has been identified in the XRD-analysis (cf. Section 9.2.2, Bentonite mineralogy) but the detection limit of this method may be too poor to detect trace minerals, and depends, among other things, on the “crystallinity” of the phase.

Magnesium in the montmorillonite structure is located in the octahedral sheet together with Al and Fe (strictly, Al is normally a minor constituent also of the tetrahedral sheet of montmorillonite). As illustrated by the plots of the oxide ratios  $Al_2O_3/MgO$  and  $Fe_2O_3/MgO$  (Figure 9-11), the concentration gradient is manifested more or less distinctly also in the relation between MgO and the other major “octahedral” elements.

The Mg-rich samples proximal to the heater are distinguished also by higher CEC values (cf. Section 9.2.2, Cation exchange capacity). However, it remains to establish whether the increase in CEC is interconnected to redistribution of Mg.

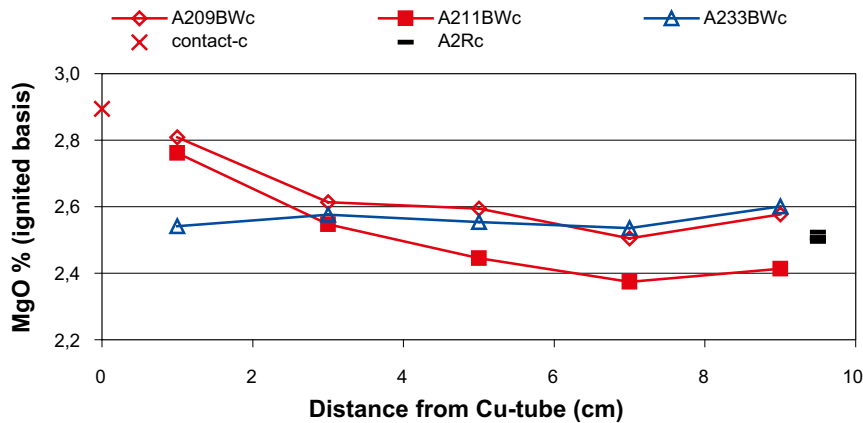


Figure 9-10. Plot of the MgO content of the Na-saturated  $<2 \mu m$  fractions (ignited basis) versus the distance from the Cu-tube for block 09, 11 and 33 of the LOT A2 parcel. Values for three reference samples are indicated at the position 9.5 cm.

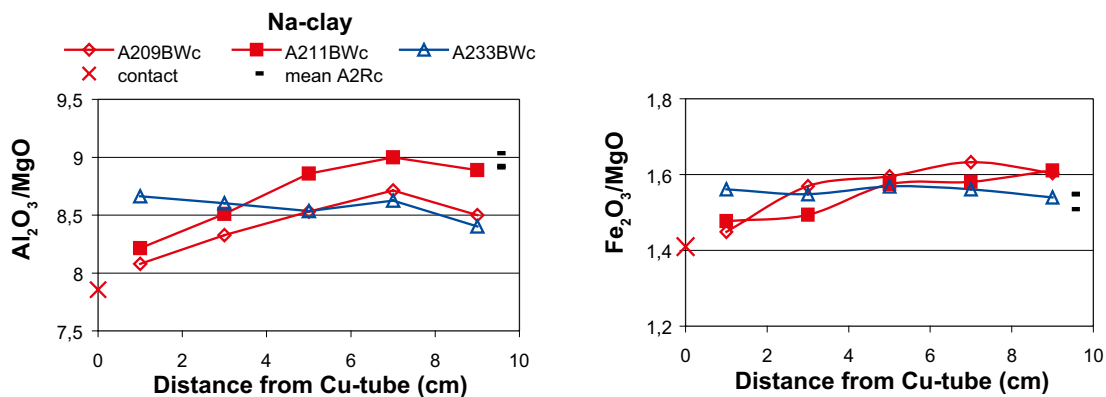


Figure 9-11. Plots of the ratios of the elements in the octahedral smectite sheet versus the distance from the Cu-tube. The Na-saturated  $<2 \mu m$  fraction of samples from block 9, 11 and 33 of the LOT A2 parcel. Values for three reference samples are plotted at the position 9.5 cm.

## Bentonite mineralogy

### The reference bentonite

The XRD-profiles of random powders of the bulk material of five LOT A2 reference samples are shown in Figure 9-12 and the mean XRD-profile of the references in Figure 9-13. The strongest peaks of the major non-phyllsilicates, i.e. quartz, cristobalite and feldspars (K-feldspar and Na-plagioclase), are indicated in Figure 9-13. Traces of gypsum are generally found in MX-80 bentonite, used for the LOT A2 parcel, and peak positions for gypsum are also indicated in Figure 9-13, but according to the chemical data the maximum amount of gypsum that can exist (i.e. if all sulfur is allocated to  $\text{CaSO}_4 \cdot 2\text{H}_2\text{O}$ ) in the reference bentonite is below 2% and close to the detection limit of the XRD analysis. Also calcite has been found in MX-80 /e.g. Karnland et al. 2000/, and is indicated in the chemical data but, again, the quantity (ca. 1.5% if all acid-soluble carbon is allocated to  $\text{CaCO}_3$ ) is close to the detection limit of the XRD method.

In the XRD-profile of Figure 9-13 also the strongest basal reflections (001) and the two-dimensional hk-bands of montmorillonite are indicated. The positions of the basal reflections (ca. 12.5 Å for (001)) are typical of the monolayer hydrate of Na-montmorillonite, which is stable at relative humidities below 60–70% /Brindley and Brown 1980/. The shoulder on the low-angle side of the first order peak suggests, however, that mixed hydration states occur, probably due to the lack of RH control during the X-ray scanning and/or due to the mixed interlayer cation pool of the reference bentonite – approximately 20% of the interlayer sites are occupied by Ca which forms a two-layer hydrate at the relative humidity of normal laboratory conditions.

In Figure 9-13 also the position of the so called (060)-peak is indicated. This reflection is useful for recognizing di- and trioctahedral sub-groups of clay minerals since it includes the *b* cell dimension which is more sensitive to the size of the cations and to site occupancy in the octahedral sheet than are the *a* or *c* cell dimensions. For smectites this peak is distinct enough to allow an estimate of the *b* parameter to an accuracy of perhaps  $\pm 0.5\%$  /Brindley and Brown 1980/. An indicated *d*(060) value of 1.49–1.50 Å ( $62^\circ 2\theta$ ) is typical of the dioctahedral sub-group of smectites, to which montmorillonite belongs.

Micaceous minerals, which have their (001) reflection at 10 Å, occur in such small quantities that basal peaks would barely be detectable in the XRD-trace of a randomly oriented preparation of good quality. No peaks can be detected in the mean XRD-profile of the references in Figure 9-13 but, depending on the degree of accidental orientation, individual samples display a peak of low intensity in the 10 Å-region, which indicates that trace amounts of mica/illite occur (Figure 9-12).

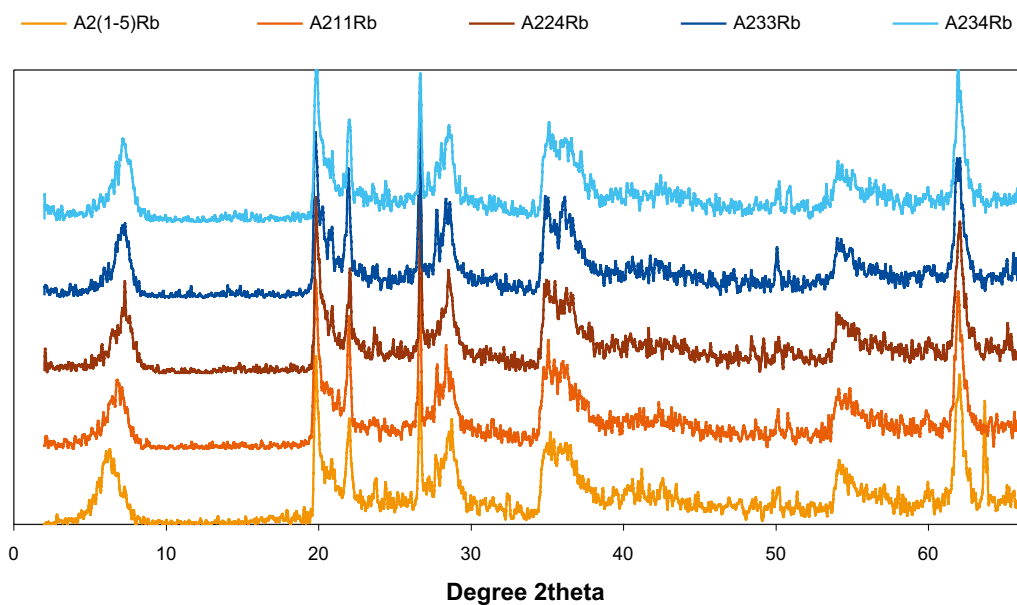


**Figure 9-12.** XRD-profiles of random powders of the bulk of five reference samples for the LOT A2 parcel. Peak positions are given in Figure 9-13. CuK $\alpha$  radiation.

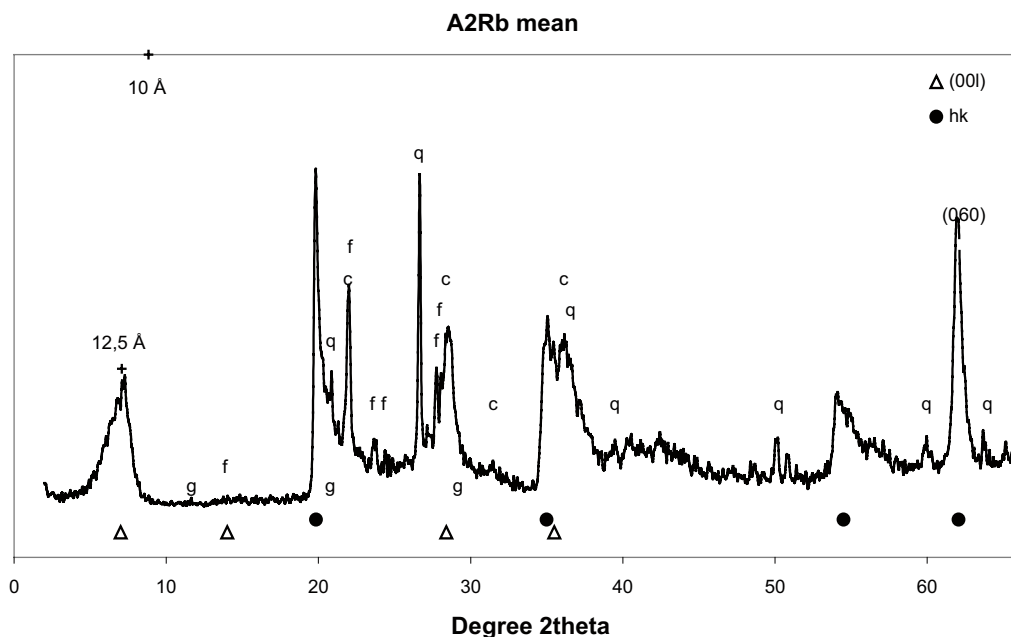


**Figure 9-13.** Mean XRD-profile of random powders of bulk material of five reference samples for the LOT A2 parcel (individual samples shown in Figure 9-12). The position of the strongest peaks of the major non-clay minerals is indicated; q=quartz, c=cristobalite, f=feldspars, g=gypsum. The position of the strongest 00l- and hk-peaks/bands of montmorillonite and the (001) mica/illite peak (10 Å) is also indicated. CuK $\alpha$  radiation.

XRD-profiles of oriented aggregates of the Mg-saturated <2  $\mu\text{m}$  fraction of the reference samples are shown in Figure 9-14 (air-dried clay) and Figure 9-15 (EG-solvated clay). The clay fractions are almost pure montmorillonite, but traces of cristobalite (4.05 Å) and quartz (3.34 Å) can be seen in the XRD-profiles of all clay samples, showing that a small fraction of these minerals are extremely fine-grained. In contrast, feldspars cannot be detected in the XRD-traces of the clay fraction, suggesting that the grain size of the feldspar is generally >2  $\mu\text{m}$ .

The homo-ionic Mg-clay has a basal spacing of 14.5–15 Å when air-dried and expands to 16.9–17 Å upon ethylene glycol treatment (EG). As can be seen in the diffractograms of EG-solvated clays (Figure 9-15), the series of basal reflections deviates little from a complete, periodic diffraction pattern, which is indicative of well-ordered stacking sequences with virtually no interstratification (in interstratified clay minerals individual crystals are composed of basic unit layers of two or more types). Similarly, the  $\Delta 2\theta_{002/003}$  value (the difference between the (002) and (003) peaks in degrees  $2\theta$ ) is 5.27–5.30 which is typical of a well-defined montmorillonite phase /cf. Moore and Reynolds 1989/. However, judged by the chemical data on the clay fraction, some illitic layers may exist – the amount of non-exchangeable potassium (0.1% K $_2$ O, Table 9-6) would correspond to 1–1.5% illite. No discrete 10-Å phase can be detected and such small amount of illitic layers in the smectite structure cannot be detected by routine XRD analysis (for comparison, ~10% illitic layers in the montmorillonite structure would give a  $\Delta 2\theta_{002/003}$  value of 5.5).

In summary, the XRD analysis of the reference bentonite shows that:

- The bulk bentonite contains montmorillonite, quartz, cristobalite, feldspars and traces of gypsum and mica/illite. No carbonate phases have been detected but are indicated in the chemistry of the solid phase. The amount is, however, close to or below the detection limit of the XRD-method.
- The clay fraction is almost pure montmorillonite but traces of quartz and cristobalite still occur. No discrete 10 Å phase, i.e. mica/illite, can be detected.
- Montmorillonite in the “as-received state” has a basal spacing of 12.5 Å at an RH of around 60% but the 001-peak tends to be broad and asymmetrical. The air-dried, homoionic Mg-exchanged clay has a basal spacing of 14.5–15 Å, and expands to 16.9–17 Å on EG-solvation, giving a complete, periodic diffraction pattern, typical of well-defined montmorillonite.

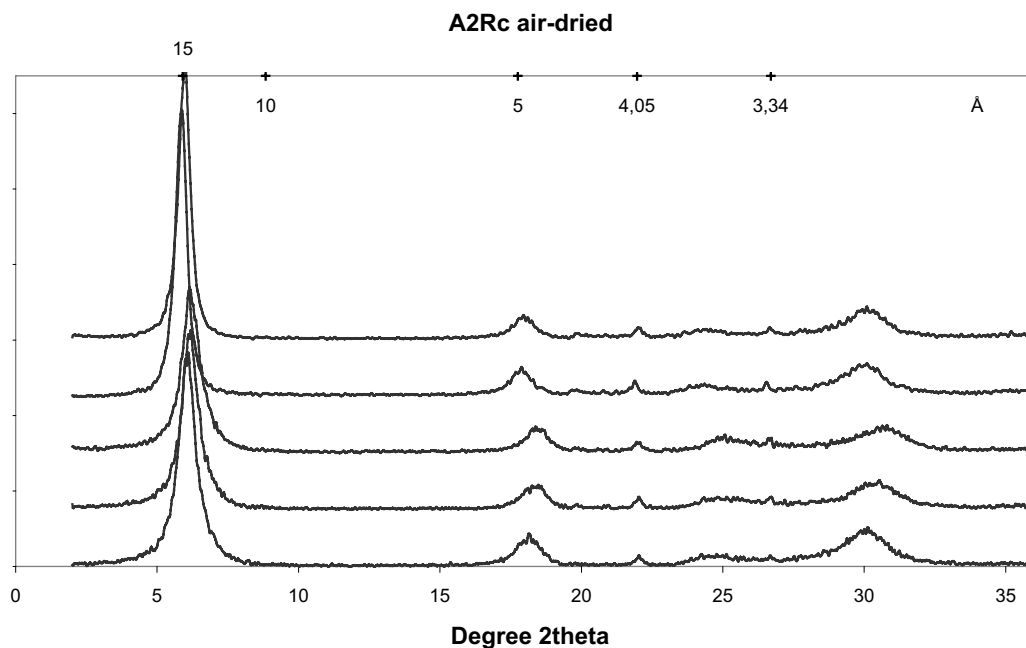


**Figure 9-14.** XRD-profiles of oriented aggregates of the air-dried, Mg-saturated clay fraction of five reference samples for LOT A2. The positions of the strongest basal reflections of montmorillonite are indicated in the upper scale together with the strongest peaks of cristobalite (4.05 Å), quartz (3.34 Å) and mica/illite (10 Å). CuK $\alpha$  radiation.

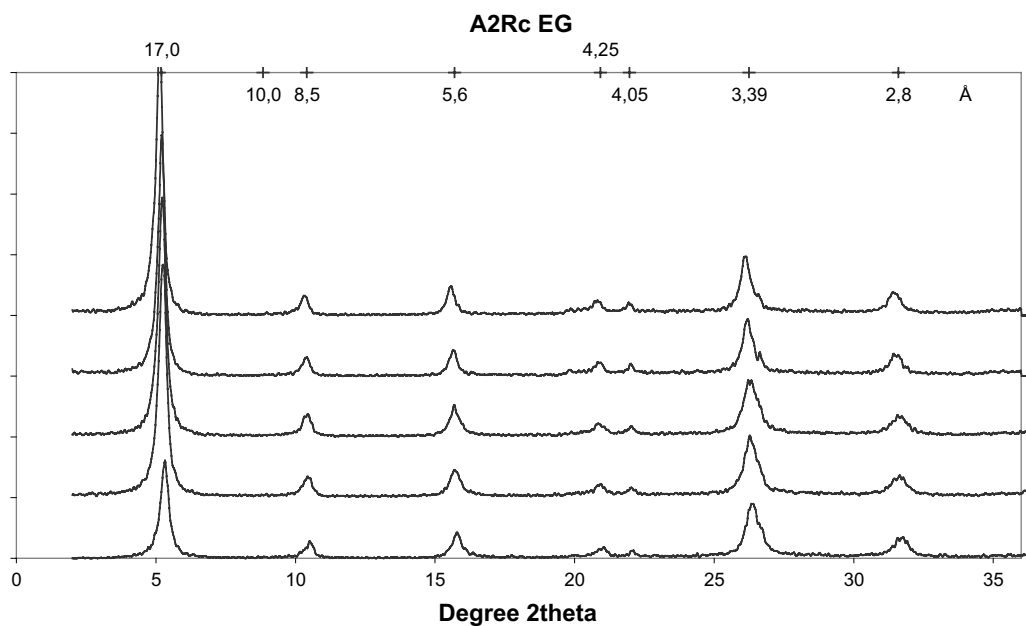


**Figure 9-15.** XRD-profiles of oriented aggregates of the clay fraction of five reference samples for LOT A2. Mg-saturated, ethylene glycol solvated samples. The positions of the basal reflections of montmorillonite are indicated in the upper scale together with the strongest peaks of cristobalite (4.05 Å), and mica/illite (10 Å). CuK $\alpha$  radiation.

### Bentonite of the LOT A2 parcel

The XRD-profiles of the bulk samples from block 33, 09, 11 and from the contact bentonite/Cu-tube are presented in Figure 9-16 to Figure 9-19. The cool block 33 (Figure 9-16) displays no significant changes compared with the reference samples, neither with respect to the type nor to the peak intensities of accessory minerals. A variation of the intensity of the feldspar peaks can be seen among the samples, but both the excellent {010} and {001} cleavage of feldspars, which promotes preferred orientation, and the coarse grain size of feldspars, may give a random variation in the peak intensities. Similarly, depending on the degree of random orientation of the preparation, some but not all samples display a 10 Å peak of low intensity produced by mica.

The shape and width of the (001) basal reflection of montmorillonite varies somewhat among the samples, most likely due to the lack of humidity control during the X-ray scanning. However, like the references, all samples have the peak centered around 12.5 Å, which is typical of the monolayer hydrate of a Na-montmorillonite and consistent with the data on the composition of the exchangeable cation pool, showing that the proportion between divalent and monovalent cations in block 33 has changed very little compared with the reference bentonite (cf. Table 9-3).

The most conspicuous mineralogical change in the hot blocks is the appearance of moderately intense peaks of anhydrite in the interval 2–6 cm from the central heater (Figure 9-17 and Figure 9-18). Accordingly, the mineralogical data match the chemical data, which clearly show that Ca-sulfate has been redistributed along the thermal gradient in the hot blocks. In some of the samples from the “anhydrite interval” the re-precipitated sulfate phase may include the hemi-hydrate bassanite ( $\text{CaSO}_4 \cdot \frac{1}{2}\text{H}_2\text{O}$ ).

It is also evident, in particular for block 9, that the basal spacing of montmorillonite has shifted from 12.5 to 15 Å in the innermost samples. This increase in the basal distance is consistent with a replacement of interlayer Na by divalent cations, as indicated in the data on the composition of the interlayer cation pool (cf. Figure 9-4) but the XRD-results are inconclusive due to the lack of humidity control during the X-ray scanning.

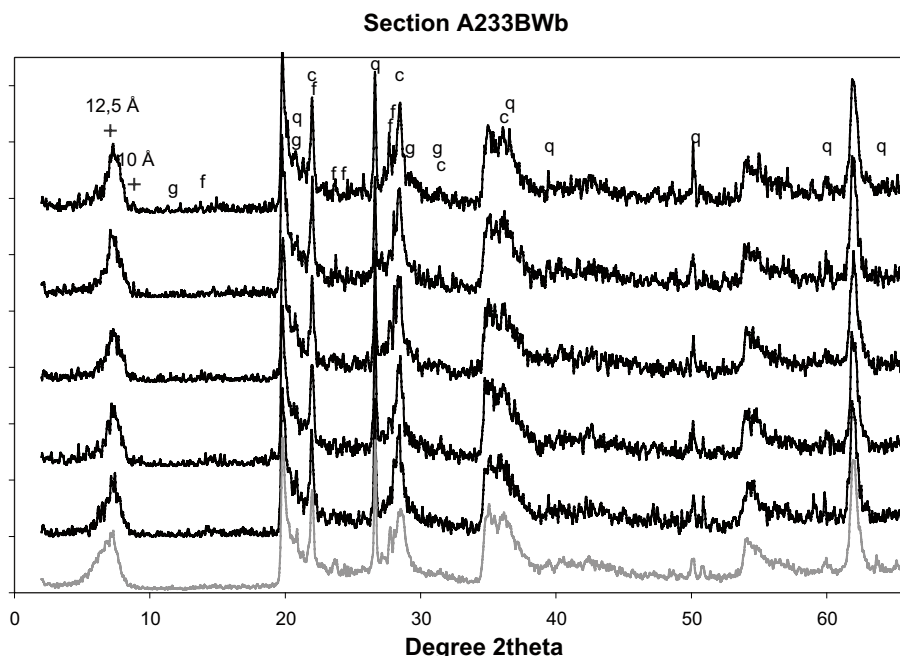


**Figure 9-16.** Black curves: XRD-profiles of sample 1 (bottom) to 9 (top) from block 33 of the LOT A2 parcel. Grey curve: mean XRD-profile of five reference samples. The position of the strongest peaks of the major non-clay minerals is indicated; q=quartz, c=cristobalite, f=feldspars, g=gypsum. The (001) peaks of mica/illite at 10 Å and of Na-smectite at 12.5 Å are also indicated. Random powder of bulk samples; CuK $\alpha$  radiation.

Section A209BWb

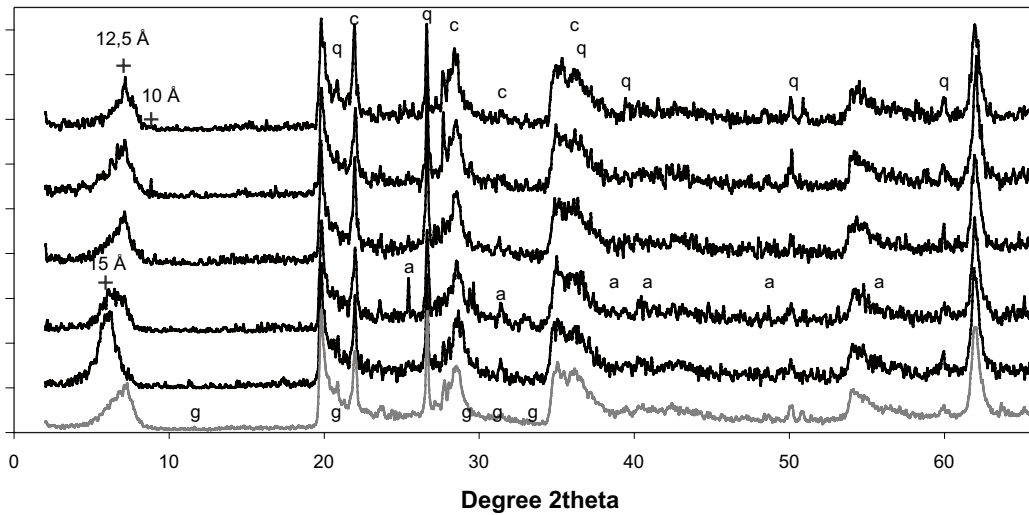


**Figure 9-17.** Black curves: XRD-profiles of sample 1 (bottom) to 9 (top) from block 9 of the LOT A2 parcel. Grey curve: mean XRD-profile of five reference samples. The position of the strongest peaks of the major non-clay minerals are indicated; q=quartz, c=cristobalite, g=gypsum, a=anhydrite ( $\text{CaSO}_4$ ). The (001) peaks of mica/illite at 10 Å and of Na-smectite at 12.5 Å are also indicated (cf. text). Random powder of bulk material; CuK $\alpha$  radiation.

Section A211BWb

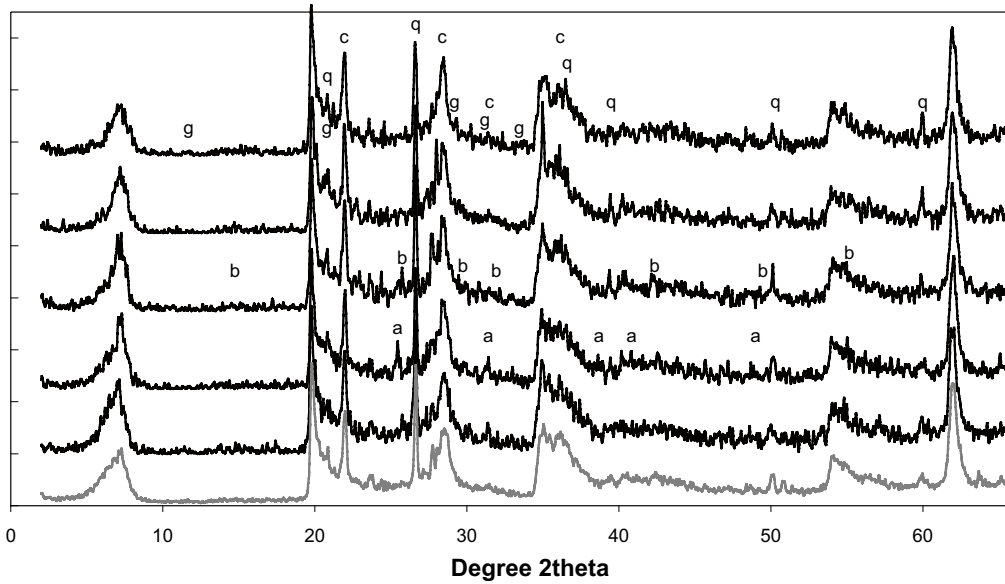


**Figure 9-18.** Black curves: XRD-profiles of sample 1 (bottom) to 9 (top) from block 11 of the LOT A2 parcel. Grey curve: mean XRD-profile of five reference samples. The position of the strongest peaks of the major non-clay minerals are indicated; q=quartz, c=cristobalite, f=feldspars, g=gypsum, b=bassanite ( $\text{CaSO}_4 \cdot \frac{1}{2}\text{H}_2\text{O}$ ), a=anhydrite ( $\text{CaSO}_4$ ). Random powder of bulk material; CuK $\alpha$  radiation.

### Contact A212(A-C)N0b

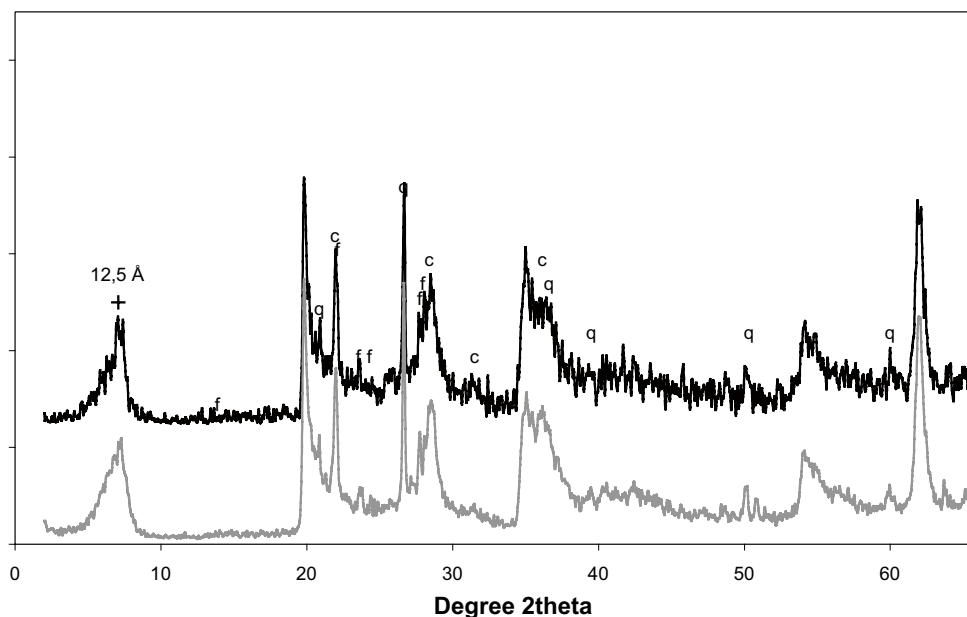


**Figure 9-19.** Black curve: XRD-profile of the contact sample Cu-tube/bentonite from block 12 of the LOT A2 parcel. Grey curve: mean XRD-profile of five reference samples. The position of the strongest peaks of the major non-clay minerals are indicated; q=quartz, c=cristobalite, f=feldspars. Random powder of bulk material; CuK $\alpha$  radiation.

A close-up of the region 60–64° 2 $\theta$  (i.e. scan resolution is not changed) of the XRD-profiles of the parcel and reference samples (Figure 9-20) shows that the d-value of the (060) peak is more or less identical in all samples (ca. 1.50 Å). Those variations that may exist appear to be random and independent of the position of the sample in the parcel. Thus, the available XRD-data provide no evidence of any significant change of the *b* cell dimension of the clay mineral, which would be an expected effect of, for instance, a change of the cations or the site occupancy in the octahedral sheet, or of a change of the amount of Al in tetrahedral coordination.

XRD-profiles of oriented mounts of the Mg-exchanged clay fraction of the individual samples from the A2 parcel are shown in Figure 9-22 to Figure 9-25 (air-dried clay) and Figure 9-26 to Figure 9-29 (EG-solvated clay) together with the corresponding average XRD profiles of the reference samples.

Traces of quartz and cristobalite occur in all clay fractions, but apart from these minerals, the clay fraction appears to be pure montmorillonite. The basal spacing of the air-dried, homo-ionic Mg-clay ranges from 14.7 to 15 Å (relative humidity 50±10%). The clay expands to 16.7–16.9 Å upon EG-solvation. A close-up of the 17 Å region of the XRD-profiles of the parcel and reference samples (Figure 9-21) shows that the d-value of the (001) peak of the expanded clay is more or less identical in all samples. Those variations that exist appear to be random and independent of the position of the sample in the parcel and are in some cases an effect of variations in preferred orientation. The expansion behavior is typical of Mg-saturated montmorillonite and similar to that of the reference clay. As can also be seen in the diffractograms of the EG-solvated clays (Figure 9-26 to Figure 9-29), the series of basal reflections deviates little from a complete, periodic diffraction pattern, which is indicative of well-ordered stacking sequences with virtually no interstratification. Similarly, the value of  $\Delta 2\theta_{002/003}$  is in the same range (5.25–5.3) as that of the references and typical of a well-defined montmorillonite phase /Moore and Reynolds 1989/.

In summary, the available XRD-data provide no clear evidence of any structural change in the montmorillonite of the LOT A2 parcel. Changes that may exist in chemical composition and in the cation exchange properties of the clay mineral do not manifest themselves in the X-ray characteristics of the clay mineral. The question is, on the other hand, whether the resolution of XRD-technique is adequate for detecting small-scaled structural changes.

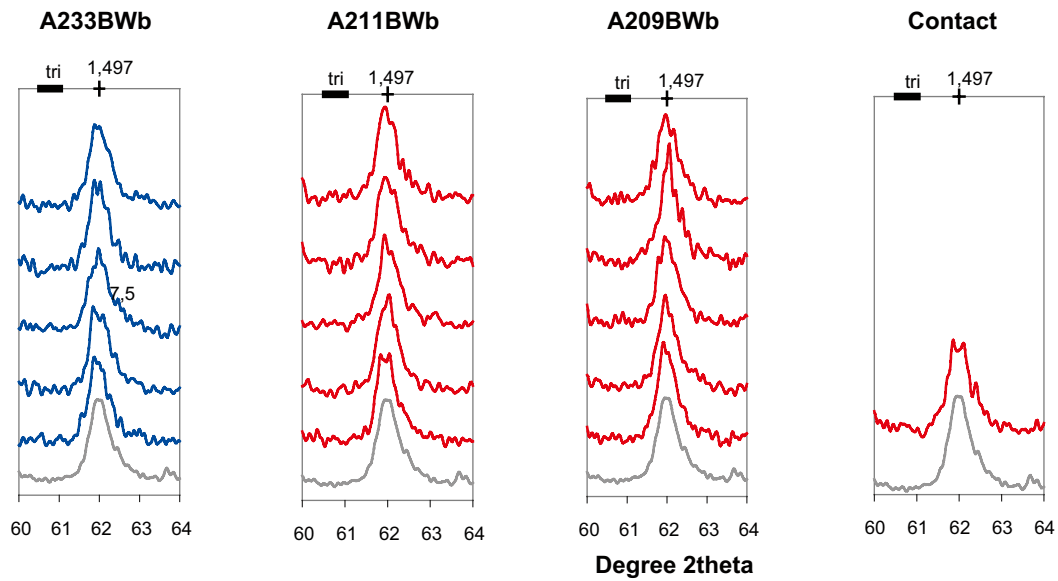


**Figure 9-20.** Close-up of the (060)-peak position. Blue curves: XRD-profiles of sample 1 (bottom) to 9 (top) from block 33; red curves: XRD-profiles of sample 1 (bottom) to 9 (top) from block 11 and 09 and from the contact bentonite/Cu-tube of the LOT A2 parcel. Grey curve: Mean XRD-profile of five reference samples. The indicated d-value (1.497 Å) of the (060)-peak is typical of dioctahedral smectites. The position of the (060)-peak of trioctahedral smectites is also indicated. CuK $\alpha$  radiation.

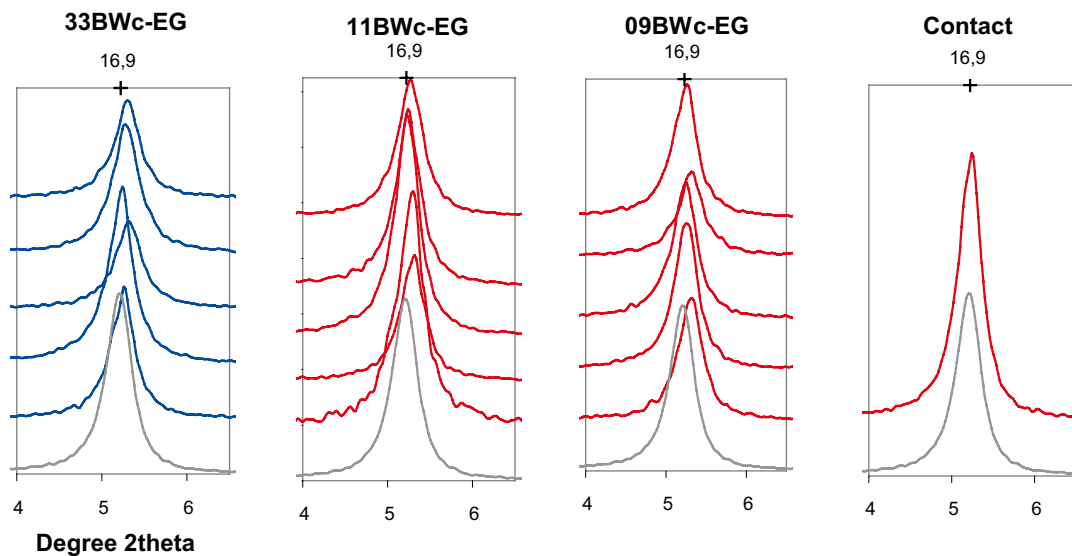


**Figure 9-21.** Close-up of the 17 Å region of EG-solvated, Mg-saturated clay fractions from the LOT A2 parcel. Blue curves: XRD-profiles of sample 1 (bottom) to 9 (top) from block 33; red curves: XRD-profiles of sample 1 (bottom) to 9 (top) from block 11 and 09 and from the contact bentonite/Cu-tube. Grey curve: Mean XRD-profile of five reference samples. The indicated d-value (16.9 Å) of the (001)-peak is typical of Mg-saturated, EG-solvated smectites. CuK $\alpha$  radiation.

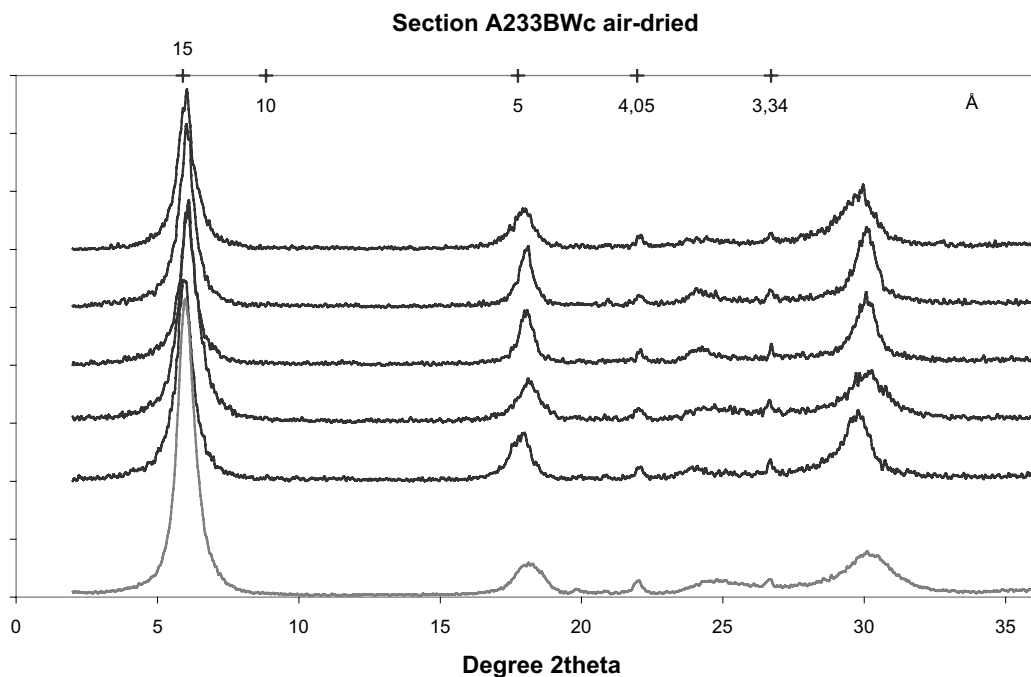


**Figure 9-22.** Black curves: XRD-profiles of oriented aggregates of the clay fraction of sample 1 (bottom) to 9 (top) of block 33 from the LOT A2 parcel. Grey curve: mean XRD-profile of the clay fraction of five reference samples. The strongest peaks of cristobalite (4.05 Å), quartz (3.34 Å) and mica/illite (10 Å) are indicated in the upper scale. Mg-saturated air-dried samples; CuK $\alpha$  radiation.

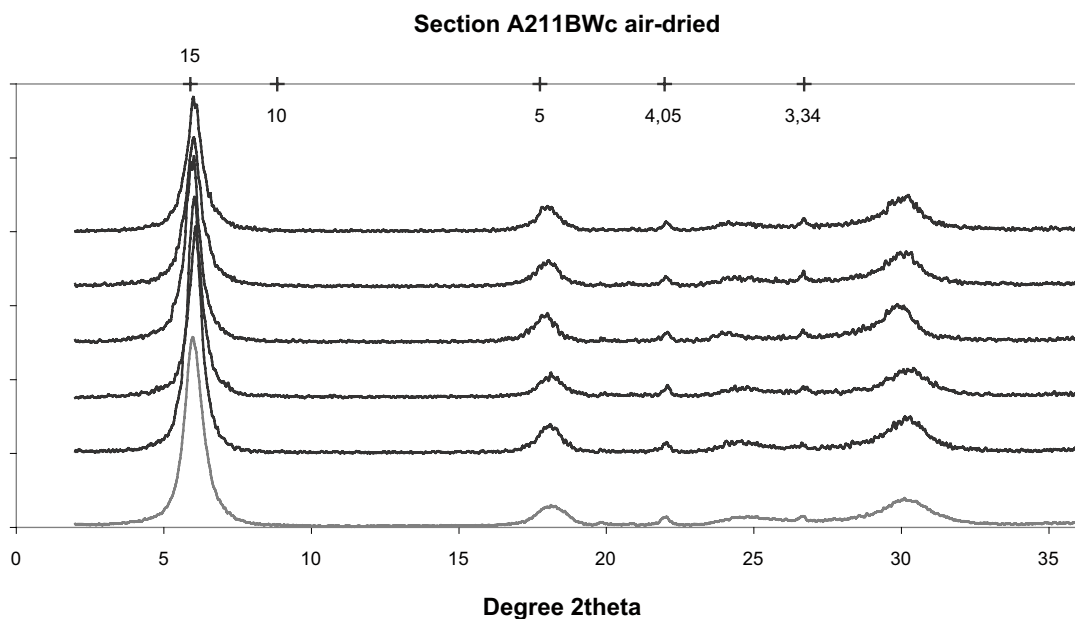


**Figure 9-23.** Black curves: XRD-profiles of oriented aggregates of the clay fraction of sample 1 (bottom) to 9 (top) of block 11 from the LOT A2 parcel. Grey curve: mean XRD-profile of the clay fraction of five reference samples. The strongest peaks of cristobalite (4.05 Å), quartz (3.34 Å) and mica/illite (10 Å) are indicated in the upper scale. Mg-saturated, air-dried samples; CuK $\alpha$  radiation.

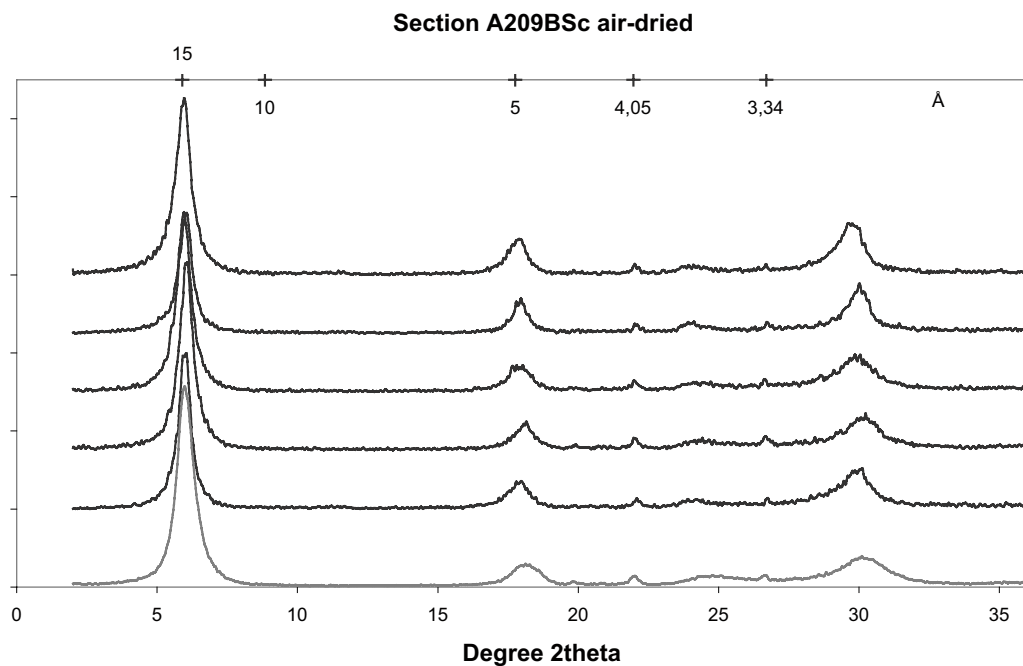


**Figure 9-24.** Black curves: XRD-profiles of oriented aggregates of the clay fraction of sample 1 (bottom) to 9 (top) of block 09 from the LOT A2 parcel. Grey curve: mean XRD-profile of the clay fraction of five reference samples. The strongest peaks of cristobalite (4.05 Å), quartz (3.34 Å) and mica/illite (10 Å) are indicated in the upper scale. Mg-saturated, air-dried samples; CuK $\alpha$  radiation.

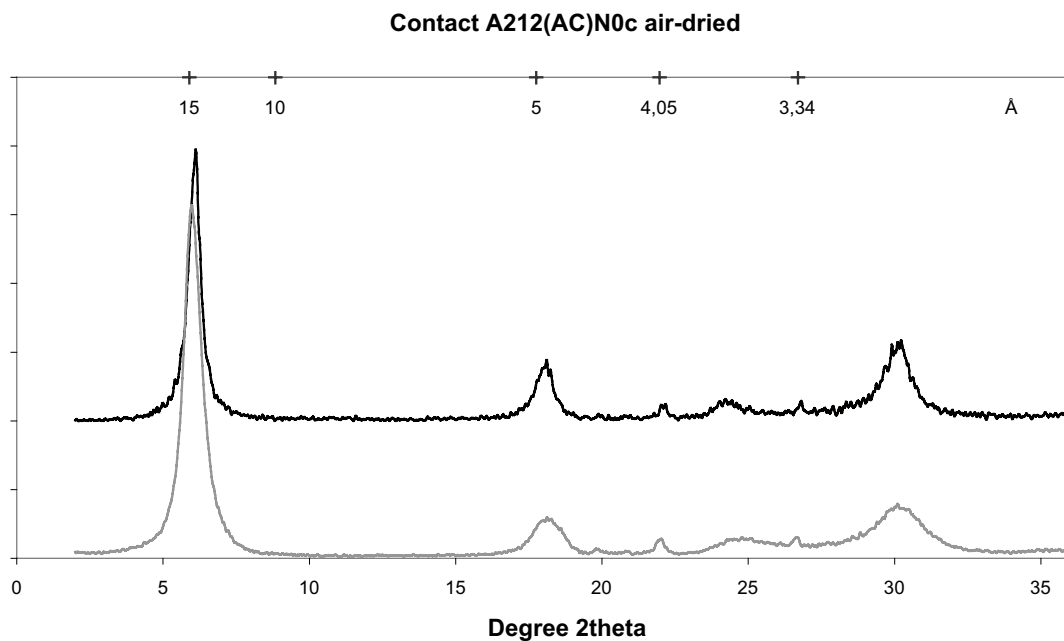


**Figure 9-25.** Black curve: XRD-profile of oriented aggregates of the clay fraction of the contact sample of block 12 from the LOT A2 parcel. Grey curve: mean XRD-profile of the clay fraction of five reference samples. The strongest peaks of cristobalite (4.05 Å), quartz (3.34 Å) and mica/illite (10 Å) are indicated in the upper scale. Mg-saturated, air-dried samples; CuK $\alpha$  radiation.

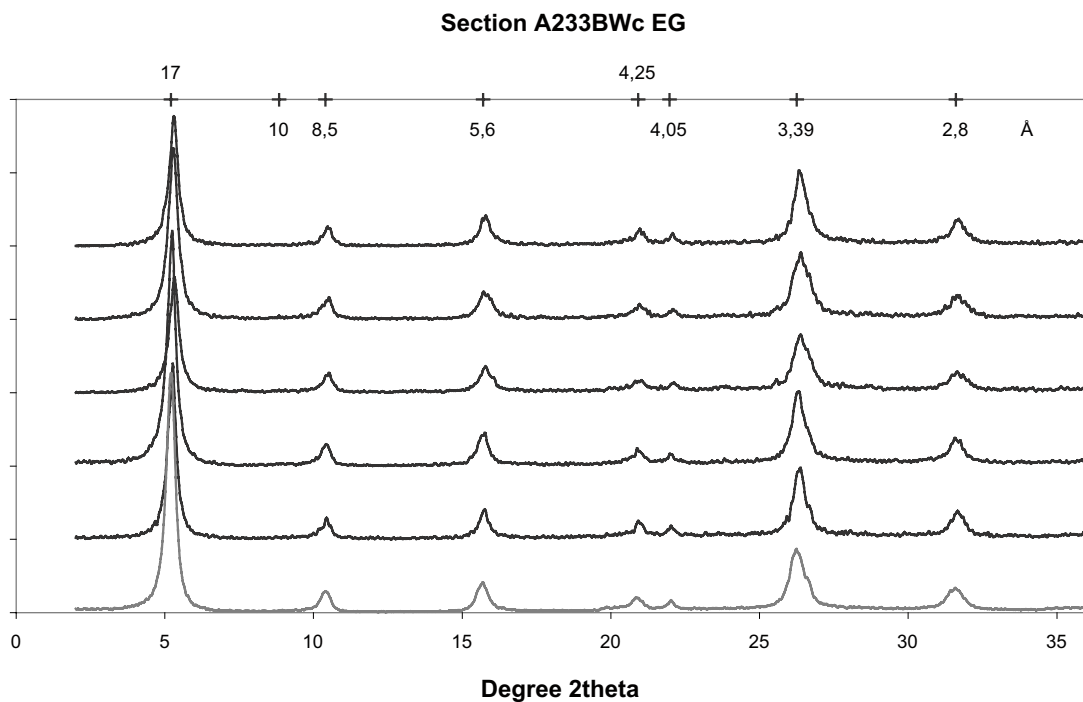


**Figure 9-26.** Black curves: XRD-profiles of oriented aggregates of the clay fraction of sample 1 (bottom) to 9 (top) of block 33 from the LOT A2 parcel. Grey curve: mean XRD-profile of the clay fraction of five reference samples. The positions of the basal reflections of montmorillonite are indicated in the upper scale together with the strongest peaks of cristobalite (4.05 Å) and mica/illite (10 Å). Mg-saturated, ethylene glycol solvated samples; CuK $\alpha$  radiation.

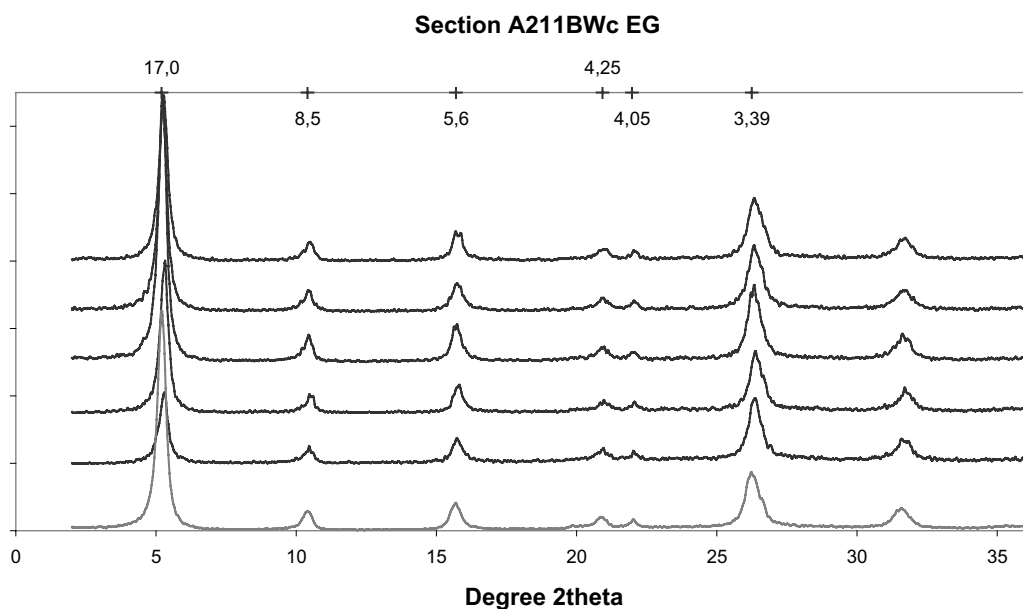


**Figure 9-27.** Black curves: XRD-profiles of oriented aggregates of the clay fraction of sample 1 (bottom) to 9 (top) of block 11 from the LOT A2 parcel. Grey curve: mean XRD-profile of the clay fraction of five reference samples. The positions of the basal reflections of montmorillonite are indicated in the upper scale together with the strongest peaks of cristobalite (4.05 Å). Mg-saturated, ethylene glycol solvated samples; CuK $\alpha$  radiation.

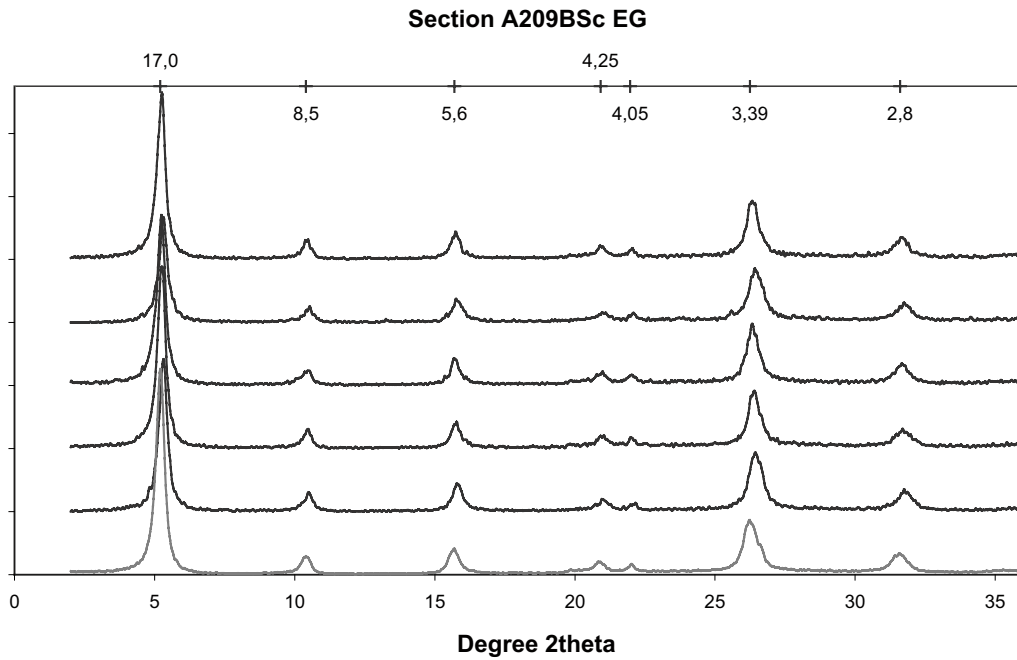


**Figure 9-28.** Black curves: XRD-profiles of oriented aggregates of the clay fraction of sample 1 (bottom) to 9 (top) of block 09 from the LOT A2 parcel. Grey curve: mean XRD-profile of the clay fraction of five reference samples. The positions of the basal reflections of montmorillonite are indicated in the upper scale together with the strongest peaks of cristobalite (4.05 Å). Mg-saturated, ethylene glycol solvated samples; CuK $\alpha$  radiation.

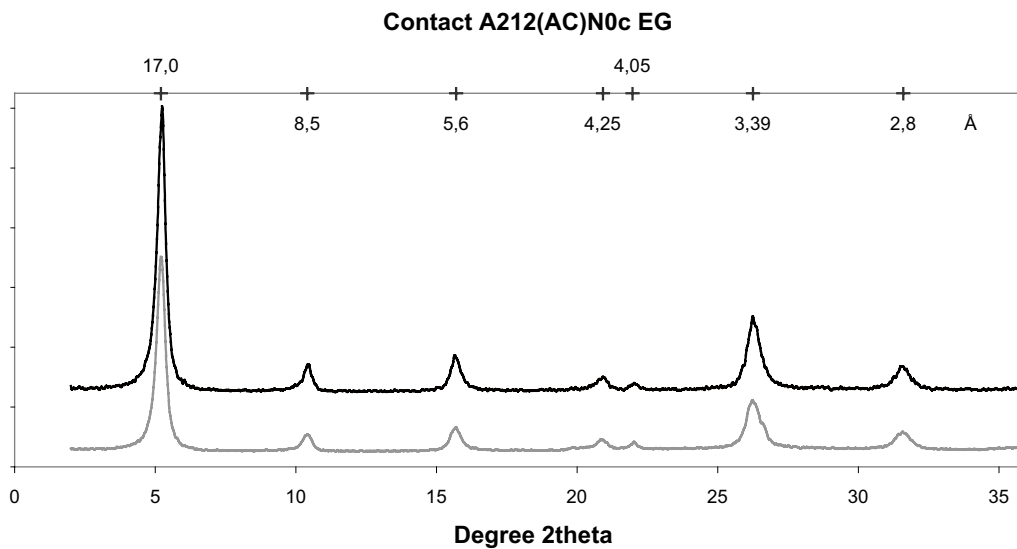


**Figure 9-29.** Black curve: XRD-profile of oriented aggregates of the clay fraction of the contact sample of block 12 from the LOT A2 parcel. Grey curve: mean XRD-profile of the clay fraction of five reference samples. The positions of the basal reflections of montmorillonite are indicated in the upper scale together with the strongest peaks of cristobalite (4.05 Å). Mg-saturated, ethylene glycol solvated samples; CuK $\alpha$  radiation.

### 9.2.3 Summary and conclusions

The chemical and mineralogical investigation of the bentonite of the standard blocks 09, 11 and 33 from the LOT A2 parcel indicates that:

- *Cu has been incorporated in the bentonite matrix proximal (0–2 cm) to the Cu-tube in all blocks.* The heated blocks have higher concentrations with a maximum of ~0.5% Cu in the mm-thick contact zone. A comparison of the results of the 5-year A2 test with those of the 1,5-year LOT A0 test /Karnland et al. 2009/ suggests that the rate of copper mobilization/incorporation is not linearly related to the duration of the test conditions but seems to have proceeded at a higher rate during an early stage of the test. The Cu concentration of the clay fractions is 20–30% of that of the corresponding bulk samples, which suggests that the major fraction of Cu is *not* incorporated in the structure of the montmorillonite. No specific investigation was made in order to identify the copper phases; however, it was noted that the major fraction of copper is not readily soluble or accessible for cation exchange.
- *Sulfates have been redistributed* along the thermal gradient in the heated blocks. Anhydrite has accumulated approximately 3–5 cm from the heater, whereas the peripheral parts of the blocks are depleted in sulfates.
- *The carbonate content decreases* with increasing temperature in the heated blocks.
- Dissolution/precipitation reactions involving sulfates and carbonates of calcium have influenced the pore water composition and, consequently, the pool of exchangeable cations. Accordingly, *some exchangeable sodium has been replaced by calcium* in the inner parts of the heated blocks.
- *Exchangeable Mg increases* with increasing temperature in the heated blocks. The trend is paralleled by an *increase in the content of non-exchangeable Mg of the clay* (Na-saturated fraction <2 µm; Figure 9-10) towards the heater whereas the peripheral parts of the blocks appear to be depleted in Mg. One possible source of Mg is the octahedral sheet of the montmorillonite, but the source of Mg has not been identified and remains to be established.
- *The proportion between exchangeable and non-exchangeable interlayer cations (the equivalent ratio  $(Ca+Na)/K$ ) has increased* in samples adjacent to the Cu-tube in the heated blocks, i.e. no relative K fixation has taken place.
- *CEC of the bulk samples and of the clay fractions tends to increase* towards the Cu-tube in the heated blocks. The differences in CEC are, however, close to the analytical resolution and should be substantiated by further testing.
- The available XRD-data provide *no evidence of a structural change of the montmorillonite*. Both the expansion behavior, a complete, periodic diffraction pattern of the basal reflections and the *b* cell dimension of the clay mineral from the parcel are typical of montmorillonite and similar to that of the reference material. Thus, those changes that exist in the chemical composition and in the cation exchange properties of the clay mineral do not manifest themselves in the X-ray diffraction characteristics of the clay mineral.

A comparison of these main observations with the results of the parallel investigations performed by the laboratories of VTT, Finland, ANDRA, France, BGR, Germany and NAGRA, Switzerland are compiled in Table 9-7.

## 9.3 Blocks with additives

### 9.3.1 Materials and methods

#### *Sampling and sample nomenclature*

The special block series comprises five blocks (10, 12, 16, 24 and 34) in which cylindrical bentonite plugs with an admixture of calcite, gypsum, K-feldspar or cement, respectively, were embedded in order to simulate various adverse chemical conditions that may accelerate alteration processes in the bentonite. The plugs had been placed in cylindrical holes, drilled in the B-level from the mantle surface of the blocks in connection with the block fabrication.

**Table 9-7. Comparison of major results obtained in the five parallel investigations of blocks from the LOT A2 parcel.**

Observation	Cu-uptake Cu-uptake at Cu-tube/bentonite interface	Cu-uptake Identification of neoformed Cu-phases	Ca-sulfate redistribution	Carbonate dissolution increase with temperature	Exchangeable Mg increase with temperature
VTT, block 18, 24 App. 5 Analytical methods			yes  dispersion of bentonite s:l ratio 1:30; squeezed porewater		
ANDRA, block 15 App. 6 Analytical methods	yes  bulk chemistry ICP-AES/MS, SEM-EDX	Cu-S phases with variable Fe-concentration  SEM-EDX; TEM-EDX; XPS	1. yes, profile identified 2. yes; CaSO <sub>4</sub> found at the Cu- tube  1.bulk chemistry ICP-AES/MS; XRD 2. SEM	yes  FTIR	yes; Mg in block samples>Mg in reference; no gradient within the block  extraction in Cl <sub>3</sub> Co(NH <sub>3</sub> ) <sub>6</sub> solution
BGR, block 15, (14) App. 7 Analytical methods	yes  bulk chemistry XRF; μ-EDXRF	CuS <sub>x</sub> phases  DTA MS 64, SEM EDX	yes  bulk chemistry XRF; MIR	yes – max. carbonate peak at rock contact but interval 4-8 cm not sampled MIR	yes  extraction in BaCl <sub>2</sub> solution
NAGRA, block 13 App. 8 Analytical methods	not studied	not studied	yes  dispersion of bentonite s:l ratio 1:10; evolved gas analysis; XRD	no; max value for inorg. C at heater  evolved gas analysis on acidification	yes, Mg in block samples>Mg in reference; max.value at heater but no clear gradient within the block Ni-ethylenediamine method corrected for salt dissolution
SKB, block 9, 11, 33 this study Analytical methods	yes  bulk chemistry ICP-AES/MS; extraction in NH <sub>4</sub> Cl - alcoholic solution	not studied	yes  dispersion of bentonite s:l ratio 1:100; bulk chemistry ICP-AES/MS+EGA; XRD	yes  evolved gas analysis on acidification	yes  extraction in NH <sub>4</sub> Cl - alcoholic solution

Table 9-7 continued.

Observation	Non-exchangeable Mg <sup>a</sup>		CEC		Smectite structure
	increase with temperature	identification of neoformed Mg-phase	CEC-range	increase with temperature	
VTT, block 18, 24 App. 5 Analytical methods					
ANDRA, block 15 App. 6 Analytical methods	1. yes, in bulk sample and <2 µm fraction 2. no; though a tendency in Figure 7. 1. bulk chemistry by ICP-AES/MS 2. TEM-EDX	not studied	bulk samples:86-100 meq/100 g <2 µm fraction: no determination  exchange in Cl <sub>3</sub> Co(NH <sub>3</sub> ) <sub>6</sub> solution	"slight augmentation in CEC from the granite to heater - not considered significant" (p.24)	no structural change  XRD; TEM-EDX; FTIR;
BGR, block 15, (14) App. 7 Analytical methods	yes  bulk chemistry by XRF	hydrotalcite-group mineral (p. 25)  XRD of magnetic separate 63 to 80 mm	bulk samples:81-88 meq/100 g  <2 µm fraction: no determination exchange in BaCl <sub>2</sub> solution	no, however interval 4-8 cm not sampled	no structural change  XRD; layer charge density; MIR
NAGRA, block 13 App. 8 Analytical methods	not studied	not studied	bulk samples:72-74 meq/100 g <2 µm fraction: no determination Na-acetate / Mg-nitrate displacement	no, rather the opposite tendency	no structural change  XRD
SKB, block 9, 11, 33 this study Analytical methods	yes, in bulk sample and in dialysed Na-clay (<2 µm) bulk chemistry by ICP-AES/MS	not identified  XRD of bulk and <2 µm	bulk samples:80-85 meq/100 g <2 µm fraction:85-94 meq/100 g Exchange in Cu-trien solution	tendency but significance uncertain? tendency but significance uncertain?	no structural change  XRD

<sup>a</sup>Data compared on ignited basis

Blocks 10 and 12 have 2-cm long plugs (Ø 20 mm) with an addition of 10% finely ground calcium carbonate and calcium sulfate, respectively, embedded in the B-level in each cardinal compass point. These blocks were sampled in the B-level between the southern plug and the inner mantle surface of the block, at two distances (0–2 cm and 2–4 cm) from the plug (Figure 9-30). The sample size was 2×2×2 cm.

Block 16 has three 2 cm long bentonite plugs (Ø 20 mm) containing 50% potassium feldspar in the B-level in each cardinal compass point. The chemical composition of the potassium feldspar used as additive is given in Table 9-8.

Blocks 24 and 34 have four 2 cm long plugs (Ø 20 mm) of cement (Aalborg white Portland cement) in the B-level to the north and south. The blocks 16, 24 and 34 were sampled at two radial positions along the southern plug and at two distances (0–2 cm and 2–4 cm) from the plug, above or below the plug (i.e. in the A/B and A- alternatively in the B/C and C-level; cf. Figure 9-30). The sample size varies from 2×2×2 to 2×2×2.5 cm.

All sampling was made by use of a band saw. A 2 mm-thick layer of the contact surface was removed from the samples that were in direct contact with plugs.

Individual samples have been given an identity code according to the general nomenclature. The code for the horizontal position of samples taken across the boundary between the A and B level (or B and C) is A/B (B/C) (Figure 9-30).

When available, bentonite used for the fabrication of the blocks has been used as reference material, supplemented with the reference material used for the standard blocks.

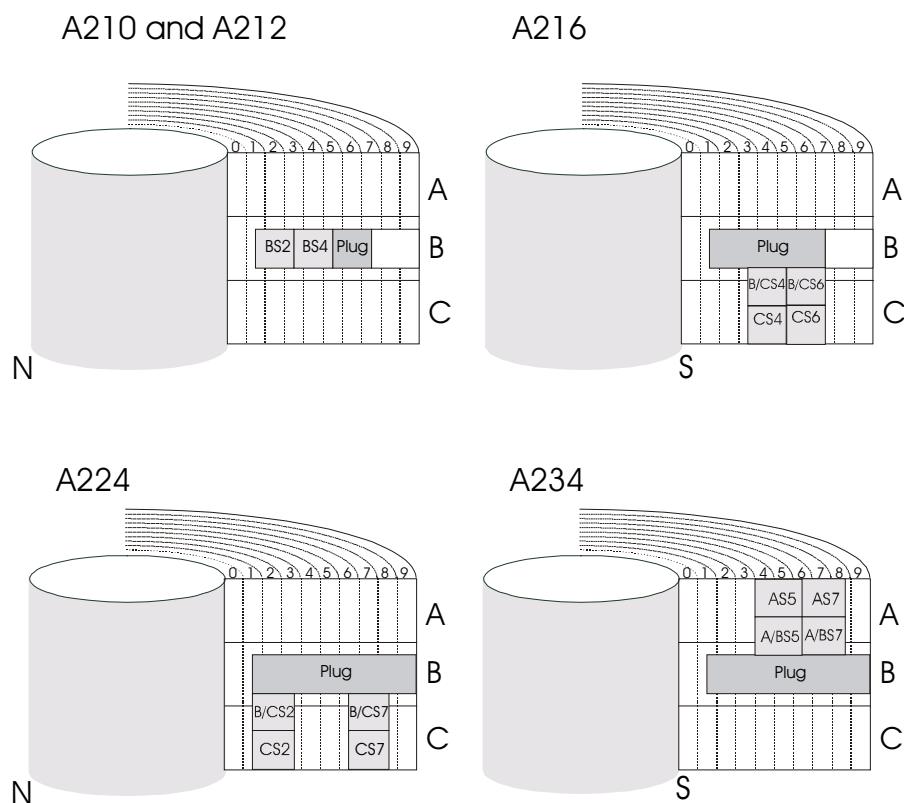


**Figure 9-30.** Sampled positions and sample nomenclature for the LOT A2 blocks 10, 12, 16, 24 and 34. Cylindrical bentonite plugs (Ø20 mm) with additives (10% calcite in 10, 10% gypsum in 12, 50% K-feldspar in 16 and cement in 24 and 34) were embedded in the B-level of the blocks.

**Table 9-8. Chemical composition of potassium feldspar used as additive in block 16, LOT A2.**

SiO <sub>2</sub>	Al <sub>2</sub> O <sub>3</sub>	Fe <sub>2</sub> O <sub>3</sub>	MgO	CaO	Na <sub>2</sub> O	K <sub>2</sub> O	TiO <sub>2</sub>	P <sub>2</sub> O <sub>5</sub>	MnO	Ba	Sr	Zr	LOI	Sum
%	%	%	%	%	%	%	%	%	%	ppm	ppm	ppm	%	%
64.2	18.7	0.42	0.01	0.37	2.74	12.6	<0.01	0.01	<0.01	124	39	7	0.9	100.1

### Methods

The analytical test protocol for the special blocks is summarized in Table 9-9. The samples have been analyzed for the same parameters as the standard blocks, i.e.:

- cation exchange capacity by exchange with Cu-triethylene tetramine,
- exchangeable cations by exchange with NH<sub>4</sub><sup>+</sup> in alcoholic solution,
- non-reactive solutes and soluble/sparingly soluble salts by aqueous leaching (s:l 1:100) followed by analysis with ICP-AES and IC. These analyses were applied for blocks 24 and 34 only,
- chemical composition of the bentonite using standard digestion techniques for silicates and analysis by ICP-AES (MS),
- carbon and sulfur by evolved-gas analysis using a Leco-furnace,
- mineralogy of the bentonite by X-ray diffraction analysis.

The methods applied are described in Section 9.2.1. Apart from block 10 and 12, both the bulk material and the clay fraction of the bentonite samples have been analyzed when relevant (cf. Table 9-9). Powders for the XRD analyses were stored at room temperature at ambient relative humidity.

## 9.3.2 Results

### **Block 10 with additive of CaCO<sub>3</sub> and block 12 with additive of CaSO<sub>4</sub>**

The inventory of calcite and gypsum is small (<1.5%) in the parent bentonite MX-80, but special attention is paid to these minerals because their solubility is temperature dependant. Under non-isothermal conditions with steep temperature gradient, dissolution and re-precipitation of these minerals can be expected to result in salt accumulations in the warmer parts of the buffer, which will affect the porosity and rheology of the bentonite. In the adverse-condition tests, the inventory of calcium carbonate and calcium sulfate had been increased by the addition of bentonite plugs containing 10% finely ground calcite and gypsum, respectively. The entire volume of block 10 and 12 has been exposed to temperatures exceeding 80°C and the sampled interval 1.5–5.5 cm from the heater to temperatures exceeding 100°C.

The chemical data on the bulk bentonite are listed in Table 9-11 (the samples have been analyzed in bulk only). Some selected parameters have been re-calculated on a molar, anhydrous basis (i.e. correction was made for LOI-(SO<sub>2</sub>+CO<sub>2</sub>)) to avoid artifacts that may arise due to variable water to solid mass ratio among the samples. The bar graph presented in Figure 9-31 shows the loss or gain in Ca, S and C relative to the average reference sample. Consistent with the trends displayed in the hot standard blocks, blocks 10 and 12 have gained sulfur at the two sampled positions. The increase in sulfur is paralleled by a more or less equivalent increase in calcium, whereas the carbon content is lower than the mean of the references. The maximum increase in S and Ca is found in sample 4 proximal to the gypsum plug in block 12. The S content of this sample is equivalent to 4% anhydrite, if all S is allocated to CaSO<sub>4</sub>.

The chemical data are supported by the XRD data which show that anhydrite has formed at all the sampled positions in block 10 and 12 (Figure 9-32 and Figure 9-33) but sample 4 proximal to the gypsum plug in block 12 is distinguished by very intense anhydrite peaks.

Calcite cannot be detected with certainty in any of the samples. In the XRD-profile of sample 4 proximal to the calcite plug in block 10, a peak of low intensity appears at the position where calcite has its most intense peak but cannot unambiguously be attributed to calcite.

**Table 9-9. Sample nomenclature and analytical test protocol for the special blocks with additives (10, 12, 16, 24 and 34) from the LOT A2 parcel.**

SICADA test code b=bulk;c=clay fraction Sample identity	Chemical analysis	Cation exchange capacity	Exchangeable cations	X-ray diffraction analysis		Aqueous leachates
	LA2EA b/c	LA2CEC b/c	LA2EC b	LA2XRD b/c random	oriented	LA2WA b
<b>Reference bentonite samples</b>						
A2(1-5)Rb	X	X	X	X		X
A2(1-5)Rc	X	X			X	
A211Rb	X	X	X	X		X
A211Rc	X	X			X	
A233Rb	X	X	X	X		X
A233Rc	X	X			X	
A224Rb	X	X	X	X		X
A224Rc		X			X	
A234Rb	X	X	X	X		X
A234Rc		X			X	
<b>Special block series</b>						
A210BS2b	X	X	X	X		
A210BS4b	X	X	X	X		
A212BS2b	X	X	X	X		
A212BS4b	X	X	X	X		
A216B/CS4b	X	X	X	X		
A216B/CS4c	X	X			X	
A216B/CS6b	X	X	X	X		
A216B/CS6c	X	X			X	
A216CS4b	X	X	X	X		
A216CS4c	X	X			X	
A216CS6b	X	X	X	X		
A216CS6c	X	X			X	
A224B/CS2b	X	X	X	X		X
A224B/CS2c	X	X			X	
A224CS2b	X	X	X	X		X
A224CS2c	X	X			X	
A224B/CS7b	X	X	X	X		X
A224B/CS7c	X	X			X	
A224CS7b	X	X	X	X		X
A224CS7c	X	X			X	
A234A/BS5b	X	X	X	X		X
A234A/BS5c	X	X			X	
A234AS5b	X	X	X	X		X
A234AS5c	X	X			X	
A234A/BS7b	X	X	X	X		X
A234A/BS7c	X	X			X	
A234AS7b	X	X	X	X		X
A234AS7c	X	X			X	

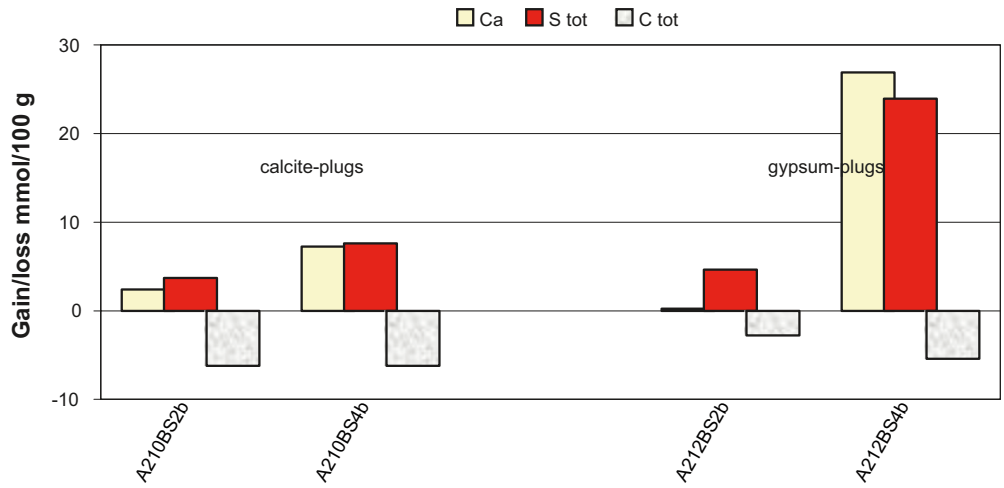


**Figure 9-31.** Bar graph showing the loss/gain (relative to the mean of the references) in total Ca, S and C in samples of blocks 10 and 12 from the LOT A2 parcel. Data are from Table 9-10 but have been re-calculated on a molar basis.

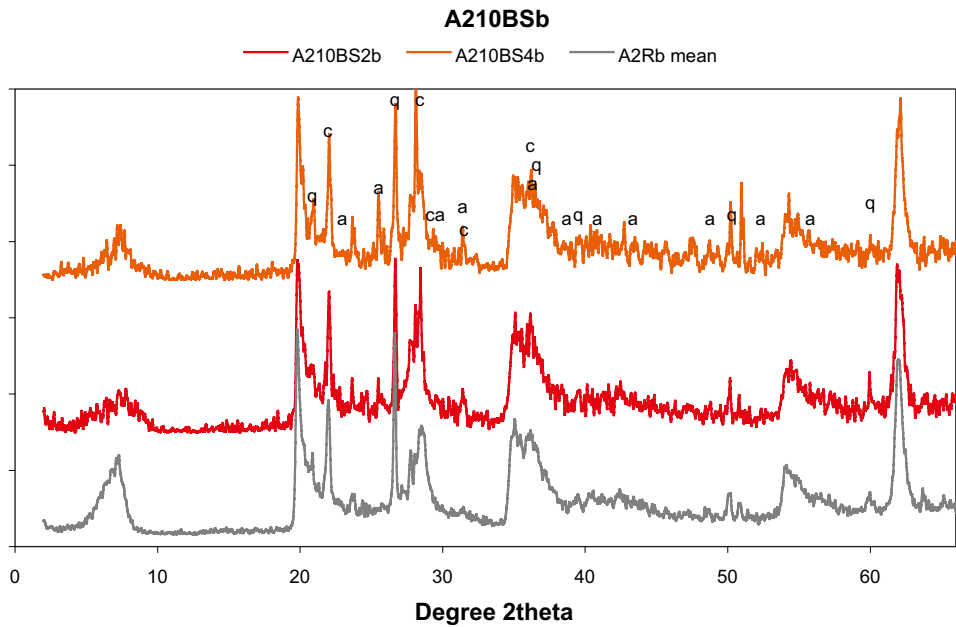


**Figure 9-32.** XRD-profiles of sample 2 (red) and 4 (orange) from block 10, with additive of calcite, of the LOT A2 parcel. Grey curve: mean XRD-profile of five reference samples. The position of the strongest peaks of the major non-clay minerals is indicated; q=quartz, c=cristobalite, a=anhydrite ( $\text{CaSO}_4$ ). The position of the strongest peak of calcite (ca) is also indicated. Random powder of bulk samples;  $\text{CuK}\alpha$  radiation.

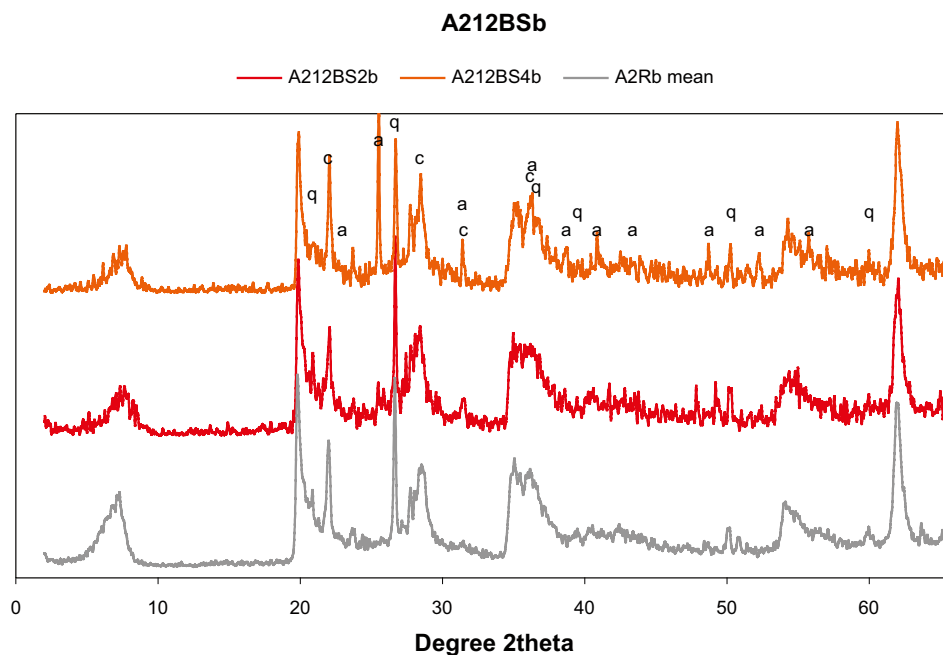


**Figure 9-33.** XRD-profiles of sample 2 (red) and 4 (orange) from block 12, with additive of gypsum, of the LOT A2 parcel. Grey curve: mean XRD-profile of five reference samples. The position of the strongest peaks of the major non-clay minerals is indicated; q=quartz, c=cristobalite, a=anhydrite (CaSO<sub>4</sub>). Random powder of bulk samples; CuK $\alpha$  radiation.

Data on the cation exchange capacity and the exchangeable cations are listed in Table 9-10 and have also been compiled in Figure 9-34. Sample 4, block 12 has the lowest CEC values, 76 cmol<sup>+</sup>/kg clay, which can be explained by the “dilution” of the bentonite with ca. 4% anhydrite. The CEC values of the rest of the samples range from 80 to 83 cmol<sup>+</sup>/kg clay, which is comparable to the mean CEC, 81 cmol<sup>+</sup>/kg clay, of the references.

All samples have essentially the same pool of exchangeable cations as the references, i.e. approximately 70% of the exchange sites are saturated with sodium and 20% with calcium. Exchangeable Mg is somewhat higher in the samples from block 10 and 12 (i.e. ca. 1–5 cm from the heater) than in the references, which is in harmony with the trend displayed in the hot standard blocks, where exchangeable Mg increases with increasing temperature.

Although the available data for block 12 are for two samples only, it seems clear that calcium sulfate has been redistributed from the plug with gypsum towards the warmer, inner part of the block. Re-precipitation (as anhydrite) has increased the sulfur content of the bentonite volume (2×2×2 cm; contact surface removed) proximal to the plug by a factor 3–4 compared to the reference bentonite. A lowering of the CEC value at this position can be explained by the “dilution” of the bentonite with anhydrite.

**Table 9-10.** Exchangeable cations and mean Cu-CEC (cmol<sup>+</sup>/kg dry matter) of blocks 10 and 12 of the LOT A2 parcel. Data for the mean of five reference samples are also included. Cations extracted by exchange with NH<sub>4</sub><sup>+</sup> in alcoholic solution.

Sample id	Additive	Ca cmol <sup>+</sup> /kg	K cmol <sup>+</sup> /kg	Mg cmol <sup>+</sup> /kg	Na cmol <sup>+</sup> /kg	Sum cmol <sup>+</sup> /kg	Mean Cu-CEC cmol <sup>+</sup> /kg
LA210BS2b	calcite	17	1.5	7.1	56	82	80
LA210BS4b	calcite	17	1.5	6.8	56	81	80
LA212BS2b	gypsum	15	1.4	6.0	54	76	83
LA212BS4b	gypsum	17	1.4	7.0	54	80	76
LA2Rb-mean	ref	16	1.3	5.30	53	76	81

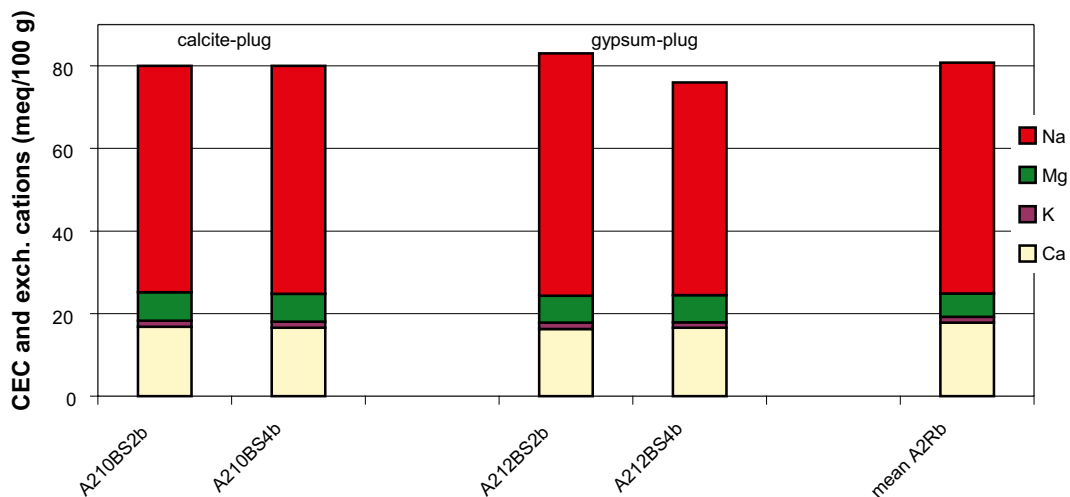


**Figure 9-34.** Bar graph showing the CEC and the relative distribution of exchangeable Na, K, Ca and Mg in samples from block 10 (additive of calcite) and 12 (additive of gypsum) of the LOT A2 parcel. The mean values of five reference samples shown to the right.

Based on the data for the two samples from the block with calcite plugs, it cannot be proved that calcium carbonate has been redistributed in a similar way as calcium sulfate. However, a sampling strategy that allows higher resolution may be necessary to verify the results.

#### **Block 16 with additive of K-feldspar**

One of the buffer alteration processes that has been considered in the long term test program is the smectite-to-illite transformation, which is believed to be accelerated by factors such as high potassium activity and elevated temperature. The entire volume of block 16 has been exposed to temperatures exceeding 80°C and the sampled interval to temperatures between 90 and 100°C.

The potassium content in the parent bentonite MX-80 is 0.53±0.02% K<sub>2</sub>O, the major sources being feldspars and mica/illite. In the adverse-condition test, the inventory of potassium was increased significantly by the addition of bentonite plugs containing 50% finely ground potassium feldspar with a K<sub>2</sub>O content of 12.65% (Table 9-9).

The chemical data on the bulk bentonite samples from block 16 (Table 9-11) indicate no significant change in the composition and the potassium content of the block samples is in the same range, 0.52 to 0.55% K<sub>2</sub>O, as that of the references. Those changes in the compositions that exist (in S and CaO) are consistent with the pattern of calcium sulfate redistribution observed in other hot blocks. The chemical data are supported by the XRD profiles of the bulk samples (Figure 9-35). Thus, anhydrite peaks appear in the sample with maximum S and CaO contents. The two samples from the least hot position 6 have a weak peak at the position of the most intense reflection of calcite, but the identification is uncertain since no other calcite reflections are detectable. The XRD-profiles display broad and indistinct first order basal reflections of the smectite (indicated by arrow in Figure 9-35). A probable explanation for this is that the re-hydration of the smectite was incomplete and variable due to the lack of strict control of humidity. As a consequence, smectite of mixed hydration states occur in the samples.

**Table 9-11. Chemical composition of the bulk bentonite samples from blocks with additives (block 10, 12, 16, 24 and 34) together with five reference samples of the LOT A2 parcel. Major and minor elements by ICP-AES, S and C by evolved gas analysis.**

Sample id	Additive	SiO <sub>2</sub> %	Al <sub>2</sub> O <sub>3</sub> %	Fe <sub>2</sub> O <sub>3</sub> %	MgO %	CaO %	Na <sub>2</sub> O %	K <sub>2</sub> O %	TiO <sub>2</sub> %	P <sub>2</sub> O <sub>5</sub> %	MnO %	Cr <sub>2</sub> O <sub>3</sub> %	LOI %	TOT/C %	TOT/S %	SUM %	Ni ppm	Sc ppm	Cu ppm	Zn ppm	Ba ppm	Co ppm	Nb ppm	Sr ppm	Ta ppm	Zr ppm	Y ppm	Ce ppm
A210BS2b	CaCO <sub>3</sub>	63.4	19.51	3.66	2.37	1.39	2.10	0.53	0.14	0.05	0.01	0.002	6.6	0.29	0.25	99.92	5	5	9	107	276	5	35	265	5	189	47	96
A210BS4b	CaCO <sub>3</sub>	63.3	19.39	3.63	2.31	1.65	2.12	0.53	0.15	0.05	0.01	0.003	6.8	0.29	0.37	100.06	5	6	7	132	361	5	35	393	5	191	46	107
A212BS2b	CaSO <sub>4</sub>	63.5	19.74	3.68	2.39	1.28	2.15	0.51	0.14	0.05	0.01	0.008	6.5	0.33	0.28	100.06	5	5	7	153	331	5	35	267	10	190	46	103
A212BS4b	CaSO <sub>4</sub>	62.0	19.00	3.50	2.24	2.70	2.00	0.50	0.14	0.05	0.01	0.004	7.6	0.30	0.87	99.93	5	5	6	110	331	5	37	516	5	187	44	104
A216B/CS4b	K-feldspar	62.9	19.41	3.76	2.25	1.45	2.10	0.54	0.14	0.05	0.01	0.001	7.2	0.36	0.18	99.92	<5	5	<10	80	446	<5	30	318	<20	197	43	84
A216CS4b	K-feldspar	62.9	19.23	3.73	2.26	1.35	2.07	0.55	0.14	0.05	0.01	0.009	7.5	0.34	0.10	99.92	12	5	<10	102	339	<5	26	283	<20	195	44	98
A216B/CS6b	K-feldspar	62.4	18.90	3.70	2.21	1.25	2.06	0.55	0.14	0.05	0.01	0.005	8.5	0.37	0.08	99.93	<5	5	<10	108	315	<5	36	246	<20	183	44	105
A216CS6b	K-feldspar	63.2	19.18	3.77	2.25	1.31	2.07	0.52	0.14	0.04	0.01	<0.001	7.4	0.36	0.09	100.06	6	5	12	88	339	<5	32	254	<20	192	43	80
A224B/CS2b	cement	63.6	19.45	3.57	2.34	1.28	2.08	0.5	0.14	0.04	0.01	0.003	6.9	0.38	0.26	100.06	5	5	72	134	282	5	32	304	6	194	46	104
A224CS2b	cement	63.6	19.71	3.64	2.31	1.32	2.12	0.52	0.14	0.05	0.01	0.001	6.5	0.38	0.21	100.07	5	5	63	86	295	5	36	309	5	194	46	105
A224B/CS7b	cement	63.4	19.78	3.71	2.34	1.26	2.19	0.52	0.14	0.04	0.01	0.001	6.5	0.39	0.17	100.06	5	5	6	106	312	5	35	263	5	191	47	109
A224CS7b	cement	63.8	19.70	3.63	2.26	1.26	2.12	0.53	0.14	0.04	0.01	0.001	6.4	0.41	0.18	100.07	5	5	8	91	311	5	36	298	6	186	45	98
A234A/BS5b	cement	61.8	19.27	3.63	3.48	1.57	2.20	0.54	0.14	0.05	0.01	0.006	7.3	0.42	0.16	100.07	5	5	5	118	290	5	32	265	5	189	45	94
A234AS5b	cement	63.8	19.58	3.64	2.16	1.42	2.13	0.51	0.14	0.04	0.01	0.002	6.5	0.39	0.19	100.07	5	5	12	76	296	5	39	293	5	194	45	98
A234A/BS7b	cement	61.9	19.12	3.51	3.58	1.87	2.18	0.55	0.14	0.05	0.01	0.001	7.0	0.42	0.15	100.05	5	5	10	115	309	5	35	258	5	190	45	103
A234AS7b	cement	63.0	19.55	3.64	2.20	1.47	2.16	0.52	0.14	0.05	0.02	0.001	7.2	0.43	0.19	100.06	5	5	9	107	308	6	35	277	5	187	46	107
A2(1-5)Rb	ref	63.5	19.03	3.81	2.38	1.35	2.08	0.55	0.15	0.06	0.01	0.005	7.2	0.38	0.26	100.08	7	5	4	76	442	1	28	289	3	206	46	130
A211Rb	ref	62.8	19.01	3.70	2.30	1.27	2.06	0.51	0.14	0.05	0.01	0.002	8.2	0.36	0.26	100.1	5	5	4	69	240	1	27	270	3	185	47	129
A224Rb	ref	63.4	19.68	3.70	2.39	1.17	2.14	0.51	0.14	0.05	0.01	0.001	6.6	0.37	0.13	99.93	<5	6	<10	74	258	<5	32	275	<20	192	45	94
A233Rb	ref	63.7	19.13	3.74	2.35	1.30	2.09	0.53	0.15	0.05	0.01	0.001	7.1	0.34	0.28	100.1	5	5	4	82	257	1	29	276	3	200	47	135
A234Rb	ref	64.1	19.28	3.64	2.33	1.21	2.09	0.53	0.14	0.04	0.01	0.002	6.4	0.37	0.14	99.93	<5	5	<10	103	395	<5	33	287	<20	187	44	90
<i>Reference mean</i>		<i>63.50</i>	<i>19.23</i>	<i>3.72</i>	<i>2.35</i>	<i>1.26</i>	<i>2.09</i>	<i>0.53</i>	<i>0.14</i>	<i>0.05</i>	<i>0.01</i>	<i>0.002</i>	<i>7.10</i>	<i>0.36</i>	<i>0.21</i>	<i>100.0</i>		<i>5.2</i>		<i>81</i>	<i>318</i>		<i>30</i>	<i>279</i>		<i>194</i>	<i>46</i>	<i>115</i>

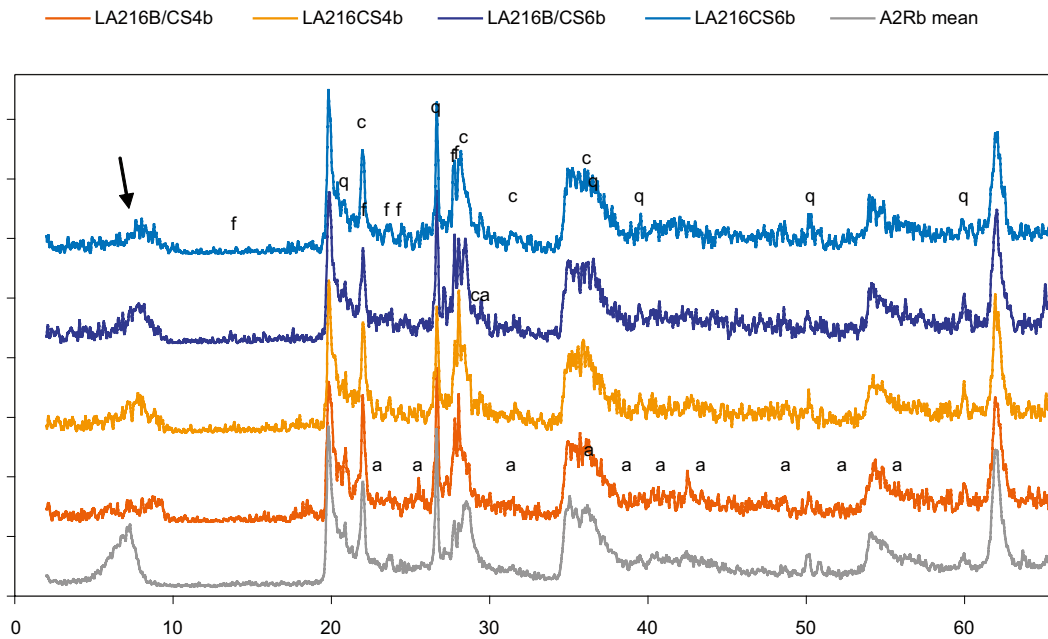


**Figure 9-35.** XRD-profiles of samples 4 and 6 from block 16 (with additive of K-feldspar) of the LOT A2 parcel. Grey curve: mean XRD-profile of five reference samples. The position of the strongest peaks of the major non-clay minerals is indicated; f=feldspar, q=quartz, c=crystalite, a=anhydrite (CaSO<sub>4</sub>). The position of the strongest peak of calcite (ca) is also indicated. Arrow indicates the normal position of the first order basal reflection of smectite (discussed in the text). Random powder of bulk samples; CuK $\alpha$  radiation.

Both the cation exchange capacity of the bulk samples and the composition of the pool of exchangeable cations (Table 9-12 and Figure 9-36) suggest that the exchange properties of the bentonite from block 16 are essentially the same as those of the reference samples.

The <2  $\mu\text{m}$  fractions of the samples from block 16 have – irrespective of the position relative the feldspar plug – a slightly higher potassium content (ca. 0.02–0.04% higher) compared to other hot blocks and compared to the references (Table 9-13 and Table 9-6). Potassium in the clay fraction probably exists mainly in a non-exchangeable form since the clay was saturated with sodium prior to the chemical analysis. Mica/illite and feldspars are the only potassium-bearing minerals that have been identified in MX-80 bentonite but their quantities in the <2  $\mu\text{m}$  fraction are below the detection limit of the XRD-method, as shown by the XRD-traces in Figure 9-37 and Figure 9-38.

**Table 9-12. Exchangeable cations and mean Cu-CEC (cmol<sup>+</sup>/kg dry matter) of bulk samples from block 16 (additive of K-feldspar) of the LOT A2 parcel. Data for the mean of five reference samples are also included. Cations extracted by exchange with NH<sub>4</sub><sup>+</sup> in alcoholic solution.**

Sample ID	Additive	Ca cmol <sup>+</sup> /kg	K cmol <sup>+</sup> /kg	Mg cmol <sup>+</sup> /kg	Na cmol <sup>+</sup> /kg	Sum cmol <sup>+</sup> /kg	Mean Cu-CEC cmol <sup>+</sup> /kg
LA216B/CS4b	K-feldspar	18	1.4	6.6	53	79	78
LA216CS4b	K-feldspar	16	1.3	5.5	52	75	80
LA216B/CS6b	K-feldspar	19	1.4	6.0	54	80	78
LA216CS6b	K-feldspar	17	1.3	5.4	53	77	79
LA2Rb-mean		16	1.3	5.30	53	76	81

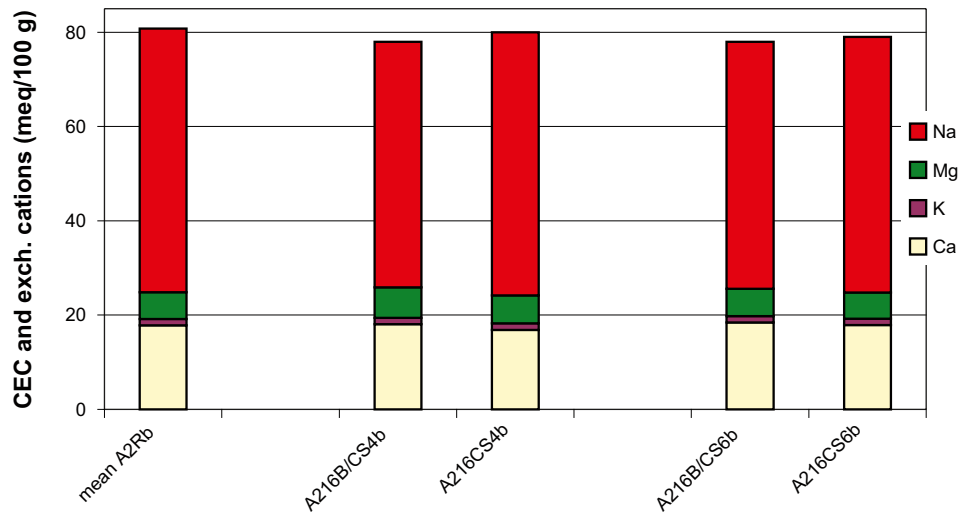


**Figure 9-36.** Bar graph showing the CEC (meq/100 g dry matter) and the relative distribution of exchangeable Na, K, Ca and Mg in samples from block 16 (additive of K-feldspar) of the LOT A2 parcel. The mean of five reference samples is shown to the left.

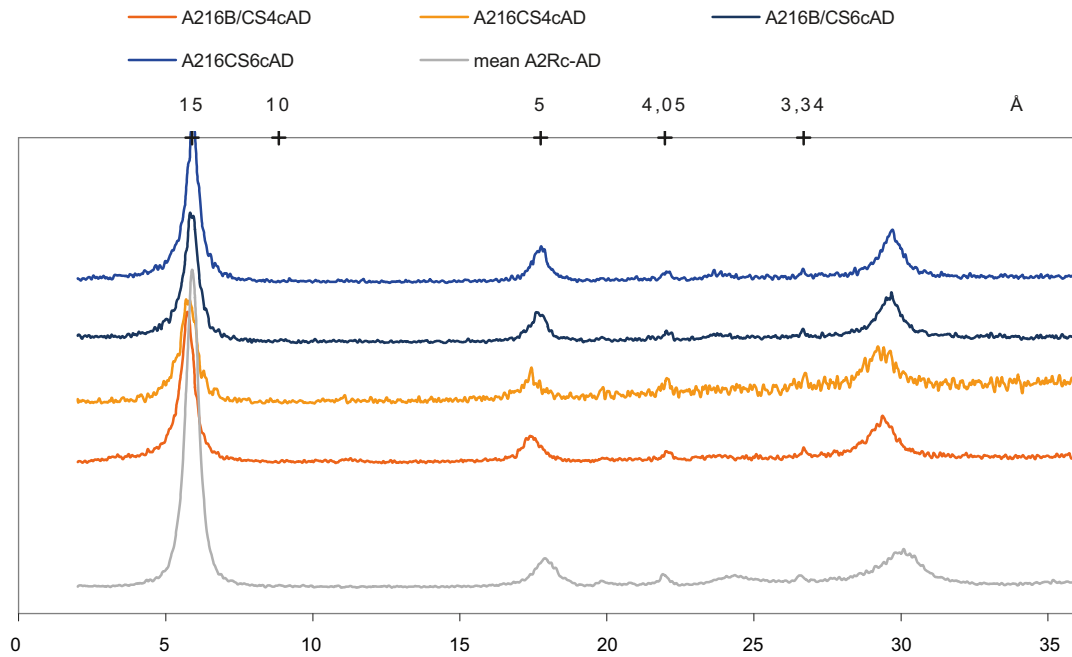


**Figure 9-37.** XRD-profiles of oriented aggregates of the Mg-saturated, air-dried (AD) clay fraction of samples of block 16 (additive of K-feldspar) from the LOT A2 parcel. Grey curve: Mean XRD-profile of the clay fraction of five reference samples. The positions of the strongest peaks of cristobalite (4.05 Å), quartz (3.34 Å) and mica/illite (10 Å) are indicated in the upper scale.; CuK $\alpha$  radiation.

**Table 9-13. Chemical composition of the Na-saturated <2 µm fraction of samples from blocks with additives (block 16 with K-feldspar, 24 and 34 with cement) together with three reference samples for the LOT A2 parcel. Major and minor elements by ICP-AES (minor elements in reference samples by ICP-MS, which explains differences in detection limits), S and C by evolved gas analysis.**

Sample id	SiO <sub>2</sub> %	Al <sub>2</sub> O <sub>3</sub> %	Fe <sub>2</sub> O <sub>3</sub> %	MgO %	CaO %	Na <sub>2</sub> O %	K <sub>2</sub> O %	TiO <sub>2</sub> %	P <sub>2</sub> O <sub>5</sub> %	MnO %	Cr <sub>2</sub> O <sub>3</sub> %	LOI %	TOT/C %	TOT/S %	SUM %	Ba ppm	Cu ppm	Zn ppm	Ni ppm	Co ppm	Sr ppm	Zr ppm	Ce ppm	Ta ppm
A216B/CS4c	63.60	20.48	3.76	2.35	0.28	2.23	0.13	0.13	0.02	<.01	0.001	6.9	0.20	<.01	99.95	33	<10	67	<5	5	22	149	111	<20
A216CS4c	64.69	20.33	3.72	2.32	0.07	2.35	0.13	0.13	0.02	<.01	<.001	6.1	0.21	0.01	99.92	37	<10	34	<5	<5	21	150	120	<20
A216CS4c-2	64.66	20.49	3.77	2.33	0.07	2.35	0.14	0.13	0.03	<.01	<.001	5.9	0.22	<.01	99.93	35	<10	35	<5	<5	21	153	93	<20
A216B/CS6c	64.88	20.83	3.72	2.34	0.06	2.37	0.12	0.13	0.02	<.01	<.001	5.4	0.21	<.01	99.93	25	<10	32	6	<5	<20	152	82	<20
A216CS6c	64.47	20.44	3.76	2.33	0.10	2.30	0.12	0.13	0.02	<.01	0.002	6.2	0.19	<.01	99.93	25	<10	53	<5	<5	20	151	81	<20
A224B/CS2c	63.02	20.43	3.64	2.37	0.03	2.37	0.08	0.13	0.02	<.01	0.001	7.8	0.24	<.01	99.93	17	21	32	<5	<5	<20	149	69	<20
A224CS2c	64.28	20.80	3.66	2.36	0.04	2.40	0.08	0.13	0.03	<.01	<.001	6.1	0.26	0.01	99.93	17	22	38	7	<5	<20	148	84	<20
A224B/CS7c	64.51	20.69	3.77	2.39	0.03	2.33	0.10	0.13	0.02	<.01	<.001	5.9	0.33	<.01	99.93	23	10	30	<5	<5	<20	154	97	<20
A224CS7c	64.09	20.36	3.67	2.32	0.03	2.34	0.10	0.13	0.03	<.01	<.001	6.8	0.28	<.01	99.92	19	23	29	<5	<5	<20	154	92	<20
A234A/BS5c	64.21	20.52	3.61	2.49	0.03	2.37	0.10	0.13	0.03	<.01	<.001	6.4	0.27	<.01	99.93	18	<10	22	<5	<5	<20	145	92	<20
A234AS5c	64.61	20.48	3.58	2.35	0.02	2.29	0.10	0.13	0.03	<.01	<.001	6.3	0.33	<.01	99.94	21	15	22	<5	<5	<20	148	96	<20
A234A/BS7c	64.26	20.39	3.64	2.53	0.02	2.29	0.09	0.13	0.02	<.01	<.001	6.5	0.34	<.01	99.91	16	13	20	<5	<5	<20	146	98	<20
A234AS7c	64.72	20.40	3.57	2.33	0.03	2.27	0.11	0.13	0.03	<.01	<.001	6.3	0.28	<.01	99.94	21	<10	23	<5	<5	<20	149	94	<20
A2(1-5)Rc	64.06	21.06	3.56	2.36	0.03	2.18	0.08	0.12	0.03	0.01	0.001	6.4	0.39	0.01	99.93	14	11	27	5	5	13	146	91	5
A211Rc	64.17	20.85	3.62	2.34	0.04	2.21	0.11	0.13	0.03	0.01	0.001	6.5	0.27	0.01	100.1	29	39	32	5	5	15	151	110	6
A233Rc	63.78	21.40	3.67	2.34	0.04	2.21	0.10	0.13	0.03	0.01	0.001	6.3	0.28	0.01	100.1	36	38	35	5	5	13	153	105	5
A233Rc-2	63.88	21.23	3.64	2.35	0.04	2.26	0.11	0.13	0.03	0.01	0.001	6.2	0.27	0.01	99.93	37	41	34	5	5	13	154	89	5
<i>Reference mean</i>	<i>63.97</i>	<i>21.14</i>	<i>3.62</i>	<i>2.35</i>	<i>0.04</i>	<i>2.22</i>	<i>0.10</i>	<i>0.13</i>	<i>0.03</i>	<i>0.01</i>	<i>0.00</i>	<i>6.35</i>	<i>0.30</i>	<i>0.01</i>	<i>100.0</i>	<i>29</i>	<i>32</i>	<i>32</i>	<i>5</i>	<i>5</i>	<i>13.5</i>	<i>151</i>	<i>99</i>	<i>5</i>

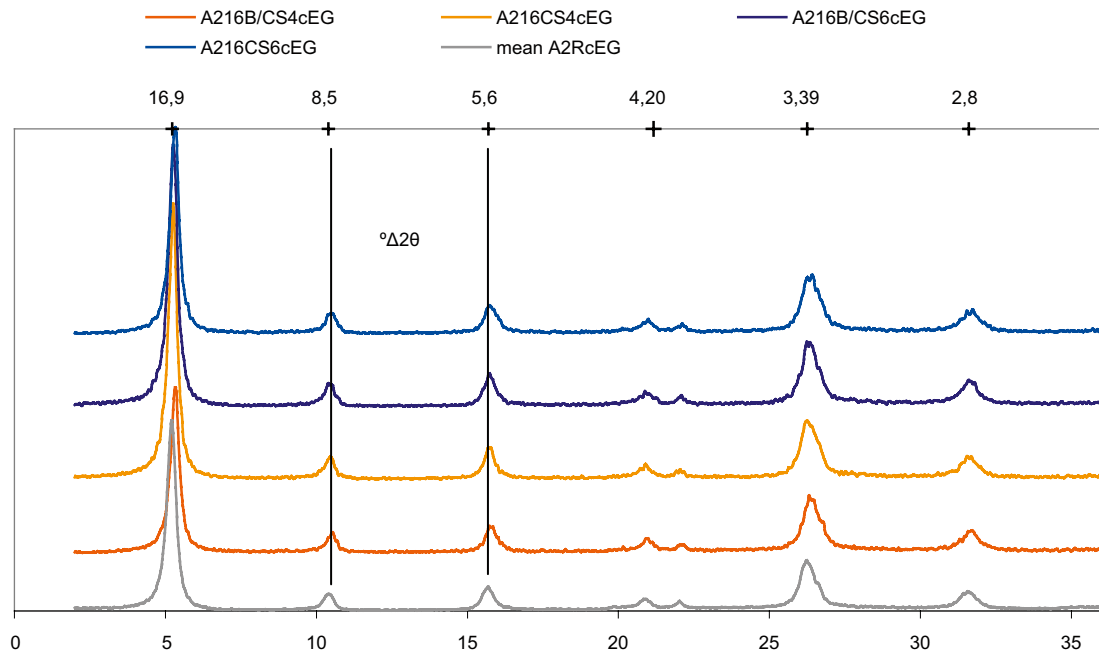


**Figure 9-38.** XRD-profiles of oriented aggregates of the Mg-saturated, ethylene glycol solvated (EG) clay fraction of samples of block 16 (additive of K-feldspar) from the LOT A2 parcel. Grey curve: mean XRD-profile of the clay fraction of five reference samples. The rational series of smectite reflections is indicated in the upper scale. The measure  $^{\circ}\Delta 2\theta$  is also indicated (cf. text). CuK $\alpha$  radiation.

A mixed-layering of the smectite with illitic layers is an alternative source of potassium and if significant enough, mixed-layering will affect the X-ray diffraction characteristics of the clay. The homo-ionic Mg-clays of both block samples and references have a basal spacing of ca. 15 Å when air-dried (relative humidity 50±10%) and expand to 16.9 Å upon ethylene glycol solvation (EG) (Figure 9-37 and Figure 9-38). A close-up of the expanded (001) basal reflections is presented in Figure 9-39. The series of basal reflections of the smectite and the parameter  $\Delta 2\theta_{002/003}$  (the difference between the (002) and (003) peaks in degrees 2 $\theta$ ) are indicated in Figure 9-38. Both the rationality of the basal reflections and a  $\Delta 2\theta_{002/003}$  value ranging from 5.24 to 5.28 indicate a smectite with virtually no interstratification /Moore and Reynolds 1989/. Thus, the diffraction characteristics give no evidence that the illitic component has increased in block 16. On the other hand, a potassium content of 0.13% K<sub>2</sub>O corresponds to ca. 2% illitic layers at most. Such small a proportion of illitic layers in an I/S structure may not be detectable by routine XRD analysis.

An increase of the fixed interlayer potassium content would also affect the exchange properties of the clay mineral. As shown in Table 9-14 the CEC values of the clay fractions of samples from block 16 are in the same range as that of the references, but, again, the effect of a gain of less than 0.05% K<sub>2</sub>O on CEC can probably not be detected in any conventional CEC determination.

### **Blocks 24 and 34 with additive of cement**

In fresh cement, extreme pH conditions will develop due to the presence of alkali bases, but pH will stabilize around 12.5 supported by portlandite (Ca(OH)<sub>2</sub>) in the matured cement. The effects on bentonite of an exposure to these hyperalkaline pore fluids are well-documented /e.g. Karnland et al. 2007, Savage et al. 2007, Trotignon et al. 2007/ and involve dissolution of both the accessory minerals and the clay minerals, which eventually may change fundamental physical and chemical properties of the buffer

The two blocks 24 and 34 with plugs of Portland cement represent different temperature regimes. Block 24 has been exposed to intermediate temperatures (50–70°C) and the two sampled radial positions to temperatures in the range 50–60 and 60–70°C, respectively. The sampled positions in block 34 were never exposed to temperatures exceeding 30°C.

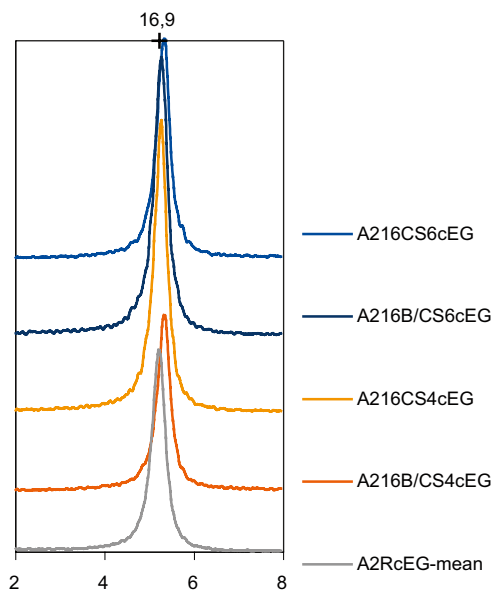


**Figure 9-39.** Close-up of the 17 Å region of EG-solvated, Mg-saturated clay fractions from block 16 of the LOT A2 parcel. Grey curve: Mean XRD-profile of the reference samples. CuK $\alpha$  radiation.

**Table 9-14. Cation exchange capacity (Cu-CEC) of the <2 µm fraction of samples from block 16 and of the reference samples for the LOT A2 parcel.**

Sample id	Cu-CEC 1 cmol <sup>+</sup> /kg	Cu-CEC 2 cmol <sup>+</sup> /kg	Mean Cu-CEC cmol <sup>+</sup> /kg
A216CS4c	87	88	88
A216B/CS4c	88	85	87
A216CS6c	89	88	88
A216B/CS6c	88	88	88
A2R(1–5)c	87	86	87
A211Rc	86	87	87
A224Rc	88	88	88
A233Rc	87	86	87
A234Rc	88	87	88
Mean reference			87

The content of soluble sulfate and chloride determined by dispersion of the bentonite in water (s:l 1:100) are given in Table 9-15 and illustrated in the bar graph in Figure 9-40. The corresponding data on the composition of the groundwater at Äspö can be found in Table 3-3. Focus is laid on the major anions chloride and sulfate since the concentrations of the cations are strongly affected by the exchange reactions that take place when cations are released from dissolving accessory minerals during the contact with water. In addition, a strong correlation between cations such as Al and Fe suggests that the source is suspended ultra-fine clay particles which the filtering method failed to remove from the solution.

**Table 9-15. Major anions (mg/g dry clay) extracted by dispersion of bentonite in deionised water in a solid:liquid ratio of 1:100. Data for blocks 24 and 34 from the LOT A2 parcel together with reference samples for the blocks.**

Sample id		S <sub>tot</sub>	Cl	NO <sub>3</sub> -N	SO <sub>4</sub> -S
		mg/g dry clay			
A224B/CS2b	cement	2.082	1.535	0.039	1.864
A224CS2b	cement	1.737	1.389	0.037	1.698
A224B/CS7b	cement	1.219	1.519	0.040	1.328
A224CS7b	cement	1.414	1.539	0.041	1.553
A234A/BS5b	cement	1.171	1.223	0.039	1.180
A234AS5b	cement	1.358	1.357	0.039	1.386
A234A/BS7b	cement	1.070	1.254	0.041	1.182
A234AS7b	cement	1.324	1.354	0.038	1.436
A224Rb	ref	1.008	0.124	0.042	1.128
A234Rb	ref	1.050	0.122	0.042	1.142

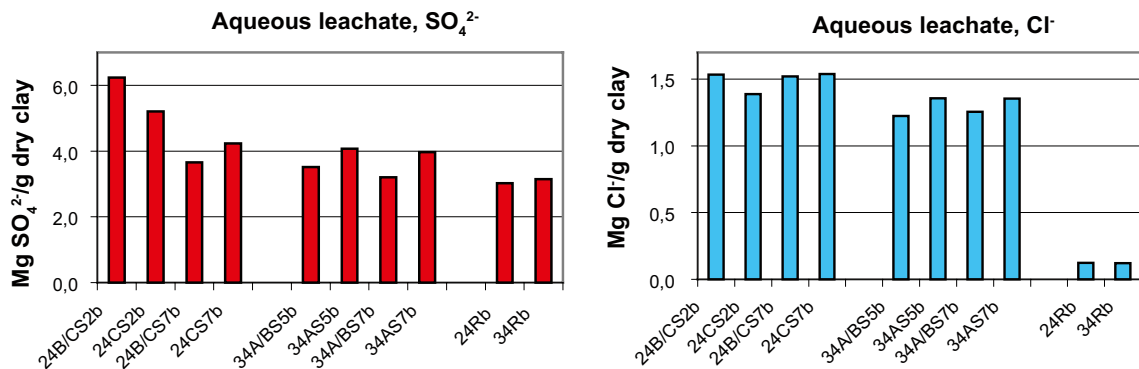


**Figure 9-40.** The concentration of Cl<sup>-</sup> and SO<sub>4</sub><sup>2-</sup> in water extracts of bulk samples from blocks 24 and 34 (additive of cement) of the LOT A2 parcel. Results for the reference samples for the blocks are shown to the right.

Consistent with the results for the standard blocks, the chloride concentration in the bentonite from blocks 24 and 34 has increased significantly due to the saturation with Äspö groundwater.

Also the sulfate distribution in the samples from block 24 and 34 appears to match the distribution pattern in the standard blocks. Thus, the sulfate concentration in the cool block 34 has changed little under the long-term-test conditions, whereas the bentonite 1.5–3.5 cm from the heater in block 24 has gained sulfate and thus appears to correspond to the “zone” of anhydrite precipitation observed in other hot standard blocks. This general pattern is confirmed by the data on total S in the bulk bentonite (Figure 9-41 and Table 9-11) but neither anhydrite nor any other Ca sulfates can be detected in the XRD traces of the samples (cf. Figure 9-42).

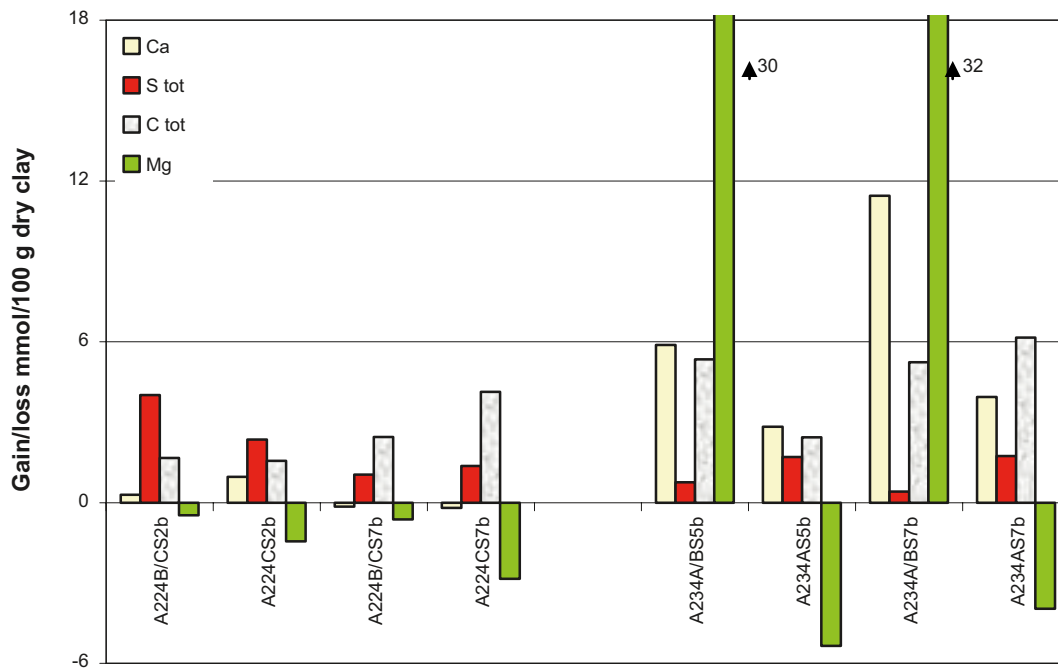


**Figure 9-41.** Bar graph showing the loss/gain relative to the mean reference in total Ca, Mg, S and C in bulk samples of blocks 24 and 34 (additive of cement) from the LOT A2 parcel.

Selected chemical data on the bulk samples (Table 9-11) have been re-calculated on a molar, water-free basis and compiled in the bar graph in Figure 9-41, which shows the loss/gain in Ca, Mg, S and C relative to the average reference sample. The most conspicuous alterations are seen in block 34, where both Ca and Mg have increased in the samples proximal to the cement plug, whereas the distal samples are depleted in Mg. Mg has most likely been supplied by dissolution of montmorillonite, which is the main source of Mg in the bentonite.

The samples have gained also some carbon, probably existing as a carbonate phase, but the balance between the cation-anion equivalents is poor, which suggests that other counter-ions, such as hydroxide, exist. Sample pH was not measured but a parallel study of the porewater composition in block 24 (see Appendix 5) demonstrates a clear gradient in pH from distal (relative the plug) to proximal positions, as can be expected.

XRD-traces of random powders of the bulk samples are presented in Figure 9-42. The XRD profiles of the contact samples from block 34 display a clear reduction in the peak intensities of cristobalite (marked by arrows in Figure 9-42), indicating dissolution. This is consistent with the results reported by /Karnland et al. 2007/ in an experimental study on the interaction of hyperalkaline solutions with compacted bentonite.

Mg-rich minerals like sepiolite, brucite and hydrotalcite have been reported as potential secondary products of the cement/bentonite interaction /e.g. Trotignon et al. 2007/, but no neoformed phases serving as sinks for magnesium have been identified with certainty. Several “new” reflections of low intensity appear in the XRD-traces of both blocks and some of these may be produced by cation-disordered, mixed carbonates, the d-values of which show an almost linear relation with composition. Tentatively, the strongest peaks of the magnesium end-member of Ca-Mg carbonates have been indicated in the trace of one of the contact samples from block 34 (Figure 9-42). It should also be emphasized that several of the potential reaction products of the interaction of cement pore fluids with bentonite (e.g. calcium silicate hydrates, CSH) tend to be X-ray amorphous due to poor crystallinity.

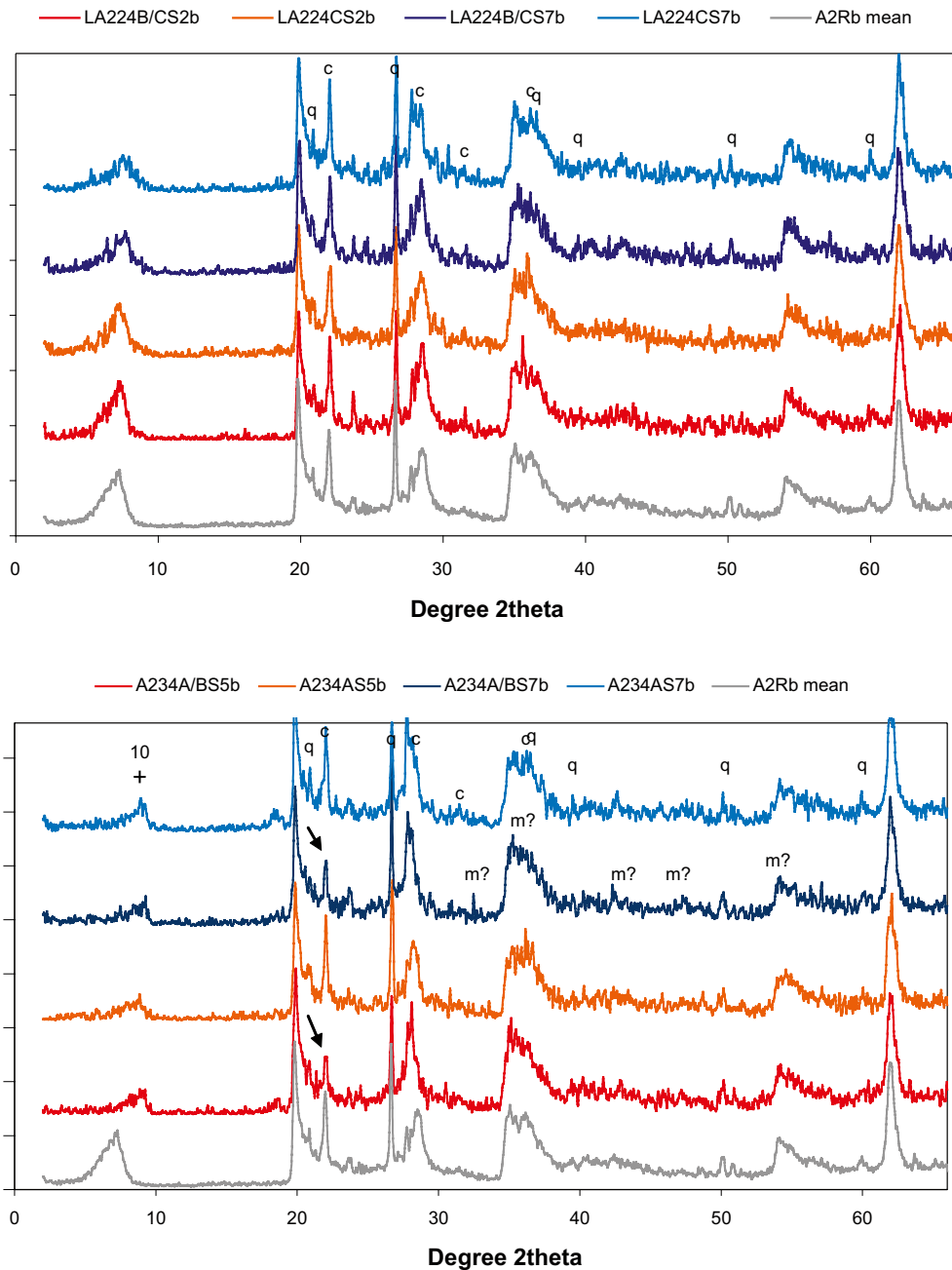


**Figure 9-42.** XRD-profiles of samples from block 24 (top) and 34 (bottom) of the LOT A2 parcel. Grey curve: mean XRD-profile of five reference samples. The position of the strongest peaks of the major non-clay minerals are indicated; q=quartz, c=cristobalite. Arrows indicate the strongest peak of cristobalite (cf. text). The position of the strongest peaks of magnesium carbonate (m?) is also indicated (cf. text). Random powder of bulk samples; CuK $\alpha$  radiation.

Data on the cation exchange capacity of the bulk samples and the exchangeable cations are listed in Table 9-16 and have also been compiled in Figure 9-43. All bulk samples from block 24 and 34 have CEC values that are 2–4 units lower than the mean reference sample. The composition of the pool of exchangeable cations has changed in both blocks but evolved differently. Exchangeable Mg has increased in block 24, whereas an increase of exchangeable Ca is paralleled by a decrease in Mg in block 34.

The low concentration of exchangeable Mg in block 34 suggests that porewater concentrations were controlled by the precipitation of some Mg-bearing phase(s) of low solubility. It is evident from the chemical composition of the <2 µm fraction (Table 9-13) that the Mg content of the clay fraction from the proximal positions remains augmented despite the pre-treatments prior to the chemical analysis (i.e. removal of carbonates, saturation by Na and dialysis). The source of this extra Mg has not been identified.

**Table 9-16. Exchangeable cations and mean Cu-CEC (cmol<sup>+</sup>/kg dry matter) of bulk samples from blocks 24 and 34 (additive of cement) of the LOT A2 parcel. The mean of five reference samples are also included. Cations extracted by exchange with NH<sub>4</sub><sup>+</sup> in alcoholic solution.**

Sample ID	Additive	Ca cmol <sup>+</sup> /kg	K cmol <sup>+</sup> /kg	Mg cmol <sup>+</sup> /kg	Na cmol <sup>+</sup> /kg	Sum cmol <sup>+</sup> /kg	Mean Cu-CEC cmol <sup>+</sup> /kg
LA224B/CS2b	cement	15	1.5	6.8	58	81	78
LA224CS2b	cement	14	1.4	6.3	56	78	77
LA224B/CS7b	cement	15	1.4	6.9	56	80	78
LA224CS7b	cement	15	1.4	6.8	58	81	78
LA234A/BS5b	cement	21	1.5	2.1	58	83	78
LA234AS5b	cement	18	1.4	2.3	54	76	78
LA234A/BS7b	cement	24	1.5	2.6	58	86	79
LA234AS7b	cement	20	1.4	2.4	53	77	79
LA2Rb-mean		16	1.3	5.30	53	76	81

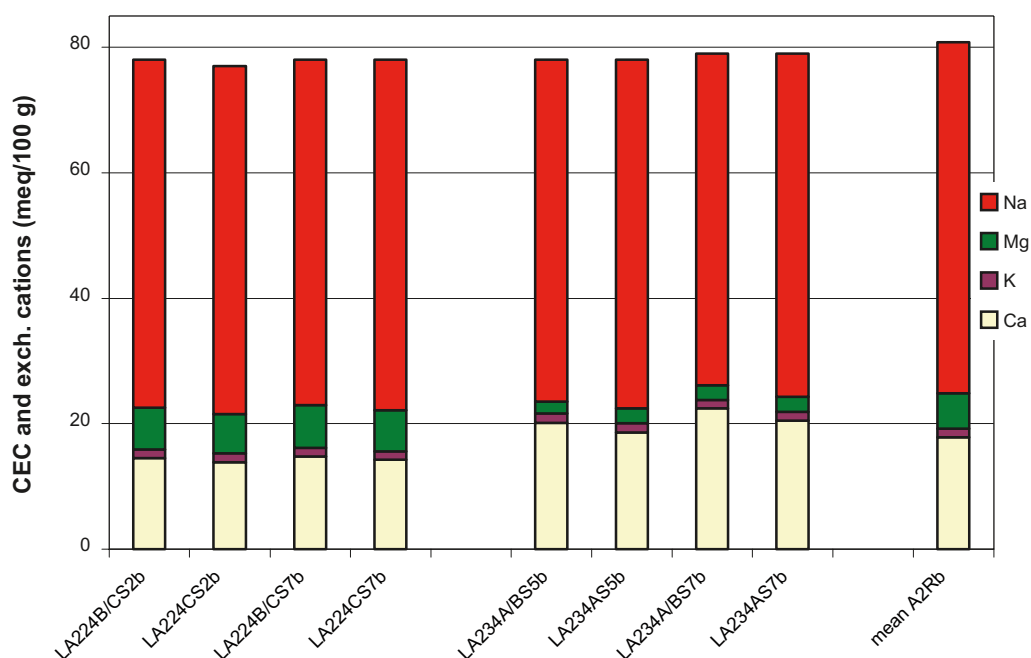


**Figure 9-43.** Bar graph showing the CEC and the relative distribution of exchangeable Na, K, Ca and Mg in samples from blocks 24 and 34 (additive of cement) of the LOT A2 parcel.

XRD-profiles of oriented mounts of the air-dried and EG-solvated clay fractions are shown in Figure 9-45 to Figure 9-48 and a close-up of the expanded first order peak is shown in Figure 9-44. The diffraction patterns of the air-dried samples from the blocks match the basic features of the pattern of the reference, but the higher order basal reflections of the two contact samples from block 34 are broader and somewhat displaced (Figure 9-47). Both peak broadening and peak displacement may be indications of mixed-layering or small crystallite size. However, the EG-solvated clays (Figure 9-44 and Figure 9-48) produce a rational series of basal reflections and the expansion behavior and d-values are essentially the same as those of the reference, indicating a more or less pure smectite.

The relative peak intensities are anomalous in some of the samples from both blocks 24 and 34 (compare, for instance, A224B/C2c and A224B/C7c). The relative intensities of the  $00l$  reflections are not only controlled by chemical composition and the positions of atoms in the unit cell, but they are also affected by properties of the sample preparation (primarily by the degree of preferred orientation of the clay minerals). Variations in preferred orientation may arise, for instance, if samples are not equally well dispersed by the pre-treatments applied.

The CEC of the  $<2 \mu\text{m}$  fractions (Table 9-17) is generally lower than the CEC of the reference samples. The contact samples from block 34 are exceptions from the trend, having higher CEC than the references. A diminished “dilution” by cristobalite due to dissolution may explain some of the increase in CEC, but more detailed analyses will be required to identify other alteration processes that may have contributed to the increase in charge. The observation reported by /Karland et al. 2007/ that increasing CEC values were connected to an increased tetrahedral charge, i.e. to a beidelitization of the montmorillonite, may be relevant also in the LOT A2 context.

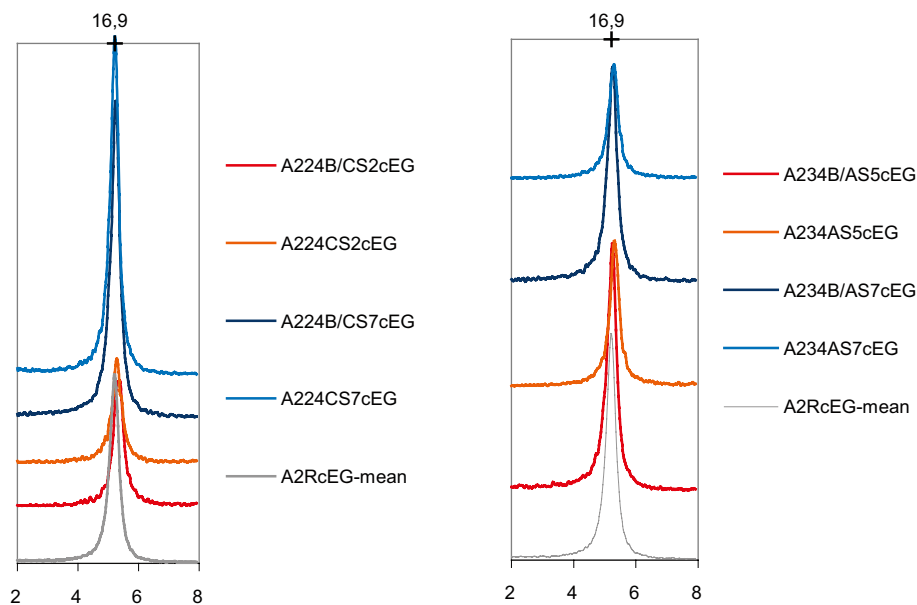


**Figure 9-44.** Close-up of the  $17 \text{ \AA}$  region of EG-solvated, Mg-saturated clay fractions from block 24 and 34 (additive of cement) of the LOT A2 parcel. Grey curve: Mean XRD-profile of the reference samples.  $\text{CuK}\alpha$  radiation.

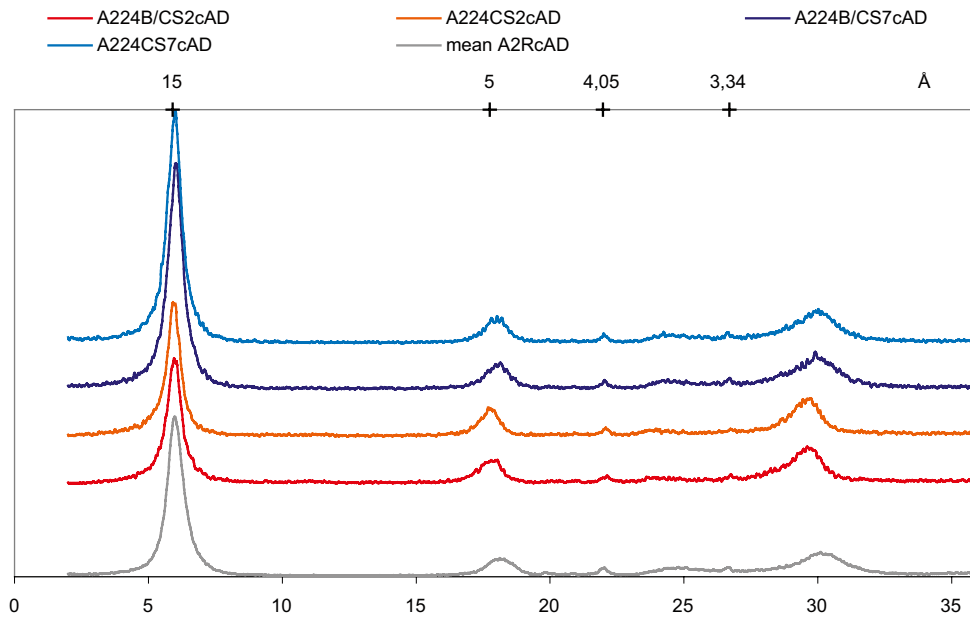


**Figure 9-45.** XRD-profiles of oriented mounts of the Mg-saturated, air-dried clay fraction of samples of block 24 (additive of cement) from the LOT A2 parcel. Grey curve: mean XRD-profile of the clay fraction of five reference samples. The positions of the strongest peaks of cristobalite (4.05 Å), quartz (3.34 Å) are indicated in the upper scale. CuK $\alpha$  radiation.

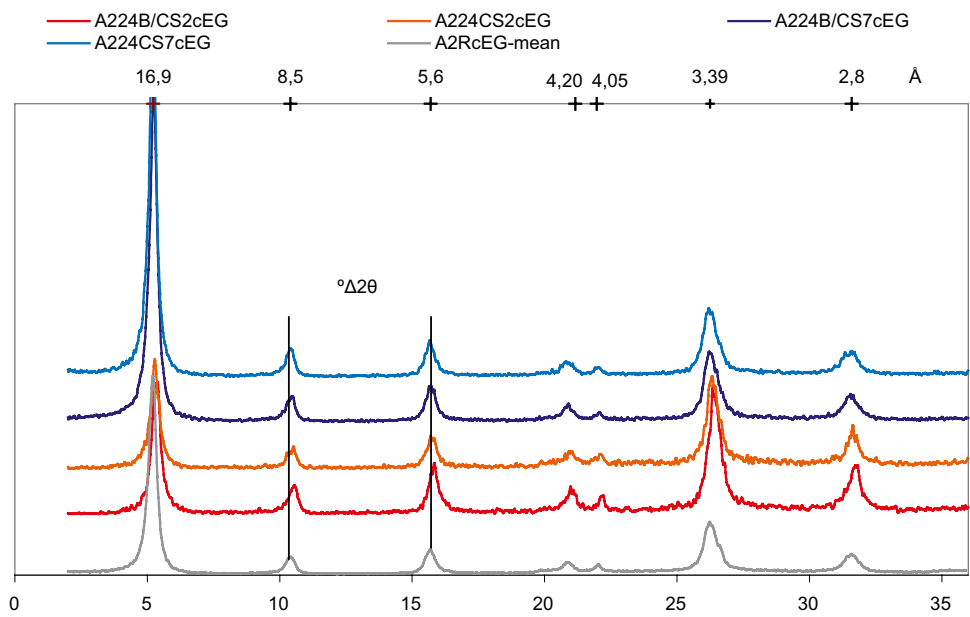


**Figure 9-46.** XRD-profiles of oriented mounts of the Mg-saturated, ethylene glycol solvated clay fraction of samples of block 24 (additive of cement) from the LOT A2 parcel. Grey curve: mean XRD-profile of the clay fraction of five reference samples. The rational series of smectite reflections is indicated in the upper scale together with the position of the strongest peak of cristobalite (4.05 Å). The measure  $^{\circ}\Delta 2\theta$  is also indicated (cf. text). CuK $\alpha$  radiation.

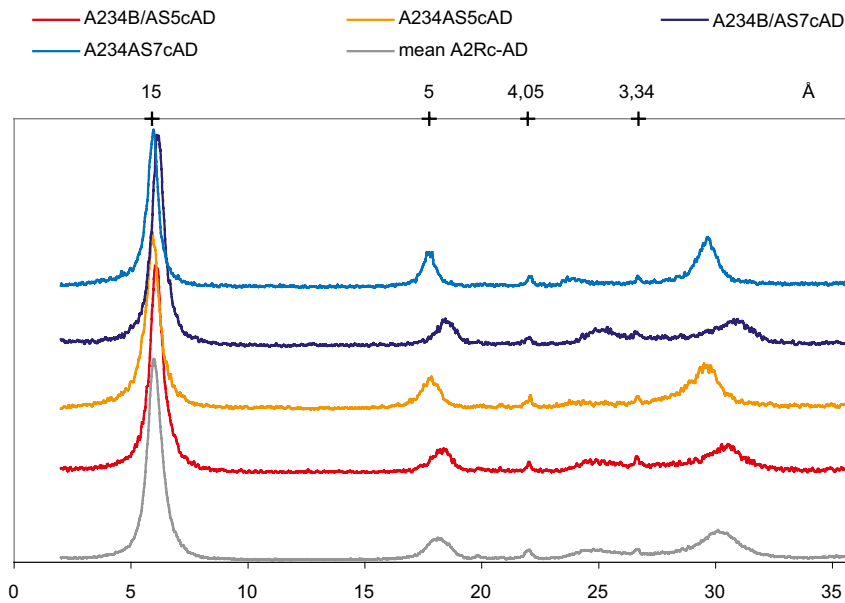


**Figure 9-47.** XRD-profiles of oriented aggregates of the Mg-saturated, air-dried clay fraction of samples of block 34 (additive of cement) from the LOT A2 parcel. Grey curve: Mean XRD-profile of the clay fraction of five reference samples. The positions of the strongest peaks of cristobalite (4.05 Å) and quartz (3.34 Å) are indicated in the upper scale. CuK $\alpha$  radiation.

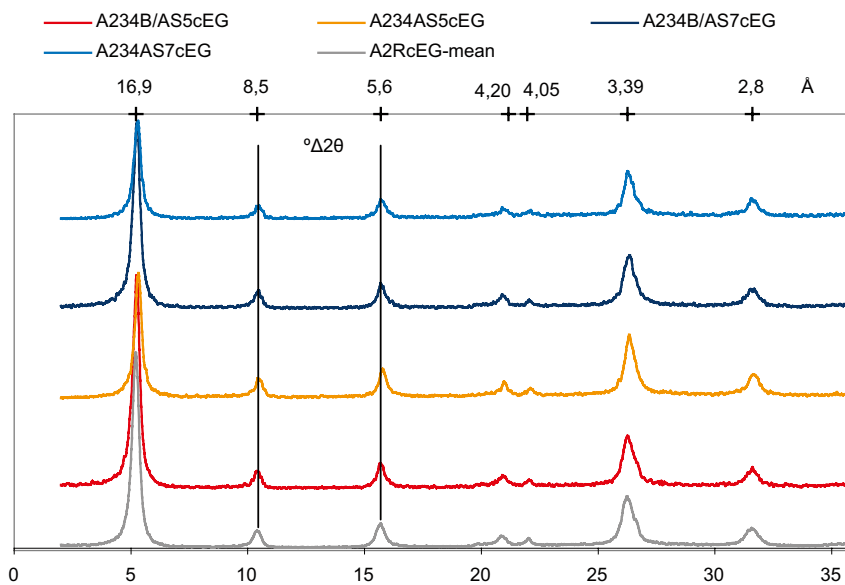


**Figure 9-48.** XRD-profiles of oriented aggregates of the Mg-saturated, ethylene glycol solvated clay fraction of samples of block 34 (additive of cement) from the LOT A2 parcel. Grey curve: Mean XRD-profile of the clay fraction of five reference samples. The series of smectite reflections is indicated in the upper scale together with the position of the strongest peak of cristobalite (4.05 Å). The measure  $^{\circ}\Delta 2\theta$  is also indicated. CuK $\alpha$  radiation.

**Table 9-17. Cation exchange capacity (cmol<sup>+</sup>/kg dry matter) of the <2 μm fraction of samples from block 24 and 34 with additive of cement from the LOT A2 parcel. The mean of the reference samples for the A2 parcel is included.**

Sample id	Cu-CEC 1 cmol <sup>+</sup> kg <sup>-1</sup>	Cu-CEC 2 cmol <sup>+</sup> kg <sup>-1</sup>	Mean Cu-CEC cmol <sup>+</sup> kg <sup>-1</sup>
A224CS2c	84	84	84
A224B/CS2c	84	84	84
A224CS7c	83	82	83
A224B/CS7c	83	81	82
A234AS5c	84	85	84
A234A/BS5c	91	92	92
A234AS7c	No data	No data	No data
A234A/BS7c	91	91	91
A2Rc-mean			87

### 9.3.3 Summary and conclusions

The mineralogy and chemical composition of bentonite samples from five blocks (blocks 10, 12, 16, 24 and 34) with additives of calcite, gypsum, K-feldspar and cement, respectively, have been studied. The major conclusions of the study are:

- Calcium sulfate has been redistributed from the gypsum plug along the thermal gradient and accumulated as anhydrite in the warmer, inner part of the block. The re-precipitation has increased the sulfur content in the bentonite volume proximal to the plug by a factor 3–4 compared to the reference bentonite.
- The data for two positions in block 10 with calcite plugs provide no evidence that calcium carbonate has been redistributed in a similar way as calcium sulfate. However, the low spatial sampling resolution may have missed minor redistribution of the carbonate.
- The addition of K-feldspar to the bentonite of block 16 seems to have had no effect on any of the clay properties investigated. Thus, the exchange properties and the exchange complex as well as the X-ray diffraction characteristics of the clay from the block are essentially the same as those of the references.
- The two blocks with cement plugs (24 and 34) represent different temperature regimes, but an influence on mineralogy is seen in the vicinity of the cement plugs in both blocks: the XRD data indicate cristobalite dissolution in the samples proximal to the cement; Ca and Mg have increased in the same samples, whereas the samples distal to the cement plug are depleted in Mg; the proportion of divalent exchangeable cations has increased in both blocks, mainly Mg in the warm block and Ca in the cold block; the clay fraction of the contact samples from block 34 are distinguished also by higher CEC than the references.

## References

- Abercrombie H J, Hutcheon I E, Bloch J D, de Caritat P, 1994.** Silica activity and the smectite-to-illite reaction. *Geology*, v. 22, 539–542
- Ammann L, Bergaya F, Lagaly G, 2005.** Determination of the cation exchange capacity of clays with copper complexes revisited. *Clay Minerals* 40, 441–453.
- Belyayeva N I, 1967.** Rapid method for the simultaneous determination of the exchange capacity and content of exchangeable cations in solonchic soils. *Soviet Soil Science*, 1409–1413.
- Birgersson M, Karnland O, 2009.** Ion equilibrium between montmorillonite interlayer space and an external solution – Consequences for diffusional transport. *Geochim. Cosmochim. Acta* (2009), doi:10.1016/j.gca.2008.11.027
- Boles J R, Frank S G, 1979.** Clay diagenesis in the Wilcox Sandstones of southwest Texas. *J. Sed. Petrol.* 49, 55–70.
- Brindley G W, Brown G, 1980.** Crystal Structures of Clay Minerals and their X-ray Identification. Mineralogical Society Mon. No. 5. 495 p.
- Börgesson L, Johannesson L-E, Sandén T, Hernelind J, 1995.** Modelling of the physical behaviour of water saturated clay barriers. SKB TR-95-20, Svensk Kärnbränslehantering AB.
- Börgesson L, Hernelind J, 1999.** Coupled thermo-hydro-mechanical calculations of the water saturation phase of a KBS-3 deposition hole. Influence of hydraulic rock properties on the water saturation phase. SKB TR-99-41, Svensk Kärnbränslehantering AB.
- Börgesson L, Johannesson L-E, Hernelind J, 2003.** Earthquake induced rock shear through a deposition hole. Effect on the canister and the buffer. SKB TR-04-02, Svensk Kärnbränslehantering AB.
- Couture R A, 1985.** Steam rapidly reduces the swelling capacity of bentonite. *Nature* 318, 50–52.
- Eberl D D, Velde B, McCormic T, 1993.** Synthesis of illite-smectite from smectite at earth surface temperatures and high pH. *Clay Minerals* 28, 49–60.
- Hower J, Eslinger E V, Hower M E, Perry E A, 1976.** Mechanism of burial metamorphism of argillaceous sediments. *Geol.Soc. Amer. Bull.* 87, 725–737.
- Huang W-L, Longo J M, Pevear D R, 1993.** An experimentally derived kinetic model for smectite-to-illite conversion and its use as a geothermometer. *Clays and Clay Minerals* 41, 162–177.
- Hökmark H, Fälth B, 2003.** Thermal dimensioning of the deep repository. SKB TR-03-09, Svensk Kärnbränslehantering AB.
- Jackson M L, 1975.** Soil chemical analysis – advanced course. Second edition. Madison, Wisconsin, 991 p.
- Johannesson L-E, Börgesson L, Sandén T, 1995.** Compaction of bentonite blocks. SKB TR-95-19, Svensk Kärnbränslehantering AB.
- Karnland O, Sandén T, Johannesson L-E, Eriksen T E, Jansson M, Wold S, Pedersen K, Motamedi M, Rosborg B, 2000.** Long term test of buffer material. Final report on the pilot parcels. SKB TR-00-22, Svensk Kärnbränslehantering AB.
- Karnland O, Birgersson M, 2006.** Montmorillonite stability. With special respect to KBS-3 conditions. SKB TR-06-11, Svensk Kärnbränslehantering AB.
- Karnland O, Olsson S, Nilsson U, 2006.** Mineralogy and sealing properties of various bentonites and smectite-rich clay materials. SKB TR-06-30, Svensk Kärnbränslehantering AB.
- Karnland O, Olsson S, Nilsson U, Sellin P, 2007.** Experimentally determined swelling pressure and geochemical interactions of compacted Wyoming bentonite with highly alkaline solutions. *Physics and Chemistry of the Earth* 32, 275–286.

- Karnland O, Olsson S, Sandén T, Fälth B, 2009 in press.** Long Term Test of Buffer Material at the Äspö HRL (LOT project) – Final report on the A0 test parcel. SKB TR-09-31, Svensk Kärnbränslehantering AB.
- Laaksoharju M, Smellie J, Nilsson A-C, Skårman C, 1995.** Groundwater sampling and chemical characterisation of the Laxemar deep borehole KLX02. SKB TR-95-05, Svensk Kärnbränslehantering AB.
- Meier L P, Kahr G, 1999.** Determination of the cation exchange capacity (CEC) of clay minerals using the complexes of copper(II) ion with triethylenetetramine and tetraethylenepentamine. *Clays and Clay Minerals* 47, 386–388.
- Moore D M, Reynolds R C, 1989.** X-ray Diffraction and the Identification and Analysis of Clay Minerals. Oxford University Press. 332 p.
- Newman A C D, Brown G, 1987.** The Chemical Constitution of Clays. In Newman, A.C.D. (ed): *Chemistry of Clays and Clay Minerals*. Mineralogical Society Mon. No. 6. 1–128.
- Pedersen K, Motamedi M, Karnland O, 1995.** Survival of bacteria in nuclear waste buffer materials. The influence of nutrients, temperature and water activity. SKB TR 95-27, Svensk Kärnbränslehantering AB.
- Perry E A, Hower J, 1970.** Burial diagenesis in Gulf Coast pelitic sediments. *Clays and Clay Minerals* 18, 165–178.
- Pusch R, Karnland O, Lajudie A, Lechelle J, Bouchet A, 1993.** Hydrothermal field test with French candidate clay embedding steel heater in the Stripa mine. SKB TR-93-02, Svensk Kärnbränslehantering AB.
- Savage D, Walker C, Arthur R, Rochelle C, Oda C, Takase H, 2007.** Alteration of bentonite by hyperalkaline fluids. A review of the role of secondary minerals. *Physics and Chemistry of the Earth* 32, 287–297.
- Slaughter M, Early J W, 1965.** Mineralogy and Geological Significance of the Mowry Bentonites, Wyoming. *Geol.Soc. Am. Spec. Pap.*, 83.
- Trotignon L, Devallois V, Peycelon H, Tiffreau C, Bourbon X, 2007.** Predicting the long term durability of concrete engineered barriers in a geological repository for radioactive waste. *Physics and Chemistry of the Earth* 32, 259–274.
- Weaver C E, 1959.** The clay petrology of sediments. *Clays and Clay Minerals* 6, 154–187.
- Wersin P, Bruno J, Spahiu K, 1993.** Kinetic modelling of bentonite-canister interaction. Implications for Cu, Fe and Pb corrosion in a repository for spent nuclear fuel. SKB TR-93-16, Svensk Kärnbränslehantering AB.
- Wersin P, Spahiu K, Bruno J, 1994.** Kinetic modelling of bentonite-canister interaction. Long-term predictions of cooper canister corrosion under oxic and anoxic conditions. SKB TR-94-25, Svensk Kärnbränslehantering AB.

## **Microbiological analyses**

Karsten Pedersen

Microbial Analytics Sweden AB and Göteborg University

Department of Cell and Molecular Biology

# 1 Sammanfattning

”Long term test of buffer material” (LOT) är en försöksserie som startades upp vid Äspö Hard Rock Laboratory (HRL) 1996. Där testas modeller och hypoteser angående stabiliteten av bentonitbufferten som skall användas vid ett eventuellt KBS-3 slutförvar av kärnbränsle. I LOT-försöken har ett antal kopparcylindrar med värmare placerats i block av bentonit och värmts till en temperatur av 90 °C. LOT-försöket inkluderar även så kallade A-försök under förhöjd temperatur (130 °C), för att accelerera de processer som kan anses skadliga för bentoniten. Det LOT-försök som undersökts i denna studie, försök A2, placerades ut 1999 (värmens slogs på i februari 2000), och avslutades i januari 2006 (värmens stängdes av i december 2005).

En del skadliga processer i bentoniten kan orsakas av mikrober. I denna rapport beskrivs mikrobiologiska analyser vad gäller totalt 20 punkter i bentoniten i toppen (block 38) och mitten (block 19–20) av LOT-paket A2. Detta paket har lagrats fem–sex år nere i berget i Äspötunneln runt en 130 °C varm kopparvärmare sedan starten av LOT-försöket. Genom att odla bakterier från bentoniten i specifika medier kunde följande bakteriella parametrar undersökas: Det totala antalet av odlingsbara heterotrofa aeroba mikroorganismer, sulfatreducerande bakterier och bakterier som producerar det organiska ämnet acetat (acetogener). Även ATP innehåll i bentoniten bestämdes. Dessutom odlades bakterier från bentoniten upp i syrefritt sulfatreducerarmedium. I dessa kulturer undersöktes närvaro av de biologiskt producerade ämnena sulfid och acetat, eftersom dessa potentiellt kan ha negativ inverkan på kopparkapseln i ett KBS-3 slutförvar. Resultaten jämfördes till viss del med data över densitet, temperatur och vatteninnehåll från Clay Technology AB. Resultaten visade att det fanns viabla sulfatreducerande och acetogena bakterier i storleksordningen  $10^0$ – $10^2$  och odlingsbara aeroba bakterier i storleksordningen  $10^3$ – $10^5$  g<sup>-1</sup> bentonit efter fem år nere i berget, så länge temperaturen och densiteten inte varit för hög och/eller vatteninnehållet för lågt. Mikroorganismer med flera olika morfologier kunde hittas i kulturerna med bentonit.

När förekomsten av bakterier undersöks i bentoniten är det viktigt att den provtas på rätt sätt. Syre är giftigt för många bakterier som lever i syrefria miljöer, däribland sulfatreducerande bakterier. För att utesluta att antalet av dessa bakterier underskattas är det viktigt att inte syre tränger in i bentoniten. Därför slussades bentoniten in i en box med syrefri atmosfär kort efter provtagning. En annan faktor som kan ge underskattade resultat är uttorkning. Genom att svepa in bentoniten i steril aluminiumfolie och plasta in den skyddades bentoniten mot detta. Samtidigt skyddades den även från kontaminering av bakterier från omgivningen. Protokollen för provtagning fungerade tillfredsställande. Det var möjligt att provta bentoniten sterilt, vilket kunde visas genom att det inte växte i alla bentonitprover utan bara i de prover där bakterierna överlevde de omgivande förhållandena i bentoniten under lagringen i A2 paketet. Att sulfatreducerande bakterier växte i odlingsmediet visar att bentoniten provtogs under syrefria förhållanden.

## 2 Abstract

”Long term test of buffer material” (LOT) is a series of experiments which was initiated at Äspö Hard Rock Laboratory (HRL) in 1996, where hypotheses and models regarding the stability of bentonite buffer in a possible KBS-3 repository for nuclear waste are tested. In the LOT experiments a number of copper canisters with heaters have been placed in blocks with bentonite and heated to a temperature of 90°C. The LOT experiments also include so-called A-tests where the temperature in the copper canister heater has been elevated to 130°C to accelerate the processes that are harmful to the bentonite buffer. The LOT parcel investigated in this study, parcel A2, was put in place in 1999 (heating turned on in February 2000) and retrieved in January 2006 (heating turned off in December 2005).

Some harmful processes in the bentonite can be caused by bacteria. In this report, the bacterial analyses regarding 20 sample points in the bentonite at the top (block 38) and middle (block 19–20) of the LOT A2 parcel are described. This parcel has been stored underground in the Äspö tunnel around a 130°C warm heater since the start of the LOT experiments five–six years ago. By culturing bacteria from the bentonite in specific media the following bacterial parameters could be examined: The total amount of culturable heterotrophic aerobic bacteria, sulphate-reducing bacteria, and bacteria that produce the organic compound acetate (acetogens). The ATP content in the bentonite was also determined. In addition, bacteria from the bentonite were cultured in different sulphate-reducing media. In these cultures, the presence of the biotic compounds sulphide and acetate was investigated, since these have potentially negative effect on the copper canister in a KBS-3 repository. The results were to some extent compared to density, water content, and temperature data provided from Clay Technology AB. The results showed that  $10^0$ – $10^2$  viable sulphate-reducing and acetogenic bacteria and  $10^3$ – $10^5$  heterotrophic aerobic bacteria  $g^{-1}$  bentonite were present after five years of storage in the rock, as long as the ambient temperature and density have not been too high, or the water content in the bentonite too low. Bacteria with several morphologies could be found in the cultures with bentonite.

When the presence of bacteria in the bentonite is investigated, it is important that the sample procedures are accurate. Oxygen is toxic to many of the bacteria that thrive in anaerobic groundwater, among them sulphate-reducing bacteria. To avoid underestimation of the number of sulphate-reducing bacteria in the bentonite it is important to exclude oxygen during sampling. Therefore, the bentonite was put in an anaerobic chamber shortly after sampling. Another factor that gives underestimated results is desiccation. By wrapping the bentonite in sterile aluminium foil and plastic bags it was possible to avoid this. The aluminium foil also served as protection against contamination of bacteria from the surroundings. The sampling procedures worked accurately. It was possible to sample the bentonite under sterile conditions, which was proved by the fact that bacteria only grew where the ambient conditions during storage in the A2 parcel allowed this. Presence of sulphate-reducing bacteria proved that the bentonite was sampled without intrusion of oxygen in levels toxic to these organisms.

## 3 Methods

### 3.1 Sampling of bentonite from the LOT A2 parcel

#### *Sampling*

The bentonite from the LOT A2 parcel was sampled according to AP TD F62-06-010. Presence of bacteria was investigated in bentonite from the middle and top part of the LOT A2 parcel in the blocks 19–20 and 38, respectively. These two bentonite blocks were wrapped in sterile aluminium foil and placed in the anaerobic box (COY Laboratory Products, Grass Lake, MI, USA) immediately after sampling. Inside the box, a triplicate of bentonite pieces of approximately 1–2 g each was collected by means of a hammer, a sterile chisel and a sterile knife. Triplicates in one cm intervals from each block were collected at a distance of 0–9 cm from the copper surface.

#### *Preparation of enrichment culture media and inoculation*

Bacteria from the bentonite were enriched in anaerobic growth media supplied with sulphate. Two types of sulphate-reducing enrichment media were produced; One medium with an organic carbon and energy source and one with inorganic carbon and energy sources. Both media contained a basal salt solution ( $l^{-1}$  milli-Q water); 7 g NaCl, 1 g  $CaCl_2 \times H_2O$ , 0.67 g KCl, 1 g  $NH_4Cl$ , 0.15 g  $KH_2PO_4$ , 0.5 g  $MgCl_2 \times 6H_2O$ , 3 g  $MgSO_4 \times 6H_2O$ . The salt solution was autoclaved and cooled under a  $N_2/CO_2$  (80/20%) atmosphere for 1 h. After that the following solutions were added: 10 ml trace element solution, 60 ml 1M  $NaHCO_3$  solution, 10 ml yeast extract solution, 10 ml vitamin solution, 1 ml thiamine solution, 1 ml vitamin  $B_{12}$  solution, 5 ml iron stock solution, 2 ml resazurin solution, 10 ml cysteine-HCl solution, and 10 ml  $Na_2S$  solution. Five ml of 50% lactate solution ( $l^{-1}$  milli-Q water) was added to the anaerobic enrichment media with organic energy and carbon source. The pH was set to 6.5–7.5 and the medium was added in 45 ml aliquots to  $N_2/CO_2$  (80/20%) filled 120-ml serum flasks sealed with butyl rubber stoppers. The serum flasks and an additional set of sterile rubber stoppers were placed in an anaerobic box.

The serum flasks were opened inside the box and 1 g bentonite pieces from each sample point were put in the anaerobic media with and without lactate, respectively. The serum flasks were resealed with new stoppers and removed from the anaerobic box. To the cultures without lactate,  $H_2/CO_2$  at 2 bars above atmospheric pressure (80/20%) was added as energy and carbon source. The enrichment cultures were left in room temperature overnight for the bentonite to disperse in the medium. After that they were vigorously shaken and incubated at 30°C for six weeks.

#### *Sampling of bentonite for ATP determination*

The third piece from each sampling point was put in a sterile 50-mL Falcon tube for ATP analysis. The tube was removed from the anaerobic box and 10 ml of B/S extraction solution (BioThema AB, Handen, Sweden), a releasing agent for intracellular ATP, was added. The bentonite was dispersed overnight in the extraction solution and frozen at  $-20^\circ C$  until analysis.

### 3.2 Presence of bacteria in the bentonite from the LOT A2 parcel

The microbial metabolites sulphide and acetate was analysed in the enrichment cultures after six weeks of incubation. The enrichment cultures were also analysed with microscopy to examine the presence of bacteria and confirm that the metabolites were of biotic origin.

#### *Microscopy*

The supernatants from the enrichment cultures were diluted 20 times in sterile water and 0.1 ml were filtered onto 0.2  $\mu m$  pore size filters stained black (Osmonics, Minnetonka, MN, US) and stained with acridine orange ( $10 \text{ mg } l^{-1}$ ) for 7 min. Bacteria on the filters were observed in an inverted microscope (Nikon Diaphot 300, Teknootik AB, Göteborg, Sweden) at 1,000 times magnification using blue light (390–490 nm) and photographed.

### ***Sulphide analysis***

The sulphide concentration was determined in enrichment cultures with lactate and H<sub>2</sub>/CO<sub>2</sub> according to /Widdel and Bak 1992/. Approximately 1 ml of the supernatant from each enrichment culture was carefully withdrawn with an anaerobic syringe and needle and 0.1 ml was added to 2 ml of 5 mM CuSO<sub>4</sub>. If sulphide was present in the sample, a brown precipitate (CuS) was formed. The absorbance of the solution was measured spectrophotometrically (Genesys 10 UV, Thermo electron corporation, Waltham, MA, USA) at λ 480 nm and the concentration was determined with an external standard curve. Sulphide is reported if bacteria were present in the cultures. The background in medium without growth was approximately 40 mg l<sup>-1</sup>.

### ***Acetate analysis***

The acetate concentration was determined in the enrichment cultures with H<sub>2</sub>/CO<sub>2</sub>. A sample from the supernatant from each enrichment culture was carefully withdrawn with an anaerobic syringe and needle. The acetate concentration in the supernatant in the bentonite enrichment cultures was determined spectrophotometrically with a kit (Boehringer Mannheim, Mannheim, Germany) which detects acetate by an enzymatic method. Acetate is reported if bacteria were present in the cultures. The background in medium without growth was approximately 6 mg l<sup>-1</sup>.

## **3.3 Enumeration of bacteria from the bentonite in the LOT A2 parcel**

As mentioned above, the enrichment cultures were left at room temperature overnight after inoculation to allow the bentonite to disperse in the medium. After dispersion of the bentonite, the enrichment cultures were used as inocula for analysis of the number of viable culturable heterotrophic aerobic bacteria (CHAB) originating from the bentonite, as well as most probable number (MPN) of sulphate-reducing bacteria (SRB) and autotrophic acetogens (AA).

### ***Culturable heterotrophic aerobic bacteria (CHAB)***

In the CHAB analysis 0.1 ml from each of the enrichment cultures was spread on a triplicate of agar plates, which contained (l<sup>-1</sup> milliQ water); peptone 0.5 g, yeast extract 0.5 g, starch 0.25 g, Na-acetate 0.25 g, CaCl<sub>2</sub> x 2H<sub>2</sub>O 0.2 g, K<sub>2</sub>HPO<sub>4</sub> 0.1 g, NaCl 10 g, trace metal solution 1 ml, agar 15 g. After one week of incubation at room temperature the number of colonies was counted. The mean and the standard deviation for the plates from both enrichment cultures from each sample point were calculated.

### ***MPN analysis of sulphate-reducing bacteria (SRB)***

In the MPN analysis of SRB 1 ml of the original enrichment cultures were inoculated into five Hungate tubes with the sulphate-reducing media with lactate. After six weeks of incubation, the sulphide concentration in the MPN tubes were determined as described above. Tubes with three times as high sulphide concentrations compared to the medium with no growth were regarded as growth positive. MPN of SRB with 99% confidence levels according to Cornish and Fischer were calculated using a computer program described in /Klee 1993/.

### ***MPN analysis of autotrophic acetogens (AA)***

In the MPN analysis of AA 1 ml of the original enrichment cultures were inoculated into five Hungate tubes with sulphate-reducing media added with H<sub>2</sub>/CO<sub>2</sub> but with the exclusion of 3 g MgSO<sub>4</sub>×6H<sub>2</sub>O. After six weeks of incubation, the acetate concentration in the MPN tubes were determined as described above. Tubes with three times as high acetate concentrations compared to medium with no growth were regarded as growth positive. MPN of AA with 99% confidence levels according to Cornish and Fischer were calculated using a computer program described in /Klee 1993/.

### **3.4 ATP content in the bentonite in the LOT A2 parcel**

The ATP in the approximately 1 g of wet bentonite was extracted with 10 ml of B/S extraction solution and frozen until analysis. At the time for analysis, the samples were thawed and the bentonite/B/S extraction solution slurry was left to sediment whereupon the ATP content in the clear liquid over the sedimented bentonite was analysed. The ATP Biomass Kit HS for determining total ATP in living cells was used (no. 266-311; BioThema, Handen, Sweden). This analysis kit was developed based on the results of /Lundin et al. 1986/ and /Lundin 2000/. The ATP biomass method used in this work has been described, tested in detail and evaluated for use with Fennoscandian groundwater, including Olkiluoto groundwater /Eydal and Pedersen 2007/ However, the bentonite interfered with the ATP analysis. Therefore, a calibration curve of ATP measurements with B/S extraction solution, bentonite (1 g/10 ml) and five different known amounts of ATP was prepared and compared to B/S extraction solution with the same ATP amounts but without bentonite. Using this calibration curve, the measurements in the bentonite samples were translated to the corresponding ATP amounts without the bentonite interference.

## 4 Results and evaluation

### 4.1 Sampling

Figure A1-1 schematically shows where the bentonite samples for microbiological analysis from the LOT A2 parcel (Figure A1-1) were extracted. Samples were taken from block 38 on the top of the A2 parcel (called TOP LOT) and block 19–20 in the middle (called MID LOT). The sample preparation was performed under anaerobic conditions with sterile equipment, which assured accurate sampling of the bentonite. The corresponding density, temperature and water content data for these positions is shown in Figure A1-2.

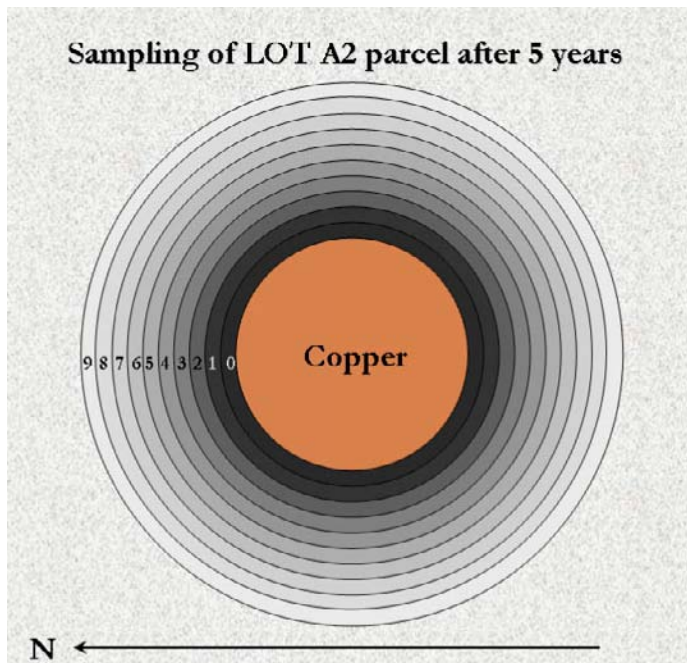


**Figure A1-1.** Schematic picture over the location of the samples from TOP LOT (block 38) and MID LOT (block 19–20) in the LOT A2 parcel.

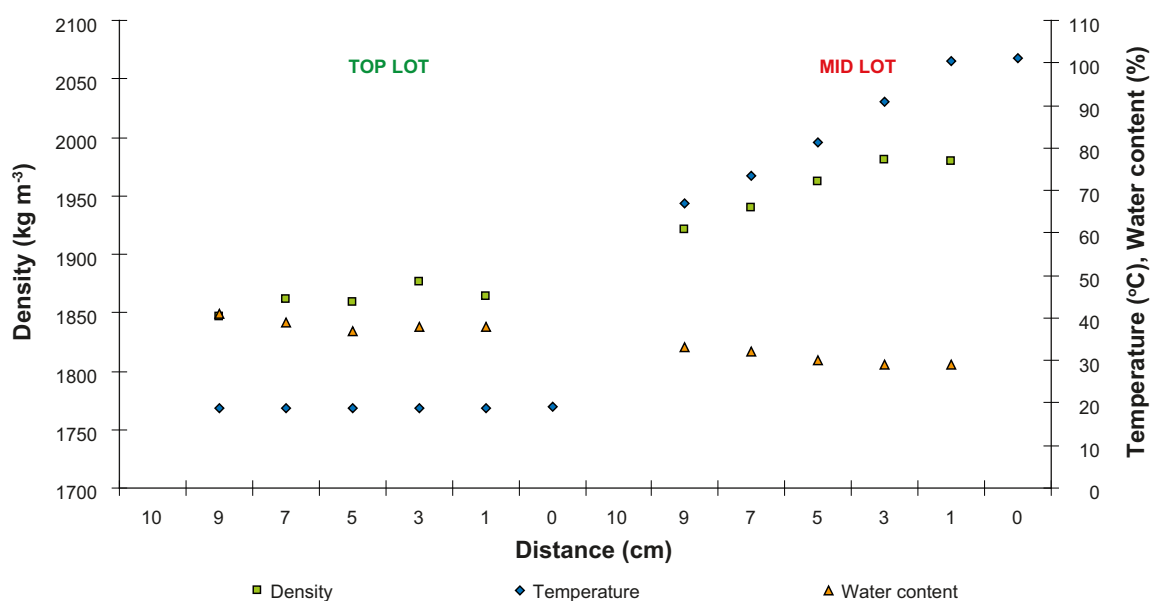


**Figure A1-2.** Density, temperature, and water content at 0–9 cm distance from the copper surface in the TOP LOT and MID LOT bentonite samples in the A2 parcel (data from Clay Technology AB).

## 4.2 Presence of bacteria in the bentonite from the LOT A2 parcel

Enrichment cultures were prepared to examine if viable bacteria were present in the sampled bentonite. When the sulphide concentrations in the bentonite enrichment cultures with addition of the organic carbon source lactate from TOP LOT and MID LOT were investigated, it was apparent that elevated sulphide concentrations (Figure A1-3, 54–507 mg l<sup>-1</sup>) could be found in most of the TOP LOT samples. Bacteria were found in all enrichment cultures with elevated sulphide concentrations. In Figure A1-4, images from microscopy analysis of two of these cultures are shown. As shown, many different bacterial morphologies were detected. In some samples (e.g. Figure A1-4A) filamentous structures with a length of more than 10 µm were found, as well as rod shaped bacteria with a length of 2–3 µm. In other samples, shorter rods with a length of approximately 1–2 µm were found to dominate the culture (e.g. Figure A1-4B).

Acetate, ranging from 23 to 318 mg l<sup>-1</sup>, was found in all the H<sub>2</sub>/CO<sub>2</sub> amended cultures with TOP LOT bentonite except one (Figure A1-6). Concomitant growth of bacteria with various morphologies was evident in all these samples. In some of these cultures the dominating morphologies were small rods, approximately 0.5–1.5 µm in length, and cocci (e.g. Figure A1-5A). In difference to the TOP LOT samples, acetate was not detected in any of MID LOT samples.

In addition to acetate, elevated sulphide concentrations with concomitant presence of bacteria were detected in some of the H<sub>2</sub>/CO<sub>2</sub> amended enrichment cultures with TOP LOT bentonite (Figure A1-7, 48–204 mg l<sup>-1</sup>). Since acetate is a carbon source used by many sulphate-reducing bacteria /Madigan et al. 2000/ and acetate was produced in the TOP LOT bentonite enrichment cultures (Figure A1-6), the sulphide in these cultures might have originated from acetate metabolism by SRB. Another possibility for SRB to gain carbon and energy is to use inorganic energy and carbon sources, H<sub>2</sub> and CO<sub>2</sub>, respectively. This might have been the case in the MID LOT culture shown in Figure A1-5B, since acetate was not detected in this culture. In this sample, the density was <1,950 kg m<sup>-3</sup>, the temperature ~70°C and the water content ~33%. As shown, the bacteria in this culture were cocci shaped and grew in chains.

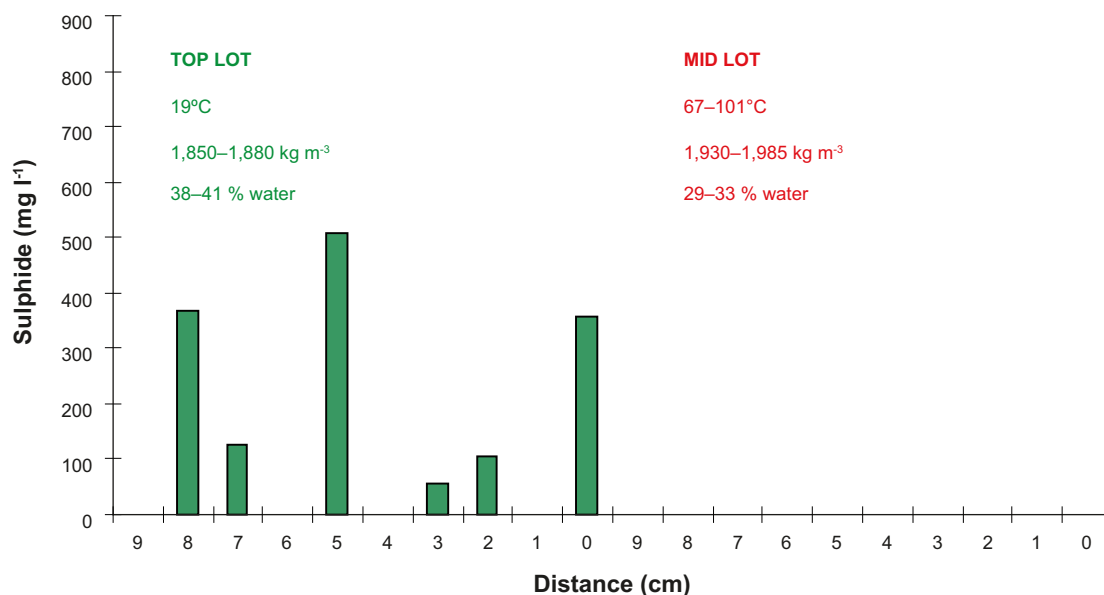


**Figure A1-3.** Sulphide concentrations in the anaerobic enrichment cultures inoculated with TOP LOT bentonite (green) and MID LOT bentonite (red) originating 0–9 cm from the copper in the A2 parcel. The medium for the enrichments contained lactate as carbon and energy source. The bentonite cultures were incubated six weeks at 30°C prior to analysis.

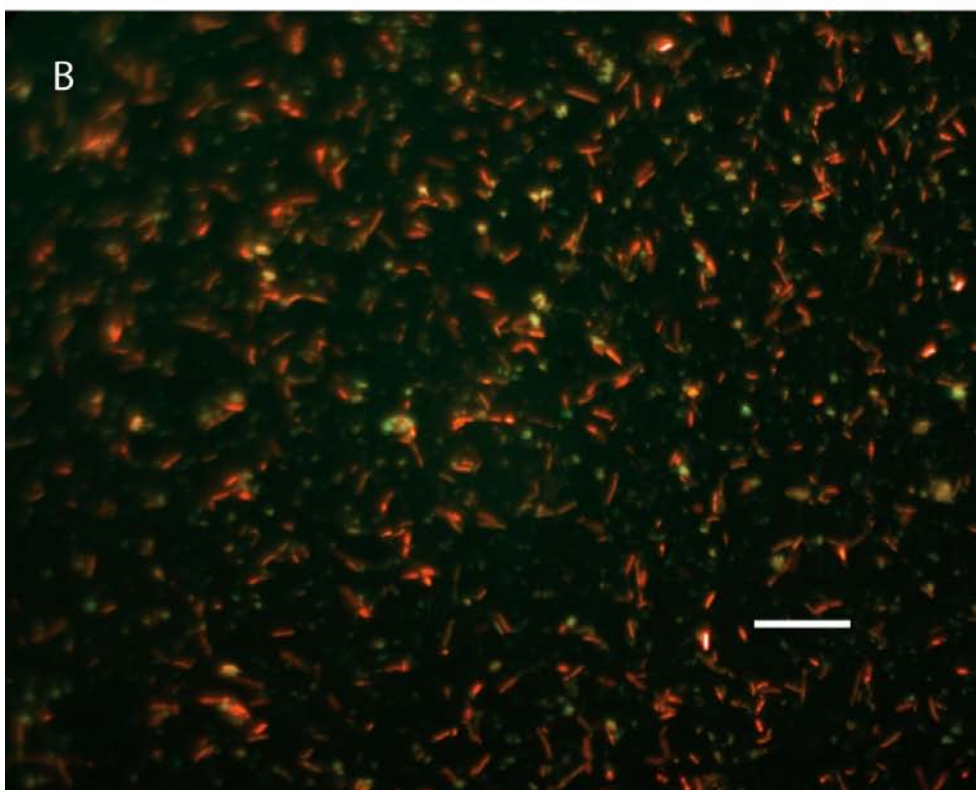
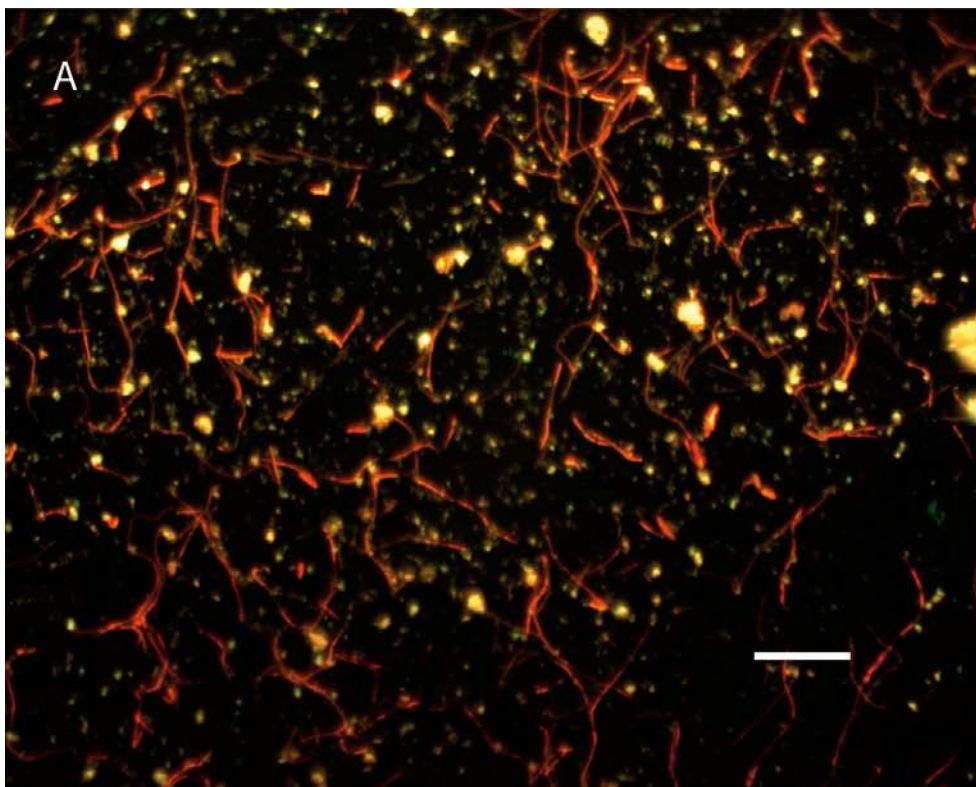


**Figure A1-4.** Images from the bentonite enrichment cultures with lactate added as energy and carbon source: A) A sulphide and acetate containing culture that was inoculated with TOP LOT bentonite situated 8 cm from the copper surface ( $\sim 1,850 \text{ kg m}^{-3}$ , temperature  $\sim 20^\circ\text{C}$ , and water content of 39%). B) A sulphide and acetate containing culture that was inoculated with TOP LOT bentonite situated 0 cm from the copper surface (density  $\sim 1,865 \text{ kg m}^{-3}$ , temperature  $\sim 20^\circ\text{C}$ , and water content of 38%). The white bar represents  $10 \mu\text{m}$ .

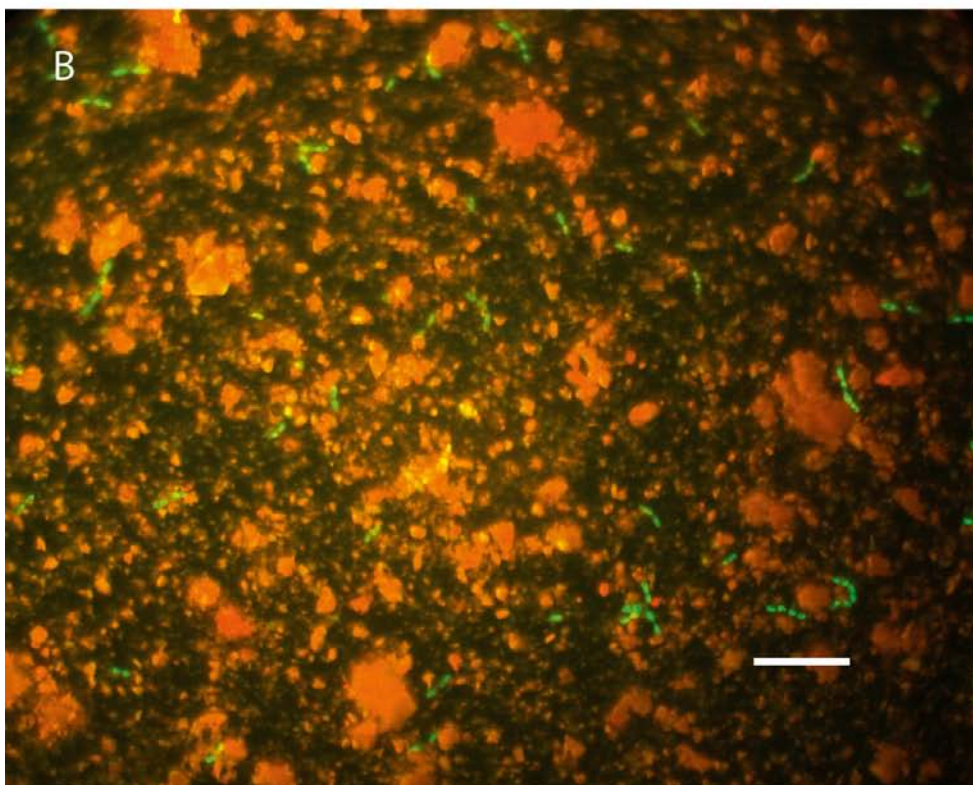
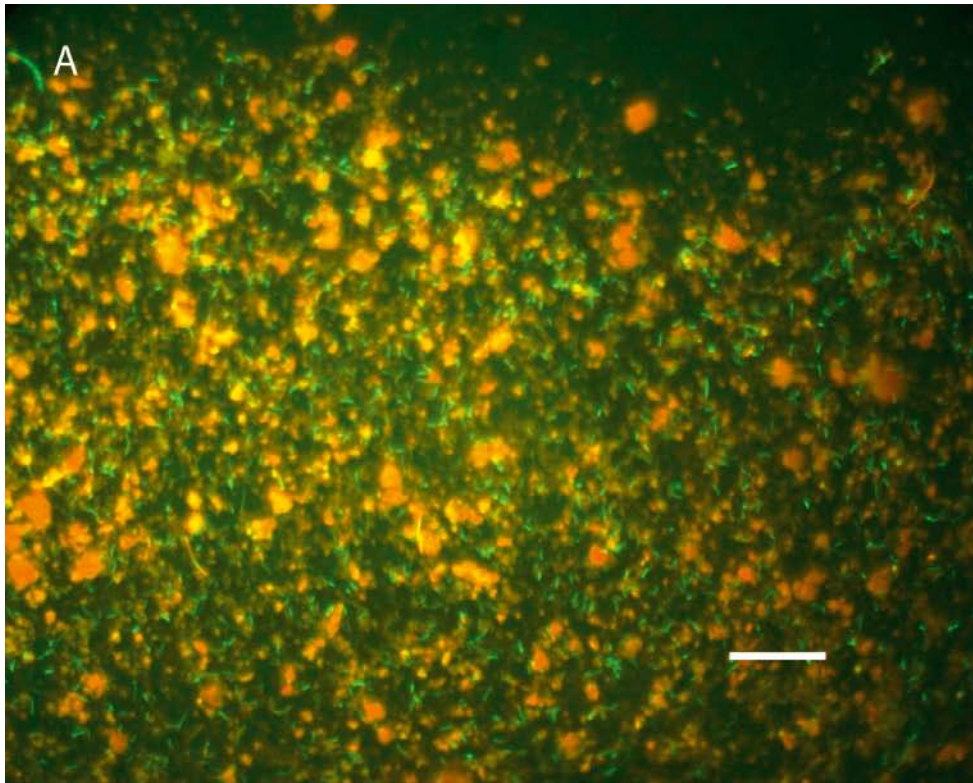


**Figure A1-5.** Images from the bentonite enrichment cultures with  $H_2/CO_2$  added as energy and carbon source for autotrophic growth: A) a sulphide and acetate containing culture that was inoculated with TOP LOT bentonite situated 1 cm from the copper surface ( $\sim 1,870 \text{ kg m}^{-3}$ , temperature  $\sim 20^\circ\text{C}$ , and water content of 38%) B) A sulphide containing culture that was inoculated with MID LOT bentonite situated 9 cm from the copper surface ( $\sim 1,930 \text{ kg m}^{-3}$ , temperature  $\sim 70^\circ\text{C}$ , and water content of 33%). The white bar represents  $10 \mu\text{m}$ .

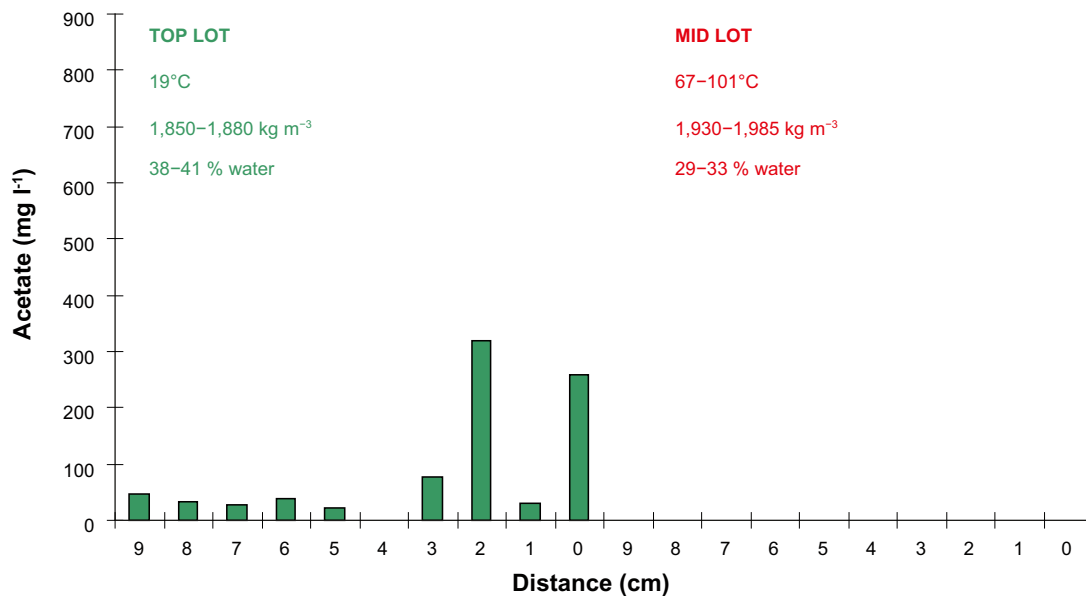


**Figure A1-6.** Acetate concentrations in the anaerobic enrichment cultures inoculated with TOP LOT bentonite (green) and MID LOT bentonite (red) originating 0–9 cm from the copper in the A2 parcel. The media for the anaerobic enrichments contained H<sub>2</sub>/CO<sub>2</sub> as energy and carbon sources for autotrophic growth. The bentonite cultures were incubated six weeks at 30°C prior to analysis.

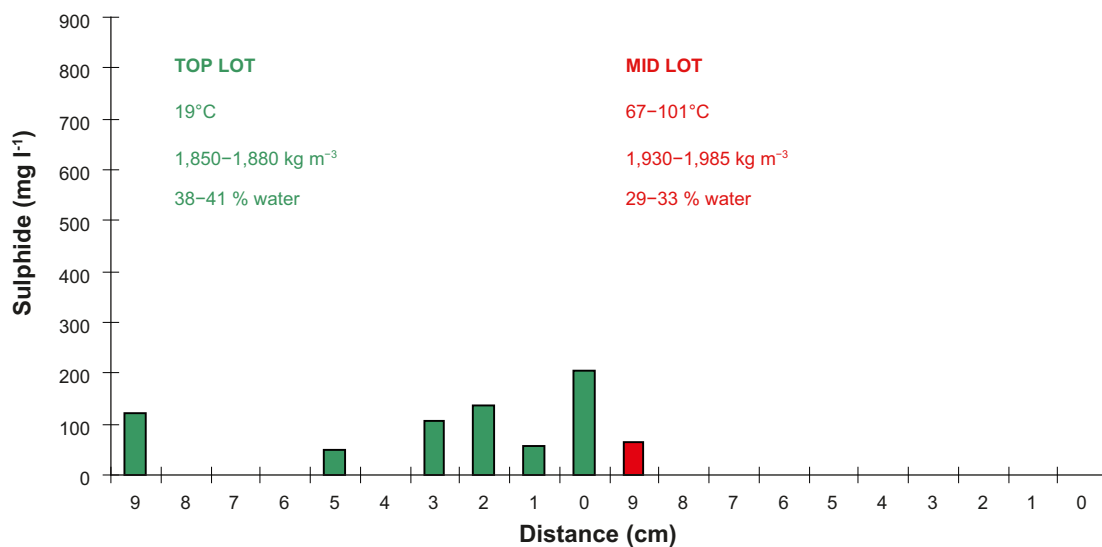


**Figure A1-7.** Sulphide concentrations in the anaerobic enrichment cultures inoculated with TOP LOT bentonite (green) and MID LOT bentonite (red) originating 0–9 cm from the copper in the A2 parcel. The media for the anaerobic enrichments contained H<sub>2</sub>/CO<sub>2</sub> as energy and carbon sources for autotrophic growth. The bentonite cultures were incubated six weeks at 30°C prior to analysis.

In Table A1-1, presence of bacteria and metabolic products in the TOP LOT and MID LOT bentonite are compared to the density, temperature and water content at the sites in the A2 parcel from where the sampled bentonite originated. The results show that bacteria were more abundant in the TOP LOT than in MID LOT samples, where the temperature and density during storage in the rock were higher and the water content lower.

**Table A1-1. Comparison of temperature, density, and water content in the sampled bentonite and bacterial growth in enrichment cultures with TOP LOT and MID LOT bentonite from the LOT A2 parcel after six weeks of incubation at 30°C. + growth – no growth.**

Measurement	Position	Carbon and energy source	Distance from Cu (cm)												
			9	8	7	6	5	4	3	2	1	0			
Temperature (°C) <sup>a</sup>	TOP LOT	–	19		19		19		19		19		19		19
Density (kg m <sup>-3</sup> ) <sup>a</sup>	TOP LOT	–	1,847		1,862		1,859		1,879		1,864				
Water content (%) <sup>a</sup>	TOP LOT	–	41		39		37		38		38				
Sulphide <sup>b</sup>	TOP LOT	Lactate	–	+	+	–	+	–	+	+	–	+			
Growth of bacteria <sup>d</sup>	TOP LOT	Lactate	+	+	+	+	+	+	+	+	+	+	+	+	+
Acetate <sup>c</sup>	TOP LOT	H <sub>2</sub> /CO <sub>2</sub>	+	+	+	+	+	–	+	+	+	+	+	+	+
Sulphide <sup>b</sup>	TOP LOT	H <sub>2</sub> /CO <sub>2</sub>	+	–	–	–	+	–	+	+	+	+	+	+	+
Growth of bacteria <sup>d</sup>	TOP LOT	H <sub>2</sub> /CO <sub>2</sub>	+	+	+	+	+	+	+	+	+	+	+	+	+
Temperature (°C) <sup>a</sup>	MID LOT	–	67		73		81		91		101		101		101
Density (kg m <sup>-3</sup> ) <sup>a</sup>	MID LOT	–	1,928		1,955		1,969		1,982		1,978				
Water content (%) <sup>a</sup>	MID LOT	–	33		30		29		29		29				
Sulphide <sup>b</sup>	MID LOT	Lactate	–	–	–	–	–	–	–	–	–	–	–	–	–
Growth of bacteria <sup>d</sup>	MID LOT	Lactate	–	–	–	–	–	–	–	–	–	–	–	–	–
Acetate <sup>c</sup>	MID LOT	H <sub>2</sub> /CO <sub>2</sub>	–	–	–	–	–	–	–	–	–	–	–	–	–
Sulphide <sup>b</sup>	MID LOT	H <sub>2</sub> /CO <sub>2</sub>	+	–	–	–	–	–	–	–	–	–	–	–	–
Growth of bacteria <sup>d</sup>	MID LOT	H <sub>2</sub> /CO <sub>2</sub>	+	–	–	–	–	–	–	–	–	–	–	–	–

<sup>a</sup> Data from Clay Technology AB, <sup>b</sup> detection limit for sulphide 1.3 mg l<sup>-1</sup>, <sup>c</sup> detection limit for acetate 15 mg l<sup>-1</sup>, <sup>d</sup> analysed with microscopy.

### 4.3 Enumeration of bacteria from the LOT A2 parcel

CHAB, SRB and AA numbers above detection limit were detected in several TOP LOT bentonite samples (Figure A1-8 to Figure A1-10). In these, the density was 1,850–1,880 kg m<sup>-3</sup>, the temperature ~20°C and the water content 38–41%.

In the samples originating from MID LOT bentonite, only one sample (located 4 cm from the copper canister) showed CHAB numbers above detection limit. In this sample, the density was >1,950 kg m<sup>-3</sup>, the temperature >80°C and the water content ~30%.

In Table A1-2, the quantitative results of bacteria in the sampled bentonite are shown. Between 10<sup>0</sup>–10<sup>2</sup> g<sup>-1</sup> AA and SRB bentonite were found. Compared to the groundwater in the area where 10<sup>1</sup>–10<sup>3</sup> ml<sup>-1</sup> AA and SRB can be detected /Pedersen 2000/, these numbers are lower. Nonetheless, it is obvious that both AA and SRB were present in almost all samples from the TOP LOT bentonite.

As shown in Table A1-1 and Figure A1-3 to A1-7, growth of bacteria with concomitant presence of sulphide and/or acetate was found in all TOP LOT (at 0–9 cm distance from the copper) and one MID LOT (at 9 cm distance from the copper) from the bentonite enrichment culture. However, growth was not always detected in the in the tubes in the MPN analysis. Theoretically, the numbers of SRB in these samples would be ~1–5 g<sup>-1</sup> bentonite. These samples are illustrated with dotted staples in Figure A1-9 and Figure A1-10.

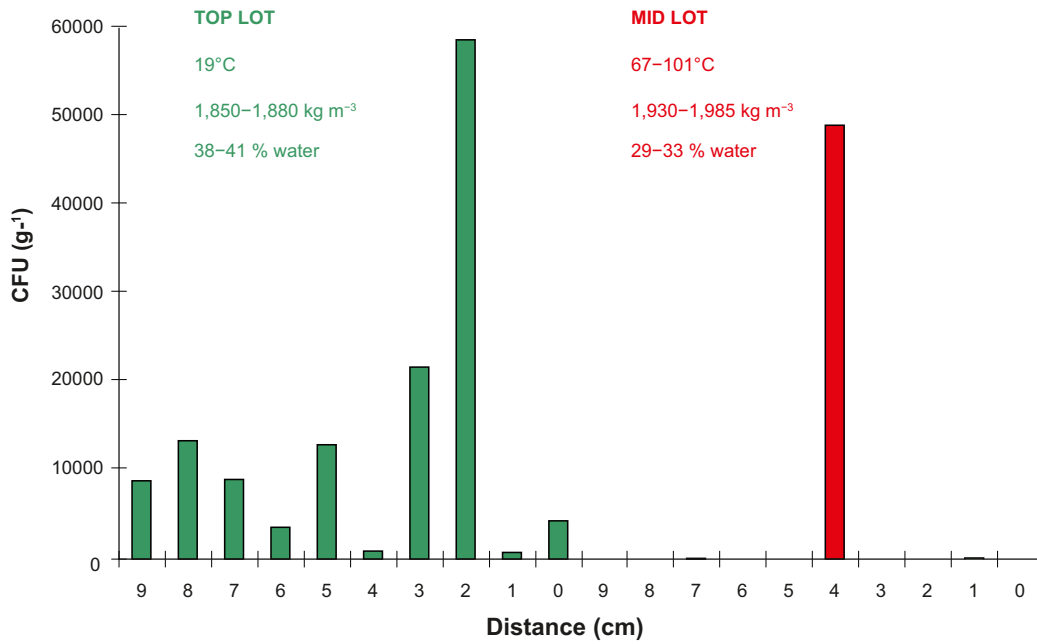


**Figure A1-8.** Culturable heterotrophic aerobic bacteria in the TOP LOT and MID LOT bentonite originating 0-9 cm from the copper in the A2 parcel after one day of dispersion of the bentonite in the anaerobic media. The numbers are means of the counts from the bentonite enrichment cultures with and without addition of organic carbon (n=2).

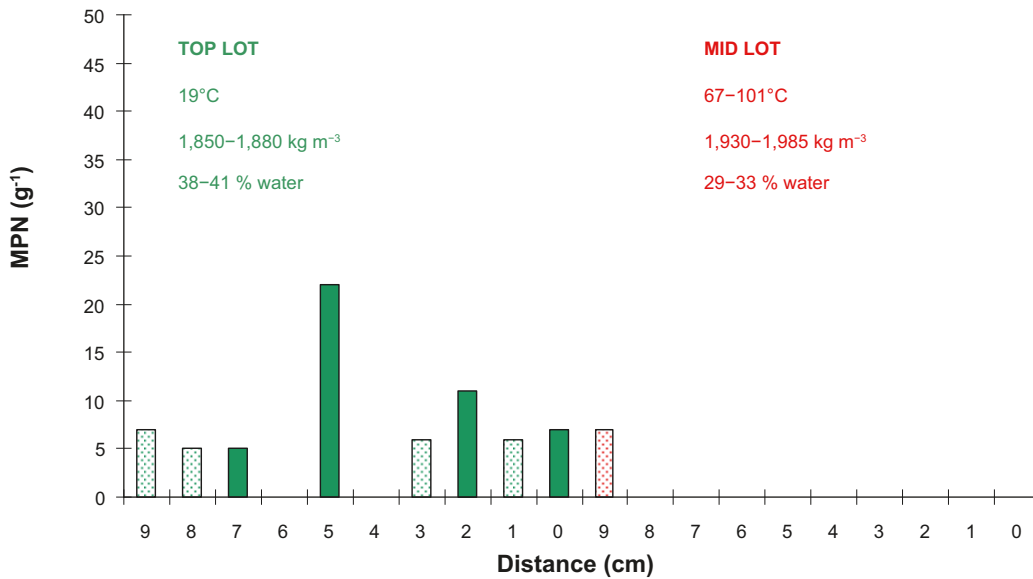


**Figure A1-9.** MPN of sulphate-reducing bacteria in the TOP LOT and MID LOT bentonite originating 0-9 cm from the copper in the A2 parcel. The dotted staples show samples where sulphate-reducing bacteria were present in the enrichment culture used as inoculum but not in the MPN tubes and represents the highest theoretical number of sulphate-reducing bacteria in the bentonite sample.

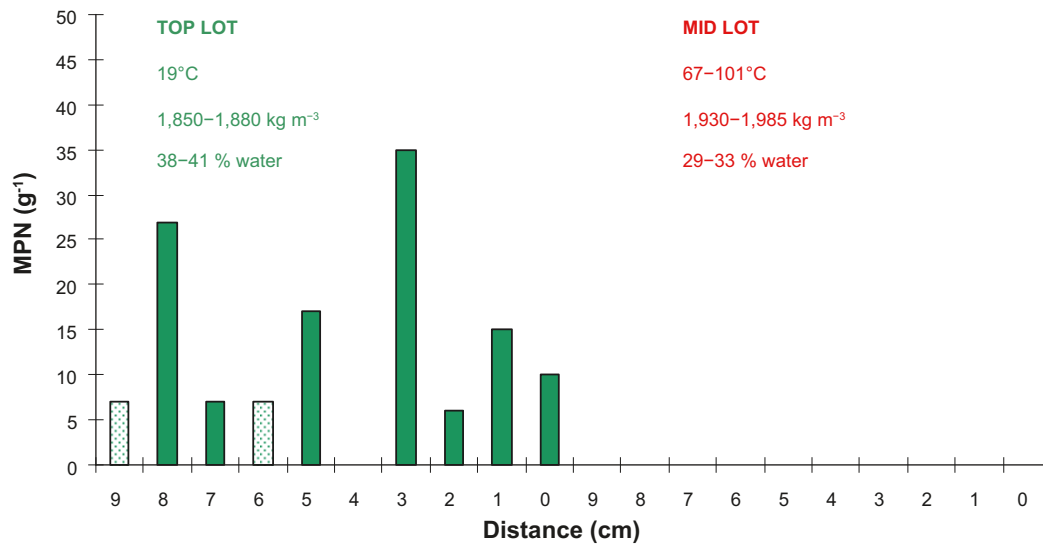


**Figure A1-10.** MPN of acetogens in the TOP LOT and MID LOT bentonite originating 0–9 cm from the copper in the A2 parcel. The dotted staples show samples where acetogens were present in the enrichment culture used as inoculum but not in the MPN tubes and represents the highest theoretical number of acetogens in the bentonite sample.

#### 4.4 ATP in the bentonite

ATP measurements showed the living bio-volume in a sample. Due to the bentonite interference in this study, the detection limit of the ATP method was relatively high compared to ATP analysis in groundwater samples /Eydal and Pedersen 2007/. All samples with bentonite from the A2 parcel except one from MID LOT contained less than  $5 \times 10^4$  amol ATP g<sup>-1</sup> (Table A1-2). This corresponds to  $10^4$ – $10^6$  cells g<sup>-1</sup>, if the ATP content in the cells in the bentonite is regarded to be the same as in anaerobic bacteria in deep granitic groundwater. These bacteria have been shown to contain 0.1–1 amoles ATP cell<sup>-1</sup> /Eydal and Pedersen 2007/.

The MID LOT sample with a detectable content of ATP also showed a high number of CHAB ( $49 \times 10^3$ ). This sample was situated in the middle a bentonite block, which basically rules out the risk for contamination during sampling. The ATP analysis and the CHAB analysis represented two independent methods both showing that bacteria were active in this sample point (the density was  $>1,950$  kg m<sup>-3</sup>, the temperature  $>80^\circ\text{C}$  and the water content  $\sim 30\%$ ). In this study, the correlation was only found in a single sampling point and can therefore not be considered a widespread phenomenon without further investigations.

**Table A1-2. Enumeration of cultivative heterotrophic aerobic bacteria (CHAB), sulphate-reducing bacteria (SRB), autotrophic acetogens (AA) and determination of the ATP content in the TOP LOT and MID LOT bentonite from the LOT A2 parcel.**

Analysis	Position	Distance from Cu (cm)									
		9	8	7	6	5	4	3	2	1	0
CHAB (CFU <sup>a</sup> × 10 <sup>3</sup> g <sup>-1</sup> ± stdev)	TOP LOT	8 ± 4	13 ± 9	9 ± 5	3 ± 2	13 ± 5	0.7 ± 0.3	22 ± 14	58 ± 7	0.6 ± 0.3	4 ± 0.4
MPN SRB (g <sup>-1</sup> with 99% confidence limits <sup>b</sup> )	TOP LOT	–	–	5 (2–30)	–	22 (3–53)	–	–	11 (2–39)	–	7 (3–41)
MPN AA (g <sup>-1</sup> with 99% confidence limits <sup>b</sup> )	TOP LOT	–	27 (3–64)	7 (3–42)	–	17 (4–64)	–	35 (2–54)	6 (3–37)	15 (3–54)	10 (2–36)
ATP (amole × 10 <sup>5</sup> g <sup>-1</sup> ± stdev)	TOP LOT	–	–	–	–	–	–	–	–	–	–
CHAB (CFU <sup>a</sup> × 10 <sup>3</sup> g <sup>-1</sup> ± stdev)	MID LOT	–	–	0.12 ± 0.08	–	–	49 ± 34	–	–	0.09 ± 0.08	–
MPN SRB (g <sup>-1</sup> with 99% confidence limits <sup>b</sup> )	MID LOT	–	–	–	–	–	–	–	–	–	–
MPN AA (g <sup>-1</sup> with 99% confidence limits <sup>b</sup> )	MID LOT	–	–	–	–	–	–	–	–	–	–
ATP (amole × 10 <sup>5</sup> g <sup>-1</sup> ± stdev)	MID LOT	–	–	–	–	–	1 ± 0.2	–	–	–	–

<sup>a</sup> CFU – colony forming units, <sup>b</sup> determined using the method of Cornish and Fischer described in /Klee 1993/.

## 5 Concluding remarks

The sampling procedures and analysis protocols in this experiment worked properly. The only cultured bacteria in the samples were the ones intrinsic in the bentonite during sampling. The origin of the bacteria in the bentonite is still to be determined but probably do they originate both from the surrounding groundwater and from the bentonite itself. Wyoming bentonite MX-80 has been shown to contain sulphate-reducing bacteria /Masurat et al. 2008/.

The numbers of AA and SRB were low compared to the surrounding groundwater, which can be expected because of the harsh conditions in the bentonite. Nevertheless, they could be found repeatedly in many of the TOP LOT bentonite samples. The results show that the bacteria inside the TOP LOT bentonite are viable and have a potential to produce both sulphide and organic carbon in form of acetate. The elevated density, temperature or/and the lower water content in the MID LOT bentonite compared to the TOP LOT bentonite obviously made it difficult for the bacteria to survive. However, the MID LOT samples were not completely sterile. In two of the MID LOT samples bacteria were viable, i.e. sulphide-producing bacteria could be enriched from a sample situated 9 cm from the copper surface with a density of  $<1,950 \text{ kg m}^{-3}$ , a temperature  $\sim 70^\circ\text{C}$  and a water content  $\sim 33\%$  and the CHAB and ATP analyses showed bacteria present in a sample situated 4 cm from the copper surface with a density of  $>1,950 \text{ kg m}^{-3}$ , a temperature  $>80^\circ\text{C}$  and a water content  $\sim 30\%$ .

## 6 References

- Eydal H S C, Pedersen K, 2006.** Evaluation of an ATP assay for biomass determination of microbial population in subsurface groundwater. Manuscript.
- Klee A J, 1993.** A computer program for determination of most probable number and its confidence limits. *J Microbial Methods* 18:91–98.
- Lundin A, 2000.** Use of firefly luciferase in ATP-related assays of biomass, enzymes, and metabolites. *Methods in Enzymology*. 305:346–370.
- Lundin A, Hasenson M, Persson J, Pousette Å, 1986.** Estimation of biomass in growing cell lines by adenosine triphosphate assay. *Methods in Enzymology*. 133:27–42.
- Madigan M T, Martinko J M, Parker J, 2000.** Chapter 15: Metabolic diversity. In: Corey PF, editor. *Brock Biology of microorganisms* 9th ed. New Jersey: Prentice Hall International Inc. pp 573–641.
- Masurat P, Eriksson S, Pedersen K, 2008.** Evidence of indigenous sulphate-reducing bacteria in commercial Wyoming bentonite MX-80. *Applied Clay Science*. doi:10.1016/j.clay.2008.07.002.
- Pedersen K, 2000.** Äspö Hard Rock Laboratory: The microbe site – Drilling, instrumentation and characterisation. SKB Internal Progress Report, IPR-00-36.
- Widdel F, Bak F, 1992.** Gram-negative mesophilic sulphate-reducing bacteria. In: Balows A, Trüper HG, Dworking M Harder W, Schleifer KH, editors. *The prokaryotes*, vol IV. Berlin: Springer-Verlag. pp 3352–3377.

## **Long term test of buffer material - in situ $\text{Co}^{2+}$ diffusion experiment**

Sara Nilsson, Trygve E Eriksen

School of Chemical Science and Engineering, Nuclear chemistry, KTH

# Introduction

Bentonite has been proposed as buffer material in several concepts for high level nuclear waste repositories. The favourable bentonite properties are closely linked to the interaction between groundwater and the main mineral montmorillonite. An experiment series, called “Long Term Test of Buffer Material” (LOT) are carried out at Äspö Hard Rock Laboratory. The main objectives of LOT are to validate models for clay performance at standard KBS-3 repository conditions and to quantify clay alteration processes under adverse conditions such as very saline groundwater, high pH and high potassium concentration in clay pore water, high temperature and temperature gradient across the buffer. Several other tests concerning copper corrosion, bacteria survival and cation diffusion are also carried out in conjunction with the buffer performance test. The LOT programme comprises seven test parcels which are exposed to KBS-3 repository conditions for 1 to >>5 years. Each test parcel (Figure A2-1) contains a heater a copper tube and pre-compacted bentonite blocks. The test parcel is placed in a vertically drilled 4-m deep borehole 450 m below ground level in Äspö Hard Rock Laboratory. When the bentonite is fully water saturated by groundwater entering the borehole through water carrying rock fissures, the copper tube is heated to simulate the temperature increase due to deposition of radionuclide decay energy.

The influence of sorption and ion exclusion on the effective and apparent diffusivity of radionuclide containing cationic and anionic species in compacted bentonite has been studied extensively in laboratory /Muurinen 1994, Eriksen and Jansson 1996, Yu and Neretnieks 1997/. Modelling diffusion and sorption are discussed in several papers /Marimon 2002, Bourg et al. 2003, Ochs et al. 2001, 2003/. Diffusion experiments with  $\text{Cs}^+$ ,  $\text{Sr}^{2+}$  and  $\text{Co}^{2+}$  have been carried out in bentonite compacted to  $1,800 \text{ kg/m}^3$  dry density and saturated with Äspö ground water using the CHEMLAB probe /Jansson and Eriksen 1998/. LOT offers the possibility of in situ studies of radionuclide migration in compacted bentonite under conditions quite different from those in laboratory; larger scale, initially dry bentonite subjected to water saturation with natural ground water, high temperature and temperature gradient across the buffer during the experiment.

The migration of the cations  $\text{Cs}^+$  and  $\text{Co}^{2+}$  were studied in earlier 1-year LOT tests /Karnland et al. 2000, Jansson et al. 2003/.

In this paper we describe a 6-year migration study within the LOT test parcel A2. Scoping calculations of expected concentration profiles of  $\text{Cs}^+$  and  $\text{Co}^{2+}$  showed that  $\text{Cs}^+$  would not be contained within the bentonite and only  $\text{Co}^{2+}$  was used in the test.

# Experimental

A 4-m deep hole was drilled vertically into the rock 445 m below ground level in the Äspö hard rock laboratory. The test parcel A2 containing a copper tube with 100 mm outer diameter surrounded by 38 cylindrical blocks with 300 mm diameter of Wyoming MX-80 bentonite pre-compacted to give a density of 2,000 kg/m<sup>3</sup> when fully water saturated is shown schematically in Figure A2-1. Two identical 20 mm long bentonite plugs with 20 mm diameter and the same density as the parcel blocks were prepared in laboratory. A 5-mm diameter hole was drilled into the centre of each plug and a few cubic millimetres of dry bentonite containing sorbed Co<sup>2+</sup> with 1MBq <sup>60</sup>Co as tracer was placed at the bottom of the hole. The top part of the hole was refilled with inactive bentonite and compacted to the plug density. The plugs were inserted into two diametrically opposite holes in the fifth bentonite block from the bottom of the test parcel immediately before lowering the parcel into the borehole.

A2-Parcel.dsf  
00-12-13

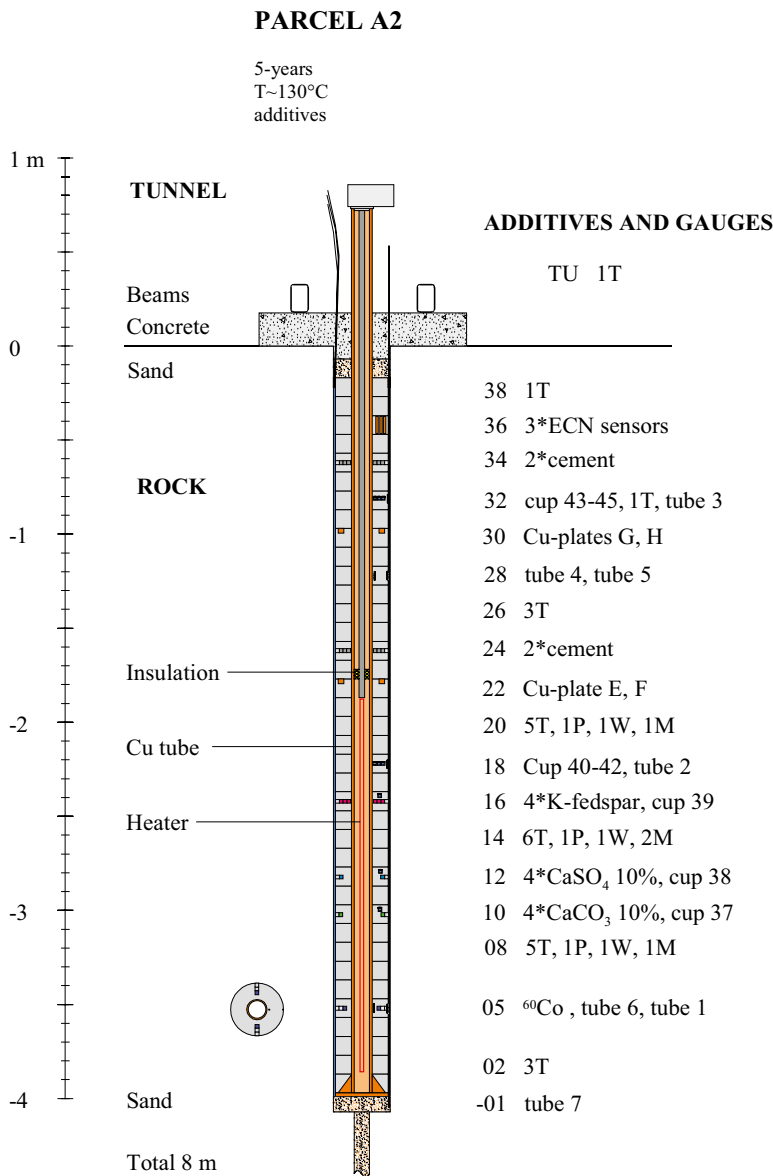


Figure A2-1. Schematics of LOT A2 parcel.

The hole was thereafter sealed with a concrete plug and the bentonite blocks left to be water saturated with ground water. The test parcel was equipped with a number of thermocouples, humidity and pressure gauges to monitor the evolution of temperature, water saturation and pressure in the bentonite. When scoping calculations as well as humidity gauges indicated that the the bentonite was fully water saturated, the temperature in the parcel was increased by heating the central copper tube to 130°C by internal electric heaters. The heating was done to simulate the increase in canister temperature due to heat generation by decaying radionuclides within the spent fuel,

At the end of the test period the parcel was removed from the bore hole by over-core drilling and the <sup>60</sup>Co containing blocks transported to a radiochemistry laboratory for profile analysis.

The experimental time schedule is given in Table A2-1.

**Table A2-1. Time schedule for LOT-2 test.**

<b>Installation</b>	<b>Heater on</b>	<b>off</b>	<b>Lift up</b>	<b>Sampling</b>
1999-10-29	2000-02-02	2005-12-05	2006-01-16	2006-02-(08-22)

## Analyses

A rectangular part containing the  $^{60}\text{Co}$  was sawn out of block five and sliced into 15 laminae and each lamina cut into small pieces, 2.5–3.5 g each, giving a total number of approximately 1,300 samples. Block 5 after transport to the radiochemistry laboratory and schematics of the sampling layout are shown in Figure A2-2.

All samples were dried overnight in an oven at  $70^\circ\text{C}$  and then weighed. The gamma activity was measured using a germanium detector and multi-channel analyzer. Every piece was measured until 10,000 pulses were reached or for maximum one hour. The mid-point of the sample with maximum specific activity (cps/g), assumed to be the position where the diffusant was originally placed, is used as reference point for determining the geometric activity distribution.

Densities of  $20\times 20\times 20$  mm samples from blocks 4 and 2 at differing distances from the copper tube were determined by weighing the samples in air and in paraffin oil.

Water ratios (water loss/dry density of bentonite) were determined for samples from blocks 4 and 6

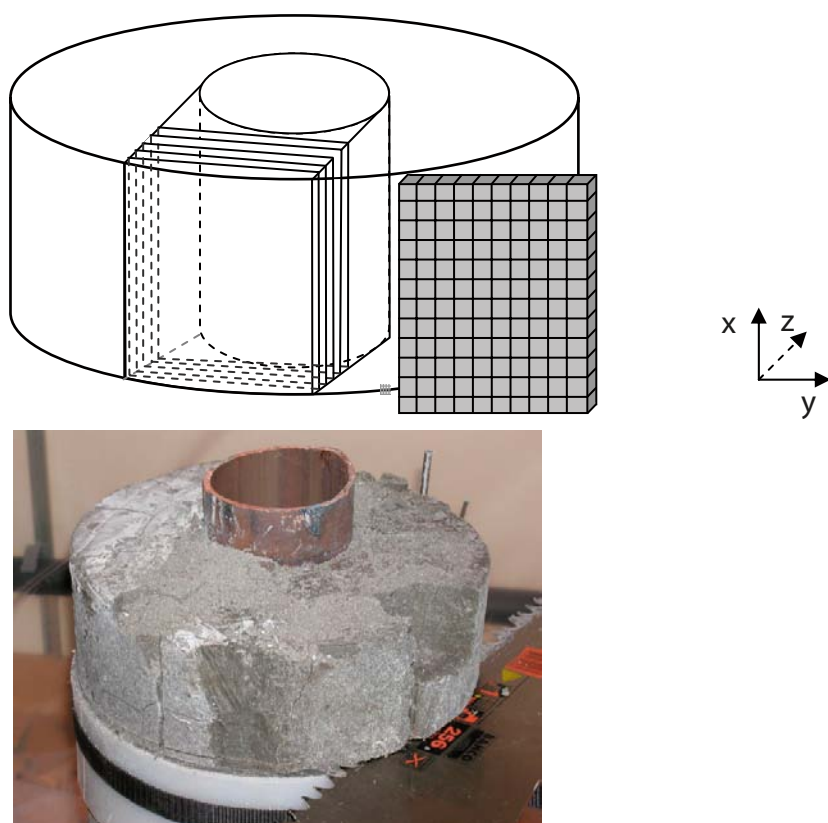


**Figure A2-2.** Block 5 after transport to radiochemistry laboratory. Schematics of sample layout.

## Results and discussion

The pressure build up due to water saturation and temperature at different distances from the copper tube in block 14 are plotted as function of time in Figures A2-3 and A2-4 respectively. Stable temperature conditions were reached after approximately one year and stable water ratio after nearly two years.

Water to solid ratios of samples from blocks 4 and 6 and wet densities of samples from block 4 are given in Table A2-2. The wet density decreases slightly and the water to solid ratio in block 4 increases with distance from the hot copper tube. The water to solid ratio in samples from block 6 is somewhat lower than the ratio in samples at the same distances from the copper tube in block 4.

The dry density and water filled porosity of the samples are calculated using equations (1) and (2) respectively:

$$\rho_d = \rho_w / (1 + R) \quad (1)$$

$$\varepsilon = (\rho_w - \rho_d) / \rho_{\text{water}} \quad (2)$$

$\rho_w$ ,  $\rho_d$  density of wet and dried bentonite sample respectively

R water to solid ratio

$\varepsilon$  porosity

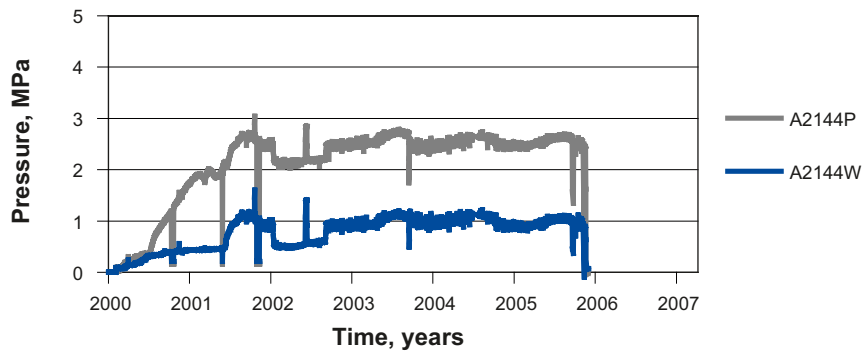


**Figure A2-3.** Pressure build-up at mid position in block 14 on saturation with ground water. Gray curve (P) shows total pressure and blue curve (W) water pressure.

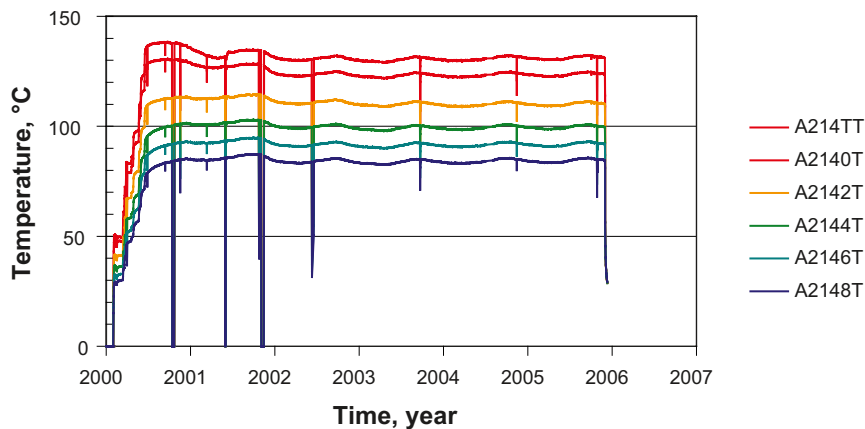


**Figure A2-4.** Temperature recordings in block 14 as function of time. Last figure denotes distance in cm from copper tube.

**Table A2-2. Water to solid ratios and wet densities measured at different distances from copper tube in blocks 4, 6 and block 4 respectively.**

Distance from copper tube (mm)	0–20	20–40	40–60	60–80	80–100
Water ratio, Block 6	0.248	0.255	0.263	0.274	0.290
Water ratio, Block 4	0.294	0.301	0.306	0.314	0.325
Wet density (g·cm <sup>-3</sup> ), Block 4	1.945	1.952	1.942	1.926	1.915

Assuming the mean value of samples from blocks 4 and 6 to be representative for the activity – containing block 5 we obtain  $\rho_d = 1.53 \pm 0.05 \text{ g}\cdot\text{cm}^{-3}$  and  $\varepsilon = 0.44 \pm 0.02$ .

Taking the density of bentonite to be  $2.73 \text{ g}\cdot\text{cm}^{-3}$  the porosity of dry compacted bentonite is given by equation (3)

$$\rho_d = 2.73(1-\varepsilon) \quad (3)$$

Using equation (3) we calculate the porosity of bentonite compacted to dry density  $1.53 \text{ g}\cdot\text{cm}^{-3}$  to be 0.44 clearly showing that the compacted bentonite in block 5 was fully water saturated. Although fully water saturation was reached after approximately two years, diffusion probably started before reaching water saturation.

The specific activity (cps/g) is plotted as a function of distance along the x,y,z axes in Figure A2-5

The specific activity of all samples from block 5 is plotted in Figure A2-6 as a function of distance from the point of maximum specific activity.

The experimental data clearly show that the <sup>60</sup>Co activity was contained within block 5. The radionuclide transport can therefore be treated as diffusion from a finite source into an infinite medium. Assuming the source to be a sphere with diameter a and initial concentration C<sub>0</sub> the concentration at distance r and time t, C(r,t), is given by equation (4) /Crank 1975/.

$$C(r,t) = \frac{1}{2}C_0 \left[ \operatorname{erf} \frac{a+r}{2\sqrt{D_a t}} + \operatorname{erf} \frac{a-r}{2\sqrt{D_a t}} \right] - \frac{C_0}{r} \sqrt{\left( \frac{D_a t}{\pi} \right)} \left[ e^{-\frac{(a-r)^2}{4D_a t}} - e^{-\frac{(a+r)^2}{4D_a t}} \right] \quad (4)$$

where D<sub>a</sub> is the apparent diffusivity.

The specific activity as a function of distance from the point of maximum activity calculated with a = 2 mm and D<sub>a</sub> = 5·10<sup>-9</sup> cm<sup>2</sup>·s<sup>-1</sup> is plotted in Figure A2-6.

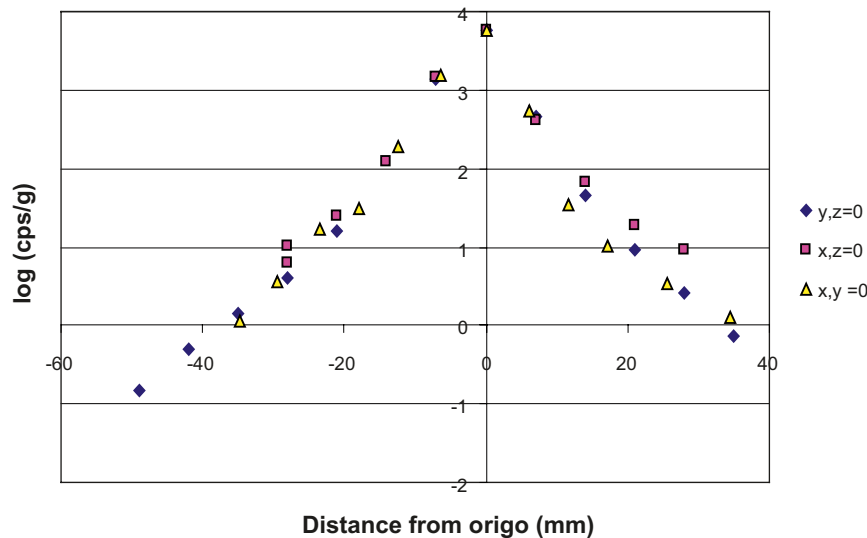


**Figure A2-5. Specific activity of samples along x,y,z axis (see Figure A2-2).**

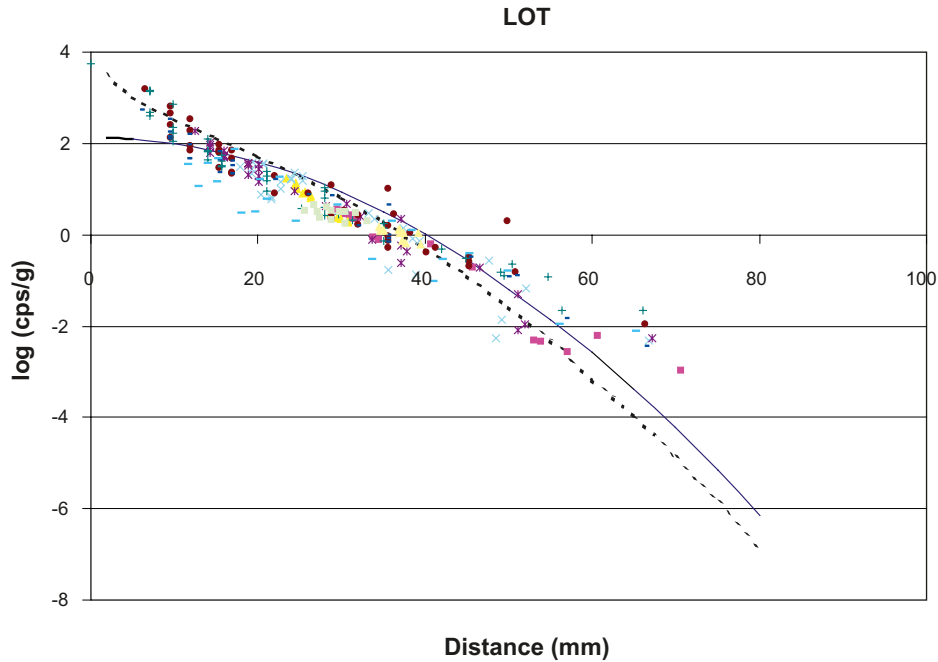


**Figure A2-6.** Specific activity of samples from block 5 plotted against distance from maximum specific activity. –  $D_a = 5 \cdot 10^{-9} \text{ cm}^2 \text{ s}^{-1}$ ,  $a = 2 \text{ mm}$ , –  $D_a = 5 \cdot 10^{-9} \text{ cm}^2 \text{ s}^{-1}$ ,  $a = 2 \text{ mm}$ , partial precipitation of Co as  $\text{Co}(\text{OH})_2$  in pore water for  $r < a$ .

The calculated activity distribution clearly underestimates the measured specific activity at short distances from the maximum. The pH in the pore water at the end of the test period was according to /Muurinen 2006/ approximately 8.3 close to the copper heater and 7.2 at the bentonite rock interface. The variation of pH with distance from the copper surface with time is not known, but the pH in the pore water at the initial position of the Co-source may have, due to slow equilibration with the ground water, been  $\geq 8.3$  during a considerable part of the test period.

One possible explanation for the difference between calculated and measured specific activity close to the position of maximum activity is precipitation of Co as  $\text{Co}(\text{OH})_2$ .

Assuming the pore water concentration for  $r < a$  to be solubility constrained and constant during the test period the specific activity  $C(r,t)$  distribution for  $r > a$  is given by equation (5), /Crank 1975/

$$C(r,t) = C(a) \frac{a}{r} \operatorname{erfc} \left[ \frac{r-a}{2\sqrt{D_a t}} \right] \quad (5)$$

As seen from Figure A2-6 the fitted specific activity distribution for  $a = 2 \text{ mm}$  and  $D = 5 \cdot 10^{-9} \text{ cm}^2 \cdot \text{s}^{-1}$  assuming partial Co precipitation corresponds better to the experimental observations.

When comparing data from the present diffusion test with data obtained in laboratory experiments it should be emphasized that several processes; water saturation, ion exchange between bentonite pore water and surrounding ground water and heating of the water saturated bentonite, have taken place during the test period.

The in situ diffusion system studied is complicated with a large temperature gradient and according to pore water analysis also an increase in pH from approximately 7.2 at the bentonite/bedrock interface to 8.3 close to the copper tube surface. The time evolution of pH in the pore water is not known and pH has probably been in the range 8–8.3, a range with great influence on  $\text{Co}^{2+}$  sorption and solubility /Bradbury and Baeyens 2005, Molera Marimon 2002/ during a considerable part of the test period.

The apparent diffusivity  $D_a$  in porous media encompassing diffusion in pore water and complete immobilization of sorbed species is, assuming the physical constrictivity to be unity, given by equation (6):

$$D_a = \frac{D_w}{\tau^2} \frac{\varepsilon}{\varepsilon + K_d \rho} \quad (6)$$

$D_w$  diffusivity in pore water

$\tau^2$  tortuosity of pore system

$\varepsilon$  porosity

$\rho$  dry density of compacted bentonite

$K_d$  sorption coefficient

/Molera Marimon 2002/ measured the apparent diffusivity of  $\text{Co}^{2+}$  at  $20^\circ\text{C}$  in bentonite compacted to  $1.2\text{--}1.8 \text{ g cm}^{-3}$  dry density and equilibrated with electrolytic solution with different ionic strength at pH 8.2 . Using equation (6) on these data we estimate  $D_a$  to be  $(3.4 \pm 1.7) \cdot 10^{-10} \text{ cm}^2 \text{ s}^{-1}$  at dry density  $1.53 \text{ g cm}^{-3}$  and  $20^\circ\text{C}$ .

The temperature profile in the LOT-2 parcel is shown in Figure A2-7. As can be seen the temperature in block 5 varies from approximately  $120^\circ\text{C}$  close to the copper tube heater to approximately  $70^\circ\text{C}$  at the bentonite/rock interface. The temperature at the position of maximum specific activity is approximately  $95^\circ\text{C}$ .

/Jansson et al. 2003/ have measured the apparent diffusivity of  $\text{Co}^{2+}$  in bentonite compacted to  $1.8 \text{ g cm}^{-3}$  dry density at  $20, 70$  and  $90^\circ\text{C}$  ( $(2 \pm 1) \cdot 10^{-14}, 8 \cdot 10^{-14}, 1.2 \cdot 10^{-13} \text{ m}^2 \text{ s}^{-1}$ ). Extrapolating these data to  $95^\circ\text{C}$  and assuming the overall activation energy for the diffusion process ( diffusion in the pore water and sorption on the bentonite) to be the same for  $1.53 \text{ g cm}^{-3}$  and  $1.8 \text{ g cm}^{-3}$  dry density we find the the ratio

$\frac{D_a(95^\circ\text{C})}{D_a(20^\circ\text{C})}$  to be 6.1 and thus the expected apparent diffusivity in the LOT-2 experiment

to be  $(2.1 \pm 0.8) 10^{-9} \text{ cm}^2 \text{ s}^{-1}$  which is within a factor 2–3 in agreement with the experimentally observed diffusivity.

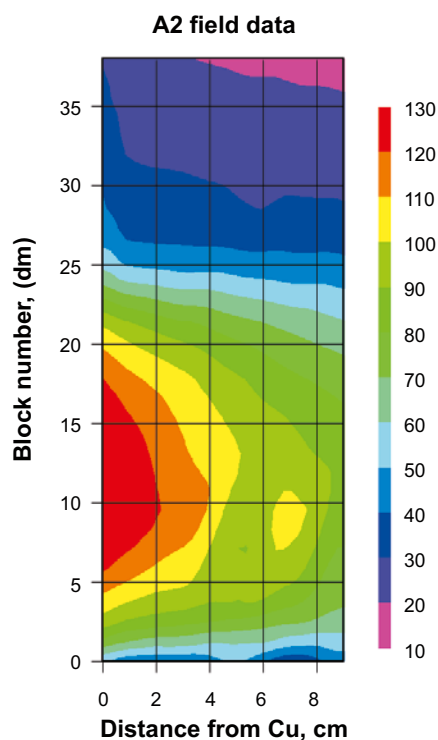


Figure A2-7. Temperature profile in the LOT-2 parcel.

## Conclusions

The apparent diffusivity is in good agreement with data from previous in situ experiments and taking into consideration differences in compaction, pH of equilibrating electrolyte solutions and temperature also within a factor 2–3 with data from laboratory experiments.

## References

- Bradbury M, Baeyens B, 2005.** Modelling the sorption of Mn(II), Co(II), Ni(II), Zn(II), Cd(II), Eu(III), Am(III), Sn(IV), Th(IV), Np(V) and U(VI) on montmorillonate: Linear free energy relationships and estimates of surface binding constants for some heavy metals and actinides. *Geochimica et Cosmochimica. Acta* 69, 875–892.
- Bourg I C, Bourg A C M, Sposito G, 2003.** Modelling diffusion and absorption in compacted bentonite: a critical review. *J. Contam. Hydrol.* 61, 293–302.
- Crank J, 1975.** *The Mathematics of Diffusion*, 2nd ed.; Oxford Univ. Press, Oxford.
- Eriksen T E, Jansson M, 1996.** Diffusion of I<sup>-</sup>, Cs<sup>+</sup> and Sr<sup>2+</sup> in compacted bentonite – anion exclusion and surface diffusion. SKB TR-96-16, Svensk Kärnbränslehantering AB.
- Jansson M, Eriksen T E, 1998.** CHEMLAB – in situ diffusion experiments using radioactive tracers. *Radiochim. Acta* 82, 153–156.
- Jansson M, Eriksen T, Wold S, 2003.** LOT –in situ diffusion experiments using radioactive tracers, *Appl. Clay Sci.* 23 77-85.
- Karnland O, Sanden T, Johannesson L-E, Eriksen T E, Jansson M, Wold S, Pedersen K, Motamedi M, Rosborg B, 2000.** Long term test of buffer material – final report on the pilot parcel. SKB TR-00-22, Svensk Kärnbränslehantering AB.
- Molera Marimon M, 2002.** On the Sorption and Diffusion of Radionuclides in Bentonite Clay. Doctoral Thesis, Department of Chemistry, Nuclear Chemistry, KTH.
- Muurinen A, 1994.** Diffusion of anions and cations in compacted sodium bentonite. Espoo Technical Research Center of Finland, Vtt Publication 168.
- Muurinen A, 2006.** Personal communication.
- Ochs M, Lothenbach B, Shibata M, Sato H, Yui M, 2001.** An integrated sorption – diffusion model for the calculation of consistent distribution and diffusion coefficients in compacted bentonite. *J. Contam. Hydrol.* 47, 283–296.
- Ochs M, Lothenbach B, Shibata M, Sato H, Yui M, 2003.** Sensitivity analysis of radionuclide migration in compacted bentonite; a mechanistic model approach, *J. Contam. Hydrol.*, 61, 313–328.
- Pusch R, Muurinen A, Lehtikoinen J, Bors J, Eriksen T, 1999.** Microstructural and chemical parameters of bentonite as determinants of waste isolation efficiency. European Commission. Nuclear Science Technology Project Report EUR 18950 EN.
- Shahwan T, Erten H N, Unugur S, 2006.** A characterization study of some aspects of the adsorption of aqueous Co<sup>2+</sup> ions on a natural bentonite clay. *J. Colloid and Interface Sci.*, 300, 447–452.
- Yu J W, Neretnieks I, 1997.** Diffusion and sorption properties of radionuclides in compacted bentonite. SKB TR-97-12, Svensk Kärnbränslehantering AB.

## **Post-test examination of copper coupons from LOT test parcel A2 regarding corrosion**

Bo Rosborg  
Rosborg Consulting

Report compiled by Bo Rosborg based upon experimental work performed at Clay Technology AB, Stockholm University and Studsvik Nuclear AB.

## Summary

Coupons of pure copper have been exposed in LOT test parcel A2 at the Äspö Hard Rock Laboratory from October 1999 to January 2006. The conditions for the coupons have been similar to those anticipated in a KBS-3 repository. This report documents the post-test examination of the copper coupons with the objective to determine the nature and extent of the corrosion.

A brownish corrosion product layer with blue-green corrosion products here and there on top of it covered most of the surface. Cuprite and paratacamite were identified as the major corrosion products.

As before the nature of the corrosion can be classified as a somewhat uneven general attack. A number of surface defects were found in the copper coupons, which are believed to originate from the manufacturing rather than being a result of corrosion. Any obvious signs of pitting cannot be claimed.

The average corrosion rate was estimated to be less than 0.5  $\mu\text{m}/\text{year}$ .

Copper was found to penetrate 500  $\mu\text{m}$  into the bentonite.

# Contents

<b>Background information</b>	147
<b>Experimental procedure</b>	148
<b>Corrosion products</b>	149
<b>Microscopy</b>	151
<b>Gravimetry</b>	155
<b>Penetration depth</b>	155
<b>Acknowledgements</b>	156
<b>References</b>	156

# Background information

The test series “Long Term Test of Buffer Material” (LOT) has been initiated at the Äspö Hard Rock Laboratory comprising conditions similar to those in a KBS-3 repository /1/. The main purpose is to study the behaviour of the bentonite clay. Wyoming bentonite with the commercial name MX-80 has been used. However, additional testing has been included, and the post-test examination of copper coupons exposed in bentonite is the subject of this report.

**Objective:** Determine nature and extent of copper corrosion.

**Attempt:** “Quantitative information about the mean corrosion rate. Qualitative information about pit corrosion and corrosion products.” See Section 2.6 in the main report.

**Hypothesis:** The average corrosion rate is less than 7 µm per year /2/.

In LOT test parcel A2 two coupons each of pure copper were as before exposed in bentonite rings 22 and 30 respectively. Furthermore three cylindrical copper electrodes for real-time corrosion monitoring were also exposed in bentonite ring 36 /3, 4/. The latter are not treated in this report.

The nominal dimensions of the copper coupons were 60×15×1.5 mm. Table A3-1 presents information about the copper coupons before start of exposure. They were manufactured by milling, and then one side was slightly polished. Test parcel A2 was emplaced on October 29, 1999. Full temperature lasted from September 2000 up to December 5, 2005. The test parcel was retrieved on January 16, 2006. The bentonite rings A222 and A230 have been exposed at temperatures of about 75°C and 30°C respectively. The total time of exposure is more than 6 years, and the time of exposure at full temperature is 5 years and 3 months.

Additional groundwater from a dedicated bore-hole in the nearby tunnel wall was added through a small titanium filter tip in the upper part of the test parcel. Full saturation was expected after less than one year at free access to water in the rock/bentonite interface. The actual full water saturation was reached within two years as interpreted from measured moisture and pressure results.

After cutting apart the bentonite rings from the test parcel at Äspö on 2006-01-17/19, they were immediately wrapped in plastic sacks which were air evacuated by means of a vacuum pump. They were then transported to Studsvik and stored in their plastic sacks until further work. The copper coupons in bentonite ring A222 were unfortunately damaged by the cutting wheel during retrieval, thus making an accurate estimation of the corrosion rate for these coupons impossible.

Copper coupons from two test series have earlier been examined. The average corrosion rate of a copper coupon in LOT pilot test parcel S1 (exposed at about 50°C) was estimated to less than 3 µm per year /1/. In LOT test parcel A0 the average corrosion rate of copper coupons (exposed at 35°C and about 80°C respectively) was estimated to less than 4 µm per year /5/. Any obvious signs of pitting were not found.

The work was carried out in accordance with activity plan SKB AP TD F62-06-012. The original data are stored in the primary database Sicada and are traceable by the Activity Plan number.

**Table A3-1. Copper coupons in LOT test parcel A2.**

Coupon	Length mm	Width mm	Thickness mm	Surface area mm <sup>2</sup>	Weight g	Micro hardness indentation
A222E	60.12	15.01	1.51	2,032	12.0564	x
A222F	60.07	15.04	1.52	2,035	12.0856	
A230G	60.09	14.99	1.52	2,030	12.1411	x
A230H	60.11	14.99	1.52	2,030	11.7696	

## Experimental procedure

Copper coupons A222E and A222F were clearly seen on the side of bentonite ring A222 due to the unfortunate damage by the cutting wheel. Thus, it was quite trivial to cut apart the bentonite ring close to the coupons and break loose the coupons. Coupons A230G and A230H were removed from bentonite ring A230 by a step-wise “fracturing” of the bentonite ring until one end of each coupon was spotted. Then the bentonite piece containing the coupon was prepared to facilitate the breaking loose of the coupon.

The experimental procedure involved the following steps:

- Photographing of bentonite rings 22 and 30 as received
- Break loose a copper coupon
- Record the position of the coupon in the bentonite block
- Photographing of the coupon and adjacent bentonite pieces
- Photographing of the coupon in a stereomicroscope
- Weighing of the coupon after spraying with pure alcohol
- Perform either SEM/EDS or scrape off corrosion products from the coupon
- Store the coupon in a desiccator until further cleaning and continued examination
- Ultrasonic cleaning in pure alcohol during 1 min
- Drying and weighing
- Photographing
- Ultrasonic cleaning in pure alcohol during 4 min
- Drying and weighing
- Photographing
- Ultrasonic cleaning in pure alcohol during another 5 min
- Drying and weighing
- Photographing
- SEM (adherent corrosion products and corrosion attack)
- Ultrasonic treatment in 10% H<sub>2</sub>SO<sub>4</sub> solution for 5 min
- Drying and weighing
- Another ultrasonic treatment in 10% H<sub>2</sub>SO<sub>4</sub> solution for 5 min
- Drying and weighing
- Microscopy (for final verification of corrosion attack)

The examination focused on copper coupons A230G and A230H. Coupons A222E and A222F were less extensively investigated. It was intended to incorporate a reference coupon in the present investigation through all cleaning procedures for the purpose of comparison. However, due to the fact that two out of four copper coupons in the test parcel were damaged during retrieval, it was decided to save the reference coupons for later investigations of copper coupons within the LOT project.

Sampling of corrosion products was performed immediately after breaking loose each copper coupon. The samples and the copper coupons were stored in a desiccator until further work.

All coupons but for coupon A222F were ultrasonically descaled in 10% H<sub>2</sub>SO<sub>4</sub> solution before final microscopy.

## Corrosion products

After breaking loose a copper coupon from the bentonite, corrosion products could as found before /1, 5/ be seen on parts of the bentonite surfaces facing the copper coupon, see Figure A3-1a, thus revealing a better adherence to the bentonite on part of the surface. A brownish corrosion product layer with blue-green corrosion products here and there on top of it covered most of the copper coupons, see Figure A3-1b. However, apparently bare copper surface was also seen. The blue-green corrosion products revealed the presence of bivalent copper.

Scraping off the brownish corrosion product layer on the bentonite revealed blue-green corrosion products below. X-ray diffraction (XRD) measurements using a Guiner-Hägg powder diffraction camera (wave length Cu  $K\alpha_1$  1.54060 Å) has confirmed that the main constituent of the brownish layer is cuprite ( $\text{Cu}_2\text{O}$ ) and that the blue-green corrosion products contain paratacamite ( $\text{Cu}_2(\text{OH})_3\text{Cl}$ ).

The blue-green corrosion products were not only unevenly distributed on the copper coupons, but also in between them. Copper coupon A230G contained the most, see Figure A3-1b through A3-1e. (It showed also the maximum weight loss, see below.) The EDS data revealed higher Al, Si and Fe contents in the blue-green corrosion products, as compared to the adjacent surface on the coupon, showing that they penetrated into the bentonite, see Table A3-2.



**Figure A3-1a.** Corrosion products seen on the adjacent bentonite after breaking loose copper coupon A230H. (The copper coupon is in place in the upper bentonite piece.)

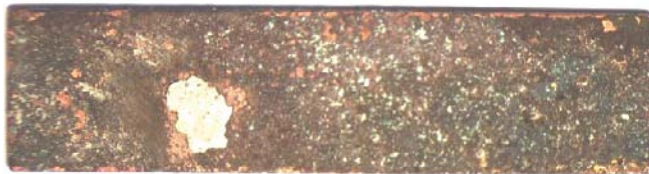


**Figure A3-1b.** Distribution of the blue-green corrosion products (almost white in the picture) on side 1 of copper coupon A230G. (The nominal dimensions of the coupon are 60×15×1.5 mm.)

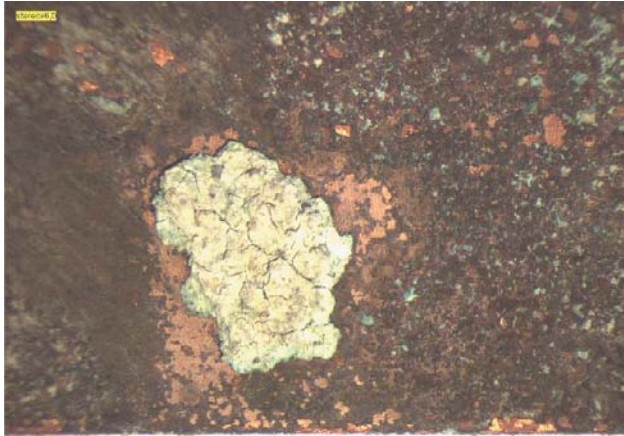


*Figure A3-1c. Part of Figure A3-1b with the blue-green “crust”.*



*Figure A3-1d. Distribution of the blue-green corrosion products (almost white in the picture) on side 2 of copper coupon A230G.*

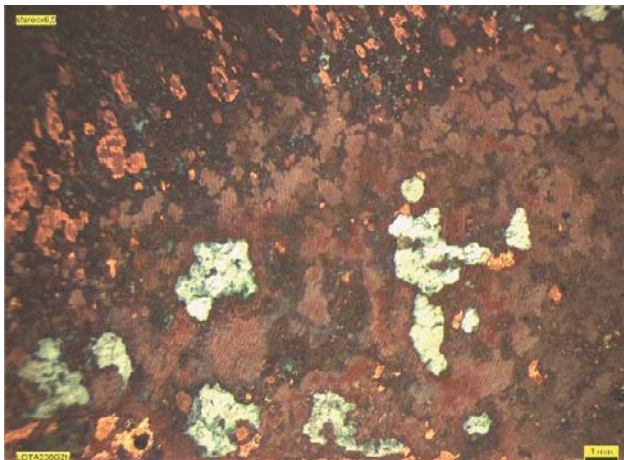


*Figure A3-1e. Part of Figure A3-1d with the blue-green corrosion products.*

**Table A3-2. SEM/EDS analysis on and next to blue-green corrosion products in copper coupon A230G (atom-%).**

	Mg	Al	Si	S	Cl	Ca	Fe	Cu
Blue-green corrosion product	2.3	16.2	42.8	0.5	11.3	0.4	1.8	24.4
Next to	0.9	2.4	5.3	0.6	7.0	2.4		81.5
Next to, another spot		2.5	6.4	0.5	6.6	1.7		82.4
Another blue-green corrosion product	1.8	13.7	45.0	0.4	9.6	0.7	1.9	26.9
Next to		1.4	2.8	0.5	7.5	0.2		87.6

## Microscopy

As in the previous investigation of the copper coupons from LOT test parcel A0 /5/ the micro hardness indentation marks on the polished side of coupons A222E and A230G made before exposure, as shown in Figure A3-2a, were not found after exposure, in spite of the fact that the identification, the milling cutter and the polishing marks are clearly seen (and that the average corrosion rate is estimated to be less than 0.5  $\mu\text{m}/\text{year}$ , see below).

Since the indentation marks were not found a series of photos were as one alternative taken in the centre of the coupon, see Figure A3-2b. As another alternative in order to visualize the extent of the corrosion attack, or rather the absence of any major corrosion, photos were also taken of the identification marks (the letters), see Figure A3-2c.

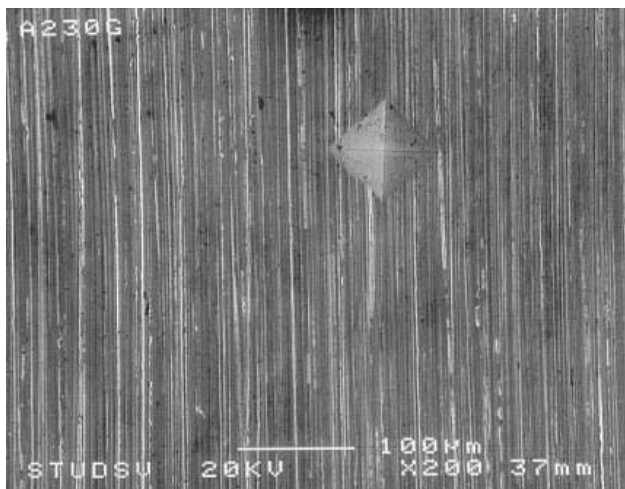


**Figure A3-2a.** The micro hardness indentation mark (a Vickers pyramid indent) in the centre of the slightly polished side 1 of copper coupon A230G before exposure.

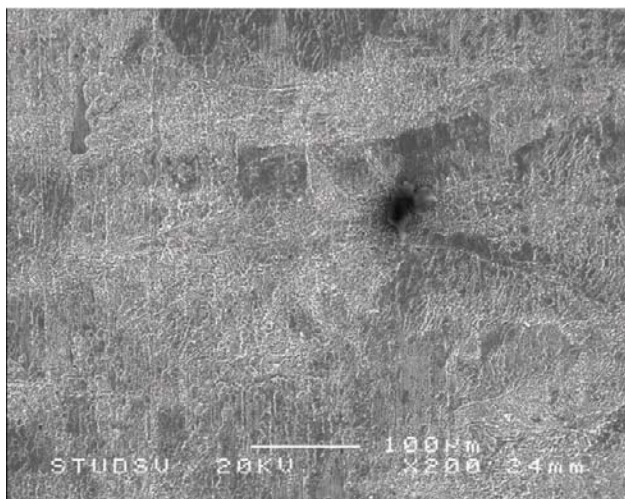


**Figure A3-2b.** The centre of the slightly polished side 1 of copper coupon A230G after exposure. (The intention was to find the indentation mark shown in Figure A3-2a after exposure and take a picture of the very same area. However, the mark was not found.)

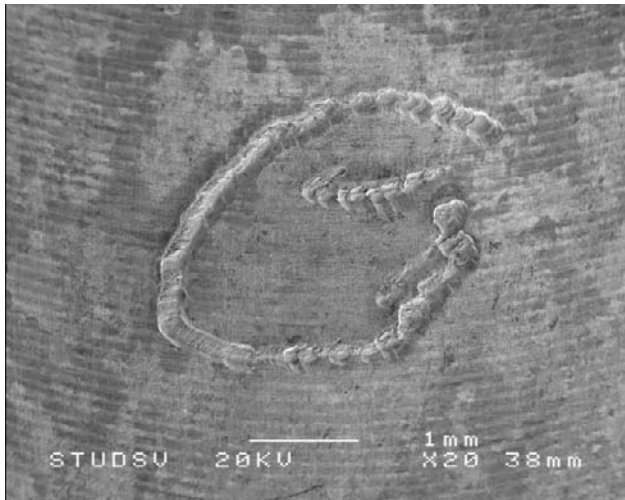


**Figure A3-2c.** The identification mark (the letter G) on side 1 of copper coupon A230G after exposure. (Do observe that the milling cutter marks, but not the polishing marks, are clearly seen.)

A number of surface defects of the kind shown in Figure A3-2d were, however, found in the copper coupons. They are believed to originate from the manufacturing rather than being a result of corrosion. Any signs of active pits could not be found.

Figures A3-2g through A3-2i show the area below and next to the crust in Figure A3-1b after descaling. The amount of corrosion is somewhat higher at the crust. However, any unambiguous signs of pitting are not obvious.

In summary, the nature of the corrosion can as before be classified as a somewhat uneven general attack. Any obvious signs of pitting cannot be claimed.

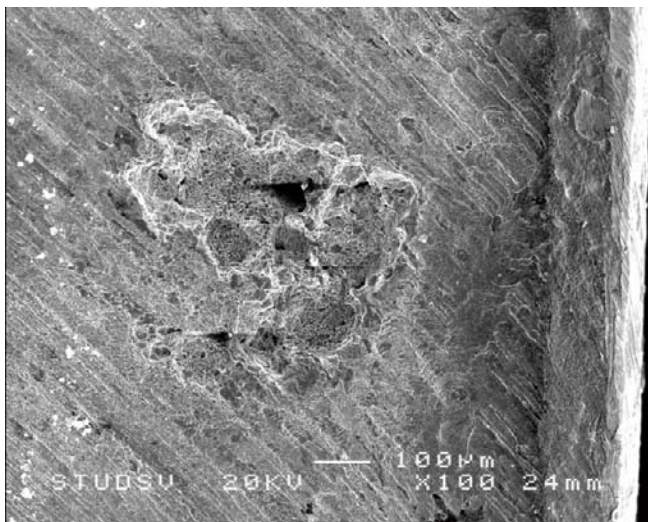


**Figure A3-2d.** Surface defect found in copper coupon A230G close to one edge.

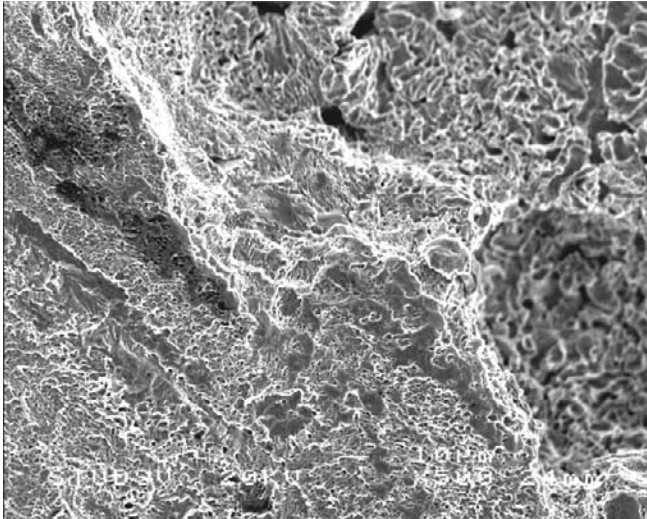


*Figure A3-2e. Detail of Figure A3-2d.*

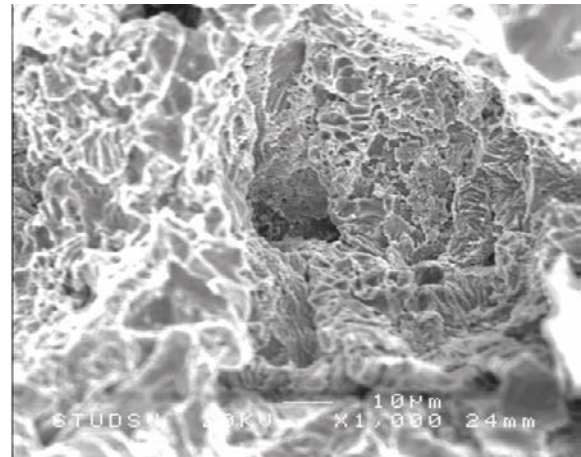
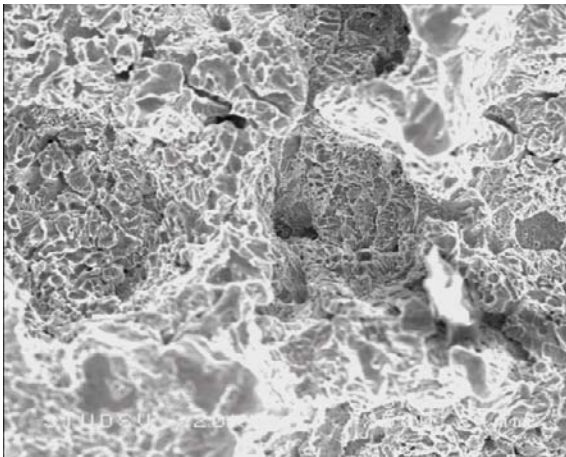


*Figure A3-2f. Another detail of Figure A3-2d in two magnifications.*

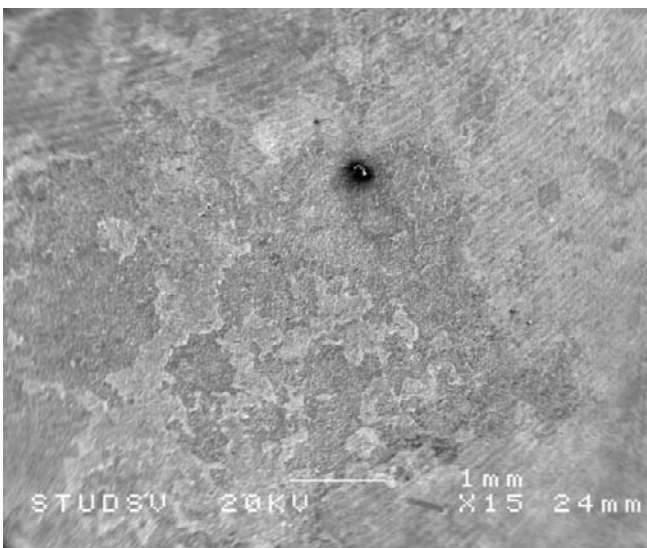


*Figure A3-2g. The area at the crust in Figure A3-1b after descaling.*

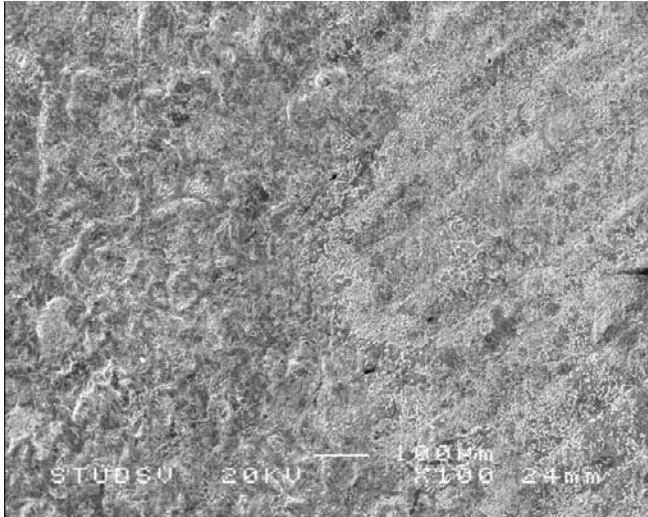


**Figure A3-2h.** Detail of Figure A3-2g showing the boundary between more corroded and less corroded area (the latter to the right where the milling cutter marks are clearly seen).

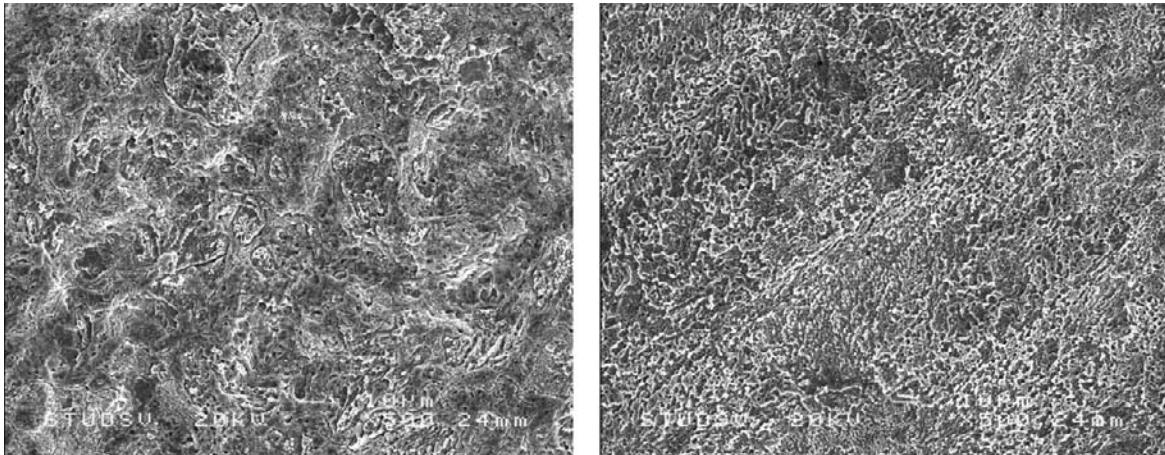


**Figure A3-2i.** The more corroded area (to the left) and the less corroded area (to the right) in higher magnification.

## Gravimetry

The weight loss data are summarized in Table A3-3. (The weight loss for coupon A222E is an estimate and coupon A222F has not been weighed.) Based upon the maximum weight loss obtained (that is for copper coupon A230G) the average corrosion rate of copper was estimated to less than 0.5  $\mu\text{m}/\text{year}$ .

**Table A3-3. Weight loss data and estimated average corrosion rate.**

Coupon	Original weight g	Final weight g	Weight loss mg	Corrosion rate $\mu\text{m}/\text{year}$
A222E	12.0564		31	
A222F	12.0856			
A230G	12.1411	12.0952	46	<0.5
A230H	11.7696	11.7426	27	

The estimated average corrosion rate is considerably lower than the values earlier obtained from LOT test parcels A0 and S1. The weight losses for the copper coupons in test parcel A2 (27–46 mg), exposed more than six years, are in fact lower than the weight losses for the coupons in test parcels A0 and S1 (77– 86 mg), exposed less than two years /1, 5/.

The estimated average corrosion rate does not contradict the earlier findings from the performed real-time corrosion monitoring in LOT test parcel A2 /3, 4/.

## Penetration depth

The penetration depth of copper into the bentonite next to copper coupon A230H has been examined. The bentonite samples were prepared by means of breaking the bentonite pieces facing the coupon in such a way that fracture surfaces perpendicular to the coupon were obtained. Bentonite sample H4b was picked for EDS.

As seen from the figure below copper was found to penetrate 500  $\mu\text{m}$  into the bentonite.

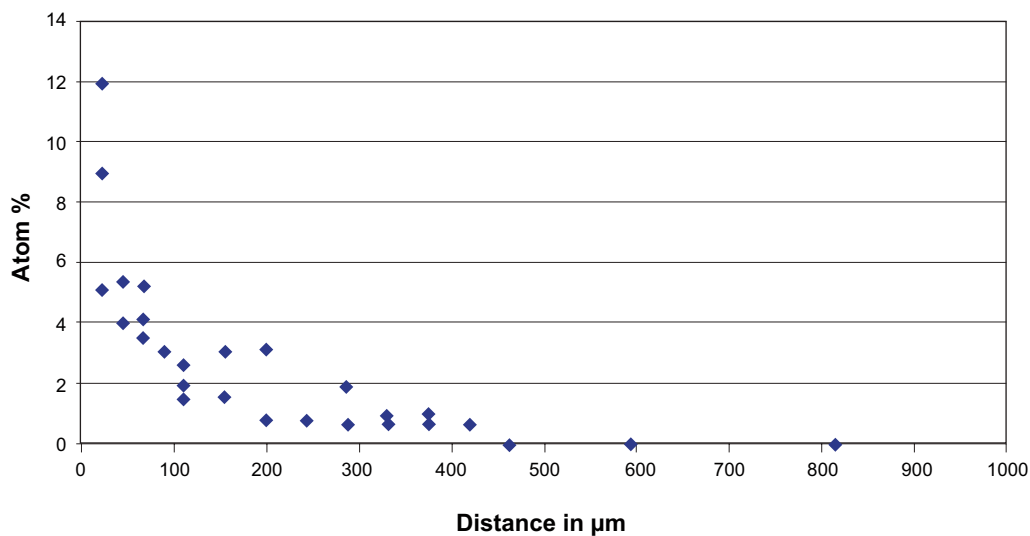


**Figure A3-3.** Copper profile in bentonite next to copper coupon A230H.

## Acknowledgements

The contributions from Martin Birgersson, Ola Karnland, Ulf Nilsson and Siv Olsson, at Clay Technology AB, Lars Göthe (XRD) at Stockholm University, and Eva Sund and Roger Lundström (SEM and stereomicroscopy) at Studsvik Nuclear AB are gratefully acknowledged.

## References

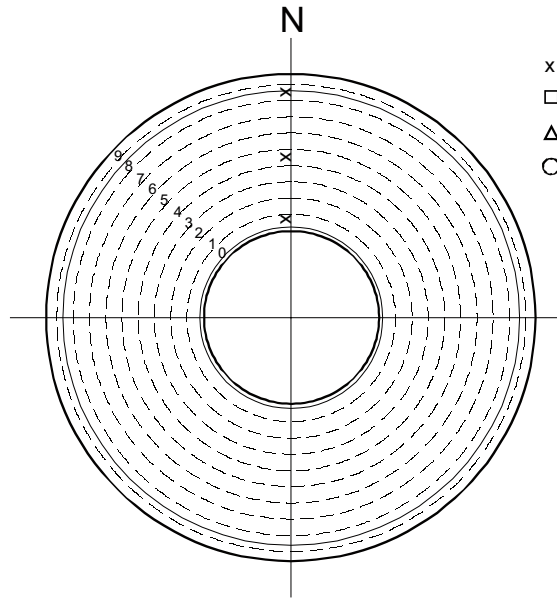
- /1/ **Karnland O, Sandén T, Johannesson L-E, Eriksen T E, Jansson M, Wold S, Pedersen K, Motamedi M, Rosborg B, 2000.** Long term test of buffer material – Final report on the pilot parcels, December 2000. SKB TR-00-22, Svensk Kärnbränslehantering AB.
- /2/ **P Wersin, K Spahiu, J Bruno, 1994.** Kinetic modelling of bentonite-canister interaction. Long-term predictions of copper canister corrosion under oxic and anoxic conditions, SKB TR-94-25, Svensk Kärnbränslehantering AB.
- /3/ **Rosborg B et al, 2004.** Real-time monitoring of copper corrosion at the Äspö HRL, Proc 2nd Inter Workshop Prediction of Long Term Corrosion Behaviour in Nuclear Waste Systems, Nice, September 2004, p 11-23. ISBN 2-9510108-6-9.
- /4/ **Rosborg B, Pan J, Eden D, Karnland O, Werme L.** Real-time monitoring of copper corrosion at the Äspö Hard Rock Laboratory, CORROSION/2004, Paper No.04687, NCE Houston, TX, 2004.
- /5/ **Karnland O, Olsson S, Sandén, Fälth B, 2009 in press.** Long term test of buffer material at the Äspö HRL (LOT project) – final report on the A0 test parcel. SKB TR-09-31, Svensk Kärnbränslehantering AB.
- /6/ **Rendahl B, 1998.** Avlägsnande av korrosionsprodukter på koppar (utkast II 98-08-18), Korrosionsinstitutet, Stockholm, 1998 (KI Rapport 65 221).

## **Bentonite block description and sensor configuration**

## A2 02

### Sensors:

A2020T  
A2024T  
A2028T

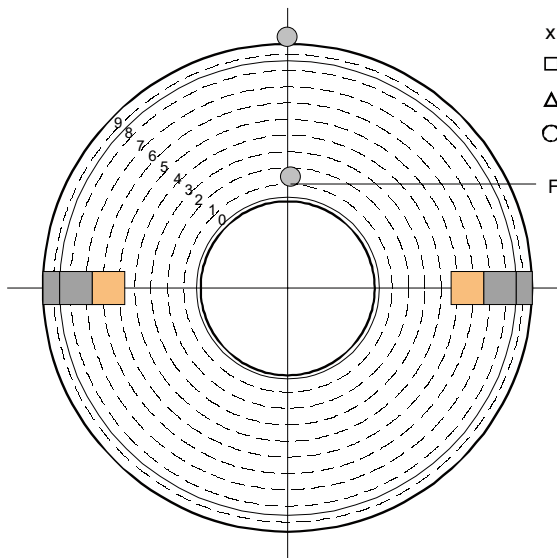


- x Thermocouple (endpoint 35 mm down in bentonite)
- Total Pressure (countersunked into the block)
- △ Water Pressure (countersunked into the block)
- Relative Humidity (countersunked into the block)

## A2 05

### Sensors:

Tracertest by filter  
and plugs



- x Thermocouple (endpoint 35 mm down in bentonite)
- Total Pressure (countersunked into the block)
- △ Water Pressure (countersunked into the block)
- Relative Humidity (countersunked into the block)

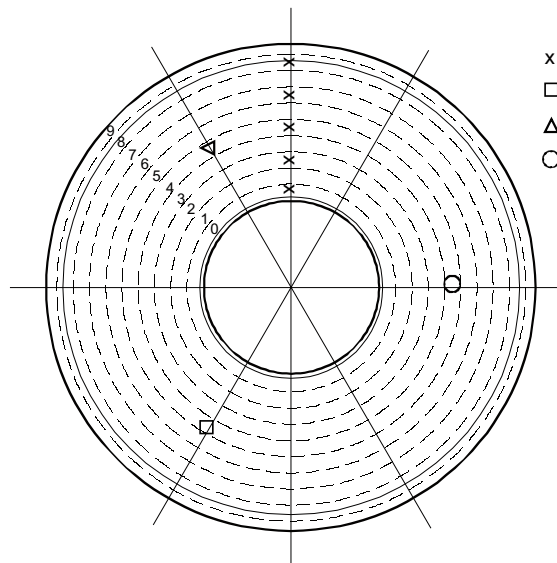
Filters for tracer and water saturation

Tracer doped plugs  $^{60}\text{Co}$

## A2 08

### Sensors:

A2080T  
A2082T  
A2084T  
A2086T  
A2088T  
  
A2084P  
A2084W  
A2084M

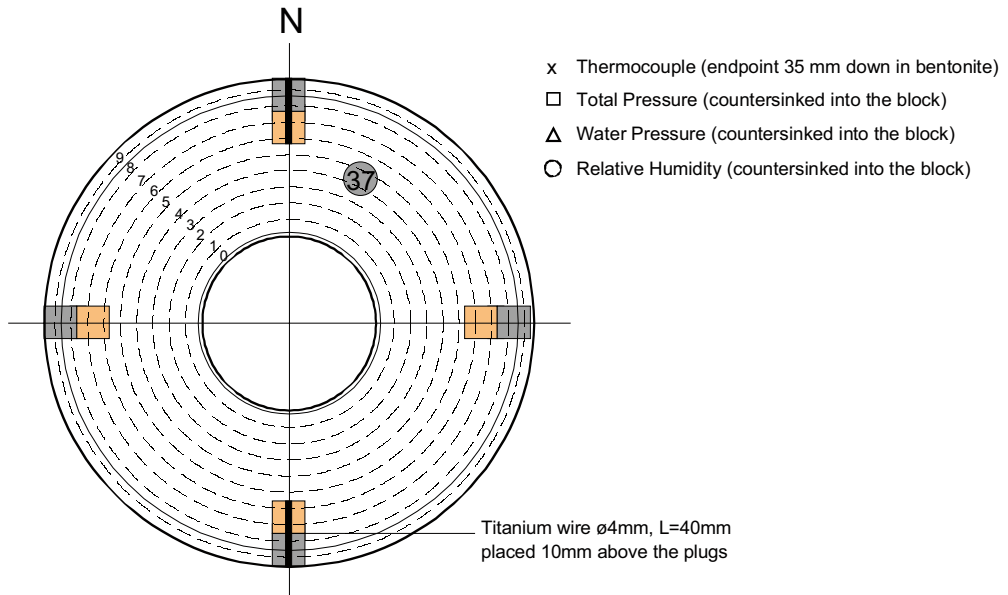


- x Thermocouple (endpoint 35 mm down in bentonite)
- Total Pressure (countersunked into the block)
- △ Water Pressure (countersunked into the block)
- Relative Humidity (countersunked into the block)

## A2 10

### Sensors:

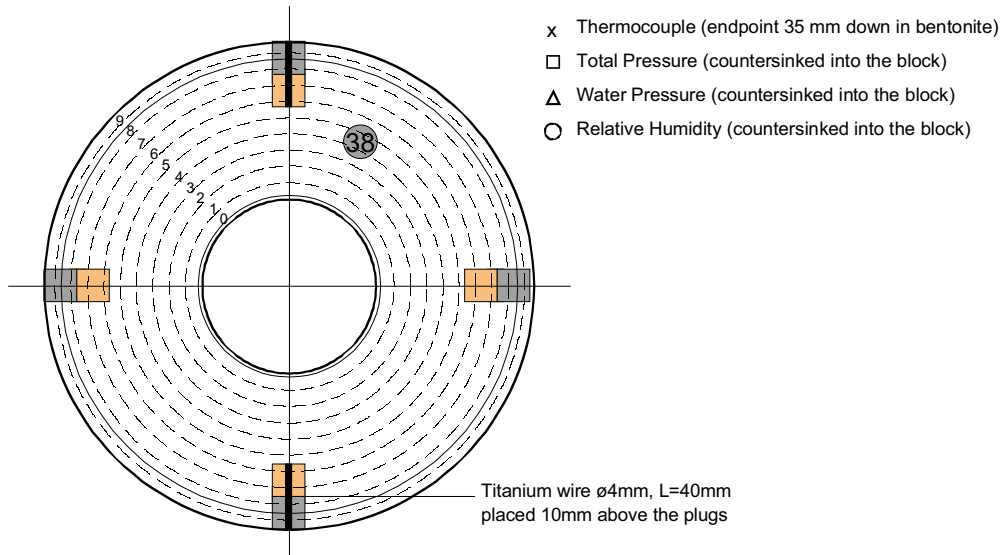
Water sampling  
10% CaCO<sub>3</sub>



## A2 12

### Sensors:

Water sampling  
10% CaSO<sub>4</sub>

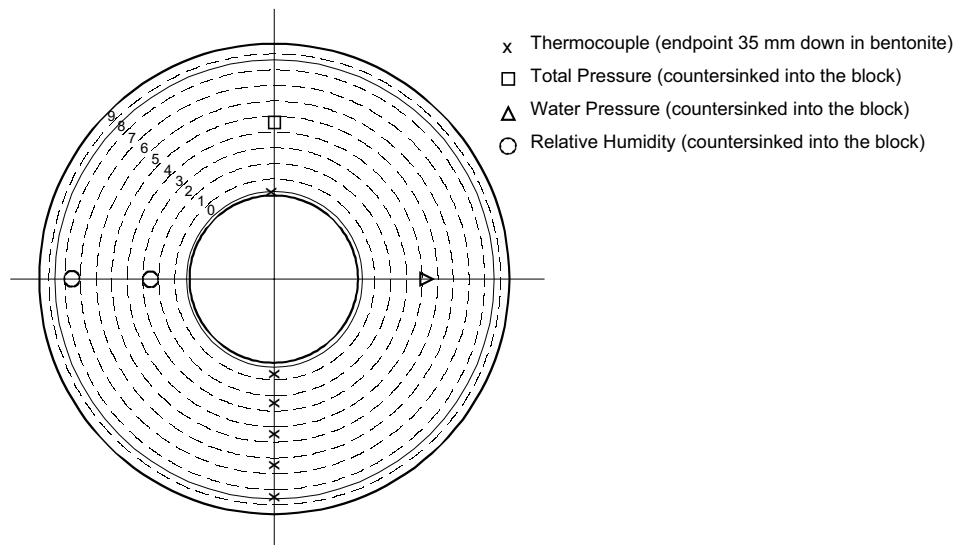


## A2 14

### Sensors:

A214TT  
A2140T  
A2142T  
A2144T  
A2146T  
A2148T

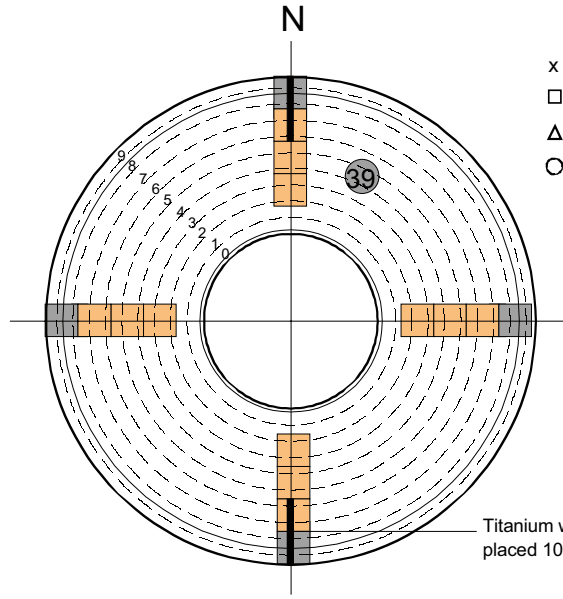
A20144P  
A2144W  
A2142M  
A2147M



## A2 16

### Sensors:

Water sampling  
50% K-feldspar

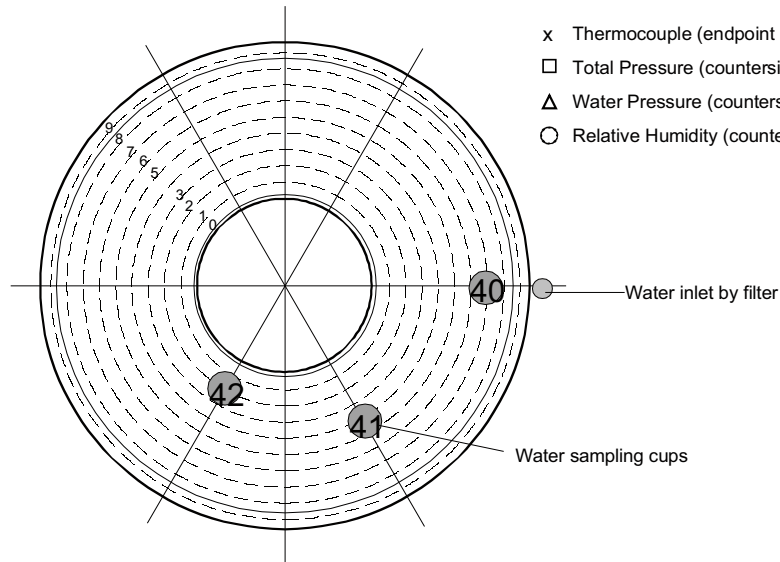


- x Thermocouple (endpoint 35 mm down in bentonite)
- Total Pressure (countersunked into the block)
- △ Water Pressure (countersunked into the block)
- Relative Humidity (countersunked into the block)

## A2 18

### Sensors:

Water sampling



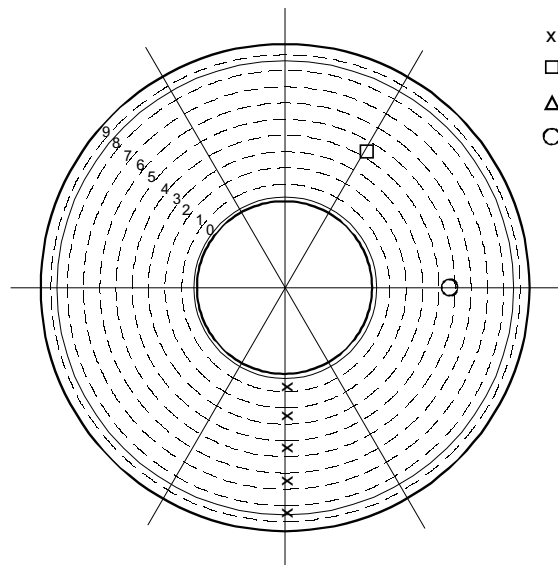
- x Thermocouple (endpoint 35 mm down in bentonite)
- Total Pressure (countersunked into the block)
- △ Water Pressure (countersunked into the block)
- Relative Humidity (countersunked into the block)

## A2 20

### Sensors:

A2200T  
A2202T  
A2204T  
A2206T  
A2208T

A2204P  
A2204W  
A2204M

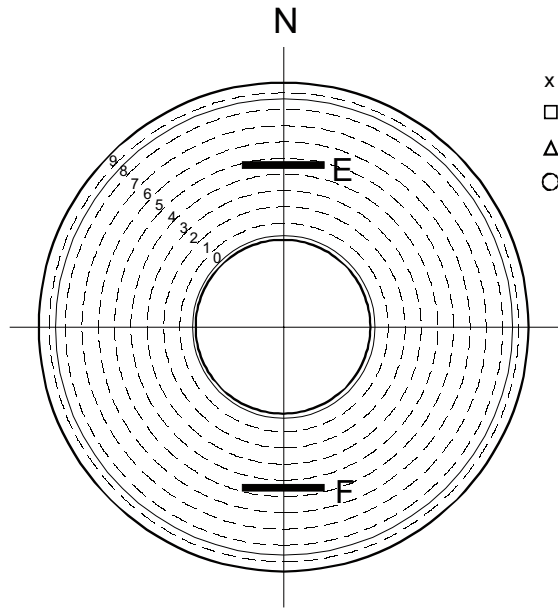


- x Thermocouple (endpoint 35 mm down in bentonite)
- Total Pressure (countersunked into the block)
- △ Water Pressure (countersunked into the block)
- Relative Humidity (countersunked into the block)

## A2 22

### Sensors:

Cu plate

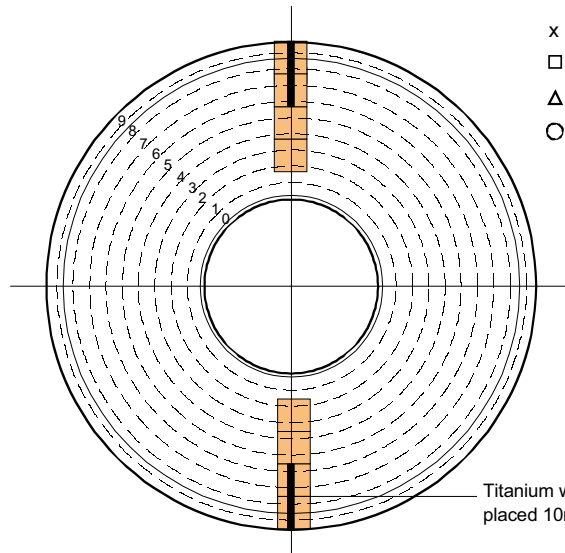


- x Thermocouple (endpoint 35 mm down in bentonite)
- Total Pressure (countersunk into the block)
- △ Water Pressure (countersunk into the block)
- Relative Humidity (countersunk into the block)

## A2 24

### Sensors:

Cement Aalborg  
AWP w/c=0.8



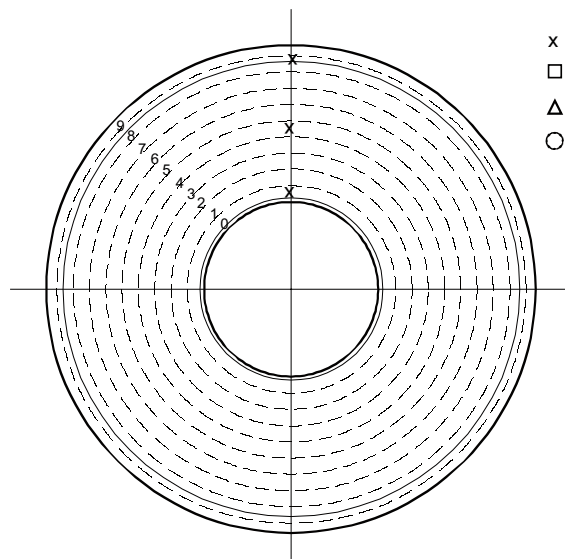
- x Thermocouple (endpoint 35 mm down in bentonite)
- Total Pressure (countersunk into the block)
- △ Water Pressure (countersunk into the block)
- Relative Humidity (countersunk into the block)

Titanium wire ø4mm, L=40mm  
placed 10mm above the plugs

## A2 26

### Sensors:

A2260T  
A2264T  
A2268T

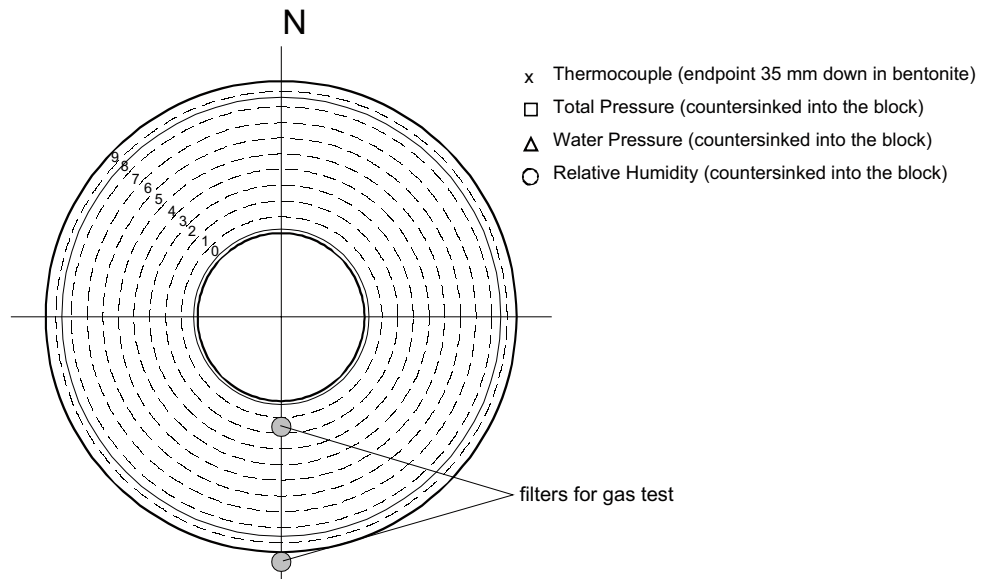


- x Thermocouple (endpoint 35 mm down in bentonite)
- Total Pressure (countersunk into the block)
- △ Water Pressure (countersunk into the block)
- Relative Humidity (countersunk into the block)

## A2 28

### Sensors:

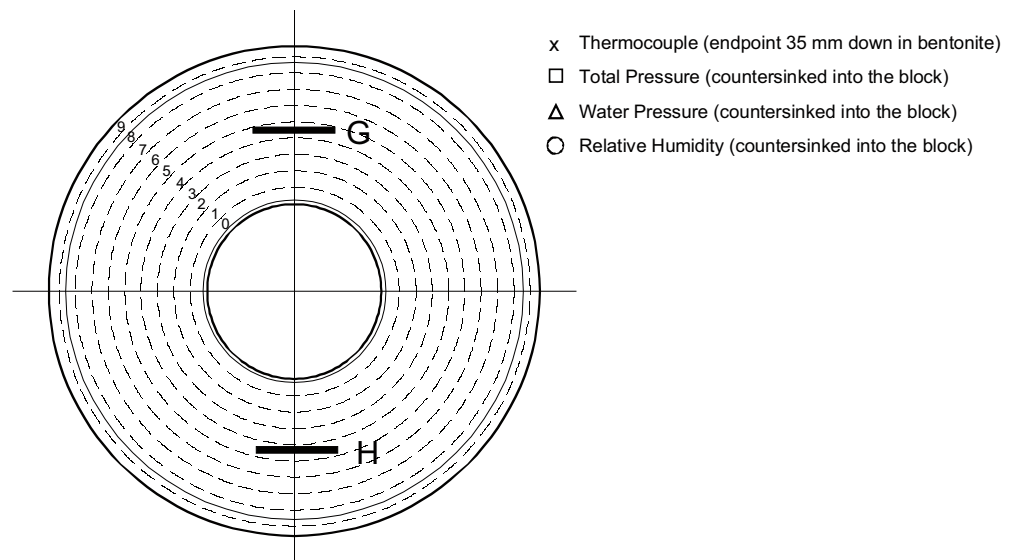
Gas test



## A2 30

### Sensors:

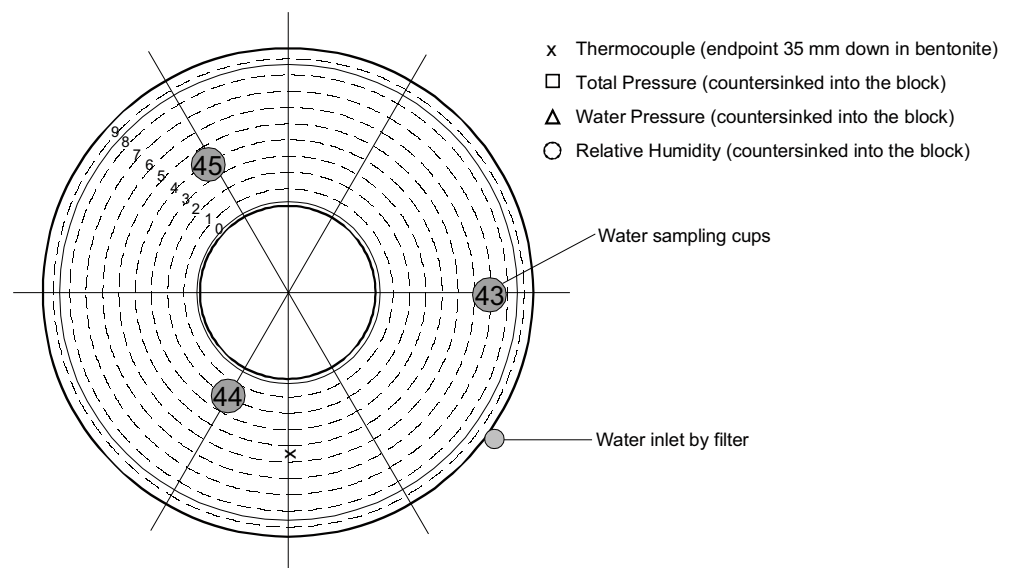
Cu plate



## A2 32

### Sensors:

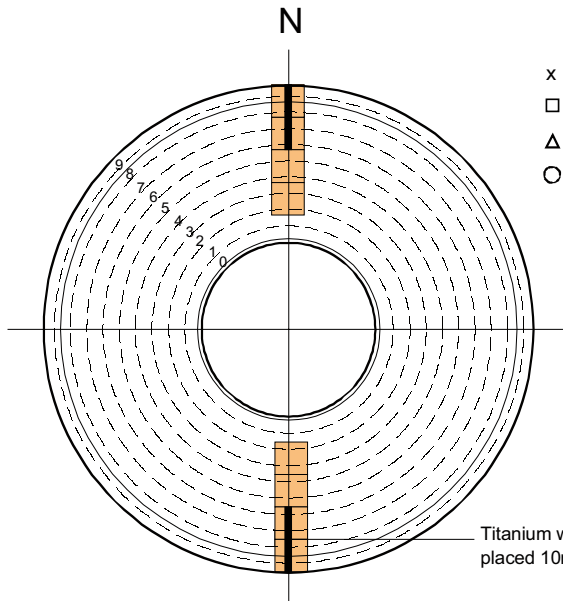
A2324T  
Water sampling



## A2 34

### Sensors:

Cement Aalborg  
AWP w/c=0.8



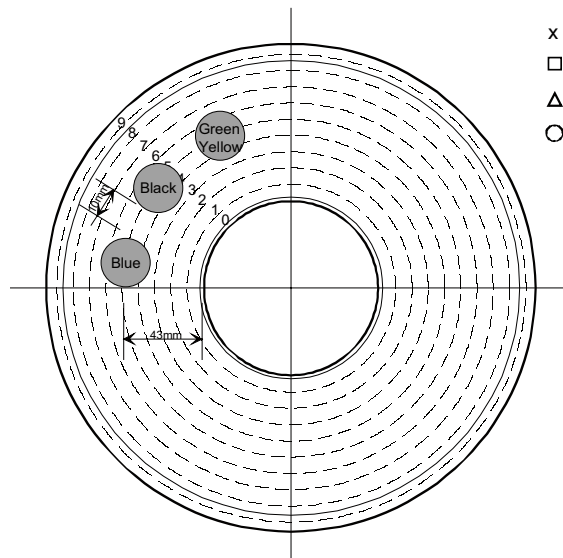
- x Thermocouple (endpoint 35 mm down in bentonite)
- Total Pressure (countersunk into the block)
- △ Water Pressure (countersunk into the block)
- Relative Humidity (countersunk into the block)

Titanium wire ø4mm, L=40mm  
placed 10mm above the plugs

## A2 36

### Sensors:

Electro chemical  
noise sensor  
Copper rods  
ø=29.7mm  
L=90.0mm

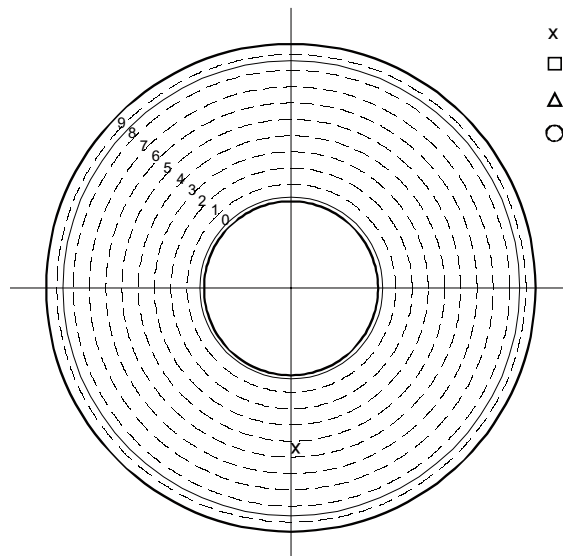


- x Thermocouple (endpoint 35 mm down in bentonite)
- Total Pressure (countersunk into the block)
- △ Water Pressure (countersunk into the block)
- Relative Humidity (countersunk into the block)

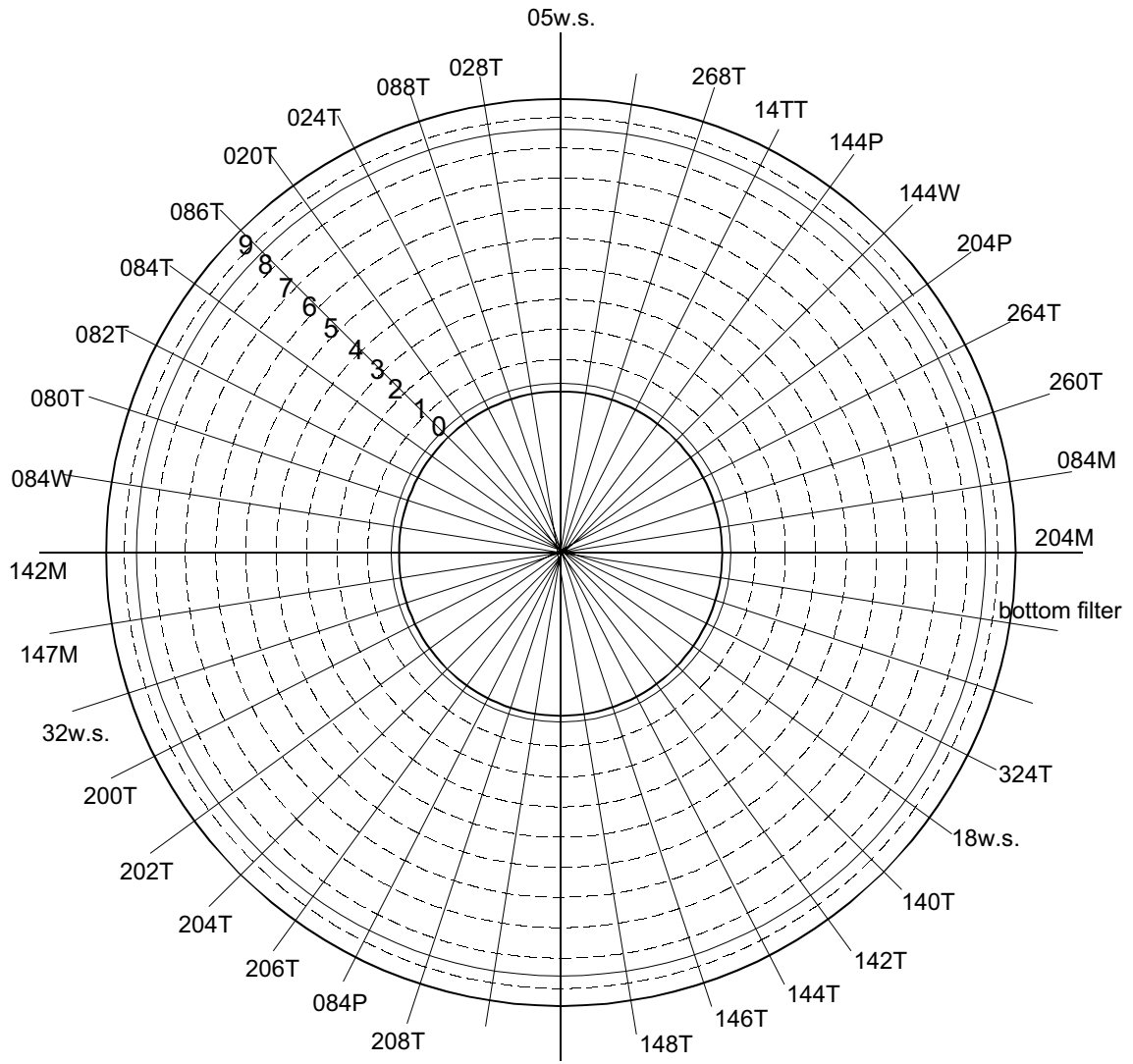
## A2 38

### Sensors:

A2384T



- x Thermocouple (endpoint 35 mm down in bentonite)
- Total Pressure (countersunk into the block)
- △ Water Pressure (countersunk into the block)
- Relative Humidity (countersunk into the block)



**Channel configuration for parcel A2.**

Channel	Tag	Manufacture ID		Description	Units
DS145	A2020T	J 026354	BICC	thermocouple	°C
DS146	A2024T	J 026355	BICC	thermocouple	°C
DS147	A2028T	J 026298	BICC	thermocouple	°C
DS148	A2080T	J 026300	BICC	thermocouple	°C
DS149	A2082T	J 026320	BICC	thermocouple	°C
DS150	A2084T	J 026353	BICC	thermocouple	°C
DS151	A2086T	J 026328	BICC	thermocouple	°C
DS152	A2088T	J 026351	BICC	thermocouple	°C
DS153	A214TT	J 026348	BICC	thermocouple	°C
DS154	A2140T	J 026347	BICC	thermocouple	°C
DS155	A2142T	J 026346	BICC	thermocouple	°C
DS156	A2144T	J 026371	BICC	thermocouple	°C
DS157	A2146T	J 026332	BICC	thermocouple	°C
DS158	A2148T	J 026321	BICC	thermocouple	°C
DS159	A2200T	J 026413	BICC	thermocouple	°C
DS160	A2202T	J 026411	BICC	thermocouple	°C
DS161	A2204T	J 026412	BICC	thermocouple	°C
DS162	A2206T	J 026410	BICC	thermocouple	°C
DS163	A2208T	J 026416	BICC	thermocouple	°C
DS164	A2260T	J 026375	BICC	thermocouple	°C
DS165	A2264T	J 026406	BICC	thermocouple	°C
DS166	A2268T	J 026373	BICC	thermocouple	°C
DS167	A2324T	J 026374	BICC	thermocouple	°C
DS168	A2384T	–	BICC	thermocouple	°C
DS170	A2084M	U3040005	Vaisala	moisture gauge	%
DS171	A2084MT	U3040005	Vaisala	Pt 100	°C
DS172	A2142M	U3040006	Vaisala	moisture gauge	%
DS173	A2142MT	U3040006	Vaisala	Pt 100	°C
DS174	A2147M	U3040007	Vaisala	moisture gauge	%
DS175	A2147MT	U3040007	Vaisala	Pt 100	°C
DS176	A2204M	U3040008	Vaisala	moisture gauge	%
DS177	A2204MT	U3040008	Vaisala	Pt 100	°C
DS178	Eff			A2	W
DS179	A2TUBE1		Druck	pressure	kPa
DS180	A2TUBE2		Druck	pressure	kPa
DS181	A2TUBE3		Druck	pressure	kPa
DS182	A2TUBE4		Druck	pressure	kPa
DS183	flow			flow	l/minM
CS11	A2144W	502326	Geokon	vibrating wire	MPa
CS12	A2144P	502337	Geokon	vibrating wire	MPa
13		P9933	Roctest		
14		P9931	Roctest		
15		P9936	Roctest		
16		P9929	Roctest		

## **Chemical conditions in the A2 parcel of the long-term test of buffer material in Äspö (LOT)**

Arto Muurinen, VTT

September 2006

### **Posiva funded part**

This part concerns a study which was conducted for Posiva within the LOT project. The conclusions and viewpoints presented are those of the authors and do not necessarily coincide with those of SKB.

## Abstract

The Long-Term Test of Buffer Material (LOT) is underway in the Äspö Hard Rock Laboratory in Sweden to test the buffer material for nuclear waste disposal. The test parcels contain prefabricated bentonite blocks placed around a copper tube. A heater is placed in the lower part of the copper tube in order to simulate the heating effect of the spent fuel. The parcels are 300 mm in a diameter and placed in 4 m-long vertical boreholes in granitic rock at a depth of 450 m. This report concerns the chemical studies performed on the parcel A2, which was excavated after about five years of experiment period. Two sample blocks were taken from the hot part of the parcel for studies. One of them was without additives while in the other one, cement plugs had been placed.

**In the block without additives** the water content, which was close to the heater 28–30 wt% of the dry bentonite, increased to 32–33 wt% close to the rock. The total concentrations of dissolving chloride and sulphate in bentonite were determined by dispersing bentonite samples in deionized water. It was obvious that sulphate had redistributed and precipitated close to the heater during the experiment. The initial chloride concentration of bentonite had increased during the experiment approximately by a factor of ten. The increase in the chloride concentration was caused by chloride in the saturating groundwater. Porewaters were squeezed out from the bentonite samples and their  $\text{Na}^+$ ,  $\text{K}^+$ ,  $\text{Ca}^{2+}$ ,  $\text{Mg}^{2+}$ ,  $\text{Cl}^-$ ,  $\text{SO}_4^{2-}$  and  $\text{HCO}_3^-$  concentrations determined. The chloride, sodium and potassium concentrations were rather independent of the distance from the heater. The calcium, magnesium and sulphate concentrations increased and bicarbonate concentrations decreased proceeding from the outer surface towards close to the heater. The chloride concentration in the squeezed porewater was slightly higher than that determined by the dispersion method, but about half of the concentration in the Äspö groundwater. The Eh and pH were measured directly in bentonite samples. Close to the outer surface, the pH in the bentonite was 7.2 and increased to 8.3 close to the heater. The Eh measurements suggest that the conditions in the bentonite were reducing. With the gold electrode, the Eh varied from –183 to –228 mV and with the Pt electrode from –287 to –366 mV, where the more negative values represent the conditions close to the heater.

**In the block with the cement plugs** the water content was somewhat higher than in the block without cement, which may be caused by the effect of the lower temperature in the block with cement. The concentrations of  $\text{Na}^+$ ,  $\text{K}^+$ ,  $\text{Ca}^{2+}$ ,  $\text{Mg}^{2+}$ ,  $\text{Cl}^-$ ,  $\text{SO}_4^{2-}$  and  $\text{HCO}_3^-$  in the squeezed porewaters were practically independent of the distance from the cement but clearly higher than in the block without cement. The pH values were generally somewhat higher than in the block without cement, and the increase was clearly seen in the measurement point closest to the cement.

**Key words:** Nuclear waste, Disposal, Bentonite, Buffer, Porewater chemistry, Rock laboratory.

## Tiivistelmä

Äspön kalliolaboratoriossa Ruotsissa on menossa pitkäaikainen puskurimateriaalin testaus n.s. LOT-koe ydinjätteen loppusijoitusta varten. Testisylinterit on tehty esivalmistetuista bentoniittipaloista, jotka on asetettu kupariputken ympärille. Kupariputken alaosaan on asetettu kuumennin. Bentoniittisylinterit ovat 300 mm halkaisjaltaan ja ne on asetettu neljä metriä pitkiin, pystysuoriin porareikiin graniittikallioon 450 metrin syvyyteen. Tässä raportissa käsitellään kemiallisia tutkimuksia, joita tehtiin sylinterille A2, joka kaivettiin ylös viisi vuotta kestäneen koejakson jälkeen. Kaksi näytepalaa otettiin tutkimuksiin bentoniittisylinterin kuumasta osasta. Toinen niistä oli ilman lisäaineita ja toiseen oli asetettu sementtisylinterejä.

**Palassa ilman lisäaineita** vesipitoisuus lämmittimen lähellä oli 28–30 paino-% bentoniitin kuivapainosta, josta se kasvoi 32–33 prosenttiin kallion läheisyydessä. Liukenevan kloridin ja sulfaatin kokonaispitoisuudet bentoniitissa määritettiin dispersoimalla bentoniittinäyte deionisoituun veteen. Sulfaattipitoisuudet olivat jakaantunut uudelleen kokeen aikana siten, että sulfaatti oli saostunut lämmittimen lähelle. Bentoniitin alkuperäinen kloridipitoisuus, oli kasvanut kokeen aikana noin kymmenenkertaiseksi. Kloridin kasvanut pitoisuus bentoniitissa aiheutui kyllästävän pohjaveden mukana tulleesta kloridista. Huokosvesiä puristettiin bentoniittinäytteistä ja niistä määritettiin  $\text{Na}^+$ -,  $\text{K}^+$ -,  $\text{Ca}^{2+}$ -,  $\text{Mg}^{2+}$ -,  $\text{Cl}^-$ -,  $\text{SO}_4^{2-}$ - and  $\text{HCO}_3^-$ - pitoisuudet. Kloridi-, natrium- ja kaliumpitoisuudet puristetussa huokosvesissä olivat melko riippumattomia etäisyydestä lämmittimestä. Kalsium, magnesium ja sulfaattipitoisuudet kasvoivat ja bikarbonaattipitoisuudet pienenevät siirryttäessä ulkopinnalta lämmittimen läheisyyteen. Kloridipitoisuus puristetussa huokosvedessä oli hiukan suurempi kuin dispersiomenetelmällä määritetty, mutta noin puolet Äspön pohjaveden pitoisuudesta. Eh ja pH mitattiin suoraan bentoniittinäytteistä. Ulkopinnan läheisyydessä pH oli 7.2, josta se kasvoi arvoon 8.3 siirryttäessä lämmittimen läheisyyteen. Eh-mittausten mukaan olosuhteet bentoniitissa olivat pelkistävät. Kultaelektrodilla Eh vaihteli –183 millivoltista –228 millivolttiin ja platinaelektrodilla –287 millivoltista –366 millivolttiin, missä negatiivisemmat arvot edustavat olosuhteita lämmittimen lähellä.

**Palassa, johon sementtisylinterejä oli lisätty**, vesipitoisuus oli hiukan korkeampi kuin palassa ilman sementtiä, mikä saattaa johtua alhaisemmasta lämpötilasta.  $\text{Na}^+$ -,  $\text{K}^+$ -,  $\text{Ca}^{2+}$ -,  $\text{Mg}^{2+}$ -,  $\text{Cl}^-$ -,  $\text{SO}_4^{2-}$ - ja  $\text{HCO}_3^-$ -pitoisuudet puristetussa huokosvesissä olivat käytännössä riippumattomia etäisyydestä sementistä. Bentoniitissa mitatut pH-arvot olivat yleensä hiukan korkeampia palassa, jossa oli sementtiä, ja kasvu oli selvästi nähtävissä mittauspisteessä, joka oli lähinnä sementtiä.

**Avainsanat:** ydinjäte, loppusijoitus, bentoniitti, puskuri, huokosvesikemia, kalliolaboratorio.

## Preface

The Long-Term Test of Buffer Material (LOT) is underway in the Äspö Hard Rock Laboratory in Sweden, which is organized by the Swedish Nuclear Fuel and Waste Management Co. (SKB). The project is coordinated by Clay Technology AB and many other partners are participating in the project. The Finnish nuclear waste company, Posiva Oy, is participating in the project through the work carried out by VTT.

# Contents

<b>1</b>	<b>Introduction</b>	173
<b>2</b>	<b>Experiment with the A2 parcel</b>	175
<b>3</b>	<b>Studies on bentonite samples</b>	176
3.1	Splitting of the bentonite blocks	176
3.2	Measurement of pH and Eh in bentonite	177
3.3	Studies on squeezed porewaters	178
3.4	Analyses with dispersion method	179
<b>4</b>	<b>Results and discussion</b>	180
4.1	Block A2 18	180
4.2	Block A2 24	184
<b>5</b>	<b>Summary</b>	186
<b>6</b>	<b>References</b>	187
<b>Appendix A</b>	Results of the Block A2 18	188
<b>Appendix B</b>	Results of the Block A2 24	189
<b>Appendix C</b>	Concentrations of different components in Äspö groundwater	190

# 1 Introduction

The Long-Term Test of Buffer Material (LOT) project is underway in the Äspö Hard Rock Laboratory in Sweden. The LOT test series may be described as a multi-task experiment in which test parcels are exposed to conditions similar to those in a KBS-3 repository and to conditions that accelerate the alteration processes, respectively. The test parcels contain prefabricated bentonite blocks placed around a copper tube, which are placed in vertical boreholes in a granitic rock structure. The diameters of the holes are 300 mm and the depths around 4 m. In total, the test series includes seven test parcels (Table A5-1) of which three are exposed to standard KBS-3 conditions and four test parcels are exposed to adverse conditions. The two pilot tests (A1 and S1) and the main test A0 have already been completed /Karnland et al. 2000, Muurinen 2003/. All five later test parcels (A0, S2, S3, A2 and A3) have in principle identical constructions, except for a number of different additives at specific locations in the bentonite blocks in the A-type parcel (Figure A5-1). Small titanium ampoules equipped with titanium filters, were also placed at strategic positions in the bentonite in order to get representative water samples from the bentonite at test termination. Temperature, total pressure, water pressure, and water contents, are measured during the heating period. At test termination, the parcels are extracted by overlapping core drilling around the original borehole, and the parcels are lifted and partitioned. Material from defined positions in the test parcels and reference material are thereafter examined by a general, well-defined set of tests and analyses in order to provide data for the different objectives.

This report concerns studies performed by VTT on the A2 parcel, which was excavated between December 2005 and January 2006 after about five years' operation. The aim of the work carried out by VTT in the LOT project is to obtain data about the chemical conditions to be developed in bentonite. Porewaters were squeezed out from the bentonite samples next to the ampoules and cement additives placed in the bentonite and their chemical compositions determined. Measurements of pH and Eh were performed directly in the bentonite samples. Dissolving chloride and sulphate in bentonite were determined by the dispersion method.

**Table A5-1. Specification of the LOT test series.**

Type	No	Type	T, °C	P <sub>c</sub>	time, y	Remark
S	1	standard	90	T		Finalized
S	2	standard	90	T	~5	Ongoing
S	3	standard	90	T	~20	Ongoing
A	0	adverse	120 <150	T, ([K <sup>+</sup> ], Am, pH)	1	Finalized
A	1	adverse	120 <150	T, ([K <sup>+</sup> ], Am, pH)	1	Finalized
A	2	adverse	120 <150	T, ([K <sup>+</sup> ], Am, pH)	~5	Analyzing
A	3	high T	120 <150	T	~5	Ongoing

S = standard conditions      A = adverse conditions  
P<sub>c</sub> = controlled parameter      C = cementation  
Ma = mineralogical alteration      Am = accessory minerals

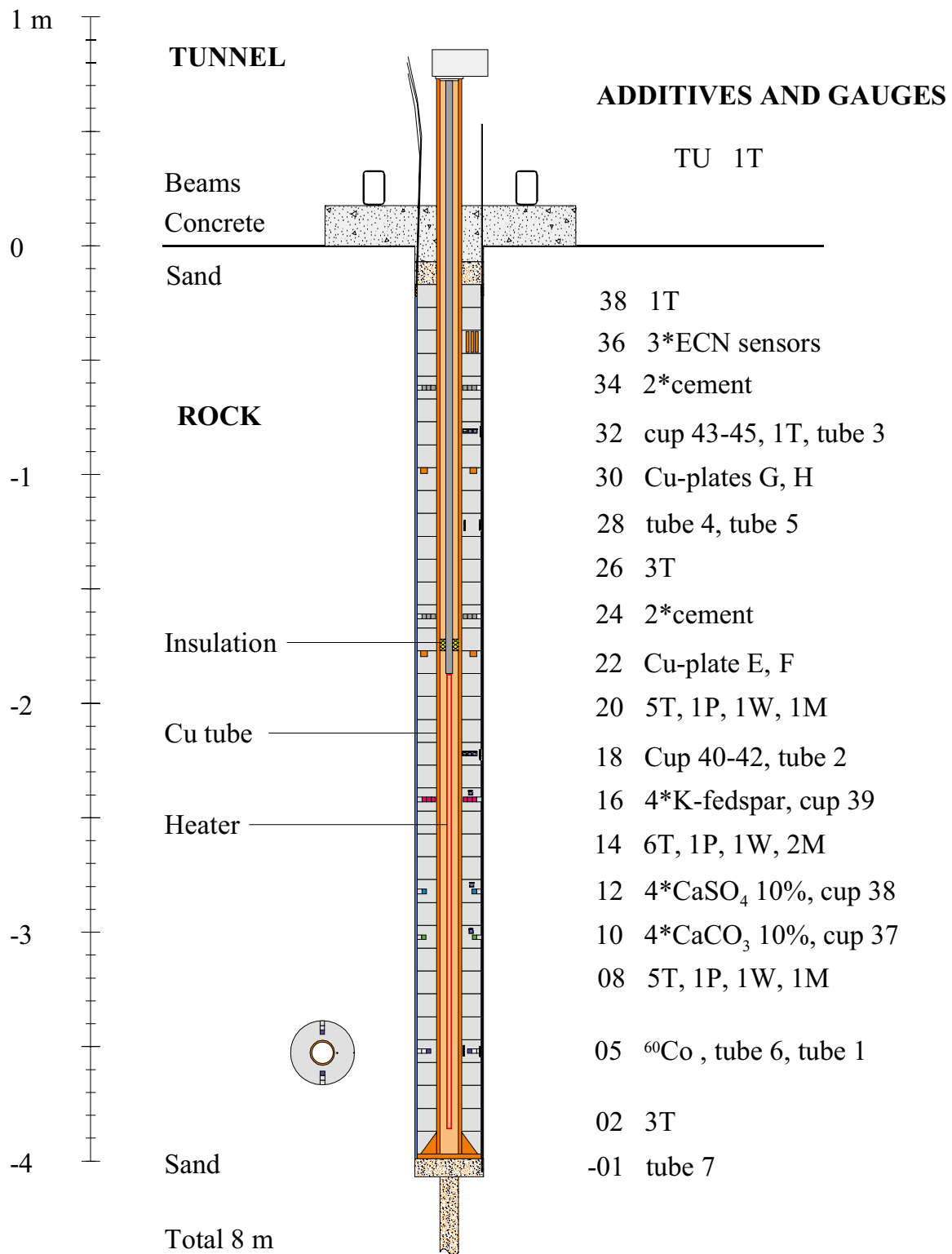


**Figure A5-1.** Principle scaled layout of the A2 test parcel. Numbers on the right-hand side of the parcel indicate the block number and the following text refers to sensors and additives.

## 2 Experiment with the A2 parcel

Figure A5-1 presents the construction of the A2 parcel. Wyoming bentonite sold under the commercial name MX-80 was the source material for all the bentonite components in the system. The bentonite material was compacted so that the intended water-saturated density was 2,000 kg/m<sup>3</sup>. In order to study the chemical changes caused by cement in the bentonite, cement plugs cast from Aalborg white Portland cement and deionized water in the cement-water ratio of 0.8 were placed in the bentonite. The plugs were placed in cylindrical holes, which were drilled from the mantle surface into the specified blocks.

The A2 parcel was placed in the KG0037G01 test hole situated in the G-tunnel at -450 m level in 29 Oct. 1999. The power to the heater was turned on 2 Feb 2000, and was increased in steps to 850 W. Stable temperature conditions were reached after one year, and the final temperature distribution shown in Figure A5-2 represents fairly well the conditions during the whole 5-year test period. The power was turned off 5 Dec 2005 in order to facilitate the uplift and sampling. Percussion drilling was started 9 Jan 2006 in order to uncover a rock column around the A2 test parcel. The column was released at the bottom by thread-sawing and finally lifted 16 Jan 2006. The rock cover was removed starting the following day 17 Jan 2006, and a rough partition of the clay was made at the test site. The remaining part was divided into sections, as similar to the original 10 cm-high blocks as possible, using saws and knives. Block 18 without additives and half of block 24 with one cement plug were carefully placed in metal vessels, flushed with N<sub>2</sub> and sent to VTT. The temperature of block 24 was somewhat lower than that of block 18, as seen in Figure A5-2, which is based on the field data of the LOT experiment.

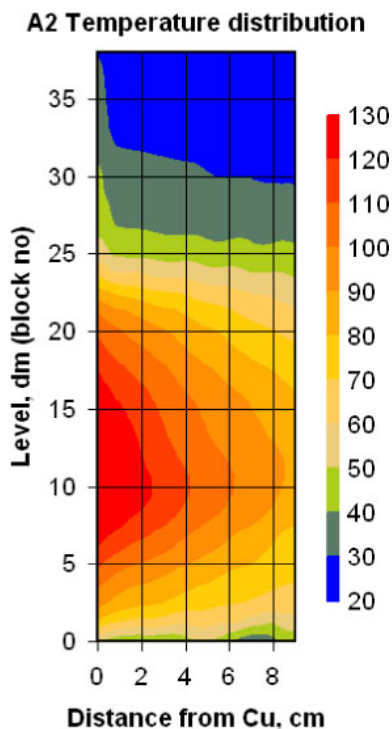


Figure A5-2. Temperature distributions in parcel A2 just before termination of the power.

### 3 Studies on bentonite samples

#### 3.1 Splitting of the bentonite blocks

The bentonite samples were sent by Clay Technology AB to VTT in metallic transportation vessels flushed with nitrogen for oxidation shielding. At VTT, the bentonite was moved into a nitrogen glove box (N-box, O<sub>2</sub> about 500 ppm) for splitting. The bentonite samples were cut in the N-box with a band saw. Sample vessels of 125 ml, which had been in nitrogen atmosphere for removal of the oxygen from their surfaces, were used for storage of the sample pieces.

Figure A5-3 presents the splitting of block 18. First the sectors containing the titanium cups were cut away and the cups removed. A hole was bored into the sinter of the cup, and through this hole a pipette was used to remove the water. However, it appeared that all the sinter cups were empty.

Sector SE between the sinter cups 40 and 41 was selected to be used in the studies and sector S between cups 41 and 42 for back-up samples. The upper and lower layers (A, C) were removed from sector SE. Then a thin horizontal layer (B2) was cut from sector SE. Two bars were cut from B2 and used for preparation of 1 cm-long dispersion samples and water content samples extending from the copper tube to the outer surface. The rest of the middle layer (B1) was cut into six sub-samples, which represent the radial distances 0–3.3 cm (SEa), 3.3–6.6 cm (SEb) and 6.6–10 cm (SEc) from the copper tube. The sub-samples were closed in plastic vessels, which were moved to an N<sub>2</sub> glove box (Braun glove-box, O<sub>2</sub> <1 ppm) and opened there for a while in order to change the gas in the vessel for one of a lower O<sub>2</sub> concentration. The vessels were then stored in the Brown glove box until used for porewater squeezing and the samples of direct pH and Eh measurements.

Figure A5-4 presents splitting of the northern half of block 24, where one of the cement plugs was placed. The upper and lower layers (A, C) were first removed and the middle layer B used for the samples. The samples to be studied were cut from both sides of the cement plug. To the left of the

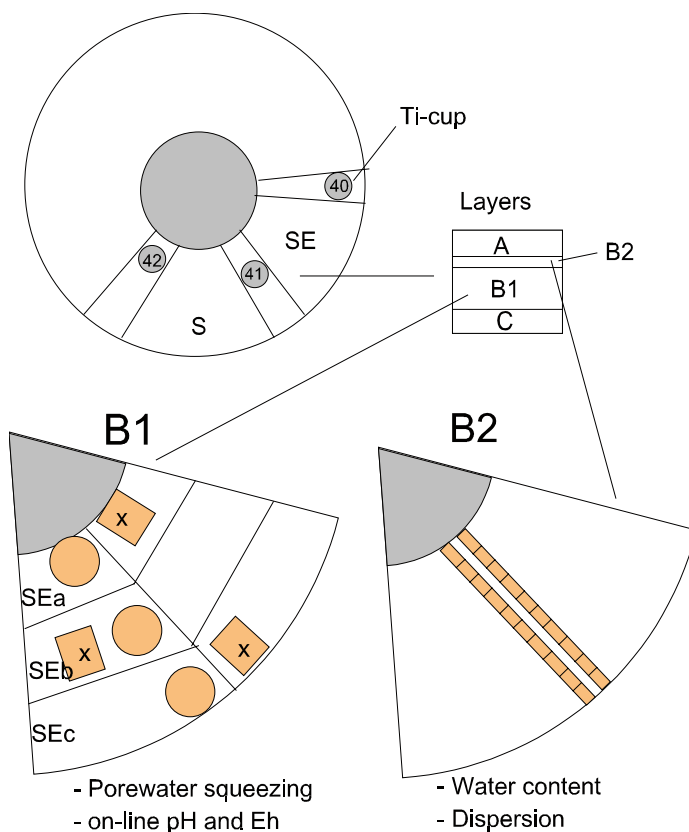


Figure A5-3. Splitting of block 18.

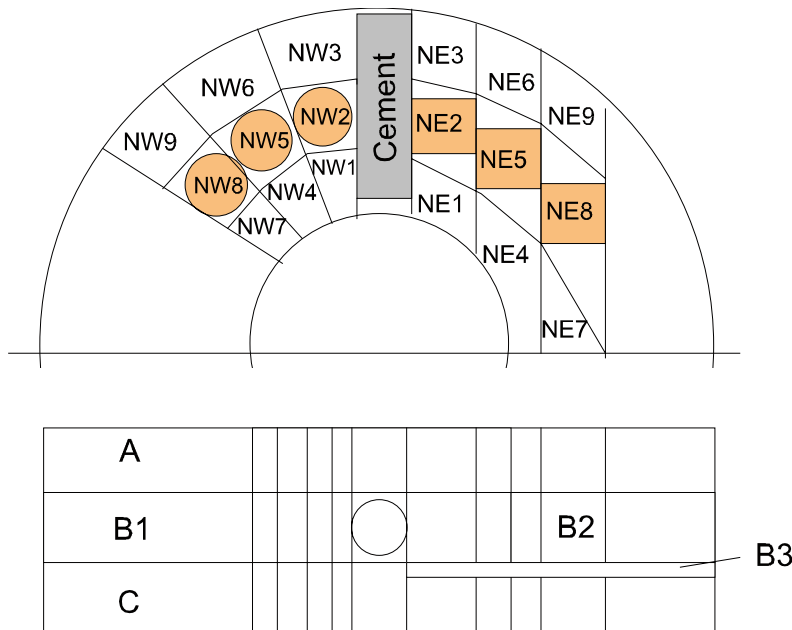


Figure A5-4. Splitting of block 24.

cement, three sectors were sawn from B1 so that the thickness of the plate was 20 mm at the radial distance of 50 mm from the copper tube. The sectors were then cut into nine sub-samples (NW1 to NW9), which represent the radial distances 0–3.3, 3.3–6.6 and 6.6–10 cm from the copper tube. The samples were stored in the Brown glove box until used for porewater squeezing.

To the right of the cement three pieces of thicknesses 2.5 cm, 2 cm and 2 cm were cut from B2. The pieces were then cut into nine sub-samples (NE1 to NE9), which represent the radial distances 0–3.3, 3.3–6.6 and 6.6–10 cm from the copper tube. The samples were stored in plastic vessels in the Brown glove box until used for pH measurement. Below B2, a thin piece B3 was cut. Two bars were cut from it and used for preparation of the water content samples extending from the copper tube to the outer surface (NE1–NE9) and from cement to the direction of NE2–NE8.

### 3.2 Measurement of pH and Eh in bentonite

The measurement cell used for the pH and Eh measurements in bentonite is presented in Figure A5-5. The cell consists of a piston, a cylindrical sample holder, a sinter and a bottom part, all made of titanium. The bottom part contains a tube, which, while filled with squeezed pore water, establishes the necessary electrical contact between the measuring electrode(s) and the reference electrode. A bentonite sample is first placed in the sample holder and compressed slightly in order to fill the sinter and the solution tube with porewater. Calibrated electrodes are then placed in the holes made in the bentonite. The bentonite is gently compacted in order to obtain a good contact between the bentonite and the electrode surface. A leak-free LF-2 reference electrode is placed in the tube and the measurement cell is placed in a metal frame, which keeps the piston in a fixed position and assures that the sample volume remains constant. Potential measurements, which normally take a couple of weeks, are carried out. Finally the electrodes are removed and recalibrated.

In block 18, three horizontal cylinders were taken at different distances from the copper tube (Figure A5-3). Each of them was placed in a measurement cell. Iridium oxide pH electrodes and Eh electrodes made of gold and platinum wires were placed in the bentonite samples at distances of 1, 5 and 9 cm from the copper tube (marked with crosses in Figure A5-3). In block 24, the pH values were measured at different distances from the cement plug. For this purpose, horizontal bentonite cylinders from NE2, NE5 and NE8 were put in one measurement cell and IrOx pH electrodes placed in the bentonite at distances of 0.5, 1.5, 3.5 and 5.5 cm from the cement and the radial distances of 4–6 cm from the copper tube.

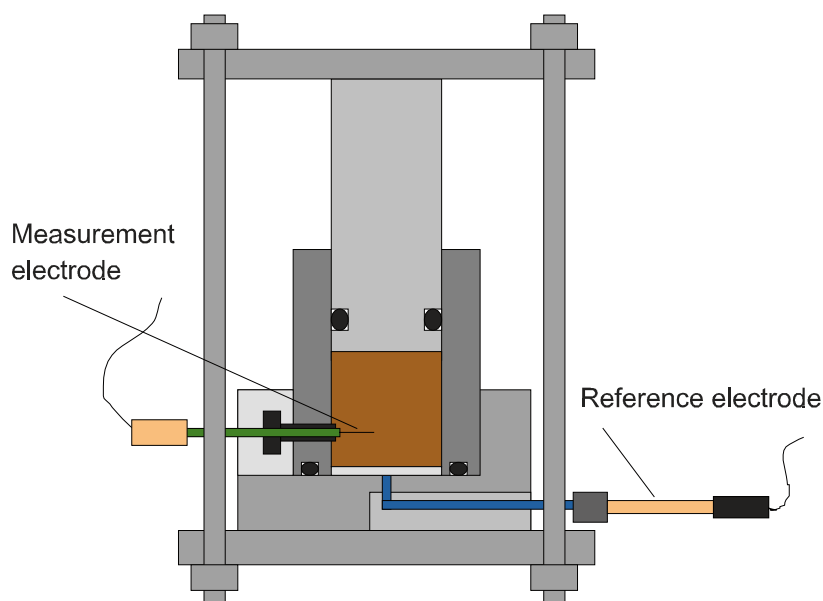


Figure A5-5. Schematic drawing of the measurement cell for pH and Eh measurements in bentonite.

### 3.3 Studies on squeezed porewaters

Squeezing of the porewaters was carried out in the nitrogen glove box (Braun box) in titanium cells, as shown in Figure A5-6. The pressure was increased stepwise to about 100 MPa and the porewater was collected in a syringe. From block 18, the bentonite samples from SE were taken at distances of 0–2, 4–6 and 8–10 cm from the copper tube. The squeezing samples of block 24 (NW2, NW5 and NW8) were taken at distances of 0–2, 2–4 and 4–6 cm from the cement, and 4–6 cm from the copper tube.

When squeezing was completed, the porewater sample was moved from the syringe into a centrifugal tube. The sample was centrifuged 15,000 rpm followed by ultrafiltering in a centrifuge filter tube (Whatmann, Vectra Spin™ Micro, MWCO 12 k). The ultrafiltered sample was used in the analyses. The concentrations of  $\text{Na}^+$ ,  $\text{Ca}^{2+}$ , and  $\text{Mg}^{2+}$  were determined with ICP-AES,  $\text{K}^+$  with FAAS,  $\text{Cl}^-$  and  $\text{SO}_4^{2-}$  with IC, and  $\text{HCO}_3^-$  with titration.

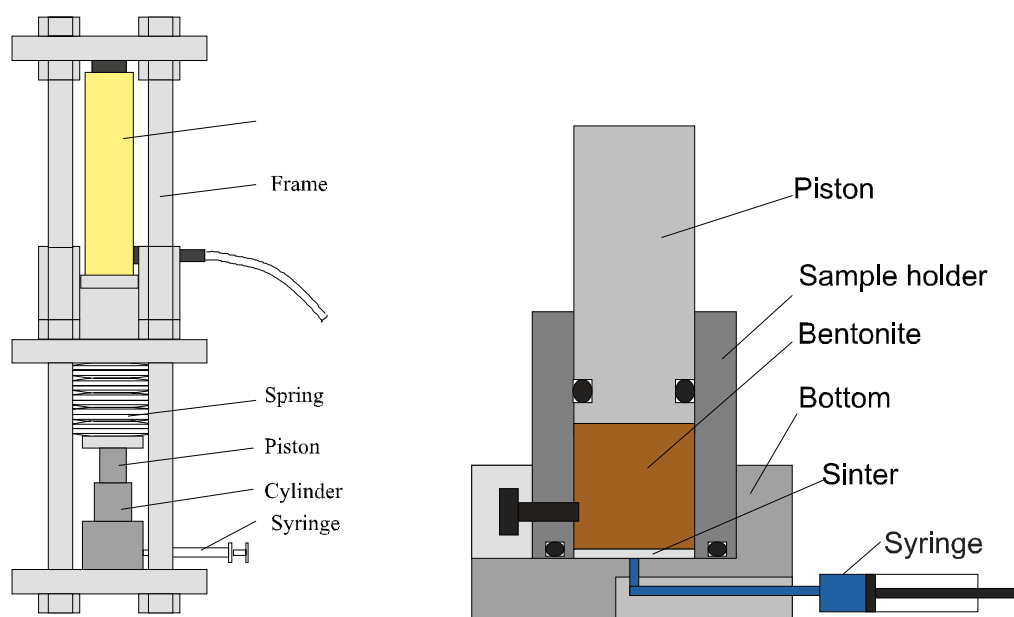


Figure A5-6. Schematic drawing of a pressing device and squeezing cell for porewater squeezing.

### **3.4 Analyses with dispersion method**

The dispersion method was used for determination of the dissolving chloride and sulphate in the bentonite. The bentonite samples were taken from block 18 at different distances from the copper tube. In the measurement, about 2 g of bentonite was dispersed in 60 ml of deionized water in centrifuge tubes. The bentonite was then separated by centrifuging. The chloride and sulphate concentrations were analysed in the ultrafiltered solution samples with IC.

## 4 Results and discussion

### 4.1 Block A2 18

The results of block 18 are presented in Appendix A. Table A5-A1 in Appendix A presents the radial distributions of water contents and chloride and sulphate concentrations determined with the dispersion method in the bentonite. The concentrations are presented both in mg per the weight of the dry clay and in mmol per the total porewater volume in the bentonite. The concentrations of different chemical components in the squeezed porewaters are presented in Table A5-A2 of Appendix A, and the pH and Eh results measured directly in the bentonite samples in Table A5-A3 of Appendix A. The composition of the Äspö groundwater is presented in Appendix C.

The radial behaviour of the water contents in block 18 is clarified in Figure A5-7. The content is lowest about 2.5 cm from the heater tube, increasing clearly while going outwards and slightly while going closer to the heater.

Figure A5-8 presents the  $\text{SO}_4^{2-}$  and  $\text{Cl}^-$  concentrations in the A2 18 SE sample of the LOT experiment together with the background values determined for MX-80, which had not been in the experiment. The sulphate and chloride concentrations determined with the dispersion method are presented in mg per the weight of the dry clay. In Figures A5-9 and A5-10 the  $\text{SO}_4^{2-}$  and  $\text{Cl}^-$  concentrations of the LOT samples are presented per the volume of the porewater in the bentonite and compared with the background concentrations coming from MX-80 and with the concentrations in the Äspö groundwater.

When the initial sulphate concentration in the bentonite was about  $4 \text{ mg/g}_{\text{dry clay}}$ , it increased during the experiment to about  $12 \text{ mg/g}_{\text{dry clay}}$  close to the heater, and decreased to about  $0.7 \text{ mg/g}_{\text{dry clay}}$  in the outer parts of the cylinder. The concentration in the Äspö groundwater is clearly lower than the concentrations coming from the dissolving sulphate in the bentonite, as seen in Figure A5-9. It is obvious that sulphate has redistributed during the experiment. This type of behaviour can be expected during non-isothermal conditions when the solubility depends on the temperature. Accumulation occurs in the area of the lower solubility. Modelling by /Domènech et al. 2004/ and /Arthur and Zhou 2005/ support this observation. The place of the concentration maximum may be affected also by other simultaneous dissolution/precipitation reactions, where the same ion participates /Arthur and Zhou 2005/.

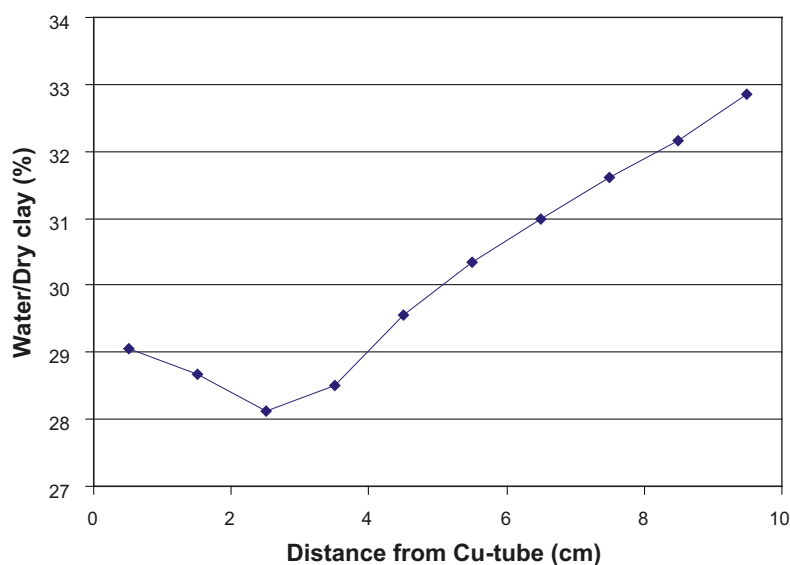
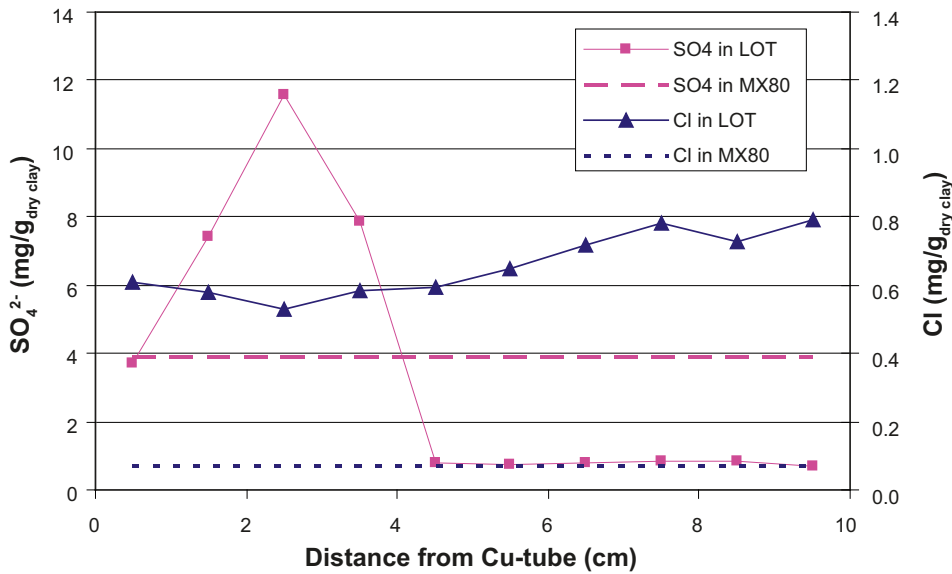
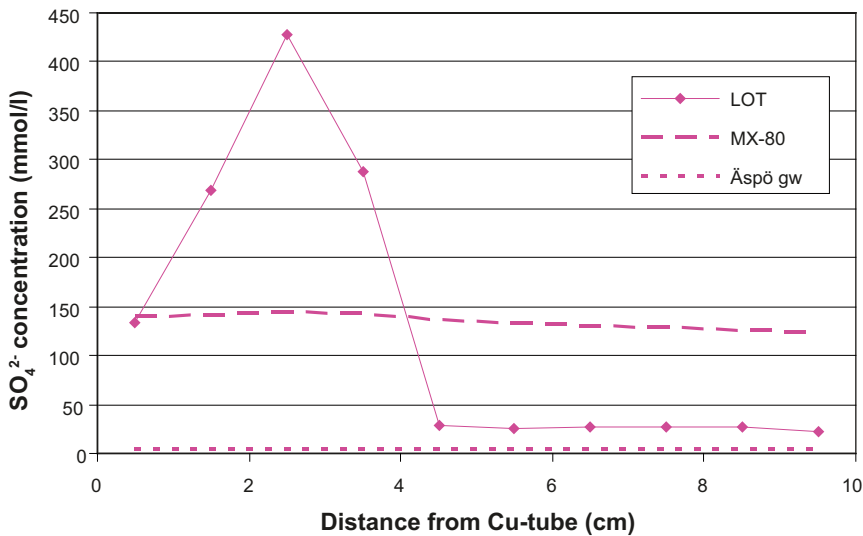


Figure A5-7. Radial distribution of water contents in the sample A2 18 B SE.



**Figure A5-8.** Sulphate and chloride concentrations in LOT sample A2 18 B SE as a function of the distance from the copper tube. The results are compared with the concentrations in MX-80 bentonite not been in the experiment. The concentrations were determined with the dispersion method and are presented per the weight of the dry clay.



**Figure A5-9.** Sulphate concentration in sample A2 18 B SE as a function of the distance from the copper tube determined with the dispersion method and presented per the volume of the porewater (LOT) concentration, which sulphate of MX-80 would cause when evenly dissolved in the porewater (MX-80), and sulphate concentration in Äspö groundwater (Äspö gw).

The initial chloride concentration ( $0.07 \text{ mg/g}_{\text{dry clay}}$ ) increased during the experiment approximately by a factor of ten (Figure A5-8). The concentration of Äspö groundwater is about three times that found in the LOT samples, as seen in Figure A5-10. It is obvious that the increased chloride in the bentonite is caused by chloride coming with the saturating groundwater. The concentration in the outer part of the bentonite is somewhat higher than that in the inner part, which may be caused by the diffusion gradient from the groundwater to the bentonite.

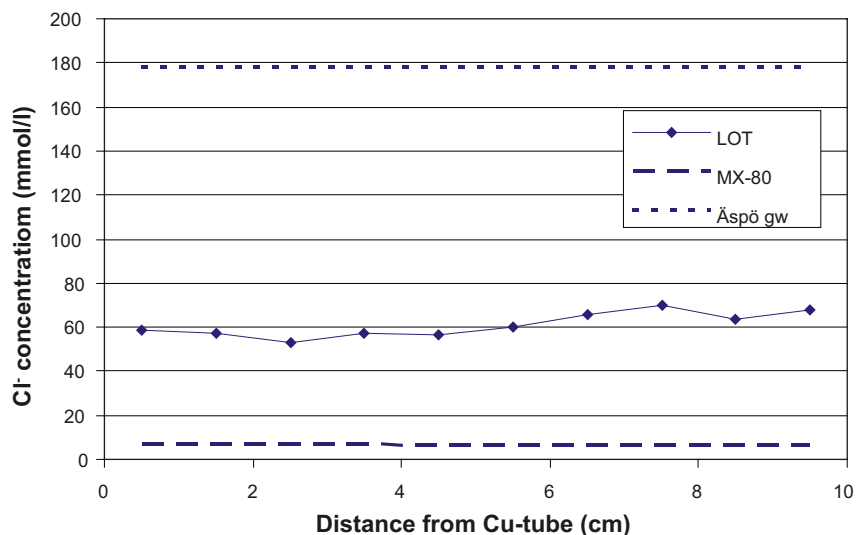


**Figure A5-10.** Chloride concentrations in sample A2 18 B SE as a function of the distance from the copper tube determined with the dispersion method and presented per the volume of the porewater (LOT) concentration, which chloride of MX-80 would cause when evenly dissolved in the porewater (MX-80), and chloride concentration in Äspö groundwater (Äspö gw).

The concentrations in the squeezed porewaters are presented in Figures A5-11 and A5-12 as a function of the distance from the copper tube. Some trends can be seen in the figures. The chloride, sodium and potassium concentrations are rather independent of the distance from the heater. The chloride concentration of the squeezed porewater is slightly higher than that determined by the dispersion method seen in Figure A5-10 but about half of the concentration in the Äspö groundwater. It is most probable that all the chloride is dissolved.

Calcium, magnesium and sulphate concentrations increase proceeding from the surface to the direction of the heater. The sulphate concentration in the squeezed porewater is much lower than the value in Figure A5-9, which assumes that all of the sulphate is dissolved. It is obvious that sulphate close to the heater is only partly dissolved and most of it is precipitated. Close to the outer surface the concentrations in the squeezed porewater approaches that in the Äspö groundwater. Bicarbonate in the squeezed porewater first increases proceeding inwards, but in the innermost sample the concentration clearly drops.

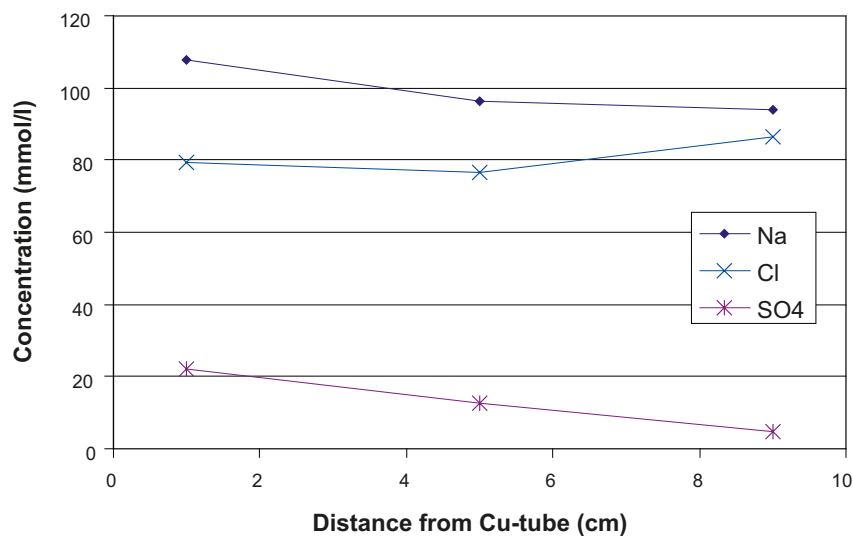


**Figure A5-11.** Radial distributions of concentrations of major components in the squeezed porewaters of samples A2 18 B SE.

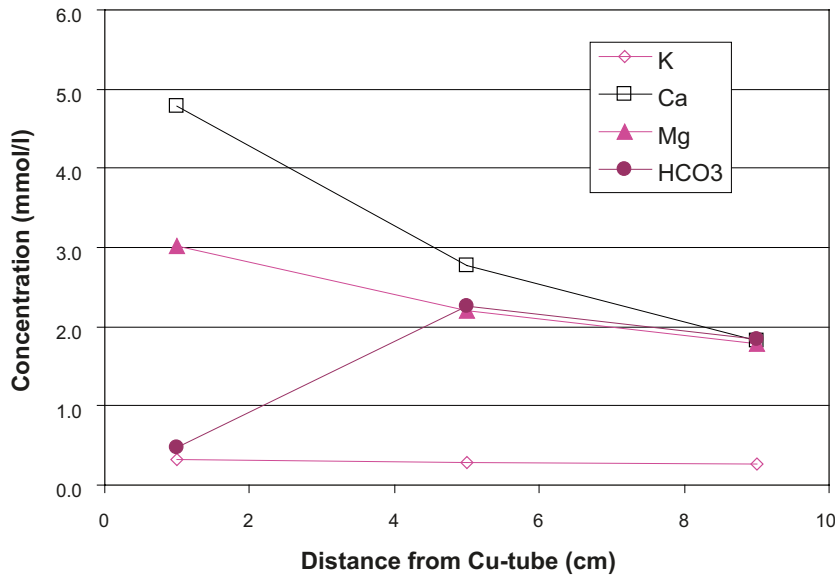


**Figure A5-12.** Radial distributions of the concentrations of the minor components in the squeezed porewaters of samples A2 18 B SE.

The radial distributions of pH and Eh determined directly in sample A2 18 B SE are presented in Figure A5-13. There seems to be variation in pH from slightly over 7 pH close to the outer surface to slightly over 8 pH close to the heater.

The Eh measurements suggest that the conditions in the bentonite were reducing. There is, however, systematic difference of about 100 mV in the Eh values determined with Pt and Au electrodes. With the gold electrode, Eh vary from -183 to -228 mV, and with the Pt electrode from -287 to -366 mV where the more negative values are close to the heater.

The complex microstructure of bentonite with different pore types (interlamellar, external), exclusion effects caused by electrical double layers and possible dissolution of solid material during squeezing make interpretation of the analysis results of the squeezed porewaters difficult. During squeezing of the LOT samples, the water content decreased from about 30 wt% to 23 wt% ( water/dry bentonite), which means that about 20% of the water has been removed and the dry density changed from 1,500 kg/m<sup>3</sup> to 1,700 kg/m<sup>3</sup>. Probably that amount of porewater cannot come only from the external pores. It can be assumed that the squeezed water is a mixture of water coming from the large

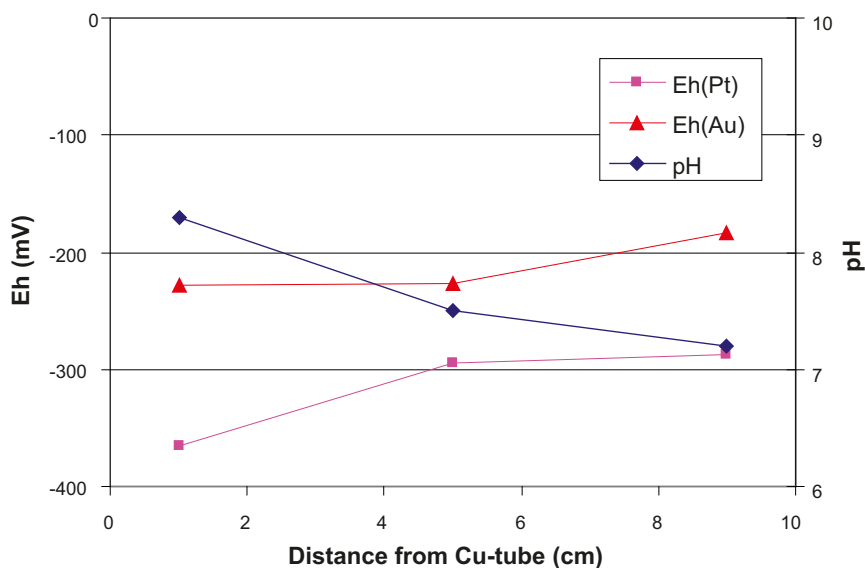


**Figure A5-13.** Radial distributions of pH and Eh determined directly in sample A2 18 B SE.

pores and that from the interlamellar space. This assumption is supported by XRD measurements performed on the bentonite samples of different densities by /Kozaki et al. 1997/. /Muurinen et al. 2004/ has evaluated that if a bentonite sample of a dry density  $1,500 \text{ kg/m}^3$  is squeezed to a density of  $1,900 \text{ kg/m}^3$  about half of the water comes from the interlamellar space. Because the concentration of free ions in the interlamellar space is very low, it dilutes the solution coming from the large pores. Owing to the electrical double layers on the montmorillonite surfaces, the free ions are not evenly distributed in the large pores either. The concentrations are higher further from the surfaces, i.e. in the middle of the pores. In squeezing, solution comes first from the middle of the pores and consequently the concentration in the solution squeezed from a large pore is higher than the average concentration in that pore. When the water coming from the external pore is diluted with that coming from the interlamellar space the concentration of some components may drop below their solubility limit. New dissolution can then occur if solid material is available. This could explain the increasing concentrations of  $\text{Ca}^{2+}$ ,  $\text{Mg}^{2+}$  and  $\text{SO}_4^{2-}$  proceeding from the outer parts closer to the heater.

## 4.2 Block A2 24

The results of block 24 are presented in Appendix B. Tables A5-B1 and A5-B2 in Appendix B present the distributions of the water contents in the bentonite as a function of the distance from the heater and as a function of the distance from the cement, respectively. Table A5-B3 in Appendix B presents the measured concentrations of different chemical components in the squeezed porewaters and Table A5-B4 shows the measured pH values in the bentonite at different distances from the cement.

The radial behaviour of the water contents in block 24 is clarified in Figure A5-14. The water content is about constant from 0 to 5 cm and then increases clearly proceeding outwards. The distribution differs from that in block 18 (Figure A5-7) such that the water content is higher in block 24 close to the heater. The increased water content is probably caused by the lower temperature in block 24. The distribution of water contents vs. the distance from the cement in sample A2 24 B NE at the radial distance of 4 to 6 cm from the heater is presented in Figure A5-15. The water content is about 1% higher at a distance of 0 to 2.5 cm from the cement.

Almost all concentrations in the squeezed porewater are higher in block 24 than in block 18. Similar difference was noticed also in parcel A0 /Muurinen 2003/. The concentrations of  $\text{Na}^+$ ,  $\text{K}^+$ ,  $\text{Ca}^{2+}$ ,  $\text{Mg}^{2+}$ , and  $\text{HCO}_3^-$  are practically independent of the distance from the cement, as seen in Figures A5-16 and A5-17. The pH values are generally somewhat higher in block 24 than in block 18, and the increase is clearly seen at the point closest to the cement (Figure A5-17).

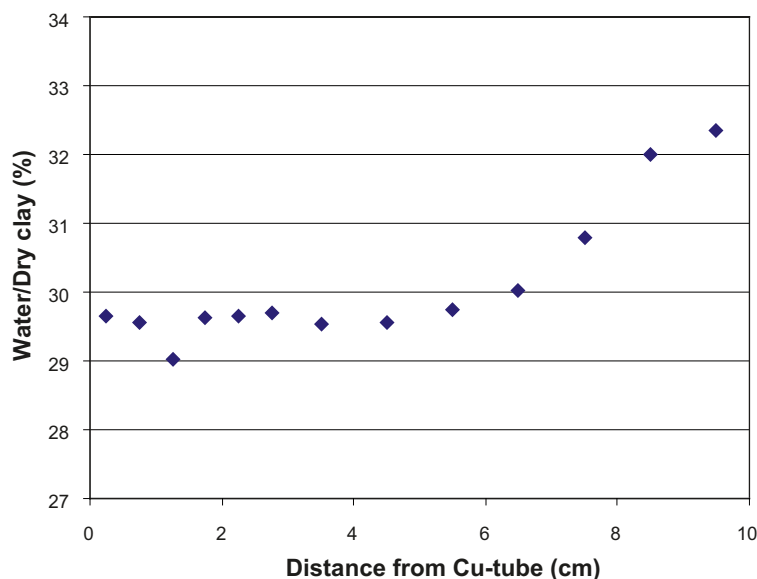
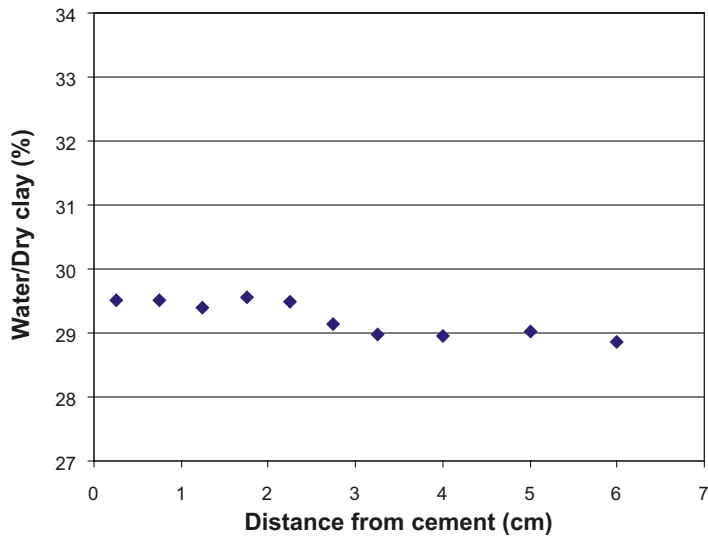
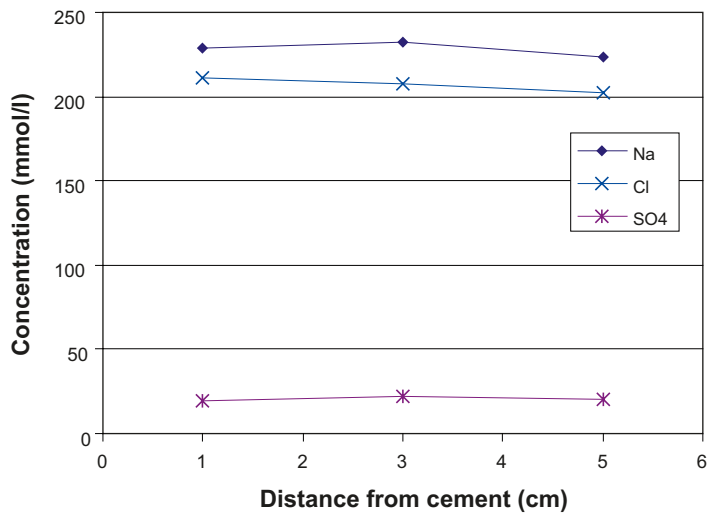


Figure A5-14. Radial distribution of water contents in sample A2 24 B NE.



**Figure A5-15.** Distribution of water contents vs. the distance from the cement in sample A2 24 B NE at the radial distance of 4 to 6 cm from the heater.



**Figure A5-16.** Concentrations of the major components in the squeezed porewaters vs. the distance from the cement plug in A2 24 B (NW2, NW5 and NW8 in Figure A5-4).

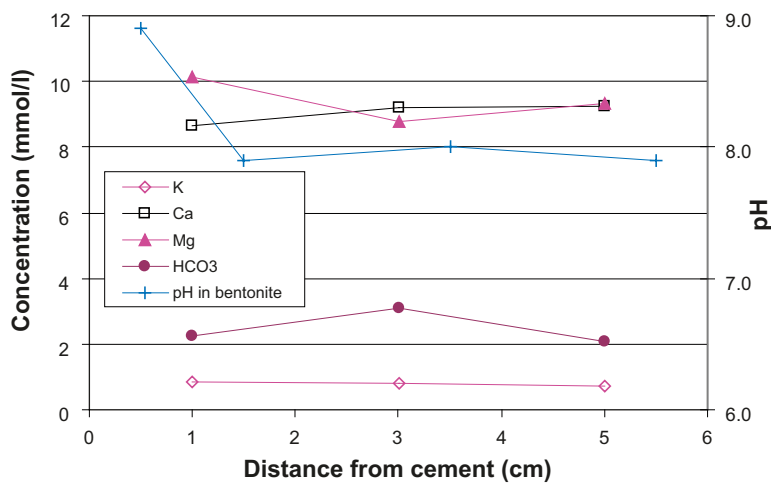


**Figure A5-17.** Concentrations of the minor components in the squeezed porewaters and pH determined directly in bentonite vs. the distance from the cement plug in A2 24 B (NW2, NW5 and NW8 in Figure A5-4).

## 5 Summary

The Long-Term Test of Buffer Material (LOT) is underway in the Äspö Hard Rock Laboratory in Sweden to test the buffer for nuclear waste disposal. The test parcels contain prefabricated bentonite blocks placed around a copper tube and a heater is placed in the lower part of the copper tube in order to simulate the heating effect of the spent fuel. The parcels are 300 mm in a diameter and placed in 4 m-long vertical boreholes in granitic rock at a depth of 450 m. This report concerns the chemical studies performed on the parcel A2, which was excavated after about five years of the experiment. Two 10 cm-high sample blocks were taken from the hot part of the parcel for studies. One of them (block 18) was without additives while in the other one (block 24), cement plugs had been placed.

**In block 18** the water content which was close to the heater 28–30 wt% of the dry bentonite, increased to 32–33 wt% close to the rock. The total concentrations of dissolving chloride and sulphate contents in bentonite were determined by dispersing bentonite samples in deionized water. The initial sulphate concentration of MX-80 bentonite, 4 mg/g<sub>dry clay</sub>, had increased during the experiment to about 12 mg/g<sub>dry clay</sub> close to the heater, and decreased to about 0.7 mg/g<sub>dry clay</sub> in the outer, colder part of the bentonite cylinder. It is obvious that sulphate had redistributed and precipitated close to the heater during the experiment. This type of behaviour can be expected during non-isothermal conditions when the solubility depends on the temperature. Accumulation occurs in the area of the lower solubility. The initial chloride concentration of bentonite, 0.07 mg/g<sub>dry clay</sub>, had increased in block 18 during the experiment approximately by a factor of ten. It was obvious that the increased chloride concentration in the bentonite was caused by chloride coming with the saturating groundwater. It is most probable that all the chloride is dissolved

Porewaters were squeezed out from the bentonite samples and their Na<sup>+</sup>, K<sup>+</sup>, Ca<sup>2+</sup>, Mg<sup>2+</sup>, Cl<sup>-</sup>, SO<sub>4</sub><sup>2-</sup> and HCO<sub>3</sub><sup>-</sup> concentrations determined. The chloride, sodium and potassium concentrations in the squeezed porewater were rather independent of the distance from the heater. The chloride concentration was slightly higher than that determined by the dispersion method but about half of the concentration in the Äspö groundwater. The calcium, magnesium and sulphate concentrations increased and the bicarbonate concentration decreased the closer to the heater.

The Eh and pH were measured directly in bentonite samples. Close to the outer surface, the pH in the bentonite of block 18 was 7.2 increasing to 8.3 close to the heater. The Eh measurements suggest that the conditions in the bentonite were reducing. There was, however, a systematic difference of about 100 mV in the Eh values determined with Pt and Au electrodes. With the Au electrode, Eh vary from -183 to -228 mV and with the Pt electrode from -287 to -366 mV, where the more negative values represent the conditions close to the heater.

**In block 24** the water content was somewhat higher close to the heater than in the block without cement. The water content was also about 1% higher close to the cement than further from it. The increased water content may be caused by the lower temperature in block 24. Almost all concentrations in the squeezed porewater were higher in block 24 than in block 18. The concentrations of Na<sup>+</sup>, K<sup>+</sup>, Ca<sup>2+</sup>, Mg<sup>2+</sup>, Cl<sup>-</sup>, SO<sub>4</sub><sup>2-</sup> and HCO<sub>3</sub><sup>-</sup> in the squeezed porewaters were practically independent of the distance from the cement. The pH values were generally somewhat higher in block 24 than in block 18, and the increase was clearly seen at the measurement point closest to the cement.

## 6 References

**Arthur R, Zhou W, 2005.** Reactive-Transport Model of Buffer Cementation. SKI Report 2005:59.

**Domènech C, Arcos D, Bruno J, Karnland O, Muurinen A, 2004.** Geochemical model of the granite-bentonite-groundwater at Äspö (LOT experiment). Mat. Res. Soc. Symp. Proc., Vol. 807, pp 855–860.

**Karnland O, Sandén T, Johannesson L-E, Eriksen T, Jansson M, Wold S, Pedersen K, Mehrdad M, 2000.** Long term test of buffer material – Final report on the pilot parcels. SKB TR-00-22, Svensk Kärnbränslehantering AB.

**Kozaki T, Sato H, Fujishima A, Saito N, Sato S, Ohashi H, 1997.** Effect of dry density on activation energy for diffusion of strontium in compacted sodium montmorillonite. In: Mat.Res. Soc. Symp. Proc., vol. 465. Pittsburgh, Pennsylvania, Materials Research Society, pp 893–900.

**Muurinen A, 2003.** Chemical Conditions in the A0 Parcel of the Long-Term Test of Buffer Material in Äspö (LOT). Olkiluoto, Finland: Posiva Oy. Working Report 2003–32.

**Muurinen A, Karnland O, Lehtikoinen J, 2004.** Ion concentration caused by an external solution into the porewater of compacted bentonite. Physics and Chemistry of the Earth 29 (2004) 119–127.

## Appendix A

### Results of the Block A2 18

**Table A5-A1. Radial distribution of water contents and  $\text{SO}_4^{2-}$  and  $\text{Cl}^-$  concentrations in sample A2 18 B SE. The  $\text{SO}_4^{2-}$  and  $\text{Cl}^-$  concentrations were determined with the dispersion method.**

Distance from Cu-tube (cm)	Water/Clay (weight%)	$\text{Cl}^-$ (mg/g <sub>dry clay</sub> )	$\text{Cl}^-$ (mmol/l <sub>porewater</sub> )	$\text{SO}_4^{2-}$ (mg/g <sub>dry clay</sub> )	$\text{SO}_4^{2-}$ (mmol/l <sub>porewater</sub> )
0.5	29.1	0.61	58.9	3.73	134
1.5	28.7	0.58	57.2	7.40	269
2.5	28.1	0.53	53.2	11.56	428
3.5	28.5	0.58	57.6	7.87	288
4.5	29.5	0.59	56.5	0.80	28.2
5.5	30.4	0.65	60.0	0.73	25.2
6.5	31.0	0.72	65.4	0.78	26.3
7.5	31.6	0.78	69.8	0.84	27.7
8.5	32.2	0.73	63.8	0.84	27.1
9.5	32.8	0.79	67.9	0.71	22.4

**Table A5-A2. Measured concentrations of different chemical components in the squeezed porewaters of block A2 18. Point explanations: level = B, compass direction = SE, radial distances from the copper tube are 1, 5 and 9 cm.**

Point	Water before squeezing (%)	Water after squeezing (%)	$\text{Na}^+$ (mmol/l)	$\text{K}^+$ (mmol/l)	$\text{Ca}^{2+}$ (mmol/l)	$\text{Mg}^{2+}$ (mmol/l)	$\text{Cl}^-$ (mmol/l)	$\text{SO}_4^{2-}$ (mmol/l)	$\text{HCO}_3^-$ (mmol/l)
B SE 1	28.9	21.4	108	0.32	4.8	3.0	79	22.3	0.5
B SE 5	29.9	22.7	96	0.28	2.8	2.2	77	12.6	2.3
B SE 9	32.5	24.3	94	0.26	1.8	1.8	87	4.6	1.8

**Table A5-A3. Measured pH and, Eh in the bentonite of block A2 18. Point explanations: level = B, compass direction = SE, radial distances from the copper tube are 1, 5 and 9 cm.**

Point	pH in bentonite	$\text{Eh}_{\text{Pt}}$ in bentonite (mV)	$\text{Eh}_{\text{Au}}$ in bentonite (mV)
B SE 1	8.3	-366	-228
B SE 5	7.5	-294	-227
B SE 9	7.2	-287	-183

## Appendix B

### Results of the Block A2 24

**Table A5-B1. Radial distribution of water contents in sample A2 24 B NE.**

Distance from Cu-tube (cm)	Water/Clay (weight%)
0.5	29.1
1.5	28.7
2.5	28.1
3.5	28.5
4.5	29.5
5.5	30.4
6.5	31.0
7.5	31.6
8.5	32.2
9.5	32.8

**Table A5-B2. Distribution of water contents vs. the distance from the cement in sample A2 24 B NE at the distance of about 5 cm from the copper tube.**

Distance from cement (cm)	Water/Clay (weight%)
0.25	8.9
0.75	8.8
1.25	9.8
1.75	8.9
2.25	9.1
2.75	9.5
3.25	10.0
4	8.9
5	9.1
6	9.2

**Table A5-B3. Measured concentrations of different chemical components in the squeezed porewaters of block A2 24. Point explanations: level = B, compass direction = NW, radial distance = 5 cm, in parentheses are the distances from the cement in cm.**

Point	Water before squeezing (%)	Water after squeezing (%)	Na <sup>+</sup> (mmol/l)	K <sup>+</sup> (mmol/l)	Ca <sup>2+</sup> (mmol/l)	Mg <sup>2+</sup> (mmol/l)	Cl <sup>-</sup> (mmol/l)	SO <sub>4</sub> <sup>2-</sup> (mmol/l)	HCO <sub>3</sub> <sup>-</sup> (mmol/l)
B NW 5(1)	29.5	24.4	228	0.86	8.6	10.1	211	19.8	2.2
B NW 5(3)	29.1	22.8	232	0.79	9.2	8.8	208	22.3	3.1
B NW 3(5)	29.0	33.3	223	0.70	9.2	9.3	202	19.9	2.1

**Table A5-B4. Measured pH values in the bentonite of block A2 24 at different distances from the cement. Point explanations: level = B, compass direction = NE, radial distance from the copper tube = 5 cm, in parentheses are the distances from the cement in cm.**

Point	pH in bentonite
B NE 5(0.5)	8.9
B NE 5(1.5)	7.9
B NE 5(3.5)	8.0
B NE 5(5.5)	7.9

## Appendix C

### Concentrations of different components in Äspö groundwater

Concentrations of different components in Äspö groundwater sample /Muurinen 2003/.  
The accuracy of the analyses is  $\pm 10\%$ .

pH	Na <sup>+</sup> mmol/l	K <sup>+</sup> mmol/l	Ca <sup>++</sup> mmol/l	Mg <sup>++</sup> mmol/l	Cl <sup>-</sup> mmol/l	SO <sub>4</sub> <sup>=</sup> mmol/l	HCO <sub>3</sub> <sup>-</sup> mmol/l
6.9 $\pm$ 0.1	100	0.28	47.3	2.4	178	4.6	0.44

## **Characterization of the LOT A2,15 test parcel**

D Rousset, R Mosser-Ruck, M Cathelineau  
G2R-CREGU Laboratory

F Villiéras, M Pelletier  
Laboratoire Environnement et Minéralurgie (LEM)  
UMR7569 INPL et CNRS, Ecole Nationale Supérieure de Géologie

### **ANDRA funded part**

This part concerns a study which was conducted for ANDRA within the LOT project. The conclusions and viewpoints presented are those of the authors and do not necessarily coincide with those of SKB.



DOCUMENT EXTERNE Nature du document / Type of document : RAPPORT	Identification / Identification : DRP 0CRE 06002/B Nom du FDR / FDR Name : HAVL Arborescence : 5.2.2
--	---

page 1/2

Émetteur Originator: CREGU-LEM	Repère support/Secrétaire : Support ref./Secretary:	Date d'origine : Original date: 31/10/2006	Page Page: 2/40
--------------------------------------	--	--	-----------------------

**ANALYSES DE MATERIAUX ARGILEUX ISSUS DE DEUX ESSAIS  
DU PROJET LOT**

*ANALYSES OF CLAY MATERIAL FROM TWO LOT TEST PARCELS*

Rapport #1 – Caractérisation de l'échantillon LOT A2/15  
*Report #1 – Characterization of the LOT A2/15 test parcel*

Documents associés / Associated documents :

Document répondant au cahier des charges mais dont le contenu traduit le point de vue du prestataire et n'engage que ce dernier / *This report concerns a study which was conducted for Andra. The conclusions and viewpoints presented in the report are those of the authors and do not necessarily coincide with those of the client.*

Observations éventuelles du prescripteur :

Titulaire / <i>Supplier</i> : CREGU BP 235 54506 Vandœuvre-lès-Nancy	N° du marché : 034780 ANDRA contract or order number:	
	Référence du titulaire : Supplier's identification:	Visa ANDRA pour diffusion OK Andra for distribution Nom / <i>Name</i> : N. MICHAU Visa / <i>Signature</i> :

Ce document est la propriété de l'ANDRA et ne peut être reproduit ou communiqué sans son autorisation  
This documents is the property of ANDRA and shall not be reproduced or distributed without its written authorisation

Ind. <i>Ind</i> :	Date : Date :	Nom et visa Rédacteur : Written by <sup>(1)</sup> :	Nom et visa Vérificateur : Reviewed by <sup>(1)</sup> :	Nom et visa Approbateur : Approved by <sup>(1)</sup> :
B	15/10/2007	F. VILLIERAS R. MOSSER-RUCK	M. CATHELINÉAU	P. SCHUHMACHER

Agence nationale pour la gestion des déchets radioactifs



DOCUMENT EXTERNE Nature du document / Type of document : RAPPORT	Identification / <i>Identification</i> : DRP OCRE 06002/B Nom du FDR / <i>FDR Name</i> : HAVL Arborescence : 5.2.2
--	---

page 1/2

(1) : Name and signature.



RÉVISIONS / <i>REVISIONS</i>	Identification / <i>Identification</i> :  Page / <i>Page</i> : 4/40 Rév. / <i>Rev.</i> : B
------------------------------	---

page 2/2

<i>Révisions / Revisions</i>		<i>Modifications / Modifications</i>
<i>Ind. / Ind.</i>	<i>Date / Date</i>	
A	31/10/2006	Version soumise à l'ANDRA pour approbation <i>Version submitted to ANDRA for approbation</i>
B	15/12/2007	<i>Finale Version</i> <i>Authorss :</i> <i>G2R: D. Rousset, R. Mosser-Ruck, M. Cathelineau</i> <i>LEM: F. Villieras, M. Pelletier</i>

# Contents

<b>1</b>	<b>Background</b>	197
<b>2</b>	<b>Methods and sampling strategy</b>	198
2.1	Sampling	198
2.2	Crystal chemistry and mineralogy	198
2.2.1	Bulk chemistry	198
2.2.2	Cation Exchange capacity (CEC)	198
2.2.3	X-Ray Diffraction (XRD)	200
2.2.4	Transmission Electron Microscopy (TEM)	201
2.2.5	Scanning Electron Microscopy (SEM)	201
2.2.6	FTIR spectrometry	201
2.2.7	XPS analyses	201
2.3	Microstructure and water status	201
2.3.1	Nitrogen absorption	201
2.3.2	Humidity and thermogravimetric analyses	202
2.3.3	Water adsorption gravimetry	202
2.3.4	Thermal analysis	202
2.3.5	Thin section by <sup>14</sup> C-MethylMethAcrylate impregnation	202
2.3.6	Thin section by resin impregnation	202
<b>3</b>	<b>Results</b>	203
3.1	Bulk chemistry	203
3.2	Mineralogical variations	206
3.3	Textural analysis and variations of morphological properties of clay aggregates	217
3.4	Thermal analyses	219
<b>4</b>	<b>Summary and prospects</b>	221
<b>5</b>	<b>References</b>	222

# 1 Background

The objectives in the “Long Term Test of Buffer Material” (LOT) test series are to validate models and hypotheses concerning long term processes in buffer material and of related processes regarding microbiology, radionuclide transport and copper corrosion under conditions similar to those in a KBS-3 repository. The objectives may be summarized in the following way:

- Produce data for validation of models concerning buffer performance under steady state conditions after water saturation, e.g. swelling pressure, cation transport.
- Validate existing models concerning buffer degrading processes, e.g. illitisation and salt enrichment.
- Study survival, activity and migration of bacteria in the buffer.
- Determine the nature and extent of possible copper corrosion.
- Serve as pilot tests for the planned full scale test series with respect to clay preparation, instrumentation, data handling and evaluation.

The general testing philosophy is to place prefabricated units of clay blocks surrounding copper tubes in vertical boreholes and to maintain the tube surfaces at defined temperatures (Figure A6-1). The test series include 7 test buffer-parcels (Table A6-1) of which 3 will be exposed to standard KBS-3 conditions in order to validate present models of clay buffer performance, and 4 test parcels which will be exposed to adverse conditions in order to validate models for buffer alteration. The buffer-parcels are placed in boreholes with a diameter of 30 cm and a length of around 4 m. The boreholes are separated from each other by 4.5 m in Äspö diorite rock structure containing water-bearing fractures in which the groundwater pressure and salinity are found acceptable.

ANDRAs contribution to the project is to analyse two LOT test series to understand the geochemical behaviour of the MX80 which has been heated and hydrated over 5 years. These analyses are carried out by two French laboratories: G2R and LEM from Nancy University (France). The LOT project will be followed by the “Alternative Buffer Material” (ABM) project. The aim of this project is to collect in situ phenomenological data over 5 years, regarding the behaviour of several clayey buffers under various conditions of temperature and hydration. Main differences of ABM project relative to LOT project are a heating system made of steel instead of copper and the use of several clayey buffers: argillite (Bure, France), GE bentonite (Georgia), FEBEX Clay (Serrata).

The present study reports the analytical characterization of the MX80 clayey buffer from LOT A2 test, slice 15 (Figure A6-1), carried out to determine the nature of physical and chemical modifications of clay material after a long term heating.

**Table A6-1. Specification of the LOT test series.**

Type	No	Type	T, °C	P <sub>c</sub>	Time, y	Remark
S	1	Standard	90	T	1	Finalized
S	2	Standard	90	T	~5	Ongoing
S	3	Standard	90	T	~20	Ongoing
A	0	Adverse	120 <150	T, ([K <sup>+</sup> ], Am, pH)	1	Finalized
A	1	Adverse	120 <150	T, ([K <sup>+</sup> ], Am, pH)	1	Finalized
A	2	Adverse	120 <150	T, ([K <sup>+</sup> ], Am, pH)	~5	Analyzing
A	3	High T	120 <150	T	~5	Ongoing

S = standard conditions.      A = adverse conditions.  
P<sub>c</sub> = controlled parameter.      C = cementation.  
Ma = mineralogical alteration.      Am = accessory minerals.

## 2 Methods and sampling strategy

### 2.1 Sampling

A sample from the LOT A2/15 test parcel has been received by CREGU in May 2006. In this block, no additives have been used (Figure A6-1). To study the evolution of the clay properties during the long term heating, the block has been divided in 5 slides with a steel saw (Figure A6-2). The slides are ca. 2-cm thick, and 10-cm wide from the Cu-MX80 boundary to the granite-MX80 contact.

Each slide has been devoted to specific characterization:

- Slide #1 has been cut in 5 sections of ca. 2-cm wide (Figure A6-3). Each section was crushed in agate mortar. The  $<2 \mu\text{m}$  size fraction was separated by sedimentation in de-ionized water. Whole rocks and size-fractions were used for bulk chemistry analysis, electron microscopy, and X-ray diffraction.
- Slide #2 was also cut in 5 sections and used for the microstructural study of the clay minerals, the FTIR spectrophotometry and the CEC determination.
- Slides #3 to #5 were dedicated to thin section fabrication. Slides #4 and #5 were processed following Pret's methodology /Prêt 2003/.

### 2.2 Crystal chemistry and mineralogy

#### 2.2.1 Bulk chemistry

After ignition and  $\text{LiBO}_4$  melting, major elements (Si, Al, total Fe, Mn, Mg, Ca, Na, K, P, Ti) of the solid fractions were obtained by ICP-AES (Jobin-Yvon JY 70), and trace and rare-earth elements by ICP-MS (Perkin Elmer 5000). The accuracy in measured solution concentrations was better than  $\pm 10\%$ . Total S content is determined by using a carbon-sulphur dosimeter (LECO SC 144DRPC) after  $\text{O}_2$ -combustion at  $1,400^\circ\text{C}$ . The accuracy ranges between  $\pm 4$  and  $\pm 12\%$  according to sample content ( $>0.5 \text{ w}\%$  and  $>0.1 \text{ w}\%$  respectively). The FeO content is determined by oxidation-reduction titration after  $\text{HF-H}_2\text{SO}_4$  digestion. The accuracy ranges between  $\pm 2$  and  $\pm 10\%$  according to sample content ( $>5 \text{ wo}\%$  and  $>0.5 \text{ wo}\%$  respectively).

#### 2.2.2 Cation Exchange capacity (CEC)

CEC values were measured using cobaltihexammonium chloride ( $\text{Cl}_3\text{Co}(\text{NH}_3)_6$ ) solutions. About 400 mg of bentonite sample were weighed and placed in polypropylene tubes. 30 ml of a cobaltihexammonium solution, with initial concentration of 0.5 mol/l, was added to the powder. The tubes were left one night under soft stirring at  $25^\circ\text{C}$ . After a centrifugation step to separate liquid and solid fractions, final concentrations were calculated using UV spectrometer measurements, including a preliminary calibration with a series of cobaltihexammonium solutions. The CEC was evaluated from the final solution, based on the adsorbed amount of cobaltihexammonium. The supernatants were simultaneously analyzed by atomic absorption spectroscopy to determine cation concentrations (Ca, Na, Mg, K and Cu). Results are normalized to dry weight ( $110^\circ\text{C}$ , overnight). CEC was determined on two separate samples to check for reproducibility and are expressed as a mean value ( $\pm 5 \text{ meq}/100 \text{ g}$ ).

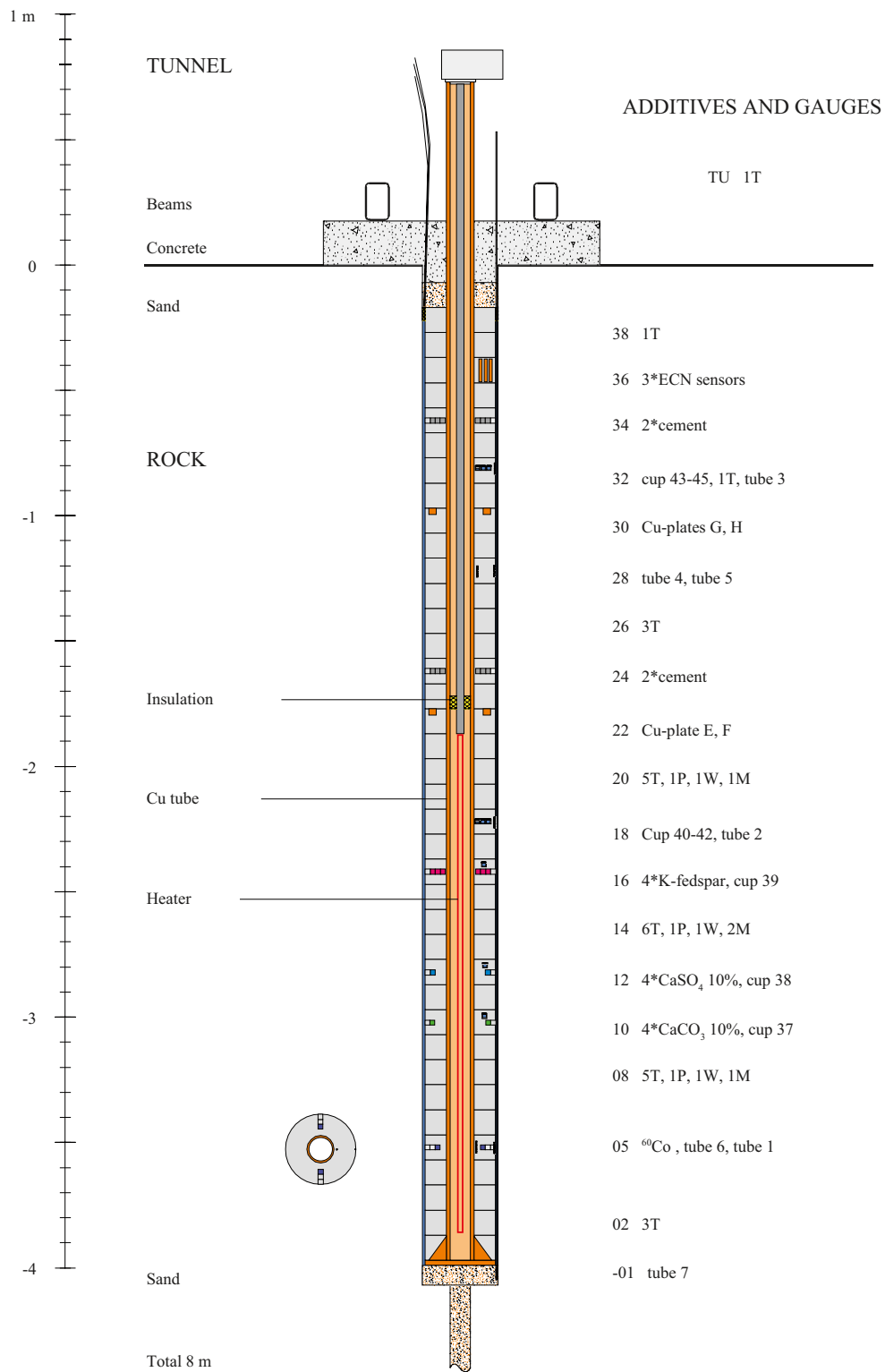


**Figure A6-1.** Principle scaled layout of the A2 test parcel. Numbers on the right hand side of the parcel indicate the block number and the following text refers to sensors and additives (from Karnland O, Clay Technology AB, LOT A2 general information, 2006-03-31).

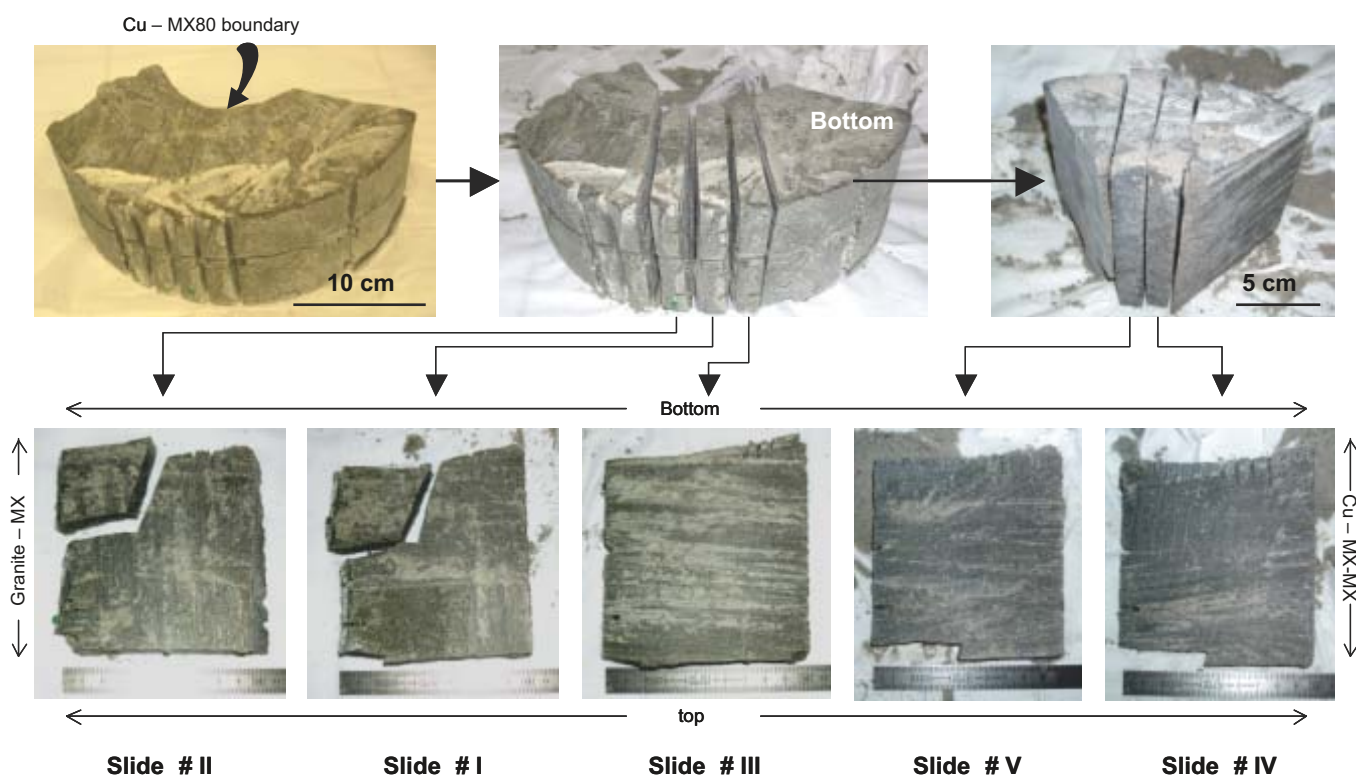


**Figure A6-2.** Sampling of the LOT A2/15 block in 5 slides of ca. 2 cm thick. The cuttings were done almost perpendicular to the MX80-Cu boundary.

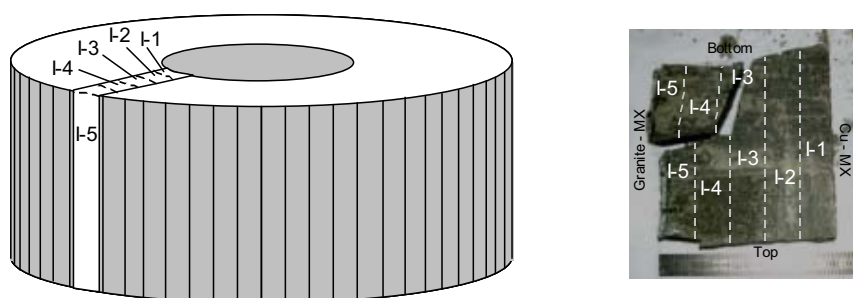


**Figure A6-3.** Five samples have been collected from the LOT A2/15 slide #1. Each sample is ca. 2×2×10 cm (L×W×H) and are labelled from 1 to 5 according to the distance from the copper-MX80 interface (Sample 1 is the nearest).

### 2.2.3 X-Ray Diffraction (XRD)

The XRD data were collected with a D8 Bruker diffractometer with Co-K $\alpha$ 1 radiation ( $\lambda = 1.7902\text{\AA}$ ). The operating conditions were 35 kV accelerating voltage, 45 mA intensity, step scanning at  $0.035^\circ(2\theta)$  intervals, 3 s counting time,  $3\text{--}70^\circ(2\theta)$  for disoriented powder and  $3\text{--}40^\circ(2\theta)$  for oriented slides. The XRD patterns of disoriented powders were carried out in atmospheric conditions to identify non-clay minerals. To identify clay minerals, X-ray diffraction patterns were also recorded on air-dried oriented samples (AD), on ethylene glycol vapour (12 h at room temperature) saturated samples (EG) and after heating at  $550^\circ\text{C}$  during 4 h. The Greene-Kelly test to distinguish montmorillonite from beidellite, saponite or nontronite was also carried out /Hoffman and Klemen 1950, Greene-Kelly 1953/: samples were Li-saturated, heated at  $400^\circ\text{C}$  during 12 h and then saturated with liquid glycerol (Gly) by covering the dry oriented slide overnight with an absorbent paper soaked with glycerol. Pure silica slides were used for oriented specimens of Li-saturated samples to avoid Na migration from the glass during heating /Byström- Brusewitz 1975/. After specific treatments, samples stayed in atmospheric conditions during 2 h maximum.

## 2.2.4 Transmission Electron Microscopy (TEM)

Micro-chemical analyses of isolated particles of the fine fractions ( $<5 \mu\text{m}$ ) oriented on carbon Ni-grids were obtained. A PHILIPS CM20 instrument operating at 300 kV with a LaB<sub>6</sub> filament as electron source and an EDAX energy dispersive X-ray analyser was used. Spectra were collected under nanoprobe mode, from an area  $\approx 10 \text{ nm}$  in diameter during 40 s. The structural formula was calculated for each EDS-TEM analysed particle on the basis of 11 oxygen for particles of the (2:1) type (illite or smectite) /Harvey 1943/. In the case of particles containing less than 10 at% iron, the valence state measurement was not possible and all the clay particles were assumed to have the same  $\text{Fe}^{3+}/\text{Fe}_{\text{Total}}$  ratio of 0.55, similar to the ratio determined in the MX80 bentonite /Guillaume 2002/.

## 2.2.5 Scanning Electron Microscopy (SEM)

Using a microscope HITACHI S2500 FEVEX, scanning electron microscopy observations were carried out on bulk bentonite fragment to characterise the general aspect of the samples at the copper–MX80 interface. One fragment has been embedded in resin and saw perpendicular to the interface to obtain a crosscut of the contact. The  $>2 \mu\text{m}$  bentonite fraction was also separated to determine the degree of alteration of the starting mineral grains and to identify by-products. Samples were prepared in atmospheric conditions.

## 2.2.6 FTIR spectrometry

Mid infrared spectra were collected in diffusive reflectance mode (Harrich attachment) using an IFS 55 Bruker Fourier Transform IR spectrometer at a resolution of  $4 \text{ cm}^{-1}$  under atmospheric conditions. For FTIR analyses, the concentration of samples in KBr was 15%.

## 2.2.7 XPS analyses

All the XPS analysis was performed at LCPME laboratory (Nancy University) on a Kratos Axis Ultra DLD (Kratos Analytical, UK) spectrometer, which employs a magnetic lens. The instrument is equipped with a monochromatic Al K $\alpha$  X-ray source operated at 90 W (15 kV, 6 mA). Charge neutralisation was provided by the Kratos charge neutralisation system and the carbon C 1 s peak (284.6 eV) was used as a reference to correct the weak charging effect ( $<1 \text{ eV}$ ). Survey scans were recorded with 1.0 eV step and 160 eV analyser pass energy and narrow scans with 0.1 eV step and 20 eV pass energy. Analysis was performed using 90° angle with operating pressure in the analytical chamber of  $10^{-9}$  mbar. The sample was fixed on a copper plate coated with a gold film before being placed in the spectrometer. The recorded lines were fitted using the Vision 2.2.0 program (Kratos Analytical, UK) after subtraction of the background (Shirley baseline).

## 2.3 Microstructure and water status

### 2.3.1 Nitrogen adsorption

Adsorption-desorption isotherms were obtained using a lab-built classical step by step volumetric setup, with successive introductions of nitrogen (purity of N<sub>2</sub>-gas  $>99.995\%$ ). The measurements were conducted at liquid N<sub>2</sub> temperature (77 K) with the samples kept in a bath of liquid N<sub>2</sub> at constant level. Pressure measurements were carried out with two absolute gauges (Edwards) in the range 0–0.01 bar and 0–1 bar. The saturation pressure of nitrogen at 77 K was recorded using a third gauge during the whole experiment. The adsorption isotherm was obtained from the measurement of equilibrium pressures before and after contact with the sample. All samples were preliminary outgassed at 120°C for 18 hours under a residual pressure of  $10^{-9}$  bar.

Specific surface areas were calculated with the BET method /Brunauer et al. 1938/ and the De Boer method /t-plot, de Boer et al. 1965/. The latter method was also used to estimate microporous and external surfaces. Micropore filling occurs at low and very low relative pressure values, during the adsorption of the first monolayer on external surface. To distinguish adsorption onto external surface from adsorption into the micropores, the experimental isotherm were compared to de Boer reference curve.

### 2.3.2 Humidity and thermogravimetric analyses

Hydration degrees of the samples were determined by using classical test (weight loss at 105°C, overnight over initial mass) and by thermogravimetric experiments. These results are considered only as indicative as it was very difficult to keep the local hydration state of the received samples (homogenization inside the sample; contact with atmosphere water).

### 2.3.3 Water adsorption gravimetry

Water vapour gravimetric adsorption experiments were carried out using a lab built quasi-equilibrium setup designed around a Setaram MTB 10-8 symmetrical microbalance. Water vapour was supplied to the sample (kept at 30°C) from a source kept at 41°C, at a slow flow rate to ensure quasi-equilibrium conditions at all times /Poirier et al. 1987/. The simultaneous recording of mass uptake and equilibrium pressure directly yields the water vapor adsorption isotherm. The experimental conditions were a sample weight of 110.7 mg and an outgassing at 110°C during 18 h under a residual pressure of 0.1 Pa.

### 2.3.4 Thermal analysis

Thermal analyses were performed on the 5 samples and also on reference sample. Experiments were carried out using a CAHN TG\_2171 microbalance, at 2°C/mn. Sample mass was around 20 mg. Buoyancy effects were corrected by running an independent experiment on a thermally stable alumina.

### 2.3.5 Thin section by <sup>14</sup>C-MethylMethAcrylate impregnation

To study the textural or microstructural features of the hydrated material, samples were impregnated with a resin allowing the filling of the interlayer of swelling clays in conditions close to water relative pressure around 98% /Prêt 2003/. In addition, <sup>60</sup>Co irradiation polymerisation of the resin allows performing autoradiography and electron microprobe mapping to derive porosity, chemical elements and minerals two-dimensional distributions.

Impregnation and irradiation durations are long for bentonite samples. Corresponding analyses are under progress and the corresponding techniques are described in annex. Results will be available at the beginning of 2008 and will be the object of a specific note.

### 2.3.6 Thin section by resin impregnation

As thin section building using the MMA impregnation is very long (see above), thin sections have been built using classical methods, not fully adapted for low-compacted materials, but allowing to go further in investigating new non-destructive methods for material characterisation (LIBS for instance).

Two experiments have been carried out for thin section building: i- impregnation under vacuum and ii- under high pressure. The size of the samples has been previously reduced to the size of a “sugar” (25×35 mm).

Samples are put in a F1809 resin bath under low vacuum ( $10^{-1}$ – $10^{-2}$  bar) for a day at room temperature, then dried on a hot plate at 100°C, and finally placed in a oven at 60°C for a week.

After drying at 80°C for 2 days, sample is placed in a glass holder filled with resin (50% araldite HY918 + 50% hardener CY192 + blue colorant), kept at 60°C for higher viscosity. The holder is put under low vacuum with frequent return in the oven to maintain the resin temperature around 60°C. After 1 h, the glass holder is placed in a stainless steel container already filled with hot resin. All the system is then closed and air-outgassed. By using a hand-pump, one can apply to the system a pressure of about 250 bars. All the system is kept at 60°C during all the experiment (5 days).

After impregnation and drying, one side of each sample was polished and stuck on a glass slide. This sample is then sawn using oil as lubricant to reduce its thickness at about 1 mm and finally polished with a 3 µm grid to reach of thickness of about 100 µm.

## 3 Results

### 3.1 Bulk chemistry

Contents in major and trace elements of the 5 slides and a SKB reference of the initial material (ref in tables) are given in Tables A6-2 to A6-5 for bulk and <2 µm fractions.

**Table A6-2. Contents in major elements for bulk fractions (LOI: loss on ignition).**

Element/Sample		15 I1 RT	15 I2 RT	15 I3 RT	15 I4 RT	15 I5 RT	15 I ref RT
SiO <sub>2</sub>	%	60.21	59.46	60.45	60.08	59.76	61.38
Al <sub>2</sub> O <sub>3</sub>	%	18.25	17.86	18.27	18.23	18.11	18.54
Fe <sub>2</sub> O <sub>3</sub>	%	2.93	2.74	2.94	2.76	2.88	3.01
FeO	%	0.57	0.68	0.57	0.69	0.59	0.57
MnO	%	0.01	0.01	0.02	0.01	0.01	0.02
MgO	%	2.40	2.26	2.21	2.17	2.14	2.24
CaO	%	1.12	1.57	1.34	1.21	1.19	1.30
Na <sub>2</sub> O	%	1.93	1.97	1.98	1.99	1.95	2.08
K <sub>2</sub> O	%	0.48	0.49	0.49	0.48	0.48	0.52
TiO <sub>2</sub>	%	0.14	0.14	0.14	0.14	0.14	0.14
P <sub>2</sub> O <sub>5</sub>	%	0.05	0.05	0.05	0.05	0.04	0.05
LOI	%	11.83	13.60	12.02	13.02	12.84	10.53
Total	%	99.91	100.92	100.55	100.91	100.20	100.44
S tot	%	0.27	0.39	0.26	0.15	0.15	0.28
Fell/FeIII		0.22	0.28	0.22	0.28	0.23	0.21

**Table A6-3. Contents in major elements for <2 µm fractions (LOI: loss on ignition).**

Element/Sample		15 I1 2 µ	15 I2 2 µ	15 I3 2 µ	15 I4 2 µ	15 I5 2 µ	15 I ref 2 µ
SiO <sub>2</sub>	%	60.11	60.32	60.27	61.45	60.83	60.85
Al <sub>2</sub> O <sub>3</sub>	%	18.11	18.33	18.27	18.28	17.88	18.19
Fe <sub>2</sub> O <sub>3</sub>	%	3.22	3.18	3.21	3.21	3.19	3.11
FeO	%	0.26	0.30	0.26	0.22	0.21	0.32
MnO	%	0.01	0.01	0.01	0.01	0.01	0.01
MgO	%	2.47	2.34	2.29	2.26	2.20	2.28
CaO	%	1.01	1.46	1.19	0.93	0.94	1.06
Na <sub>2</sub> O	%	1.41	1.46	1.44	1.53	1.46	1.49
K <sub>2</sub> O	%	0.22	0.38	0.30	0.22	0.21	0.31
TiO <sub>2</sub>	%	0.13	0.13	0.14	0.14	0.14	0.14
P <sub>2</sub> O <sub>5</sub>	%	0.03	0.04	0.04	0.04	0.04	0.05
LOI	%	13.72	12.85	12.85	12.05	13.10	12.91
Total	%	100.73	100.85	100.28	100.36	100.23	100.73
S tot	%	0.09	0.18	0.12	0.11	0.06	0.13
Fell/FeIII		0.09	0.11	0.09	0.08	0.07	0.12

**Table A6-4. Contents in trace elements for bulk fractions.**

Element/Sample		15 I1 RT	15 I2 RT	15 I3 RT	15 I4 RT	15 I5 RT	15 I ref RT
As	ppm	12.160	10.300	11.800	12.310	11.310	12.600
Ba	ppm	239.100	294.900	381.000	256.300	251.300	333.700
Be	ppm	1.781	1.808	1.810	1.754	1.731	1.664
Bi	ppm	0.984	0.949	0.961	0.977	0.973	0.966
Cd	ppm	0.300	0.436	0.529	0.421	0.344	0.422
Ce	ppm	105.900	104.600	107.800	105.700	103.600	104.700
Co	ppm	1.094	1.077	1.086	1.087	0.897	1.031
Cr	ppm	11.480	50.620	29.710	13.370	18.350	67.530
Cs	ppm	0.427	0.411	0.450	0.443	0.419	0.421
Cu	ppm	2,110.000	9.012	6.147	6.138	448.500	4.474
Dy	ppm	7.835	7.811	8.088	7.943	7.766	7.741
Er	ppm	3.927	3.921	4.040	3.976	3.807	3.924
Eu	ppm	0.657	0.666	0.669	0.670	0.651	0.698
Ga	ppm	27.630	27.100	28.270	28.000	27.710	27.820
Gd	ppm	8.508	8.470	8.723	8.658	8.463	8.650
Ge	ppm	0.660	0.634	0.657	0.677	0.589	0.655
Hf	ppm	7.113	7.233	7.400	7.398	7.376	7.181
Ho	ppm	1.426	1.428	1.492	1.497	1.446	1.444
In	ppm	0.090	0.101	0.107	0.099	0.098	0.096
La	ppm	50.920	50.170	52.300	51.800	50.000	50.760
Lu	ppm	0.527	0.521	0.547	0.534	0.541	0.538
Mo	ppm	6.113	4.143	3.834	3.937	4.317	4.455
Nb	ppm	26.000	25.910	26.180	26.420	25.560	25.780
Nd	ppm	46.340	45.830	46.660	46.900	44.750	45.250
Ni	ppm	39.390	9.075	14.510	50.610	169.500	4.075
Pb	ppm	36.670	45.658	43.136	43.711	37.782	43.041
Pr	ppm	12.420	12.290	12.670	12.690	12.420	12.430
Rb	ppm	11.800	12.280	12.160	12.120	11.850	12.050
Sb	ppm	1.532	1.550	1.545	1.650	1.455	1.541
Sm	ppm	10.050	10.180	10.460	10.330	9.959	9.992
Sn	ppm	8.624	8.155	8.554	8.662	8.466	8.453
Sr	ppm	207.000	287.500	301.300	206.500	211.600	247.500
Ta	ppm	3.214	3.119	3.281	3.294	3.226	3.182
Tb	ppm	1.344	1.360	1.404	1.372	1.349	1.389
Th	ppm	37.810	37.480	38.940	38.360	37.990	37.960
Tm	ppm	0.560	0.576	0.595	0.586	0.580	0.591
U	ppm	12.470	12.460	12.890	12.910	12.740	12.590
V	ppm	5.187	5.387	5.306	5.131	5.041	5.583
W	ppm	0.321	0.269	0.280	0.281	0.276	0.306
Y	ppm	40.340	38.540	39.470	40.530	39.380	39.620
Yb	ppm	3.730	3.703	3.840	3.818	3.709	3.787
Zn	ppm	86.390	112.700	106.800	126.400	116.500	122.100
Zr	ppm	183.500	187.300	185.200	189.800	189.300	179.400

**Table A6-5. Contents in trace elements for <2 μm fractions (L.D.: detection limit).**

Element/Sample		15 I1 2 μ	15 I2 2 μ	15 I3 2 μ	15 I4 2 μ	15 I5 2 μ	15 I ref 2 μ
As	ppm	6.397	8.839	7.005	4.468	5.316	8.064
Ba	ppm	98.300	234.400	231.200	96.160	114.300	188.800
Be	ppm	1.617	1.665	1.687	1.757	1.590	1.763
Bi	ppm	0.799	0.823	0.794	0.799	0.822	0.916
Cd	ppm	<L.D.	0.305	<L.D.	<L.D.	<L.D.	<L.D.
Ce	ppm	126.000	106.000	115.100	139.100	146.400	118.000
Co	ppm	0.877	0.984	0.909	0.881	0.695	0.913
Cr	ppm	<L.D.	8.570	<L.D.	<L.D.	<L.D.	<L.D.
Cs	ppm	0.387	0.405	0.427	0.410	0.453	0.391
Cu	ppm	1229.000	8.004	5.955	5.571	235.200	5.822
Dy	ppm	9.128	7.785	8.370	9.717	10.250	8.674
Er	ppm	4.434	3.844	4.167	4.833	4.955	4.318
Eu	ppm	0.639	0.629	0.651	0.737	0.749	0.649
Ga	ppm	27.680	27.940	27.760	27.230	27.590	27.130
Gd	ppm	10.210	8.644	9.445	11.180	11.740	9.609
Ge	ppm	0.524	0.649	0.594	0.589	0.603	0.574
Hf	ppm	6.698	6.859	6.839	6.905	6.550	6.673
Ho	ppm	1.668	1.428	1.559	1.796	1.852	1.583
In	ppm	0.098	0.092	0.099	0.125	0.131	0.082
La	ppm	60.090	51.500	55.950	67.130	70.100	56.640
Lu	ppm	0.556	0.489	0.519	0.578	0.611	0.535
Mo	ppm	4.034	2.610	2.150	1.460	1.863	1.811
Nb	ppm	25.870	24.210	24.840	26.800	27.160	25.460
Nd	ppm	54.770	46.480	51.350	60.210	63.600	51.830
Ni	ppm	35.090	12.160	12.830	43.690	137.000	4.289
Pb	ppm	29.421	36.270	33.385	29.097	30.124	30.851
Pr	ppm	14.890	12.530	13.710	16.530	17.150	13.920
Rb	ppm	7.036	9.637	8.366	7.045	7.274	8.502
Sb	ppm	1.178	1.195	1.019	0.835	0.979	1.006
Sm	ppm	12.100	10.310	11.210	13.200	13.880	11.400
Sn	ppm	8.518	8.578	8.586	8.425	8.491	8.140
Sr	ppm	195.800	286.100	298.100	194.800	198.100	228.400
Ta	ppm	3.658	3.279	3.503	3.888	3.856	3.422
Tb	ppm	1.635	1.382	1.516	1.771	1.836	1.509
Th	ppm	47.300	40.040	44.010	52.520	54.310	44.680
Tm	ppm	0.630	0.560	0.596	0.676	0.704	0.608
U	ppm	14.990	13.030	14.110	16.460	17.300	14.290
V	ppm	4.548	4.690	4.628	4.464	4.533	4.692
W	ppm	0.265	0.277	0.269	0.309	0.288	0.268
Y	ppm	44.290	37.870	41.030	48.470	49.470	41.500
Yb	ppm	4.064	3.598	3.787	4.289	4.514	3.950
Zn	ppm	67.340	93.690	50.340	37.920	47.630	56.270
Zr	ppm	146.500	158.400	152.000	150.600	147.300	154.500

The main conclusions of chemical analyses are that variations in major elements are negligible. One noticeable variation is observed for bulk sample 2 with a slight decrease in silica and aluminium and a slight increase in calcium. Ti, generally considered as stable upon leaching remains constant in all the sample, showing that dissolution of bentonite minerals or precipitation of new phases are negligible in amounts.

Concerning traces, copper is as expected the element showing enrichments at the bentonite/heater interface (sample 1) in bulk sample and in its clay fraction. The same result is obtained for the bentonite/granite interface (sample 5), but with a lower extent. Concomitantly, samples located between these two interfaces show low concentrations in Cu, close to the reference sample, suggesting that Cu transfer from heater to granite does not occurs through the migration in the porosity of the bentonite. The amount of copper in the clay fraction of bentonite/heater interface is half of the sodium one (mol/mol) suggesting possible cation exchange in the clay. Other elements show little variations in concentration between the heater and the granite particularly in samples 1 and 4, which are depleted in Mo, Cr, Sr, Ba and Zn. It can also be noticed that bentonite is enriched in Ni at the two bentonite surfaces, mostly at the bentonite/granite interface.

### 3.2 Mineralogical variations

Bulk fraction mainly consists of clay minerals with little amounts of quartz and feldspars. XRD patterns show no evidence of any mineralogical variation among the samples relative to the reference material (Figure A6-4). Nevertheless, FTIR patterns indicate progressive disappearance of an absorption band centred at  $1,440\text{ cm}^{-1}$  (Figure A6-5). This band can be related to the occurrence of very small amounts of carbonates (<1%), not identified by XRD. The decrease of this band for samples close to the heating body can be interpreted as a progressive decarbonatation of the bentonite with increasing temperature. This observation proves the sensitivity of diffuse reflectance FTIR spectroscopy for some accessory minerals that could not be identified by XRD because of their low amount. In the bending vibration region ( $1,000\text{ to }600\text{ cm}^{-1}$ ) the absence of spectra modification shows that octahedral composition of the clay remains unchanged. Sulphates (gypsum...) are not observed.

The fine fraction ( $<2\text{ }\mu\text{m}$ ) consists only on a Ca-Na-montmorillonite. Typically, the XRD pattern shows a broad peak around  $13\text{--}14\text{ \AA}$  for the air-dried sample (due to the occurrence of cations with different hydration state in interlayer position), shifted towards  $17.4\text{ \AA}$  for glycolated samples (Figure A6-6a). Between the samples, one can distinguish a slight evolution for air-dried samples: the main peak is shifted towards smaller angles (higher d) as the sample is getting closer to the heating system (Figure A6-6b). This shift could be explained by a slight substitution Na à Ca in the interlayer. Ca could origin from carbonate destabilisation as shown by FTIR spectroscopy.

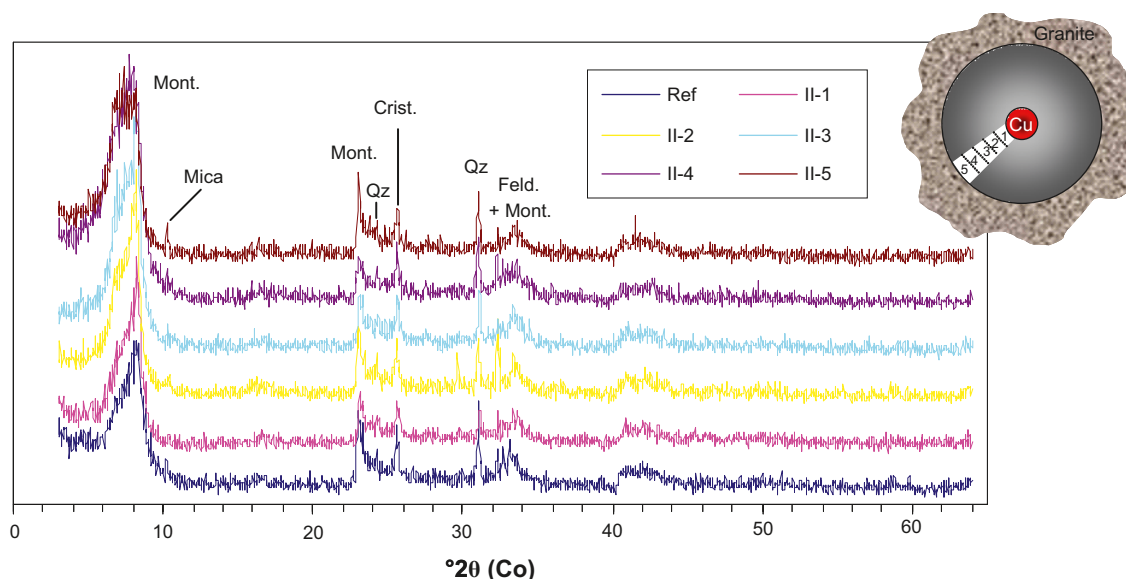


**Figure A6-4.** XRD patterns of bulk disoriented samples (LOT A2/15 test parcel). Mont. = montmorillonite, Qz = quartz, Feld. = Feldspars, Crist. = cristobalite.

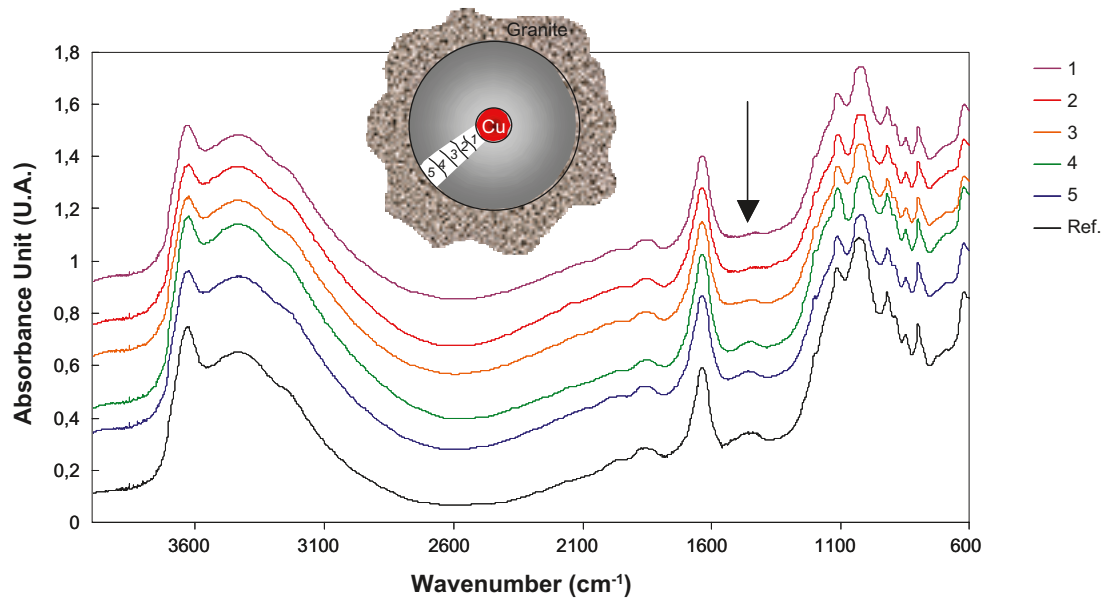


**Figure A6-5.** FTIR patterns of LOT A2/15 test parcel which shows the decrease of the carbonate content with increasing temperature (sample 5 to 1).

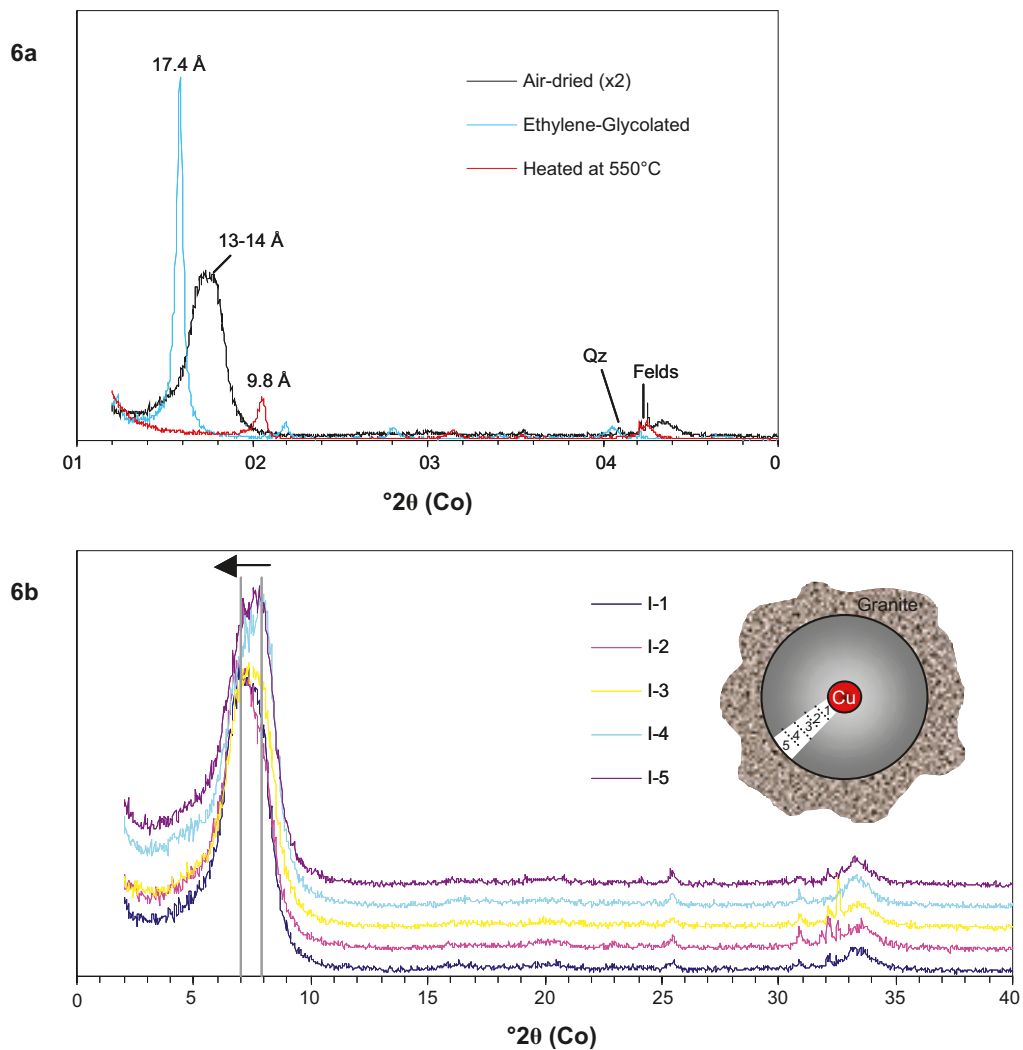


**Figure A6-6.** Oriented clay-size fraction (<2 μm) XRD patterns. (6a) Typical patterns for the 3 treatments (sample I-3): occurrence of Quartz (Qz) and Feldspars (Felds). (6b) Air-dried samples: shift of the main peak towards lower angles with increasing temperature.

Nevertheless, the Ca-Na substitution should have involved a trend in the particle chemistry obtained by TEM-EDX analysis. This is not the case as all the analytical data points plot in same area with the same scattering (Figure A6-7). The particle chemistry does not evolve according to the distance with the heating system. Specifically, clay mineral copper content does show any enrichment from the copper barrel to the granite (Figure A6-8), which is not in agreement with chemical analyses of clay fractions. Clay particles appear unaffected during the experiment whatever the temperature they have undergone.

CEC results are given in Table A6-6 and show that CEC remains constant for all samples. The measured CEC of the starting bentonite is more important than the value obtained for MX-80 sample of ANDRA. In addition, it can be observed that the balance Na-Ca in the LOT sample is in favour of Na (Na/Ca = 1.8 and 3.5 for ANDRA and LOT samples, respectively). The slight augmentation in CEC from the granite to heater, compared to starting bentonite, is not considered as significant. The nature of exchangeable cations is not changed, as well as their proportions.  $\text{Cu}^{2+}$  was not found among the released cations showing that Cu associated to the clay fraction does is not exchanged with interlayer cations of montmorillonite particles. In the case of sample 2, the difference in CEC between UV and chemical analysis of exchanged cations can be related to the occurrence of a soluble mineral such as a calcium sulfate (as observed by /Karnland 2005/)

**Table A6-6. Cationic exchange capacity of the studied samples, expressed as a function of initial weight (wet samples) and dry weight (110°C, overnight). Unit: meq/100 g.**

Sample	CEC <sup>a</sup>	CEC <sup>b</sup>	Na	K	Ca	Mg	Cu	Total <sup>b</sup>
Reference	79	86	52.8	1.5	29.3	6.0	0	89
Zone 5	77	92	50.7	1.4	28.4	9.7	0	90
Zone 4	87	100	52.4	1.6	29.0	12.7	0	95
Zone 3	79	95	52.8	1.6	29.9	9.9	0	94
Zone 2	79	95	52.7	1.8	47.7	9.8	0	112
Zone 1	77	91	51.7	1.6	31.7	10.2	0	95

<sup>a</sup> Wet samples. <sup>b</sup> Dry samples.

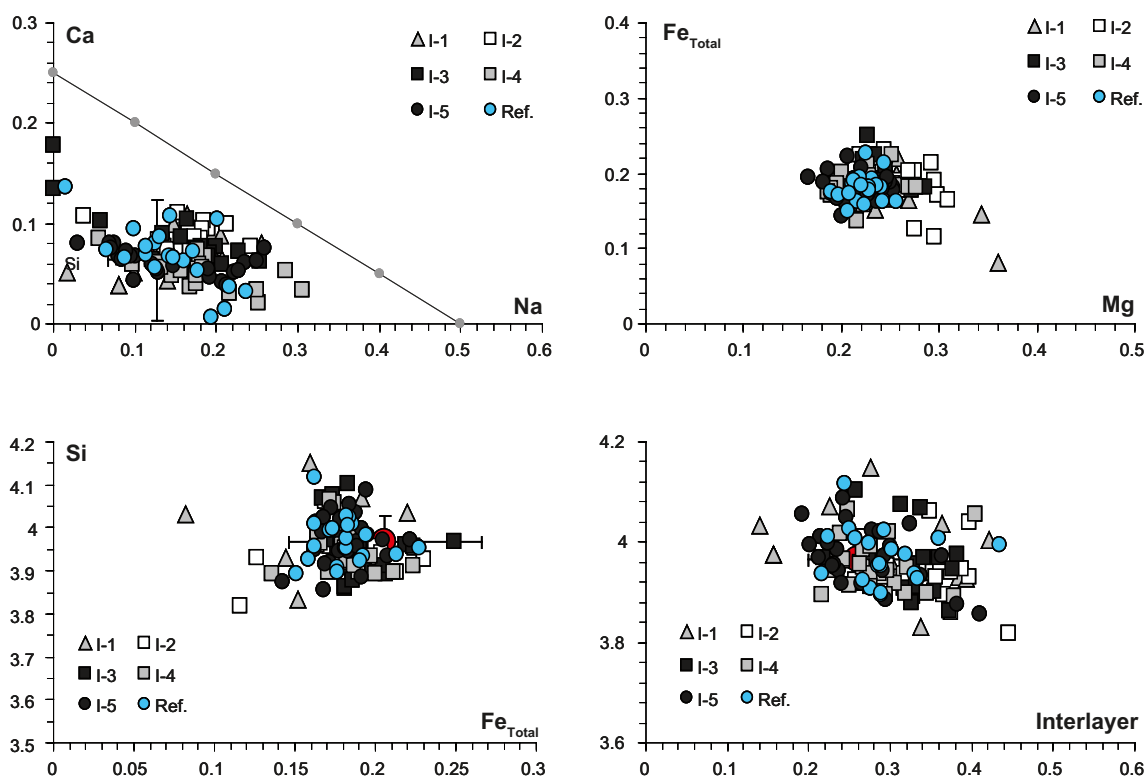


**Figure A6-7. Crystal chemistry by TEM-EDX showing no evolution relative to temperature (samples 1 to 5 from the heater to the granite respectively). The red data point stands for ANDRA MX80 /Rousset et al. 2005/.**

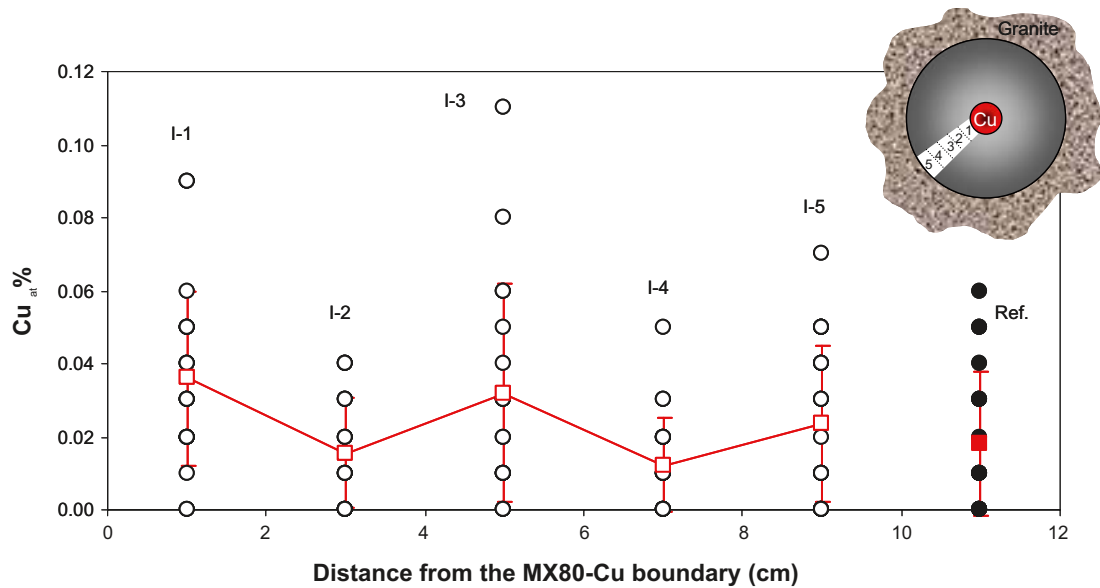


**Figure A6-8.** Evolution of the copper content in the clay particles. No significant increase can be shown in the vicinity of the copper-made heater. Open circle = data points, open square = standard deviation ( $\pm 1 \sigma$ ).

The studied reference sample contains more calcium as exchangeable cation than expected from the unit cell formula given by SKB ( $\text{Na}/\text{Ca} = 9.4$ ). The reason of this discrepancy is not known for the moment. The high amount in Ca can not be accounted to the presence of soluble minerals such as gypsum or carbonates as such a presence systematically results in a UV CEC lower than those calculated from chemical analysis of exchanged cations (see for instance the effect for sample of zone 2). This could suggest additional Ca fixation in the interlayer position of clay particles as already assumed from XRD patterns

Various accessory minerals have been identified by SEM in all the samples including iron oxides, pyrite, zircon, baryte, and apatite. Two types of secondary mineral neoformation have been observed by SEM:

- 1) Calcium sulphates
  - 2) Copper sulphides
- 1)  $\text{CaSO}_4$  is only found in the vicinity of the Cu-MX80 contact (Figure A6-9), as already observed by /Karnland 2005/. Ca required for the precipitation could origin from carbonate dissolution. Sulphur could come either from pyrite oxidation or from in situ geological fluids with which bentonite was equilibrated prior to the experiment.
  - 2) The copper sulphides have been observed only in the closest sample from the heater. These phases are easily identified by SEM using retro-diffused electrons because of high contents in heavy elements such as Fe or Cu (e.g. Figure A6-9).

These phases are Cu-S association with various amounts of Fe (Figure A6-10). They form small aggregates of about  $5 \mu\text{m}$  in diameter. SEM cartography shows an apparent repartition of these elements within aggregates and the absence of O, so these phases can be considered as sulphides (Figure A6-10). The homogeneous repartition has to be confirmed by TEM as the size of these aggregates is in the range of the low limit of SEM analytical resolution.

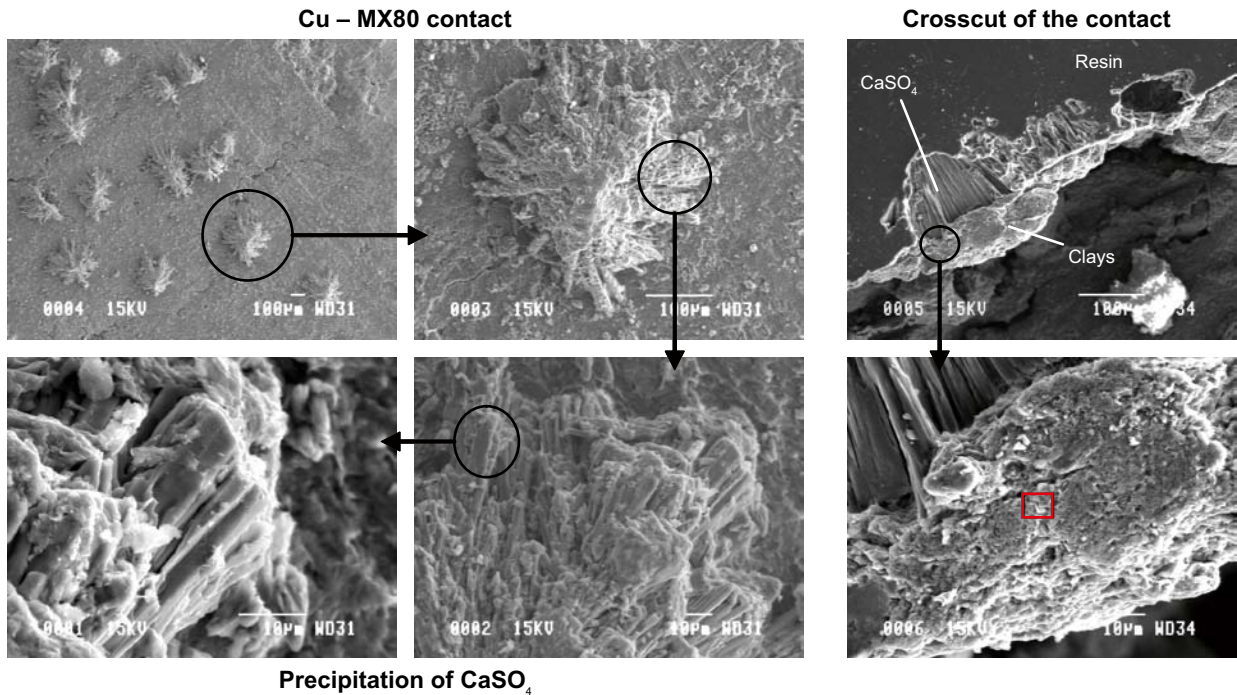


**Figure A6-9.** SEM photographs of  $\text{CaSO}_4$  precipitation at the MX80-Cu interface. Note the occurrence of Cu-rich phases within clay aggregates (square, bottom right photograph).

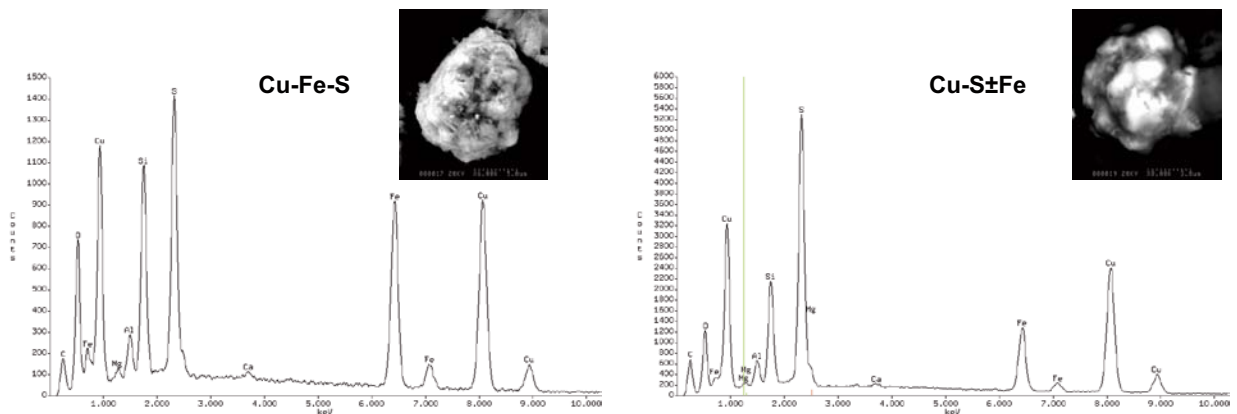


**Figure A6-10.** SEM-EDX patterns of Cu-rich phases.

Cu-rich phases have then been analysed at higher resolution by TEM to obtain accurate cartography and profile of the elementary repartition in the aggregates (Figures A6-11 to A6-14). One can thus distinguish 3 types of sulphides according to the iron content:

- i) *High Fe content*: heterogeneous sulphides with Fe-S in the centre of the particle and Cu-S on the edge (Figure A6-12). These particles probably form from pyrite dissolution and precipitation of new Cu-S phase.
- ii) *Medium Fe content* ( $\text{Fe} < \text{Cu}$ ): the repartition of S and Cu is homogeneous, and Fe is present where Cu and S contents decrease and O contents increase (Figure A6-13), probably reflecting a mixture between copper sulphides and iron oxides. The conditions of formation of these aggregates remain unclear.
- iii) *Low Fe content*: precipitation of Cu sulphides.

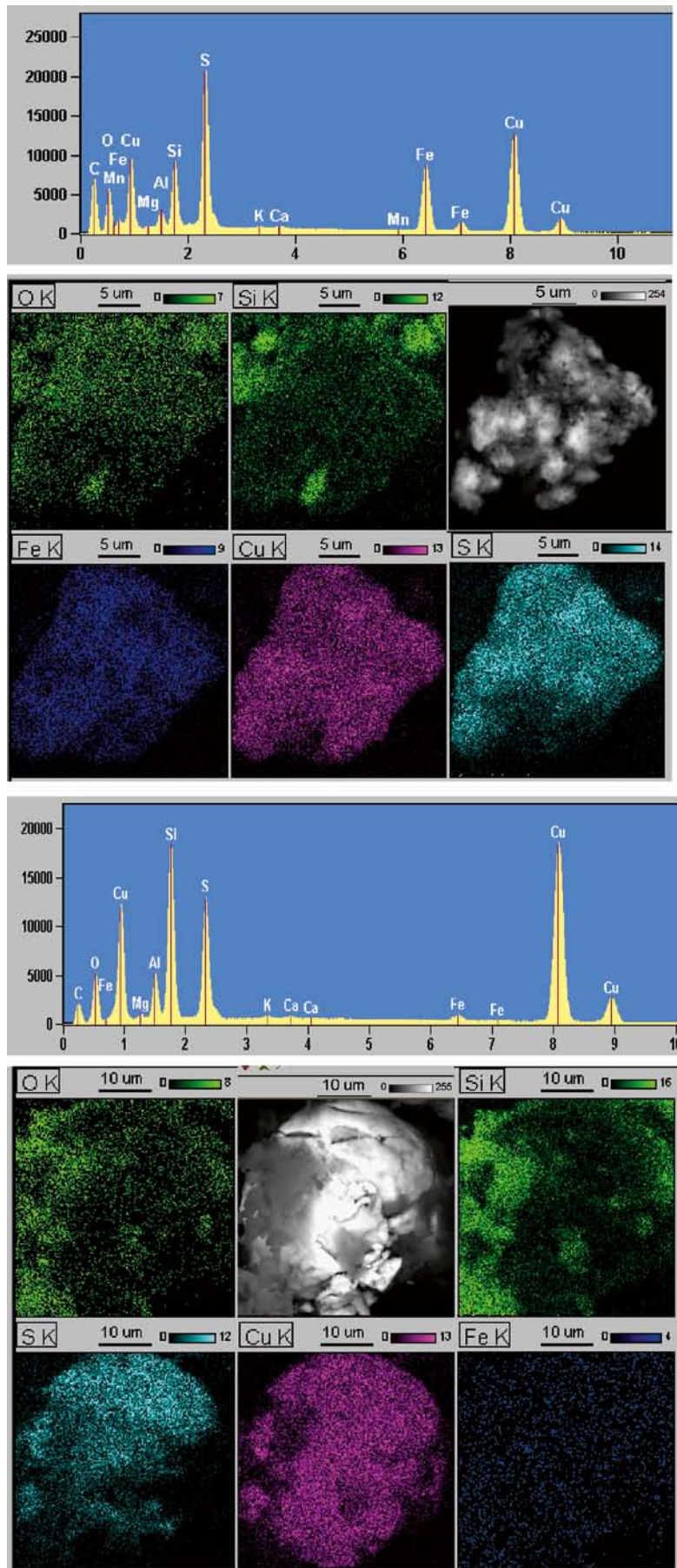


Figure A6-11. SEM-EDX patterns and cartography of Cu-rich phases.

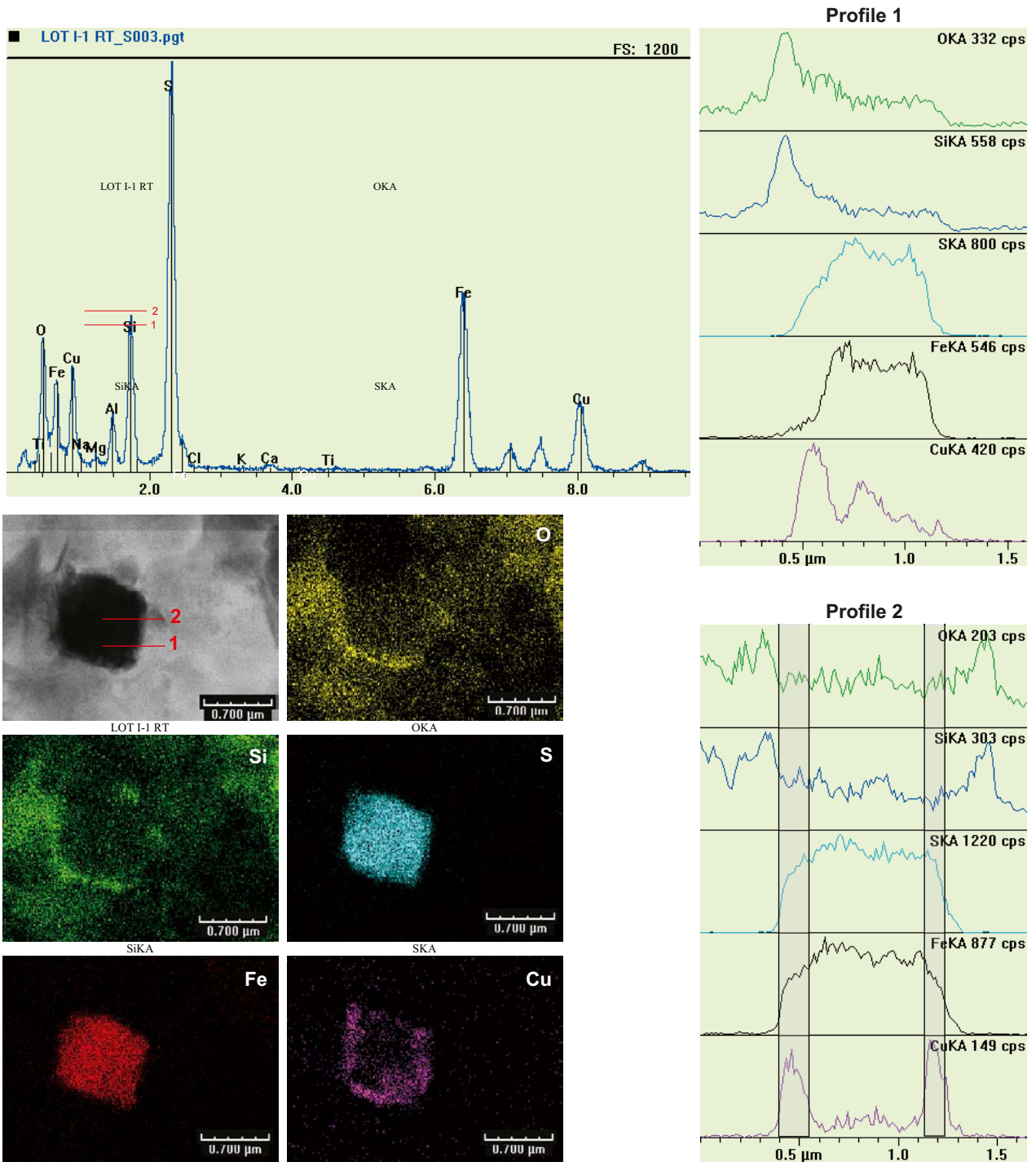


Figure A6-12. TEM-EDX patterns, cartography and profiles of Cu-rich heterogeneous sulphides.

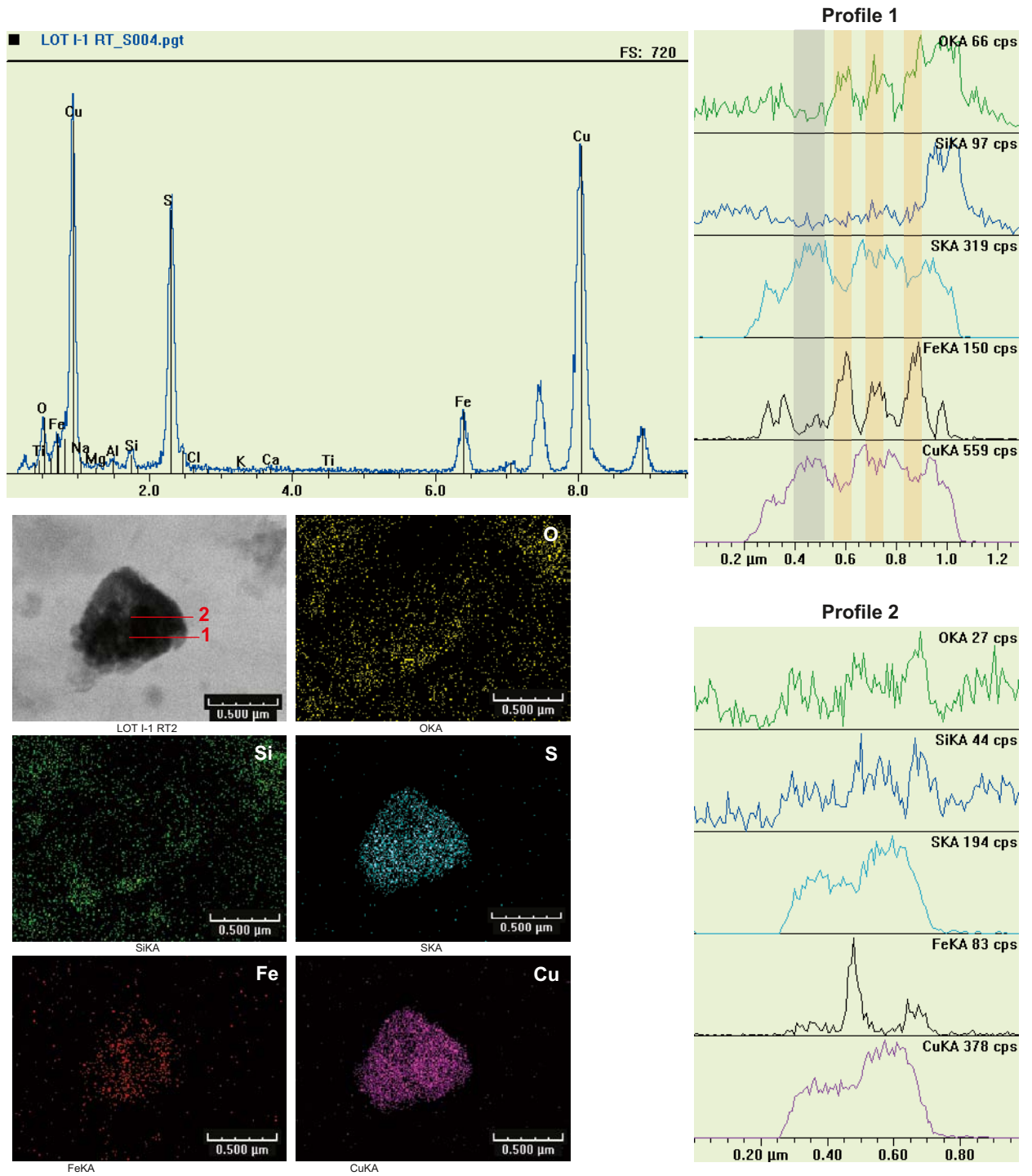
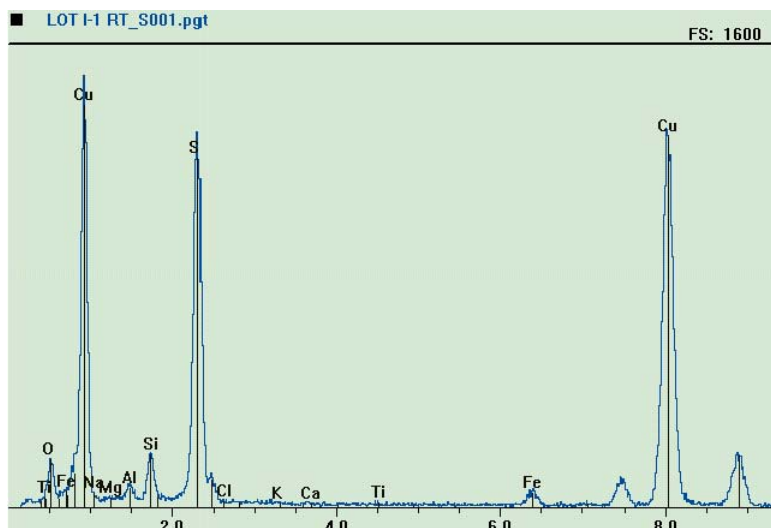


Figure A6-13. TEM-EDX patterns, cartography and profiles of Cu-rich homogeneous sulphides.



**Figure A6-14.** TEM-EDX patterns of Cu sulphides.

XPS analyses have been performed in order to evaluate the interest of this technique for the detection of copper at the surface of the sample. For this test, a small fragment corresponding to the interface between the bentonite and the heater was chosen (Figure A6-15). Wide spectrum and images was recorded on a surface aggregate.

The XPS spectrum presented on Figure A6-16 shows the different observed elements and it can be noticed that copper is observed. Although XPS is generally used to obtain quantitative chemistry of the surface (around 5 nm depth), the fine analysis allowing the corresponding calculations have not been carried out as the studied surface was not flat. To go deeper in the potential interest of XPS, the mapping of different elements was tested for the studied area (Figure A6-17).

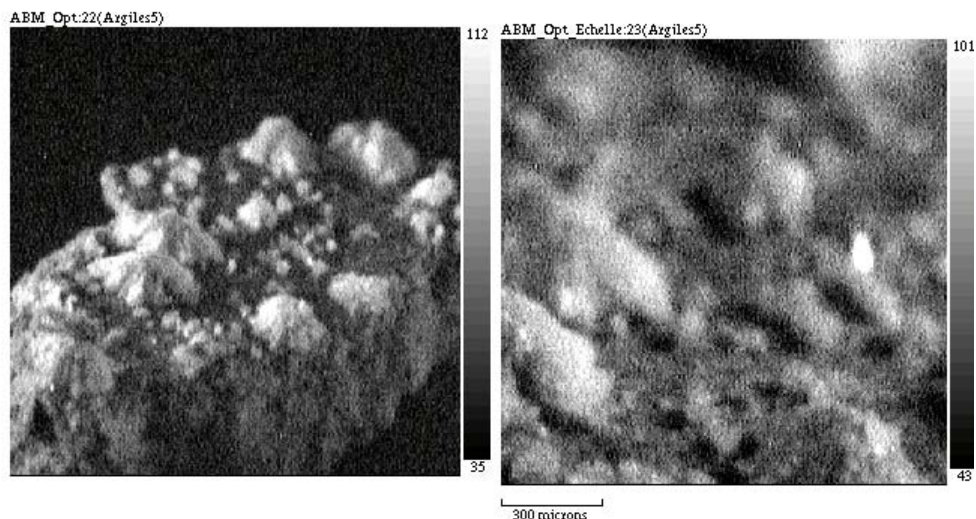


**Figure A6-15.** Photographs of XPS studied areas.

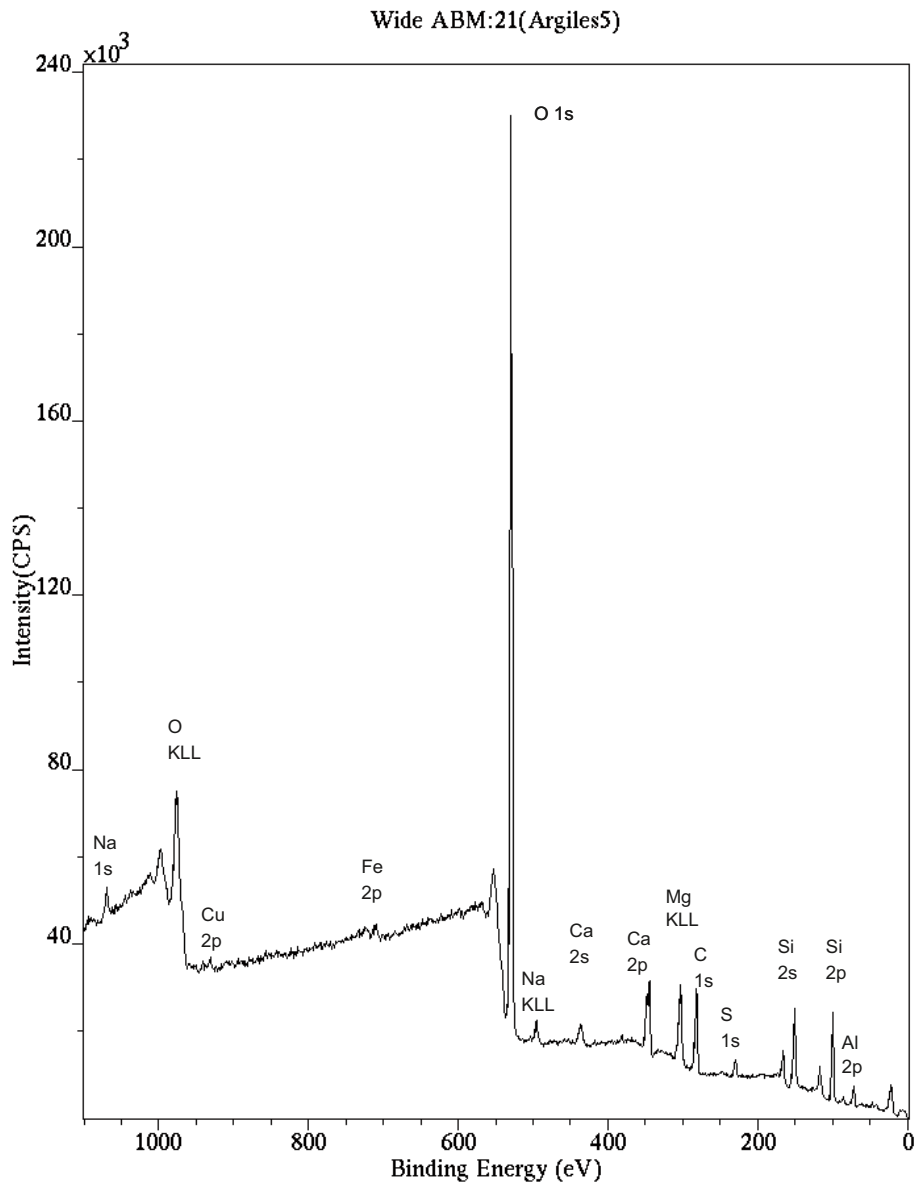


**Figure A6-16.** XPS spectrum obtained on a test sample taken at the interface between the heater and bentonite.

The maps of Figure A6-17 show that at the surface of the test sample, copper is systematically associated to iron. In addition, areas with different chemical associations are observed:

- S, Ca, Fe and Cu, consistent with the precipitation of sulfates, as observed by SEM on Figure A6-9;
- Si, Fe, Cu, as observed at the periphery of iron sulphides on Figure A6-12. On the present case, Si and Cu repartitions seem more homogeneous than on Figure A6-12 showing that the corresponding phase is located at the surface of another material but without information on the different Si, Fe and Cu profiles as obtained by TEM (Figure A6-12);
- Cu and Fe without significant amounts of other mapped elements. This may correspond to oxides.

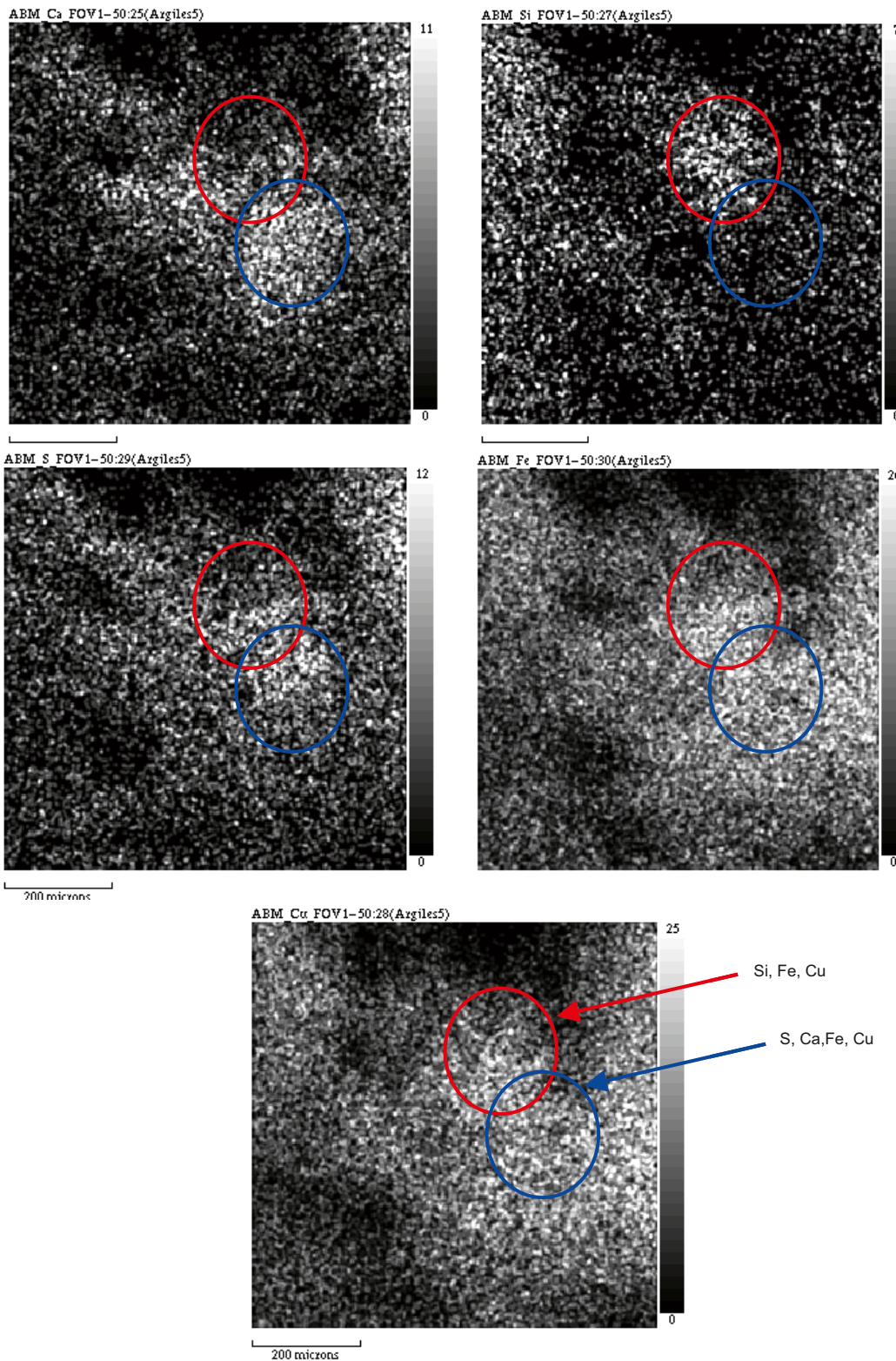


**Figure A6-17.** XPS mapping of Ca, Si, S, Fe and Cu on trest sample located at the interface between the heater and bentonite.

The XPS analysis confirms that copper is heterogeneously distributed at the interface between the heater and bentonite. This technique can be considered as complementary to SEM and TEM to obtain information on the first nanometers of the bentonite surface. The present results should be considered as preliminary tests demonstrating the potentiality of XPS. Indeed, a better control

of sample geometry and experimental conditions are required to derive accurate results. This is particularly the case for iron and copper as their peak intensities are low compared to the baseline and specific signal acquisition and treatment should be considered in future works.

### 3.3 Textural analysis and variations of morphological properties of clay aggregates

Humidity results are given in Figure A6-18. The humidity of the sample contacting granite (zone 5) is very close to the humidity of the sample in contact with the heater. This results is in the same range as for FEBEX bentonite /Montarges-Pelletier et al. 2003, Villar et al. 2004/, except that in that case, samples of each zone were separately collected and protected during dismantlement.

Adsorption-desorption isotherms are shown on Figure A6-19 and are typical of bentonites. For the 5 samples, the curves are closely superimposed; no modification of the pore size distribution is then clearly evidenced. However differences could be noticed at the very beginning, suggesting modification in the microporosity. In addition, high relative pressure adsorption ( $>0.5$ ) is slightly lower and the hysteresis between the adsorption and desorption branches decreases slightly for the samples located in the vicinity of the heater (zone 1 and 2), indicating a slightly more open network of intra-aggregate mesopores (a similar behaviour was observed in the case of FEBEX samples /Montarges-Pelletier et al. 2003, Villar et al. 2004/).

The BET analysis shows that the monolayer capacity and corresponding specific surface area decrease slightly from granite to heater (Table A6-7 and Figure A6-20) and remain very close to results obtained for MX-80 sample from ANDRA (33 m<sup>2</sup>/g) /Sauzéat et al. 2001/. T-plot total specific surface areas are higher than BET ones, which is classical when the studied solids contain some micropores. In the present case, the external surface area (or out of micropores surface area) can be considered as constant (mean value = 28.2 m<sup>2</sup>/g; standard deviation = 1.1 m<sup>2</sup>/g) while microporosity clearly decreases from granite to heater. This behaviour suggests that main textural features of the studied clay remain unchanged. The main effect, the decrease in microporosity, can be related to the local reorganization of tactoids as a function of dehydration/rehydration conditions in the vicinity of the heater /Neaman et al. 2003/.

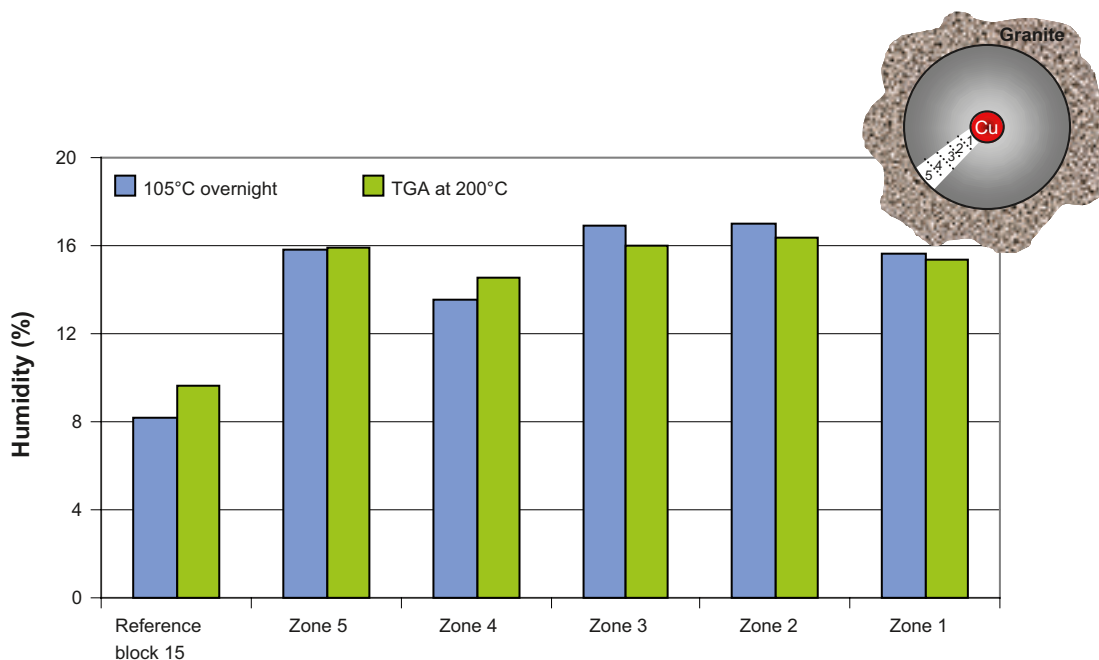


**Figure A6-18.** Humidity of the studied samples (Zone 1 to 5: mean: 15.8%, standard deviation 1.4%).

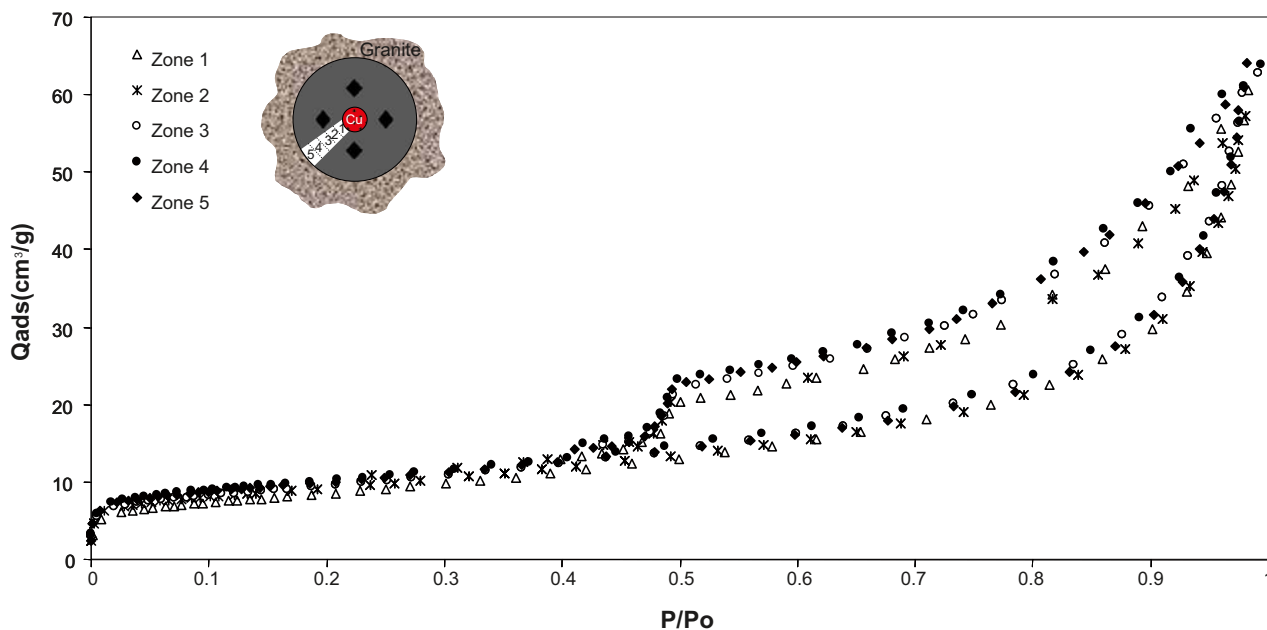


**Figure A6-19.** Nitrogen adsorption/desorption isotherms at 77 K on bentonite samples from granite (zone 5) to heater (zone 1).

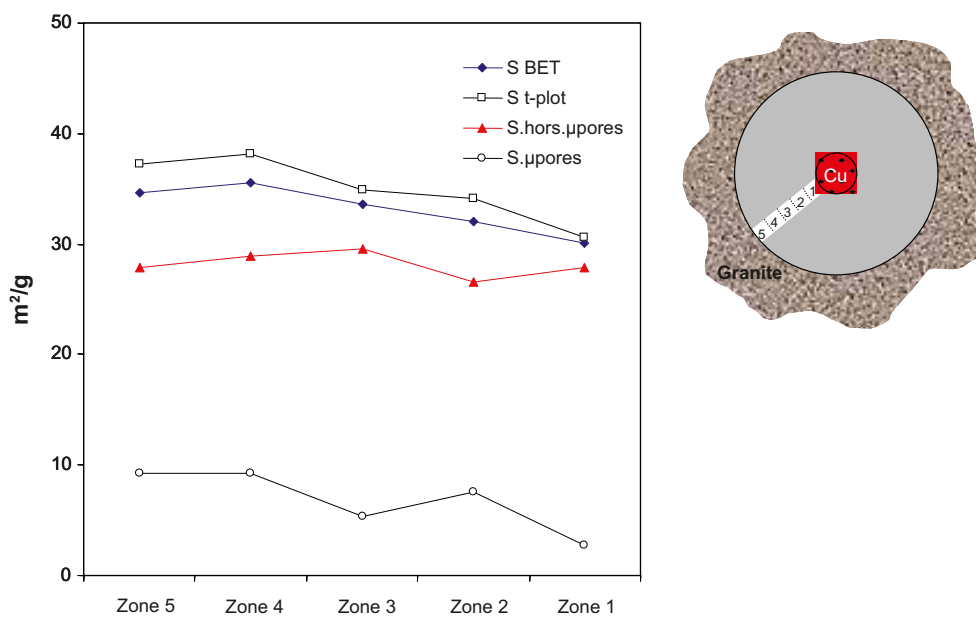


**Figure A6-20.** Evolution of specific surface areas (SSA) in  $m^2/g$  ( $\pm 1$ ) as obtained from BET and t-plot analyses of nitrogen adsorption isotherms on bentonite samples from granite (zone 5) to heater (zone 1).

**Table A6-7.** Evolution of specific surface areas (SSA) in  $m^2/g$  ( $\pm 1$ ) as obtained from BET and t-plot analyses of nitrogen adsorption isotherms on bentonite samples from granite (zone 5) to heater (zone 1).

	Zone 5	Zone 4	Zone 3	Zone 2	Zone 1
BET SSA	34.6	35.6	33.6	32.1	30.1
t-plot SSA	37.2	38.1	34.9	34.1	30.6
External SSA	27.9	28.9	29.6	26.6	27.9
Micropores SSA	9.3	9.2	5.3	7.5	2.7
% micropores	25.0	24.1	15.2	22.0	8.8

Figure A6-21 presents water adsorption curves obtained for samples close to the granite (zone 5) and close to the heater (zone 1). This figure clearly shows that water vapour adsorption process is the same for the two samples, suggesting that crystalline swelling properties of the sample are not significantly affected by the local environment. The obtained adsorption curves are typical of Na-smectites /Villieras et al. 1997, Michot and Villieras 2006/, which is in agreement with the composition in cations of the interlayer.

### 3.4 Thermal analyses

Figure A6-22 shows the weight loss vs temperature obtained on reference sample. The obtained curve is very close to the one obtained for MX <80 sample of Andra /Sauzeat 2001/, with an initial weight loss between room temperature and 200°C, corresponding to interlayer hydration water of the smectite and a weight loss between 500 and 750°C corresponding to smectite dehydroxylation. Small amounts were also outgassed between 200 and 550°C and were assigned by /Sauzeat et al./ to accessory minerals. Calcite decarbonation was not observed on the analysed samples, confirming that corresponding amount is very low. Thermal curves are very similar for all the other samples, except at the very beginning due to different contents in interlayer hydration water.

On differential curves the dehydroxylation peak is identical for all samples except for zone 4 (Figure A6-23). This phenomenon is reproducible as duplicate runs were performed for samples 4 and 3. The temperature of dehydroxylation peak is centred around 635°C for sample 4 and 655°C for all the other samples (Table A6-8). The specific behaviour of sample 4 may be associated to the migrations of different cations as observed in Tables A6-4 and A6-5. It is however not fully understood for the moment.

The amount of hydration water (expressed as a function of initial sample mass) compares very well with sample humidity measured at 110°C overnight (Figure A6-18). Weight loss determined for the different parts of the curves are reported on Table A6-5 as a function of final sample mass (1,000°C). It can be seen that the content in smectite is high as the amount of dehydroxylated water is close to theoretical value for pure smectite (5%). It is however not possible to give precise content in smectite for the studied samples due to the overlap of dehydroxylation of smectite with the thermal decomposition of accessory minerals between 200 and 550°C.

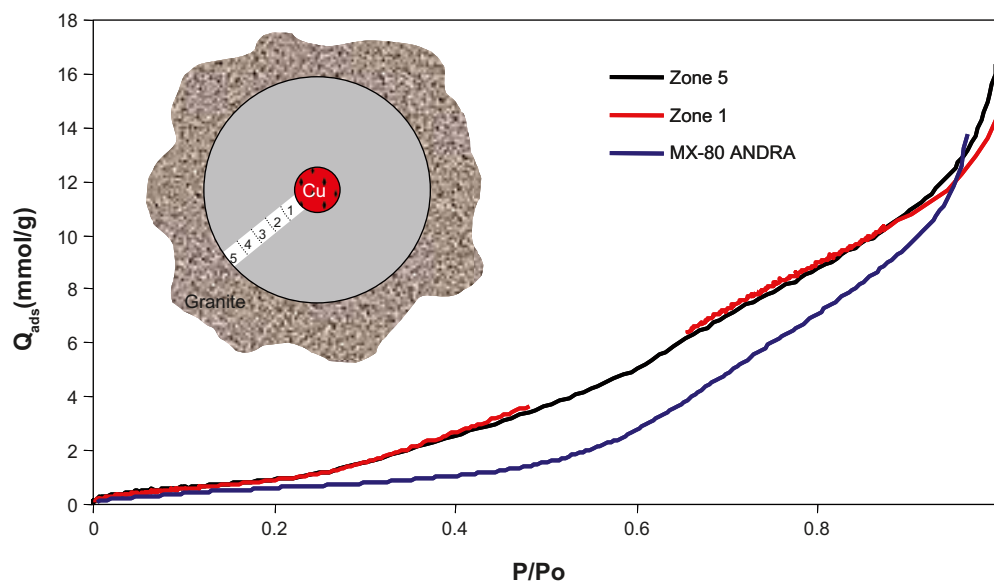


**Figure A6-21.** Water vapour adsorption isotherm at 303 K on bentonite samples at granite (zone 5) and heater (zone 1) interfaces and comparison with ANDRA MX-80 sample.

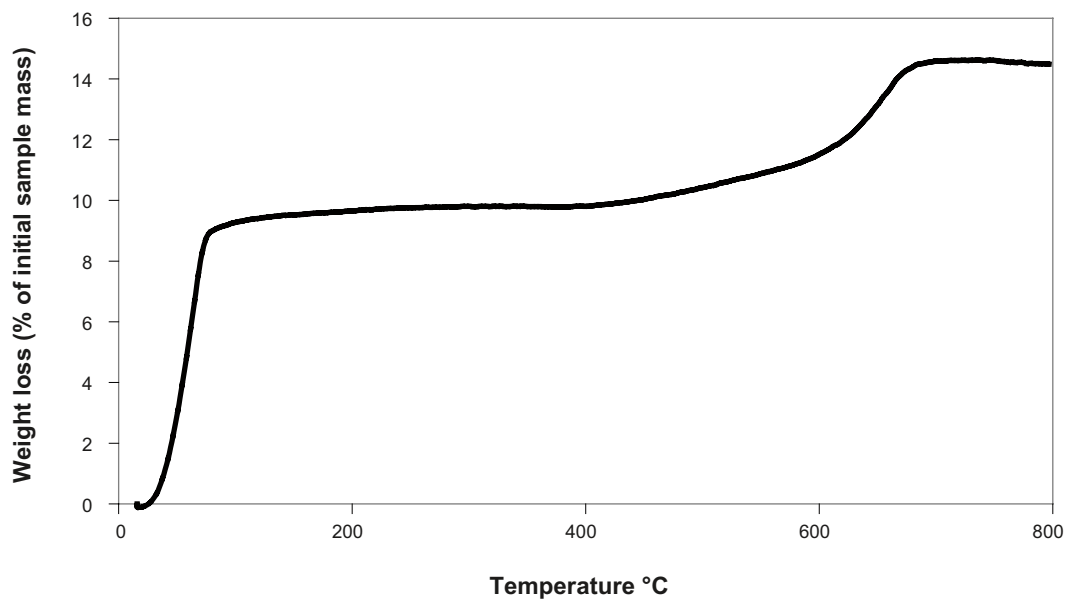


Figure A6-22. Weight loss as a function of temperature of the reference sample.

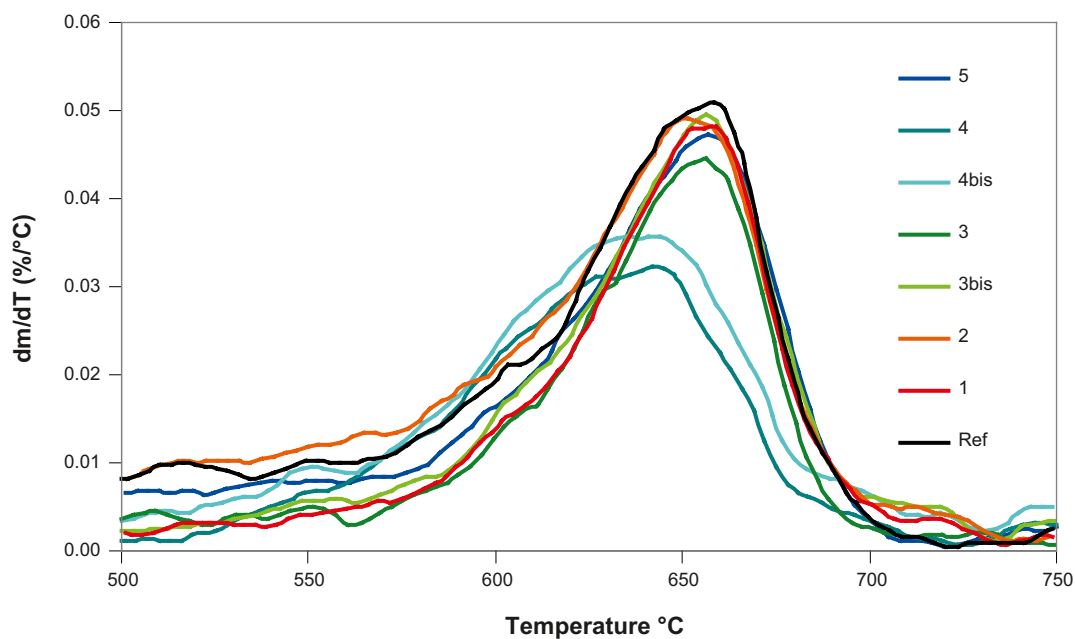


Figure A6-23. Differential weight loss as a function of temperature of the analysed samples. Analyses for samples 4 and 3 have been performed twice to check for reproducibility.

Table A6-8. Weight loss (% ,  $\pm 0.1\%$ ) expressed as a function of final mass (sample mass at 1,000°C) and peak temperature ( $^{\circ}\text{C}$ ,  $\pm 3^{\circ}\text{C}$ ) obtained from thermal analyses.

	0–200°C	200–500°C	500–750°C	T° Endo
Reference	11.3	0.9	4.9	658
Zone 5	20.3	2.1	4.8	657
Zone 4	17.7	0.7	3.4	638
Zone 3	19.9	0.5	3.8	656
Zone 2	20.8	0.7	5.6	653
Zone 1	19.0	0.2	4.1	656

## 4 Summary and prospects

These results have clearly shown that the long-term heating of MX80 bentonite did not modify, from a chemical and textural point of view, the main properties of the bulk material. Very slight modifications have been recorded by the clayey buffer, mainly in relation with temperature and hydration degree (decrease in microporosity, decarbonation). The copper is only provided by the heating system and these modifications affect mainly the very first centimetres of the buffer. Chemical analyses reveal also the presence of copper at the interface between granite and bentonite, suggesting complex fluid circulations. In enriched parts, copper is associated to bulk material and to the clay fraction. It seems however that copper does not interact directly with the phyllosilicates and occurs likely as small particles of oxide or sulphide.

The destabilisation of primary minerals (pyrite and carbonates) has led to formation of secondary phases such as Ca sulphates, Cu sulphides and Fe oxides. This report has shown occurrence of mixture of Cu-Fe-S but formation processes of these phases remain unclear. Synchrotron-based investigations could lead to determine such processes in studying more carefully either inter-atomic distance or oxidation-reduction state of iron in these phases.

On a methodological point of view, the most useful methods for such investigations are those allowing to realize element mapping and profiles. This is particularly the case of SEM and TEM. XPS also seems also attractive but its interest (complementarity) is not clearly demonstrated. The impregnation realized following Prêt /Sammartino et al. 2002, Prêt 2003, Prêt et al. 2004/ method also represents an additional and complementary way of investigation of both textural and chemical evolution of clayey material at an upper scale and will be the object of a separated report.

## 5 References

- Brunauer S, Emmett P H, Teller E, 1938.** Adsorption of gases in multimolecular layers. *Journal of American Chemical Society*, 60, 309.
- Byström-Brusewitz A M, 1975.** Studies of the Li test to distinguish beidellite and montmorillonite. *Proceedings of the International Clay Conference, Mexico City. Applied Publishing Ltd., Wilmette, Illinois*, pp. 419–428.
- de Boer J H, Linsen B G, Osinga T J, 1965.** Studies on pore systems in catalysts. VI. The universal t-curve – *Journal of Catalysis*, 4, 643.
- Greene-Kelly R, 1953.** The identification of montmorillonoids in clays. *Journal of Soil Science* 4, 233–237.
- Guillaume D, 2002.** Etude expérimentale du système fer-smectite en présence de solution à 80°C et 300°C. Ph.D. Thesis, Université Henri Poincaré, Nancy.
- Harvey C O, 1943.** Some notes on the calculation of molecular formulae for glauconite. *American Mineralogist* 28, 541–543.
- Hoffman U, Klemen E, 1950.** Loss of exchange-ability of lithium ions in bentonites on heating. *Zeitschrift für Anorganische und Allgemeine Chemie* 262, 95–99.
- Karland O, 2005.** Long Term Test of Buffer Material – LOT project, 2005-11-02, Clay Technology AB. “ABM Karland Lot 2005-11-02.pdf”, 47 slides.
- Michot L J, Villieras F, 2006.** Critical assesment of analytical techniques: Surface area and porosity. In *Handbook of Clay Science*, F. Bergaya, B.K.G. Theng and G. Lagaly Eds., Elsevier, Amsterdam, 2006, ISBN 0080441831, chap. 12.9, 975–988.
- Montarges-Pelletier E, Devineau K, Villieras F, Bouquet E, Pelletier M, Razafitianamaharavo A, Barrès O, Lambert P, Charpentier D, Mosser-Ruck R, Cathelineau M, 2003.** Post-mortem FEBEX bentonite samples: Mineralogical and textural analysis. ANDRA Report, CRPIENG033, 37 p.
- Neaman A, Pelletier M, Villieras F, 2003.** The effects of exchanged cations, compression and heating on textural properties of MX-80 bentonite and its corresponding purified montmorillonite. *Applied Clay Science*, 22, 153–168.
- Poirier J E, Francois M, Cases J-M, 1987.** Study of water adsorption on Na-Montmorillonite/ New data owing to the use of a continuous procedure. In : *Fundamentals of adsorption*, Liapis A.T. Ed. A.I. Ch. E. New York, pp 473–482.
- Prêt D, 2003.** Nouvelles méthodes quantitative de cartographie de la minéralogie et de la porosité dans les matériaux argileux : application aux bentonites compactées des barrières ouvragées. Ph.D. Thesis, Université de Poitiers, Poitiers.
- Prêt D, Sardini P, Beaufort D, Zellagui R, Sammartino S, 2004.** Porosity distribution in a clay gouge by image processing of <sup>14</sup>C-PolyMethylMethAcrylate (<sup>14</sup>C-PMMA) autoradiographs. Case study of the fault of St Julien (Basin of Lodève, France). *Applied Clay Science*, 27, 107–108.
- Rousset D, Mosser-Ruck R, Cathelineau M, 2005.** Expression du besoin relatif à la compréhension du comportement à long terme d’une barrière ouvragée en argile pour le stockage de déchets radioactifs en formation géologique profonde. Final Report ANDRA, DRP0CRE.05-002, 132 p.
- Sauzeat E, Guillaume D, Neaman A, Dubessy J, François M, Pfeiffert C, Pelletier M, Mosser-Ruck R, Barrès O, Yvon J, Villieras F, Cathelineau M, 2001.** Caractérisation minéralogique, cristalochimique et texturale de l’argile MX-80. Rapport ANDRA C RP 0LEM 01-001, 82 p.
- Sammartino S, Siitari-Kauppi M, Sardini P, Bouchet A, Tevissen E, 2002.** An imaging method for the porosity of sedimentary rocks: adjustment of PMMA method – Example of a characterisation of calcareous shale. *Journal of Sedimentary Research*, 72, 937–943.

**Villar M V, Fernandez A M, Rivas P, Loret A, Daucausse D, Montarges-Pelletier E, Devineau K, Villieras F, Hynkova E, Cechova Z, Montenegro L, Samper J, Zheng L, Robinet J C, Muurinen A, Weber H P, Børgesson L, Sanden T, 2004.** Postmortem bentonite analysis. Technical report 70-IMA-M-67-6-7, European Program FIKW-CT-2000-00016 FEBEX II, 159 p.

**Villieras F, Michot L J, Cases J M, Berend I, Bardot F, François M, Gérard G, Yvon J, 1997.** Static and dynamic studies of the energetic surface heterogeneity of clay minerals. In “Equilibria and Dynamics of Gas Adsorption on Heterogeneous Solid Surfaces”, W. Rudzinski, W.A. Steele and G. Zgrablich Eds., Studies in Surface Science and Catalysis, Elsevier Science Publishers B. V., Amsterdam, 104, 573–623.

## **Mineralogical and geochemical alteration of the MX80 bentonite from the LOT experiment**

### **Characterization of the A2 parcel**

Kaufhold S, Dohrmann R

BGR Bundesanstalt für Geowissenschaften und Rohstoffe

LBEG Landesamt für Bergbau, Energie und Geologie

Email of corresponding author: [s.kaufhold@bgr.de](mailto:s.kaufhold@bgr.de)

#### **BGR funded part**

This part concerns a study which was conducted for BGR within the LOT project. The conclusions and viewpoints presented are those of the authors and do not necessarily coincide with those of SKB.

## Abstract

Bentonites are believed to represent a suitable geotechnical barrier in HLRW repositories and, therefore, are investigated with respect to long term stability under the conditions expected. In order to identify the type and extend of possible bentonite alteration processes long term tests have to be performed. Particularly valuable information is gained from in situ tests which are commonly conducted in underground rock laboratories (URL). The LOT test performed by SKB is one of the outstanding tests due to the long test period accounting for 6 years including 5 years heating period. In this study chemical and mineralogical alteration processes of the bentonite after the 5 years heating period are investigated.

By in situ  $\mu$ -EDXRF an increased Cu concentration was detected at the surface and along a profile until a depth of ca. 2 cm. By standard bulk XRF a slightly increased Cu concentration was found even in 4 cm distance from the Cu tube. Surprisingly, Cu was not detected on the exchange sites of the smectite. Accordingly, Cu has to be present as a separate phase. On the surface of the bentonite sample which was in direct contact with the Cu tube a bluish phase with metallic glance was found by light microscopy. SEM-EDX proved the dominance of Cu and S within this phase. In addition, by thermal analysis in combination with evolved gas analysis (DTA-MS) the presence of Cu-sulphides within the first cm is indicated. This raises the question about the S source. In the bentonite applied (MX80 from Wyoming) S predominantly occurs as sulphate (gypsum). Alternatively S could stem from dissolved sulphate of the pore water which entered the system during the experiment. Regardless of the two possible S sources it can be concluded that Cu corrosion directly or indirectly led to sulphate reduction. Based on the available data it is impossible to decide whether  $\text{SO}_4$  from the external water or from the gypsum of the bentonite was reduced by Cu corrosion. It can be concluded – regardless of this open question – that the selection of a bentonite being poor in  $\text{SO}_4$  (not containing sulphides or sulphates) would lead to reduction of the corrosion rate.

Parallel studies conducted by SKB, ONDRAF, and NAGRA proved the redistribution of water extractable  $\text{SO}_4$  over the entire bentonite block distance (10 cm). Surprisingly, a  $\text{SO}_4$  depletion was found both in the inner part (contact to Cu tube) and in the outermost 5 cm. On the other hand, a  $\text{SO}_4$  peak was found at appr. 3 cm distance from the heater. During the experiment water flew at the inner and outer surface of the bentonite block. Hence it is conceivable that this water dissolved the partially soluble gypsum which has been homogenously distributed over the 10 cm of the bentonite block as the experiment started. Such dissolution – precipitation processes conceivably affect porosity and in turn the hydraulic conductivity. Therefore, the selection of a bentonite being poor in partly soluble minerals as calcite or gypsum would help to reduce the extend of dissolution – precipitation processes.

No unambiguous evidence for (structural) alteration of the montmorillonite was found. However, a slight increase of Mg nearby the heater could be detected indicating that some Mg was released from the montmorillonite. Interestingly, this result corresponds to the results obtained from the Mont Terri Heater project /Plötze et al. 2007/. It is concluded that Mg release occurred to such a small extend that structural changes (e.g. change of layer charge density) could not be detected by IR, XRD, CEC and Alkylammoniummethod.

## Introduction

Bentonite is a candidate material as geotechnical barrier in high level radioactive waste (HLRW) repositories. However, one important open question with respect to safety assessment of the whole system is the long term stability. Bentonite properties are known to be affected by high pH solutions (e.g. cement pore water), highly saline waters, and by extensive drying. In this context illitization and/or the irreversible collapse of smectitic layers are particularly considered. Long term tests have to be performed in order to identify such processes and to learn more about the stability of bentonites under the conditions expected in a HLRW repository. However, bentonite cannot be considered as instable material even though different bentonite alteration processes are known. Therefore, either exaggerated conditions or a long time period have to be applied. Exaggerated conditions might lead to alteration processes which would not occur under realistic conditions. Therefore, performing long term tests covering a significant period of time are particularly valuable for bentonite research. In this respect, the LOT test as conducted by SKB represents a currently outstanding in situ test. Detailed information about this test is given by /Karnland et al. 2000/.

In this paper the mineralogical and chemical alteration processes which occurred within the first 5–6 years (5 years heating) are investigated.

# Materials and methods

In the LOT experiment conducted by SKB, different scenarios were included in the experimental setup. As an example, Cu plates were inserted as well as potassium feldspar. Therefore, the exact location of investigated samples has to be known in order to ensure comparability of results obtained by different laboratories.

BGR received a sample from the extensively heated part (15) of the A2 parcel. The experimental setup, temperature distribution at equilibrium conditions, and a photograph of the investigated sample are shown in Figure A7-1.

The analyses conducted by BGR focused on mineralogical and chemical processes at the Cu-bentonite interface. This was thought to be most interesting since Cu corrosion was already evident from the macroscopic inspection of the Cu tube. It was decided to first continuously measure the Cu distribution by in situ  $\mu$ -EDXRF.

During the LOT experiment the bentonite has been in contact with excess water which led to the slow but steady increase of swelling pressure in turn indicating ongoing water saturation. The water content of the sample, therefore, was comparably high and the tendency to release water at ambient laboratory conditions was obvious. For  $\mu$ -EDXRF analysis the block, except for the profile, was protected with plastic foil in order to prevent the slice from falling apart. This protection was sufficient to measure two replicates. Thereafter, the block was sampled (appr. 5 g/sample) according to Figure A7-1. The sample called ‘1<sup>st</sup> mm’ was collected by scraping off ca. 2 g from the very surface. The samples were dried at 60°C until constancy of weight and subsequently ground by a laboratory mortar mill.

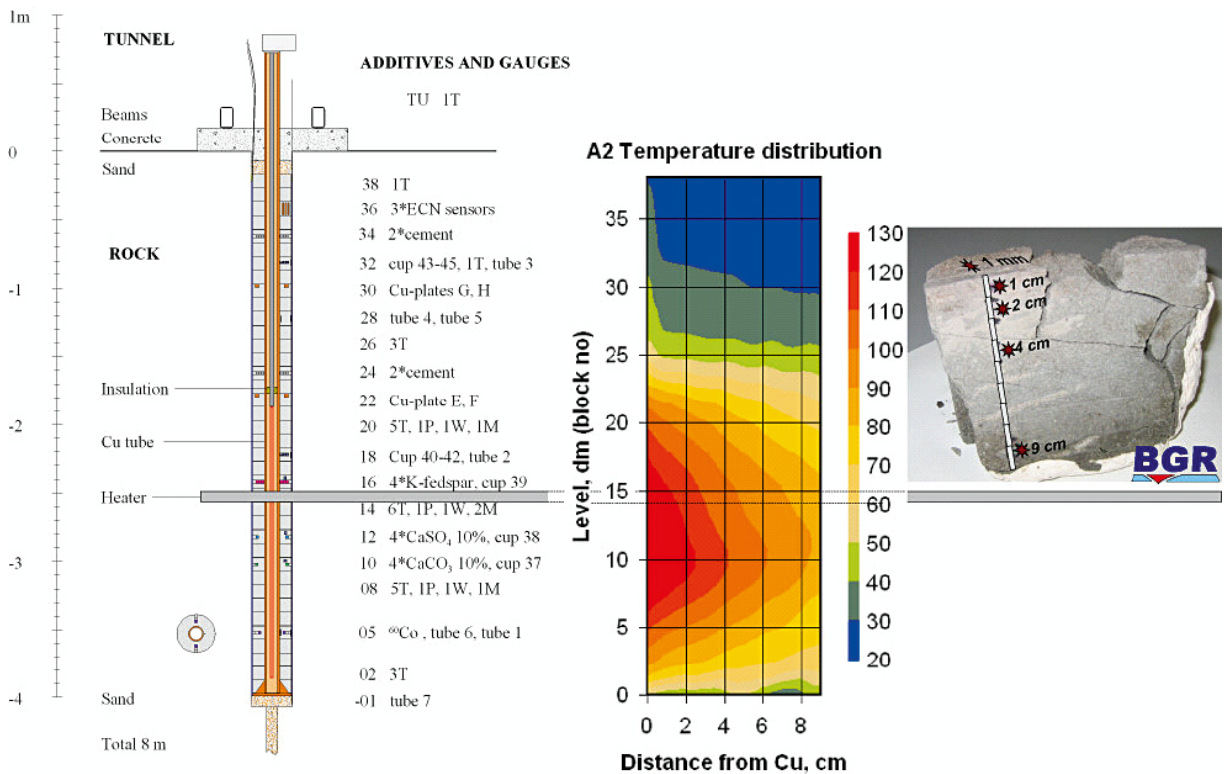


**Figure A7-1.** Experimental setup, temperature distribution at equilibrium conditions (source: SKB). The sampling of the slice of block 15 sent to BGR is shown in the photograph.

The **in situ- $\mu$ EDXRF** measurements were performed by the combination of an ITRAX microscope and a geoscanner, as it is distributed by COX analytical systems.

The chemical composition was determined by **XRF** using a PANalytical Axios and a PW2400 XRF spectrometer.

For **XRD** analysis oriented mounts were produced by suction of a suspension (60 mg of clay dispersed in 2 ml of deionised water) through porous ceramic plates. XRD pattern were recorded on a Seifert 3003 TT diffractometer, using  $\text{CuK}_\alpha$  radiation before and after exposure to an ethyleneglycol atmosphere.

The cation exchange capacity was determined by the **BaCl<sub>2</sub>** method according to /Mehlich 1948/ but without buffering and using a batch technique instead of percolation.

For recording mid **infrared** (MIR) spectra the KBr pellet technique (1 mg sample/200 mg KBr) was applied. Spectra were collected on a Thermo Nicolet Nexus FTIR spectrometer (beam splitter: KBr, detector DTGS TEC).

Near infrared (NIR) spectra were recorded using the DRIFT-technique, beam splitter  $\text{CaF}_2$ , detector InGaS. Both MIR and NIR spectra consist of 32 scans each. The resolution was adjusted to  $2 \text{ cm}^{-1}$ .

**Thermoanalytical** investigations were performed by a Netzsch 409 PC thermobalance equipped with a DSC/TG sample holder linked to a Balzers ThermoStar quadrupole mass spectrometer (MS). 100 mg of powdered material previously equilibrated at 53% r.H. is heated from 25–1,000°C with a heating rate of 10 K/min.

Scanning electron microscopy (**SEM**) was performed on an ESEM (environmental scanning electron microscope) from FEI Quanta 600 FEG.

The specific surface area (**SSA**) was determined by  $\text{N}_2$  adsorption using a 5 point BET method. Measurements were performed by a Micromeritics Gemini III 2375 surface area analyzer with ca. 300 mg weight.

The **water uptake capacity** was determined gravimetrically. Defined temperature and humidity were provided by a climate oven. Approximately 0.5 g sample was weighed in an Al crucible and equilibrated at 50, 60, and 70% RH for one week each.

The layer charge density (**LCD**) was determined by the alkylammonium method /Lagaly 1994/. Lagaly proposed to use a set of n-alkylammonium ions ( $n_c = 6-18$ ) which provides information about layer charge density distribution. However, in some cases only a value for the mean layer charge density is desired. Accordingly, /Olis et al. 1990/ suggested using the dodecylammonium ion, only. In this study we applied chain lengths 11, 12, and 13, in order to increase statistical significance. For the calculation of LCD values from the different d-spacing own unpublished calibrations were used. These calibrations were established by considering 13 different bentonites which covered a LCD range from 0.30 to 0.35 eq/FU.

# Results and discussion

## XRF

Chemical analyses based on XRF, in contrast to common quantitative mineralogical methods, provide precise values indirectly reflecting the mineralogical composition. These values are very useful for the identification of mineral alteration processes. Particularly relative differences are considered to be mineralogically meaningful even within the 1% range. The chemical composition as determined by XRF of all samples is given in Table A7-1.

The sample from the first mm, in contrast to samples 1–4 cm, reveals an appr. 1% higher loss on ignition (LOI) whereas the LOI of the sample at 9 cm is appr. 1% lower. This affects XRF values of all elements/oxides and in turn pretends meaningless trends. One example is given in Figure A7-2. To avoid this misinterpretation in the following only values which were normalized to LOI = 0 are considered.

Using these corrected data in case of SiO<sub>2</sub> and Al<sub>2</sub>O<sub>3</sub> slightly lower values of ‘sample 4 cm’ were observed (Figure A7-3). No systematic deviation of the Fe<sub>2</sub>O<sub>3</sub> content could be observed. In contrast, the MgO content increased nearby the Cu tube (Figure A7-4). Figure A7-5 shows a CaO and SO<sub>3</sub> peak at 4 cm which cannot be attributed to material heterogeneity which was proved before the experiment to be significantly lower. It is tentatively concluded that gypsum redistributed during the 5 (6) years of the project. Other studies conducted by Andra, SKB (a.o. yet unpublished) report a maximum gypsum concentration at 3 cm. However, in this study no sample was collected at this depth. In conclusion, the maximum gypsum concentration at 4 cm observed in this study probably represents the right shoulder of the actual peak.

With respect to the trace element composition three significant systematic variations were observed.

First of all a surprisingly high content of Cu was found even within the 1<sup>st</sup> cm indicating that Cu corrosion a) occurred and b) led to penetration of Cu into the bentonite. Even the 50 mg/kg which were observed in the ‘40 mm sample’ likely result from Cu migration (Wyoming bentonites commonly are poor in Cu).

The high Mo content in ‘sample 1 mm’ is supposed to also result from tube corrosion. A third effect was found for Ba displaying the same trend as was found for gypsum (CaO and SO<sub>3</sub>). This can be explained either by gypsum containing small amounts of Ba or by the presence of traces of baryte being present already in the precursor material.

**Table A7-1. Major element composition (XRF) normalized to LOI = 0 (LOI values given separately).**

		1 mm 1 <sup>st</sup> block	1 cm 1 <sup>st</sup> block	2 cm 1 <sup>st</sup> block	4 cm 1 <sup>st</sup> block	9 cm 1 <sup>st</sup> block
SiO <sub>2</sub>	[wt-%]	68.3	68.3	68.3	67.7	68.4
TiO <sub>2</sub>	[wt-%]	0.2	0.2	0.2	0.2	0.2
Al <sub>2</sub> O <sub>3</sub>	[wt-%]	20.7	20.8	20.7	20.5	20.7
Fe <sub>2</sub> O <sub>3</sub>	[wt-%]	3.9	4.0	4.0	4.0	4.0
MnO	[wt-%]	0.0	0.0	0.0	0.0	0.0
MgO	[wt-%]	3.0	2.7	2.7	2.5	2.4
CaO	[wt-%]	1.2	1.2	1.3	1.8	1.3
Na <sub>2</sub> O	[wt-%]	2.0	2.0	2.0	2.1	2.1
K <sub>2</sub> O	[wt-%]	0.5	0.5	0.5	0.5	0.5
P <sub>2</sub> O <sub>5</sub>	[wt-%]	0.1	0.1	0.0	0.0	0.1
(SO <sub>3</sub> )	[wt-%]	0.2	0.2	0.3	0.7	0.3
(Cl)	[wt-%]	0.0	0.0	0.0	0.0	0.0
(F)	[wt-%]	<0.05	<0.05	<0.05	<0.05	0.06
Sum	[wt-%]	100.0	100.0	100.0	100.0	100.0
LOI	[wt-%]	11.1	10.4	10.1	10.1	9.2

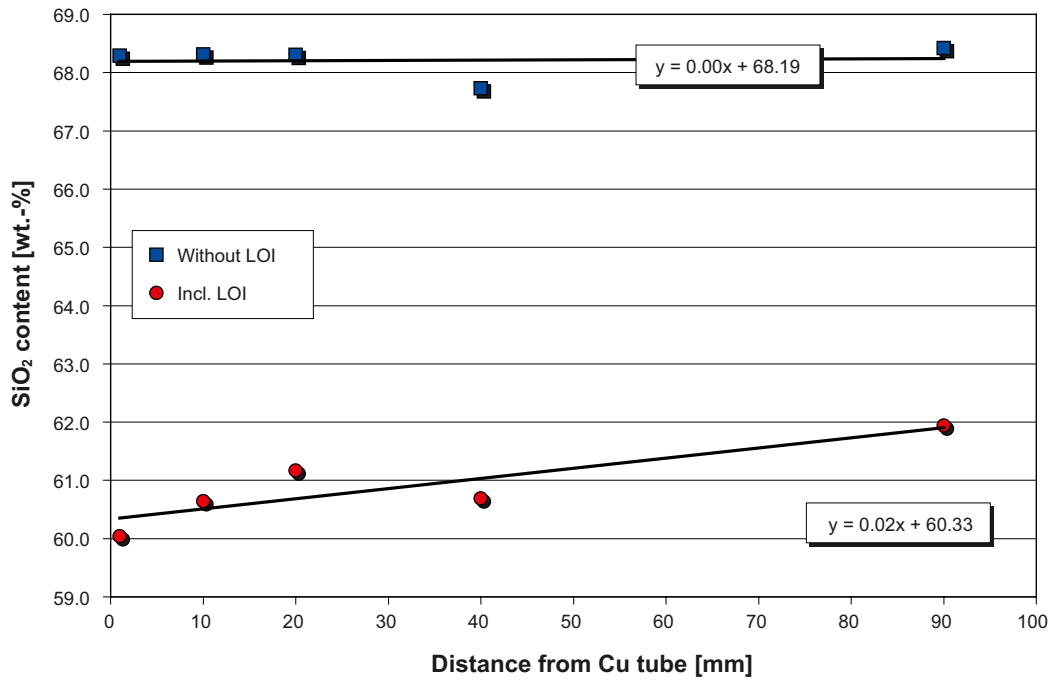


Figure A7-2. Comparison of SiO<sub>2</sub> content before and after correction of XRF data for the loss on ignition (LOI).

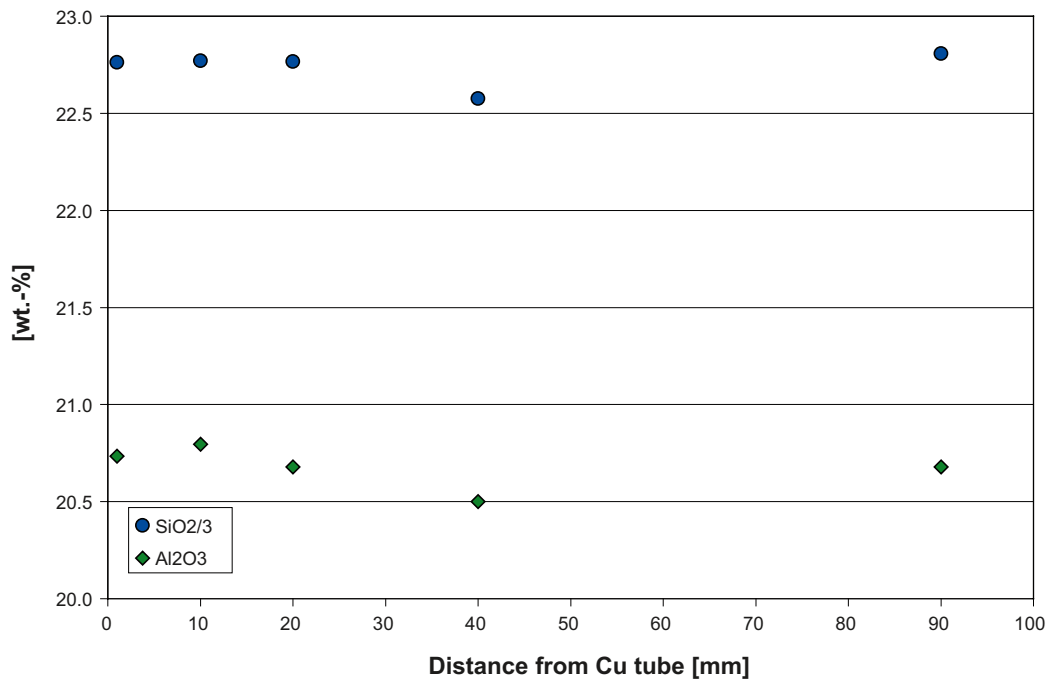


Figure A7-3. Al<sub>2</sub>O<sub>3</sub> and SiO<sub>2</sub> content (SiO<sub>2</sub> content is divided by 3) depending on the distance from the Cu tube.

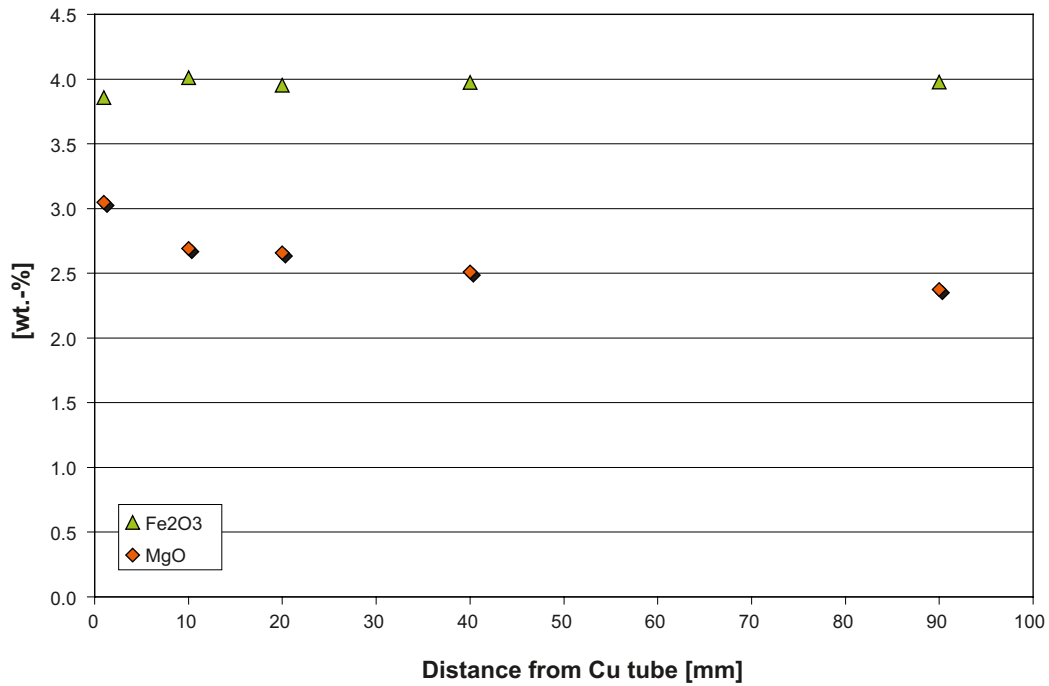


Figure A7-4. MgO and Fe<sub>2</sub>O<sub>3</sub> content depending on the distance from the Cu tube.

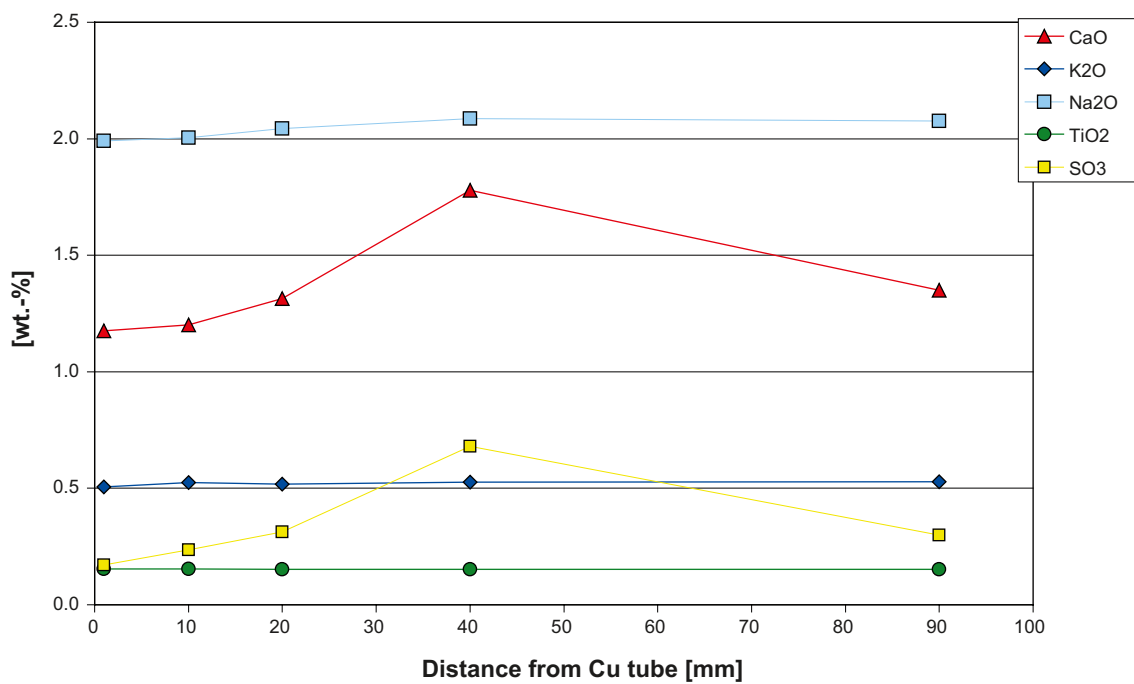


Figure A7-5. CaO, K<sub>2</sub>O, Na<sub>2</sub>O, TiO<sub>2</sub>, and SO<sub>3</sub> (XRF) content depending on the distance from the Cu tube.

In summary,

- an increased Cu and Mo content even in 2 cm distance,
- a CaO, Ba, and SO<sub>3</sub> peak at appr. 40 mm, and
- a higher MgO content nearby the Cu tube was found.

In conclusion, a) indicates corrosion, b) indicates sulphate redistribution, and c) raises the suspicion that something happened to the montmorillonite (cation exchange or structural alteration).

**Table A7-2. Trace element composition (XRF).**

		mm 1	mm 10	mm 20	mm 40	mm 90
As	[mg/kg]	13	14	11	11	13
Ba	[mg/kg]	<b>177</b>	<b>215</b>	<b>328</b>	<b>331</b>	<b>271</b>
Bi	[mg/kg]	<3	<3	<3	<3	<3
Ce	[mg/kg]	104	112	111	116	116
Co	[mg/kg]	<3	<3	<3	<3	<3
Cr	[mg/kg]	11	60	27	72	10
Cs	[mg/kg]	<5	<5	<5	<5	<5
Cu	[mg/kg]	<b>5,764</b>	<b>4,075</b>	<b>240</b>	<b>50</b>	<b>&lt;10</b>
Ga	[mg/kg]	26	27	27	27	28
Hf	[mg/kg]	8	5	8	7	7
La	[mg/kg]	38	32	32	31	38
Mo	[mg/kg]	<b>27</b>	<b>6</b>	<b>&lt;2</b>	<b>3</b>	<b>3</b>
Nb	[mg/kg]	27	26	27	30	27
Nd	[mg/kg]	<50	<50	55	<50	<50
Ni	[mg/kg]	<b>&lt;3</b>	5	<3	<3	<3
Pb	[mg/kg]	27	32	44	46	42
Rb	[mg/kg]	10	12	9	10	10
Sb	[mg/kg]	<5	<5	<5	5	<5
Sc	[mg/kg]	5	5	5	5	6
Sm	[mg/kg]	<50	<50	<50	<50	<50
Sn	[mg/kg]	9	11	8	9	7
Sr	[mg/kg]	213	220	233	301	215
Ta	[mg/kg]	10	7	<5	7	<5
Th	[mg/kg]	45	41	43	41	43
U	[mg/kg]	18	15	20	17	20
V	[mg/kg]	9	<5	<5	7	10
W	[mg/kg]	<5	<5	<5	<5	<5
Y	[mg/kg]	37	39	39	37	38
Zn	[mg/kg]	93	59	125	109	101
Zr	[mg/kg]	179	184	175	181	181

***In situ*  $\mu$ -EDXRF**

The in situ  $\mu$ -EDXRF as applied provides continuous but only relative intensity information. Therefore, the curves were roughly fitted to the XRF Cu values. The quality of calibration does not allow for the accurate interpretation of  $\mu$ -EDXRF data. However, it could be clearly proved that Cu penetrated the clay until a depth of 2–2.5 cm. From Figure A7-6 it is evident that bulk XRF data were confirmed with respect to Cu penetration depths.

In addition the Fe concentration was measured by in situ  $\mu$ -EDXRF. No systematic Fe redistribution could be detected (Figure A7-7).

***XRD***

By XRD a trace of gypsum was found in the 4 cm sample (Figure A7-8) which confirms the trend observed by XRF (Figure A7-5). In addition a slightly more distinct and relatively sharp illite 001 reflection was found in sample 4 cm likely indicating material heterogeneity or texture effect. Small differences of the 001 reflection of the dried material can be attributed to varying (re-)hydration state. The differences in peak positions of the first and second order of the basal reflections observed after EG solvation are relatively small and hence do not allow to suppose structural changes. The intensity differences are quite large. However, this is assumed to stem from typical problems with sample preparation of these clays.

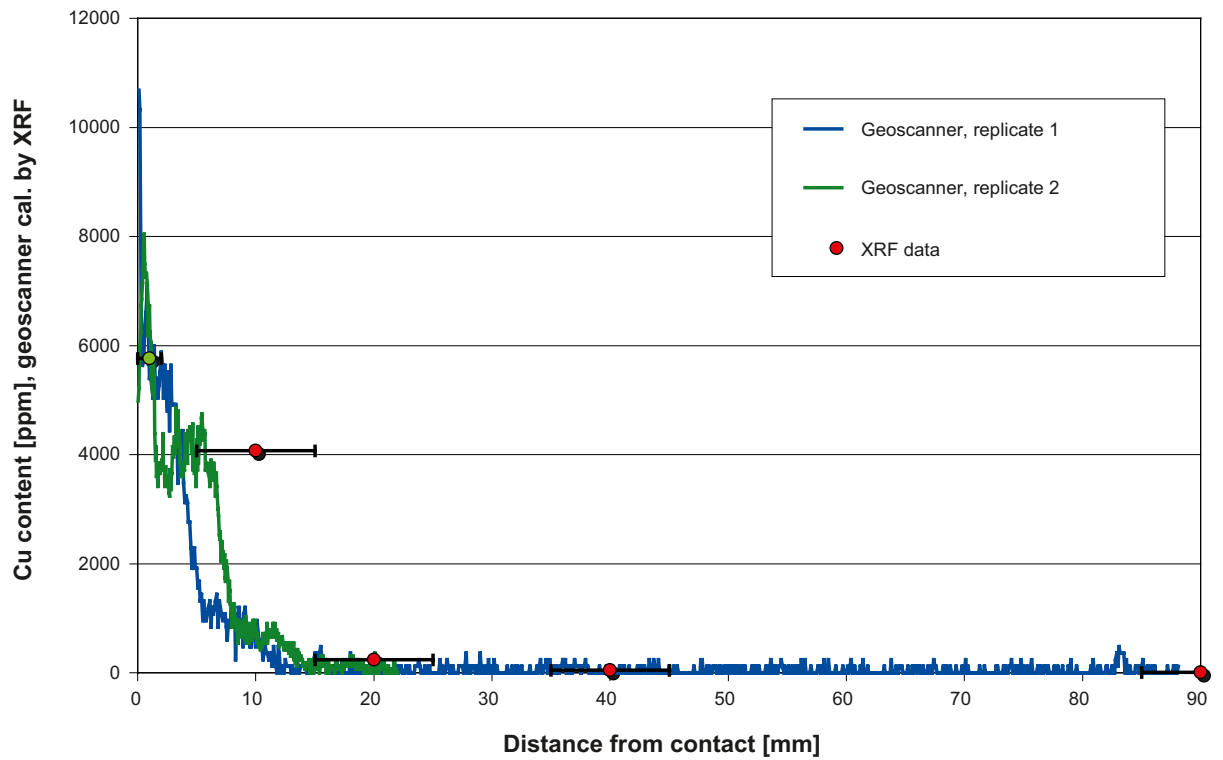


Figure A7-6. In situ  $\mu$ -EDXRF investigation of Cu-concentration of LOT bentonite block A2 (15).

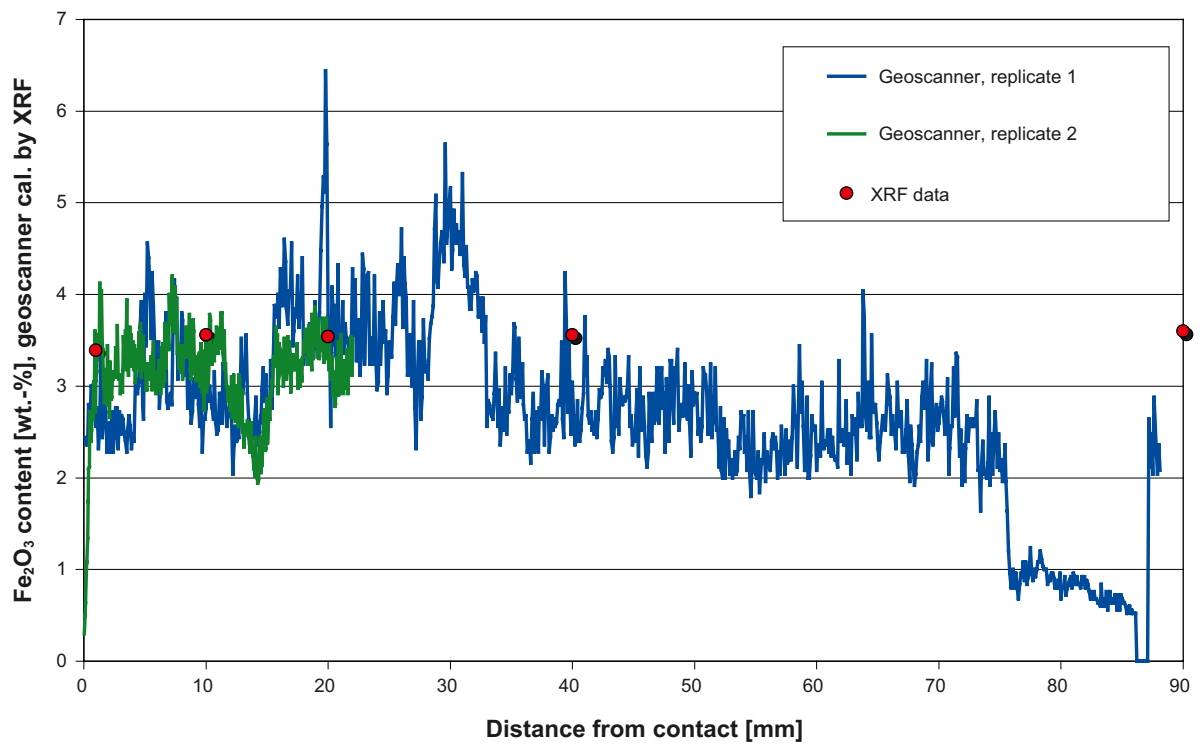
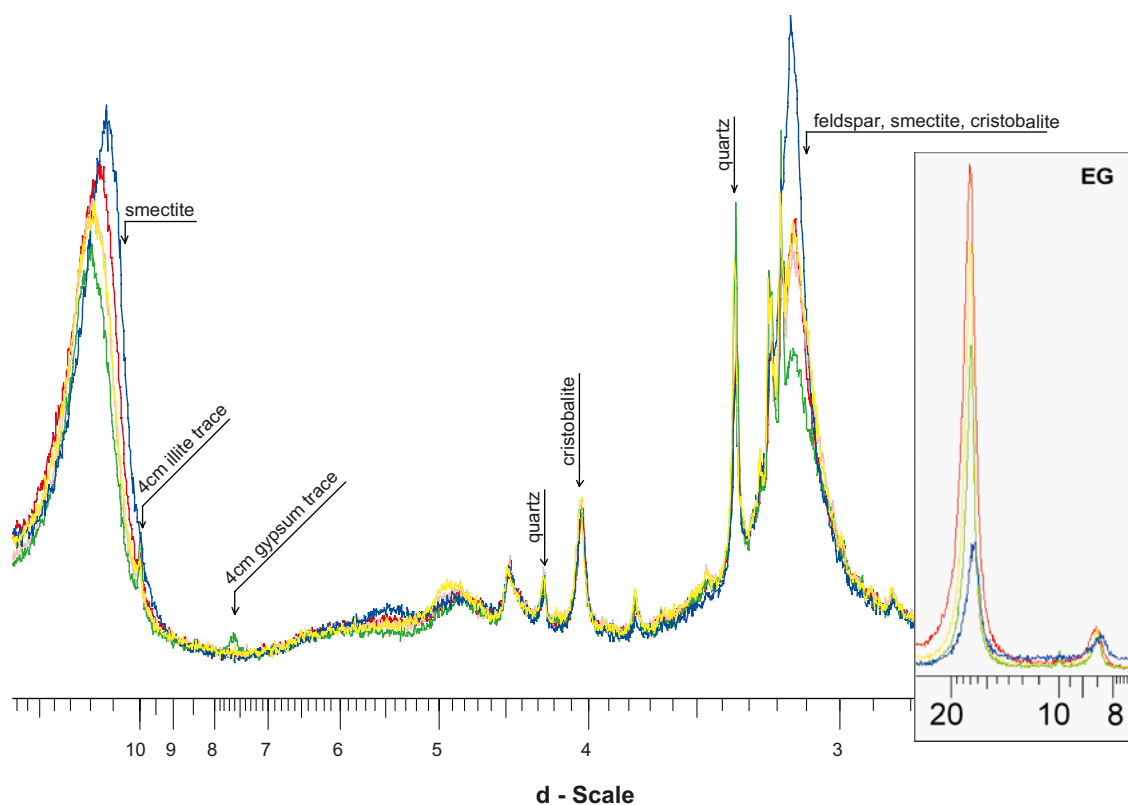


Figure A7-7. In situ  $\mu$ -EDXRF investigation of Fe-concentration of LOT bentonite block A2 (15).



**Figure A7-8.** XRD pattern of oriented mounts dried at 60°C and 001 and 002 reflection of EG saturated material (red = 1 mm, orange = 1 cm, yellow = 2 cm, green = 4 cm, blue = 9 cm).

### CEC

At the BGR clay laboratory commonly the Cu triene method is used for CEC determination. In this study the BaCl<sub>2</sub> method was selected since Cu was believed to play an important role and triethylenetetramine as strong complexing agent for Cu could facilitate dissolution of possible Cu corrosion products. With respect to the present study it is important to note that the BaCl<sub>2</sub> requires the repeated addition of different solutions which leads to the extensive dissolution of relatively soluble mineral phases as calcite or gypsum. The specific problems of this method are discussed in detail by /Dohrmann 2006/. However, in the present study the CEC method was mainly conducted in order to a) identify the fate of Cu released from the tube by corrosion (did it exchange for Na<sup>+</sup> ?) and b) identify possible montmorillonite alterations.

For answering these questions the BaCl<sub>2</sub> method was thought to be applicable (results are presented in Table A7-3).

**Table A7-3.** Exchangeable cations (including Cu), sum of cations and total Ba<sup>2+</sup> which was exchanged representing CEC (BaCl<sub>2</sub> method). Average values of different initial weights of samples (0.300 and 0.500 g).

Sample	K <sup>+</sup> [meq/100g]	Na <sup>+</sup> [meq/100g]	Ca <sup>2+</sup> [meq/100g]	Mg <sup>2+</sup> [meq/100g]	Cu <sup>2+</sup> [meq/100g]	Sum cations [meq/100g]	Ba <sup>2+</sup> [meq/100g]
1 mm	2.5	60.4	28.6	11.9	0.0	103.4	87.5
1 cm	1.7	63.2	28.5	11.7	0.1	105.2	86.5
2 cm	1.5	60.6	28.6	11.2	0.0	101.9	85.5
4 cm	1.2	59.0	32.3	11.0	0.0	103.5	80.5
9 cm	1.5	60.0	29.1	10.1	0.0	100.7	86.0

The sum of exchangeable cations, expectedly exceeds the CEC ( $\text{Ba}^{2+}$ ) by 15–20 meq/100 g. This difference can be explained by dissolution of gypsum in the exchange solutions applied. We used different initial weights (0.300 and 0.500 g) in order to find out, if the total fraction of gypsum was dissolved. In case of presence of gypsum or calcite higher  $\text{Ca}^{2+}$  values are obtained for the lower initial weight /Dohrmann 2006/. In the present study no such dependence was observed which clearly indicates the complete dissolution of gypsum throughout the CEC experiment.

In Figure A7-9 the maximum of the concentration of exchangeable  $\text{Ca}^{2+}$  should correspond to the increase in CaO (XRF data, Figure A7-5). The increase of appr. 3.5 meq/100 g as observed in ‘sample 4 cm’ corresponds to appr. 0.3 wt% gypsum or 0.1 wt% CaO. In contrast, by XRF (Table A7-1) an increase of 0.5 wt% CaO was found. This indicates the presence of an additional Ca-phase being less soluble than gypsum.

In addition, by XRF an increased MgO content was found near to the Cu tube. This result, qualitatively, could be confirmed by the exchangeable Mg analysis (Figure A7-9) which increased by appr. 1 meq/100 g. However, by XRF a difference of appr. 0.4 wt% was observed which, theoretically, would correspond to 5 meq/100 g. Therefore, the slight increase of exchangeable Mg is not sufficient to explain the total increase of MgO near to the Cu tube. It can be concluded that the additional Mg either occurs in newly precipitated hardly soluble phases or in the montmorillonites’ structure.

Generally, it is questionable whether such small XRF and CEC differences should be considered quantitatively. However, the results presented above should be kept in mind when investigating the LOT A3 parcel.

In Table A7-3 a slightly higher content of exchangeable  $\text{K}^+$  was found in the 1 mm sample. It is at least conceivable that  $\text{K}^+$  was adsorbed from the water at the Cu-bentonite interface.

CEC methods are sensitive towards changes of charges commonly caused by structural alterations. As can be seen in Figure A7-9 only the ‘4 cm sample’ has a slightly lower CEC than the others. This cannot be explained only by the slightly lower montmorillonite content (due to higher gypsum/montmorillonite ratio; see chapter XRF). In addition, the CEC is known to be influenced by the pH

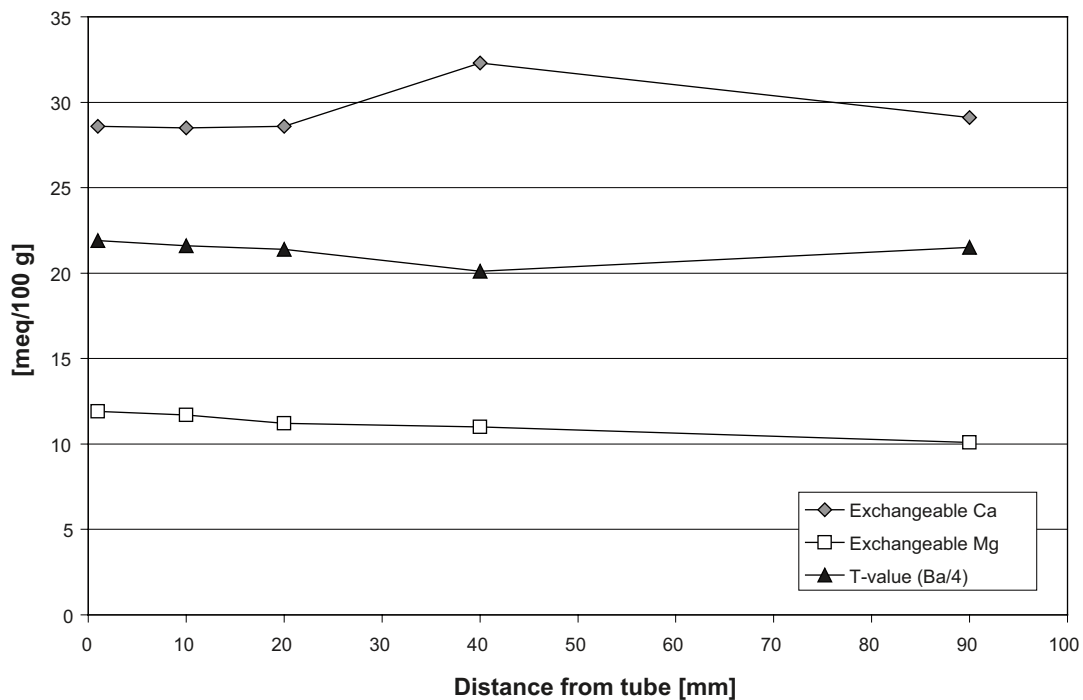


**Figure A7-9.** Distribution of exchangeable  $\text{Ca}^{2+}$ ,  $\text{Mg}^{2+}$ , and  $\text{Ba}^{2+}$  (divided by 4), the latter representing the CEC.

value of the suspensions during cation exchange. However the slightly lower pH value of the '4 cm sample' (pH 9.7) compared to the others (pH 9.9) is not supposed to influence the CEC by more than 1 meq/100 g. Accordingly, the lower CEC value of the '4 cm sample' can not be explained unambiguously.

Despite the different CEC value of the 4 cm sample no montmorillonite alteration processes nearby the Cu tube can be deduced from the CEC values of the '1 mm' and '1 cm' sample.

### DTA

Differential thermal analysis represents a suitable complementary analytical tool for the identification of specific minerals, especially if the gases evolved are characterized either by infrared spectroscopy or mass spectrometry. The differential scanning calorimetry curves of the BGR LOT samples is given in Figure A7-10. The corresponding mass spectrometer curves (mass 64) are given in Figure A7-11. All samples show the typical dehydration, dehydroxylation, and recrystallization reactions of smectites and the other minerals of MX 80 bentonite. In addition all curves show distinct peaks at ca. 900°C. These peaks can be assigned to the SO<sub>2</sub> release from gypsum and hence are clearly visible in the MS 64 curve (Figure A7-11).

The samples '1 mm' and '1 cm' in contrast to the others, exhibit one distinct peak at appr. 360°C. This peak was clearly observed in the MS curve indicating the presence of a S phase. According to /Maurel 1964/ this peak could represent the presence of covelline (CuS) or a related phase. This indicates that the corrosion product is a sulphide. The '1 cm sample', in contrast to the '1 mm sample', shows an additional peak at appr. 400°C indicating the presence of an additional phase in 1 cm depths. From the oxidation zones in Cu porphyry ore deposits it is known that a number of different CuS<sub>x</sub> phases exist varying in the Cu:S ratio depending on the geochemical milieu. The existence of different CuS<sub>(x)</sub> phases depending on the distance from the heater, therefore, is possible.

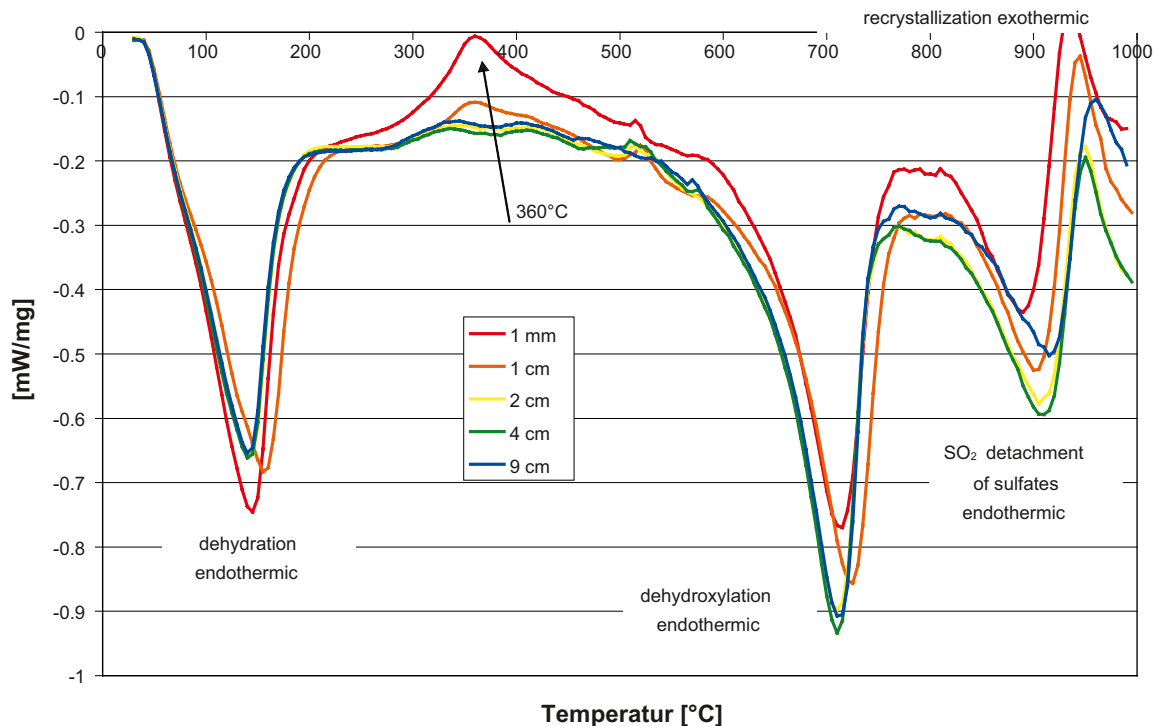
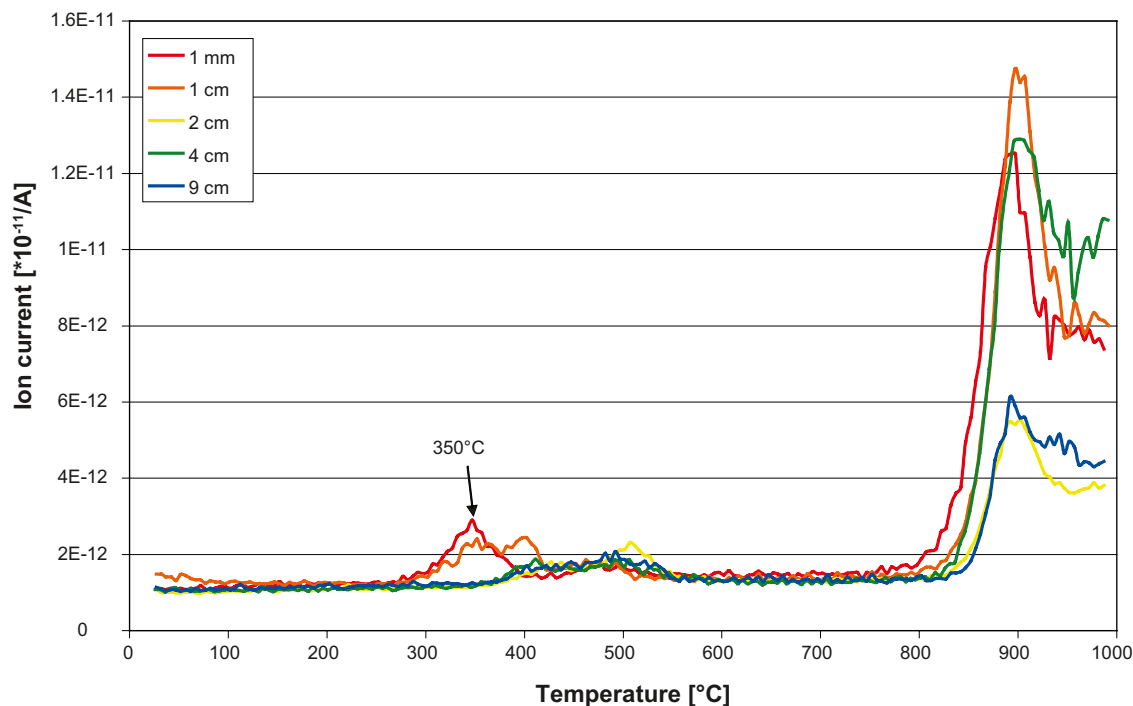


Figure A7-10. Differential scanning calorimetry (DSC) curves of all samples.



**Figure A7-11.** Mass spectrometer curves (mass 64) of all samples.

## **IR**

By infrared spectroscopy information about both the composition of smectites and the presence of some minor constituents can be gained. The most interesting MIR spectral range is shown in Figure A7-12. In the '9 cm sample' traces of carbonate were found either representing material heterogeneity or carbonate from the outside water.

From XRF and CEC data the presence of gypsum was concluded. In the MIR spectra the main gypsum ( $\text{SO}_4$ ) vibration at ca.  $1,145 \text{ cm}^{-1}$  could not be observed. However, very small bands at  $680$  and  $600 \text{ cm}^{-1}$ , which were particularly observed in the '4 cm sample', likely indicate the higher gypsum content in the '4 cm sample' compared to the others. Additionally, the presence of cristobalite and quartz as already found by XRD was confirmed. Considering the structural OH groups of the smectite (montmorillonite) no alterations could be detected. It is worth mentioning that changes in the %-range of the discussed minerals can not be identified by this method.

NIR spectra were collected to complement to CEC results. This is possible because the NIR band at  $5,025 \text{ cm}^{-1}$  (+  $5,100 \text{ sh cm}^{-1}$ ) is sensitive to the type of cation (mono or divalent). As can be seen in Figure A7-13 no significant differences of the NIR spectra and particularly of the  $5,025 \text{ cm}^{-1}$  band could be observed.

## **BET**

Alteration processes including dissolution and precipitation may influence the specific surface area (SSA) which in case of bentonites mainly results from microporosity. It is at least conceivable that dissolution of specific mineral constituents leads to deblocking of pores and hence to an increase of SSA. Mineral precipitation, in turn, may lead to a decrease of SSA.

This theoretical process would explain the observed SSA distribution (Figure A7-14) showing a SSA minimum between 2–4 cm. In this distance a higher gypsum concentration was found possibly indicating precipitation of gypsum.

Based on the model explained above it is at least conceivable that the SSA values reflect gypsum redistribution.

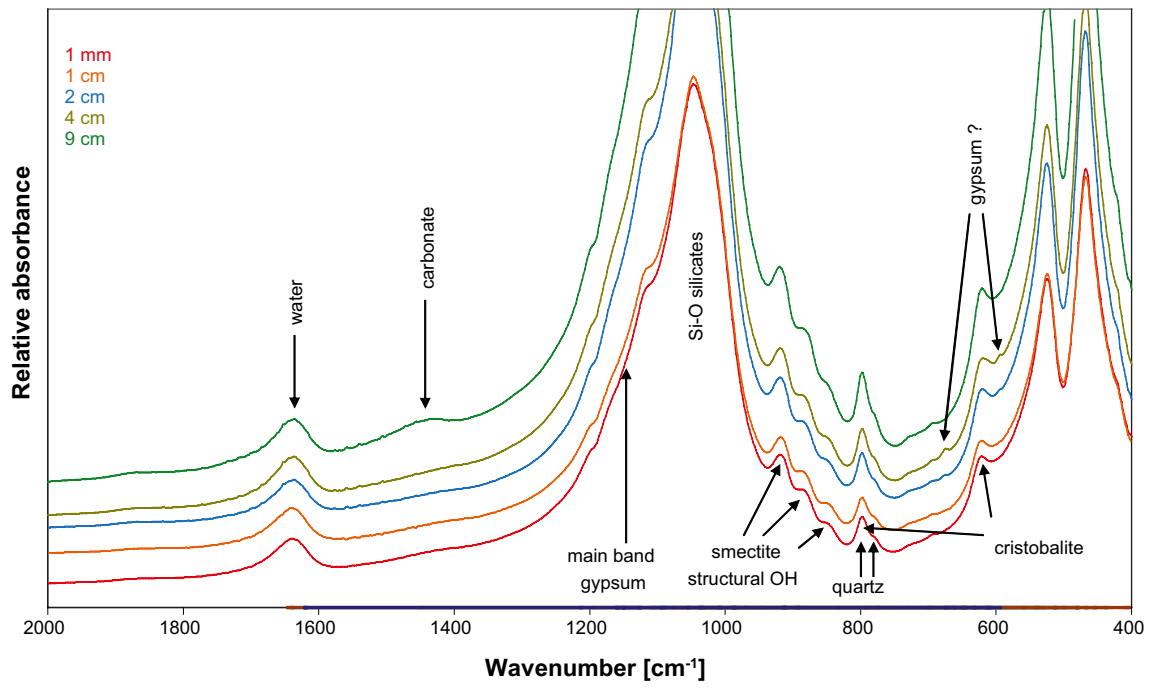


Figure A7-12. MIR spectra (400–2,000 cm<sup>-1</sup>) of all samples.

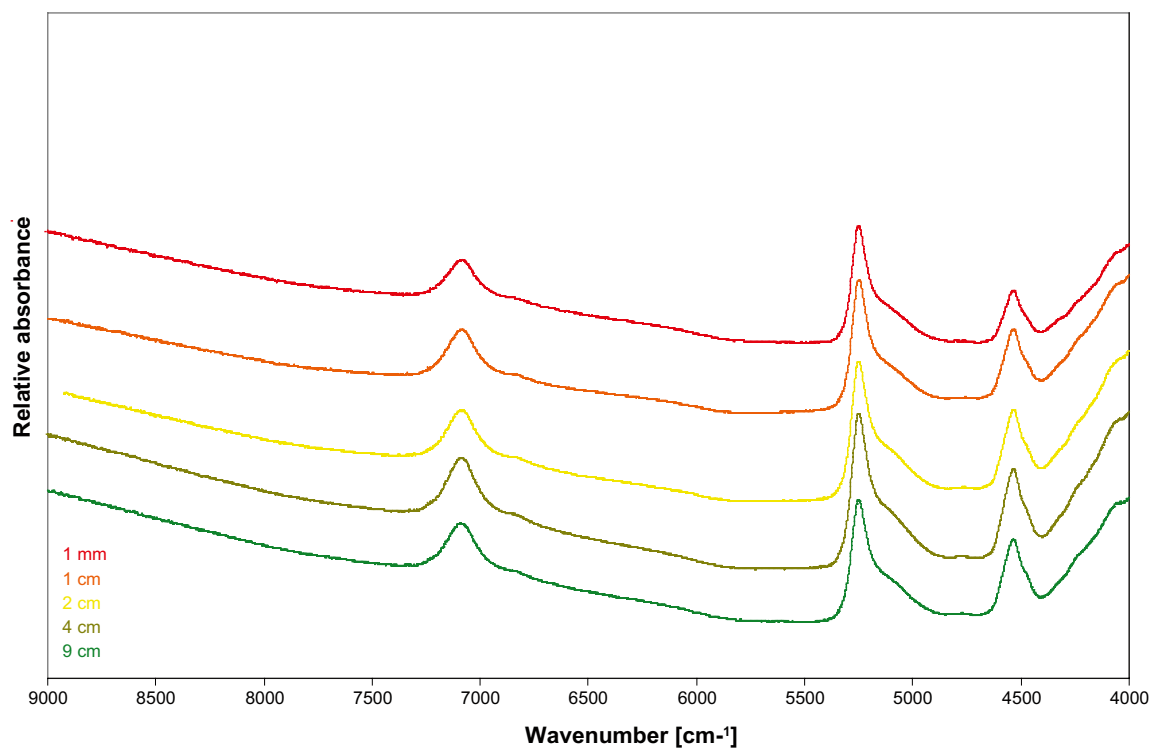
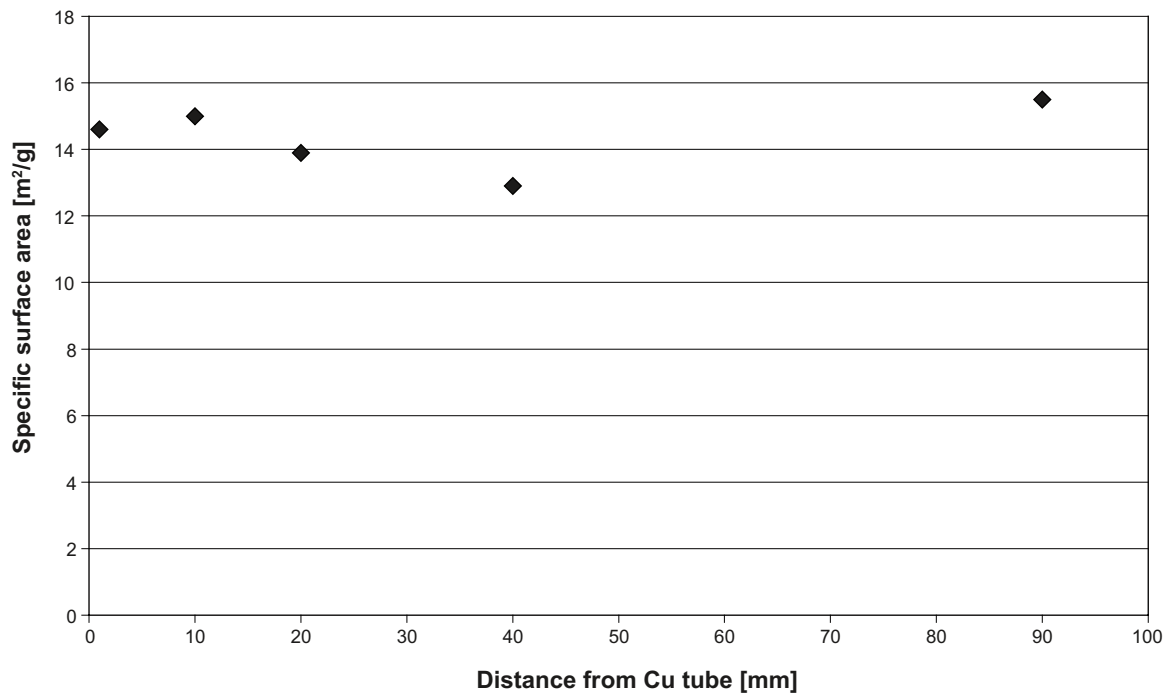


Figure A7-13. NIR spectra of all samples.



*Figure A7-14. specific surface area (from N<sub>2</sub> adsorption according to BET method).*

#### **Light and electron microscopy**

The surface of the bentonite block which has been in direct contact to the Cu tube was investigated by light microscopy. Clearly a bluish phase distinctly showing metallic glance could be observed (Figure A7-15). This grain was investigated by SEM (Figure A7-16).



*Figure A7-15. Light microscopy image of the bentonite-Cu tube contact surface (image width appr. 4 cm).*

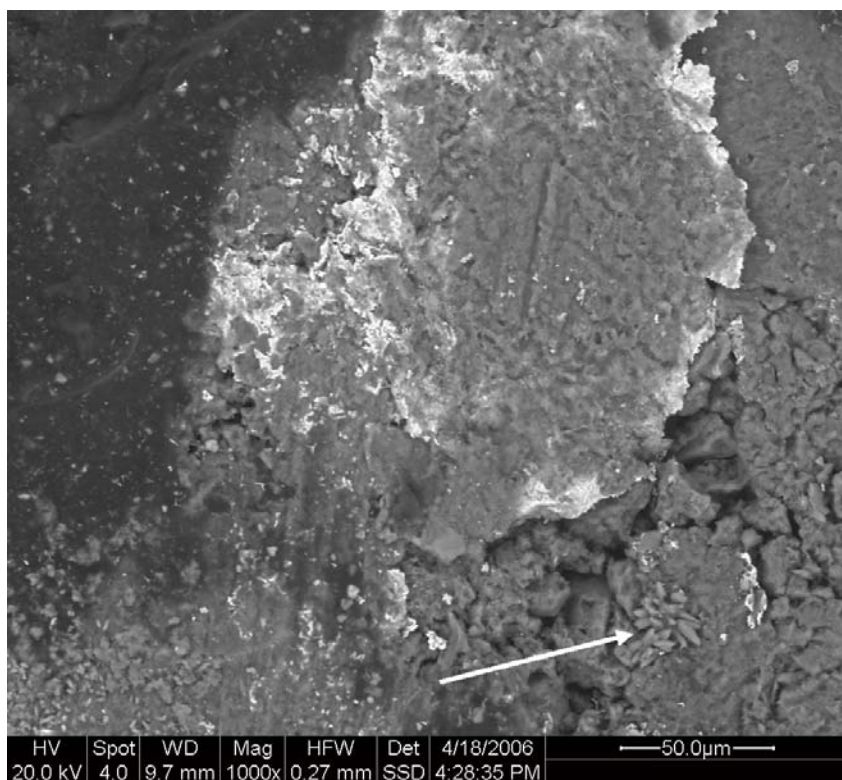


**Figure A7-16.** Electron microscopy image of the bluish metallic phase primarily identified in the light microscope.

By EDX the dominance of Cu and S of this grain was measured indicating that it is either a Cu sulphide or sulphate. The brightness of this grain is striking and results from high electrical conductivity being typical for metals and metal sulphides or oxides. This, together with the metallic glance observed by light microscopy, strongly indicates the presence of Cu sulphides rather than sulphates. Furthermore, small idiomorphic calcite crystals could be identified in the vicinity of the Cu sulphide grain (white arrow in Figure A7-16). In Figure A7-17 an example for the systematic EDX investigation of the bentonite sample is presented. In this figure small Cu sulphide particles as well as freshly appearing calcite grains could be identified by the qualitative elemental composition. However, the EDX spectra are affected by the underlying smectites which is caused by the small grain size of the calcite and the Cu sulphides ('matrix effect'). Hence, the structural elements, mainly Si and Al, can be observed in all spectra.

### **Water uptake capacity**

The water uptake capacity strongly depends on type and amount of exchangeable cation. Any collapse of the montmorillonite interlayer would result in a reduced water uptake capacity. Additionally, the pore system is believed to influence the water uptake capacity particularly at high relative humidity. Measuring the water uptake capacity, therefore, is a sensitive method for the determination of bentonite or clay alteration processes. The water uptake capacity of the LOT bentonite samples is shown in Figure A7-18.

Surprisingly, the samples which were close to the heater show a slightly higher water uptake capacity. This might be due to small differences of the cation occupation or changes of porosity. However, it is important to note, that the swelling ability, here determined by measuring the water uptake capacity, obviously was not affected by the extensive heating.

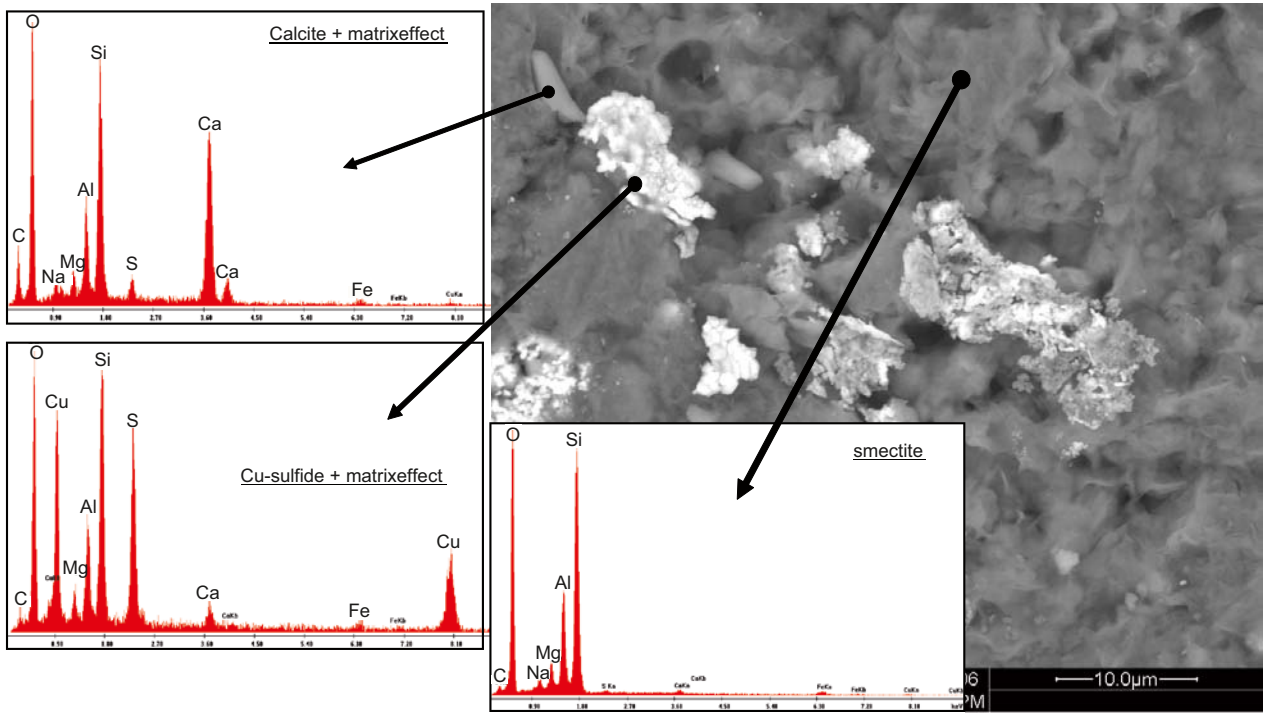


Figure A7-17. EDX investigation of the bentonite sample which was close to the Cu tube.

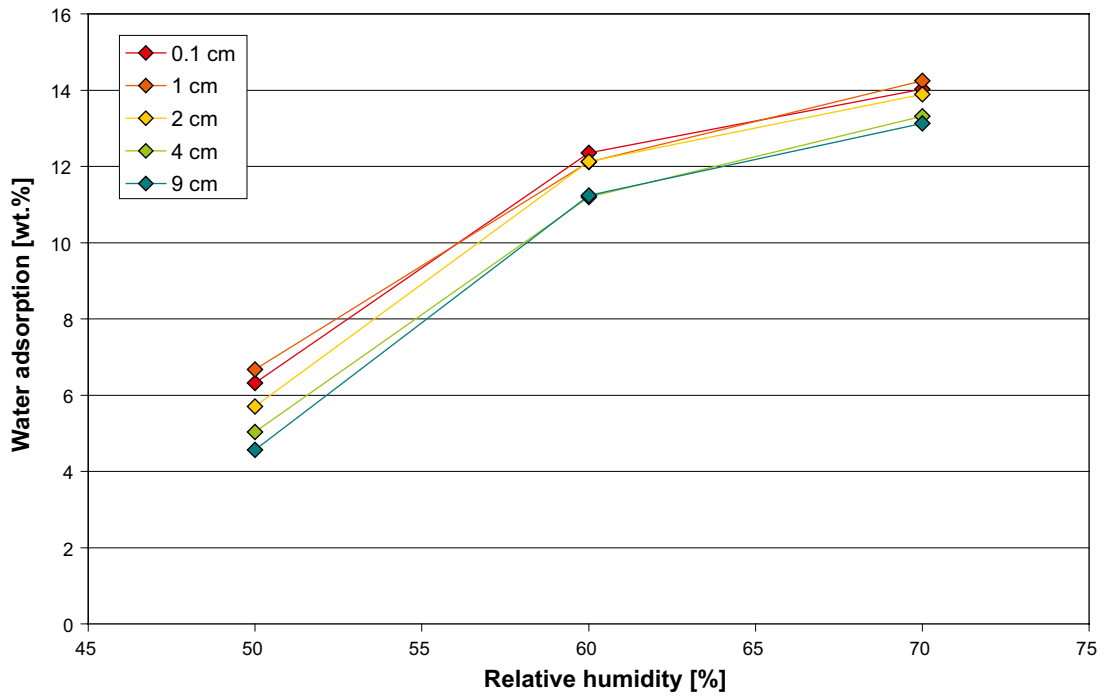


Figure A7-18. Water uptake capacity at 50, 60, and 70% RH.

### Layer charge density (LCD)

For measuring the layer charge density with the whole set of alkylammonium chains the mass of material gained by sampling the A2 15 block was insufficient. Therefore, an additional block (A2 14N) was sampled and investigated by the alkylammonium method based on /Lagaly 1994/ and /Olis et al. 1990/. In the present study three different chain lengths of the alkylammonium ions were used ( $n_c = 11, 12, 13$ ).

Macroscopically, this second block revealed a higher gypsum concentration at the surface which has been in contact with the copper tube.

**Table A7-4. Comparison of the chemical composition of the second block (used for alkylammonium method) with the first block mainly considered in this study.**

		1 mm	1 mm	1 cm	1 cm	2 cm	2 cm	3 cm	3 cm	4 cm	4 cm	9 cm	9 cm	
		1 <sup>st</sup> block	2 <sup>nd</sup> block											
SiO <sub>2</sub>	[wt-%]	68.3	67.7	68.3	68.4	68.3	68.3		68.0	67.7	67.5	68.4	68.4	
TiO <sub>2</sub>	[wt-%]	0.2	0.2	0.2	0.2	0.2	0.2		0.2	0.2	0.2	0.2	0.2	
Al <sub>2</sub> O <sub>3</sub>	[wt-%]	20.7	20.6	20.8	20.7	20.7	20.7		20.5	20.5	20.4	20.7	20.7	
Fe <sub>2</sub> O <sub>3</sub>	[wt-%]	3.9	3.9	4.0	4.0	4.0	4.0		4.0	4.0	3.9	4.0	4.0	
MnO	[wt-%]	0.0	0.0	0.0	0.0	0.0	0.0	no sample taken	0.0	0.0	0.0	0.0	0.0	
MgO	[wt-%]	3.0	2.9	2.7	2.6	2.7	2.6		2.6	2.5	2.4	2.4	2.4	2.4
CaO	[wt-%]	1.2	1.5	1.2	1.2	1.3	1.2		1.5	1.8	1.9	1.3	1.3	1.3
Na <sub>2</sub> O	[wt-%]	2.0	2.1	2.0	2.1	2.0	2.2		2.2	2.1	2.2	2.1	2.2	2.2
K <sub>2</sub> O	[wt-%]	0.5	0.5	0.5	0.6	0.5	0.6		0.6	0.5	0.6	0.5	0.6	0.6
P <sub>2</sub> O <sub>5</sub>	[wt-%]	0.1	0.1	0.1	0.0	0.0	0.0		0.0	0.0	0.0	0.1	0.1	0.1
(SO <sub>3</sub> )	[wt-%]	0.2	0.5	0.2	0.2	0.3	0.2		0.3	0.7	0.7	0.3	0.3	0.2
(Cl)	[wt-%]	0.0	0.0	0.0	0.0	0.0	0.0		0.0	0.0	0.0	0.0	0.0	0.0
(F)	[wt-%]	<0.05	<0.05	<0.05	<0.05	<0.05	<0.05		0.00	<0.05	<0.05	0.06	0.06	0.06
Sum	[wt-%]	100.0	100.0	100.0	100.0	100.0	100.0		100.0	100.0	100.0	100.0	100.0	100.0
LOI	[wt-%]	11.1	8.3	10.4	7.6	10.1	7.6		7.6	10.1	7.8	9.2	7.3	
(As)_SI	[ppm]	13	12	14	9	11	12		9	11	9	13	12	
Ba_SI	[ppm]	177	188	215	300	328	311		332	331	358	271	323	
Bi_SI	[ppm]	<3	4	<3	4	<3	<3		4	<3	<3	<3	4	
Ce_SI	[ppm]	104	111	112	109	111	112		114	116	122	116	99	
Co_SI	[ppm]	<3	<3	<3	<3	<3	<3		<3	<3	<3	<3	<3	
Cr_SI	[ppm]	11	18	60	23	27	27		30	72	17	10	14	
Cs_SI	[ppm]	<5	<5	<5	<5	<5	<5		<5	<5	<5	<5	<5	
Cu_SI	[ppm]	5,764	5,853	<b>4,075</b>	<b>1,053</b>	240	62		12	50	<10	<10	54	
Ga_SI	[ppm]	26	27	27	28	27	30		29	27	29	28	28	
Hf_SI	[ppm]	8	13	5	6	8	<5		5	7	8	7	<5	
La_SI	[ppm]	38	52	32	51	32	52		48	31	49	38	55	
Mo_SI	[ppm]	27	27	6	4	<2	9		4	3	5	3	5	
Nb_SI	[ppm]	27	28	26	30	27	27		29	30	28	27	28	
Nd_SI	[ppm]	<50	<50	<50	51	55	57		55	<50	56	<50	66	
Ni_SI	[ppm]	<3	<b>1572</b>	5	409	<3	149		53	<3	24	<3	9	
Pb_SI	[ppm]	27	24	32	38	44	48		49	46	45	42	44	
Rb_SI	[ppm]	10	16	12	16	9	14		15	10	16	10	15	
Sb_SI	[ppm]	<5	5	<5	<5	<5	<5		<5	5	<5	<5	<5	
Sc_SI	[ppm]	5	5	5	5	5	6		6	5	5	6	6	
Sm_SI	[ppm]	<50	<50	<50	<50	<50	<50		<50	<50	<50	<50	<50	
Sn_SI	[ppm]	9	9	11	7	8	7		6	9	6	7	7	
Sr_SI	[ppm]	213	202	220	221	233	230		279	301	353	215	224	
Ta_SI	[ppm]	10	8	7	<5	<5	6		<5	7	<5	<5	<5	
Th_SI	[ppm]	45	40	41	39	43	41		40	41	40	43	40	
U_SI	[ppm]	18	12	15	11	20	8		13	17	14	20	14	
V_SI	[ppm]	9	<5	<5	7	<5	<5		<5	7	6	10	<5	
W_SI	[ppm]	<5	<5	<5	<5	<5	<5		<5	<5	<5	<5	<5	
Y_SI	[ppm]	37	43	39	42	39	43		42	37	40	38	41	
Zn_SI	[ppm]	93	80	59	92	125	135		108	109	108	101	102	
Zr_SI	[ppm]	179	188	184	194	175	190		191	181	184	181	195	

The comparability of both blocks was investigated by XRF:

- 1) The higher gypsum content at the bentonite tube contact surface is displayed by the CaO content (slightly higher in the 2<sup>nd</sup> block, sample 1 mm).
- 2) Slight deviations of the Cu content in samples 1 cm and 2 cm were found, which are likely due to small deviations of sampling distances.
- 3) Surprisingly, an elevated Ni content has been found in the second block. Here, a systematic difference between the first and the second block is evident. The Ni is supposed to stem from the cupro nickel shielding which surrounded the thermocouples (pers. comm. Karnland, 2007).

Overall, XRF strongly indicates the comparability of both blocks by considering the main element distribution, and in particular the distribution of 'structural elements' of smectites (such as Mg).

It is essential to note, that the LCD calculation from the  $d_{001}$  spacing is possible between the n-alkylammoniummono- and bilayer. The minimum d-spacing required is 13.7 Å. The MX 80 bentonite from the LOT test obviously contains low charged smectites. This is reflected by the low d-spacings of  $n_c = 11$  and 12. Only for  $n_c = 13$  a calculation of the LCD is reasonable. The differences are very small and vary between 13.8 and 13.8 Å.

Based only on the results presented in Table A7-5 it is impossible to determine an accurate mean value for the layer charge density. However, the following can be deduced:

- a) the LOT MX80 bentonite contains montmorillonites with a particularly low LCD. Three different MX80 samples which were investigated at BGR show higher LCD values.
- b) Despite the analytical problems caused by the low LCD it is impossible to unambiguously prove structural montmorillonite alteration because chain length 12 of the '1 mm sample' indicates a slight LCD increase whereas chain length 13 does not.

The accuracy of the alkylammoniummethod is approximately  $\pm 0.01$  eq/FU. Therefore it has to be concluded that *within this range* no systematic dependency of LCD on the distances between the bentonite and the Cu tube could be identified.

### **Magnetic fractionation**

Magnetic fractionation was applied in order to obtain a sample with increased content of the Cu sulphide phase. The intention was to raise the concentration of this phase above the XRD detection limit in to get structural information about this phase. Accordingly, ca. 20 g of the first 2 cm of the second A2 block (A2 14N) were carefully broken and sieved. These different grain size fractions were subjected to a magnetic separator ('Franz Scheider') and analyzed by XRD, DTA, and IR. Surprisingly, in the magnetic 63–80 µm fraction a high content of a hydrotalcite-group mineral could be identified by XRD (Figure A7-19). However, it remains unclear why this phase was enriched in the magnetic fraction.

**Table A7-5.  $D_{001}$  spacing of three different n-alkylammonium-montmorillonites of the 6 samples and three reference MX80 samples. Calculation of LCD is only reasonable >13.6 Å.**

Sample	n = 11 d-value [Å]	LCD [eq/FU]	n = 12 d-value [Å]	LCD [eq/FU]	LCD /Olis et al. 1990/ [eq/FU]	n = 13 d-value [Å]	LCD [eq/FU]
1 mm	13.5		14.1	0.28	0.26	13.8	0.23
1 cm	13.4		13.7	0.27	0.25	13.8	0.23
2 cm	13.4		13.6			13.7	0.23
3 cm	13.5		13.6			13.7	0.23
4 cm	13.6		13.9	0.27	0.25	13.8	0.23
9 cm	13.5		13.6			13.7	0.22
MX80 IB20 SKB	13.7	0.31	14.3	0.28	0.27	14.7	0.26
MX80 IB33 SC	13.8	0.31	14.3	0.28	0.27	14.7	0.26
MX80 GRS	13.4		13.5			14.6	0.25

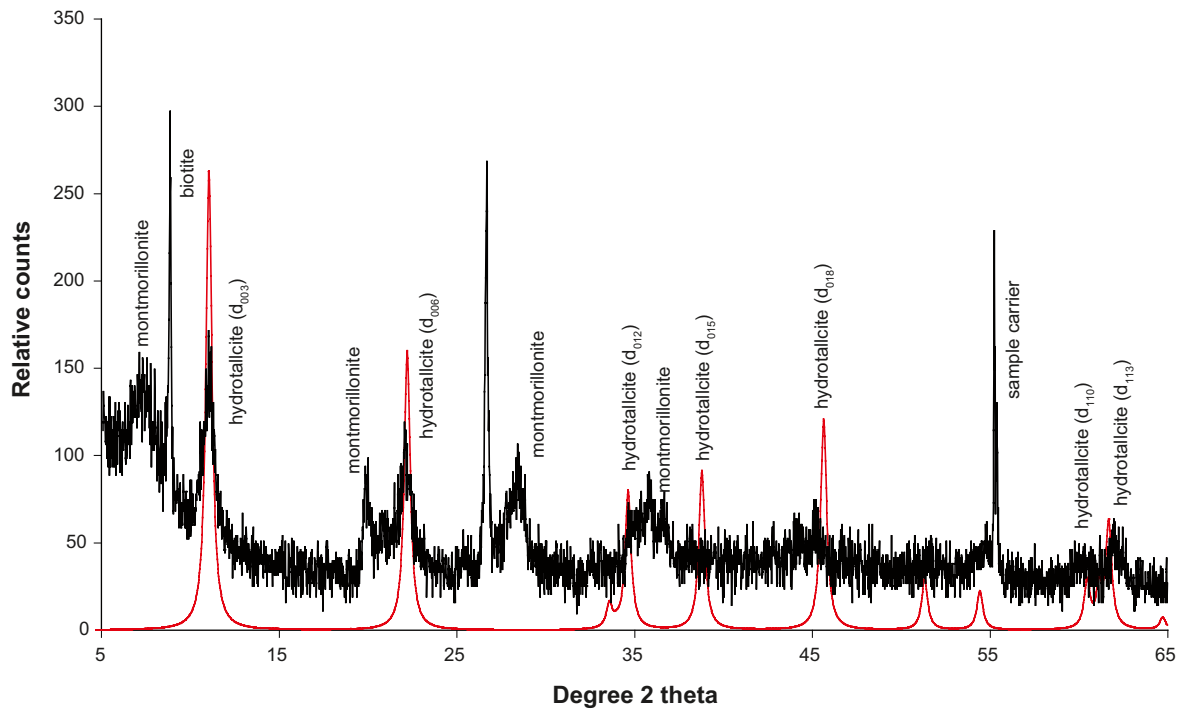


**Figure A7-19.** XRD pattern of the magnetic 63–80 μm fraction compared to a hydrotalcite XRD pattern calculated according to /Ennadi 2000/.

## Summary and discussion

Chemical and mineralogical investigations of the LOT bentonite presented in this and other studies indicate that:

- a) gypsum redistributed by dissolution and precipitation,
- b) Cu was liberated from the tube and migrated into the bentonite, and
- c) no unambiguous evidence for structural alteration of the montmorillonite could be found.

All results being relevant with respect to the three main findings are summarized in Table A7-6.

a) A variety of methods proved a gypsum peak at 4 cm. Since the gypsum distribution was homogenous at the beginning of the experiment it has to be concluded, that gypsum redistributed during the test period, most probably by dissolution and precipitation. From the first LOT sample which was considered in this study (except for LCD and magnetic fractionation) no sample was collected at 3 cm depth. Therefore, it was thought that the gypsum peak concentration at 4 cm likely represents the right shoulder of the peak at 3 cm of this study. The second LOT sample (considered for LCD and magnetic fractionation) revealed the gypsum peak at 4 cm (Table A7-4). However, the actual position of the gypsum peak concentration is less important for the understanding of corrosion and alteration processes. It is most important that its existence was proved unambiguously (even by different working groups). Both the  $\text{Al}_2\text{O}_3$  and the  $\text{SiO}_2$  content as determined by XRF show a minimum at 4 cm which was interpreted as relative decrease caused by gypsum precipitation. However, it can not yet be explained why the other elemental concentrations do not reveal this minimum and if other Ca- and/or Mg- phases precipitated. We conclude that the actual mechanism for the redistribution of gypsum is not clear, yet.

b) Cu corrosion led to the release of Cu from the tube which migrated into the bentonite block. XRF analysis, having the lowest Cu detection limit of the methods applied, proved an increased Cu concentration even in the '4 cm sample'. Surprisingly, Cu was not found in the interlayer of the montmorillonites. Instead, Cu sulphides could be found. Gypsum, a natural minor constituent of the bentonite (appr. 1.3 wt%), is believed to be the S source, since it is the only S bearing mineral within

**Table A7-6. Summary of analytical results being relevant with respect to the three main findings.**

Method/value	Figure/Table	Brief description of finding	Gypsum redistrib.	Cu corrosion	Structural alteration
1 XRF $\text{Al}_2\text{O}_3$ , $\text{SiO}_2$	Fig. 3	Minimum at 4 cm	??		
2 XRF $\text{Fe}_2\text{O}_3$	Fig. 4	No minimum	??		
3 XRF MgO	Fig. 4	Increase towards Cu tube			??
4 XRF CaO / $\text{SO}_3$	Fig. 5	Maximum at 4 cm	+		
5 XRF Cu	Tab. 2	Increased Cu content until min. 4 cm		+	
6 XRF Mo	Tab. 2	Increased Mo content until 1 cm		+	
7 $\mu$ -EDXRF	Fig. 6	Increased Cu content until 2 cm		+	
8 XRD	Fig. 8	Gypsum peak only in 4 cm	+		no
9 CEC $\text{Ca}^{2+}$	Fig. 9	Maximum at 4 cm	+		
10 CEC $\text{K}^+$	Tab. 3	Slight increase towards Cu tube			??
11 CEC $\text{Mg}^{2+}$	Fig. 9	Increase towards Cu tube			??
12 DTA MS 64	Fig. 11	Cu sulphide indicated		+	
13 MIR	Fig. 12	Gypsum band only in 4 cm	+		no
14 Light Microsc.	Fig. 15	Bluish grains with metallic glance		+	
15 SEM EDX	Fig. 16, 17	Cu and S bearing grains		+	
16 $\text{H}_2\text{O}$ uptake cap.	Fig. 18	$\text{H}_2\text{O}$ uptake cap. not affected by heating			no
17 LCD AAM	Tab. 5	No systematic differences within range of precision			no
18 Magnetic separation	Fig. 19–21	Hydrotalcite-group phase was found			??

the bentonite. It has to be concluded that sulphate, either from gypsum or from surrounding water, was reduced upon corrosion. A by-product of this reaction is  $\text{Ca}^{2+}$  which conceivably precipitates as carbonate together with  $\text{HCO}_3^-$  likely present in the surrounding water. This proposed corrosion mechanism is presented in Figure A7-20.

c) XRF and CEC revealed a Mg increase nearby the Cu tube. The MgO increase as determined by XRF exceeds the MgO content as calculated from the increased CEC  $\text{Mg}^{2+}$  value appr. 5 times. This indicates, that the Mg peak cannot be explained by an increase in exchangeable  $\text{Mg}^{2+}$ , only. Accordingly, Mg either precipitated from pore water as hardly soluble phase (a higher solubility would have led to complete dissolution during the CEC experiment – XRF and CEC values would correspond to each other) or at least partly entered the montmorillonite structure. The latter possibility would have led to an increase of LCD which could not be detected neither by CEC nor AAM. Therefore, the Mg increase likely reflects the precipitation of Mg phases. It is at least conceivable that this phase is the hydrotalcite which was found by magnetic separation. The slight increase of exchangeable  $\text{Mg}^{2+}$ , in turn, indicates that this phase is partly soluble (keeping in mind the high liquid/solid ratio applied during the  $\text{BaCl}_2$  method). Yet, it could not be proved that the hydrotalcite was formed by alteration of the montmorillonite (e.g. beginning incongruent dissolution of edge octahedral sheets). Hence it cannot be concluded that it indicates structural alteration of the montmorillonite. Additionally, the slight increase of exchangeable  $\text{K}^+$  nearby the Cu tube is particularly interesting, because  $\text{K}^+$  adsorption is believed to initiate illitization. Yet, no illitization (structural alteration of montmorillonite) could be detected.

It is worth mentioning that /Plötze et al. 2007/ reported a slight Mg increase in the bentonite nearby the heater of the Mont Terri heater project. Hence, it is at least conceivable that montmorillonites (in general) tend to release a small amount of Mg from octahedral sheet. From the results presented in the present study it is concluded that the Mg release of the LOT bentonite occurred to such a small extent that structural changes (e.g. change of layer charge density) could not be detected by IR, XRD, CEC and Alkylammoniummethod.

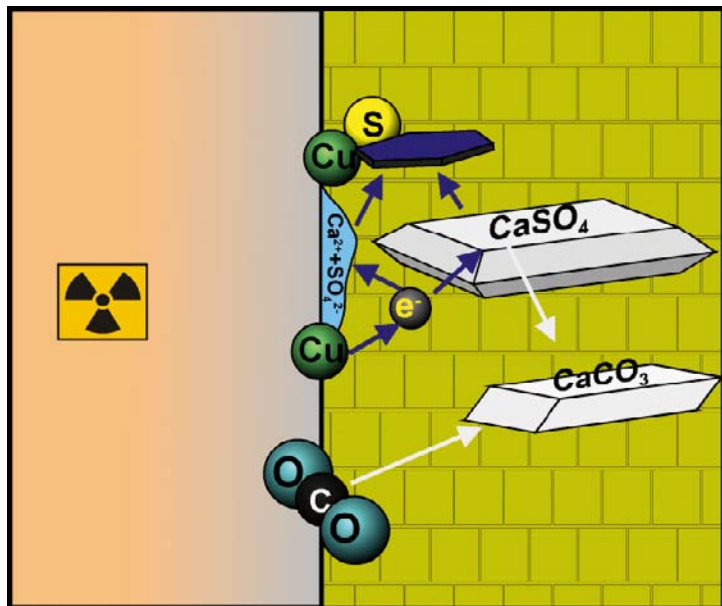


**Figure A7-20.** Sketch of model for corrosion mechanism (explanations are given in the text).

## Conclusions

In order to minimize mineral redistribution processes, which possibly lead to the formation of diffusion pathways, bentonites not containing relatively soluble minerals as calcite and gypsum should be used as geotechnical barrier material. Furthermore, the application of a bentonite not containing gypsum would lead to a reduction of the corrosion rate since the corrosion mechanism as observed is impossible without a S source.

The A3 parcel will be excavated after even longer time than the A2 parcel investigated in the present study. When the A3 parcel is analyzed, particular attention should be paid to K<sup>+</sup> fixation nearby the Cu tube as well as the formation of alteration products such as hydrotalcite.

## References

- Dohrmann R, 2006.** Cation Exchange Capacity Methodology I: An Efficient Model for the Detection of Incorrect Cation Exchange Capacity and Exchangeable Cation Results. *Appl. Clay Science*, 34, 31–37.
- Ennadi A, Legrouri A, De Roy A, Besse J P, 2000.** Shape and size determination for zinc-aluminum-chloride layered double hydroxide crystallites by analysis of X-ray diffraction line broadening. *J. Mater. Chem.*, 10, p 2337–2341.
- Karnland O, Sandén T, Johannesson L-E, Eriksen T, Jansson M, Wold S, Pedersen K, Motamedi M, Rosborg B, 2000.** Long term test of buffer material. Final Report on the pilot parcels. SKB TR-00-22, Svensk Kärnbränslehantering AB.
- Lagaly G, 1994.** Layer charge determination by alkylammonium ions. In: Mermut, A.R., editor: Layer charge characteristics of 2:1 silicate clay minerals, CMS Workshop Lectures Vol. 6, Boulder, CO, Clay Miner. Soc., p 1–46.
- Maurel C, 1964.** *Bull. Soc. Franç. Minéral. Crist.*, 87, p 377.
- Mehlich A, 1948.** Determination of cation- and anion-exchange properties of soils. *Soil Science* 66, 429–445.
- Olis A C, Malla P B, Douglas L A, 1990.** The rapid estimation of the layer charge of 2:1 expanding clays from a single alkylammonium ion expansion. *Clay Min.* 25, p 39–50.
- Plötze M, Kahr G, Dohrmann R, Weber H, 2007.** Hydro-mechanical, geochemical and mineralogical characteristics of the bentonite buffer in a heater experiment. The HE-B project at the Mont Terri rock laboratory. *Physics and Chemistry of the Earth*, accepted for publication.

## **Geochemical analysis of samples of MX-80 compacted bentonite from Block 13, parcel A2 of the LOT Experiment, Äspö Hardrock Laboratory, Sweden**

Raúl Fernández, Urs Mäder, Margarita Koroleva  
Rock-Water Interaction Group, Institute of Geological Sciences  
University of Bern

NAB 08-08  
September 2008

*Keywords:* MX-80, Clay, Compacted bentonite, EBS, In situ experiment, Analytical techniques, LOT Experiment, Äspö.

### **NAGRA funded part**

This part concerns a study which was conducted for Nagra within the LOT project. The conclusions and viewpoints presented are those of the authors and do not necessarily coincide with those of SKB.

# Contents

<b>1</b>	<b>Introduction and objectives</b>	254
<b>2</b>	<b>Sample material</b>	255
2.1	LOT parcel A2 and Block 13	255
2.2	Recovery of Block 13	257
2.3	Generic information on bentonite used for LOT	260
<b>3</b>	<b>Physico-chemical conditions during the LOT experiment</b>	261
<b>4</b>	<b>Analytical program, methods, sample preparation</b>	264
4.1	Analytical program	264
4.2	Analytical methods	264
4.2.1	Water content	264
4.2.2	XRD analysis	264
4.2.3	Wet and dry density	264
4.2.4	Aqueous leachates	265
4.2.5	Exchangeable cations	265
4.2.6	Sum of measured exchangeable cations	265
4.2.7	Cation exchange capacity by Na-acetate/Mg-nitrate displacement	266
4.2.8	Analysis of total carbon and sulfur	266
4.3	Sample preparation	267
4.3.1	Sample preparation at the Äspö URL	267
4.3.2	XRD analysis	269
4.3.3	Wet and dry density	270
4.3.4	Aqueous leachates	270
4.3.5	Exchangeable cations	270
4.3.6	Cation exchange capacity by Na-acetate/Mg-nitrate displacement	270
4.3.7	Total carbon and sulfur	270
<b>5</b>	<b>Results</b>	271
5.1	Water content	271
5.2	XRD analysis	272
5.3	Wet and dry density	273
5.4	Aqueous leachates	273
5.5	Exchangeable cations	274
5.6	Sum of measured exchangeable cations	275
5.7	Cation exchange capacity determined by Na/Mg displacement	275
5.8	Total carbon and sulfur	276
<b>6</b>	<b>Comments and discussion</b>	278
6.1	Water content	278
6.2	XRD analysis	278
6.3	Wet and dry density	278
6.4	Aqueous leachates	279
6.5	Exchangeable cations and sum of cations	279
6.6	Cation exchange capacity by Na/Mg displacement	279
6.7	Carbon and sulfur	280
6.8	Additional issues	281
6.9	Recommendations	282
	Acknowledgments	282
	<b>References</b>	282
	<b>Appendix A</b> Water content data	283
	<b>Appendix B</b> XRD data	288
	<b>Appendix C</b> Aqueous extract data	295
	<b>Appendix D</b> Exchangeable cation data	296

# 1 Introduction and objectives

The Rock-Water Interaction Group of the Institute of Geological Sciences at the University of Bern was contracted by Nagra to perform analytical work for bentonite samples from the LOT experiment (Äspö Hardrock Laboratory) within the framework of a Nagra-SKB cooperation.

The aim of this work is to apply the analytical techniques tested and developed for the analysis of claystone (Opalinus Clay from Mont Terri and the Zürcher Weinland area, Switzerland; Callovo-Oxfordian claystone from the Bure area, France), and compare them with the techniques and procedures employed by Clay Technology AB that is performing most of the analytical work for the various parcels of the LOT experiment. This effort is expected to broaden the data basis and strengthen its interpretation. The resolution of any inconsistencies will help to optimize analytical techniques, and better assess their relative merits.

This report emphasises the results of the analytical work and methods used, and offers limited interpretation. The report is intended as a basis for discussion regarding the in-depth interpretation and the assessment of the relative merits of alternate analytical techniques.

The objectives of SKB in the LOT test series are to validate models and hypotheses concerning long term processes in the bentonite buffer material and of related processes regarding microbiology, radionuclide transport and copper corrosion under conditions similar to those expected in a KBS-3 repository design foreseen by SKB for deep disposal of high-level radioactive waste.

The Parcel A2 of the LOT Experiment was excavated in January 2006. The analytical work reported here was performed during 2006, and a draft data report was issued in January 2007. The report was completed, reviewed and revised during 2007. Results were presented at the LOT Project Meetings in Äspö (Nov. 2006) and Lund (Nov. 2007).

## 2 Sample material

The LOT experiment, carried out at the Äspö Hardrock Laboratory in Sweden, consists of seven parcels emplaced in large-diameter vertical boreholes in granite, each one consisting of a central heater surrounded by a stack of compacted bentonite blocks (doughnuts). The stack is instrumented for monitoring physical conditions during the experiment, and contains a variety of special-purpose doughnuts designed for specific tasks such as corrosion studies, or for obtaining geochemical information. The parcels are left in place for a desired length of time (years) and are then excavated, dissected and prepared for analysis (see below).

### 2.1 LOT parcel A2 and Block 13

The layout of the LOT parcel A2 is shown in Figure A8-1. The parcel was emplaced at the end of October, 1999, and the heater was turned on February 2, 2000. The heater was turned off December 5, 2005, and the parcel was excavated between January 9 and 16, 2006. The duration of the experiment was therefore approximately 6 years, whereby a steady-state heat flow condition was reached after the 1<sup>st</sup> year. The experimental site was located in the G-tunnel at the -450 m level of the Äspö Laboratory.

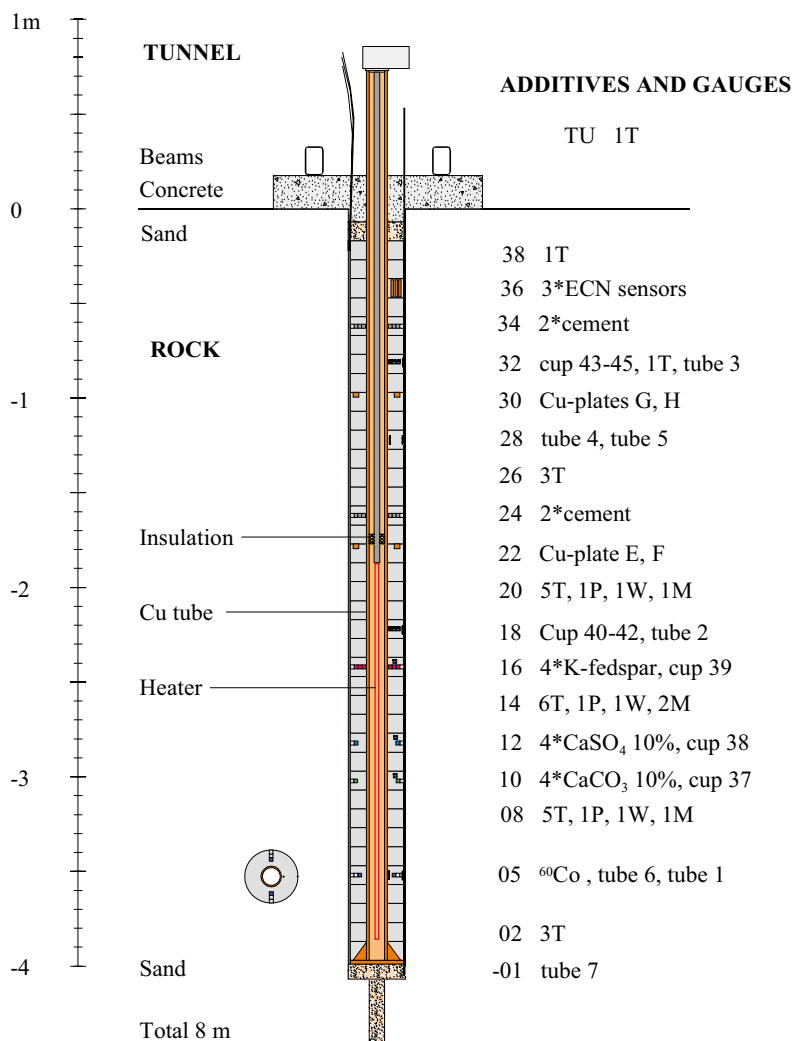


**Figure A8-1.** Layout of the LOT parcel A2. Blocks equipped with sensors or test materials are numbered, from bottom to top. Block 13 (barren, not numbered) is located at a depth of 2.7 m (scale on left) (figure from O. Karnland, Clay Technology).

Block 13 (sample label LA2-13) is located at a depth of approximately 2.7 m (Figure A8-1) measured from the floor of the gallery and is contained within the hottest zone of the experiment (see below). The underlying block, No 12, contains 10% anhydrite ( $\text{CaSO}_4$ ) as discrete embedded plugs as well as a sampling cup for porewater (if present). The overlying block, No 14, is barren, except for 6 temperature sensors and several pressure sensors (contacting materials are Ti and CuNi alloy).

The central heater is contained in a heavy-walled copper tube (11 cm outer diameter), and the diameter of the borehole is 30 cm. The bentonite blocks were only slightly undersized to fit into the borehole snugly, and they have a radial width after swelling of 9.5 cm, and a height of 10 cm.

Initially, an annular gap of approximately 10 mm existed between the bentonite blocks and the borehole wall in the granite (partially occupied by Ti and CuNi tubing containing the sensor connections). This gap was filled with formation water after sealing of the parcel and before the heater was turned on. This water was intended to induce rapid initial swelling of the outermost part of the bentonite blocks in order to close the gap. It can also be assumed that the small annular gap between the copper heater and the bentonite doughnuts was wetted as well when the outer free volume was filled with formation water. It may therefore be assumed that the contact between the heater and the bentonite as well as that between the bentonite and the granite was already tight when the heater was turned on 3 months after installation.

The standard analytical program set up by Clay Technology (not including this study) includes the following, with methods indicated in parentheses:

- Water ratio (oven drying).
- Density (weighing in paraffin oil).
- Hydraulic conductivity (oedometer).
- Swelling pressure (oedometer).
- Swelling capacity (free swelling in test tube).
- Shear strength (uniaxial compression tests, triaxial tests).
- Element concentration in porewater (chemical analysis).
- Element content in the bulk and clay fraction material (ICP-AEM).
- Cation exchange capacity (Cu-trien).
- Distribution of exchangeable ions (ammonium exchange).
- Mineralogical composition of bulk and clay fraction (XRD, SEM-EDX).
- Microstructure (TEM and SEM-EDX).

The sample orientation scheme for the LOT experiment was also used in this study, and sample numbers according to this scheme are also provided in addition to our internal sample numbers. Figure A8-2 illustrates the sample orientation and labelling scheme.

An example illustrates the method: 08ASE3 where:

- 08 block number (counted from the bottom of the parcel),
- A vertical level in the block (A or B or C),
- SE direction of compass in the test hole,
- 3 radial distance in centimeters from the inner mantle surface to the center of the specimen.

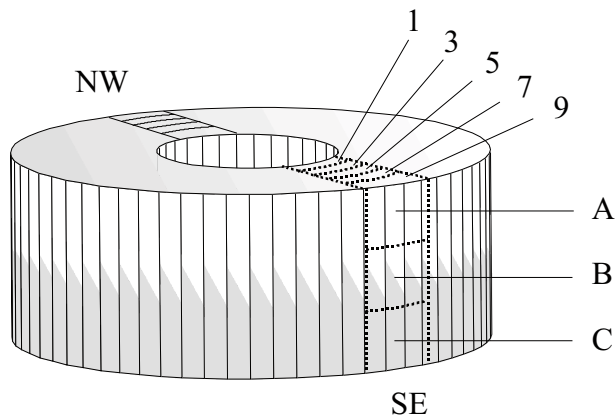


**Figure A8-2.** Sample orientation and labeling scheme used in the LOT series of experiments. SE and NW denote the directions of compass in the test-hole, figures denote the radial position of the centre of the specimens expressed in centimetres measured from the block inner mantle surface (interface to heater), and A, B and C denote the analysed three vertical positions in the blocks (figure from O. Karnland, *Clay Technology*).

## 2.2 Recovery of Block 13

The LOT parcel A2 was extracted as a cylindrical block preserving a rind of granite (Figures A8-3 and A8-4). The excavated cylinder was dissected near the experimental location by first gradually removing the enclosing granite, followed by separating the bentonite blocks. Drying out was minimized by covering the parcel in between working episodes (Figure A8-5), by wrapping samples immediately after removal from the central heater tube, and also by the relatively high ambient humidity.



**Figure A8-3.** LOT parcel A2 ready to be lifted. The stack of bentonite blocks is completely contained in an outer rind of granite (image from O. Karnland, *Clay Technology*).



**Figure A8-4.** The lower part of the LOT parcel A2. The diameter of the bentonite blocks is 30 cm, stacked on the central copper tube. Sensor wires are located along the outside of the bentonite blocks (peeled back before dissection). The deep end is still contained within a rind of granite.



**Figure A8-5.** Protection of the bentonite section from drying out between the 1<sup>st</sup> and 2<sup>nd</sup> day of sampling.

Block 13 was removed in the same way as all other blocks, by measuring the thickness of 10 cm, and cutting the block with a power saw to very close to the copper tube (Figure A8-6). The block could then be pried loose and slid off the central tube in a single piece (Figures A8-7 and A8-8). The block was tightly wrapped for short interim storage before it was carried to the surface to be further processed in one of the laboratory rooms at the Äspö Laboratory surface facilities.



*Figure A8-6. Block 13 secured with a supporting nylon strap, and marked for cutting. The thickness of a block is 10 cm, the outer diameter 30 cm, and the inner diameter 11 cm. The radial width is 9.5 cm.*



*Figure A8-7. The removal of the “doughnut” block 13.*

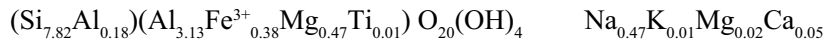


*Figure A8-8. Martin Birgersson from Clay Technology with the successfully removed block 13. The groove marks the top of the block and the North orientation. North is also marked by a red pin placed on the side of the block.*

## 2.3 Generic information on bentonite used for LOT

Na-exchanged Wyoming bentonite (MX-80) was used for fabricating the bentonite blocks for all of the LOT parcels. Table A8-1 is a summary of mineralogy (data from O. Karnland, presented at a LOT meeting 2006) as determined by X-ray diffraction analysis.

The chemical formula of the Na-montmorillonite of the reference material is (O. Karnland, Clay Technology):



The composition is indicated in Figure A8-9 within the nomenclature adopted by Clay Technology /Karnland and Birgersson 2006/.

**Table A8-1. Mineralogical composition of the Wyoming bentonite material used for fabricating the bentonite blocks. (data from O. Karnland, Clay Technology).**

Minerals %	MX-80
Albite	7
Cristobalite	3
Gypsum	1
Muscovite	1
Quartz	5
Na-Montmorillonite	83
	100

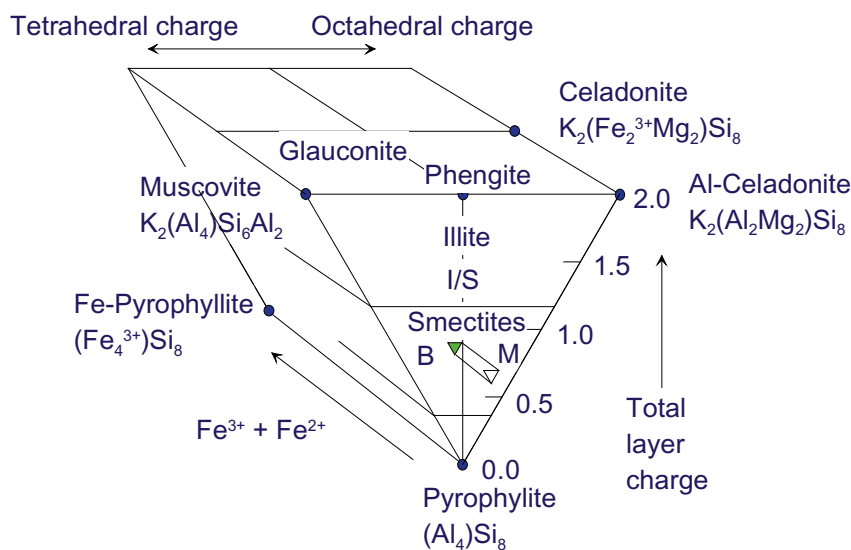


**Figure A8-9.** Composition of Na-montmorillonite of the Wyoming bentonite reference material indicated as a triangle in the Beidellite (B) – Montmorillonite (M) range. The basis is  $\text{O}_{20}(\text{OH})_4$  /Karnland and Birgersson 2006/, modified from /Newman and Brown 1987/.

### 3 Physico-chemical conditions during the LOT experiment

Parcel A2 of the LOT experiment reached stable temperature conditions after 1 year, and remained at constant temperature for an additional 5 years. The overall temperature distribution in the LOT parcel A2 is synthesized in Figure A8-10. The temperature distribution in block 14 (just 10 cm above block 13) is shown in Figure A8-11. Block 13 was therefore subject to temperatures of  $\sim 135^{\circ}\text{C}$  at the contact to the heater, and  $\sim 85^{\circ}\text{C}$  at the contact to the granite.

The heater was turned off on December 5, 2005, and left to cool until excavation started on January 9 and ended on January 16, 2006. There was therefore a 4–5 week period during which temperatures were decreasing, and some chemico-physical re-adjustments may have occurred.

Preliminary data from Clay Technology on water content (Table A8-2), density (Table A8-3) and degree of saturation (Table A8-4) are shown below for reference.

The bentonite may be assumed to be fully saturated in the entire parcel, including the hottest zone. The tendency towards saturation values slightly below 1.00 observed in the hottest zone (Table A8-4) may reflect the effect of thermal contraction after cooling. It should be noted that there is a strong correlation between water content and density, and thus full saturation does not imply a uniform water content.

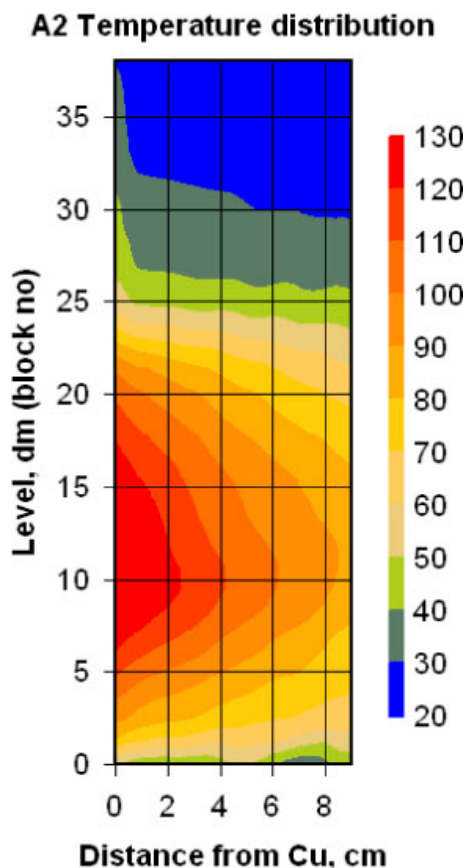


*Figure A8-10. Vertical section displaying the radial stable temperature distribution. Temperatures are constrained at the level of block 14, just 10 cm above block 13. It can be inferred that block 13 was exposed to temperatures of  $130\text{--}140^{\circ}\text{C}$  at the interface to the central copper tube (data and graph from O. Karnland, Clay Technology).*

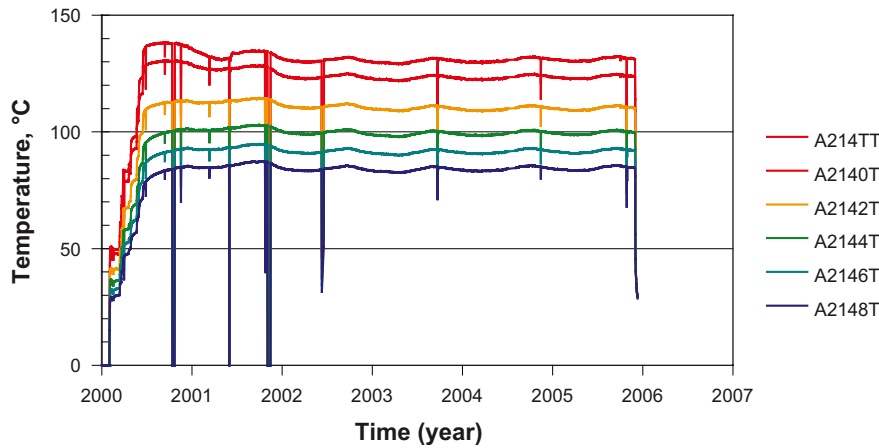


**Figure A8-11.** Temperature distributions in block no 14. The denomination A2141T indicates the temperature 1 cm from the central copper tube (in parcel A2, block 14), and A2148T indicates the temperature 8 cm from the copper tube, which is 1–2 cm from the rock (data and graph from O. Karnland, Clay Technology).

**Table A8-2.** Water ratio of bentonite material from different positions in parcel A2 relative to dry mass. Position indicates radial distance [cm] from Cu-tube (data from O. Karnland, Clay Technology).

Position Block no	1	3	5	7	9
38	0.376	0.380	0.374	0.393	0.408
33	0.321	0.321	0.320	0.325	0.337
31	0.309	0.305	0.309	0.316	0.336
29	0.301	0.299	0.304	0.314	0.331
27	0.309	0.303	0.304	0.312	0.333
25	0.299	0.301	0.304	0.320	0.340
23	0.293	0.293	0.299	0.313	0.332
21	0.285	0.289	0.293	0.304	0.326
19	0.287	0.285	0.303	0.317	0.333
17	0.282	0.278	0.295	0.308	0.324
<b>15</b>	<b>0.280</b>	<b>0.279</b>	<b>0.300</b>	<b>0.316</b>	<b>0.330</b>
<b>11</b>	<b>0.268</b>	<b>0.271</b>	<b>0.279</b>	<b>0.297</b>	<b>0.316</b>
9	0.269	0.271	0.282	0.303	0.318
7	0.275	0.274	0.283	0.298	0.314

**Table A8-3.** Density of bentonite material from different positions in parcel A2. Position indicates radial distance [cm] from Cu-tube. All data values in kg/m<sup>3</sup> (data from O. Karnland, Clay Technology).

Position Block no	1	3	5	7	9
38	1,864	1,876	1,859	1,862	1,847
33	1,923	1,922	1,920	1,918	1,897
31	1,941	1,948	1,943	1,930	1,898
29	1,955	1,962	1,954	1,941	1,912
27	1,954	1,962	1,957	1,945	1,912
25	1,965	1,960	1,953	1,916	1,890
23	1,977	1,971	1,964	1,943	1,917
21	1,982	1,978	1,969	1,955	1,928
19	1,979	1,981	1,962	1,940	1,921
17	1,983	1,987	1,948	1,951	1,928
<b>15</b>	<b>1,977</b>	<b>1,985</b>	<b>1,959</b>	<b>1,942</b>	<b>1,919</b>
<b>11</b>	<b>1,987</b>	<b>1,993</b>	<b>1,979</b>	<b>1,950</b>	<b>1,933</b>
9	1,990	1,988	1,975	1,951	1,934
7	2,000	1,991	1,975	1,954	1,936

**Table A8-4. Degree of saturation of bentonite material from different positions in parcel A2.  
Position indicates radial distance [cm] from Cu-tube (data from O. Karnland, Clay Technology)**

<b>Position Block no</b>	<b>1</b>	<b>3</b>	<b>5</b>	<b>7</b>	<b>9</b>
38	1.007	1.024	0.998	1.024	1.026
33	0.995	0.993	0.990	0.995	0.991
31	0.996	0.998	0.998	0.994	0.990
29	0.999	1.004	1.003	1.004	0.998
27	1.011	1.010	1.006	1.005	1.000
25	1.006	1.004	1.002	0.985	0.987
23	1.011	1.004	1.005	1.004	1.004
21	1.003	1.006	1.001	1.005	1.007
19	1.004	1.001	1.010	1.008	1.011
17	1.000	0.997	0.982	1.005	1.005
<b>15</b>	<b>0.988</b>	<b>0.995</b>	<b>1.002</b>	<b>1.008</b>	<b>1.004</b>
<b>11</b>	<b>0.979</b>	<b>0.990</b>	<b>0.989</b>	<b>0.986</b>	<b>0.998</b>
9	0.984	0.986	0.990	0.998	1.003
7	1.007	0.993	0.993	0.993	0.998

## 4 Analytical program, methods, sample preparation

### 4.1 Analytical program

The analytical program for the analysis at the University of Bern included the following parameters. The aim was not to perform a complete or most optimal analytical program, but to apply those methods that were used previously for the analysis of claystones, and thus allow for some comparison with the analytical program of Clay Technology.

- Measurement of water content.
- XRD on bulk samples and grain size fractions.
- Wet and dry density measured in paraffin oil on select samples.
- Cations and anions on aqueous leachates.
- Exchangeable cations using the Ni-ethylenediamine method corrected for disturbing effects.
- Sum of measured exchangeable cations.
- Cation exchange capacity by Na-acetate/Mg-nitrate displacement.
- Content of C(inorganic), C(total), and S(total) in select samples.

### 4.2 Analytical methods

#### 4.2.1 Water content

Water content was measured by heating the clay samples in a drying oven. All samples were placed in plastic containers and dried at 40°C for 20 days. After this period the samples were changed to glass dishes and the temperature increased to 70°C, maintaining this temperature for 5 days to reach constant mass. This was repeated to higher temperatures, and drying times were: 1 day at 90°C, 6 days at 105°C, and 19 days at 150°C.

The water content was calculated relative to the dry mass obtained at 105°C by the following equation:

$$\text{Water content (\%)} = \frac{m_{\text{initial}} - m_{105^{\circ}\text{C}}}{m_{105^{\circ}\text{C}}} \times 100$$

The mass of the samples was weighed periodically, recording all mass losses. The water loss as a function of temperature was also evaluated, whereby the measurements were extended to constant mass at each temperature.

#### 4.2.2 XRD analysis

Mineralogical analyses of the bulk sample and different clay fractions were made by X-ray diffraction analysis on disoriented and oriented rock powders using a PHILIPS PW-3710 diffractometer. The system uses  $\text{Cu}_{K\alpha}$  radiation with a wavelength of 1.54Å. Current intensity and voltage were 30 mA and 40 kV, respectively.

Total bulk samples and clay fraction samples were determined by scanning from 2 to 70° and from 2 to 40° 2 $\theta$ , respectively, with 0.02° step size and 1 second counting time per step.

#### 4.2.3 Wet and dry density

Bulk wet density ( $\rho_{b,\text{wet}}$ ) was measured in duplicate using the paraffin oil displacement method. The principle of the method is the calculation of bulk wet density from the sample mass and its volume. The volume was determined by weighing a sample first in air, and then weighing it while immersing the sample in paraffin oil ( $\rho_p = 0.86 \text{ g/cm}^3$  at 20°C), making use of Archimedes' principle. The mass of a beaker filled with paraffin oil was measured before ( $m_p$ ) and after ( $m_{p+r}$ ) immersion of

the sample, which was let hang freely on a thin thread fixed to a tripod. The bulk wet density was calculated according to:

$$\rho_{b,wet} = \frac{\rho_p \times m_{rock+pw}}{m_{p+r} - m_p}$$

where  $m_{rock+pw}$  is the mass of the wet rock sample,  $m_p$  is the mass of the beaker with paraffin oil and  $m_{p+r}$  is the measured mass of the beaker with paraffin oil and the immersed freely hanging sample.

Two separate homogeneous and physically intact samples of 2–3 cm<sup>3</sup> volume were measured.

Bulk dry density ( $\rho_{b,dry}$ ) was calculated from the water content and the bulk wet density according to:

$$\rho_{bdry} = \frac{\rho_{b,wet}}{1 + 0.01 \times WC}$$

where WC is the water content value (%).

#### 4.2.4 Aqueous leachates

6 g of dried bentonite was added to 60 ml of distilled water (S:L ratio 1:10) and shaken end-over-end for two days. The mix was centrifuged two times for 1 hour, and the supernatant solution filtered with a 0.2  $\mu$ m filter. Additional centrifuging yielded approximately one more milliliter of solution that was not used, however, for analysis. Sample W-4B was centrifuged three times before filtration to increase the initially low yield.

Alkalinity (by titration) and pH were determined immediately after termination of the extraction procedure. Major cations (Na<sup>+</sup>, K<sup>+</sup>, Ca<sup>2+</sup> and Mg<sup>2+</sup>) and anions (F<sup>-</sup>, Cl<sup>-</sup>, Br<sup>-</sup>, SO<sub>4</sub><sup>2-</sup> and NO<sub>3</sub><sup>-</sup>) were determined using a Metrohm 861 Compact Ion Chromatograph with a relative error of  $\leq \pm 5\%$ . Sr<sup>2+</sup> was measured by Atomic Absorption Spectroscopy (AAS) in a Varian SpectrAA 300 instrument because its concentrations were below the detection limit for ion chromatography.

#### 4.2.5 Exchangeable cations

Samples were mixed with 30.0 ml of a nickel ethylenediamine (Ni-en) 0.5 M solution using a S:L ratio of 0.5:1. All samples were shaken end-over-end for 2 days in polypropylene tubes. After phase separation by centrifuging (1 hour at 5,200 rpm), the supernatant leachate was removed using a syringe and filtered to <0.2  $\mu$ m.

The exchangeable cation population was displaced with Ni(en) as proposed by /Bradbury and Baeyens 1998/. The method takes advantage of the high selectivity of the Ni(en) complex which displaces all exchangeable cations from the clay minerals into solution. The pH of the Ni(en) solution is buffered to 8.1–8.2 by adding HNO<sub>3</sub> Titrisol™ solution which is equivalent to the pH of a calcite saturated solution at a of 10<sup>-3.5</sup> bar and consequently a solution in equilibrium with air. Then, the solution is filtered and analyzed.

Analyses of major cations (Na<sup>+</sup>, K<sup>+</sup>, Ca<sup>2+</sup>, Mg<sup>2+</sup> and Sr<sup>2+</sup>) and nickel were performed by AAS. The Cumulative error of the measurements is approximately  $\pm 5\%$ .

The obtained Ca<sup>2+</sup> and Na<sup>+</sup> exchangeable cation concentrations should be corrected for the contributions from the porewater or any soluble salts with the chloride and sulfate concentrations measured in the aqueous leachates to obtain “true” amounts on the exchanger (see results and discussion).

#### 4.2.6 Sum of measured exchangeable cations

It has been assumed that some calcium and sodium measured as exchangeable cations by AAS actually originate from the dissolution of NaCl and CaSO<sub>4</sub> soluble salts contained in the dried sample. This has been corrected by combining all chloride with sodium and all sulfate with calcium, and considering the remaining concentrations as exchangeable. No correction has been performed to potassium, magnesium or strontium. This issue – and some alternative assumptions – are discussed below.

Thus, the sum of exchangeable cations is taken as the sum of extracted  $K^+$ ,  $Mg^{2+}$  and  $Sr^{2+}$  plus the sum of remaining  $Na^+$  and  $Ca^{2+}$  after corrections.

#### 4.2.7 Cation exchange capacity by Na-acetate/Mg-nitrate displacement

The method used is a modification of the one proposed by /Rhoades 1982/ developed for soils. It was refined and used for bentonite at the University Autónoma de Madrid within the Geochemistry of Clays research group.

0.25 g of dry sample were weighed and placed in a centrifuge tube, and 20 ml of sodium-acetate buffer solution were added (AcONa, 1M, pH = 8.2). This was done on duplicate samples. The mixture was let reacting for 24 hours in an end-over-end shaker. During this period  $Na^+$  saturates the exchangeable cation positions while displacing the original cation population to the solution. The selected pH in solution is supposed to minimize the dissolution of any accessory minerals, calcite in particular, or salt precipitates formed during drying of the sample.

After this, the tube was ultrasonically agitated for 5 minutes and stirred for 30 minutes in an orbital stirrer. Then, the tube was centrifuged for 10 minutes at 4,500 rpm. Right afterwards, the solution was decanted and discarded, and the solid sample was washed two more times with 20 ml of AcONa 1M, again including ultrasonic and orbital agitation and centrifuging.

Then, the sample was washed with 20 ml of ethanol to remove the excess of salts, again 3 times, following the method described above with ultrasonic and orbital stirring steps and centrifuging. For the third time, just 10 ml of ethanol were added.

Finally, sodium was displaced from the exchangeable positions by saturation with magnesium by washing with a  $Mg(NO_3)_2$  1M solution (pH ~ 5). 15 ml of magnesium nitrate solution were added to the remaining solid sample, following again the same method for three times (5 minutes of ultrasonic agitation, 30 minutes in the orbital stirrer, and 5 minutes of centrifugation) but now collecting all the solution in a 50 ml flask.

The flask with the collected solutions was filled to the 50 ml level with distilled water. The solid sample can be discarded.

Finally,  $Na^+$  was measured by AAS and the CEC calculated as:

$$CEC (meq / 100g) = \frac{Na^+ (mmoles)}{m_{dry}} \times 5$$

A small density correction was applied in order to account for the density of the Mg-nitrate solution, depending on the concentration units used.

#### 4.2.8 Analysis of total carbon and sulfur

Between 50 and 100 mg of dried sample (at 105°C) was used to measure total and inorganic carbon and total sulfur in the West profile.

Total sulfur and total carbon were determined by coulometry in a CS-MAT-5500 carbon and sulfur analyzer (Ströhlein Instruments). The principle of the method is based on the oxidation of carbon and sulfur species to  $CO_2$  and  $SO_2$  by applying oxidative atmosphere at high temperature (1,350–1,550°C). The solid sample for analysis is combusted in a high frequency furnace in a ceramic crucible in an oxygen stream. The reaction gases  $CO_2$  and  $SO_2$  produced during combustion are quantified by Non-Dispersive Infrared (NDIR) spectroscopy, giving the results of total carbon and sulfur. Inorganic carbon is determined by acidification. Organic carbon was obtained by subtracting inorganic carbon from the total carbon.

The detection limit for S is approximately 0.1 wt%, and that for C likely better than 0.5 wt%, a quantity established for carbon-rich samples. The detection of organic carbon in carbon-poor materials such as bentonite is therefore difficult if not impossible by this method.

### 4.3 Sample preparation

All sample preparation and handling (crushing, leaching, etc) of air-dried rock material was performed under ambient laboratory conditions. Two North to South profiles (30 samples in total) were cut to measure the water content, and these samples were prepared on-site at Äspö a short time after the recovery of Block 13. A profile extending towards the West (4 samples) was cut for all other analytical measurements, and these samples were prepared at the University of Bern.

#### 4.3.1 Sample preparation at the Äspö URL

Four sample profiles were prepared on site at Äspö for water content measurements. Two profiles extend to the North, and two profiles to the South, whereby one of each profiles represents the lower half of the doughnut (relative to its position in the borehole), and the other one the upper half (Figure A8-12).

The bentonite block was cut with an electric band-saw (Figure A8-13). The radial sections were further cut into an upper and lower half, and segmented into 7 and 8 subsamples, respectively (Figure A8-14). The marks on the plastic wrapping shown in Figure A8-14 are only schematic and do not represent the cutting as carried out.



**Figure A8-12.** Sample block 13 (LA2-13) wrapped in plastic foil marked and ready for cutting. The top surface is oriented up in the experiment, and the radial orientation is relative to North. Two radial slabs were first cut, labelled N and S.

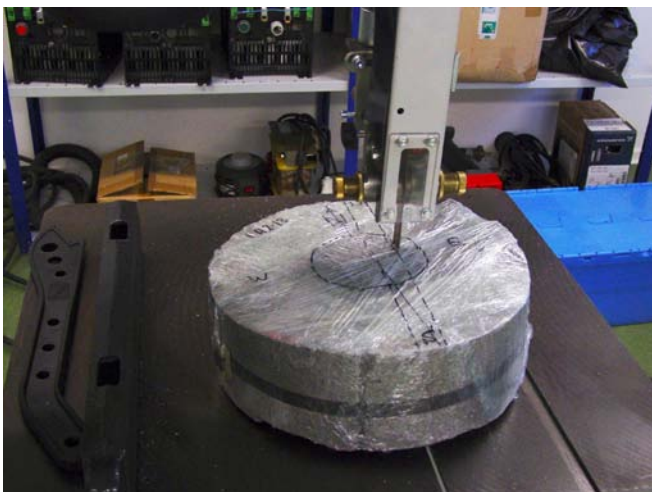


**Figure A8-13.** Cutting block 13 with a brand new band-saw in one of the surface laboratories at Äspö.



**Figure A8-14.** Two slabs marked for cutting 4 radial profiles for the measurement of water content. The profiles are labelled NU (North, upper profile), NL (North, lower profile), SU (South, upper profile), and SL (South, lower profile). The lines marking the cuts for the segments are only approximate

All samples were immediately weighed after cutting and enclosed in vials. The vials were packed under a slight vacuum for transport, and brought to Bern by Urs Mäder by air plane. The two large off-cuts of block 13 were also vacuum-packed and transported to Bern for further analysis. The vacuum packaging technique allows for easy inspection of the tightness of the seal simply by the state of preservation of the vacuum. The vacuum need not be strong (avoid evaporation) and corresponds to that achieved by a commercial household vacuum sealing device used for general food wrapping and preservation.

The radial width of the samples used for the water content analysis is given in Table A8-5, including 8 segments for the North profile and 7 segments for the South profile. The mass of the samples varies between 11 and 60 g depending on radial width, all having approximately the same thickness and height.

The sample ID (Table A8-5) would correspond to the following nomenclature adopted for LOT by Clay Technology (see Figure A8-2): 13CNx.x for the North lower profile, 13ANx.x for the North upper profile, 13ASx.x for the South upper profile, and 13CSx.x for the South lower profile, where x.x denotes the radial distance (in cm) from the heater surface to the middle of the sample.

**Table A8-5. Sample labels and radial width of the subsamples of the N and S profiles.**

Position	Sample ID	Sample width [mm]						
Heater	NL-1	12	NU-1	12	SL-1	11	SU-1	13
	NL-2	12	NU-2	14	SL-2	13	SU-2	15
	NL-3	14	NU-3	15	SL-3	13	SU-3	15
	NL-4	14	NU-4	15	SL-4	16	SU-4	15
	NL-5	12	NU-5	14	SL-5	15	SU-5	16
	NL-6	13	NU-6	12	SL-6	19	SU-6	15
	NL-7	11	NU-7	8	SL-7	8	SU-7	6
Outer rim	NL-8	6	NU-8	5				

### 4.3.2 XRD analysis

The samples used for XRD studies, as well as for cation exchange properties, wet and dry density, and for aqueous leaching analysis were cut from a profile oriented towards the West. The radial slab was cut in 4 radial segments, with the dimensions given as radial thickness in Table A8-6.

The samples were cut with a small electric band-saw. Cutting was done through the plastic foil to minimize drying of samples (Figure A8-15). The cut segments are shown in Figures A8-16 and A8-17.

**Table A8-6. Sample labels and radial width of the subsamples of the West profile.**

Orientation	Label	Length (mm)
Heater	W-1	12
	W-2	24
	W-3	30
Outer rim	W-4	30



**Figure A8-15.** Western half of block 13 (LOT parcel A2) used to cut a vertical profile oriented towards the West (tip of pen).



**Figure A8-16.** Cut profile from block 13. The heater was in contact along the right side (curved surface), and the contact to granite was along the left side. The lower edge represents the base of block 13.



**Figure A8-17.** Cut profile from block 13 after subsampling. The larger pieces were processed to perform the CEC, ion selectivity and XRD analyses. Some reference samples were kept sealed and refrigerated (for water content, density).

Whole-rock samples were powdered to a size approximately below 60  $\mu\text{m}$  by gentle manual crushing in an agate mortar. The clay fraction ( $<2 \mu\text{m}$ ) was obtained from granulated material by sedimentation in a water column with an ammonium phosphate dispersant solution. Sedimentation time was extended to 18 and 72 hours using a column length of 20 cm.

#### **4.3.3 Wet and dry density**

The density measurements had been conducted using the samples from the West profile. The samples were preserved from atmosphere in closed containers stored in a refrigerated room until measurement in order to minimize evaporation, and to preserve the original moisture content.

#### **4.3.4 Aqueous leachates**

Dried solid samples processed as described in Section 4.3.2 (XRD) were shaken in distilled water for two days, then filtered to  $<2 \mu\text{m}$ . Different solid:liquid ratios were tested initially, and based on this, a S/L of 1:10 was used for all aqueous leachates.

#### **4.3.5 Exchangeable cations**

15 g of powdered rock material, previously air-dried at  $105^\circ\text{C}$ , was used and prepared in the same fashion as for XRD analysis (Section 4.3.2).

#### **4.3.6 Cation exchange capacity by Na-acetate/Mg-nitrate displacement**

The samples were previously dried for 48 hours at  $105^\circ\text{C}$ , whereby the cation exchange capacity in the clay can be referred to the dry sample mass. Samples were mildly ground manually in an agate mortar before processing.

#### **4.3.7 Total carbon and sulfur**

Approximately 2 g of gently ground (agate mortar) and dried sample (at  $105^\circ\text{C}$ ) from the West profile were used to measure total and inorganic carbon as well as total sulfur.

## 5 Results

### 5.1 Water content

The water content was measured in 30 samples, corresponding to 2 different profiles carried out in duplicate (lower and upper sections), comprising 8 samples from the North Upper profile, 8 from the North Lower, 7 from the South Upper and 7 from the South Lower. The results have been plotted as function of the radial distance from the copper heater and also as function of drying time and temperature (see figures in Appendix A). 105°C has been considered the reference temperature for dry mass of the samples. Water content relative to this temperature as reference is shown in Table A8-7.

The water content is lowest in the samples adjacent to the heater and is identical in all four sections, 27.6–27.8 wt% relative to a dry mass determined at 105°C. Towards the outer margin, water contents increase to 31.7–33.5 wt%, showing a slight asymmetry with the South profiles containing 1–2 wt% less water compared to the North profiles. The water content forms a plateau over the first inner 40 mm of radial section, and then is increasing in approximate linear fashion towards the margins. The sample closest to the heater in each profile contains consistently slightly more water than the adjacent samples to a distance of 40 mm.

The water loss as a function of temperature is increasing from that measured at 40°C by 2–2.5 wt% to 105°C, and only negligibly to a final temperature of 150°C.

Additionally, the water content in samples W-3 and W-4 were determined in duplicate several months after measuring the North-South profile, to get a reference dry mass (105°C) for the cation exchange capacity (CEC) measurements. Results are shown in Table A8-8. The measured water content of the outermost sample (W-4) is consistent with the measurements of the more detailed N and S profiles documented above.

**Table A8-7. Water content relative to 105°C and radial width of the subsamples of the N and S profiles.**

Profile Position	North Lower		North Upper		South Lower		South Upper	
	Sample width [mm]	Water content [wt%]						
Heater	12	27.5	12	27.8	11	27.5	13	27.6
	12	27.4	14	n.d.	13	27.3	15	27.4
	14	27.5	15	n.d.	13	27.3	15	27.4
	14	28.4	15	28.6	16	27.8	15	28.1
	12	30.0	14	30.5	15	29.2	16	29.7
	13	31.7	12	32.0	19	30.9	15	31.4
	11	33.2	8	33.3	8	32.0	6	31.7
	Outer rim	6	33.5	5	33.0			

n.d.: not determined.

**Table A8-8. Measured water content in samples W-3 and W-4 relative to 105°C (/1 and /2 denote duplicates).**

Sample	Water Content (%)
W-3/1	28.78
W-3/2	28.93
W-4/1	31.53
W-4/2	31.11

## 5.2 XRD analysis

The nomenclature adopted for the samples determined by XRD and some comments to clarify their treatment and origin are shown in Table A8-9. All diffractograms (Figures A8-32 to A8-44) are included in Appendix B.

Quartz, cristobalite and montmorillonite peaks have been detected in all samples. Likely feldspars were detected in one of the test samples (LOT-3.RD, Figure A8-32, Appendix B). The feldspars have been detected in a sample where a portion of the clay fraction had been removed (LOT-1.RD). Very small amounts of illite were detected in the test sample (fractions LOT-3.RD and LOT-4.RD, Figure A8-33, Figure A8-42, Appendix B). No new minerals have been formed above the detection limit of XRD. There were no special efforts made to optimize the detection of pre-existing or any newly formed accessory minerals.

Superposition of X-ray diffractograms made on sedimentary clay fraction samples at 18 and 72 hours (Figures A8-37 to A8-40, Appendix B) do not reveal any clear tendency on the clay behaviour as a function of the distance from the heater.

Na-montmorillonite is observed in all oriented clay samples (reference and profiles) but no Ca-montmorillonite has been detected.

Diffractograms of the bulk samples show some difference in peak asymmetry: samples W1, W3 and W4 look alike, but distinctly different from sample W2 and the unreacted reference sample for Block 13, with the latter two showing an asymmetry towards higher  $2\theta$  values. The interpretation of this feature is unclear: assuming that equal humidity prevailed (data recorded on the same day in an air-conditioned room) this might indicate that the samples with peaks shifted towards higher  $2\theta$  values represent more Na-rich montmorillonite. See Section 6 for further comments on this issue.

**Table A8-9. Measured XRD samples.**

Sample	Profile location	Sedimentation time (h)	Figure, App. B	Remarks
REF-Bulk			32	LOT A2. Disoriented reference bulk sample for Block 13 (not subject to the LOT experiment)
REF-18.RD		18	34, 36	LOT A2. Oriented clay fraction of reference material for Block 13
REF-72.RD		72	35, 36	LOT A2. Oriented clay fraction of reference material for Block 13
LOT-1.RD		18	33	Oriented test sample, clay fraction
LOT-2.RD		24	33	Oriented test sample, clay fraction
LOT-3.RD			33	Oriented test sample. Residual sand and clay fraction taken after withdrawal of LOT-1.RD.
LOT-4.RD			33	Oriented test bulk sample without sedimentation.
w1-Bulk	W1		32	Disoriented bulk sample
w2-Bulk	W2		32	Disoriented bulk sample
w3-Bulk	W3		32	Disoriented bulk sample
w4-Bulk	W4		32	Disoriented bulk sample
W1-18.RD	W1	18	34, 40	Oriented sample, clay fraction
W2-18.RD	W2	18	34, 39	Oriented sample, clay fraction
W3-18.RD	W3	18	34, 38	Oriented sample, clay fraction
W4-18.RD	W4	18	34, 37	Oriented sample, clay fraction
W1-72.RD	W1	72	35, 40	Oriented sample, clay fraction
W2-72.RD	W2	72	35, 39	Oriented sample, clay fraction
W3-72.RD	W3	72	35, 38	Oriented sample, clay fraction
W4-72.RD	W4	72	35, 37	Oriented sample, clay fraction
LOT_Wnx.RD	W2,3,4		41, 42, 43, 44	Oriented dry sample, $n = 2,3,4$
LOT_Wny.RD	W2,3,4		41, 42, 43	Oriented sample saturated in ethyleneglycol
LOT_Wnz.RD	W2,3,4		41, 42, 43	Oriented sample heated at 550°C for 2 hours

### 5.3 Wet and dry density

The bulk wet density of the West profile was measured. From the obtained values, the bulk dry density was calculated from the measured water content, and the average values are summarized in Table A8-10.

The value of bulk dry density varies between 1.42 and 1.52 g/cm<sup>3</sup>. The lower densities are measured in the samples farther away from the heater (sample W-4) which also contain more water compared to those from near the heater. Consequently, values of bulk dry density are higher close to the heater. The distribution of the bulk density (packing of the rock particles in samples) along the profile is in accordance with the water content along the profile (Table A8-7).

### 5.4 Aqueous leachates

The aqueous leachates are dominated by sodium, chloride and sulfate, which is typical for a montmorillonite. Sample W-2 displays anomalously high concentrations of Na and SO<sub>4</sub> as well as K, Ca and Mg (Figure A8-18). The charge balance for the elevated cation concentrations is mainly compensated by sulfate. Chloride displays a regular distribution, increasing slightly from the heater towards the outer margin. The concentrations on the outermost sample are lower for all ions compared to the unreacted reference sample for Block 13 with the exception of chloride. The seemingly anomalously high concentrations found in sample W-2 are confirmed by the measurements in duplicate. All measured concentrations in aqueous leachates are shown in Appendix C.

**Table A8-10. Measured Bulk Densities.**

Sample ID	Bulk wet density (g/cm <sup>3</sup> )	Bulk dry density (g/cm <sup>3</sup> )
W-1	1.92	1.51
W-2	1.95	1.52
W-3	1.93	1.46
W-4	1.89	1.42

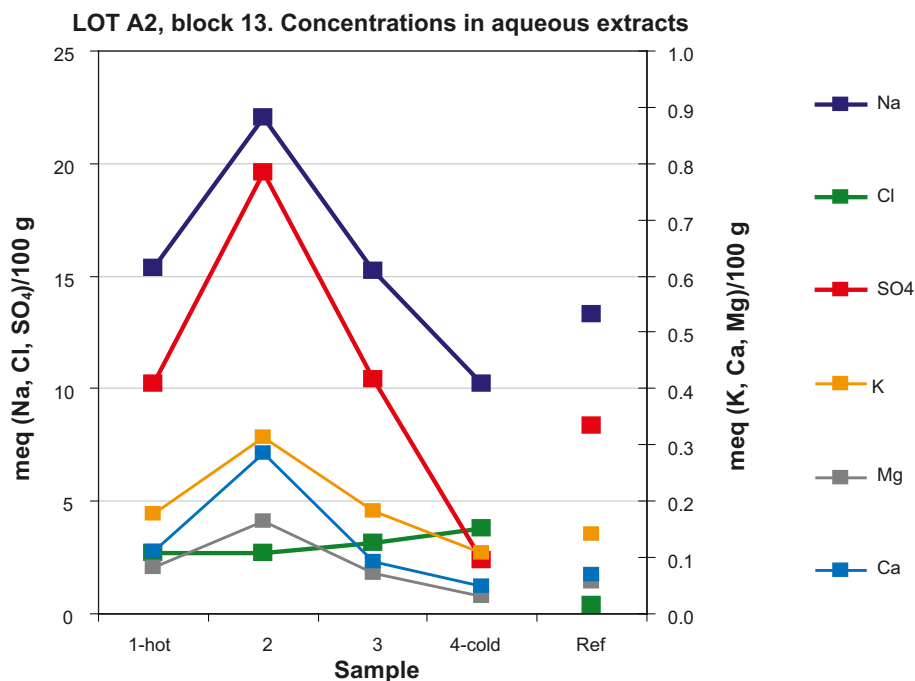


**Figure A8-18.** Aqueous species distribution in the aqueous leachates as function of their proximity to the cooper heater (meq/100 g dry mass).

## 5.5 Exchangeable cations

The cations measured as exchangeable must be corrected for cations originating from dissolution of soluble salts (residues from dried porewater and/or accessory minerals) to obtain “true” values. /Bradbury and Baeyens 1998/ proposed two cases to estimate the in situ cation occupancies. As case I, they considered to combine all chloride measured in the aqueous leachates with sodium and all sulfate with calcium and conceive these concentrations as a result of dissolution of the salts sodium chloride and calcium sulfate. As case II, they considered to combine both, chloride and sulfate, with sodium, and subtracting equivalent amounts from the exchangeable sodium. Potassium, magnesium and strontium extracted with the nickel method and measured by AAS are considered to maintain the same concentration without any correction.

Following this argument, data applying a correction according to cases I and II are presented in Table A8-11. All samples are reported in duplicate analysis (/1 and /2). The 0.5 in the sample label refers to the solid:liquid ratio used. Ni LOT A2-13 is the reference material. The uncorrected values for the concentrations of the exchangeable cations are listed in Appendix D.

The results for the corrected values applying both cases, I and II, are shown in Figure A8-19, displaying only the major cations Ca, Na, Mg and K:

**Table A8-11. Corrected distribution of exchangeable cations (meq/100 g dry mass).**

Sample	Correction case I: NaCl/CaSO <sub>4</sub>						Total	Correction case II: NaCl/Na <sub>2</sub> SO <sub>4</sub>						Total
	Ca	Na	Mg	K	Sr	Cu		Ca	Na	Mg	K	Sr	Cu	
Ni LOT A2-13 0.5/1	8.7	57.7	4.2	1.4	0.5	N.D.	72.5	17.0	49.4	4.2	1.4	0.5	N.D.	72.5
Ni LOT A2-13 0.5/2	9.1	57.7	4.1	1.4	0.5	N.D.	72.8	17.5	49.3	4.1	1.4	0.5	N.D.	72.8
Ni W-1B 0.5/1	15.1	52.7	6.1	1.3	0.5	1.64	77.3	25.0	42.9	6.1	1.3	0.5	1.64	77.3
Ni W-1B 0.5/2	14.4	52.5	6.3	1.3	0.5	1.63	76.6	25.0	41.9	6.3	1.3	0.5	1.63	76.6
Ni W-2B 0.5/1	8.0	56.4	5.1	1.5	0.5	1.51e-2	71.5	27.7	36.7	5.1	1.5	0.5	1.51e-2	71.5
Ni W-2B 0.5/2	7.8	56.6	5.1	1.5	0.5	1.52e-2	71.5	27.3	37.1	5.1	1.5	0.5	1.52e-2	71.5
Ni W-3B 0.5/1	12.1	55.9	5.0	1.4	0.5	1.49e-3	74.9	23.0	45.0	5.0	1.4	0.5	1.49e-3	74.9
Ni W-3B 0.5/2	13.0	56.0	5.1	1.4	0.5	1.53e-3	76.0	22.8	46.1	5.1	1.4	0.5	1.53e-3	76.0
Ni W-4B 0.5/1	13.8	56.8	5.5	1.3	0.5	6.98e-2	78.0	16.2	54.4	5.5	1.3	0.5	6.98e-2	78.0
Ni W-4B 0.5/2	13.9	55.9	5.3	1.3	0.4	5.05e-2	76.9	16.2	53.6	5.3	1.3	0.4	5.05e-2	76.9

N.D. = not detectable.

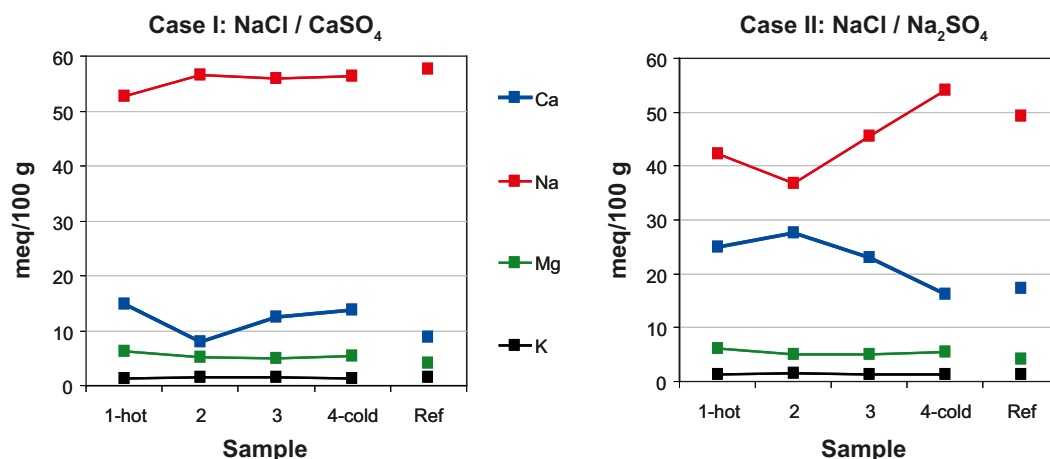


**Figure A8-19.** Distribution of exchangeable cations as a function of sample position relative to the copper heater for case I (Na corrected for aqueous Cl equivalents and Ca for aqueous SO<sub>4</sub>) and case II (Na corrected for aqueous Cl + SO<sub>4</sub> equivalents).

Cu was also measured in the extracted Ni solutions. It was found to be below a detection limit of  $10^{-3}$  meq/100 g in the reference sample, but was measurable in all samples of the profile. Highest values of 1.6 meq/100 g were found adjacent to the Cu-heater, decreasing to a minimum of  $1.5 \cdot 10^{-3}$  meq/100 g in sample W-3 and increasing again to  $\sim 6 \cdot 10^{-2}$  meq/100 g at the margin adjacent to the granite. The measurements are corrected for a small blank of Cu concentration contained in the Ni solution. The data are tabulated in Appendix D.

## 5.6 Sum of measured exchangeable cations

The sum of exchangeable cations in equivalents (81–94 meq/100 g) is  $\sim 21.5\%$  less than the Ni consumption (107–116 meq/100 g). The data is presented in Appendix D. The sum of the exchangeable cations is listed in Table A8-11 and is shown in Figure A8-20. Because the correction is based on milliequivalents, the total value is the same in both cases.

## 5.7 Cation exchange capacity determined by Na/Mg displacement

The total CEC measured in duplicate by the Na-Mg displacement method in the samples of the West profile is shown in Table A8-12. The value obtained for the reference material from Block 13 does agree very well with the sum of the measured exchangeable cations after correction (cases I and II, above).

In addition, aqueous calcium was measured in the final magnesium nitrate solution. Results just confirm the dissolution of significant calcite and/or gypsum/anhydrite, but the calcium concentration measured is not conclusive because some of this calcium may have been retained from previous extraction steps with sodium acetate, and also because some calcite might remain in bentonite to be continuously dissolved. Calcium measured in solution is also shown in Table A8-12.

The results of the direct CEC measurements are compared in Figure A8-21 with the sum of the exchangeable cations after correction for  $\text{Cl}^-$  and  $\text{SO}_4^{2-}$ .

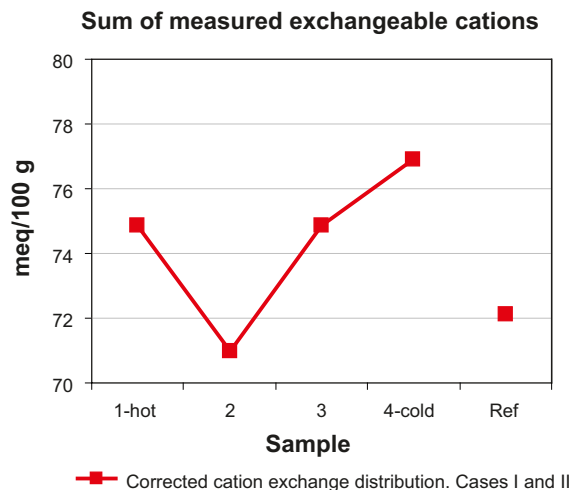


**Figure A8-20.** Sum of measured exchangeable cations as function to the sample position relative to the copper heater applying corrections (cases I and II) as described above.

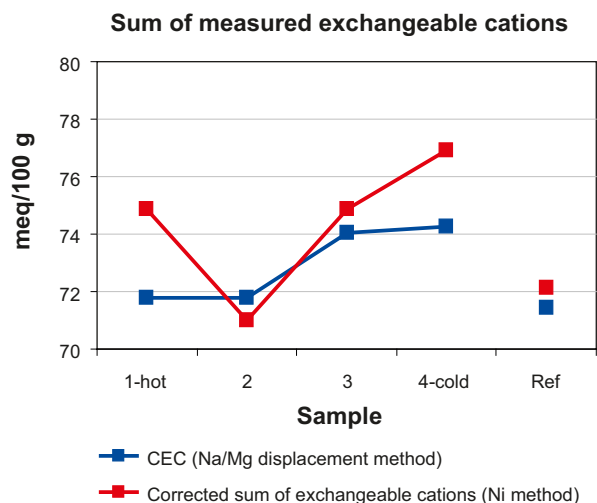


**Figure A8-21.** Comparison between the sum of measured exchangeable cations by the Ni(en) method (average of duplicate analyses) and the cation exchange capacity measured by the Na/Mg displacement method related to the sample position from the copper heater.

**Table A8-12.** Cation exchange capacity and calcium dissolved from calcite (meq/100 g).

Sample	CEC (meq/100 g)	Ca <sup>2+</sup> (meq/100 g)
Ni LOT A2-13 0.5/1	71.6	14.7
Ni LOT A2-13 0.5/2	71.3	14.7
Ni W-1B 0.5/1	72.1	14.3
Ni W-1B 0.5/2	71.5	14.2
Ni W-2B 0.5/1	70.0	14.1
Ni W-2B 0.5/2	73.6	14.0
Ni W-3B 0.5/1	74.6	14.9
Ni W-3B 0.5/2	73.5	15.3
Ni W-4B 0.5/1	74.1	14.9
Ni W-4B 0.5/2	74.4	14.8

## 5.8 Total carbon and sulfur

Results of total, inorganic and organic carbon and total sulfur are shown in Table A8-13. These values transformed to equivalents per 100 g are used further in the discussion.

In accordance with the observed distribution in the aqueous sulfate, the total amount of sulfur present in the second sample (W-2) is significantly higher than the rest of the sections. The detection limit for the sulfur content is ~ 0.1 wt%.

Although the detection limit for C by the method used might be better than 0.5 wt% for carbonate-poor materials, such as the MX-80 bentonite, the unexpected relatively high amount of organic carbon (by difference) in the section closest to the heater (W-1) is most likely not significant because of the large combined errors.

**Table A8-13. Total, inorganic and organic carbon and total sulfur on the West profile samples.**

Sample	Total C (%)	Inorganic C (%)	Organic C (%)	Total S (%)
LOT A2-13 0.5/1	0.6	0.6	<0.1	0.3
LOT A2-13 0.5/2	0.7	0.6		0.3
W-1B 0.5/1	0.9	0.6	0.3	0.4
W-1B 0.5/2	0.9	0.6		0.4
W-2B 0.5/1	0.4*	0.4*	0.1	0.5
W-2B 0.5/2	0.7	0.5		0.5
W-3B 0.5/1	0.5	0.5	<0.1	0.3
W-3B 0.5/2	0.5	0.5		0.2
W-4B 0.5/1	0.6	0.5	<0.1	0.2
W-4B 0.5/2	0.5	0.5		0.2

\*Possibly below a detection limit of 0.5 wt%. Organic C is computed by difference.

## 6 Comments and discussion

An in-depth discussion of optimal analytical procedures and the analytical results will be part of a collaborative effort of the partners involved in the LOT experiment and the analysis of parcel A2. The following sections contain a brief discussion just of the data of this report. By the same reason, the discussion is limited in some cases because results from other studies are not included at this stage.

### 6.1 Water content

In general, the water content is decreasing as a function of the proximity to the heater. It can be observed in Figures A8-23 to A8-31 (Appendix A) that the water content distribution in Sections 2 and 3 (11 to 40 mm from the copper heater) in all profiles is slightly lower than the water content in the section immediately adjacent to the heater. This anomaly could have been caused during the cooling of the parcel after turning off the heater, combined with either a re-distribution of water, or an external source of water. The effect of volume contraction during cooling may also be significant to consider, and this would be more significant for samples close to the heater.

In terms of temperature effect on drying, most of the water is lost up to 70°C. Small losses are observed from 70 to 150°C. A reference temperature of 105°C appears reasonable for relating data to dry mass. The important point is that samples – especially small blocks – have to be dried until a constant mass is reached rather than just for a fixed duration of time (e.g. 24 hrs).

### 6.2 XRD analysis

There is no difference observed in the oriented XRD patterns of the clay fraction – the clay material appears to be unchanged in comparison to the reference sample regardless of grain size and position relative to the heater. The idea was to separate and compare a very fine grained clay fraction (72 hrs) because this fraction would presumably be the most sensitive one to display any effects of thermal modification.

The differences observed in the disoriented bulk samples of the West profile compared to the reference sample (diffractogram 1, Appendix B) in the 5–10° 2 $\theta$  region need to be further discussed. It is striking that sample W2 is more like the unreacted bulk sample of Block 13, compared to the three other samples of the profile (Figure A8-32, Appendix B). This correlates with lower Ca-contents in the exchangeable cation populations in the former two samples (see details below). It can therefore be inferred that the reference sample and sample W2 should be more Na-montmorillonite rich compared to the other samples of the profile. This would result in a peak shift towards higher 2-theta values as observed.

### 6.3 Wet and dry density

The measured wet density of 1.92–1.95 g/cm<sup>3</sup> adjacent to the heater is somewhat lower than that reported by Clay Technology on nearby Blocks 15 and 11 as 1.98 g/cm<sup>3</sup> (Table A8-3). The value measured for a sample at the cold end of the profile is 1.89 g/cm<sup>3</sup> and compares to values of 1.91–1.92 g/cm<sup>3</sup> from blocks 15 and 11 (data by Clay Technology). It should be noted that Clay Technology determined densities shortly after sampling.

It should be noted that it was not planned to measure densities systematically for this study. The measurements represent a mere test for the paraffin oil immersion method and were carried out several month after sampling on samples that had been kept in closed containers in cold storage, but that may have undergone some volumetric relaxation. Nevertheless, the agreement is reasonable, but the density data for the samples of this study should not be used to calculate a degree of saturation. Instead, the degree of saturation for Block 13 should be assumed to be similar to that determined for nearby Blocks 15 and 11 by Clay Technology.

## 6.4 Aqueous leachates

The distribution of the cations and anions displayed in the profile of aqueous leachates is not straightforward to interpret, in particular the seemingly anomalously high  $\text{SO}_4$  content in sample W-2 (and associated elevated Na and Ca concentrations). The underlying Block 12 did contain heterogeneous packages of anhydrite (10%, as discrete embedded plugs), and this may have locally influenced the sulfate content in the overlaying Block 13. It may also be plausible, that heterogeneities in the content of accessory sulfate minerals do exist. This issue was not further resolved within the scope of this project, but could be addressed by analyzing additional profiles in a different orientation. The observations on this profile are, however, in agreement with studies by other partners that also document a sulfate accumulation towards the hot part of the profile.

## 6.5 Exchangeable cations and sum of cations

The appearance of the profile of the measured exchangeable cations is strongly influenced by the anomalously high sulfate concentration and its associated correction to the exchangeable cations, either to Na and Ca (case I) or only Na (case II). The favored correction is that of associating Cl concentrations with Na, and sulfate concentrations with Ca. The “true” correction may be a mixed correction composed of the two end-members, I and II. The existence of the low Ca population on the exchanger in sample W-2 is therefore uncertain, and should be confirmed with additional measurements.

The chloride profile shows an increase towards the outer margin as may be expected from contact with the saline groundwater. The values (and those of the other ions) should be compared to the actual composition of the infiltration groundwater to the LOT Parcel A2.

By reasons not yet determined, the sum of exchangeable cations in equivalents (81–94 meq/ 100 g) is ~ 21.5% less than the Ni consumption (107–116 meq/100 g). Proton exchange on permanent charge sites hasn't been measured, but this is not expected to be significant enough to explain this discrepancy due to the small surface area for edge sites (8.5 m<sup>2</sup>/g) compared to the total surface area (788 m<sup>2</sup>/g) in a compacted Na-MX-80 clay fraction studied by /Tournassat et al. 2004/. This same discrepancy between the sum of exchangeable cations and the exchange capacity was described by /Bradbury and Baeyens 1998/ for Opalinus clay core samples drilled up to 20 m into the wall rock of a reconnaissance gallery associated with the Mont Terri motorway tunnel in Canton Jura, Switzerland.

The sum of the exchangeable cations corrected for by case I or II varies along the profile with a tendency to be slightly higher values by less than 2 meq/100 g on average compared to the reference sample, with the exception of sample W-2. Such a variation is, however, within the combined analytical uncertainties. There is therefore no significant change in the exchange capacity evident between the reference sample and those of the hot zone of the LOT Parcel A2.

The presence of Cu (1.6 meq/100 g) measured in the sample adjacent to the heater is not surprising. It is notable, however, that small concentrations of Cu were measured throughout the profile that were distinctly higher compared to the reference material for Block 13. The increased value for Cu in the outermost sample can be reasoned by the presence and corrosion of many CuNi tubes along the bentonite-bedrock interface used for protection of the electric connections to the sensors (see Figure A8-4, for example). It has not been demonstrated if the Cu is present entirely on the exchanger, or as a secondary precipitate. This could probably have been achieved by doing additional extracts with formic acid that would dissolve any residual Cu-phase. It may also be possible that Cu present on the exchanger may enter the octahedral sheet at elevated temperature. This would modify the layer charge (small change). If this could be detected by measurements is questionable.

## 6.6 Cation exchange capacity by Na/Mg displacement

The Na/Mg method may underestimate the CEC for at least two reasons: (1) small amounts of the finest size fraction may be lost during repeat decanting (likely not significant), and (2) any calcite

or Ca-sulfate dissolution occurring during the Na-acetate exchange may leave some Ca on the exchanger despite repeat exchange steps. Ca-phases did clearly and significantly dissolve during the last step of the repeat Mg-nitrate displacement, as was seen by the measured Ca concentrations (Table A8-12).

The reproducibility between the duplicate samples is excellent and the data set does show a slight tendency in the distribution of the total cation exchange capacity to increase by ~2 meq/100 g from the heater towards the outer rim, but again, this is within the combined analytical uncertainty.

The CEC values obtained by direct measurement (Na-acetate/Mg-nitrate) agree very well with the sum of the exchangeable cations (Ni-en, corrected) for samples W-2, W-3 and the reference. This is providing confidence in the two methods and supports the assumptions underlying the corrections applied to the sum of the cations based on the anion concentrations obtained by the aqueous extracts. The sum of the cations is approximately 3 meq/100 g larger compared to the CEC for samples W-1 and W-4. The combined measurement uncertainties are estimated to about 4% relative, equivalent to 2.9 meq/100 g at a level of 72 meq/100 g.

We may therefore conclude that the two methods employed for estimating the CEC are largely in agreement, and that the CEC did not change significantly during the experiment in Block 13. The possible slight increase permitted by the data would have to be substantiated by a large data set, and some more testing of the individual steps of the analytical procedures.

## 6.7 Carbon and sulfur

The measurement values obtained for inorganic carbon and total sulfur, as well as the amount of calcium, chloride, sulfate and alkalinity (as  $\text{CO}_3^{2-}$ ) extracted in the aqueous leaches, and the exchangeable calcium have been transformed to equivalents, assuming 100 g of dry sample mass (Table A8-14). Total inorganic carbon and sulfur and aqueous  $\text{CO}_3^{2-}$  and  $\text{SO}_4^{2-}$  are also plotted in Figure A8-22 to compare the values and discuss some assumptions on the reactivity of accessory mineral phases in bentonite.

It is observed that the amount of sulfate extracted in the aqueous leachates has a similar distribution as the total amount of sulfur determined in the bulk sample, arising from accessory sulfates and minor dissolved sulfate. It is therefore reasonable to infer that hydrated (e.g. gypsum, bassanite) or dehydrated  $\text{CaSO}_4$  (anhydrite) and possibly also  $\text{Na}_2\text{SO}_4$  (residual of dried porewater) are dissolving relatively rapidly during aqueous extractions until complete dissolution or saturation. These observations are in support of associating  $\text{Ca}^{2+}$  with  $\text{SO}_4^{2-}$  when performing the corrections on the determinations of exchangeable cations.

In contrast to sulfur, the total inorganic carbon is one order of magnitude higher compared to the dissolved carbon (measured as alkalinity) in the aqueous extracts. There is evidence of substantial dissolution of calcite during the CEC measurement ( $\text{Ca}^{2+}$  measured in the CEC  $\text{MgNO}_3$  solution), but for the aqueous extracts the dissolution of calcite is much smaller than that for Ca-sulfate. The solutions used during the Ni-en exchange for obtaining exchangeable cations are pH-buffered to minimize calcite dissolution.

**Table A8-14. Averaged values of duplicates of the West profile: aqueous and exchangeable calcium, inorganic and aqueous carbon (as  $\text{CO}_3^{2-}$ ), total and aqueous sulfur (as  $\text{SO}_4^{2-}$ ) and aqueous chloride. All values relate to 100 g of dry sample.**

Sample	Aqueous Ca (eq)	Exchang. Ca (eq)	Inorg. C or $\text{CO}_3^{2-}$ (eq)	Alkalinity as $\text{CO}_3^{2-}$ (eq)	Total S or $\text{SO}_4^{2-}$ (eq)	Aqueous $\text{SO}_4^{2-}$ (eq)	Aqueous Cl (eq)
LOT ref.	2.3E-04	1.7E-02	1.0E-01	8.7E-03	1.9E-02	8.4E-03	4.0E-04
W-1	3.7E-04	2.5E-02	1.0E-01	5.2E-03	2.5E-02	1.0E-02	2.7E-03
W-2	9.5E-04	2.8E-02	7.5E-02	3.2E-03	3.1E-02	2.0E-02	2.7E-03
W-3	3.0E-04	2.3E-02	8.3E-02	4.4E-03	1.6E-02	1.0E-02	3.1E-03
W-4	1.6E-04	1.6E-02	8.3E-02	6.9E-03	1.3E-02	2.4E-03	3.8E-03

While it may be possible that different amounts of gypsum and calcite are dissolving during aqueous extraction and the exchange procedures, the consistency of the direct CEC determination and the sum of exchangeable cations (after corrections) lend support to the method and justifications adopted here.

Some other combinations for applying corrections to the exchangeable cations may also be envisaged – but cannot be further constrained or evaluated by the data available.

The presence of significant amounts of carbonates and sulfates in bentonite suggests that equilibrium with respect to calcite and gypsum in the pore solution may be established after bentonite saturation. These accessory phases will also form significant inventories of anions and cations, as well as buffering capacity (calcite) during porewater-bentonite interaction. The amounts of aqueous chloride are also relatively high (Table A8-14), suggesting the presence of soluble salts and/or impurities.

Relatively little emphasis was placed in the past on tracking and using the mineralogical changes of the accessory minerals during long-term laboratory and field experiments on compacted bentonite systems. The authors suggest that it would be important to more carefully examine the role and nature of the accessory minerals as these will exert an important control on the evolution of porewater chemistry and related mass transfer processes.

## 6.8 Additional issues

The possibility of any textural changes of the compacted bentonite has not been addressed in this study. Generally, it is assumed that compacted bentonite will largely behave as a homogeneous medium after full saturation. Cementation effects as a result of thermal gradients may, however, affect very locally grain distribution, porosity distribution, surface area, water uptake, and swelling properties.

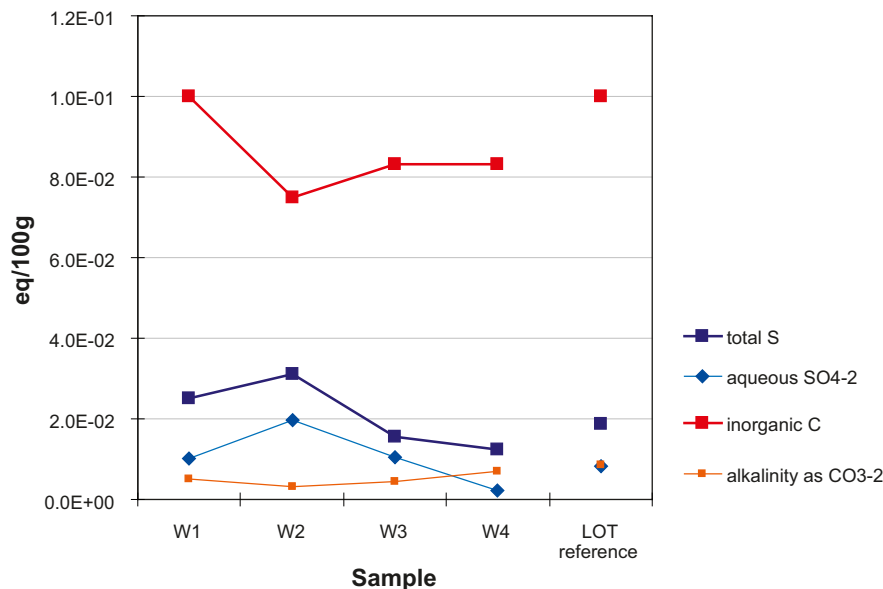


**Figure A8-22.** Inorganic and aqueous carbon (soluble as  $\text{CO}_3^{2-}$ ) and total and aqueous sulfur (soluble as  $\text{SO}_4^{2-}$ ) distribution related to the sample position from the copper heater.

## 6.9 Recommendations

The presence of relatively sharply bound chemical heterogeneities (sample W2 of the West profile, and observed by other investigators as well) as evident in the cation occupancy must also link to variations in the content and distribution of accessory minerals. It is therefore important from a geochemical point of view to better characterize these heterogeneities as these are likely to exert chemical controls on porewater composition, and hence, also mass transport and local swelling behavior. This would require the application of optimized non-aqueous separation methods to increase the resolution of XRD methods, and also to perform further studies on the separated material.

## Acknowledgments

The authors like to acknowledge the excellent management of the LOT Project by Clay Technology (Ola Karnland). Hanspeter Weber and Paul Wersin of Nagra initiated and financed this project. Michael Plötze (ETH Zürich) kindly reviewed a draft version and provided many comments and suggestions. Ruth Mäder (RWI, University of Bern) performed the CEC determinations and aqueous extracts. Analytical work was supported by the teams of Urs Eggenberger (XRD) and Niklaus Waber (IC analytics) at RWI, University of Bern. Martin Mazurek and Niklaus Waber (RWI, University of Bern) contributed to the data interpretation.

## References

- Bradbury M H, Baeyens B, 1998.** A Physicochemical Characterisation and Geochemical Modelling Approach for Determining Porewater Chemistries in Argillaceous Rocks. *Geochimica et Cosmochimica Acta* 62, 783–795.
- Karnland O, Birgersson M, 2006.** Montmorillonite stability, with special respect to KBS-3 conditions. SKB TR-06-11, Svensk Kärnbränslehantering AB.
- Newman A C D, Brown G, 1987.** The Chemical Constitution of Clays, Mineralogical Society Monograph No.6, ed. A.C.D. Newman, 1987.
- Rhoades J D, 1982.** Cation Exchange Capacity. A.L. Page, R.H. Miller and D.R. Keeney Eds., *Methods of Soil Analysis, Part 2. Chemical and Microbiological Properties*. ASA-SSSA, Madison, Wisconsin, USA, 2nd ed, 149–157 pp.
- Tournassat C, Greneche J-M, Tisserand D, Charlet L, 2004.** The titration of clay minerals: I. Discontinuous backtitration technique combined with CEC measurements. *Journal of Colloid and Interface Science*, 273, 224–233.

## Water content data

## Appendix A

Water content measurements of Block 13 of Parcel A2 of the LOT Experiment are summarized in Tables A8-15 and A8-16 and depicted in Figures A8-23 to A8-31.

**Table A8-15. Water content as a function of temperature and distance from the copper heater in the North profile (Lower and Upper).**

Water content [mass ratio] in profile "North Lower"					Water content [mass ratio] in profile "North Upper"				
Distance (mm)	40°C	70°C	90°C	105°C	Distance (mm)	40°C	70°C	90°C	105°C
0–12	0.258	0.271	0.273	0.275	0–12	0.260	0.274	0.276	0.278
12–24	0.259	0.270	0.272	0.274	12–26	n.d.	n.d.	n.d.	n.d.
24–38	0.260	0.271	0.273	0.275	26–40	n.d.	n.d.	n.d.	n.d.
38–52	0.270	0.281	0.283	0.284	40–55	0.272	0.283	0.285	0.286
52–65	0.287	0.297	0.299	0.300	55–69	0.292	0.302	0.304	0.305
65–77	0.304	0.314	0.316	0.317	69–81	0.307	0.317	0.319	0.320
77–89	0.319	0.329	0.331	0.332	81–90	0.320	0.330	0.332	0.333
89–95	0.324	0.332	0.334	0.335	90–95	0.318	0.327	0.328	0.330

n.d.: not determined.

**Table A8-16. Water content as a function of temperature and distance from the copper heater in the South profile (Lower and Upper).**

Water content [mass ratio] in profile "South Lower"					Water content [mass ratio] in profile "South Upper"				
Distance (mm)	40°C	70°C	90°C	105°C	Distance (mm)	40°C	70°C	90°C	105°C
0–11	0.258	0.271	0.273	0.275	0–13	0.258	0.272	0.274	0.276
11–24	0.257	0.269	0.272	0.273	13–28	0.256	0.270	0.272	0.274
24–38	0.258	0.270	0.272	0.273	28–43	0.258	0.270	0.272	0.274
38–53	0.264	0.274	0.276	0.278	43–58	0.266	0.278	0.279	0.281
53–68	0.278	0.289	0.290	0.292	58–74	0.284	0.294	0.296	0.297
68–87	0.292	0.306	0.307	0.309	74–89	0.300	0.311	0.313	0.314
87–95	0.308	0.317	0.319	0.320	89–95	0.305	0.314	0.316	0.317

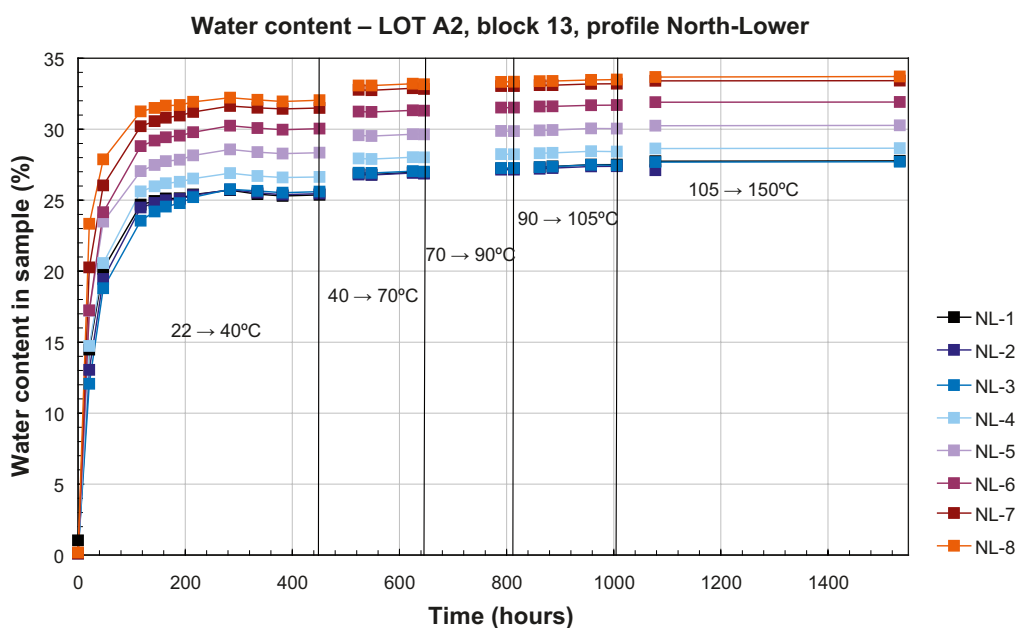


**Figure A8-23.** Water content in the North-Lower profile as a function of time of drying and drying temperature augmented incrementally.

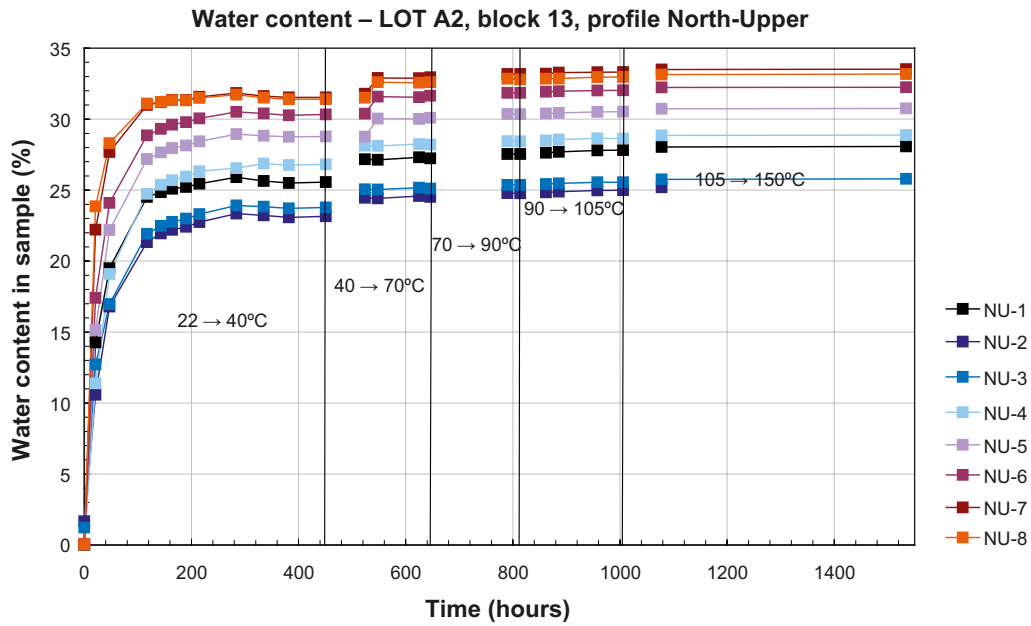


Figure A8-24. Water content in the North-Upper profile as a function of time of drying and drying temperature augmented incrementally.

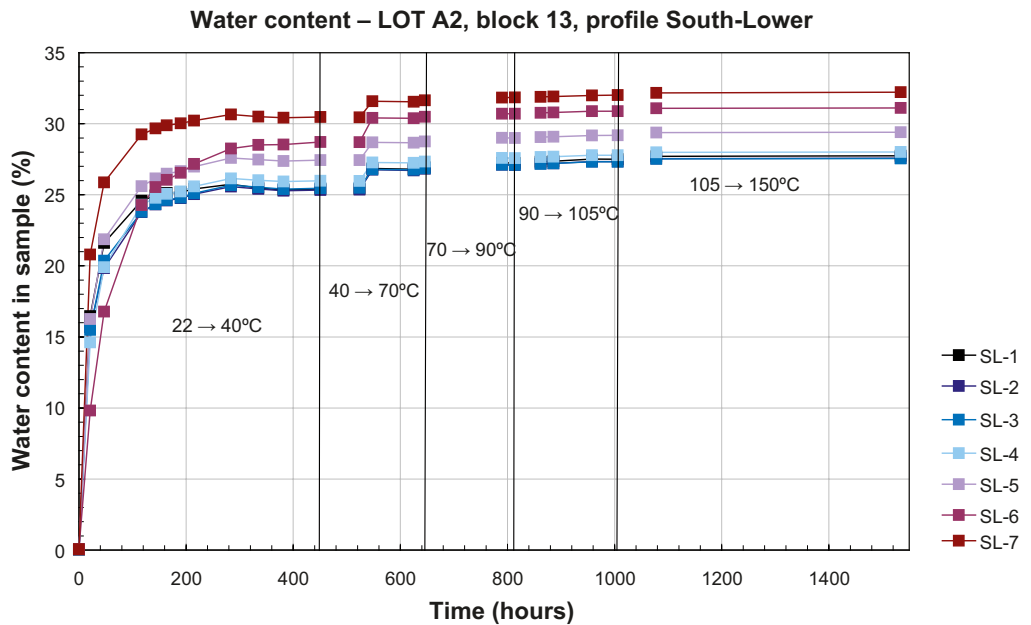


Figure A8-25. Water content in the South-Lower profile as a function of time of drying and drying temperature augmented incrementally.

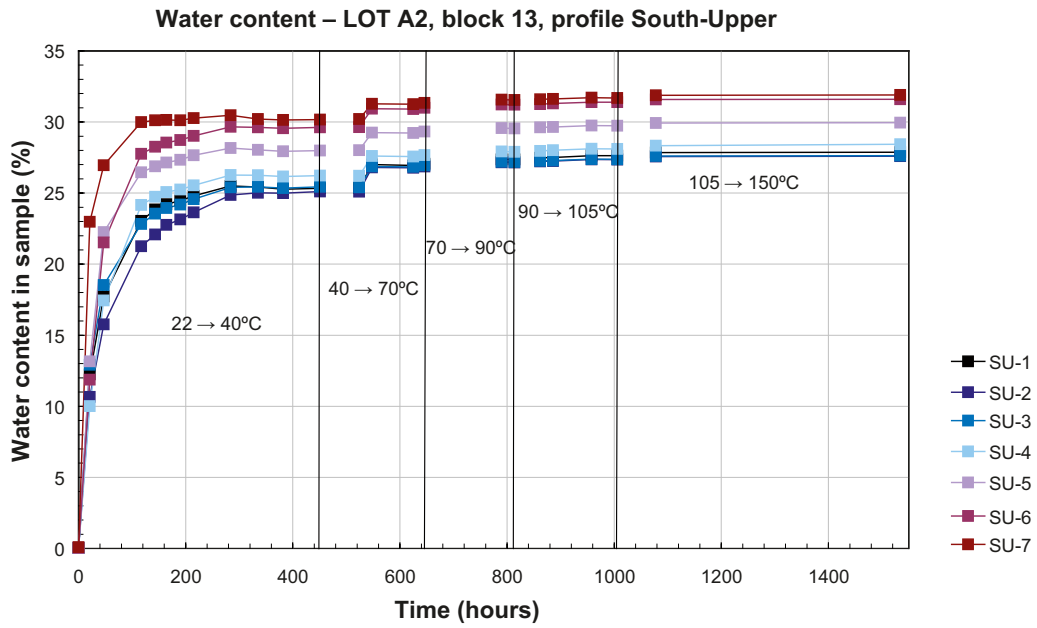


Figure A8-26. Water content in the South-Upper profile as a function of time of drying and drying temperature augmented incrementally.

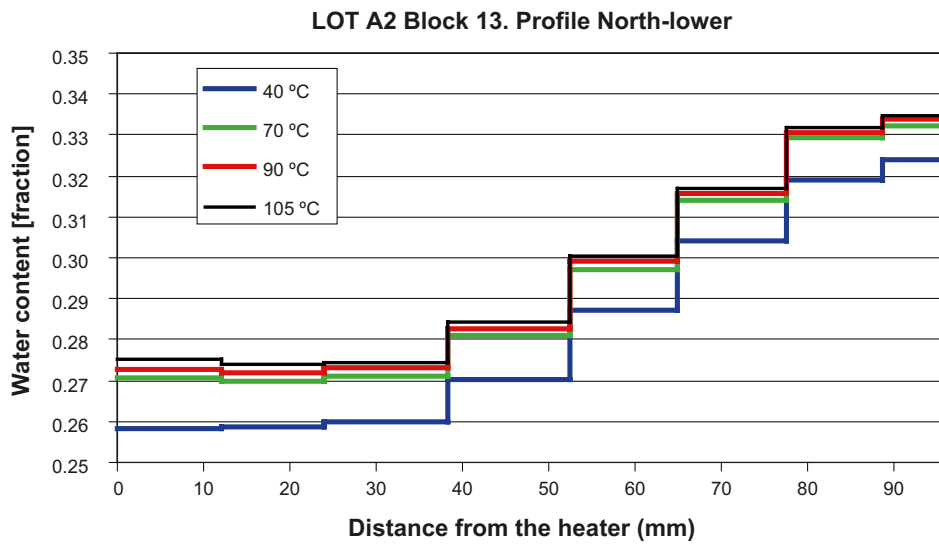


Figure A8-27. Water content at selected temperatures in the North-Lower profile in function of the distance from the heater.

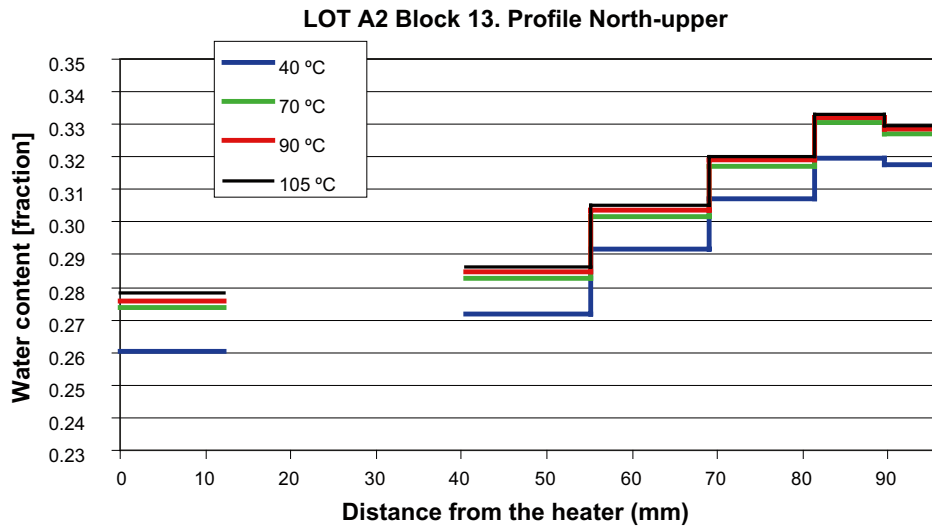


Figure A8-28. Water content at selected temperatures in the North-Upper profile in function of the distance from the heater.

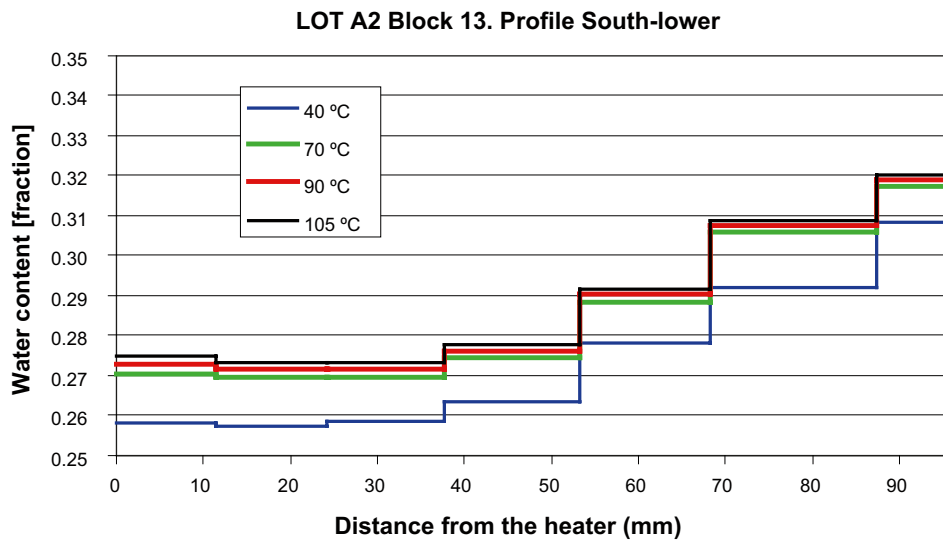
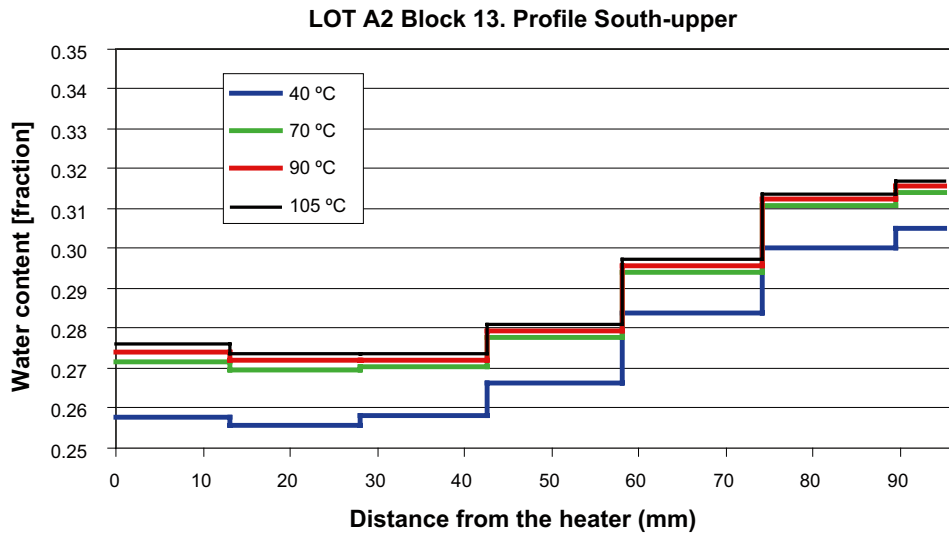
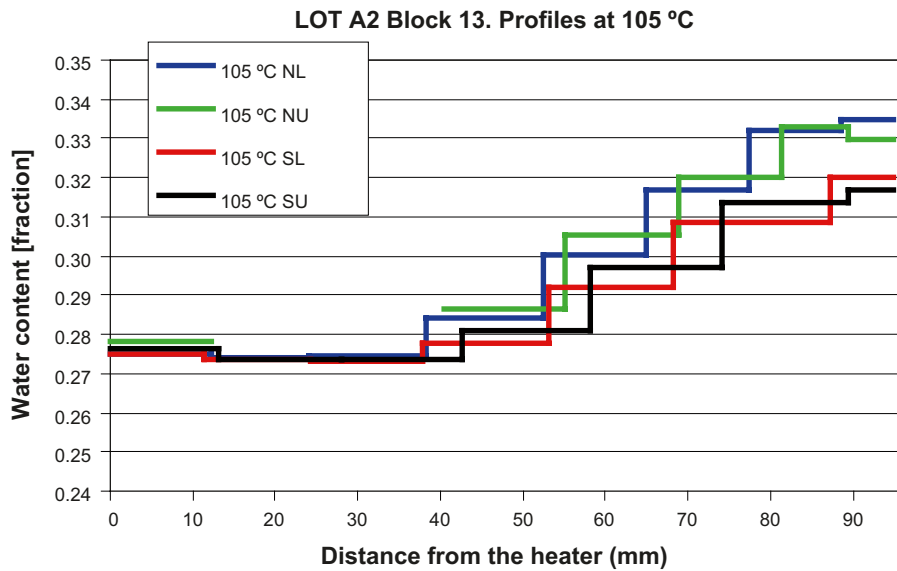


Figure A8-29. Water content at selected temperatures in the South-Lower profile in function of the distance from the heater.



*Figure A8-30. Water content at selected temperatures in the South-Upper profile in function of the distance from the heater.*



*Figure A8-31. Comparison of the water content in all profiles at 105°C, in function of the distance from the heater.*

## Appendix B

### XRD data

The XRD patterns are displayed in Figures A8-32 to A8-44. See Table A8-9 for a summary and overview of samples and sample preparation.

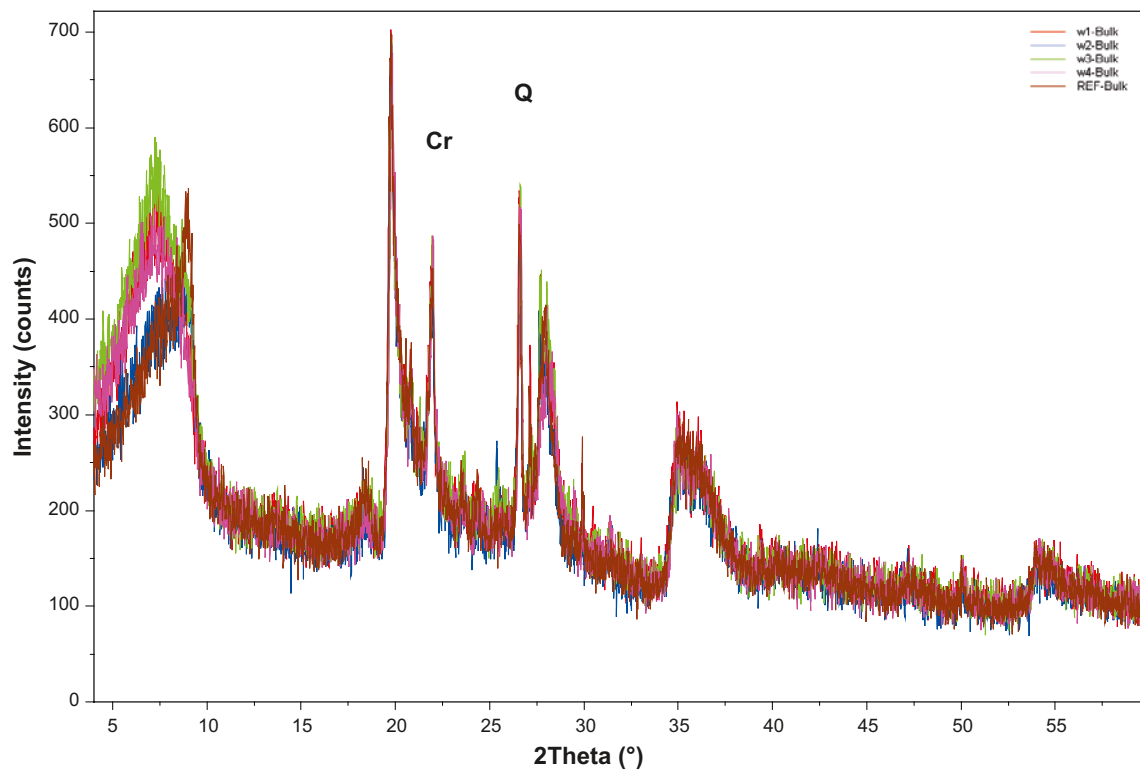


**Figure A8-32.** Disoriented bulk samples: Profile W1 to W4 compared to reference sample (REF-Bulk). Cr = cristobalite; Q = quartz.

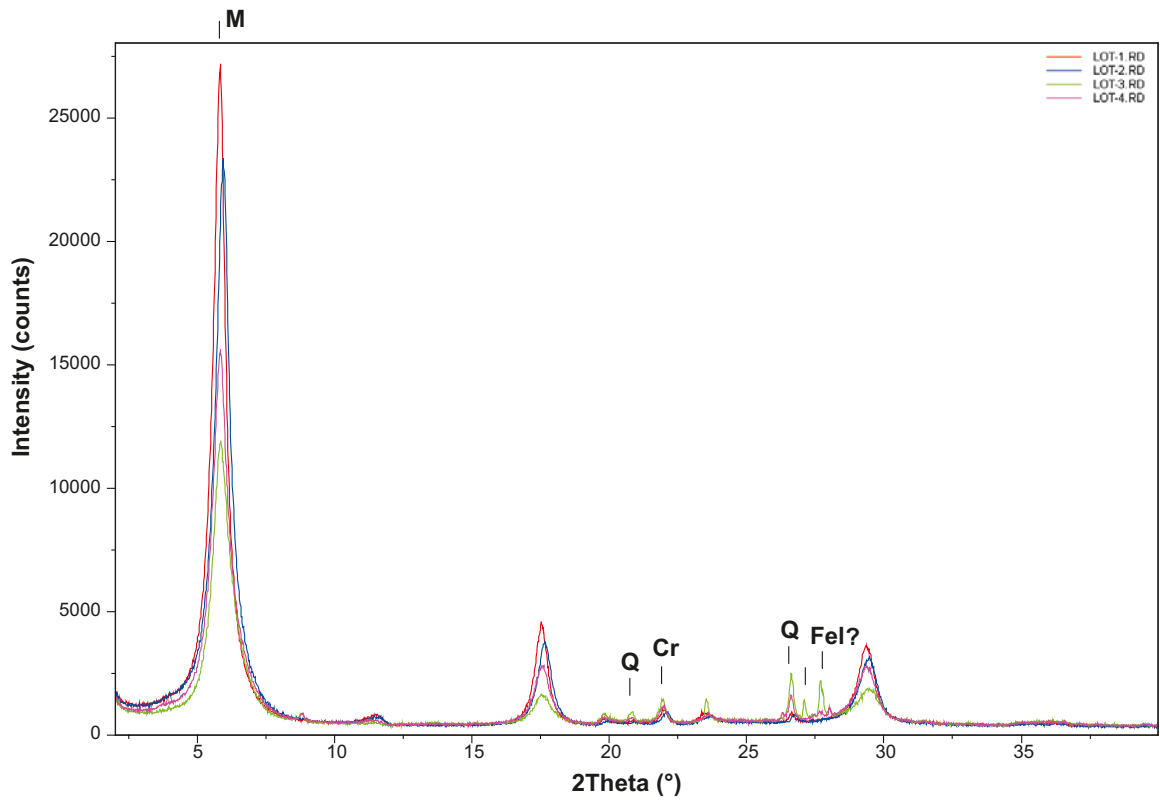


Figure A8-33. Test samples for optimizing measurement conditions. Cr = cristobalite; Q = quartz; Fel = feldspars; M = montmorillonite.

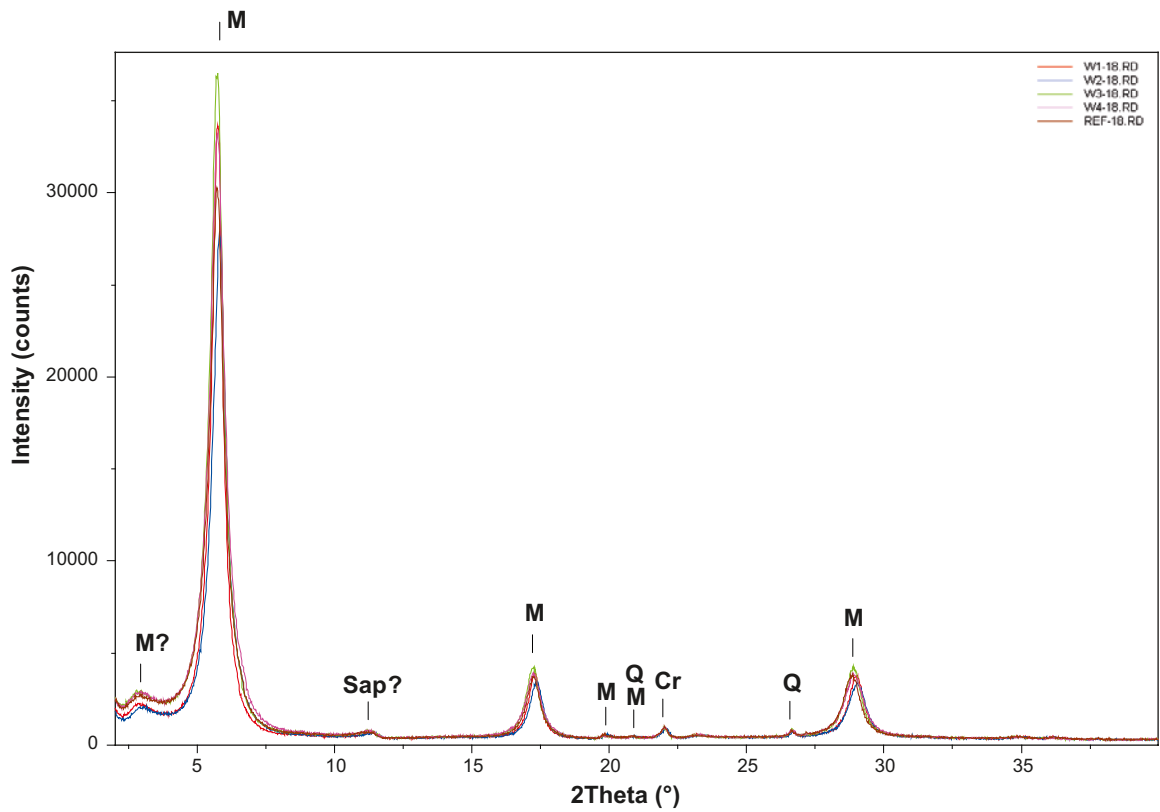
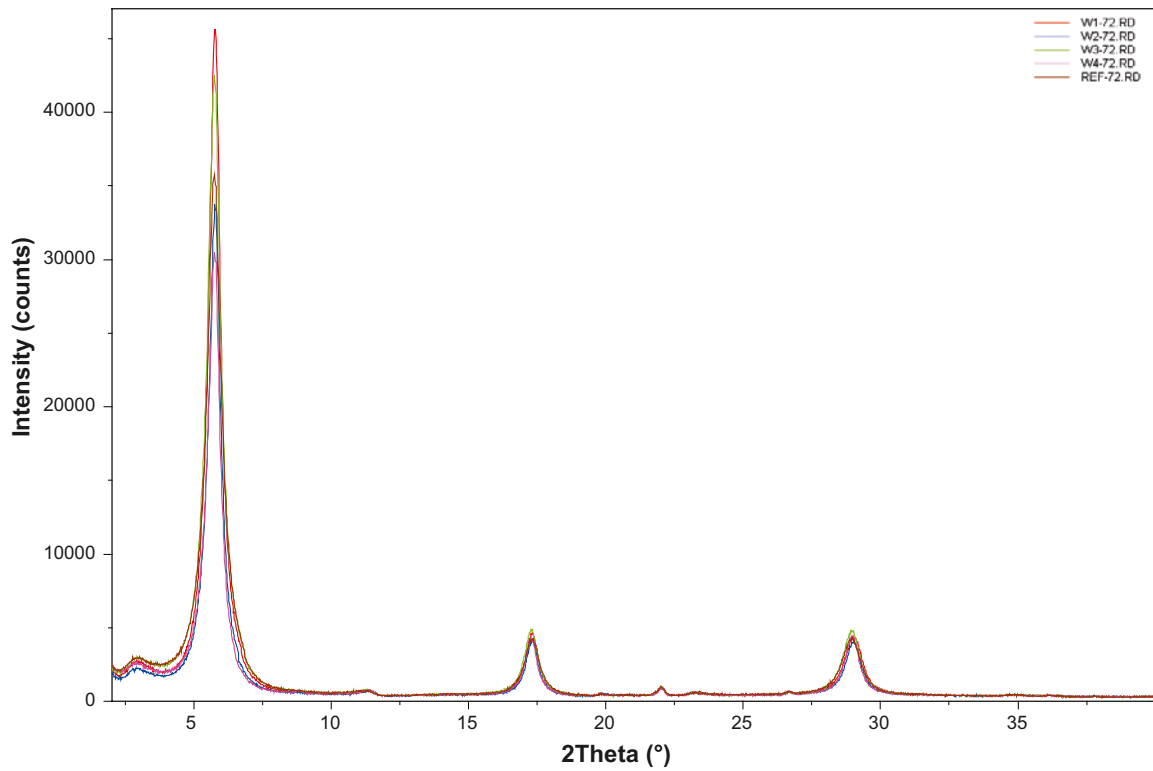
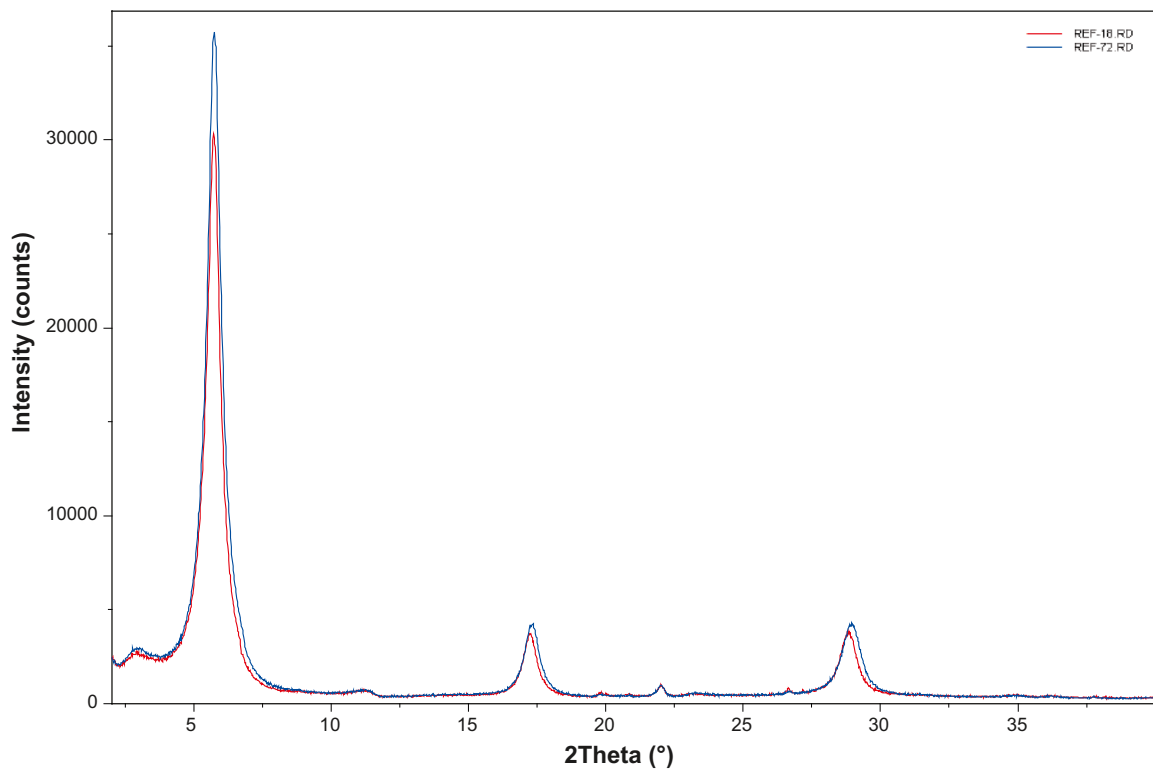


Figure A8-34. Oriented clay samples, 18 hours of sedimentation. Profile W1 to W4 compared to reference. Cr = cristobalite; Q = quartz; M = montmorillonite; Sap = saponite.



**Figure A8-35.** Oriented clay samples, 72 hours of sedimentation. Profile W1 to W4 compared to reference. See Figure A8-34 for peak labels.



**Figure A8-36.** Comparison between 18 and 72 hours of sedimentation, reference sample. See Figure A8-34 for peak labels.

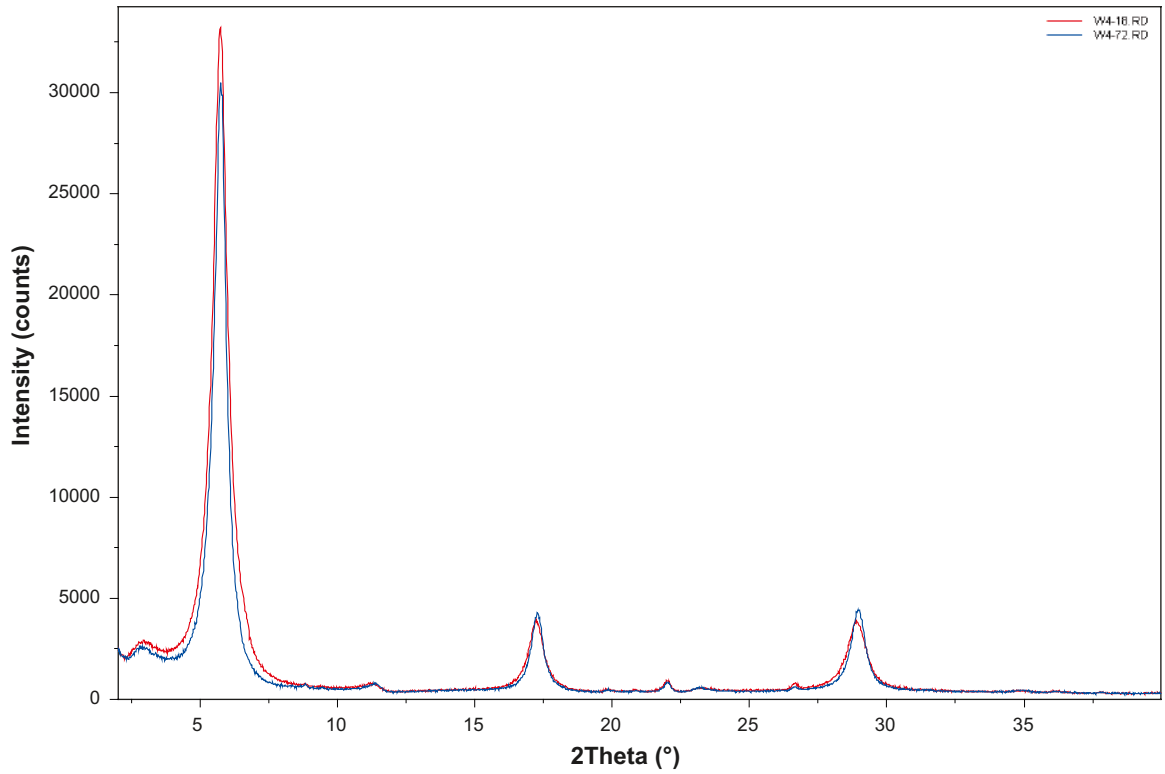


**Figure A8-37.** Comparison between 18 and 72 hours of sedimentation, profile sample W4 (cold end). See Figure A8-34 for peak labels.

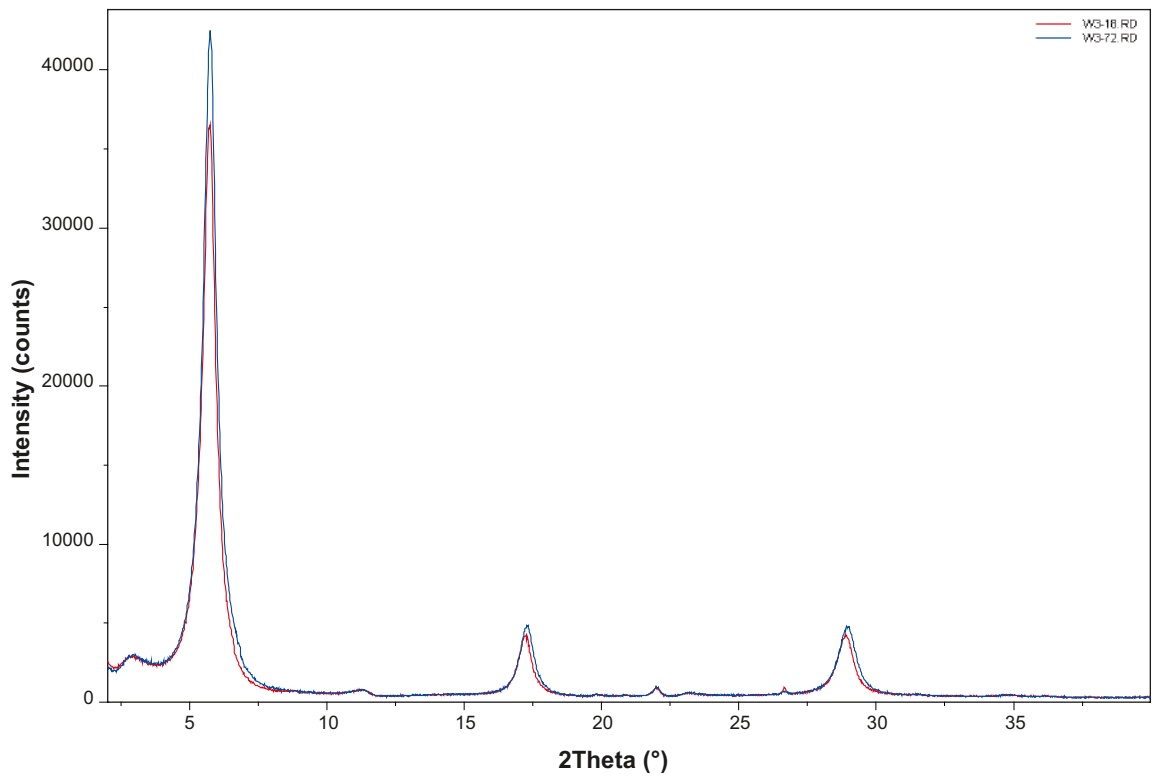


**Figure A8-38.** Comparison between 18 and 72 hours of sedimentation, profile sample W3. See Figure A8-34 for peak labels.

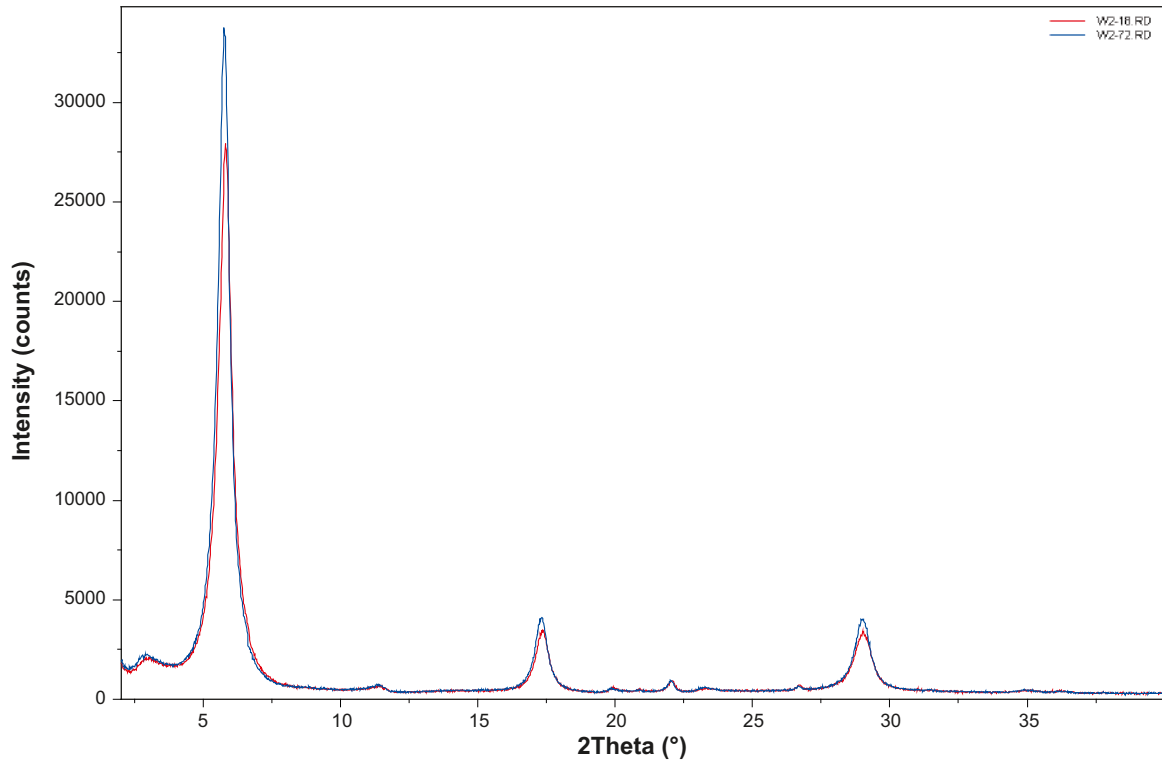


**Figure A8-39.** Comparison between 18 and 72 hours of sedimentation, profile sample W2. See Figure A8-34 for peak labels.

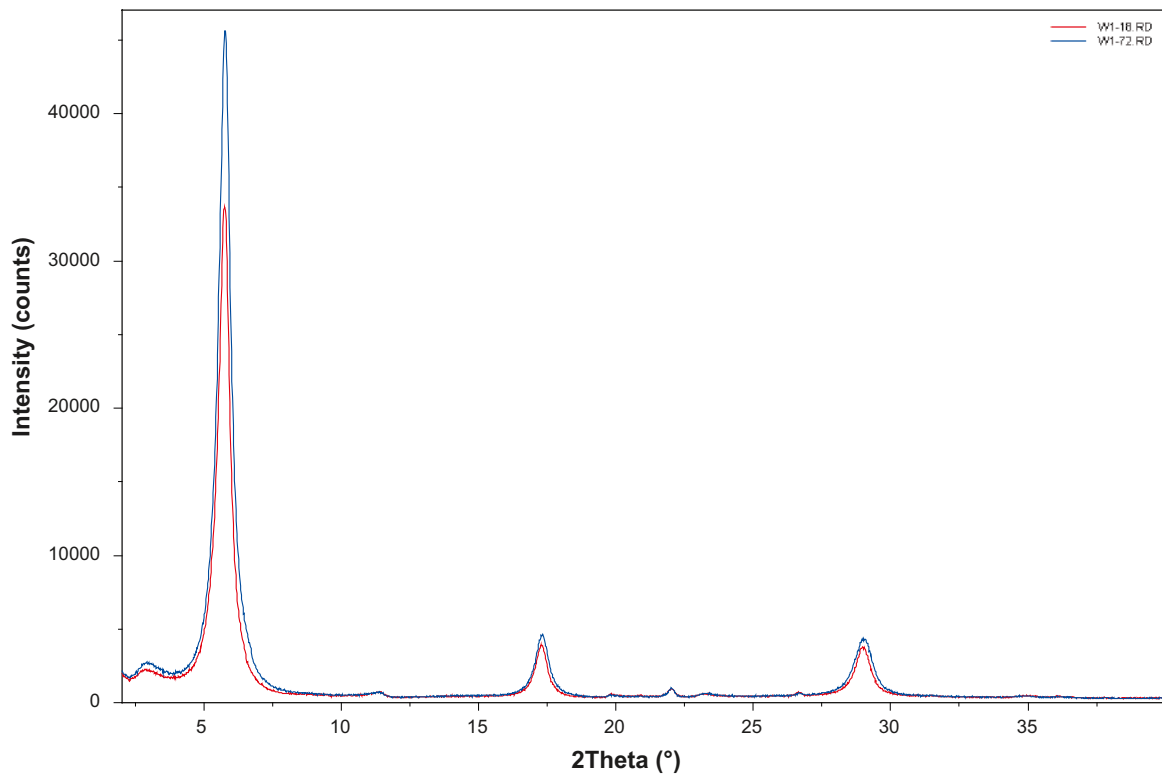


**Figure A8-40.** Comparison between 18 and 72 hours of sedimentation, profile sample W1 (hot end). See Figure A8-34 for peak labels.

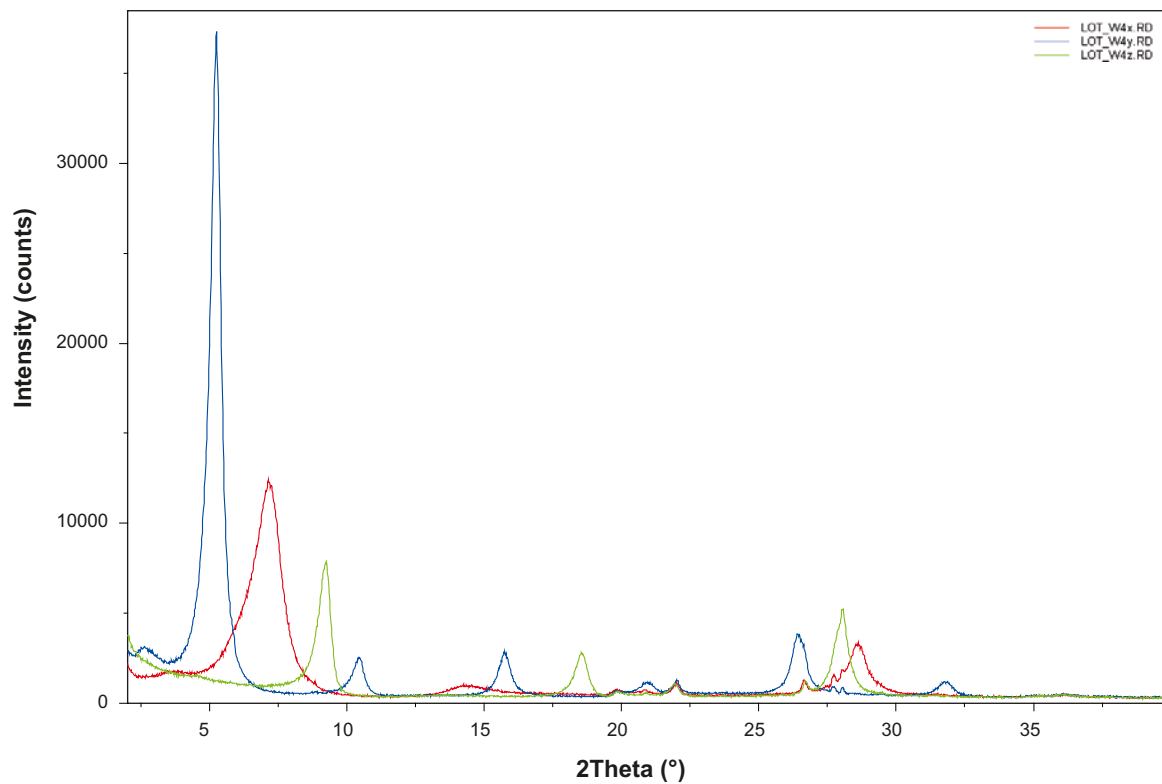


**Figure A8-41.** Profile sample W4 (cold end): *x* = dry sample; *y* = ethylenglicol saturated; *z* = heated at 550°C for 2 h.

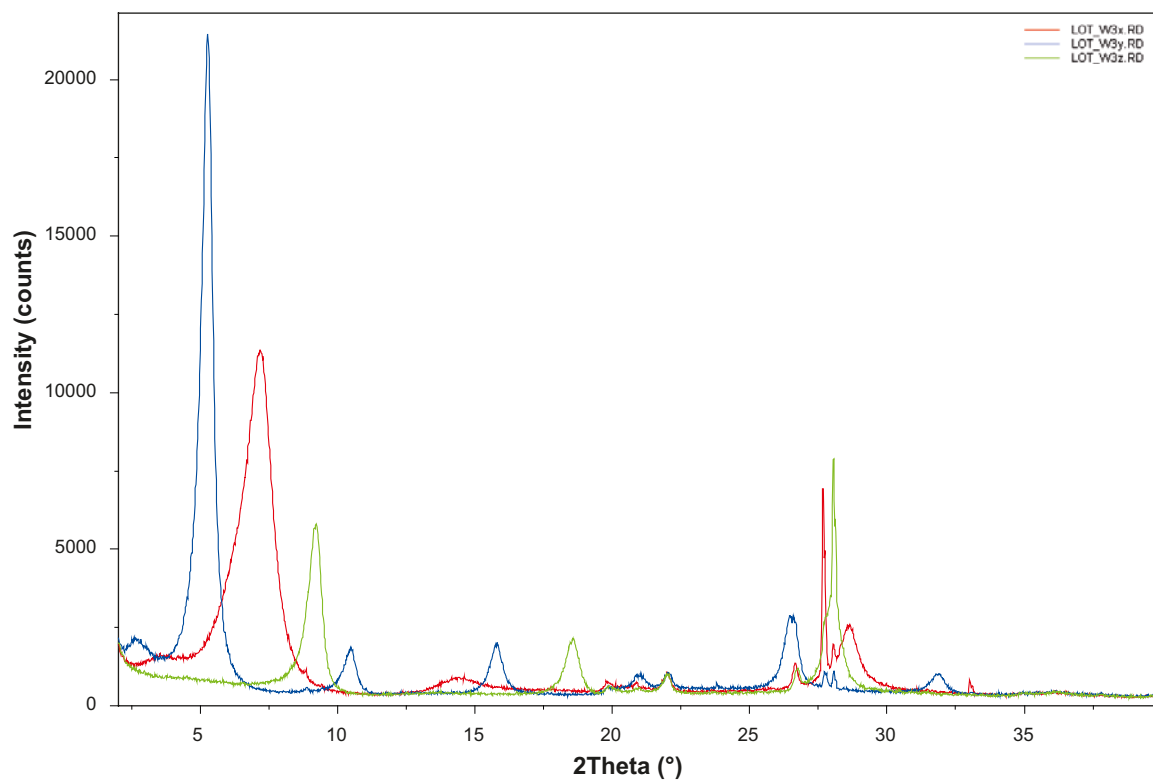


**Figure A8-42.** Profile sample W3: *x* = dry sample; *y* = ethylenglicol saturated; *z* = heated at 550°C for 2 h.

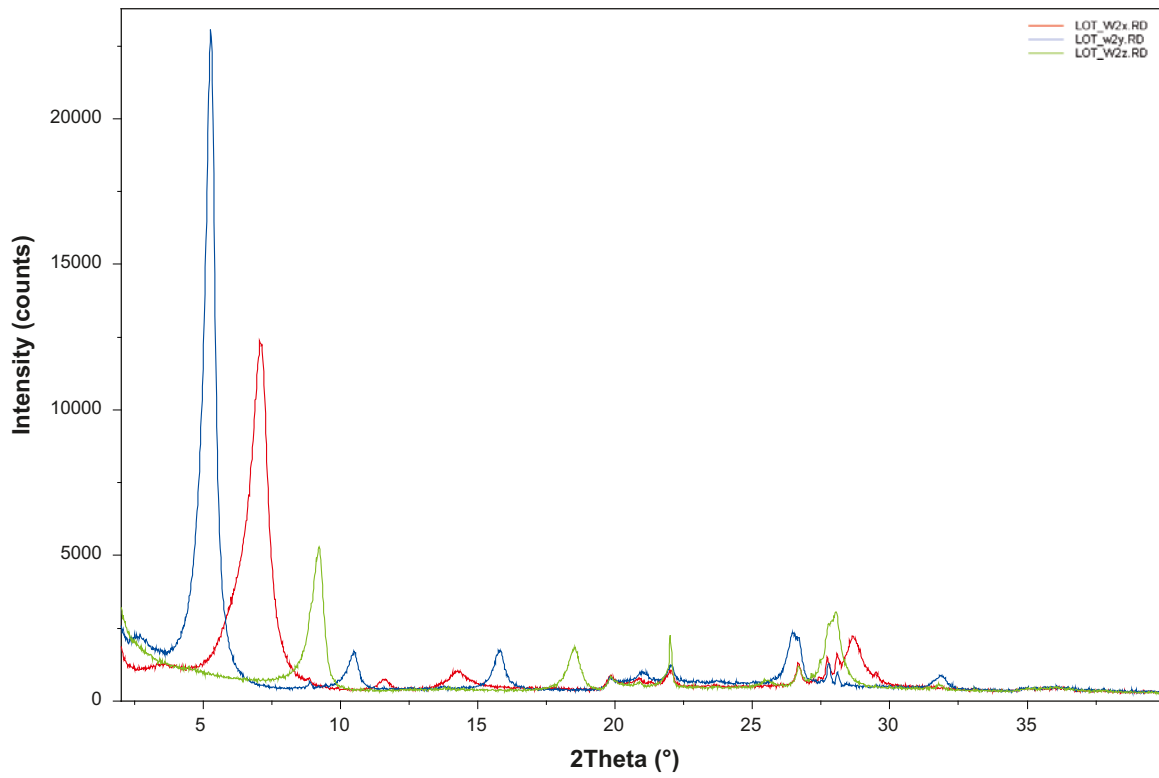


Figure A8-43. Profile sample W2:  $x$  = dry sample;  $y$  = ethylenglicol saturated;  $z$  = heated at 550°C for 2 h.

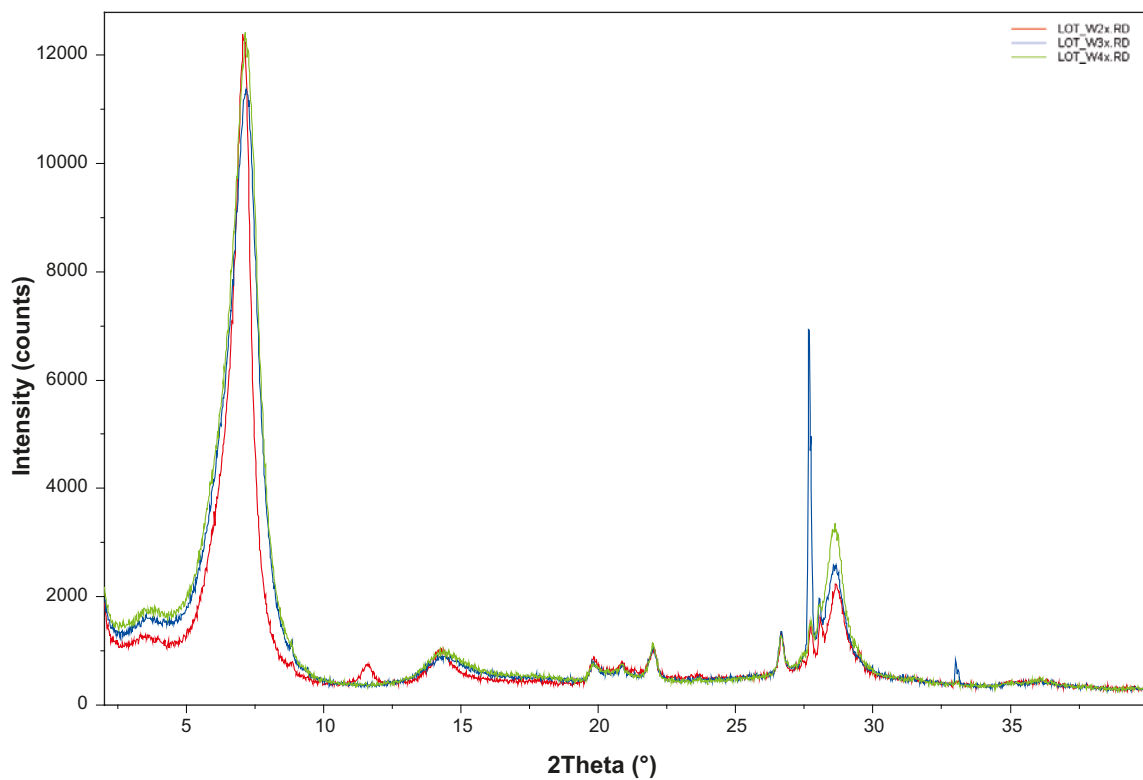


Figure A8-44. Profile sample W2, W3 and W4 (cold end): oriented dry samples.

## Aqueous extract data

Cation and anion concentrations of aqueous extracts from Block 13 of Parcel A2 of the LOT Experiment are summarized in Table A8-17.

**Table A8-17. Aqueous extract concentrations in samples from LOT A2, Block 13 (mmol/l).**

Sample (S:L = 0.1:1)	Na <sup>+</sup>	K <sup>+</sup>	Mg <sup>+2</sup>	Ca <sup>+2</sup>	Sr <sup>+2</sup>	F <sup>-</sup>	Cl <sup>-</sup>	Br <sup>-</sup>	SO <sub>4</sub> <sup>2-</sup>	NO <sub>3</sub> <sup>-</sup>	Alkal- inity (as HCO <sub>3</sub> <sup>-</sup> )	pH	Charge balance error (%)
LOT A2-13-1	13.31	0.15	0.04	0.12	1.63E-03	0.06	0.40	6.50E-03	4.17	1.30E-01	4.40	9.19	1.60
LOT A2-13-2	13.28	0.13	0.02	0.11	1.68E-03	0.06	0.40	N.D.	4.20	1.30E-01	4.31	9.16	1.35
W-1B-1	14.98	0.17	0.04	0.19	1.97E-03	0.05	2.69	6.53E-03	4.93	1.54E-02	2.60	8.73	1.22
W-1B-2	15.69	0.19	0.05	0.18	2.00E-03	0.05	2.71	6.57E-03	5.30	1.70E-02	2.55	8.95	1.24
W-2B-1	22.09	0.31	0.09	0.48	6.29E-03	0.04	2.74	N.D.	9.84	1.24E-02	1.65	8.91	1.26
W-2B-2	22.03	0.31	0.08	0.47	6.36E-03	0.04	2.66	N.D.	9.78	1.25E-02	1.52	8.96	0.73
W-3B-1	15.64	0.19	0.04	0.16	2.53E-03	0.06	3.14	N.D.	5.46	1.36E-02	2.14	9.18	0.15
W-3B-2	14.86	0.18	0.03	0.14	2.73E-03	0.06	3.13	N.D.	4.94	1.35E-02	2.23	9.11	0.24
W-4B-1	10.21	0.12	0.01	0.08	6.86E-04	0.10	3.78	6.52E-03	1.20	1.39E-02	3.41	9.30	4.05
W-4B-2	10.28	0.10	0.02	0.08	6.93E-04	0.10	3.81	5.35E-03	1.16	1.31E-02	3.45	9.26	4.61

N.D. = not detected.

## Appendix D

### Exchangeable cation data

Uncorrected cation concentrations derived from Ni-en extracts expressed in meq per 100 g dry mass from Block 13 of Parcel A2 of the LOT Experiment are summarized in Table A8-18. Also included is the sum of the cations and the total Ni consumption.

**Table A8-18. Uncorrected concentrations of exchangeable cations recalculated to dry mass (meq/100 g) and total Ni consumption.**

Sample S:L	pH	Ca	Mg	K	Na	Sr	Cu	meq cat./100 g	meq Ni/100 g
Ni LOT A2-13 0.5/1	7.86	17.0	4.19	1.38	58.1	4.71e-1	N.D.	81.14	110.8
Ni LOT A2-13 0.5/2	7.87	17.5	4.09	1.36	58.1	4.67e-1	N.D.	81.52	111.0
Ni W-1B 0.5/1	8.25	25.0	6.06	1.30	55.4	4.51e-1	1.64	89.85	107.7
Ni W-1B 0.5/2	8.24	25.0	6.26	1.28	55.2	4.49e-1	1.63	89.82	107.1
Ni W-2B 0.5/1	8.14	27.7	5.14	1.54	59.1	5.08e-1	1.51e-2	94.00	115.1
Ni W-2B 0.5/2	8.13	27.3	5.12	1.54	59.3	5.20e-1	1.52e-2	93.80	116.2
Ni W-3B 0.5/1	8.09	23.0	4.97	1.37	59.0	4.92e-1	1.49e-3	88.83	115.0
Ni W-3B 0.5/2	8.08	22.8	5.09	1.36	59.1	4.84e-1	1.53e-3	88.84	115.7
Ni W-4B 0.5/1	8.05	16.2	5.47	1.29	60.6	4.50e-1	6.98e-2	84.08	113.3
Ni W-4B 0.5/2	8.05	16.2	5.33	1.25	59.7	4.46e-1	5.05e-2	82.98	114.8

N.D. = not detected.

ISSN 1404-0344

CM Gruppen AB, Bromma, 2009